NASA Conference Publication 3190

The Evolution of Galaxies and Their Environment

Proceedings of the Third Teton Summer School on Astrophysics Sponsored by the Universities of Colorado and Wyoming Grand Teton National Park, Wyoming USA July 5-10, 1992

NASA

NASA Conference Publication 3190

The Evolution of Galaxies and Their Environment

Edited by
David Hollenbach
Ames Research Center
Moffett Field, California

Harley Thronson
Wyoming Infrared Observatory
University of Wyoming

J. Michael Shull
Joint Institute for Laboratory Astrophysics
University of Colorado

Proceedings of the Third Teton
Summer School on Astrophysics
Sponsored by the Universities of
Colorado and Wyoming
Grand Teton National Park, Wyoming USA
July 5-10, 1992

National Aeronautics and
Space Administration

Ames Research Center
Moffett Field, California 94035-1000

1993

Abstract

The Third Teton Summer School on Astrophysics entitled "The Evolution of Galaxies and Their Environment" was held on July 5-10, 1992, to discuss the formation of galaxies, star formation in galaxies, galaxies and quasars at high redshift, and the intergalactic and intercluster medium and cooling flows. Observational and theoretical research on these topics was presented at the meeting and summaries of the contributed papers are included in this volume.

The papers covered a broad range of research on galaxy environment and evolution and focused on such topics as the Cosmic Background Explorer (COBE) observations of the microwave background, the evolution of the large scale structure of the universe, the formation of galaxies, stellar population synthesis and galaxian spectral evolution, the nature of high redshift objects, X-ray observations of galaxies, the intergalactic medium, quasar absorption lines, cooling flows, mergers and interactions among galaxies, galactic clusters and their evolution, star formation in galaxies, galactic winds, and the central energy source for active galaxies. A number of papers examined galaxy morphology and luminosity functions.

Some emphasis was given to the origin and evolution of quasars. A number of papers examined the origin of the Lyman alpha forest of absorption lines from distant quasars, and the implications for the conditions in the intergalactic medium.

Scientific Organizing Committee

M. Begelman

J. Binney

A. Heavens

D. Hollenbach

R. Kron

S. Kulkarni

C. Norman

P. Shapiro

J. M. Shull (Co-Chairman)

H. Spinrad

J. Stocke

H. A. Thronson (Co-Chairman)

A. Wolfe

Local Organizing Committee

D. Barnaby

K. Bella

J. Dove

E. Haskell

M. Mitchum

J. Moser

J. M. Shull (Co-Chairman)

H. A. Thronson (Co-Chairman)

Sponsors

University of Colorado

University of Wyoming

National Science Foundation

National Aeronautics and Space Administration

Preface and Acknowledgements

The Third Teton Summer School on Astrophysics was held during early July, 1992, at the Jackson Lake Lodge near the center of Grand Teton National Park, Wyoming. While the University of Colorado had informally supported the University of Wyoming during the first two conferences at this location, for the first time this year the two universities joined formally to host a gathering of about 310 astronomers and another 50 or so spouses, friends, guests, and children.

As with past meetings, there was a deliberate effort to include younger colleagues in all aspects of the meeting: as invited speakers, moderators, support personnel, and of course in the audience. Perhaps one area where we continue to neglect the advantages of new blood is in the Scientific Organizing Committee, where we continue to benefit from the contributions from many of the same people who have assisted so ably for the preceding two meetings. And all of us continue to grow older, despite a few external behavior patterns to the contrary.

We are especially grateful to the administration of the Universities of Colorado and Wyoming, including deans and department chairs, for continuing support for these conferences over the years. Once again, both the National Aeronautics and Space Administration and the National Science Foundation provided substantial aid. The NSF support went mainly for small grants to allow younger people to attend and the NASA support went primarily for support for invited speakers and to defray the costs of publication, including of course this volume.

Once again we enjoyed working with the staff of the Jackson Lake Lodge, which makes hosting a major scientific conference appear almost effortless.

We also took advantage of the support staff of both Universities: Marce Mitchum, Darcy Collins, Evelyn Haskell, Kim Bella, and Jo Moser. The meeting was ably supported by graduate students from both schools: David Barnaby, Jim Dove, Theresa Calovini, Steve Martin, Jim Dove, Kara Peterson, and Steve Penton.

Finally, we appreciate the advice and support of our colleagues, who serve to remind us how wonderfully human is the scientific enterprise.

The Editors

October, 1992

TABLE OF CONTENTS

Day 1: Monday, 6 July 1992

Day 2: Tuesday, 7 July 1992

Day 3: Wednesday, 8 July 1992

Day 4: Thursday, 9 June 1992

Additional Papers

How to get Unlimited Observing time on a 4 metre Telescope.

S.P.Driver.

Physics Department, University of Wales College of Cardiff,

PO Box 913, Cardiff, CF1 3TH,

Wales, UK.

Abstract

As the astronomical community moves ever more towards fewer and larger telescopes it is not just desirable but essential to make the maximum possible use of these new facilities. The Hitchhiker parallel CCD camera has been specially designed to increase the scientific output of a large telescope by imaging the off-axis field of view. The large data set collected by this instrument consists of deep CCD multicolour data of the distant Universe and is extremely well suited to the study of faint galaxies and their evolution, as well as other areas. The instrument's design and some of its projects are briefly discussed below and demonstrates the scientific value such instruments could have if incorporated on all new telescopes.

Introduction

Unlimited observing time on a 4 metre telescope, sounds like an astronomers dream come true. But at Cardiff this dream has been turned into reality. For over a year now students and staff have been able to collect high quality CCD data whenever desired. This has been made possible by a new step forward in instrument technology and telescope efficiency. The camera known as hitchhiker was installed on the William Herschel Telescope (WHT) at La Palma in November 1990 and fully operational by February 1991. This novel instrument contains two unique features in the realm of CCD imaging. Firstly, it images the off-axis field of view allowing it to be operated whenever small field of view or spectroscopic instruments are being used. Secondly, it uses two CCD's to image one 6 by 4 arcmin field in two broadband colours simultaneously.

So, not only does Hitchhiker increase the scientific output of the telescope by collecting otherwise wasted light, but doubles up again because of its dual colour capability. As the majority of work on a large telescope tends to be spectroscopic Hitchhiker can be used for most nights of the year. The obvious constraints on the instrument are that its direction and exposure time are governed by the spectroscopic observer who always has priority. However the amount of data potentially available is enormous and this allows us to pick and choose which programs to observe with and at which times of the year. For example Hitchhiker is currently only run during darktime when the galactic plane is not overhead. Even so the dataset collected is still large and suitable to a wide range of survey projects.

Camera design

In essence the Hitchhiker parallel CCD camera (Disney et al 92) uses two P88200 EEV CCDs (770 x 1152) to image a single 6 x 4 arcmin field of view, through two broadband filters by using a beam splitter. This gives 0.3 arcsecond resolution pixels and the center of the field of view is 7 arcmins from the WHT field center. The CCD system is controlled by a 386 IBM compatible PC and is completely independent of the WHT control computers. Inside the camera itself are six motors, also controlled from the PC, which move the focussing optics, filter wheels and dichroic slide. Currently Hitchhiker can observe in B and R, V and I or B and I broadband filters, this combination allows for accurate colour measurement with only one calibration point necessary.

Science projects underway

Hitchhiker has now covered about 1.3 square degrees of sky in two or more filters and in exposure times varying from 10 minutes to 2 hours. For comparison a single half hour exposure by Hitchhiker will sample a similar volume to a half hour schmidt plate. This reflects the much greater depth to which Hitchhiker can observe as its field of view is only about $\frac{1}{7000}^{th}$ of a schmidt plate. The data is suitable for any survey program where there are few constraints on the direction from which the data comes. The Cardiff group have a large number of scientific projects in mind, most important amongst these at the moment are;

- **Searching for very low surface brightness galaxies** — Cardiff have always been heavily involved in the survey for low surface brightness objects (Davies 92) and Hitchhiker data surveys a considerably deeper/fainter portion of the sky than other surveys. Careful reduction techniques have been developed which preserve structure on scales upto an arcminute.

- **Studying faint galaxies and clusters** — Recently (Tyson 88; Metcalfe 91; Lilly et al 91) there has been much work on matching the observed number counts to predicted cosmological models. Whilst Hitchhiker is unlikely to achieve the very deep number counts obtained from long integration CCD frames it is able to survey a large fraction of a square degree to greater depth than before and with accurate relative colours. Already Hitchhiker is obtaining multicolour number counts for objects upto blue magnitudes 26.5 and red magnitudes 26.0 (Driver 92). See pictures below.
- **Supernova candidates** — A number of supernova candidates are observed and provided they are quickly identified spectroscopic follow ups could be made.
- **Searching for primaeval galaxies** — As well as specific survey projects along established areas of research it is hoped that Hitchhiker will uncover a number of serendipitous discoveries. Very similar to the search for high luminosity low surface brightness galaxies is the search for primaeval galaxies (Uson 91) and this area of research can be carried out within the LSB program.
- **Searching for gravitational lenses** — Many groups in the UK and abroad are interested in studying the very distant universe via gravitational lenses and Hitchhiker should be capable of detecting many new lensing candidates.
- **Faint stars** — Although the group at Cardiff are primarily concerned with the study of faint and LSB galaxies collaborators are intending to use Hitchhiker data to study the halo distribution of faint stars and brown dwarves.

The images below show the same 5 by 3.5 arcmin field but in three broadband colours B, V and R, the exposure times are 2 hours, 30 mins and 2 hours respectively. In excess of 1000 galaxies have been identified on all three frames and there broadband colours measured (Driver 92). Finally recall that this data was collected whilst simultaneous spectroscopic observations were in progress.

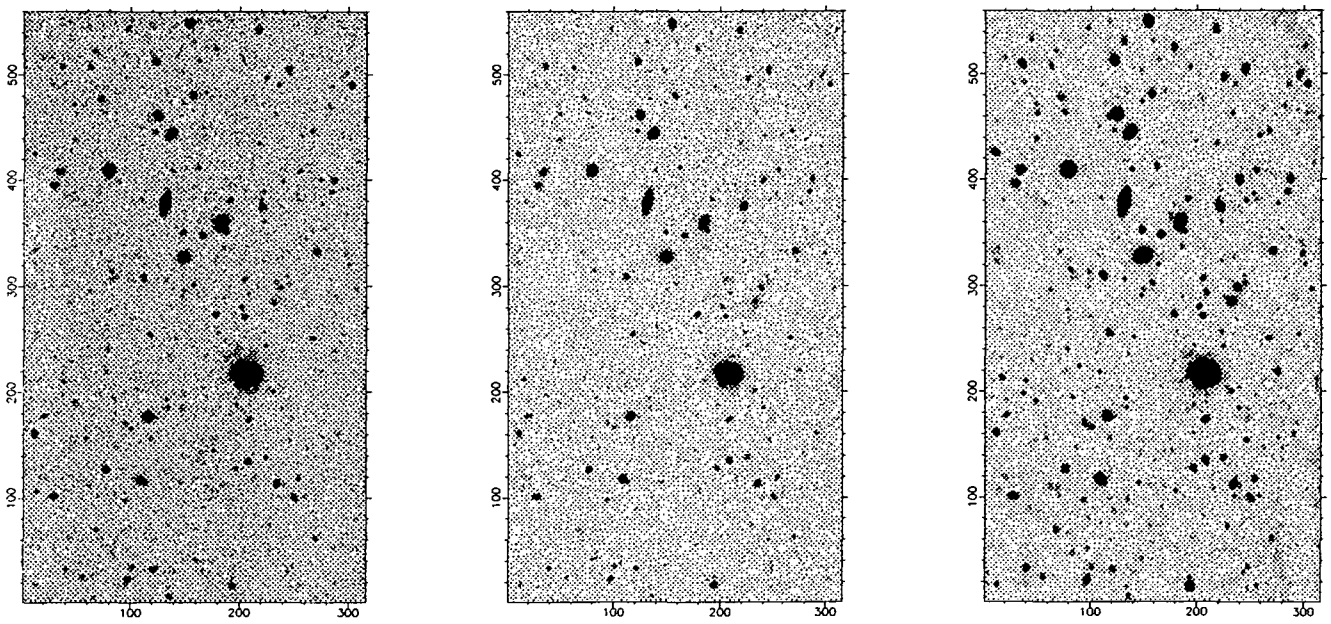

Conclusion

The Hitchhiker camera offers us a unique opportunity to sample large volumes of the Universe with multi-colour CCD exposures. Parallel observing works and is an efficient cost-effective way for sky surveys to keep in touch with the development of very large telescopes. These large telescopes and their on-axis instruments need to be fed a diet of comparable survey data if they are to be fully utilized. Overall, we think it is essential to consider incorporating similar instruments in the design and construction of all new, large telescopes — not doing so can be viewed as an excessive waste of money and potential scientific knowledge.

References

Davies, J.D., 1992. Invited Review this conference.
Disney, M.J. et al 1992. Mon. Not. R. astr. Soc submitted.
Driver, S.P. et al 1992 *Colours of Faint Galaxies* In preparation.
Lilly, S.J. et al 1991. Astrophys. J., **369**, 79.
Metcalfe, N. et al 1991 Mon. Not. R. astr. Soc., **249**, 498.
Tyson, J.A. 1988. Astr. J., **96**, 1.
Uson, M.J. et al 1991. Physical Review Letters., **Vol 67, No 24**, 3328.

Cosmology with Liquid Mirror Telescopes

David W. Hogg, Brad K. Gibson, Paul Hickson
(University of British Columbia)

Liquid mirrors provide an exciting means to obtain large optical telescopes for substantially lower costs than conventional technologies. The liquid mirror concept has been demonstrated in the lab with the construction of a diffraction limited 1.5m mirror (Borra et al. 1989). The mirror surface, using liquid mercury, forms a perfect parabolic shape when the mirror cell is rotated at a uniform velocity. An f/1.9 2.7m liquid mirror observatory is now nearing completion at a site near Vancouver, B.C.. The *UBC/Laval liquid mirror observatory* is expected to begin a survey of quasars and galaxies in the fall of 1992. The successful demonstration of the 2.7m observatory may usher in an era of 4-8m liquid mirror telescopes (LMTs).

The primary disadvantage of liquid mirrors is their inability to point, being restricted to observations at the zenith. The use of large format CCD's, read out using the time-delay and integrate (TDI) technique (McGraw et al. 1986) compensates for the earth's rotation as the image crosses the telescope's field of view. The telescope than has access to the strip of sky that passes overhead over the course of a year. The disadvantage of being restricted to observations at the zenith is mitigated in cosmological studies, where surveys of any strip of sky can provide valuable information.

A liquid mirror must be able to support a heavy mercury load with minimal flexure and have a fundamental resonant frequency that is as high as possible, to suppress the amplitude of surface waves caused by small vibrations transmitted to the mirror. To minimize the transmission of vibrations to the liquid surface, the entire mirror rests on an air bearing. This necessitates the mirror cell being lightweight, due to the limited load capabilities of the air bearing. The mirror components must also have physical characteristics which minimize the effects of thermal expansion with ambient temperature fluctuations in the observatory. In addition, the 2.7m mirror construction is designed so that the techniques used may be readily extended to the construction of larger mirrors.

To attain the goals of a lightweight, rigid mirror, a composite laminant construction (such as is found in the aerospace industry) was used (Hickson et al. 1992). The mirror consists of a foam core cut to the desired parabolic shape, with an accuracy of a few mm. An aluminium hub serves as an anchor for the foam and skin, and allows precise centering of the mirror on the air bearing and drive system. Several plys of Kevlar, covered in an epoxy matrix, are then applied to the foam. A final layer of pure epoxy is formed by spin casting. This final layer is parabolic to within a fraction of a mm. An aluminium ring bonded to the circumference of the mirror retains the mercury, and incorporates stainless-steel hard-points for the attatchment of balance weights.

The mirror cell is covered with a 1-2mm layer of liquid mercury. A transparent monomolecular layer on the surface of the mercury suppresses sufrace waves and virtually eliminates evaporation. The reflectivity of mercury is about 79% from 3100 $\rightarrow$ 8700Å as compared to 92% for a fresh aluminium layer in the visible. However, it is pointed out

that the aluminium coating deteriorates as it oxidizes, while mercury oxidizes very slowly and is easy to clean (Borra et al. 1992).

To obtain high image quality, the angular velocity of rotation must be uniform to within 10^{-7}. This is achieved by driving the mirror with a synchronous motor, controlled by a quartz-oscillator.

A preleminary survey is expected to begin in the fall of 1992. The total survey area will be approximately 20 deg^2, consisting of a strip of sky 21′ wide, at a declination of 49°04′. A Loral 2048×2048 CCD wil be used, read out using the TDI technique clocked at the siderial rate (Gibson et al. 1992). This will provide an integration time of approximately 2 minutes per filter.

Spectrophotometry will be obtained by multiband imaging through a series of 40 intermediate band filters, each with a bandwidth of $\Delta\lambda/\lambda_c \approx 0.046$, uniformly sampling the entire optical spectrum: $14.87 \leq \log\nu_c \leq 14.48(4000 \rightarrow 10000\text{Å})$ where the filter central wavelength separation is $\Delta \log\nu_c = 0.01$. A different filter will be used each night, building up over a two-year period spectral energy distributions (SEDs) of all detectable objects down to a limiting magnitude of $V \sim 21.4(S/N \approx 3)$. Theoretically this will yield SEDs for $\sim$ 20000 galaxies and $\sim$ 1000 QSOs. Photometric calibration will be derived from a sequence of secondary spectrophotometric standards in this region of the sky. The SEDs may then be used for determining redshifts and morphological type.

References

Borra, E.F., Content, R., Drinkwater, M.J., and Szapiel, S. 1989, ApJ, 346, L41

Borra, E.F., Content, R., Girard, L., Szapiel, S., Tremblay, L.M., and Boily, E. 1992, ApJ, 393, in press

Gibson, B.K., and Hickson, P. 1992, MNRAS, in press

Hickson, P., Gibson, B.K., and Hogg, D.W. 1992, PASP, submitted

McGraw, J.T., Cawson, M.G.M., and Keane, M.J., 1986, in Instrumentation in Astronomy VI, edited by D.L. Crawford (SPIE, Bellingham), p.60

HEAVY ELEMENT ABUNDANCES AND MASSIVE STAR FORMATION

Boqi Wang and Joseph Silk
Astronomy Department, University of California, Berkeley, CA 94720

The determination of the stellar initial mass function (IMF) remains a great challenge in astronomy. In the solar neighborhood, the IMF is reasonably well determined for stellar masses from about 0.1 $M_\odot$ to 60 $M_\odot$ (Scalo 1986). However, outside the solar neighborhood the IMF is poorly known. Among those frequently discussed arguments favoring a different IMF outside the solar neighborhood are the estimated time to consume the remaining gas in spiral galaxies, and the high rate of forming massive stars in starburst galaxies. An interesting question then is whether there may be an independent way of testing possible variations in the IMF. Indeed, the heavy elements in the interstellar medium are mostly synthesized in massive stars, so increasing, or decreasing, the fraction of massive stars naturally leads to a variation in the heavy element yield, and thus the metallicity. The observed abundance should severely constrain any deviations of the IMF from the locally determined IMF. We focus on element oxygen, which is the most abundant heavy element in the interstellar medium. Oxygen is ejected only by massive stars that can become Type II supernovae, and the oxygen abundance is therefore a sensitive function of the fraction of massive stars in the IMF. Adopting oxygen (rather than, *e.g.,* Fe) enables us to avoid uncertainties in Type I supernovae.

The ejected oxygen mass in the supernova event for a given stellar mass has been calculated for stars with solar metallicity by Arnett (1978), and more recently by Woosley and Weaver (1986), and Thielemann, Nomoto, and Hashimoto (1992). The agreement of the ejected oxygen mass for stars with masses larger than about 15 $M_\odot$ is fairly good among these authors, despite the difference in their adopted $^{12}C(\alpha,\gamma)^{16}O$ rate. There is, however, some discrepancy in the ejected oxygen mass at $m \simeq 12\ M_\odot$, presumably due to differences in stellar structure and different treatments of the convection (overshooting) in the different supernova models. The oxygen abundance yield weighted by the IMF, however, does not differ significantly among different models. This is primarily because the ejected oxygen mass increases very rapidly with stellar mass (approximately $\propto m^4$) at $m \simeq 12 - 20\ M_\odot$, and therefore for any reasonable IMF with a slope $x \lesssim 4$, the ejected oxygen is dominated by stars with masses $m \gtrsim 20\ M_\odot$. We use the nucleosythesis results to calculate the oxygen yield for given IMF. We then calculate the oxygen abundance in the interstellar medium assuming instantaneous recycling of oxygen.

We found that (1) Given that the oxygen abundance in our Galaxy as well as in many normal spiral galaxies is approximately solar, there is no evidence of variations in the IMF outside the solar neighborhood. (2) Both infall and ejection of interstellar gas can change the metallicity somewhat, but they at most can change the heavy element abundance by a factor of 2 in normal spiral galaxies as long as the infall or ejection rates are proportional to the rate of star formation. Ejection can be important in dwarf galaxies where the gravitational potential wells are shallow. This may partly explain the observed low metallicities of dwarf galaxies. (3) For starburst galaxies, truncation of the IMF at large m_l results in an abundance at least an order of magnitude over the solar value. Since the available observations of the oxygen abundance suggest otherwise, a truncated IMF alone cannot explain the starburst activity. If indeed the IMF is truncated in starburst galaxies, extremely efficient mass ejection from the starburst regions has to occur in order to dilute the metallicity. This is however a non-trivial task since the ejected material would amount

to many times the amount of matter existing in the starburst regions. Future observations of gas outflows in starburst galaxies should test models of a varying IMF. (4) Our method of using oxygen abundance can also be applied to extremely low-mass stars (*e.g.*, baryonic dark matter considered in galaxies) since their abundance determines the relative fraction of massive stars that can become supernovae, and thus the oxygen abundance. Clearly the slope of the IMF differs at low masses from that at high masses, therefore a useful constraint would require some knowledge of the slope of the IMF at low masses.

Arnett, D. 1978, Ap. J., 219, 1008.
Scalo, J.M. 1986, Fund. Cos. Phys., 11, 1.
Thielemann, F., Nomoto, K., and Hashimoto, M. 1992, in Supernovae, Les Houches, Session LIV 1990, eds J. Audouze, S.R. Bludman, R. Mochkovitch, J. Zinn-justin (Elsevier Science Publ.), in press.
Woosley, S.E., Weaver, T.A. 1986, in Radiation Hydrodynamics, IAU Colloq. No 89, eds D. Mihalas, and K.H. Winkler (Reidel, Dordrect), 91.
Wang, B, and Silk, J. 1992, Berkeley Preprint.

SURVEY INCOMPLETENESS AND THE EVOLUTION OF THE QSO LUMINOSITY FUNCTION

STEVEN R. MAJEWSKI
The Observatories of the Carnegie Institution of Washington,
813 Santa Barbara Street, Pasadena, CA 91101

JEFFREY A. MUNN, RICHARD G. KRON,
MATTHEW A. BERSHADY, JOHN J. SMETANKA
Yerkes Observatory, P.O. Box 258, Williams Bay, WI 53191-0258

DAVID C. KOO
Lick Observatory, UCSC, Nat. Sci. 2, Santa Cruz, CA 95064

It is a commonly held notion that there is a significant amount of evolution in the QSO luminosity function at relatively low redshifts ($z <\sim 2$). However, analyses of the QSO luminosity function often make use of data gathered heterogenously at different redshifts. Surveys are usually optimized for finding either low redshift ($z <\sim 2$) QSOs (e.g. Boyle *et al.* 1990; Schmidt & Green 1983) or high redshift ($z >\sim 2$) QSOs (e.g. Warren *et al.* 1991; Schmidt, Schneider & Gunn 1986), so that the redshift where the strong evolution is thought to begin is suspiciously coincident with the point at which survey strategies change. Before claims of rapid evolution at low redshifts can be made reliably, one must be confident that the apparent deficint in low redshift quasars compared to expectations from mildly evolving the high redshift population is not simply an artifact of sample incompleteness.

Are QSO surveys missing a significant fraction of low redshift QSOs? Recently Goldschmidt *et al.* (1992) have shown the Palomar-Green survey has a factor of 3.4 fewer quasars in one field in common between these two UV-excess surveys (which are most sensitive to QSOs with $z <\sim 2.2$). Hazard (1991) points out that the low redshift ($z = 2$) counterparts to the brightest $z \geq 4$ QSOs have apparent magnitudes of $16 < B < 17.5$ and therefore have spectra which are saturated (and therefore neglected) in typical objective prism surveys. Here we concentrate on a third type of survey which depends on selecting QSO candidates based on combinations of colors. Since QSOs have emission lines and power-law continua, they are expected to yield broadband colors unlike those of stellar photospheres. Previously, the fraction of QSOs expected to be hiding (unselected) within the locus of stellar $(U-J, J-F)$ colors was estimated at about 15% (Koo & Kron 1988, KK88 hereafter; Marano *et al.* 1988). We have now verified that the KK88 survey is at least 11% incomplete, but have determined that it may be as much as 34% incomplete. The "missing" QSOs are expected to be predominantly at $z \leq 2.2$.

We have studied the proper motion and variability properties of all stellar objects with $J \leq 22.5$ or $F \leq 21.5$ in the SA 57 field (0.3 degrees^2) which has previously been surveyed with a multicolor QSO search by KK88. The high precision proper motions (Majewski 1992) have the potential of identifying ALL

extragalactic, compact objects since most stars will have measureable, telltale proper motions. We find 223 candidate objects with proper motions less than 4σ (including *all* of the 31 previously found QSOs), of which a majority are still contaminating stars. In order to improve our efficiency at isolating QSOs, we make a further requirement of variability within the candidate sample. We have (Majewski 1992) high precision, profile-fitted photometry (random errors less than 0.02 over most of the magntude range surveyed) of all stellar objects in SA 57 at 16 epochs over 16 years which allows us to check for variability on timescales of years to decades. Of the 31 spectroscopically-confirmed SA 57 QSOs previously found by KK88, we find 30 to be variable; it appears that all QSOs are variable over a 16 year baseline. The total number of variable objects with proper motions less than 4σ is 81, including: (a) the 30 known QSOs from KK88, (b) 3 compact, narrow-emission line galaxies (NELGs) found in KK88, (c) 1 confirmed star, (d) 27 objects identified by KK88 as QSO candidates but still lacking spectroscopic confirmation, but also (e) 20 new candidates which were not previously identifed by KK88. Seventeen of these fall within the blue end of the stellar locus in the $(U-J, J-F)$ color diagram. By modelling the change in colors through redshifting typical QSO spectra we find that this region of color space is most likely to be inhabited by QSOs with $z < 2.3$.

We have obtained spectra for 4 candidates in the stellar locus: 3 are QSOs - with redshifts 0.71, 0.74 and 1.61 - and one is an NELG (redshift 0.16). An additional new QSO which is not in the stellar locus was also found at a redshift of 3.54. Thus, based on the 35 known SA 57 QSOs, the KK88 survey is 4/35 = 11% incomplete. We might project that of the total new 20 candidates, 16 will be QSOs. Then at worst, KK88 will be 16/(31+16) = 34% incomplete. However, there are candidates selected by both KK88 and the proper motion + variability survey which still lack spectroscopic confirmation. Presently, the QSO:NELG:star breakdown is 35:4:1, so that we might project that in the entire sample of 81 proper motion + variability objects we might have 70 QSOs, or a density of 233 degree^{-1} to $J = 22.5$. In this case, the incompleteness of the multicolor survey is 16/70 = 23%. Based on their colors, a majority of these new QSOs will be at $z < 2.3$. However, based on their apparent magnitudes and under the assumption that they are at $z < 2.3$, a majority of these new QSOs would lie on the fainter ($M_B > -25$), flatter part of the luminosity function. Thus, while it does appear that the multicolor surveys are missing QSOs in the redshift range of interest, at present it does not appear that these QSOs will significantly alter the perception of a significant amount of evolution at low redshifts in the currently-fashionable pure luminosity evolution models.

Boyle, B. J., Fong, R., Shanks, T., and Peterson, B. A. 1990, MNRAS 243, 1.

Goldschmidt, P., Miller, L., La Franca, F., & Cristiani, S. 1992, *preprint*

Hazard, C. 1991, in *The Space Distribution of Quasars*, David Crampton (ed.), (Provo:ASP), 170.

Koo, D. C., and Kron, R. G. 1988, *Ap. J.*, 325, 92 (KK88).

Majewski, S. R. 1991, *Ap. J. Suppl.*, , 78, 87.

Marano, B., Zamorani, G., and Zitelli, V. 1988, MNRAS 232, 111.

Schmidt, M. & Green, R. F. 1983, *Ap. J.*, 269, 352.

Schmidt, M., Schneider, D. P. & Gunn, J. E. 1986, *Ap. J.*, 310, 518.

Warren, S. J., Hewett, P. C., Irwin, M. J., and Osmer, P. S. 1991, *Ap. J. Suppl.*, 76, 1.

Omega from the Anisotropy of the Redshift Correlation Function

A. J. S. Hamilton
Joint Institute for Laboratory Astrophysics
and Department of Astrophysical, Planetary and Atmospheric Sciences
University of Colorado, Boulder

ABSTRACT. Peculiar velocities distort the correlation function of galaxies observed in redshift space. In the large scale, linear regime, the distortion takes a characteristic quadrupole plus hexadecapole form, with the amplitude of the distortion depending on the cosmological density parameter Ω. Preliminary measurements are reported here of the harmonics of the correlation function in the CfA, SSRS, and IRAS 2 Jansky redshift surveys. The observed behavior of the harmonics agrees qualitatively with the predictions of linear theory on large scales in every survey. However, real anisotropy in the galaxy distribution induces large fluctuations in samples which do not yet probe a sufficiently fair volume of the Universe. In the CfA 14.5 sample in particular, the Great Wall induces a large negative quadrupole, which taken at face value implies an unrealistically large $\Omega \sim 20$. The IRAS 2 Jy survey, which covers a substantially larger volume than the optical surveys, and is less affected by fingers-of-god, yields a more reliable and believable value, $\Omega = 0.5^{+.5}_{-.25}$.

1. Theory

Peculiar velocities distort the pattern of clustering of galaxies in redshift space. The most familiar distortion is the finger-of-god effect, caused by large orbital velocities of galaxies in the virialized cores of clusters. A more subtle effect, which is the subject of this paper, is the squashing effect induced on large scales by peculiar infall towards overdense regions. Both finger-of-god and squashing effects are illustrated in Figure 1.

The same distortions affect the redshift correlation function. Hamilton (1992), building on work by Kaiser (1987), showed that the anisotropy of the redshift correlation function $\boldsymbol{\xi}$ in the linear regime has a characteristic quadrupole plus hexadecapole form (the redshift correlation function $\boldsymbol{\xi}$ is printed in bold face to distinguish it from the true underlying correlation function ξ)

$$\boldsymbol{\xi}(r,\mu) = \boldsymbol{\xi}_0(r)P_0(\mu) + \boldsymbol{\xi}_2(r)P_2(\mu) + \boldsymbol{\xi}_4(r)P_4(\mu) \qquad (1)$$

Here r is the separation of a pair, μ is the cosine of the angle of the pair relative to the line of sight, and P_l are Legendre polynomials. The quadrupole harmonic $\boldsymbol{\xi}_2$ of the redshift correlation function should be negative in the linear regime, reflecting the line of sight compression of overdense regions caused by peculiar motions toward them. The hexadecapole harmonic $\boldsymbol{\xi}_4$, which is induced by the dispersion of peculiar infall velocities, should be small and positive. All the higher order harmonics, $\boldsymbol{\xi}_l$ for

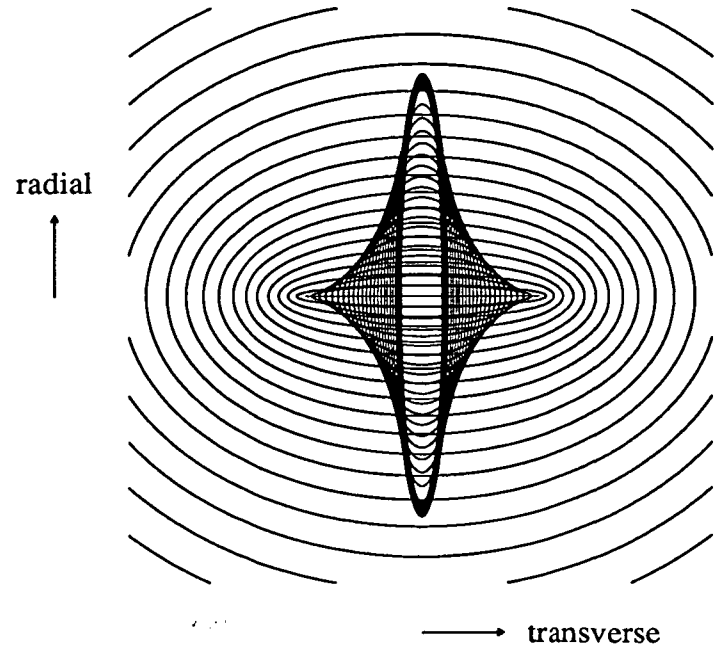

Figure 1. A spherical overdense region appears distorted by peculiar velocities when observed in redshift space. On large scales (linear regime) the region appears squashed, producing a negative quadrupole harmonic. On small scales (nonlinear regime), fingers-of-god appear, producing a positive quadrupole harmonic.

$l \geq 6$, should be zero in the linear regime. Note that non-zero azimuthal harmonics, $m \neq 0$, vanish identically by symmetry about the line of sight, while odd l harmonics vanish by pair exchange symmetry.

The relative amplitudes of the monopole, quadrupole, and hexadecapole harmonics $\boldsymbol{\xi}_l$ depend on the dimensionless growth rate f of growing modes in linear theory, which in the standard gravitational instability picture in the standard pressureless Friedmann cosmology is (Peebles 1980, eq. [14.8])

$$f \approx \Omega^{0.6} \tag{2}$$

where Ω is the density of the Universe relative to the critical density. The relative amplitudes of $\boldsymbol{\xi}_l$ also depend on the shape of the underlying correlation function $\xi(r)$, but by weighting the harmonics in an appropriate fashion, it is possible to eliminate this shape dependence. An appropriately weighted set of harmonics $\tilde{\boldsymbol{\xi}}_l$ is (Hamilton 1992):

$$(1 + {}^2/_3 f + {}^1/_5 f^2)[\overline{\xi}(r) - \xi(r)] = \tilde{\boldsymbol{\xi}}_0(r) \equiv -\boldsymbol{\xi}_0(r) + 3\int_0^r \boldsymbol{\xi}_0(s)(s/r)^3 ds/s \tag{3}$$

$$({}^4/_3 f + {}^4/_7 f^2)[\overline{\xi}(r) - \xi(r)] = \tilde{\boldsymbol{\xi}}_2(r) \equiv -\boldsymbol{\xi}_2(r) \tag{4}$$

$${}^8/_{35} f^2 [\overline{\xi}(r) - \xi(r)] = \tilde{\boldsymbol{\xi}}_4(r) \equiv -\boldsymbol{\xi}_4(r) + 7\int_r^\infty \boldsymbol{\xi}_4(s)(r/s)^2 ds/s \tag{5}$$

where $\overline{\xi} \equiv 3r^{-3}\int_0^r \xi s^2 ds$ denotes the mean correlation function interior to r. The ratio

of any pair of the weighted harmonics $\tilde{\xi}_l$ yields a value of f, hence Ω through equation (2). The dependence of the ratios on Ω is illustrated in Figure 4. In practice, the ratio $\tilde{\xi}_2/\tilde{\xi}_0$ is the important one, since $\tilde{\xi}_4$ is small and its relative uncertainty therefore large.

2. Results — Optical Surveys

Figure 2 shows the harmonics of the redshift correlation function measured in a number of optical redshift surveys: the CfA 14.5 survey (Huchra et al. 1983; Huchra 1991); the first CfA slice (Huchra 1991); and the Southern Sky Redshift Survey (da Costa et al. 1991). All the surveys show qualitatively the expected behavior. On small scales the quadrupole harmonic, along with all the other harmonics, becomes large and positive, which is the nonlinear finger-of-god effect. The quadrupole harmonic goes negative somewhere around 5-10h^{-1}Mpc, which is the squashing effect. In linear theory, the quadrupole harmonic is expected to become more negative to smaller scales, so the separations in Figure 2 up to the point where the quadrupole goes through its minimum are presumably contaminated by nonlinearity. In the northern samples, CfA 14.5 North, and CfA Slice, the nonlinear contamination by fingers-of-god apparently extends to separations of around 20h^{-1}Mpc, whereas in the southern samples, CfA 14.5 South, and SSRS, the nonlinear contamination extends only to about 8h^{-1}Mpc.

Judged from the scatter in the higher order harmonics, the least noisy of the optical samples is the CfA 14.5 North sample. A calculation of Ω in this sample using equations (2)-(5) yields $\Omega \sim 20$, an implausibly large value. Analysis of various angular and radial cuts from CfA 14.5 North reveals that the large negative quadrupole and large positive hexadecapole visible in Figure 2 arises almost entirely from a radial shell 60-80h^{-1}Mpc away. The region coincides physically with the location of the Great Wall (Geller & Huchra 1989). This result highlights what may be the main problem with this method for measuring Ω, which is that real anisotropic structure in the galaxy distribution can mimic the effect of peculiar velocities.

The results shown in Figure 2 should be regarded as preliminary, since error analyses are still in progress, and there is at least one important source of bias which has not been removed. This is a bias caused the local overdensity, which is not a random piece of the Universe (see Hamilton 1993 for a discussion).

3. Results — IRAS 2 Jansky Survey

Figure 3a shows the harmonics of the redshift correlation function measured in the IRAS 2 Jansky survey (Strauss et al. 1990, 1992; Strauss 1992). To exclude the local bias (Hamilton 1993), only galaxies with recession velocities $> 2{,}500 \mathrm{km\,s^{-1}}$ have been retained. As in the optical surveys, the quadrupole harmonic in the IRAS survey is large and positive at small separations, which is the finger-of-god effect, and it goes negative at about 5h^{-1}Mpc, which is the squashing effect.

Although the number of galaxies, 2658, in the IRAS 2 Jy survey is not much greater than in any of the optical surveys discussed in §2, it covers a substantially larger volume, albeit in a substantially sparser fashion. The larger volume means that the correlation function is more accurately measured in the IRAS survey on the larger scales which are the focus of this paper. The IRAS survey has the further advantage

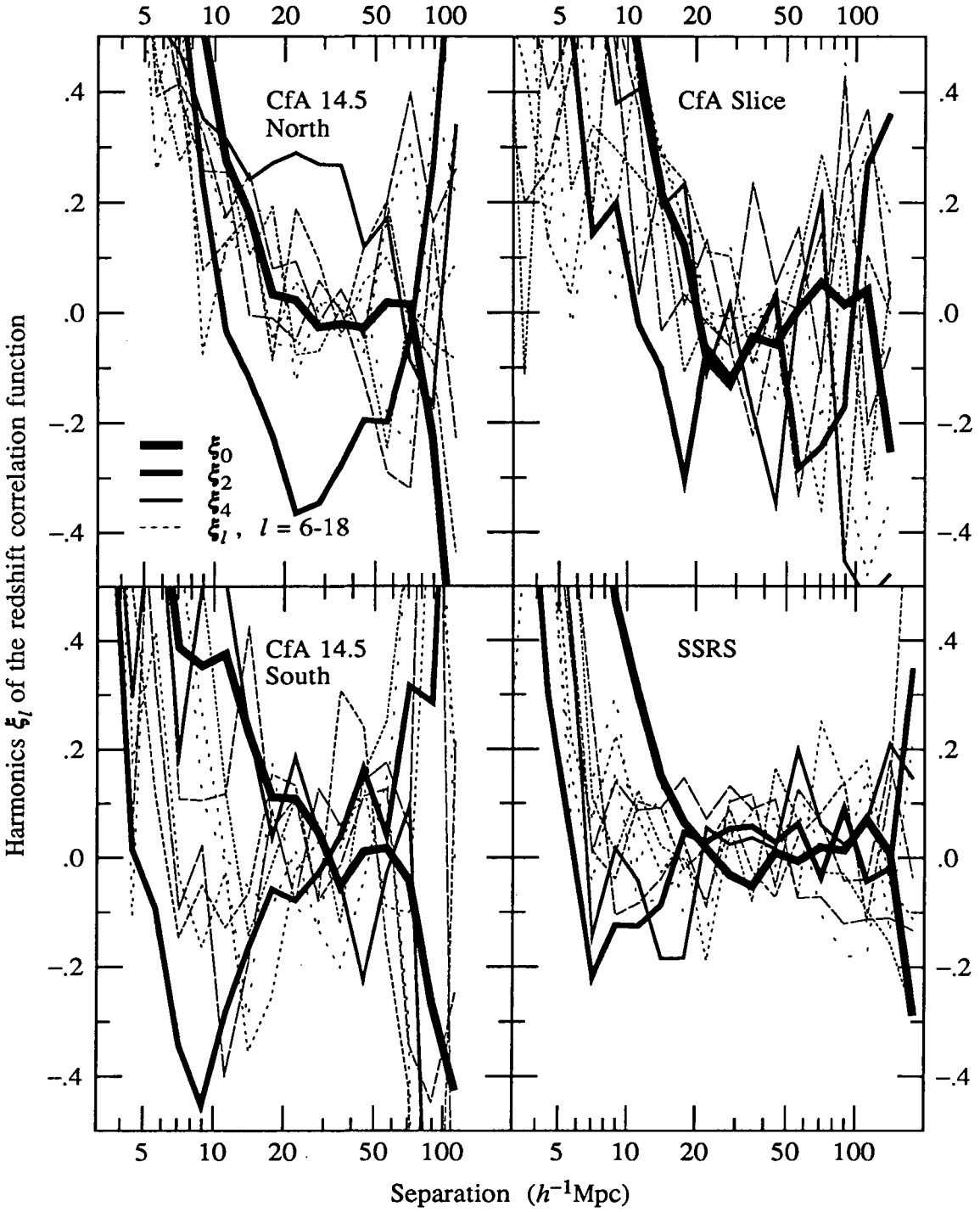

Figure 2. Harmonics ξ_l of the redshift correlation function from several optical surveys: the northern and southern parts of the CfA 14.5 survey, the first CfA slice, and the Southern Sky Redshift Survey. The thickest line is the usual monopole redshift correlation function; successively thinner and less complete lines are higher order harmonics, up to $l = 18$.

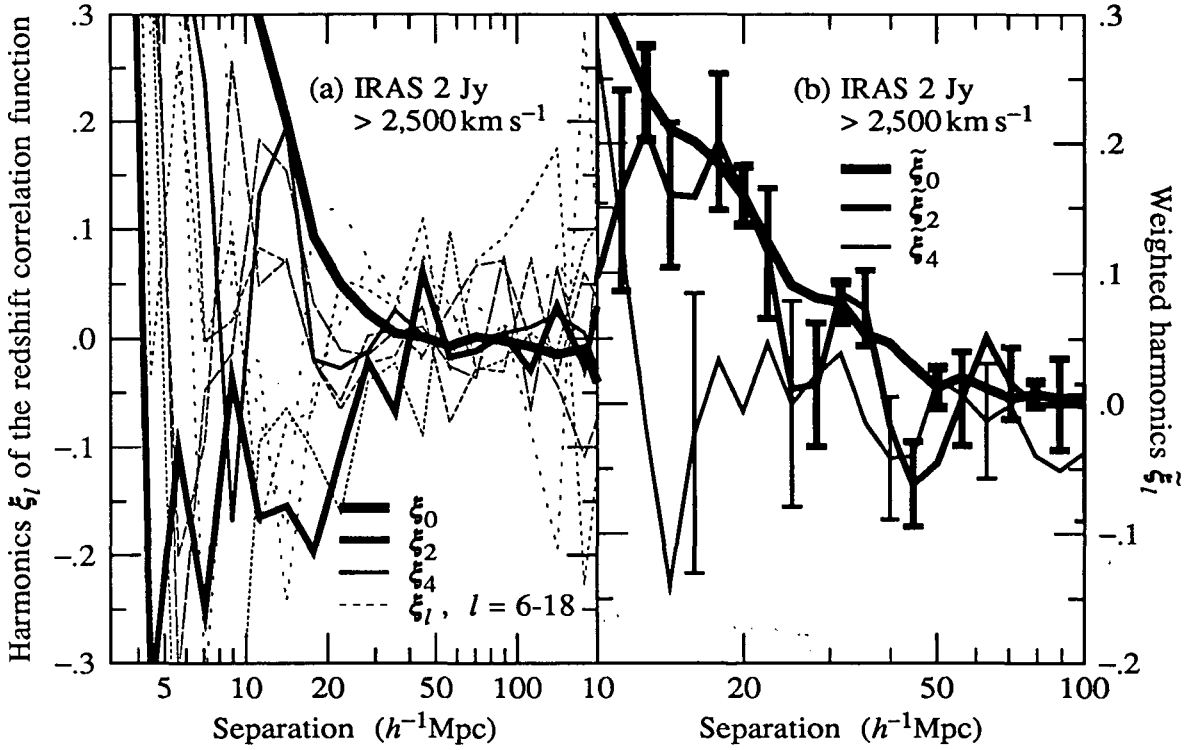

Figure 3. Harmonics of the redshift correlation function in the IRAS 2 Jy survey. (a) The harmonics ξ_l. (b) Weighted harmonics $\tilde{\xi}_l$, weighted in accordance with equations (3)-(5).

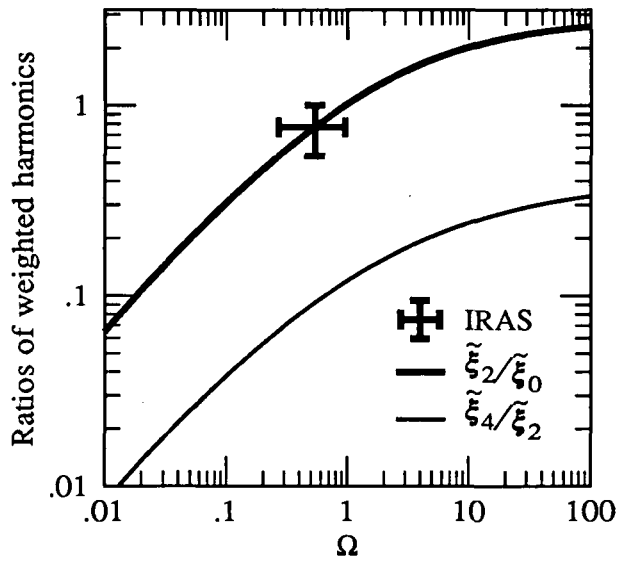

Figure 4. Relation between Ω and the ratios of the weighted harmonics $\tilde{\xi}_l$, from equations (2)-(5). The ratio $\tilde{\xi}_2/\tilde{\xi}_0$ measured from the IRAS 2 Jy sample is plotted as a cross with error bars.

over optical samples that it is likely to be subject to fewer systematic uncertainties arising for example from galactic absorption, or from calibration of fluxes/magnitudes. In addition, since IRAS galaxies tend to avoid the cores of rich clusters, fingers-of-god are less prominent than in optical samples. All of these considerations lead to the conclusion that IRAS samples are likely to yield more reliable values of Ω using the present method than are optical samples. Whether this view is borne out by future work remains to be seen.

Figure 3b shows the harmonics of the correlation function in the IRAS 2 Jy survey weighted in accordance with equations (3)-(5). The prediction of linear theory is that these weighted harmonics $\tilde{\xi}_l$ should be proportional to each other, with their ratios depending on the value of Ω. The predicted proportionality appears to hold approximately on scales $\gtrsim 12h^{-1}$Mpc.

Stacking the data shown in Figure 3b over $12.5\text{-}45h^{-1}$Mpc, below which nonlinearity is important, and above which there is no signal to speak of, yields $\tilde{\xi}_2/\tilde{\xi}_0 = 0.77 \pm .23$, which is plotted on Figure 4. The corresponding value of the parameter f, equation (1), is $f = 0.69^{+.27}_{-.23}$, and the inferred value of Ω is, in round numbers, $\Omega = 0.5^{+.5}_{-.25}$.

More details of the analysis of the IRAS 2 Jy survey are given by Hamilton (1993).

References

da Costa, L. N., Pellegrini, P. S., Davis, M., Meiksin, A., Sargent, W. L. S., & Tonry, J. L. 1991, ApJS, 75, 935.

Geller, M. J., & Huchra, J. P. 1989, Science, 246, 879.

Hamilton, A. J. S. 1992, ApJ, 385, L5.

Hamilton, A. J. S. 1993, ApJ Letters, submitted.

Huchra, J. P. 1991, private communication.

Huchra, J. Davis, M., Latham, D., & Tonry, J. 1983, ApJS, 52, 89.

Kaiser, N. 1987, MNRAS, 227, 1.

Peebles, P. J. E. 1980, The Large Scale Structure of the Universe (Princeton: Princeton University Press).

Strauss, M. A. 1992, private communication.

Strauss, M. A., Davis, M., Yahil, A., & Huchra, J. P. 1990, ApJ, 361, 49.

Strauss, M. A., Davis, M., Yahil, A., & Huchra, J. P. 1992, ApJ, 385, 421.

Ways to Improve Your Correlation Functions

A. J. S. Hamilton
Joint Institute for Laboratory Astrophysics
and Department of Astrophysical, Planetary and Atmospheric Sciences
University of Colorado, Boulder

ABSTRACT. This paper describes a number of ways to improve on the standard method for measuring the two-point correlation function of large scale structure in the Universe. Issues addressed are: (1) The problem of the mean density, and how to solve it; (2) How to estimate the uncertainty in a measured correlation function; (3) Minimum variance pair weighting; (4) Unbiased estimation of the selection function when magnitudes are discrete; (5) Analytic computation of angular integrals in background pair counts.

1. The Mean Density Problem

It is widely thought that the accuracy of the correlation function ξ is fundamentally limited by uncertainty in the mean density. Actual, this notion is *false* (§1.2), although it is true for the commonly used estimator of ξ (§1.1).

1.1 The Problem

The statistic commonly used to estimate ξ from a catalog of galaxies is (e.g. Davis and Peebles 1983)

$$\xi_{\rm est} = \frac{<NN><W>}{<NW><N>} - 1 \qquad (1)$$

where N represents real galaxies, W is the catalog window, and $<>$ denotes averaging over all points in the catalog; for $<NN>$ and $<NW>$ the averaging is over all pairs lying in an interval of separations r. The observed galaxy density N is the true galaxy density n times the catalog window W (strictly, observed discrete galaxies are taken to be a Poisson process superimposed on this). In terms of the true galaxy overdensity $\delta \equiv (n - \bar{n})/\bar{n}$, where $\bar{n}$ is the true mean galaxy density of the Universe, the observed galaxy density N is

$$N = \bar{n} W (1 + \delta) \quad . \qquad (2)$$

To see how good the estimate (1) of ξ is in a realistically unfair sample, introduce the following notations (3)-(5). Let $\bar{\delta}$ be the mean overdensity in the catalog

$$\bar{\delta} \equiv \frac{<W\delta>}{<W>} \qquad (3)$$

and let ψ denote the galaxy-catalog correlation function

$$\psi_{12} \equiv \frac{<W_1 \delta_1 W_2>}{<W_1 W_2>} \quad . \tag{4}$$

In a fair sample, the mean overdensity $\bar{\delta}$ and the galaxy-catalog correlation function ψ would be identically zero, but they are not necessarily zero in reality. Let $\hat{\xi}$ denote the windowed galaxy-galaxy correlation function

$$\hat{\xi}_{12} \equiv \frac{<W_1 \delta_1 W_2 \delta_2>}{<W_1 W_2>} \quad . \tag{5}$$

While $\hat{\xi}$ is not necessarily equal to the true correlation function ξ of the Universe, it is at least the 'true' correlation function of the sample, which is presumably the next best thing.

In terms of $\bar{\delta}$, ψ, and $\hat{\xi}$, the standard estimate (1) of the correlation function ξ is

$$\xi_{est}(r) = \frac{\hat{\xi}(r) + \psi(r) - \bar{\delta} - \psi(r)\bar{\delta}}{(1 + \psi(r))(1 + \bar{\delta})} \quad . \tag{6}$$

The problem with equation (6) is that it contains not-necessarily-vanishing terms $\psi(r) - \bar{\delta}$ which are of first order in overdensity δ, whereas the thing you want, the sample correlation function $\hat{\xi}$, is of second order in δ. This is a severe drawback of the estimator (1) for ξ in the linear regime of small δ.

1.2 A Solution, Part 1

A better estimate of ξ is

$$\xi_{est} = \frac{<NN><WW>}{<NW>^2} - 1 \tag{7}$$

in which the brackets $<>$ in both numerator and denominator denote averaging over pairs in an interval of separations r. In terms of the galaxy-catalog correlation function ψ and the sample galaxy-galaxy correlation function $\hat{\xi}$ defined by equations (4) & (5), the estimate (7) is

$$\xi_{est}(r) = \frac{\hat{\xi}(r) - \psi(r)^2}{(1 + \psi(r))^2} \tag{8}$$

which differs from the sample correlation function $\hat{\xi}$ only by terms which are of second order in overdensity δ.

The advantages of the estimator (7) over the standard estimator (1) for ξ are:

(a) Accuracy, especially in the large scale, linear regime;

(b) Reliability in the presence of unfairness, especially with not-unbiased (e.g. minimum variance, §3) pair weightings;

(c) Peace of mind: there is no need to measure the mean density $<N>/<W>$ as a separate operation; equation (7) specifies that the 'correct' mean density to use in place of the $<N>/<W>$ in equation (1) is $<NW>^2/<WW>$, a quantity which it is to be noted varies with separation r.

1.3 SOLUTION, PART 2

The ψ^2 term in equation (8) represents large scale variance which is inevitably missing in a finite catalog; its presence is symptomatic of the familiar problem that using the sample mean leads to an underestimate of the sample variance. Although the galaxy-catalog correlation ψ should be zero in the mean over many samples, its variance $<\psi^2>$ should be positive in the mean. Physically, $<\psi^2>$ represents the mean fractional excess of galaxies clustered around a galaxy on the scale of the catalog. If one imagines evaluating the correlation function by sitting on galaxies and counting neighbors, the mean density at infinity should be determined not from the total number of galaxies in the catalog volume, but rather from the number of galaxies less the mean excess of galaxies clustered around a galaxy.

One way to correct for the missing variance is to use an alternate estimator

$$\xi_{\rm est} = \frac{<NN><WW>}{<NW>^2 - <\Delta(NW)^2>} - 1 \qquad (9)$$

which in terms of $\hat{\xi}$ and ψ and its variance $<\psi^2>$ is

$$\xi_{\rm est}(r) = \frac{\hat{\xi}(r) - \psi(r)^2 + <\psi(r)^2>}{(1+\psi(r))^2 - <\psi(r)^2>} \quad . \qquad (10)$$

The variance $<\Delta(NW)^2>$ in equation (9) may be computed from the fluctuations in $<NW>$, using methods similar to those described in §2. Another way to correct for missing large scale variance is given by Hamilton (1993).

2. Estimating Errors in the Correlation Function

2.1 MATHEMATICS

The window W can be imagined as a set of weights W_i attached to every tiny volume element of the Universe. For an observed subsample, the weights W_i are nonzero only over the observed region. For the entire population, the Universe, the weights $W_{i,\rm pop}$ are finite everywhere, but infinitesimal compared to the sample weights W_i.

The correlation function $\xi(W_i)$ measured in a sample differs from the true correlation function $\xi(W_{i,\rm pop})$ by an error $\Delta\xi$

$$\Delta\xi = \xi(W_i) - \xi(W_{i,\rm pop}) \quad . \qquad (11)$$

Expanding the error $\Delta\xi$ as a Taylor series to second order in the weights gives

$$\Delta\xi = \sum_i (W_i - W_{i,\rm pop}) \frac{\partial\xi}{\partial W_i}\bigg|_{\rm pop} + \frac{1}{2}\sum_{ij}(W_i - W_{i,\rm pop})(W_j - W_{j,\rm pop}) \frac{\partial^2\xi}{\partial W_i \partial W_j}\bigg|_{\rm pop} \quad . (12)$$

Using the facts that (a) $\xi(W_i)$ is unchanged by rescaling $W_i \to \lambda W_i$, (b) ξ is a quadratic function of the weights W_i (at least for the estimator [7]), and (c) $W_{i,\rm pop}$ is infinitesimal compared to W_i, eliminates most of the terms in equation (12), reducing it to

$$\Delta\xi = \frac{1}{2}\sum_{ij} W_i W_j \frac{\partial^2\xi}{\partial W_i \partial W_j}\bigg|_{\rm pop} \qquad (13)$$

which then reduces further to

$$\Delta\xi = \sum_{\text{distinct } ij} W_{ij} \frac{\partial \xi}{\partial W_{ij}}\bigg|_{\text{pop}} \qquad (14)$$

where $W_{ij} \equiv W_i W_j$. Expression (14) makes clear the fact that the error $\Delta\xi$ is truly a derivative with respect to *pairs*. Approximating the population derivative of ξ in (14) by the sample derivative, and again using the fact that $\xi(W_i)$ is quadratic in W_i, permits equation (14) to be rearranged as a sum over volume elements i rather than pairs ij:

$$\Delta\xi = \sum_i \Delta\xi_i \qquad \text{with} \qquad \Delta\xi_i = \frac{1}{2} W_i \frac{\partial \xi}{\partial W_i} \quad . \qquad (15)$$

Note the important factor of $^1/_2$ in equation (15), which in effect causes pairs to be counted once, not twice. The variance of ξ is then

$$<\Delta\xi^2> = \sum_{ij} \Delta\xi_i \Delta\xi_j \quad . \qquad (16)$$

Characteristically, the variance (16) increases as pairs ij of greater and greater separation are included, reaches a maximum, then declines to exactly zero when all pairs are included. The declining to zero is a consequence of approximating the population derivatives of ξ with the sample derivatives of ξ. To solve the problem, only pairs ij separated by some finite distance should be included.

For the estimator (7), the contribution $\Delta\xi_i$ to the error in ξ from volume element i is

$$\Delta\xi_i = (1 + \xi_{\text{est}}) \left[\frac{<N_i N>}{<NN>} - \frac{<N_i W>}{<NW>} - \frac{<NW_i>}{<NW>} + \frac{<W_i W>}{<WW>} \right] \quad . \qquad (17)$$

2.2 Suggested Step-by-Step Error Analysis

(a) Divide the catalog into many subregions i.

(b) Estimate ξ from equation (7), and compute $\Delta\xi_i$ for each subregion from equation (17).

(c) Compute the variance $<\Delta\xi^2>$ from equation (16), including pairs ij of subregions of greater and greater separation, until the variance reaches a maximum.

(d) The 1-sigma error in ξ is the square root of this variance.

3. Minimum Variance Pair Weighting

3.1 Mathematics

An unbiased estimate of the correlation function ξ is gotten in principle by weighting each point inversely with the selection function Φ at the point, so that all volume elements count equally. Unfortunately this leads to a noisy estimate of ξ from regions where the selection function Φ is small. To the extent that the selection function is uncorrelated with the true galaxy density, the most accurate estimate of ξ is obtained by reweighting the unbiased weighting of pairs inversely with the variance $<\Delta\xi^2>$ of ξ, so that a (real or background) pair 12 is weighted

$$w_{12} = \frac{1}{\Phi_1 \Phi_2 <\Delta\xi^2>} \quad . \qquad (18)$$

If the only source of uncertainty in ξ comes from the fact that the sample is a finite subset of the Universe, then the expected covariance between ξ's at separations r_{12} and r_{34} is

$$\begin{aligned} <\Delta\xi_{12}\,\Delta\xi_{34}> &= <\delta_1\delta_2\delta_3\delta_4> - <\delta_1\delta_2><\delta_3\delta_4> \\ &\propto \int (\xi_{13}\xi_{24} + \xi_{14}\xi_{23} + \eta_{1234})\, dV_3 \end{aligned} \tag{19}$$

the integral being carried over all possible separations of point 3 from point 1. An important point to notice is that the ξ's in the integrand of (19) have delta functions at zero separation, because of the discreteness of galaxies. These delta functions cause equation (19) to take the general form

$$<\Delta\xi^2> \propto \Phi^{-2} + 2\Phi^{-1}J + K \tag{20}$$

in a region where the selection function is Φ. The Φ^{-2} term in equation (20) comes the case where pairs 12 and 34 coincide, the Φ^{-1} term from cases where 12 and 34 share a point in common, and the constant term from cases where 12 and 34 are disjoint pairs. Equation (20) yields the pair weighting

$$w_{12} = \frac{1}{1 + 2\Phi J + K\Phi^2} \quad . \tag{21}$$

Generally one is interested not in ξ at some precise separation, but rather averaged over some range of separations; or one might be interested in the power spectrum, or the harmonics of ξ, or such like. In that case equation (19) should be integrated with the desired kernel functions over the desired ranges of separations. The result is again equations of the form (20) and (21), but with different values of the coefficients J and K. The bad news is that a calculation of J and K from equation (19) is generally tricky and uncertain, and in any case suspect because an observationally measured ξ may be subject to other sources of uncertainty ignored in equation (19). The good news is, the calculation is unnecessary. A practical solution is to proceed empirically, using the form (21) as a template for an approximate pair weighting, the free parameters of which would be determined empirically by minimizing the observed variance $<\Delta\xi^2>$ computed for example using the method of §2. This is the approach suggested in §3.2 below.

3.2 Suggested Near Minimum Variance Weighting

A simple approximation to the minimum variance pair weighting which should not be too bad in practice would be to weight every (real and background) pair 12 by $w_{12}=w_1w_2$, the weight w_i at each point i where the selection function is Φ_i being

$$w_i = \frac{1}{1 + \Phi_i J} \quad . \tag{22}$$

The quantity J in equation (22) is likely to be different for different pair separations r. Consideration of the behavior of the integral (19) suggests that a reasonable guess would be to take

$$J = Cr^c \tag{23}$$

with $c \approx 3-\gamma$ if $\xi \propto r^{-\gamma}$. The free parameters C and c in (23) would be determined empirically by varying them until the computed variance $<\Delta\xi^2>$ of ξ, or of whatever integral over ξ is the quantity of interest, is minimized. Clearly the approximation (23), and perhaps also (22), could be refined if deemed necessary.

4. The Selection Function and the Discreteness of Magnitudes

4.1 PROBLEM

Turner's (1979) classic inhomogeneity-insensitive method of measuring the selection function is found empirically to be sensitive to bin size.

4.2 DIAGNOSIS

Strauss, Yahil & Davis (1991) correctly attribute the sensitivity of Turner's method to bin size to the fact that magnitudes given in catalogs are discretely, not continuously, distributed.

The periodicity of listed magnitudes (e.g. Zwicky gives magnitudes mostly to 0.1) translates into a periodic ripple in the derived selection function (with period 0.1 magnitudes in Zwicky's case).

4.3 SOLUTION

The fix is simple: just choose a bin size equal to the period (0.1 magnitudes in Zwicky's case), so the periodic ripple has no effect. Note that the worst possible binning is exactly half a period, since successive samplings of the selection function are then maximally out of phase.

5. Better Backgrounds

Oftentimes a catalog window is the product of a radial selection function and an angular window which is one inside, zero outside, a boundary composed of a set of arc segments. Angular integrals in such a case can be done *analytically*, and backgrounds can then be integrated quickly and accurately.

[At the conference, a binder was exhibited containing listings of Fortran code to compute angular integrals analytically. The relevant mathematics is given by Hamilton (1993, Appendix).]

References

Davis, M., & Peebles, P. J. E. 1983, ApJ 267, 465.
Hamilton, A. J. S. 1993, ApJ, submitted.
Strauss, M. A., Yahil, A., & Davis, M. 1991, PASP, 103, 1012.
Turner, E. L. 1979, ApJ, 231, 645.

PRIMEVAL GALAXIES IN THE SUB-MM AND MM

J. RICHARD BOND & STEVEN T. MYERS
Canadian Institute for Theoretical Astrophysics

ABSTRACT. *Although the results of COBE's FIRAS experiment[1] constrain the deviation in energy from the CMB blackbody in the 500-5000μ range to be $\Delta E/E_{cmb} < 0.005$, primeval galaxies can still lead to a brilliant sub-mm sky of non-Gaussian sources that are detectable at 10″ resolution from planned arrays such as SCUBA on the James Clerk Maxwell Telescope and, quite plausibly, at sub-arcsecond resolution in planned mm and sub-mm interferometers. Here we apply our hierarchical peaks method[2] to a CDM model to construct sub-mm and mm maps of bursting PGs appropriate for these instruments with minimum contours chosen to correspond to realistic observational parameters for them and which pass the FIRAS limits.*

Where does the waste heat from galaxy formation lie? The nuclear energy output of stars with efficiency ϵ_{nuc} (which is less than 0.004, but not by very much for massive stars) radiating at redshift z_* with an abundance Ω_* relative to the CMB is $\Delta E_*/E_{cmb} \sim 0.03\ (\Omega_* h^2/10^{-3})[(1+z_*)/5]^{-1}\ \epsilon_{nuc}/0.004$. The radiant energy release from stars which eject a mass $Z_{ej}M$ in metals when they undergo supernova explosions is limited by the metal fraction Z they contribute to a gas of density Ω_{gas}, $E_{preSN*}/E_{cmb} \sim 0.0008\ (Z/10^{-3})(\Omega_{gas}h^2/10^{-2})\ [(1+z_*)/5]^{-1}\ (Z_{ej}/0.2)\ (M/20\,M_\odot)^{0.5}$. Radiation generated by mass accreting onto black holes with an efficiency ϵ_{acc}, typically taken to be about 0.1 for quasar models, delivers energy $\Delta E_{BHacc}/E_{cmb} \sim 0.0008(\Omega_{BHacc}h^2/10^{-6})[(1+z_{acc})/5]^{-1}\ \epsilon_{acc}/0.1$. We expect $\Omega_*\epsilon_{nuc}$, $Z\Omega_{gas}$ and $\Omega_{BHacc}\epsilon_{acc}$ to be significantly larger than the normalizations given, and quite possibly in conflict with the FIRAS limits.

One way out of the FIRAS dilemma is to have no dust of course, so the radiation is just redshifted. It would then lie in the near infrared and the constraints are still not very restrictive there, even from COBE's DIRBE experiment, which is plagued by difficult foreground subtractions before it can get to the residual cosmological signal. Although it may well turn out that extensive dust production in early galaxies covers only a small fraction of its overall scale ($z \sim 2$ 'Wolfe disks' being relatively metal poor), so most lines of sight to high redshift do not pierce through a significant optical depth of dust (*c.f.* ref. 3), we would be surprised if there were no analogue of the dust-shrouded starburst phenomenon in galactic cores at high redshifts. To allow a large energy generation with dust, one could make the grains hot: for example, 70K dust delivers its peak at about $50\mu(1+z_{gf})$ which might just have missed the FIRAS band for a galaxy formation redshift $z_{gf} \lesssim 7$. However, moderate energy releases which satisfy the FIRAS constraint can still lead to interesting sub-mm skies as we now show.

To focus the discussion, we give a concrete example using the CDM model with amplitude factor $\sigma_8 = 0.67$ ('bias' factor $\sigma_8^{-1} = 1.5$). We first must identify primeval galaxy sites and secondly choose how much energy is produced and in what wavebands. Although we think we can be reasonably confident about the first stage, by using the hierarchical peaks method[2] for identifying galaxy halos at these high redshifts, unfortunately there are too many parameters at our disposal to be definitive about how the energy is released in galaxy formation, even in a supposedly well defined model like CDM. We constructed a 2-component peak model (using 2 filter scales) consisting of fiducial dwarf galaxies (mass in baryons $\sim 3 \times 10^9\,M_\odot$ and halo radius ~ 18 kpc) and 'normal' galaxies (mass in baryons $\sim 4 \times 10^{10}\,M_\odot$ and halo radius ~ 42 kpc).

The dust was assumed to be of a 'normal' (Galactic) variety, distributed in randomly oriented exponential disks with e-folding radii $r_e = 1.8$ kpc and 4.2 kpc respectively, with a dust-to-baryon fraction in the galaxies of 0.2%, and was assumed to be emitting with a λ^{-1} opacity law at a characteristic temperature of 30K (leading to an intensity peak at $\sim 600\mu$). The total luminosities are then star-burst level, $\sim 10^{44}S$ erg/s and $\sim 10^{45}S$ erg/s, respectively, where S is a scale factor that we are free to choose as long as we satisfy the FIRAS constraint; *e.g.*, S increases linearly with the dust-to-baryon ratio and is quite sensitive to dust temperature changes. (If $S \approx 10$ then the normal galaxies would all be emitting at an Arp 220 level).

We assume these primevals were bursting between their formation (but do not include any generation earlier than $z = 6$) and an arbitrary cutoff redshift we chose to be $z = 4$. With these parameters, the energy in the background from these objects would be $\Delta E/E_{cmb} \sim 0.01S$, hence $S \lesssim 1/2$ is required. The metallicity that results from such luminosities over such times is not a great restriction on these models.

The maps in Figure 1 correspond to SCUBA, a submm interferometer and a mm interferometer. Experiments that have already looked for PGs in the mm, at IRAM[4] (λ=1.3mm, 11″ *fwhm* beam), and in

the submm, at JCMT[5] (λ=760μ, 18″ *fwhm* beam), have placed 95% upper limits on the strength of *rms* intensity fluctuations of 0.9 mJy/beam and 12 mJy/beam, respectively. Although these limits can be used to constrain the source density and clustering of some PG models that satisfy FIRAS limits,[3,5] they do not significantly constrain the starburst models considered here. SCUBA, which should come on line within a year, will have *much* higher sensitivity than the Church *et al.* JCMT experiment.[5] Indeed, it is clear from Figure 1 that SCUBA-like instruments will be invaluable for identifying promising PG candidates, but will be confusion-limited because of the beam size. Higher resolution studies will be essential for unraveling the nature of the sources. Sub-mm interferometers appear to be the most promising in terms of signal, but how strongly the atmosphere will limit the sensitivity is not well known at this early stage of their development. Interferometers at mm wavelengths can achieve the assumed sensitivities of Fig. 1(c), but the extrapolation of the flux into the mm depends upon the opacity law and the distribution of dust temperatures.

References

1. Mather, J. *et al.* (1992), preprint.
2. Bond, J.R. and Myers, S. (1991), in *Trends in Astroparticle Physics*, ed. D. Cline and R. Peccei (Singapore: World Scientific).
3. Bond, J.R., Carr, B.J. and Hogan, C.J. 1986, *Ap. J.*, **306**, 428 [BCH1]; 1991, *Ap. J.*, **367**, 420 [BCH2].
4. Kreysa, E. and Chini, A. 1988, *Proc. 3rd ESO-CERN Symp. on Astronomy, Cosmology and Fundamental Particles*, Bologna; 1989, *Proc. Particle Astrophysics Workshop, Berkeley*, (Singapore: World Scientific).
5. Church, S., Lasenby, A. and Hills, R. 1992, *M.N.R.A.S.*, in press.

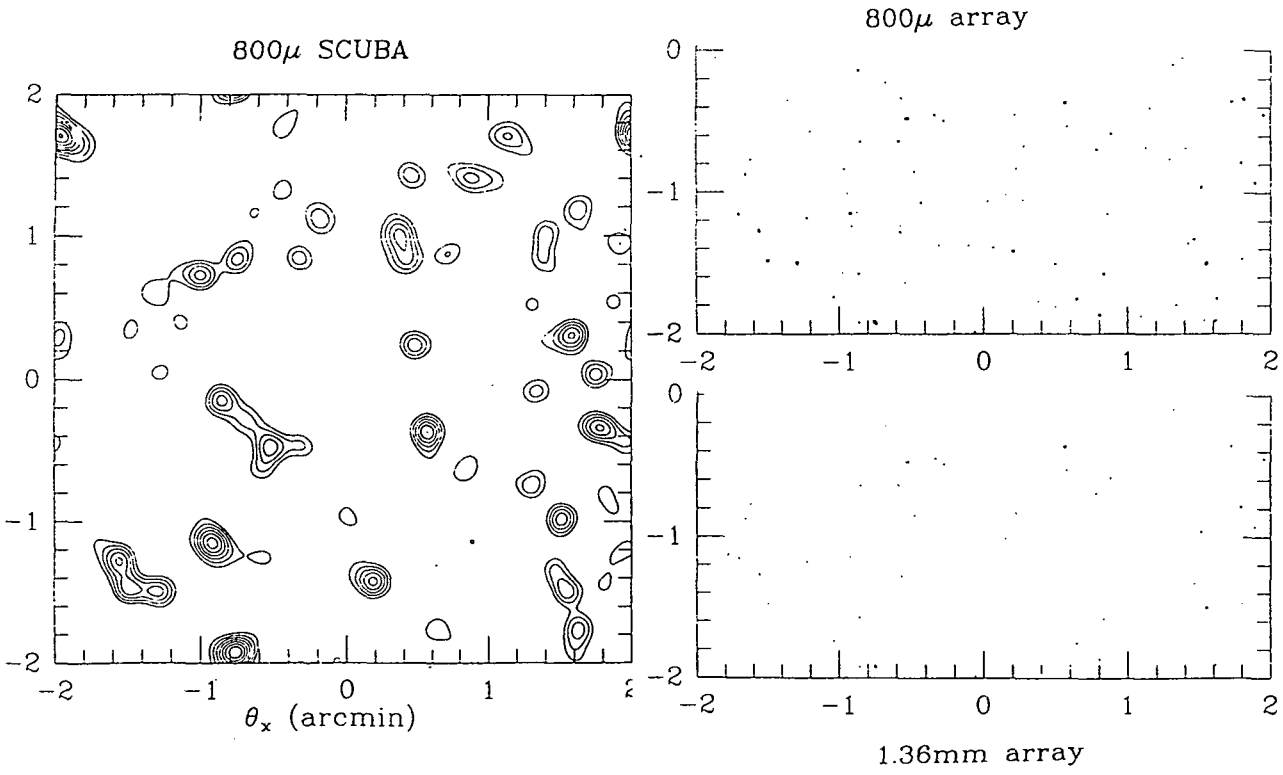

Figure 1. *(a) A 4′ × 4′ contour map for dust-emission from primeval galaxies at $z \sim 5$ convolved with a 12″ beam appropriate for the 855μ 37-pixel SCUBA array. The minimum contour is 1000S μJy/beam and subsequent contours increase linearly in 250S μJy/beam steps. SCUBA has a 2′ × 2′ FOV and is expected to achieve 470 μJy/beam at the 1σ level in just one hour of integration. (b) shows the lower half of the same map seen with a 1″ beam with 250S μJy/beam contours for an 800μ sub-mm array. (c) shows the lower half for a 0.86″ beam with 200S μJy/beam contours for a 1.36 mm array, which can be reached in ∼ a day with the upgraded OVRO mm interferometer.*

Two Searches for Primeval Galaxies

D. Thompson and S. Djorgovski (Caltech)
and J. Trauger (Jet Propulsion Laboratory)

A number of active galaxies are now known at very large redshifts, some of them even have properties suggestive of galaxies in the process of formation. They commonly show strong Lyα emission, at least some of which appears to be ionized by young stars. Inferred star formation rates are in the range $\sim 100 - 500\ M_\odot\ \mathrm{yr}^{-1}$. An important question is: are there radio-quiet, field counterparts of these systems at comparable redshifts? Whereas we are probably already observing some evolutionary and formative processes of distant radio galaxies, the ultimate goal is to observe *normal galaxies* at the epoch when *most* of their stars form. We have thus started a search for emission-line objects at large redshifts, ostensibly young and forming galaxies. Our method is to search for strong line emission (hopefully Lyα) employing two techniques: a direct, narrow-band imaging search, using a Fabry–Perot interferometer; and a serendipitous long-slit spectroscopic search.

The Fabry-Perot Survey: The experiment consists of deep imaging of selected high-latitude "empty" fields in a series of adjacent narrow bands, with spectroscopic follow-up of objects which show a probable line emission excess in one or more bands. A special, low-resolution Fabry-Perot imaging interferometer was designed for this purpose. A three-dimensional data cube (two spatial dimensions plus redshift) is built up by stepping the Fabry-Perot by an amount equal to the instrumental FWHM, chosen to be ~1000 km/s in the restframe for Lyα at any redshift (about 20 – 25 Å), between successive exposures. The field of view is $\sim$ 5.5 arcmin square. We search in several redshift intervals (2.80 – 2.98, 3.27 – 3.45, 4.42 – 4.61, and 4.75 – 4.90), chosen to avoid the night sky emission lines.

To date we have surveyed 3 fields (~0.03 deg^2) in the redshift range 4.42 – 4.61, and 6 fields (~0.06 deg^2) in the redshift range 4.74 – 4.90, down to a limit of $AB_\nu \sim 23$. This corresponds to a surface density of less than $\sim$ 13 objects/deg^2 down to the limiting Lyα flux of $\sim 10^{-16}$ erg/cm^2/s, declining to a surface density of less than $\sim$ 2600 objects/deg^2 down to the limiting Lyα flux of $\sim 3.2 \times 10^{-17}$ erg/cm^2/s, for compact objects ($\leq$ 2 arcsec); for extended objects, the limits are less stringent (about a factor of two worse in the integrated flux).

No immediately obvious primeval galaxy candidates were found, although many faint emission line objects were detected. In a typical data cube, we find 3 or 4 excellent candidates, and up to a couple of dozen other faint emission line galaxies worth following up spectroscopically. We are now trying to obtain their slit spectra. One low-z AGN was detected and confirmed spectroscopically so far, as well as half a dozen starburst galaxies at intermediate redshifts.

The Serendipitous Long-Slit Survey: Our second experiment is a serendipitous long-slit spectroscopic search, using data obtained in the course of other projects. After two-dimensional sky subtraction, the spectroscopic CCD frames are examined carefully for any possible emission-line objects which may have been covered by the slit.

An average set–up for the various runs would cover a wavelength range of 4000–8000 Å, corresponding to a Lyα redshift of 2.3–5.6. One hour exposures reach flux limits comparable to the Fabry–Perot survey, which vary with wavelength, depending on the night sky spectrum. Whereas these exposures have a large, continuous redshift coverage, they cover a much smaller area, typicaly about 2 arcsec by 2 arcmin for a long slit.

To date, about 100 long exposures have been examined carefully, and at least a dozen interesting objects were found, including an apparently normal field galaxy at $z > 1$ (Thompson & Djorgovski 1991, ApJL, 371, L55). They are mostly star forming or mildly active galaxies at moderate redshifts. We anticipate that several tens of additional 1-hour-class exposures will be added to this search over the next year or two.

Even if none of the candidates so far are actually primeval galaxies, our preliminary limits are comparable to, or better than, the best limits obtained to date in other similar experiments. We may already be in conflict with the CDM model predictions by Baron & White (1987), although to do an honest comparison, one must look at the redshift distributions, as well as surface density and flux limits.

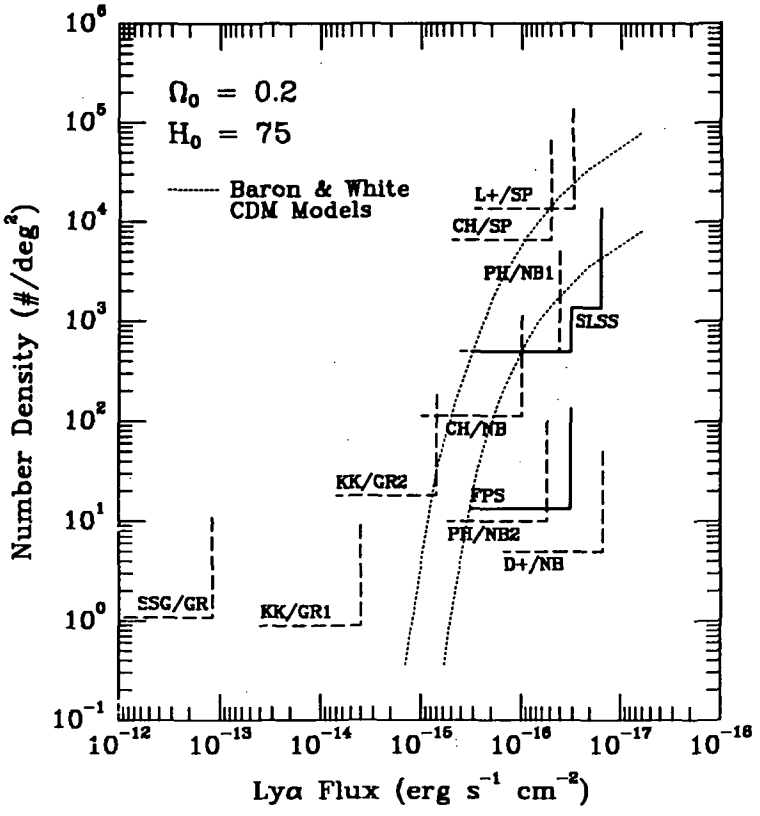

Some Effects of Dust on Photometry of High-Z Galaxies: Confounding the Effects of Evolution

H. A. Thronson, Jr.[1] A. N. Witt,[2], and J. Capuano[2]

Photometric observations of very distant galaxies — e.g., color vs. z or magnitude vs. z — have been used over the past decade or so in investigations into the evolution of the stellar component. Numerous studies have predicted significant color variations as a result of evolution, in addition to the shifting of different rest wavelengths into the band of observation. Although there is significant scatter, the data can be fit with relatively straightforward, plausible models for galaxian evolution. In very few cases are the effects of dust extinction included in the models. This is due in a large part to the uncertainty about the distribution and optical properties of the grains, and even whether or not they are present in significant numbers in some types of galaxies such as ellipticals. It is likely that the effects of dust on broadband observations are the greatest uncertainty in studies of very distant galaxies.

We use a detailed Monte Carlo radiative transfer model within a spherical geometry for different star/dust distributions to examine the effects of dust on the broadband colors of galaxies as a function of redshift. The model fully accounts for absorption and angular redistribution in scattering. In this summary, we consider only the effects on color vs. redshift for three simple geometries each with the same total dust optical depth. Elsewhere at this conference, Capuano, Thronson, & Witt consider other effects of altering the relative dust/star distribution.

Some of our results are shown in the following figure, where we have plotted (heavy lines) the V-R colors vs. redshift adapted from the galaxian evolution models of Yoshii & Takahara (1988; ApJ, 326,1), which do not include effects of dust (heavy lines). The caption describes the characteristics of each model. Our results are the three lighter lines which show the effects of extinguishing the "A" model for three plausible geometries each with $\tau_V = 1$.

From $z \approx 0 \rightarrow 0.6$ our models show very little effect on the observed color, as expected: for modest optical depths, the reddening effects of absorption are almost exactly canceled by the bluing effects of scattering. Furthermore, for all optical depths, the composite stellar light remains dominated by the relatively unobscured stars closest to the observer (e.g., Mathis 1970; ApJ, 159, 263). Consequently, large amounts of dust may be present with little effect on the observed colors. Note, however, that significant absorption of stellar radiation by dust is possible. Thus, our models trivially produce high ratios of infrared-to-visual (i.e., dust-to-stellar) light in systems that are only slightly red.

However, beginning at $z \approx 0.7$ the UV is shifted into the V passband. For these rest wavelengths, conventional grains have a much lower albedo than at longer visual wavelengths. All other things being equal, distant galaxies will appear distinctly redder than closer systems. We note that in these (vastly oversimplified) models, galaxies may change color very significantly for a modest change in z as the wavelength regime most heavily affected by the dust is shifted into the passbands of observation. Such a sudden color change might be partially masked by the effects of stellar evolution, although as the figure indicates, broadband evolutionary effects may be much smaller than those of dust.

For clarity, we have not included the effects of different cosmological models in this figure. However, the effects of dust in our models are also larger than the effects of cosmology for $z \geq 0.7$. We emphasize that in addition to very poorly known geometries, the most significant uncertainty in our models are the grain optical parameters in the ultraviolet.

[1]Wyoming Infrared Observatory, University of Wyoming
[2]Ritter Observatory, University of Toledo

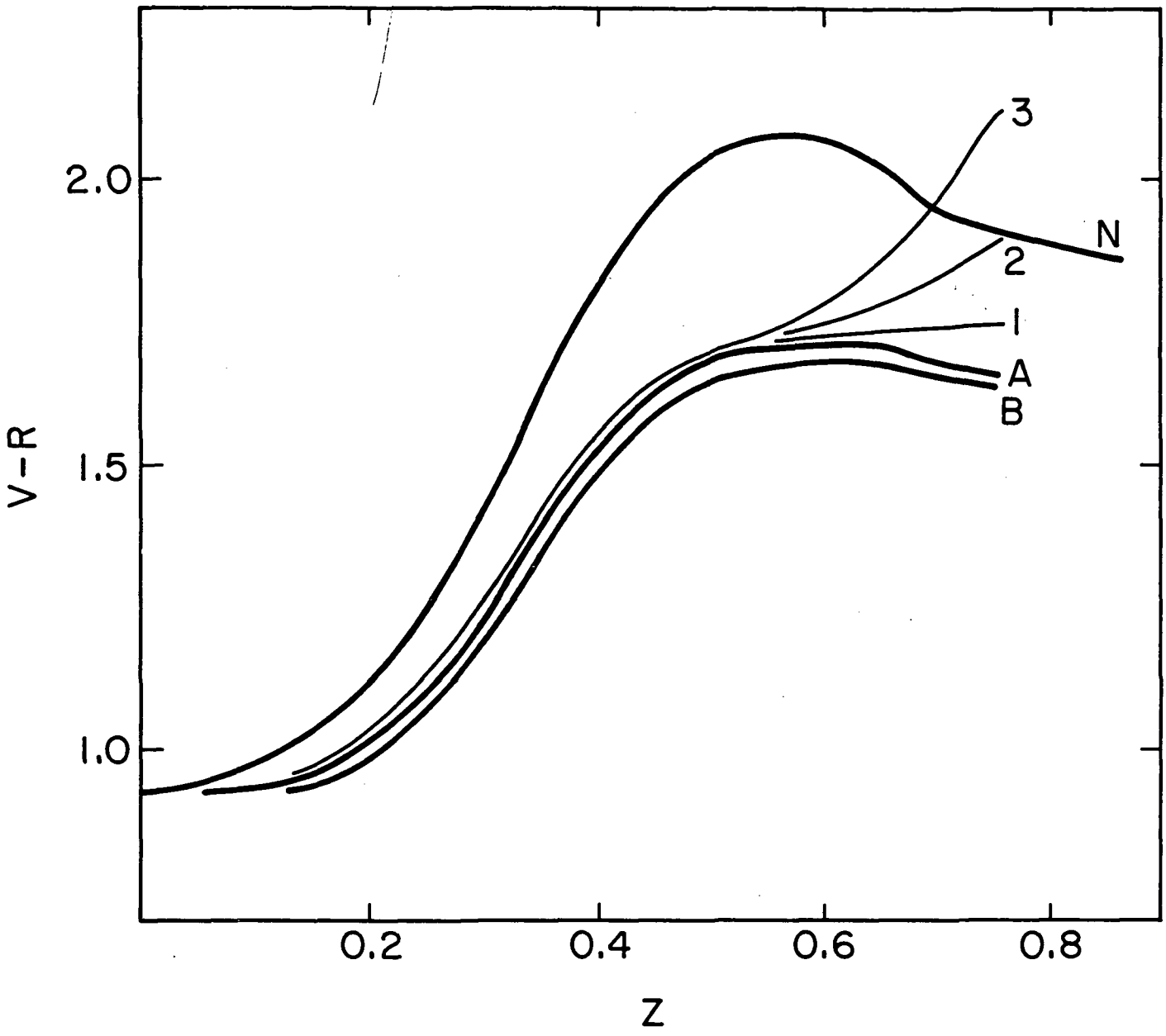

Figure 1: The effects of dust on the spectral energy distribution of galaxies may be both significant and difficult to predict. The three heavy lines show the predicted V-R colors as a function of z from the models of Yoshii & Takahara (1988), where "N" refers to no evolution and "A" and "B" represent colors predicted for systems formed at $z = 5$ and 3, respectively. The results of our spherical model transfer calculations are shown as the numbered lighter lines representing changes to "A" depending upon the dust/star geometry. Model "1" has a small sphere of dust centered on a larger sphere of stars; "2" is our model elliptical galaxy with a r^{-3} stellar distribution and r^{-1} dust distribution; "3" is a uniform mixture of stars and dust. In all cases $\tau_V = 1$ measured from the center to the surface.

The Nature of Faint Emission-line Galaxies

John J Smetanka
Center for Astrophysical Research in Antarctica
and
University of Chicago, Department of Astronomy and Astrophysics

One of the results of faint (B > 20) galaxy redshift surveys is the increased fraction of galaxies which have strong emission-line spectra (Broadhurst *et al.*, 1988 (BES); Colless *et al.*, 1990 (LDSS); Cowie *et al.*, 1991; Broadhurst *et al.*, 1992). These faint surveys find that roughly 50% of the galaxies have an equivalent width of [OII], W_{3727}, greater than 20Å while this fraction is less than 20% in the DARS (B < 17) survey. This has been interpreted as evidence for strong evolution in the galaxy population at redshifts less than 0.5 (BES; Broadhurst *et al.*, 1992; Cowie *et al.*, 1992).

In order to further investigate the properties of the galaxies in faint redshift surveys two important factors must be addressed. The first is the observed correlation between color, luminosity, and W_{3727}. There is a correlation between color and the strength of emission-lines, bluer galaxies having stronger emission features, as evident for Markarian galaxies (Huchra, 1977) and for galaxies in Kennicutt's spectrophotometric atlas (Kennicutt, 1992). This correlation also applies to galaxies in faint redshift surveys (see Figure 2) (Koo and Kron, unpublished). In addition, low luminosity galaxies have a larger average W_{3727} (and bluer colors) than higher luminosity galaxies. This is illustrated in Figure 1a for Kennicutt's low z late-type galaxies (Kennicutt, 1992), 1b for the Durham Faint Surveys (BES and LDSS), and 1c for galaxies in SA68 (B < 23).

The second factor which must be incorporated into any interpretation of the faint emission galaxies is the different luminosity functions for galaxies depending on color. This is usually modeled by varying M^* for different color classes (or morphological types); however, the **shape** of the luminosity function is different for galaxies with different colors. Low luminosity, blue galaxies have a much larger number density than low luminosity, red galaxies (Shanks, 1990). Furthermore, the low luminosity end of the blue galaxy luminosity function is not well fit by a Schechter function (Shanks, 1990).

These two factors have been included in a very simple, no-evolution, model for the galaxy population. This model uses the luminosity functions from Shanks (1990) and spectral energy distributions (SEDs) from Bruzual (1988). W_{3727} is predicted using the correlation (including dispersion) with color shown in Figure 2. Although this model is very simple, utilizing a small number of SEDs and luminosity functions, preliminary results show that the observed distribution of W_{3727} is reproduced without evolution. For 16 < B < 17 the fraction of galaxies with strong emission-lines is roughly 18% while this fraction is 52% for 20 < B < 21.5 (the range of BES) and 54% for 21.5 < B < 22.5 (the range of LDSS). Unfortunately, this model does not reproduce the observed median redshift of these samples. The model's median redshift is too small by 20% compared to faint redshift surveys. Some of this difference is likely to be due to the small number of SEDs used. The limited success of this model indicates that the differences between the luminosity functions for different classes of galaxies and color-luminosity-W_{3727} effects are important in the interpretation of faint galaxy data. An observational program is currently underway to determine the luminosity function and emission-line characteristics of faint blue galaxies to better precision.

Figure 1: W_{3727} *v.* Luminosity

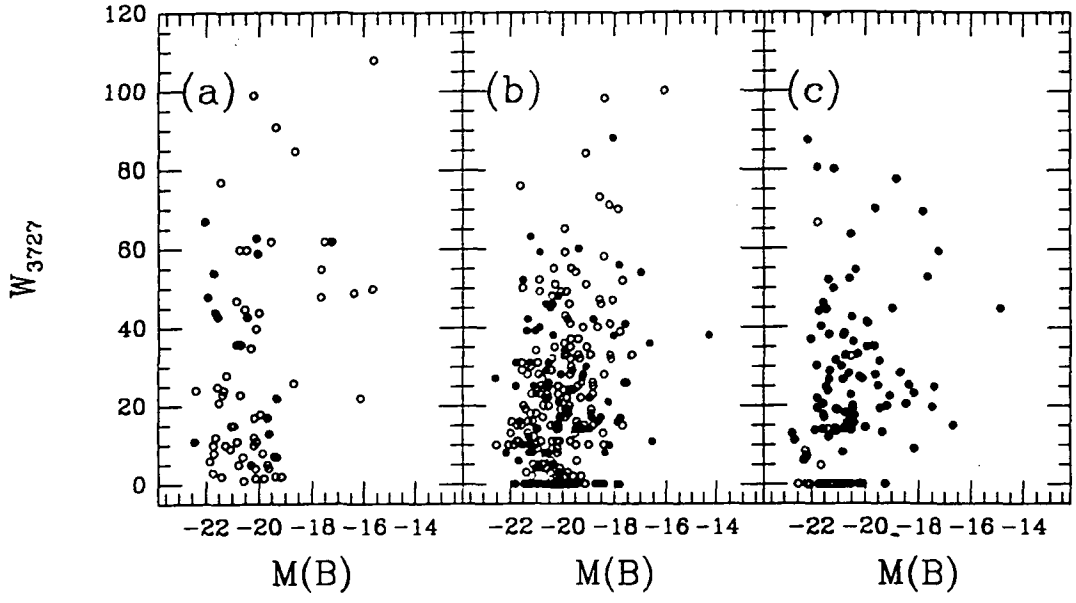

Figure 1: Luminosity *v.* W_{3727} for three galaxy surveys. (a): Late-type galaxies (Sa-I0) from Kennicutt (1992). Solid symbols represent peculiar and/or Markarian galaxies. (b): Galaxies in the DFS. Open symbols represent galaxies from BES. Solid symbols represent galaxies from LDSS. (c): Galaxies in SA68. Solid symbols represent galaxies with U-R < 1.

Figure 2: W_{3727} *v.* Color

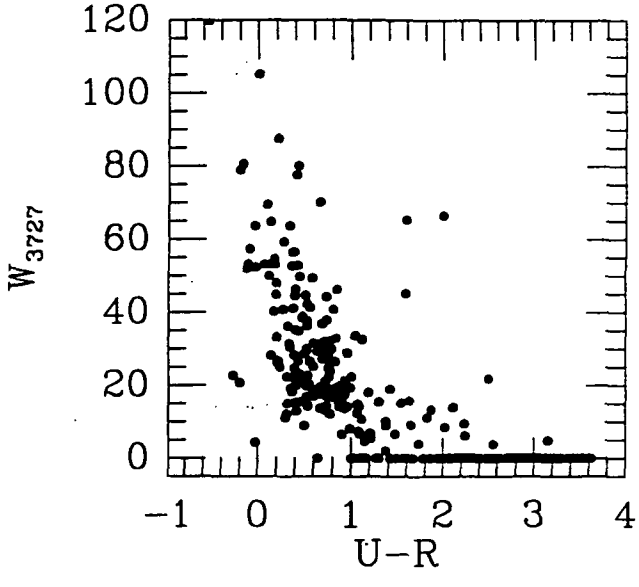

Figure 2: The correlation between U-R color and W_{3727} for galaxies in SA68. A color-selected (U-R < 1) redshift survey to B < 21.5 which allows increased statistics for blue galaxies is included along with the galaxies observed in the color-independent Koo-Kron redshift survey.

References

Broadhurst, T.J., Ellis, R.S., & Glazebrook, K. (1992) *Nature* **355**:55.

Broadhurst, T.J., Ellis, R.S., & Shanks, T. (1988) *M.N.R.A.S.* **235**:827. (BES)

Bruzual, G. (1988) in *Toward Understanding Galaxies at Large Redshift*, eds. R.G. Kron and A. Renzini (Dordrecht:Kluwer), p161.

Colless, M., Ellis, R.S., Taylor, K., & Hook, R.N. (1990) *M.N.R.A.S.* **244**:408. (LDSS)

Cowie, L.L., Songaila, A., & Hu, E.M. (1991) *Nature* **354**:460.

Huchra, J.P. (1977) *Ap. J. Suppl.* **35**:171.

Kennicutt, R.C. (1992) *Ap. J.* **388**:310.

Shanks, T. (1990) in *Galactic and Extragalactic Background Radiation: Optical, Ultraviolet and Infrared Components. IAU Symp. 139* eds. S. Bowyer and Ch. Leinert (Dordrecht:Kluwer), p269.

Two Protogalaxy Candidates in One Night

Peter Eisenhardt, JPL/Caltech, and Mark Dickinson, UC Berkeley

On 20 March 1992 our ongoing program of infrared imaging of high redshift galaxies with the KPNO 4m turned up evidence for the flat spectrum considered characteristic of protogalaxies in two radio galaxies: B2 0902+34 at z=3.395 (hereafter 0902), and 3C 256 at z=1.819.

In spite of a lookback time of 77 to 89% (qo=0 - 0.5) of the age of the universe, Lilly provided evidence that the dominant stellar population in 0902 was surprisingly old, over 1 Gyr. This age estimate was based on the values K=18.8 and I-K=4.5 in the central 3.5 x 3.5". At Lilly's suggestion, we reobserved 0902 at K, and in initial reductions of our data found only an upper limit (K > 19.5). After extensive experimentation with reduction techniques and correction for low-level systematic effects, we succeeded in extracting a four sigma detection at K=19.9 in a 4" diameter circular aperture (see Figure 1). The morphology and location of this detection were more reminiscent of the Ly alpha image (Dickinson et al. 1992) than of CCD continuum images, and in March 1992 we obtained a narrow band image which included redshifted [OIII] 4959,5007 Angstrom line emission at 2.20um. This [OIII] image gave a strong detection which demonstrates that most of the central K flux, already reduced by a magnitude, is due to line emission. Our formal line corrected values in a 4" aperture are K=21.5 and R-K=1.9 (vs. a flat spectrum value R-K=1.7). Hence 0902 has been transformed from relaxed maturity into unsettled youth.

The morphology in each of the four images shown in Figure 1 is somewhat different, although there is a general east-west orientation. Since the radio morphology is generally north-south (van Breugel and McCarthy 1990), 0902, unlike most high redshift radio galaxies, does not have aligned radio and UV/optical emission. The difference between the K and [OIII] morphologies suggests that some K continuum flux distinct from the [OIII] emission is present. In fact our data may indicate the presence of an extended (>10" diameter) halo of K emission which would be consistent with the brighter K values found by Lilly in larger apertures using a single element photometer. However, the halo is not seen in [OIII] emission and could be a systematic error in the K data. If the halo is real our line corrected values become K=20 and R-K=3.4, but modelled ages are still much younger than those based on I-K=4.5.

In comparison, 3C 256 is a much more straightforward case for a protogalaxy. Despite its extreme faintness (K=19.1, 5000 times fainter than the sky) our K image (Figure 2) shows that the (rest frame 0.8um) light is highly elongated and aligned with the radio lobes, similar to the CCD R light (rest 0.23 um). The low ratio of K/R light (R-K=2.4), lack of a central red core, and dynamically young morphology all imply that 3C 256 is forming its first major generation of stars:, i.e. it is a protogalaxy. The excellent radio alignment suggests that radio jets triggered this formation.

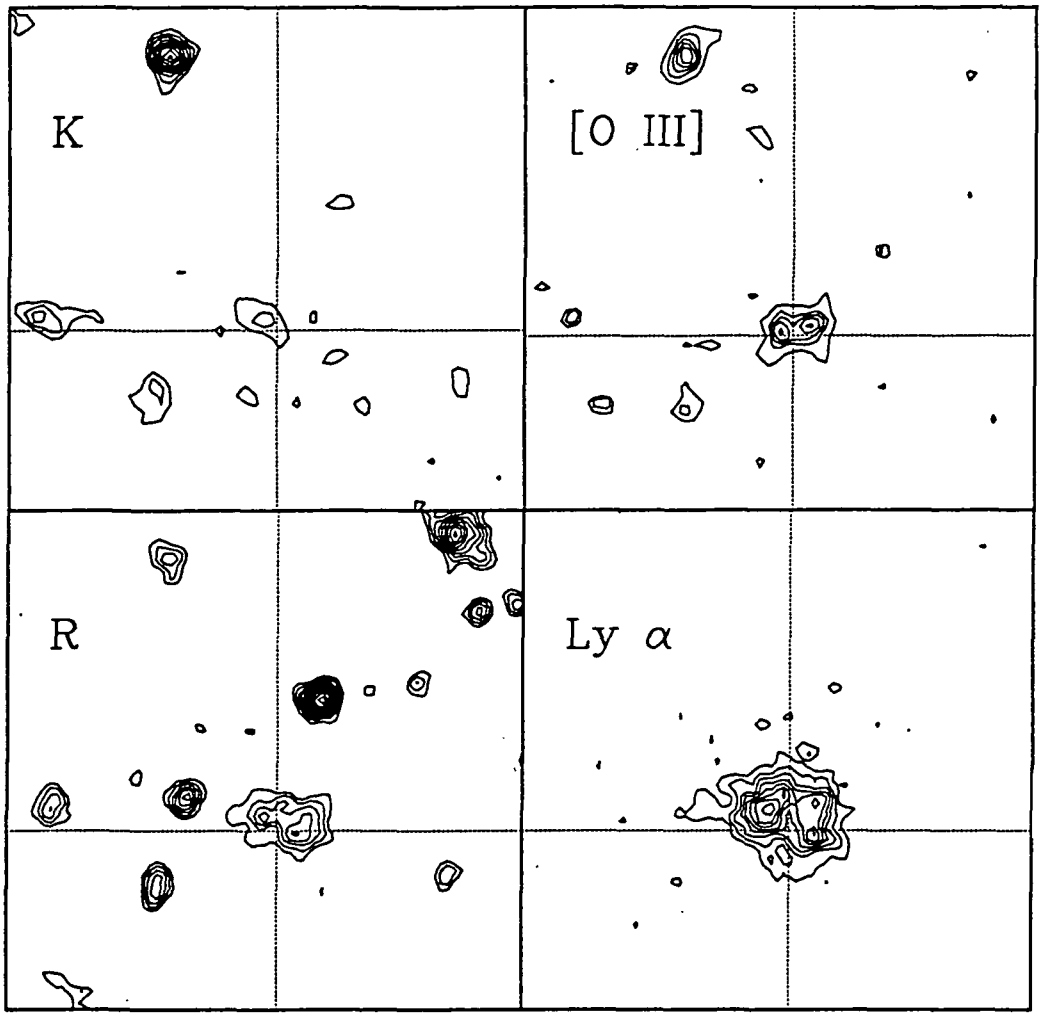

Figure 1: Montage of IR and optical imaging data for 0902+34. The upper panels show the K and narrow band 2.21um images. The latter includes flux from both the K band continuum and the redshifted [OIII] 4959,5007 Angstrom emission lines; no attempt has been made to subtract the continuum from the line image. The deep CCD R and Ly alpha images are taken from Dickinson et al. (1992). The field of view is 25 arcseconds on a side for each panel, and the 0902 radio core position (9h02m24.796s, 34o19'56.58") is marked by the intersection of the dotted lines. North is up and East is to the left.

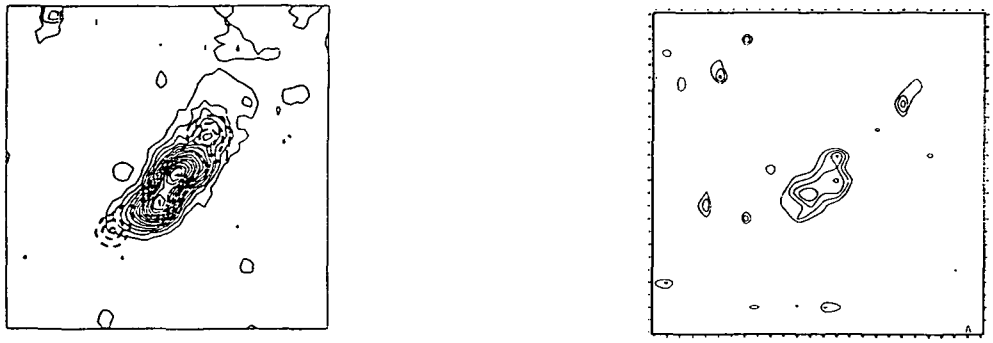

Figure 2: 3C 256 in R (left panel), with the radio data superimposed (from van Breugel and McCarthy 1990), and in K (right). The panels are 10" wide, north is up, east is to the left.

A Comparison of the Near-Infrared Spectral Features of Early-Type Galaxies in the Coma Cluster, the Virgo Cluster and the Field

Mark L. Houdashelt and Jay A. Frogel
Department of Astronomy, The Ohio State University

Aaronson *et al.* (1981) derived the relative distance between the Coma and Virgo clusters from color-magnitude relations of the early-type galaxies in each cluster. They found that the derived distance was color-dependent and concluded that the galaxies of similar luminosity in the two clusters differ in their red stellar populations. More recently, the color-dependence of the Coma-Virgo distance modulus has been called into question by Bower *et al.* (1992a, 1992b). However, because these two clusters differ so dramatically in their morphologies and kinematics, it is plausible that the star formation histories of the member galaxies also differed. If the conclusions of Aaronson *et al.* are indeed correct, then some signature of the resulting stellar population differences should appear in the near-infrared and/or infrared light of the respective galaxies.

We have collected near-infrared spectra (6600 - 9200 Å) of 17 Virgo and 10 Coma early-type galaxies; this sample spans about four magnitudes in luminosity in each cluster. Seven field E/S0 galaxies have been observed for comparison. Pseudo-equivalent widths have been measured for all of the field galaxies, all but one of the Virgo members, and five of the Coma galaxies. The features examined are sensitive to the temperature, metallicity and surface gravity of the reddest stars. These include the Ca II triplet (8498, 8542 and 8662 Å) as defined by Delisle & Hardy (1992), the Na I doublet (8183 and 8195 Å) as defined by Faber & French (1980), the TiO band indices I(7100), I(7450), I(7890), I(8197) and I(8460) of Terndrup *et al.* (1990), and the TiO1 and TiO2 bands of Carter *et al.* (1986).

A *preliminary* analysis of these spectral features has been performed, and, with a few notable exceptions discussed below, the measured pseudo-equivalent widths agree well with previously published values. In particular, our I(8197) indices support those of Boroson & Thompson (1991) and Delisle & Hardy (1992), both of whose I(8197) strengths disagree with the Terndrup *et al.* (1990) values. However, we have had some difficulty reproducing the Na I measurements of Delisle & Hardy, and our sample of galaxies does not show the correlation between Na feature strength and luminosity which they see. This is undoubtedly due to the very narrow continuum bands used to determine the Na I width; they span only one or two pixels at our spectral resolution. We have also found some of the feature measurements to be highly sensitive to the removal of the telluric O_2 and H_2O absorption bands present in this spectral region. This is especially true of the Na doublet and I(8197) band.

The pseudo-equivalent widths of the E/S0 galaxies in the Coma cluster and in the field do not appear to be systematically different from those of the Virgo cluster members of similar luminosity and/or color. There are two significant trends evident in the Virgo data, and the field and Coma galaxies tend to scatter about the Virgo relations.

For the Virgo galaxies, the strength of the Ca II triplet weakens as the TiO band at 7890 Å gets stronger. This trend is shown in Figure 1; it is consistent with the inverse correlation between the widths of the TiO band at 8145 Å and the Ca II 8662 Å line seen in Galactic bulge stars and solar neighborhood M giants by Sharples *et al.* (1990). However, due to the measurement uncertainties in our data and the fact that our observed trend greatly depends upon the two or three galaxies with the strongest Ca lines, the Ca II strengths are also consistent with the galaxies having an intrinsically small spread in Ca II width, as predicted by Terlevich *et al.* (1990) for a metal-rich, giant-dominated stellar population.

Figure 2 illustrates that the indices of the two most prominent TiO bands in the near-IR, I(7100) and I(7890), tend to be stronger in redder galaxies, with their strengths becoming constant for the reddest galaxies. Since the color of an early-type galaxy is known to be a function of metallicity, this would indicate that, at least for the bluest galaxies in our sample, the TiO band strengths trace the average metallicity of the underlying late-type stellar population.

Reduction of the remaining near-IR spectra is in progress, and this project will soon move on to an analysis of infrared (*K* band) and optical (4300 - 7000 Å) spectra which have already been obtained.

Aaronson, M., Persson, S. E., and Frogel, J. A. 1981, ApJ, 245, 18.
Boroson, T. A. and Thompson, I. B. 1991, AJ, 101, 111.
Bower, R. G., Lucey, J. R. and Ellis, R. S. 1992a, MNRAS, 254, 589.
Bower, R. G., Lucey, J. R. and Ellis, R. S. 1992b, MNRAS, 254, 601.
Carter, D., Visvanathan, N., and Pickles, A. J. 1986, ApJ, 311, 637.
Delisle, S. and Hardy, E. 1992, AJ, 103, 711.
Faber, S. M. and French, H. B. 1980, ApJ, 235, 405.
Sharples, R., Walker, A., and Cropper, M. 1990, MNRAS, 246, 54.
Terlevich, E., Díaz, A. I., and Terlevich, R. 1990, MNRAS, 242, 271.
Terndrup, D. M., Frogel, J. A., and Whitford, A. E. 1990, ApJ, 357, 453.

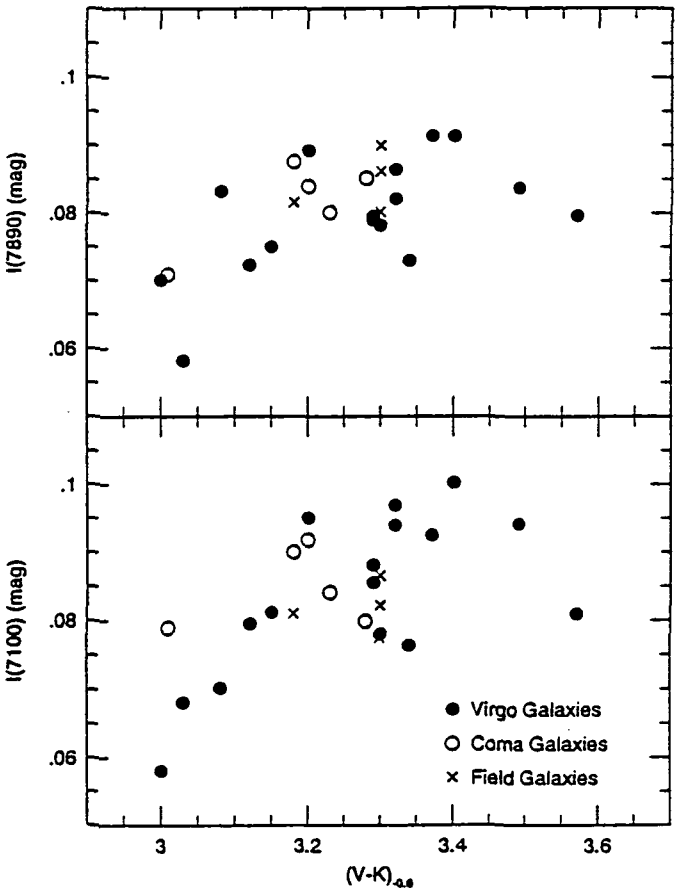

Fig 1. - The correlation of the strength of the TiO band index I(7890) with the pseudo-equivalent width of the Ca II triplet. Ca II is the sum of the Ca lines at 8542 and 8662 Å.

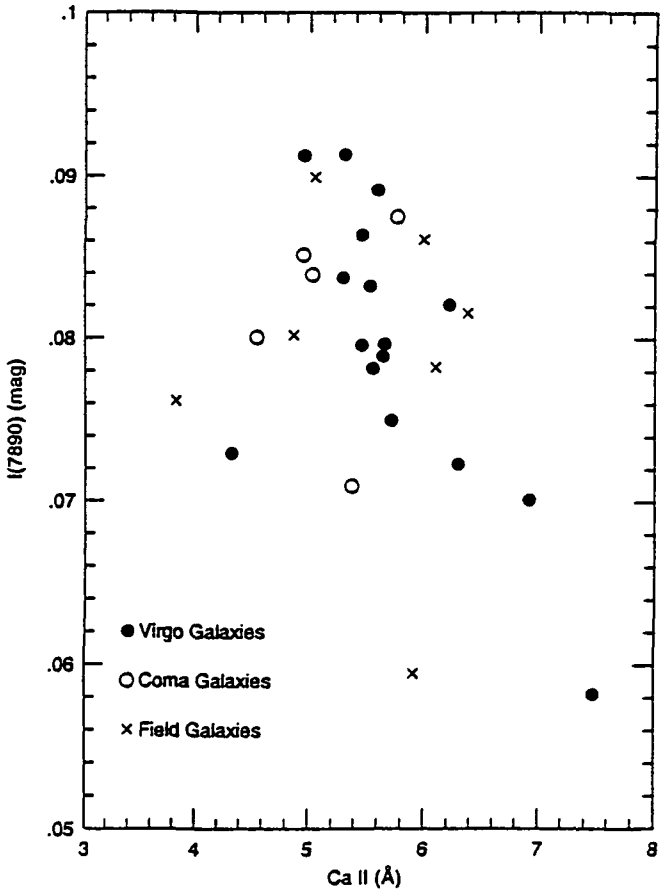

Fig. 2. - The strengths of the TiO band indices I(7100) and I(7890) as a function of galaxy color. $(V\text{-}K)_{-0.6}$ is the *V-K* color at log (Å/D_0) = -0.6 taken from Aaronson *et al.* (1981).

Everything you ever wanted to know about

The Ultraviolet Spectra of Star-forming Galaxies

but were afraid to ask.

A.L. Kinney, R. Bohlin, D. Calzetti, N. Panagia, and R. Wyse

I. ABSTRACT

We present ultraviolet spectra of 143 star-forming galaxies of different morphological types and activity classes including S0, Sa, Sb, Sc, Sd, irregular, starburst, blue compact, blue compact dwarf, Liner, and Seyfert 2 galaxies. These IUE spectra cover the wavelength range from 1200 to 3200 Åand are taken in a large aperture ($10'' \times 20''$).

The ultraviolet spectral energy distributions are shown for a subset of the galaxies, ordered by spectral index, and separated by type for normal galaxies, Liners, starburst galaxies, blue compact (BCG) and blue compact dwarf (BCDG) galaxies, and Seyfert 2 galaxies. The ultraviolet spectra of Liners are, for the most part, indistinquishable from the spectra of normal galaxies. Starburst galaxies have a large range of ultraviolet slope, from blue ($F_\lambda \propto \lambda^{-1.85\pm0.06}$) to red ($F_\lambda \propto \lambda^{0.26\pm0.14}$). The star-forming galaxies which are the bluest in the optical (BCG and BCDG), also have the "bluest" average ultraviolet slope of $\beta = -1.75 \pm 0.63$. Seyfert 2 galaxies are the only galaxies in the sample that consistently have detectable UV emission lines.

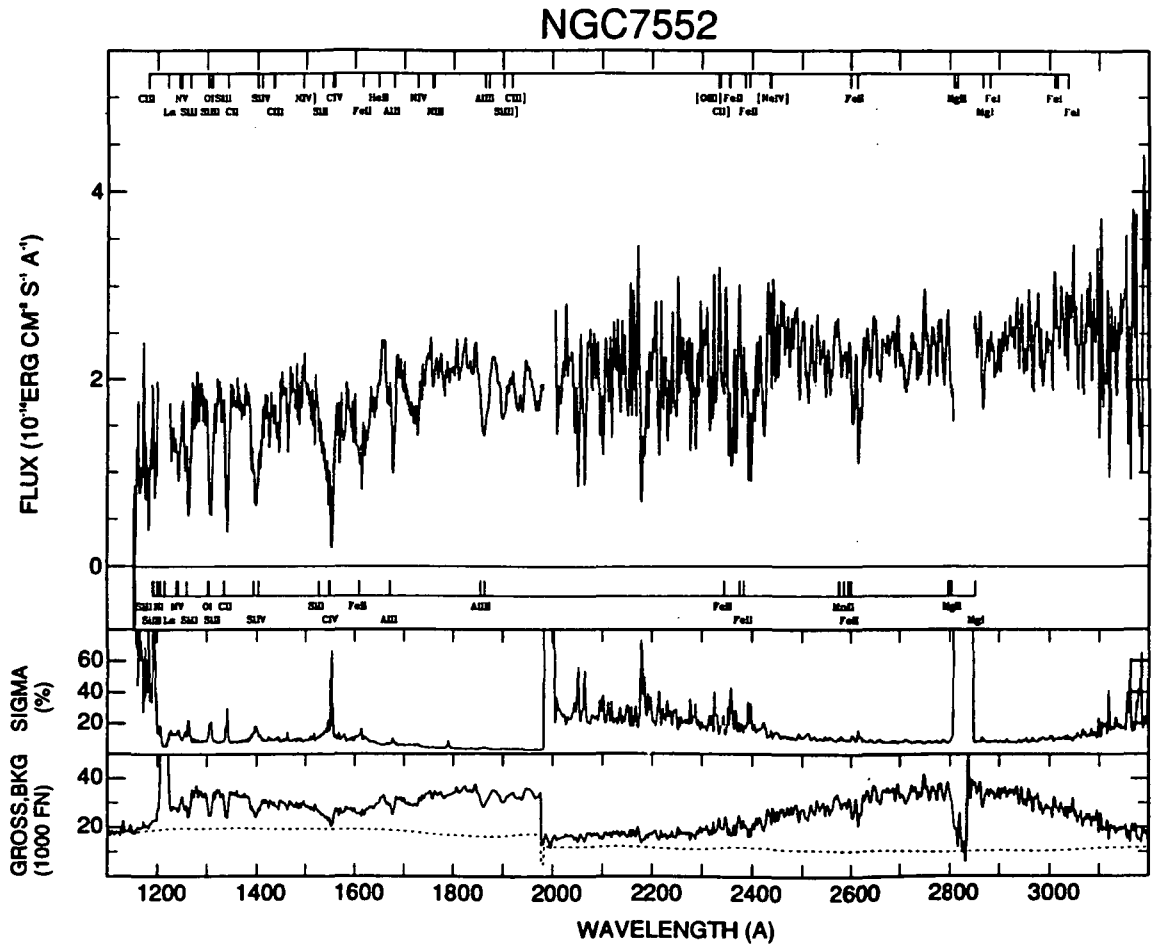

THE ULTRAVIOLET SIGNATURE OF MASSIVE STARS IN STARBURST GALAXIES

CARMELLE ROBERT, CLAUS LEITHERER[1], AND TIMOTHY M. HECKMAN[2]
Space Telescope Science Institute, 3700 San Martin Dr., Baltimore, MD 21218
[1] Affiliated with the Astrophysics Division of ESA
[2] Johns Hopkins University, Dept. of Physics and Astronomy

ABSTRACT We present a progress report of a study of the massive star population in starburst galaxies using the UV spectral region.

INTRODUCTION

Studies in different spectral regimes of starburst galaxies clearly indicate the presence of hot, massive stars (see *STScI Sym. 5: Massive Stars in Starbursts*, 1991). However, only the UV spectral region can be used to directly identify the spectroscopic signature of these stars. The typical contributor to the integrated continuum at $\sim$ 1400 Å of a starburst is from the hot B stars. More massive stars (O stars and their descendants, the Wolf-Rayet [W-R] stars) are responsible for the majority to the UV lines which are broad (compared to the interstellar [IS] lines) photospheric absorption lines and wind emission or P Cygni profiles.

POPULATION SYNTHESIS MODELS

The line profiles of SiIV λ1397 and CIV λ1549 are synthesized with the latest generation of stellar evolution models (Maeder 1990, *A&AS* 84, 139), stellar atmospheres (Kurucz 1992, *IAU 142*, p. 225; Schmutz *et al.* 1992, *PASP* in press), and a line profile library based on IUE **high** dispersion spectra of massive stars (except for the B stars for which we use low dispersion spectra at the moment). Stellar populations for continuous and instantaneous bursts are calculated given a certain slope (α) and cut-off masses (M_l and M_u) for the initial mass function (IMF). An interpolation is done for a mass interval of 1 $M_\odot$ and a time resolution of 10^4 yr.

RESULTS

Figure 1 shows the relative number of massive stars in an instantaneous burst. As one can see, the most massive stars, O and W-R stars, disappear after $\simeq 10^7$ yr. The number of BV-IV stars slightly decreases with time while the number of BI-III stars is increasing.

In figure 2, we present the SiIV and CIV profiles synthesized for the stellar population described in figure 1. At $t \simeq 10^{6.5}$ yr, the SiIV doublet has a P Cygni type profile (over which the IS component is superposed). This wind profile shape is due to an increased number of O supergiants and W-R stars. At $t \geq 10^{6.8}$ yr, the SiIV doublet is broad but not blue shifted anymore. B stars, which have become the dominant contributors, are responsible for this profile shape (along with

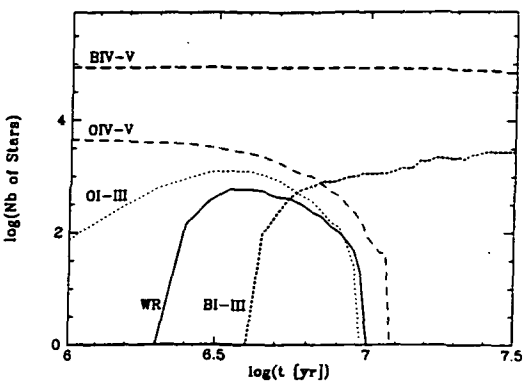

FIGURE 1. Number of stars as a function of time for an instantaneous burst of total mass 10^6 $M_\odot$ ($Z = Z_\odot$, $\alpha = 2.35$, $M_l = 1$ $M_\odot$, and $M_u = 120$ $M_\odot$).

the IS medium). Massive main sequence stars have a CIV doublet which already shows a P Cygni type profile. This profile increases in strength and become narrower as the winds from O supergiants becomes more important ($t \simeq 10^{6.5}$ yr). Later on, B stars and the IS medium are responsible for a weak CIV feature.

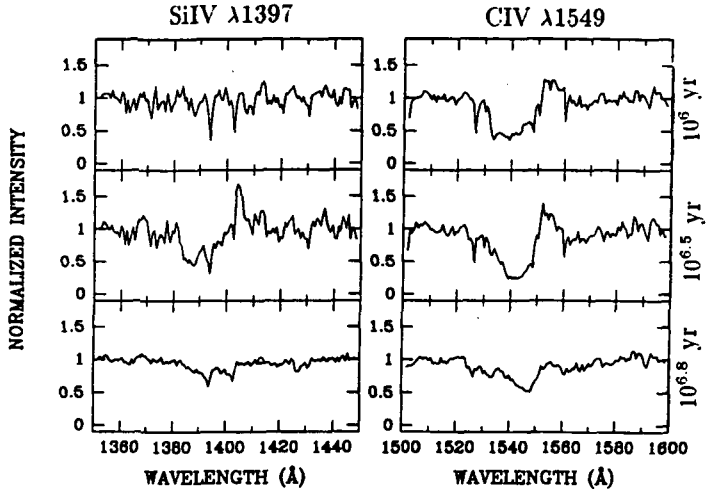

FIGURE 2. Synthetic SiIV and CIV line profiles of a burst at three evolutionary phases. (Model parameters are as in fig. 1.)

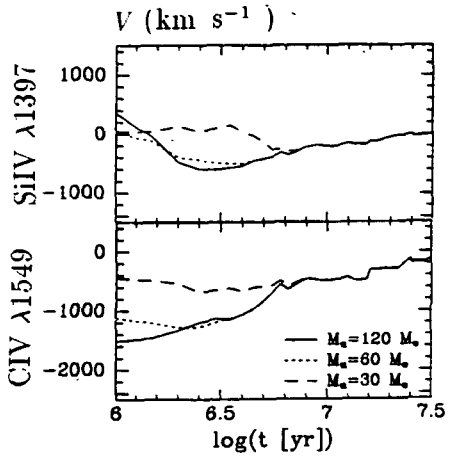

FIGURE 3. Synthetic SiIV and CIV velocity shift as a function of time for three upper cut-off mass limits. (Model parameters are as in fig. 1.)

The velocity shifts described in the synthetic profile of figure 2 are quantitatively presented in figure 3 (solid line for $M_u = 120\ M_\odot$). One can clearly see the blue shift of SiIV after $\simeq 10^{6.5}$ yr due to stellar winds from massive stars. CIV is shifted back to the laboratory wavelength as time passes, *i.e.* as massive stars are dying.

In figure 3, the velocity shifts are presented for 3 models using different values of M_u. For $M_u = 60\ M_\odot$, the main sequence star contribution to CIV is reduced at early phases. For $M_u = 30\ M_\odot$, most massive stars are absent and the profiles are virtually unshifted. No important dependences of the SiIV and CIV velocity shifts with α (*i.e.* from 1.5 to 3) are observed.

OBSERVATIONS OF STARBURST GALAXIES

We have selected a sample of 49 starburst galaxies from IUE archives based on their high signal-to-noise ratio. For this sample, we calculate an average velocity shift of -490 and -745 km s^{-1} for SiIV and CIV, respectively. No significant shifts (larger than ± 200 km s^{-1}) are seen for simple lines formed in the IS medium. Based on our models, the large blue shifts observed for SiIV and CIV clearly indicate the presence of massive stars, $> 30\ M_\odot$, in most of our galaxies. In the case of NGC3256, for which Joseph (1991, *Massive Stars in Starbursts*, p. 259) estimated $M_u = 25$-$30\ M_\odot$ based on IR data, we obtain large blue velocity shifts for SiIV and CIV (-611 and -1125 km s^{-1}). This result argues in favor of a large value for M_u.

The full potential of our method will be exploited on the basis of Hubble Space Telescope data of several galaxies available in a near future.

We gratefully thank Kinney, Bohlin, Prinja, Howarth, St.-Louis, and Fanelli for the use of their reduced IUE spectra. T. H. and C. L. acknowledge NASA for support of this research in the form of ADP and LTSA grants. C. R. thank CRSNG (Canada) for a post-doctoral fellowship and STScI's Director's Research Fund for travel support.

A Search for Quasar Protoclusters at z > 4

J.D. Smith, D. Thompson, and S. Djorgovski
Palomar Observatory
California Institute of Technology

Introduction: In the CDM and many other hierarchical scenarios for the origins of large scale structure, the existence of luminous quasars at very high redshifts ($z > 3$ or 4) is difficult to understand, unless such objects form at the very highest peaks of the density field. One then might expect a strong clustering of quasars at large redshifts. This is a generic prediction for practically any reasonable primordial density fluctuation spectrum. For CDM, Efstathiou & Rees (1988) predicted that quasars at $z > 4$ should be clustered as strongly as the bright galaxies at $z \sim 0$. Cole & Kaiser (1989) suggest that $z > 4$ quasars might represent $\gtrsim 4\sigma$ peaks of the density field, and thus should be clustered more strongly than galaxies at $z \sim 0$.

We are performing the following experiment: A search for quasars, AGN, or other discrete objects, e.g., starforming galaxies, near *known*, $z > 4$ quasars. In other words, use the early quasars as markers of possible protoclusters. This is a fairly basic test of our understanding of the formation of galaxies, large-scale structure, and the origin of the first quasars themselves.

The Experiment: A quick and simple way to search for high-z quasars is through multicolor imaging. We obtain multicolor CCD images on and around the fields containing known $z > 4$ quasars, and use discrepant colors to select other quasar candidates near them. Such putative faint AGN may have ecsaped detection due to some selection effect (e.g., brightness, weaker lines, not being a strong radio source, etc.) The known target quasar itself provides an immediate empirical calibration as to what kind of a color discrepancy may be expected. A simple setup is to use the Gunn-Thuan *gri* bands, and look for objects where Lyα is in the r band; the line, and the continuum change between the g and i bands would leave a distinct color-color signature. This implies a redshift range $\sim 4.05 - 4.9$. Promising color-selected candidates will be followed up spectroscopically.

Whereas this method should work for AGNs where the continuum is well detectable, it may be insufficient to pick out very faint galaxies at these redshifts. Actively star-forming galaxies (which, at these redshifts, could well be identified as primeval galaxy candidates) should perhaps be even more numerous than faint AGNs. For them, the optimal detection technique may be Lyα narrow-band imaging, where they should stand out, regardless of what their continuum level is. Many high-z Lyα galaxies (but usually with active nuclei) have already been found using this method and its derivatives.

Data: So far, we have obtained multicolor images of the following quasar fields using the 4-Shooter imager at the Palomar 200-inch telescope: PC 0307+0222 ($z = 4.373$), PC 0751+5623 ($z = 4.285$), PC 0910+5625 ($z = 4.036$), PC 1158+4635 ($z = 4.733$), PC 1247+3406 ($z = 4.897$), and QSO 2203+292 ($z = 4.399$). This imaging data has been

(almost) fully reduced. Multicolor data on the following fields has also been obtained at the Palomar 60-inch telescope: PC 0104+ 0215 ($z = 4.171$), PC 0953+4749 ($z = 4.457$), PC 1233+4752 ($z = 4.447$), PC 1301+4747 ($z = 4.004$), and PC 2331+0216 ($z = 4.093$). Only the data on PC 1233+4752 has been reduced. Multicolor data on two southern quasar fields have been obtained at the CTIO 4-meter telescope and fully reduced: QSO 0000–26 ($z = 4.098$) and QSO 0051–279 ($z = 4.402$). We have also obtained one set of imaging data (PC 1233+4752) at the Palomar 200-inch telescope using the COSMIC imager which has not been reduced.

The photometry was done using *Daophot*. For the 4-Shooter, the photometry is complete down to $r \sim 24^m - 24.5^m$, and reliable detections extend even to $r \lesssim 25^m$. Typically about 2000 objects are detected in each 4-Shooter field. For the Palomar 60-inch, the photometry is complete down to $r \sim 23.5^m$ with about 350 objects detected. The CTIO data on QSO 0000–26 is complete to $r \sim 23^m$ with 650 objects detected while the data on QSO 0051–279 is complete to $r \sim 24.5^m$ with 2000 objects detected. All color-selected candidates are examined visually on a workstation. Some are resolved (galaxies), but with a strong excess in the r band; some are (quasi?)stellar in appearance. At this point, we do not discriminate against galaxies (extended objects), since we are interested in *any* objects at these redshifts. The best candidates are selected for follow-up spectroscopy.

Narrow band imaging has been obtained at the CTIO 4-meter for PC 0307+0222 and QSO 0051–279, and at the Palomar 60-inch for PC 0953+4749, and PC 1233+4752.

Results: At these redshifts, the 4-Shooter fields ($\sim$ 8.5 arcmin sq.) correspond to a comoving area of about $126 h_{75}^{-2}$ Mpc^2 (for $\Omega_0 = 1$), or about $632 h_{75}^{-2}$ Mpc^2 (for $\Omega_0 = 0$), with $\Delta z \simeq 0.8$, i.e., a depth of a few hundred Mpc. The distance moduli at these redshifts, for $H_0 = 75$ km/s/Mpc, are about about 46.9 (for $\Omega_0 = 1$), or about 48.1 (for $\Omega_0 = 0.2$). Thus, we are probing the AGN luminosity function nearly to the Seyfert 1 level. Based on *very* uncertain extrapolations of the comoving density and quasar luminosity function from lower redshifts, we estimate that the probablity of detecting another quasar (down to our magnitude limit) for each of these fields is $\sim 10^{-1 \pm 1}$. There are between 0 and 3 highly promising candidates per quasar field, and an additional half-dozen objects per field, whose spectra may be worth obtaining.

We have selected 41 objects for follow-up spectroscopy using the multicolor technique, with $\approx$ 10 of those being high-priority candidates. So far, we have obtained follow-up spectroscopy on six objects. Five of the objects have $z < 1$. However, one object in the PC 0910+5625 field has a tentative redshift of $z = 4.06$. More spectrocopy is needed on this object to confirm this result. Twelve candidates have been chosen from the narrow-band imaging but we have been unable to obtain spectra of any of them. Our Lyα flux limits achievable in $\sim$ 20 minute integrations ($\sim 10^{-17}$ erg/cm^2/s) at these redshifts correspond to unobscured line luminosities powered by star formation of $SFR \lesssim 5 M_\odot$/yr, and thus any unobscured, star-forming young galaxies in these fields should be detectable.

In the future, we hope to cover several additional fields using the multicolor technique. Most of all, we need spectra of the candidates already in hand.

Wide-Field Direct CCD Observations Supporting the Astro-1 Space Shuttle Mission's Ultraviolet Imaging Telescope

Paul Hintzen[1,3], Ron Angione[2], Freddie Talbert[2],

K.-P. Cheng[3], Eric Smith[3], and Theodore Stecher[3]

[1] Department of Physics, University of Nevada, Las Vegas, NV

[2] Department of Astronomy, San Diego State University

[3] Laboratory for Astronomy and Solar Physics, NASA-Goddard Space Flight Center

Summary

Wide field direct CCD observations are being obtained to support and complement the vacuum-ultraviolet (VUV) images provided by Astro's Ultraviolet Imaging Telescope (UIT) during a Space Shuttle flight in December 1990. Because of the wide variety of projects addressed by UIT, the fields observed include (1) Galactic supernova remnants such as the Cygnus Loop and globular clusters such as Omega Cen and M79; (2) the Magellanic Clouds, M33, M81, and other galaxies in the Local Group; and (3) rich clusters of galaxies, principally the Perseus cluster and Abell 1367. Ground-based observations have been obtained for virtually all of the Astro-1 UIT fields. The optical images allow identification of individual UV sources in each field and provide the long baseline in wavelength necessary for accurate analysis of UV-bright sources. To facilitate use of our optical images for analysis of UIT data and other projects, we plan to archive them, with the UIT images, at the National Space Science Data Center (NSSDC), where they will be universally accessible via anonymous FTP.

The UIT, one of three telescopes comprising the Astro spacecraft, is a 38-cm f/9 Ritchey-Chretien telescope on which high quantum efficiency, solar-blind image tubes are used to record VUV images on photographic film. Five filters with passbands centered between 1250A and 2500A provide both VUV colors and a measurement of extinction via the 2200A dust feature. The resulting calibrated VUV pictures are 40 arcminutes in diameter at 2.5 arcseconds resolution. The capabilities of UIT therefore complement HST's WFPC: The latter has 40 times greater collecting area, while UIT's usable field has 170 times WFPC's field area.

During the Astro mission, UIT obtained data for a wide variety of scientific projects. Low redshift galaxies were major targets for UIT, as study of their OB associations should yield fundamental information on the initial mass function for massive star formation, the resulting supernova rates, and ionizing radiation fields. At larger distances, UIT surface brightness observations are similarly being used to study the initial mass functions for star formation in a sample of nearby galaxies, since integrated VUV colors and color profiles provide the most sensitive available measure of the formation rate of massive stars. The blue stages later in stellar evolution are also being studied, e.g. UIT observations at 1500A detected 1300 hot horizontal branch stars (HHB) in Omega Cen. Such a large statistical sample is necessary to place constraints on mass loss during the red giant phase, which is probably the dominant factor determining the future evolution of these stars as well as a central issue in the chemical enrichment of the interstellar medium. These data will also allow more accurate determination of the helium abundances and metallicities of HHB stars.

In all of these projects, supporting ground-based data are critical. Depending on the type of object, optical images have been obtained in some combination of filters which may include U, B, V, R and/or narrow-band H-alpha and [OIII] 5007A. A mere three years ago, only photographic plates would have allowed coverage of the 40 arcminute diameter UIT fields. However, the fortuitous development of a new generation of large-format CCDs has allowed us to acquire optical observations with seeing-limited resolution and linear flux response while still covering a substantial fraction of each UIT frame with one to four integrations. Objects accessible from the Northern Hemisphere were observed from Kitt Peak National Observatory or SDSU's Laguna Observatory; their complementary observing seasons allow year-round coverage. Objects accessible only from the Southern Hemisphere, including the Magellanic Clouds and 47 Tucanae, were observed from Cerro Tololo Interamerica Observatory. Data from the National Observatories were taken with Tek 2048 CCDs on 0.9-meter telescopes, yielding seeing-limited resolution over fields of 20+ arcminutes (KPNO) and 14 arcminutes (CTIO). At Laguna Observatory, a focal reducer was used in conjunction with a TI 800 CCD, providing fields of 11 to 18 arcminutes depending on the field lens used. All data were reduced using standard IRAF routines. The reduced, photometrically calibrated data, in FITS format, will be distributed by the NSSDC to interested investigators upon request.

RESULTS ON THE EVOLUTION OF GALAXIES AND THEIR ENVIRONMENT FROM THE ULTRAVIOLET IMAGING TELESCOPE ON ASTRO-1

Theodore P. Stecher
Laboratory For Astronomy and Solar Physics
NASA/Goddard Space Flight Center
Greenbelt, MD 20771

The Ultraviolet Imaging Telescope, part of the Astro-1 Spacelab Mission was used to obtain high-resolution surface brightness distribution data in six ultraviolet wavelength bands for the bright reflection nebula NGC 7023. The quantitative comparison of the measured surface brightness profiles with corresponding data from the visible leads us to conclude that the scattering in the near and far ultraviolet in this nebula is more strongly forward directed than it is in the visible. The dust albedo for wavelengths longer than 1400 A is identical to that in the visible, with the exception of the 2200 A bump in the extinction curve. In the wavelengh of the bump the albedo is approximately 30% reduced compared to both longer and shorted wavelength regions,which is consistent with the true absorption nature of this feature. This means that there will be more penetration of ultraviolet radiation in the molecular clouds where star formation is proceeding. This higher radiation field changes the concentration of ions in the clouds and therefore the chemical formation rates.

The Ultraviolet Imaging Telescope also obtained near-UV and far-UV images of the giant OB association NGC 206 in M31. Photometry was obtained for thirty massive stars. Their colors and magnitudes agree, after correcting for extinction, with evolutionary predictions. The brighter stars are systematically redder than the fainter stars indicating that they are supergiants whose age is about 4 million years; the fainter bluer stars probably just formed.

We analyze UV imagery of two Sb bulges and two E galaxies obtained with UIT. The UV brightness of these systems is not produced by recent massive star formation but in relatively low luminosity objects. We also find extended, large amplitude UV color gradients which are probably related to abundance gradients within the galaxies.

For NGC 1275 the measured UV colors indicate a mass function which extends to eight solar masses but no higher. This indicates either a cessation of star formation during the last 50 million years or a truncated initial mass function.

The Ultraviolet Imaging Telescope is funded by NASA's Spacelab Office.

The Peculiar Velocities of Rich Clusters in the Hot and Cold Dark Matter Scenarios

George F. Rhee[1], Michael J. West[2], and Jens V. Villumsen[3]

[1]Department of Astronomy, New mexico State University,
[2]Sterrewacht Leiden, The Netherlands,
[3]Department of Astronomy, Ohio State University

We present the results of a study of the peculiar velocities of rich clusters of galaxies. The peculiar motion of rich clusters in various cosmological scenarios is of interest for a number of reasons. Observationally one can measure the peculiar motion of clusters to greater distances than galaxies because cluster peculiar motions can be determined to greater accuracy. One can also test the slope of distance indicator relations using clusters to see if galaxy properties vary with environment. We have used N-body simulations to measure the amplitude and rms cluster peculiar velocity as a function of bias parameter in the hot and cold dark matter scenarios. In addition to measuring the mean and rms peculiar velocity of clusters in the two models we determine whether the peculiar velocity vector of a given cluster is well aligned with a)the gravity vector due to all the particles in the simulation and b)the gravity vector due to the particles present only in the clusters.

We have investigated the peculiar velocities of rich clusters of galaxies in the cold dark matter and hot dark matter galaxy formation scenarios. We have derived peculiar velocties and associated errors for the scenarios using four values of the bias parameter b ranging from $b = 1$ to $b = 2.5$. The growth of the mean peculiar velocity with scale factor has been determined and compared to that predicted by linear theory; we find a larger growth rate for clusters over that predicted by linear theory. In addition we have compared the orientation of force and velocity in these simulations to see if a program such as that proposed by Bertschinger and Dekel (1989) for elliptical galaxy peculiar motions can be applied to clusters. The method they describe enables one to recover the density field from large scale redshift distance samples. The method makes it possible to do this when only radial velocities are known by assuming that the velocity field is curl free. Our analysis suggests that this program if applied to clusters is only realizable for models with a low value of the bias parameter i.e. models in which the peculiar velocities of clusters are large enough that the errors do not render the analysis impracticable.

A Revised Catalog of CfA Galaxy Groups in the Virgo/Great Attractor Flow Field

(Ap. J. submittal)

Richard Nolthenius
UCO/Lick Observatory
University of California, Santa Cruz

A new identification of groups and clusters in the CfA1 Catalog of Huchra, *et al.* (1983) is presented, using a percolation algorithm to identify density enhancements. The procedure differs from that of the original Geller and Huchra (1983; GH) catalog in several important respects; galaxy distances are calculated from the Virgo - Great Attractor flow model of Faber and Burstein (1988), the adopted distance linkage criteria is only ~1/4 as large as in the Geller and Huchra catalog, the sky link relation is taken from Nolthenius and White (1987), correction for interstellar extinction is included, and "by-hand" adjustments to group memberships are made in the complex regions of Virgo / Coma I / Ursa Major and Coma / A1367 (to allow for varying group velocity dispersions and to trim unphysical "spider arms"). Since flow model distances are poorly determined in these same regions, available distances from the IR Tully-Fisher, D_n-σ, planetary nebula luminosity function, and surface brightness resolution methods are adopted if possible.

The percolation algorithm's link criteria are cast in terms of a new determination of the galaxy luminosity function ϕ, using the inhomegeneity-independent procedure of deLapparent, Geller and Huchra (1989). The resulting Schechter parameters are; α = -1.01 and M^* = -19.45; about 0.2 brighter than earlier determinations (α = -0.77, M^* = -19.00 after correction for Malmquist bias). The sky D_L and redshift V_L link criteria are ($V_F \equiv$ 5000 km s^{-1}; $\Phi \equiv$ integrated ϕ visible at distance V):

$$D_L(V) \propto \left[\frac{\Phi(V)}{\Phi(V_F)}\right]^{-1/2} L^{-1/6} = 1.12\ Mpc \left[\frac{\Phi(V)}{\Phi(V_F)}\right]^{-1/2} \left(\frac{V}{V_F}\right)^{-1/3}. \quad (1)$$

$$V_L(V) = 350\ km\ s^{-1} \left[\frac{\Phi(V)}{\Phi(V_F)}\right]^{-1/3}, \quad (2)$$

Table 1 compares the global properties of the original GH and new group catalogs. GH's higher mass-to-light and velocity dispersion values and low crossing times are caused by their much higher velocity link criterion. Most groups appear in both catalogs, although GH groups often contain extra members. The new catalog does better at resolving the complex Virgo / Coma I / Ursa Major / Coma Cluster areas into associated and infalling smaller groups. The group luminosity function is roughly a power law with a possible turn-over at low luminosity.

Table 1: Group Catalog Global Properties

Quantity	Value	GH Value
total no. groups	173	176
Fraction grouped	1146/2404=48%	1451/2390=61%
Fraction N=3/4/5 grps	.40/.21/.09	.33/.21/.10
$\langle M/L_B \rangle_{med}$	148	551
$\langle t_c H_o \rangle_{med}$	0.444	0.271
$\langle \sigma \rangle_{med}$	116 km s^{-1}	231 km s^{-1}
$\langle r_h \rangle_{med}$	0.48 Mpc	0.55 Mpc
$\langle r_p \rangle_{med}$	0.72 Mpc	---
$\langle \delta\rho/\rho \rangle_{med}$	119	---
$\langle V_{grp}-V_{brt} \rangle_{med}$	6 km s^{-1}	30 km s^{-1}
$\langle V_{grp}-V_{brt} \rangle_{avg}$	5 km s^{-1}	108 km s^{-1}

Contamination by interlopers has been significantly reduced. Figure 1 and Table 1 shows that the GH groups' brightest member tends to be at lower redshift than the group mean, implying comtamination by interlopers in the Hubble flow. The new groups' close V_{grp} - V_{brt} symmetry about zero implies minimal contamination.

References

deLapparent, V., Geller, M. J., and Huchra, J. 1989, ApJ **343**, 1

Faber, S. M., and Burstein 1988, in Large Scale Motions in the Universe, Proceedings of the Pontifical Academy of Sciences Study Week no. 27 (FB)

Geller, M., and Huchra, J. 1983, ApJS **52**, 61 (GH)

Huchra, J., Davis, M., Latham, D., and Tonry, J. 1983, ApJS **52**, 89

Nolthenius, R., and White, S. D. M. 1987, MNRAS **225**, 505 (NW)

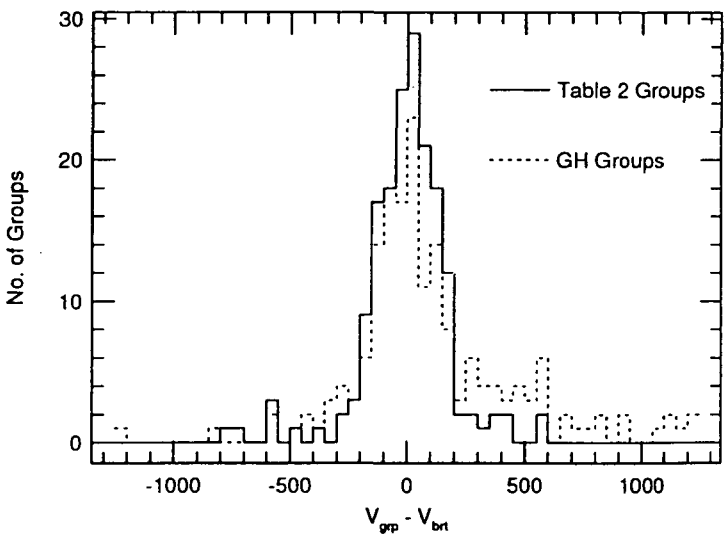

Figure 1. The distribution of residuals V_{grp}-V_{brt} for the GH and new groups. The GH catalog's excess of positive V_{grp}-V_{brt} groups implies significant interloper contamination compared to the new groups, whose distribution is symmetric about zero.

WHAT DETERMINES THE MORPHOLOGICAL FRACTIONS IN CLUSTERS OF GALAXIES?

BRADLEY C. WHITMORE
Space Telescope Science Institute
3700 San Martin Dr., Baltimore, MD 21218

A reexamination of Dressler's (1980) sample of nearly 6000 galaxies in 55 clusters shows that the morphology-clustercentric radius relation is more fundamental than the morphology-local density relation. This conclusion is supported by improved correlations when the projected clustercentric radius is used as the independent parameter, and by a comparison of galaxies with the same normalized clustercentric radii but different values of the projected local density (Figure 1).

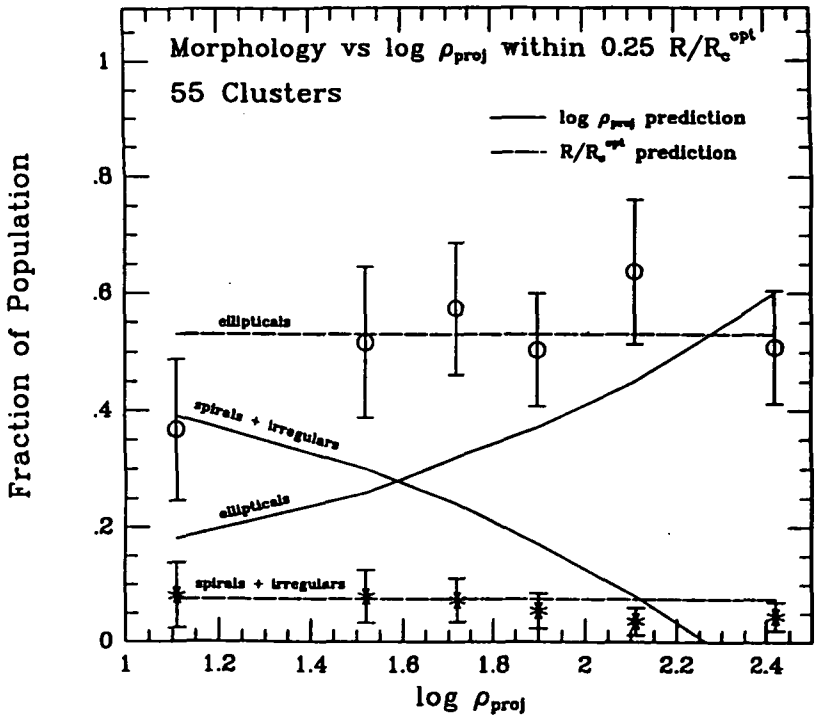

Figure 1 - The morphology-density relation for the galaxies within 0.25 R/R_c^{opt} of the cluster centers (where R_c^{opt} is the radius where the cumulative density falls below 20 galaxies Mpc^{-2}). The solid lines are the predictions for the morphology-density relation; the dashed lines are the predictions for the morphology-radius relation. Only the ellipticals and the spiral + irregular galaxies are shown for clarity. The data clearly favor the morphology-radius relation.

Figure 2 shows that the elliptical fraction in the outer regions of clusters is relatively constant for all types of clusters, with a slight rise from about 10% in the outermost regions to about 16% at R = 0.5 Mpc. For smaller radii, the elliptical fraction rises rapidly, reaching values of 60 - 70 % near the center of the cluster. The S0 fraction rises moderately as the center is approached, and then falls sharply within about 0.2 Mpc of the center. The spiral fraction falls moderately as the clustercentric radius decreases. The spiral fraction is essentially zero at the cluster center, even though spirals dominate everywhere else in the universe.

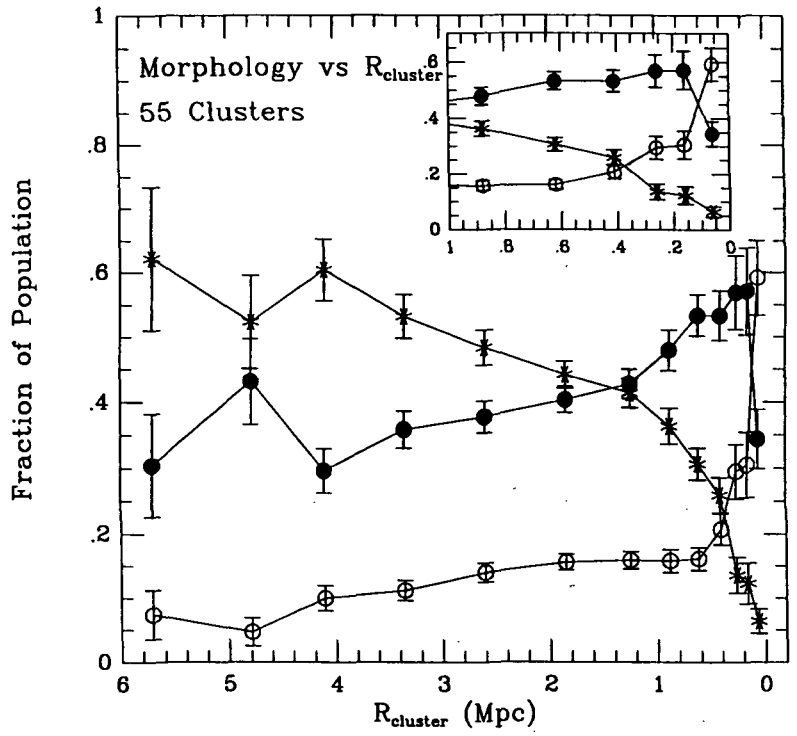

Figure 2 - The morphology-clustercentric radius relation for Dressler's (1980) 55 clusters.

The morphology-radius relation, when normalized by a characteristic cluster radius, R_c^{opt}, does not vary as a function of the number density within 0.5 Mpc, the x-ray luminosity, or the velocity dispersion of the cluster. This surprising result means that only one parameter is needed to determine the morphological fractions in clusters, namely R/R_c^{opt}.

These results indicate that some property of the cluster center plays the key role in determining the morphological fractions in clusters, and suggests the possibility that a destructive mechanism is controling the morphological fractions rather than a formation mechanism. Based on these results, we have developed the following simple model. The three basic assumptions are: 1) the intrinsic morphological mix of galaxies is E/S0+S+I = 10/90 %, 2) elliptical galaxies form first, followed by the cluster collapse, S0 galaxies, and finally, spiral and irregular galaxies, 3) during the cluster collapse, galaxies which are still protogalactic clouds of gas are destroyed, and the gas from these failed galaxies forms most of the intracluster medium. This simple model can explain a wide range of observations, and suggests that roughly half of the intracluster gas resulted from "failed" galaxies.

I would like to thank Diane Gilmore (STScI) and Christine Jones (CfA) who collaborated on various aspects of this project. Further details are available in Whitmore and Gilmore (1991) and Whitmore, Gilmore, and Jones (1992).

Dressler, A. 1980, *Ap. J.*, **236**, 351.
Whitmore, B. C. and Gilmore, D. 1991, *Ap. J.*, **367**, 64.
Whitmore, B. C., Gilmore, D., and Jones, C. 1992, in preparation.

ENVIRONMENTAL INFLUENCES ON GALAXY EVOLUTION

Stephen E. Zepf, *University of Durham*

and

Brad Whitmore, *Space Telescope Science Institute*

Abstract

We investigate the role of mergers and interactions in the evolution of galaxies by studying galaxies in compact groups. Compact groups of galaxies have high spatial densities and low velocity dispersions making these regions ideal laboratories in which to study the effect of interactions and mergers. Based on a detailed spectroscopic and multi-color imaging study, we find that both the isophotal shapes and the stellar kinematics indicate that many of the elliptical galaxies in compact groups have been affected by tidal interactions. At the same time however, we find that the only a few elliptical galaxies in compact groups have evidence for the young stellar populations that would be expected if they are the result of recent merger of two spiral galaxies. Therefore we conclude that tidal interactions affect galaxy properties at the current epoch, but the bulk of basic galaxy formation and transformation must have occurred at much higher redshift.

1. Colors and Recent Mergers

Elliptical galaxies recently created from the mergers of spiral galaxies are expected to have relatively blue colors because of their younger stellar populations. Therefore, if mergers of spiral galaxies are common in compact groups, a population of elliptical galaxies should exist in these groups with bluer than normal colors. In order to address this question, we undertook an extensive multicolor imaging survey of 76 early-type galaxies in compact groups (Zepf *et al.* 1991). The primary result of this survey is that three of the elliptical galaxies and one of the S0 galaxies have blue colors indicative of recent interactions and mergers.

A complementary study of the number of currently interacting systems, as determined from far-infrared colors, optical morphology, and emission-line rotation curves, finds that roughly 7% of the galaxies in compact groups are currently merging (Zepf 1992). Therefore, mergers are occurring in compact groups, but the timescale for the evolution of the groups through merging is significantly longer than the observed crossing time. Moreover, these results suggest caution in attributing all of the enhanced activity observed at higher redshifts to changes in environment, as not even in compact groups is the level of starbursting and

other phenomena often associated with interactions and mergers as high as that apparently observed in samples of galaxies at moderate redshifts (e.g. Broadhurst *et al.* 1988) .

2. Structure and Dynamics

Although dramatic mergers which result in a transformation of galaxy type are rare in compact groups, the elliptical galaxies appear to be affected by tidal interactions within the groups. These tidal interactions manifest themselves as differences in both the isophotal structure and the stellar kinematics of ellipticals in compact groups compared to ellipticals in other environments. The isophotal shapes of elliptical galaxies in compact groups differ from those in other environments in several ways. They are less likely to have perfectly elliptical isophotes and more likely to have isophotes with irregular shapes than galaxies in other regions. These two differences are consistent with the more frequent encounters expected in compact groups. The third difference is that elliptical galaxies with boxy isophotes are rarer in compact groups. This result argues against a connection between interactions and mergers and boxy isophotes.

The stellar kinematics of the elliptical galaxies in compact groups also appear to be different than those of elliptical galaxies in other regions. We have obtained velocity dispersions of 20 ellipticals in compact groups and find that these galaxies have systematically lower velocity dispersions than ellipticals in other environments (Zepf & Whitmore 1992). These low velocity dispersions cause the compact group ellipticals to lie off of the "fundamental plane" defined by other ellipticals. Although the sample size is unfortunately small, there are several factors which support the hypothesis that elliptical galaxies in compact groups have low velocity dispersions. The first is that distance errors are unlikely to be a factor since the compact group ellipticals have low velocity dispersions for their colors. The second factor is that the central velocity dispersions correlate with the isophotal shape, such that disky ellipticals have lower velocity dispersions than boxy ellipticals. This trend also suggests that the same physical phenomenon may be responsible for the differences in isophotal shape and the low velocity dispersions.

References

Broadhurst, T.J., Ellis, R.S., & Shanks, T. 1988, MNRAS, 235, 827

Zepf, S.E. 1992, ApJ, submitted

Zepf, S.E., Whitmore, B.C., & Levison, H.F. 1991, ApJ, 383, 524

Zepf, S.E., & Whitmore, B.C. 1991, ApJ, 383, 542

Zepf, S.E., & Whitmore, B.C. 1992, ApJ, in preparation

GLOBULAR CLUSTER SYSTEMS AS CLUES TO GALAXY EVOLUTION

Stephen E. Zepf, *University of Durham*

and

Keith M. Ashman, *CITA*

Abstract

We investigate the properties of systems of globular clusters in light of the hypothesis that galaxy mergers play a major role in galaxy evolution. In a previous paper we presented a model in which the formation of globular clusters occurs during galaxy interactions and mergers. We discussed several predictions of the model, including the existence of young globular clusters in currently merging galaxies and the presence of two or more metallicity peaks in the globular cluster systems of normal elliptical galaxies. Here we present recent observational evidence which supports both of these predictions and suggests that mergers may have a significant influence on the formation and evolution of galaxies and their globular clusters.

1. Introduction

The great age of many globular clusters and their presence around nearly all galaxies make them excellent fossils through which the process of galaxy evolution can be traced. If galaxy mergers play a major role in galaxy evolution, then the properties of globular cluster systems must reflect these processes. In particular, if elliptical galaxies are formed by mergers of spiral galaxies, then the formation of new globular clusters during mergers is necessary to explain the higher number of clusters around ellipticals relative to spirals of the same luminosity. Ashman & Zepf (1992) examined the implications of such a model and found that many well-known properties of globular clusters are consistent with such a hypothesis. For example, a thick disk population of globular clusters similar to that present in our Galaxy and M31 is predicted by this model. Moreover, the globular clusters are required to be metal-poor compared to the underlying light of an elliptical galaxy as is observed. Ashman & Zepf (1992) also made several new predictions. Among these were that young globular clusters should be found in mergers of gas-rich galaxies, and that there should be at least two peaks in the metallicity distribution of the globular cluster systems of elliptical galaxies.

2. Young Clusters in Merging Galaxies

The most obvious prediction of a model in which globular cluster formation occurs during mergers and interactions is that young globular clusters should be found in galaxies

which are now experiencing this phenomenon. Until recently, this prediction seemed at odds with the belief that all globulars are old (although there has been an ongoing debate about the nature of the young clusters in the LMC and the "populous" blue clusters discussed by Kennicutt & Chu 1988). However, observational evidence is now mounting which suggests that some globular clusters are young. For example, Zepf & Ashman (1992) suggest that in NGC 5128 several of the very blue globular clusters near the center of the galaxy may be young rather than extremely metal poor clusters. Another example is the observation by Lutz (1991) of compact blue objects in the ongoing merger NGC 3597. The properties of these objects are consistent with those expected of young globular clusters, although the spatial resolution of the ground-based data is not quite sufficient to show that these clusters are as compact as galactic globular clusters. Recently, Holtzman *et al.* (1992) have reported the detection of young globular clusters in NGC 1275, which they interpret as being the result of a recent merger. Further HST observations of merging galaxies are likely to be very fruitful.

3. Metallicity Distributions of Globular Cluster Systems of Elliptical Galaxies

One of the interesting results to come out of recent surveys of the globular cluster systems of elliptical galaxies is that the metallicity distributions are not smooth and uniform but appear to have two or sometimes three peaks (Zepf & Ashman 1992). These distributions provide dramatic support for our models which predict that the metallicity distribution of the globular cluster system of an elliptical galaxy should have at least two peaks. These peaks correspond to the two populations of globular clusters: the low metallicity clusters formed during the collapse of the progenitor disk galaxies, and the higher metallicity clusters which form during the merger. More generally, the metallicity distribution of globular clusters around normal ellipticals is a powerful tool for understanding the evolution of these galaxies. In particular, the multi-peak prediction of the merger scenario contrasts sharply with the rather uniform and single-peaked distribution expected if elliptical galaxies (and their globular clusters) have a single formation phase.

References

Ashman, K.M, & Zepf, S.E. 1992, ApJ, 384, 50

Holtzman, J.A. *et al.* 1992, AJ, 103, 691

Kennicutt, R.C., & Chu, Y.-H. 1988, AJ, 95, 720

Lutz, D. 1991, A&A, 245, 31

Zepf, S.E., & Ashman, K.M 1992, ApJ, in preparation

Globular Cluster Formation in Merging Galaxies?

D. Lutz
MPI für extraterrestrische Physik
Giessenbachstraße
D-W8046 Garching
Germany

The properties of a population of luminous blue clusters in the merging galaxy NGC 3597 are discussed, and the observability of the signature of such a population in later evolutionary stages of a merger is assessed.

NGC 3597 is an advanced merger which has already developed into an elliptical-like object with a de Vaucouleurs brightness distribution, but intense star formation is continuing in the central 4 kpc. A population of unresolved blue objects that are concentrated towards the central region is identified as clusters belonging to NGC 3597.

The luminosities and colours of these luminous blue clusters in NGC 3597 are those expected for young luminous globular clusters. After evolution to an age of 10 Gyr, they will resemble the most luminous globulars of the Milky Way (Lutz 1991).

New Hα narrowband data do not show line emission from the clusters, confirming that the clusters already have passed the stage of active star formation (Fig. 1). Although the upper limit of about 100 pc for the size of the clusters is insufficient to distinguish unambiguously between compact globulars and more diffuse associations, the observations indicate that the specific globular cluster frequency of galaxies is not conserved during merging. The more recent observation of similar young luminous clusters in NGC 1275 (Holtzman et al. 1992) strengthens the argument for significant late additions of new clusters to the globular cluster systems of some galaxies, which has also been discussed by Ashman and Zepf (1992).

Simulated colour–magnitude diagrams for the globular cluster system of a merger are used to assess the further evolution of NGC 3597–like cluster sytems. The signature of a mixture of old globulars and globulars newly formed during merging is observationally evident only in early stages. Taking foreground stars, background galaxies and observational errors into account, the colour–magnitude diagram of such a mixed globular cluster system will be indistinguishable from that of ordinary ellipticals at the time when other indicators of the merger origin (tidal tails) have dispersed (Fig. 2). The situation is complicated further by partial compensation of age and metallicity effects on the colurs of a mixed system.

References:

Ashman, K.M., Zepf, S.E., 1992, Astrophys. J. 384,50
Holtzman, J.A., et al., 1992, Astron. J. 103,691
Lutz, D., 1991, Astron. Astrophys. 245,31

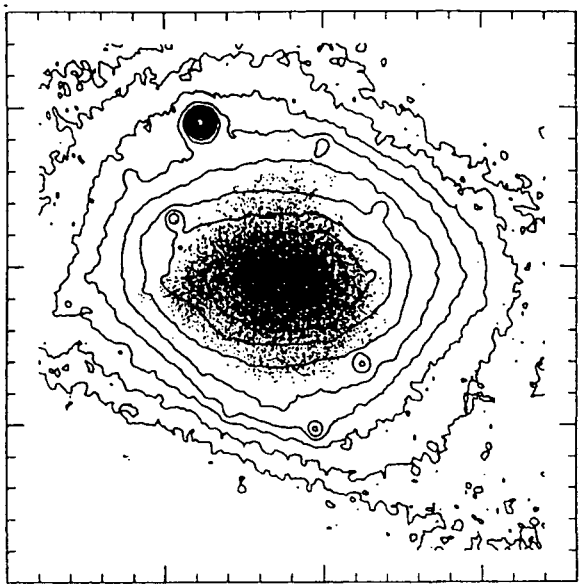

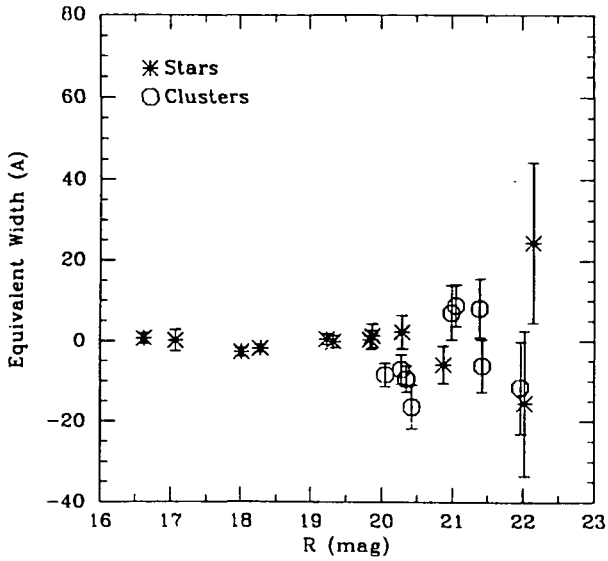

Fig. 1: Left: Continuum-subtracted Hα image of the central region of NGC 3597 (greyscale), superposed on a narrowband continuum image at a wavelength close to Hα (contours). The unresolved blue clusters seen in continuum light do not show up in Hα. The brightest unresolved object is presumably a foreground star. Right: Equivalent width of Hα+[N II] for the brightest clusters and foreground stars. Data are derived from DAOPHOT analyses in the light of the line and at two neighbouring continuum wavelengths, and are corrected for differences in continuum colour. The equivalent width in the clusters is certainly lower than 20Å, or the line even in absorption, implying that none of the clusters is still actively forming stars.

Fig. 2: Simulated colour-magnitude diagram for the globular cluster system of a merger that has been allowed to evolve for 5 Gyr. It is assumed that half of the clusters have been formed during the merging event, and now are on average 1 mag brighter and 0.1 mag bluer than the old clusters (mean B-V=0.7). No clear signature of the merging event can be seen, the reddening of the average colour from the bright end towards fainter magnitudes is marginal above the limit where errors and background contamination start to interfere.
Assumptions for this plot: Total number of clusters 2000, Virgo distance modulus, (excellent) limiting magnitudes B=26.5 and V=26. Different symbols denote "young" globulars (squares), "old" globulars (circles), foreground stars (asterisks) and unresolved background galaxies (crosses).

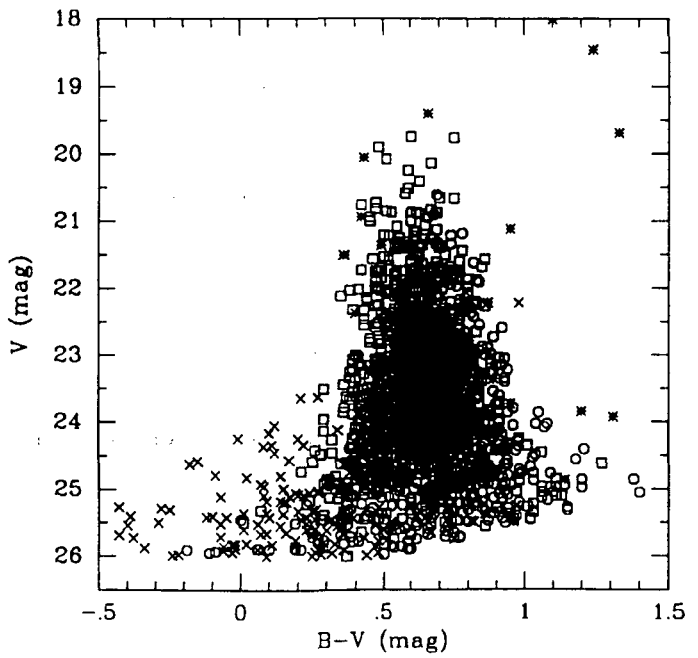

CLUSTER EVOLUTION AS A PROBE OF PRIMORDIAL DENSITY FLUCTUATIONS

J. RICHARD BOND & STEVEN T. MYERS
Canadian Institute for Theoretical Astrophysics

ABSTRACT. *Although COBE's detection of large angle microwave background anisotropies[1] fixes the amplitude of density fluctuations on length scales* $k^{-1} \sim (300 - 6000)\,h^{-1}$Mpc, *what is crucial for the level of large scale clustering is the amplitude of density fluctuations on scales* $(5 - 50)\,h^{-1}$Mpc. *The level of dynamical clustering is usually parameterized by the size of the mass fluctuations in* $8\,h^{-1}$Mpc *spheres,* σ_8. *For the cold dark matter model, COBE gives* $\sigma_8 \sim 1$, *while models with extra large scale power give* $\sigma_8 \sim 1/2$. *The most massive clusters of galaxies* ($\gtrsim 10^{15}\,M_\odot$) *form from rare 'peak patches' found in the initial mass density distribution. Their abundance as a function of redshift is a sensitive probe of the wavenumber band* $k^{-1} \sim (3 - 8)\,h^{-1}$Mpc, *hence of* σ_8, *and so cluster evolution can discriminate among models allowed by the COBE results. We use our Hierarchical Peaks Method[2], which accurately reproduces the results of* P^3M *N-body simulations, to calculate the evolution of cluster X-ray flux counts, luminosity and temperature functions as a function of* σ_8 *for CDM models and those with more large scale power. We find that the EMSS and Edge et al. cluster samples support* σ_8 *in the range from* $\sim 0.6 - 0.9$, *and that models with more large scale power (and hence flatter fluctuation spectra in the cluster regime) fit the X-ray bright end better.*

It has long been recognized that the abundances of clusters can be used to constrain the 'biasing factor' $1/\sigma_8$. However, it was unclear how accurate the theoretical estimates of the mass functions of such rare events were. Although the Press-Schechter (PS) mass function for Gaussian hierarchical theories is widely used for estimating the distribution of cluster properties and accords reasonably well with N-body mass functions,[2,4] it has little theoretical support[4] and gives no information on spatial fluctuations. Hydrodynamical studies probe 3D volumes too small to use for a complete statistical description. Pure N-body calculations can now approach the large volumes required for a useful cluster sample at the expense of resolution. We find the peaks associated with a hierarchy of filter scales and calculate the virial masses, velocities v_{3D} and gas temperatures T_X using the local properties of the density field about the peaks. Subclustering within peaks, the influence of tidal forces on peak collapses, the merging of peaks and the motion of the surviving peaks using the Zeldovich approximation are included. We also have an accurate analytic counterpart to the Monte Carlo method. We have calibrated our peaks catalogues with those constructed from N-body simulations of the CDM model[3] and find excellent agreement. An important issue for PS and peak approaches is the relationship between the mass, T_X and the dark matter velocity dispersion v_{3D}. We have found that N-body velocity dispersions are about 16% higher than the N-body binding energy values, which would be appropriate if isolated virial equilibrium prevails in the clusters. High resolution hydrodynamical calculations are required to settle which is the appropriate T_X estimator to use. A further uncertainty arises in our estimates of cluster luminosity L_X and flux S_X through their (squared) dependence upon the gas density, which in turn depends upon the primordial density of baryons and the fraction of them which remain as hot intracluster gas. For the graphs we have taken $\Omega_B = 0.05$, and the X-ray core radius to be $0.15\,h^{-1}$Mpc.

We have compared our results for CDM-like models with the available X-Ray data[5,6] and find that the luminosities and fluxes support a fluctuation amplitude σ_8 between 0.7 and 0.9 using the binding energy measure for T_X, while slightly smaller values are indicated if we use the N-body velocity dispersions. The key feature, generic to a wide class of extra power models, is the flattening of the power law index of the density fluctuations on the wavelengths that cluster counts probe, which gives more clusters with large values of L_X than the CDM slope gives and fits the data reasonably well for σ_8 in the 0.6-0.9 range. However, matching such models to COBE[1,7] gives $\sigma_8 \lesssim 0.5$, which would give too few clusters at moderate redshifts to match the Gioia *et al.* data. We have also made predictions for the ROSAT and microwave background sky for these models.[2] The non-standard models [C–F] were chosen to reproduce the large scale galaxy clustering data with linear biasing (which the CDM model does not). Model [F] is an example of a class of models with extra large-scale power, parameterised by the factor Γ,[7] which ranges from 0.15–0.3 to explain the large scale clustering, to 0.5 for standard CDM. Models with $\Lambda \neq 0$ can give $\Gamma \sim 0.2$, though for this paper we assume a flat cosmology. If the EMSS data at $z = 0.2$–0.4 is used, no CDM-like models in the $\Omega = 1$ cosmology are viable. Our conclusions are strongly dependent upon the details of the gas dynamics within the clusters, but it is highly unlikely that $b_8 > 1.5$ models can survive. Flat cosmologies with $\Lambda \neq 0$ provide good fits to the galaxy clustering data for $\Omega_\Lambda \approx 0.75$ (h=0.8), and COBE then gives $\sigma_8 \sim 1$.

References

1. Smoot, G. *et al.* (1992), Wright, E. *et al.* (1992) *Ap. J. Lett.*, in press
2. Bond, J.R. and Myers, S. (1991), in *Trends in Astroparticle Physics*, ed. D. Cline and R. Peccei (Singapore: World Scientific).
3. Couchman, H.C. (1991), *Ap.J.*, **368**, L23.
4. Bond, J.R., Cole, S., Efstathiou, G. and Kaiser, N. (1991), *Ap.J.*, **379**, 440.
5. Edge, A.C., Stewart, G.C., Fabian, A.C. and Arnaud, K.A. (1990), *M.N.R.A.S.*, **245**, 559.
6. Gioia, I.M. *et al.* (1990), *Ap. J.*, **356**, L35.
7. Efstathiou, G., Bond, J.R. and White, S.D.M. (1992), *M.N.R.A.S*, in press.

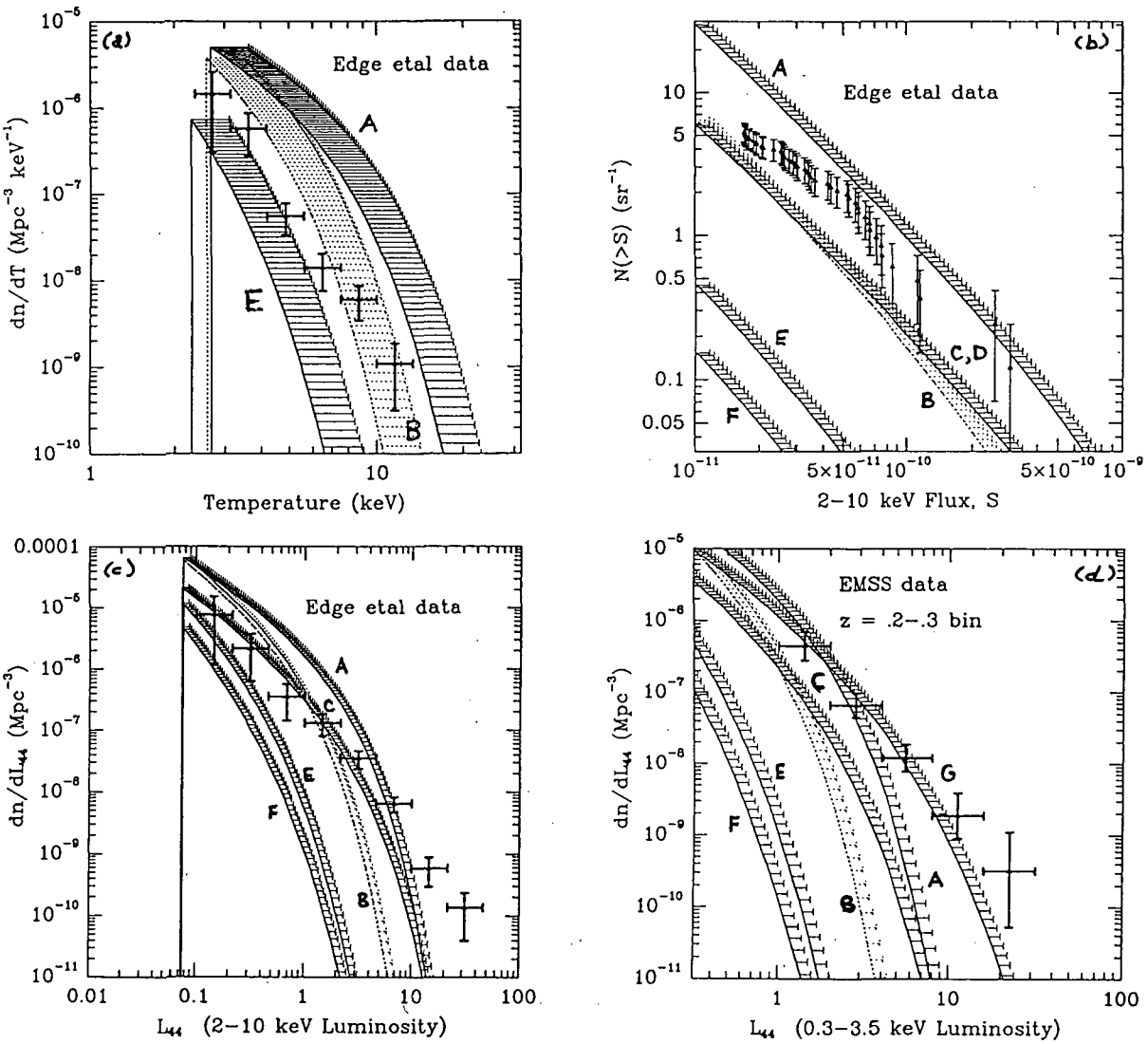

Figure 1. *Comparison of the Peaks analytic predictions with X-Ray data for Edge et al. and EMSS. The models are: $b_8 = 1$ [A] and $b_8 = 1.4$ [B] standard CDM models, $b_8 = 1.4$ HDM-CDM hybrid models ($\Omega_\nu = 0.3, \Omega_{cdm} = 0.7, m_\nu = 7\,eV$) [C] and ($\Omega_\nu = 0.13, \Omega_{cdm} = 0.87, m_\nu = 3\,eV$) [D], a $b_8 = 2.0$ CDM model with non-Zeldovich spectral index $n = 0.6$ [E], and an extra-power model ($b_8 = 2.2, \Gamma = 0.2$) [F]. For the peaks model curves, the spread represents the 16% uncertainty assumed for the velocity dispersion only. Panels (a–c) show the X-ray temperature, flux counts, and 2–10 keV luminosity function for the Edge data. The best-fit model appears to be the $b = 1.4$ hot-cold hybrid [C], though all models show a deficiency on the high end. In panel (d), the models are compared with the EMSS $z = 0.2$–0.3 luminosity function (0.3–3.5 keV). All our models fall short of reproducing the flat luminosity function in the EMSS data. To demonstrate what is required to obtain agreement, we have included another extra-power model ($b_8 = 1, \Gamma = 0.1$) [G], which does NOT match the COBE or low-redshift X-Ray data. High bias models fail miserably on all counts.*

Clustering of Very Luminous Infrared Galaxies and their Environment

Yu Gao
Astronomy Program, SUNY at Stony Brook

The IRAS survey reveals a class of ultraluminous infrared (IR) galaxies (ULIRGs) with IR luminosities comparable to the bolometric luminosities of quasars. The nature, origin, and evolution of ULIRGs are attracting more and more attention recently (cf. Sanders et al 1988, hereafter S88; Solomon et al 1992a; 1992b; Kormendy & Sanders 1992). Since galaxy morphology is certainly a function of environment (e.g. Postman & Geller 1984), morphological observations show that ULIRGs are interacting/merging galaxies (S88; Melnick & Mirabel 1990), and some ULIRGs might be the dust-enshrouded quasars (S88) or giant ellipticals (Solomon et al 1992a; Kormendy & Sanders 1992), the study of ULIRGs environment and large scale clustering effects should be worthwhile.

ULIRGs ($L_{IR} \geq 10^{12}\ L_{\odot}$; $H_0 = 75\ km/s/Mpc$ and $q_0 = 0$) and very luminous IR galaxies (VLIRGs; $L_{IR} \geq 2 \times 10^{11}\ L_{\odot}$) have been selected from the 2Jy IRAS redshift survey, which is complete to a redshift of 10,000 km/s and might be complete to a redshift of 30,000 km/s at high galactic latitudes (Strauss et al 1990; Yahil et al 1991). Meanwhile, a catalog of IRAS groups of galaxies has been constructed using a percolation-like algorithm. Therefore, whether ULIRGs and/or VLIRGs have a group environment can be checked immediately. Surprisingly, most VLIRGs ($\sim 90\%$) are not IRAS group members, in marked contrast to the fact that $\sim 50\%$ of IRAS galaxies are in groups of galaxies. Also, only a few percent of group member galaxies are VLIRGs and no group member galaxies are ULIRGs (see Figure 1), which is extremely different from the situation that $\sim 20\%$ of field IRAS galaxies are VLIRGs and a few percent of field IRAS galaxies are ULIRGs.

The two-point spatial correlation functions have been estimated for the some *volume-limited* subsamples of luminous IR galaxies and U/VLIRGs. Preliminary results show that there is no luminosity segregation in the correlation functions for IRAS galaxies if $L_{IR} \leq 10^{11}\ L_{\odot}$, which should be consistent with the conclusions of Davis et al (1988). However, for U/VLIRGs, the more IR-luminous they are, the stronger correlations they have and ULIRGs have the strongest correlations which is comparable with that of poor clusters of galaxies (Figure 2).

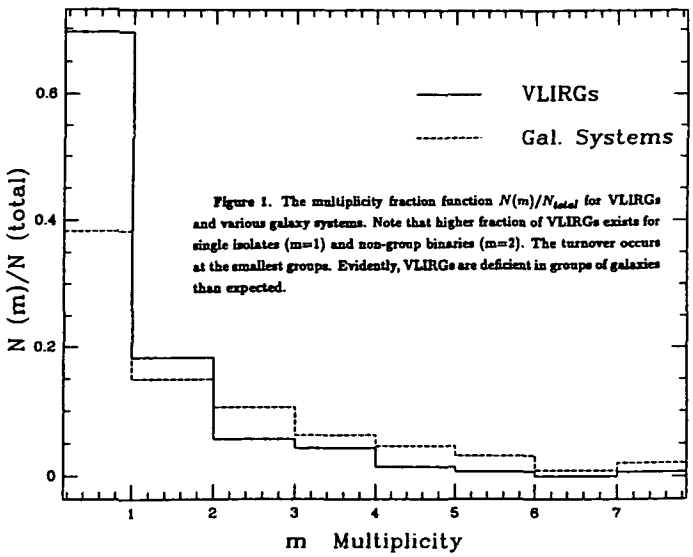

Figure 1. The multiplicity fraction function $N(m)/N_{total}$ for VLIRGs and various galaxy systems. Note that higher fraction of VLIRGs exists for single isolates (m=1) and non-group binaries (m=2). The turnover occurs at the smallest groups. Evidently, VLIRGs are deficient in groups of galaxies than expected.

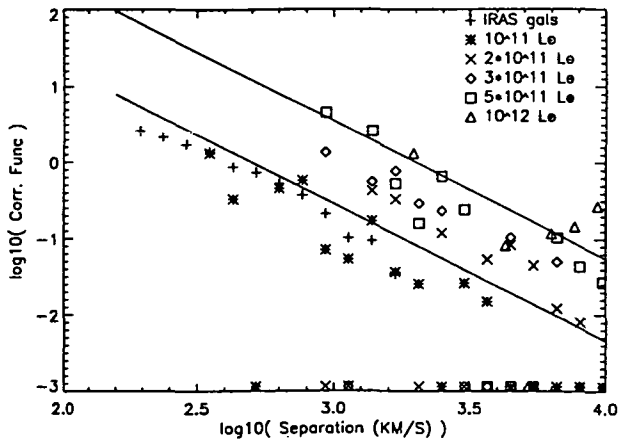

Figure 2. The correlation functions for various subsamples of IRAS galaxies as indicated by their IR luminosities. The lower and upper straight lines are the correlation functions for optical galaxies and clusters of galaxies respectively: $\xi_{gg}(r) = (\frac{r}{5000\,KM/S})^{-1.8}$; $\xi_{cc}(r) = (\frac{r}{5000\,KM/S})^{-1.8}$ (cf. Bahcall 1988).

Our correlation results have also been checked by selecting various subsamples within a redshift of 30,000 km/s. We can select subsamples with the same IR luminosity constraints

to check the luminosity dependence and compare the results for all the five *volume-limited* subsamples. The results are essentially the same and the conclusion of stronger clustering of more luminous VLIRGS remains unchanged.

U/VLIRGs will be the dominant population in the local universe among other objects with bolometric luminosity $L_{bol} \geq 3 \times 10^{11}\ L_{\odot}$. However, most of them in nearby universe are not members of clusters or groups of galaxies. Thus, the distribution of VLIRGs is avoiding the concentrations of galaxies, yet show stronger clustering effects than less luminous IRAS galaxies. Strong clustering of VLIRGs might imply their preferential location in groups as Bahcall & Chokshi (1991; 1992) suggest that the origin of the observed correlations of quasars and radio-galaxies, which is intermediate in strength between that of galaxies and of rich clusters of galaxies, is the preferential locations of quasars in small groups and of radio-galaxies in groups of galaxies of intermediate richness. According to this picture, having the same correlation amplitudes as that of groups or poor clusters of galaxies, the U/VLIRGs should have the corresponding group or cluster environments. However, most U/VLIRGs are merging galaxies and we have shown that most of them are not the members of galaxy groups now in the nearby universe. This apparent contradiction might indicate that U/VLIRGs may be the remnants of the evolution of groups of galaxies due to their advanced merging, thus losing their present properties as groups of galaxies but still have stronger correlations in spatial distribution as that of groups or clusters of galaxies. Some cosmological implications on the origin and evolution of ULIRGs and groups of galaxies might be implied.

In conclusion, there is an over population of isolated VLIRGs in the nearby universe. Most VLIRGs (especially the most luminous VLIRGs) are not members of groups of galaxies (only $\sim 10\%$ VLIRGs are in groups, whereas $\sim 50\%$ IRAS galaxies are group members) and they are deficient at small redshift of $\sim$ 5,000 kms^{-1}. However, U/VLIRGs show stronger correlation than all IRAS galaxies. The more luminous the VLIRGs are, the stronger clustering they have. The correlation strength of ULIRGs is comparable to that of poor clusters of galaxies. The U/VLIRGs' properties of stronger correlation and deficiency in galaxy groups might suggest they are probably the remnants of the evolution of groups of galaxies due to the advanced merging of member galaxies.

ACKNOWLEDGEMENTS

I thank Phil Solomon for support and suggestions. Amos Yahil is also thanked for his suggestions. I am very grateful to Michael Strauss for sending me the 2Jy IRAS redshift catalog prior to publication. I appreciate the helpful discussions with Yi-peng Jing. Finally, I wish to thank the organizers of this summer school for partial support.

REFERENCES

Bahcall, N.A. & Chokshi, A. 1991, Ap. J. Lett., **380**, L9.

Bahcall, N.A. & Chokshi, A. 1992, Ap. J. Lett., **385**, L33.

Davis, M., Meiksin, A., Strauss, M.A., da Costa, L.N., & Yahil, A. 1988, Ap. J. Lett., **333**, L9.

Kormendy, J. & Sanders, D.B. 1992, Ap. J. Lett., **390**, L53.

Melnick, J. & Mirabel, I.F. 1990, Astron. Astrophys., **231**, L19.

Postman, M. & Geller, M. 1984, Ap. J., **281**, 95.

Sanders, D.B., Soifer, B.T., Elias, J.H., Madore, B.F., Matthews, K., Neugebauer, G., Scoville, N.Z. 1988, Ap. J., **325**, 74. (S88)

Solomon, P.M., Downes, D. & Radford, S.J.E. 1992a, Ap. J. Lett., **387**, L53.

Solomon, P.M., Radford, S.J.E. & Downes, D. 1992b, Nature, in press.

Strauss, M.A., Davis, M., Yahil, A., & Huchra, J.P. 1990, Ap. J., **361**, 49.

Yahil, A., Strauss, M.A., Davis, M., & Huchra, J.P. 1991, Ap. J., **372**, 380.

Galaxy Tracers in N-body Simulations

F J Summers[1,4], August E. Evrard[2], and Marc Davis[1,3,4,5]

N-body simulations of large scale structure have sometimes been referred to as 'experimental cosmology'. Indeed, at the heart of these efforts is the desire to provide stringent tests of various theories of structure development. Much progress has been made in determining which theories produce structure similar to what is observed, but a major obstacle to this progress is the identification of where galaxies would reside in a dark matter only simulation. Various ideas for biasing the galaxies relative to the dark matter have been proposed and these schemes provide a large amount of flexibility when comparing simulation and observation. Developing a well defined, reliable galaxy tracer method that would cut through the veil of biasing is an important, but complex problem.

Collisionless simulations, which follow only the dark matter component interacting via gravity, are successful in describing large scale structure, but do not adequately track the clustering of galaxies. The unknown correlation between the dark matter and the observed luminous galaxies is especially troublesome on smaller scales, where physics other than gravity is known to have strong effects. A more direct problem for identifying galaxies is that a collisionless gas is very efficient at erasing substructure when merging. In low density regions, one may make a one to one correspondence between dark matter halos and galaxies. However, in clustered regions, standard grouping algorithms pick out only the common cluster halo and can not identify the individual galaxies within the cluster. More sophisticated techniques or analysis are required.

The straightforward way to follow the luminous matter is to add a baryonic species to the simulation. Using the method of smoothed particle hydrodynamics, we have modelled the formation of a compact group of galaxies with sufficient resolution to trace galaxies. Radiative cooling allows the baryons to dissipate their thermal energy and collapse to overdensities characteristic of real galaxies. With their cross section greatly reduced, these galaxy tracers remain distinct during cluster formation while their dark matter halos merge. In addition, the number density, the mass distribution function, and even the morphology of these objects are similar to those of observed galaxies. A viable population of galaxy tracers can be unambiguously defined.

SPH simulations, however, carry a hefty price tag. Many questions remain about how best to implement the smoothing procedures. One must also develop and refine algorithms to model unresolved or unknown physical processes such as viscosity or star formation and associated feedback. SPH computing requirements stretch both memory and CPU to the

[1] Department of Astronomy, University of California at Berkeley
[2] Department of Physics, University of Michigan
[3] Department of Physics, University of California at Berkeley
[4] Center for Particle Astrophysics
[5] Theoretical Astrophysics Center

limits on even the biggest supercomputers. In addition, there is evidence that the mass resolution necessary to achieve sufficient cooling and form galaxy tracers may limit current simulations to box sizes too small to make adequate measurements of large scale structure. Simpler methods for tracing galaxies are desirable and these ideas can be checked for consistency with the SPH results.

One method we have investigated is to try to follow galaxy tracers through the merging process in a collisionless only simulation. The idea is that one can tag individual halos before merging and then later examine these particles within the cluster halo to identify galaxy tracers. Utilizing a collisionless only simulation with the same initial conditions as our collisionless plus SPH model, two algorithms have been studied. Neither method finds enough substructure within the cluster halo, especially in the central region. In fact, most of the groups of particles identified are not gravitationally bound. These results disagree with the findings of Carlberg, Couchman, and Thomas chiefly because the baryons in their SPH simulation, due to insufficient mass resolution, did not cool and collapse to the very high overdensities we observe. Our results support the notion that collisionless galaxy tracer algorithms will always fail due to the fact that groups of collisionless particles lack a dissipational mechanism for maintaining spatial and kinetic coherence during merging.

Methods of tracing galaxies should be devised, extended, and examined carefully. A star formation algorithm is being developed and tested for inclusion in the SPH code. Perhaps a suitable collisionless tracer mechanism can be found, though the current results are not encouraging. Collisionless n-body codes have been successfully coupled to Eulerian (grid based) hydrodynamics codes, but fixed grid hydrodynamics simulations do not yet have the dynamic range necessary to resolve galaxies within clusters and there is little *a priori* knowledge of where to place a refined grid. Having the SPH results in hand, one may be able to modify collisionless codes to mimic the cooling processes via an expert system. Such techniques may yield good results in the future. For the present, one concludes that SPH methods, though costly, are required to reliably trace galaxies in simulations.

N93-26733

The Large-Scale Morphology of IRAS Galaxies

ARIF BABUL[1], GLENN D. STARKMAN[1], & MICHAEL A. STRAUSS[2]
[1] *Canadian Institute for Theoretical Astrophysics, Toronto, Canada.*
[2] *Institute for Advanced Study, Princeton, NJ.*

Introduction: At present, visual inspection is the only method for comparing the large-scale morphologies in the distribution of galaxies to those in model universes generated by N-body simulations. To remedy the situation, we have developed a set of three structure functions (S_1, S_2, S_3) that quantify the degree of large-scale prolateness, oblateness and sphericity/uniformity of a 3-D particle distribution (*c.f.* Babul & Starkman 1992, preprint) and have applied them to a volume-limited ($\leq 4000\,\mathrm{km\,s^{-1}}$) sample of 699 IRAS galaxies with $f_{60} > 1.2$ Jy (Fisher 1992, Ph.D. Thesis, U.C. Berkeley).

To determine the structure functions, we randomly select 500 galaxies as origins of spherical windows of radius R_w, locate the centroid of the galaxies in the window (assuming all galaxies have equal mass) and then, compute the principal moments of inertia (I_1, I_2, I_3) about the centroid. Each S_i is a function of I_2/I_1 and I_3/I_1. S_1, S_2 and S_3 tend to unity for highly prolate, oblate and uniform distributions, respectively and tend to zero otherwise. The resulting 500 values of S_i at each scale R_w are used to construct a histogram.

IRAS Sample: In analyzing the IRAS sample, we restrict ourselves to windows with radius $1100\,\mathrm{km\,s^{-1}} \leq R_w \leq 1700\,\mathrm{km\,s^{-1}}$. Smaller windows contain too few galaxies while larger windows are rejected due to the scarcity of window origins for which the window lies entirely within the sample volume. A set of histograms for S_1, S_2 and S_3 in windows of radius $1300\,\mathrm{km\,s^{-1}}$ is shown in panel 1 of Figure 1. The structures in the IRAS galaxy distribution do not appear to be highly prolate or oblate.

Model Distributions: We compare the IRAS results to analyses of eight galaxy distributions discussed by Weinberg & Cole (1991, preprint). The eight distributions correspond to particles identified as galaxies according to biased and unbiased schemes from simulations of an $\Omega = 1$ universe characterized by the initial 1-point probability distribution, $P(\delta)$, which is either Gaussian, or has a long tail of positive fluctuations (skew-positive), a long tail of negative density contrasts (skew-negative), or both negative and positive tails (broad). The non-Gaussian initial conditions were generated by a local transformation of the Gaussian field with power spectrum $P(k) \propto k^{-1}$. In order to ensure that S_i for the models are comparable to those for the IRAS galaxies, we analyze four subsets (spheres of radius $4000\,\mathrm{km\,s^{-1}}$) of each of the simulation volumes, each containing 400—1000 galaxies. Placing the observer at the centre of the spheres, we transform the simulations from real space to redshift space. For each of the four volumes, we compute the S_i histograms at $R_w = 1100$, 1300, 1500, and $1700\,\mathrm{km\,s^{-1}}$. For each S_i, the four histograms at a given R_w are then averaged to obtain the mean "model" histogram. Panels 2 and 3 of Figure 1 show the mean histograms for the unbiased Gaussian and the unbiased skew-positive models ($R_w = 1300\,\mathrm{km\,s^{-1}}$).

Comparison: As a prelude to comparing the IRAS histograms to those for the models, we interpret the mean model histograms (for each S_i and at each R_w) as the underlying probability distributions and compute the likelihood (using the multinomial likelihood function) of obtaining the corresponding IRAS histogram. We also compute the likelihood for obtaining the histograms for each of the four spherical sub-volumes from the mean. The results for the two least unlikely models (unbiased skew-positive and unbiased Gaussian) are presented in Figure 2. The skew-positive model is preferred; its likelihood is the largest of any of the models and it is the only one for which the IRAS results are comparable to the likelihoods of individual volumes for all three S_i and at all R_w. The results of our likelihood analysis are evident in the histograms themselves. For example, in the Gaussian model, the histogram for S_1 ($R_w = 1300\,\mathrm{km\,s^{-1}}$) has a tail extending to $S_1 = 0.3$ while both the skew-positive and IRAS histograms (compare panels in Figure 1) are narrower. The differences between the S_3 histograms are even more pronounced, with the Gaussian histogram being noticeably broader than either the IRAS or the skew-positive. The histograms for the latter two are similar. As an aside, we note that four out of five colleagues, when asked to visually compare unlabelled particle plots of the model galaxies to those for IRAS galaxies, also selected the unbiased skew-positive model as the most likely match.

Conclusions A preliminary comparison of the large-scale morphology of IRAS galaxies with those present in the eight simulated galaxy distribution suggests that the distribution of IRAS galaxies is most like the distribution of galaxies in an unbiased, evolved skew-positive model. This result suggests that either the initial conditions that gave rise to the IRAS galaxies are non-Gaussian or the nature of biasing associated with their formation gives such an impression.

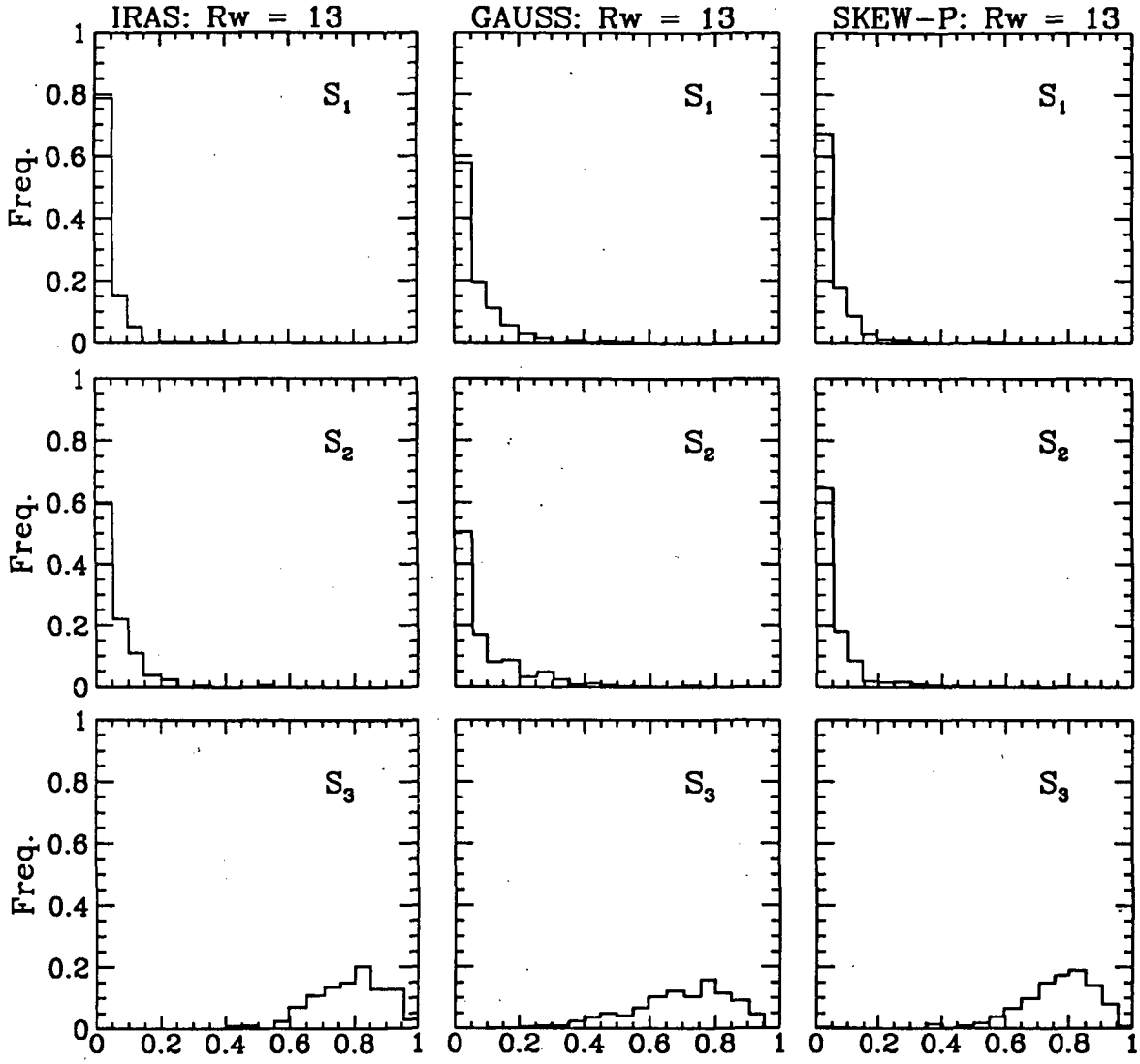

Fig. 1. Histograms for the normalized frequency distribution of S_i for IRAS galaxies (left column of panels) as well as for the galaxy distribution (unbiased) from simulations with Gaussian (middle column) and positively skewed (right column) initial 1-point probability distribution, $P(\delta)$.

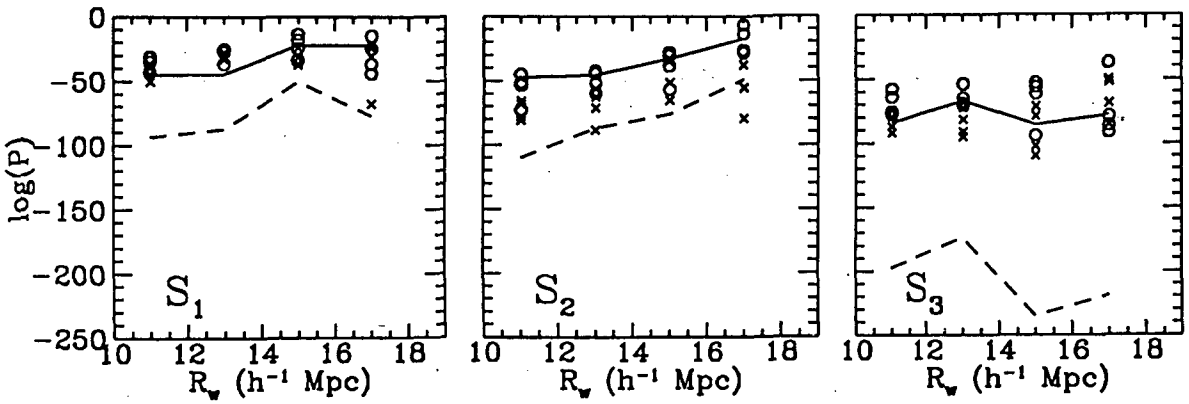

Fig. 2. The value of the likelihood function for obtaining the IRAS S_i histograms at R_w = 1100, 1300, 1500, and 1700 km s^{-1} from the histograms for the skew-positive model (solid line) and for the Gaussian model (dashed line). The points show to the likelihood of obtaining the histograms for the four sub-volumes for each model from the mean histogram. The open circles correspond to the skew-positive model and should be compared to the solid line; the crosses correspond to the Gaussian simulation and should be compared to the dashed line.

Subclustering in the Hierarchical Model of Galaxy Formation

Satoshi Yoshioka

Department of Physics, Tokyo University of Mercantile Marine
Etchujima, Koto, Tokyo 135, Japan

ABSTRACT

We investigate the process of subclustering in the hierarchical model of galaxy formation. We construct density field around peaks of density fluctuations using the path integral method and investigate their nature.

I. INTRODUCTION

Methods studying formation process of individual galaxies particularly numerically are so far divided into two types. First, galaxy-scale density perturbations are assumed and their gravitational collapses are followed. However, assumed density perturbations are usually top-hat models, and then unrealistic. In the second type galaxy-scale objects are chosen from large-scale simulations and their evolution is followed. This method is in principle the best. We must however represent an individual galaxy by at most several hundred meshes or particles owing to present limitation of computational ability, which leads to low resolution of computations. Therefore, we study galaxy formation basing upon a more realistic model.

In clustering model of galaxy formation galaxies are thought to form at or near peaks of density fluctuations. We construct density field around peaks of density fluctuations using path integral method (Bertschinger 1987) and investigate their nature. Advantage of this method is that it can produce density fields satisfying certain constraints, *e.g.*, a density peak with a given amplitude at a given position.

II. SUBCLUSTERING

We investigate the process of subclustering in galaxies by applying an object search algorizm to the density field produced by the path integral method.

The algorizm of searching objects from a given density field is a modified version of Press and Schechter (1974) method. First, the density field produced by the path integral method is smoothed using Gaussian filter with the scale R_f: $\tilde{P}(k) = P(k)\exp(-R_f^2 k^2)$. R_f is made gradually smaller from a sufficient large value. When the value of a peak of the smoothed density field reaches a critical value ($\delta_c \approx 1$), we identify it as an object corresponding to such a scale. We can find objects with various mass by applying this algorizm for the density field with various R_f. In addition, we can investigate the history of subclustering in galaxies by comparing the objects found from density fields at different epochs.

We here present the results of three-dimensional simulation. We take a cube whose length of sides is l. The cube is divided into 32^3 meshes. We assume the power spectrum obeys power law: $P(k) \propto k^n$. As a constraint, we put a peak with $\delta/\sigma(< 0.5\mathrm{Mpc}) = 3$ in the center of the cube. In the simulation, we took l as 2.5Mpc. Thus, this peak corresponds to an object with the mass of $M \simeq 3 \times 10^{11}\mathrm{M}_\odot$ in the cosmology of $\Omega = 1$ and $h = 0.75$.

Number evolution of subclumps in the case of $n = -2$ is shown in Fig. 1. From considerably early epoch the clumps form, which is natural in the clustering models. Since star formation can occur in these clumps, the formation epoch of these stars will be much earlier than those of galaxies to which the stars will belong at the late epoch.

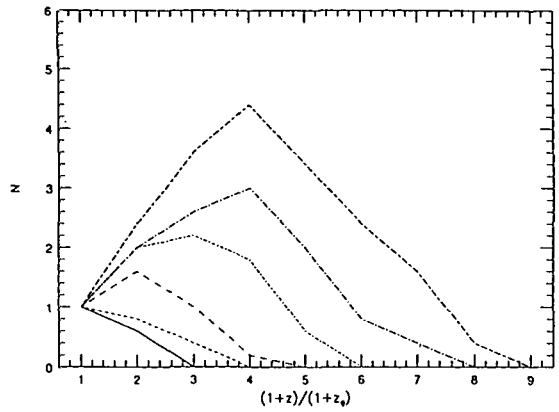

Fig. 1.–number evolution of subclumps. $n = -2$ case. Six lines indicate number of subclumps with mass larger than $10^9 M_\odot$, $10^{9.5} M_\odot$, $10^{10} M_\odot$, $10^{10.5} M_\odot$, $10^{11} M_\odot$, and $10^{11.5} M_\odot$ from the top. z_g is the epoch 0.5Mpc perturbation goes nonlinear, *i.e.*, the perturbation becomes an isolate galaxy.

III. N-BODY SIMULATIONS

We perform N-body simulations whose initial conditions are given by the density field produced by the path integral method. The density field is translated into particle distribution using the Zeldovich approximation. We follow gravitational evolution of particles using the tree code.

As a constraint, we put a peak with $\delta/\sigma(< 0.2L) = 3$ in the center of the cube as section 2. Initial redshift is $z_i = 20$. We scale amplitudes of perturbations in the way the density perturbation goes nonlinear at $z = 5$.

An example of calculations is shown in Fig. 2. This is the case that $n = -2$. The number of particles is $N \simeq 2 \times 10^4$. First, several clumps form, which merge into a single galaxy.

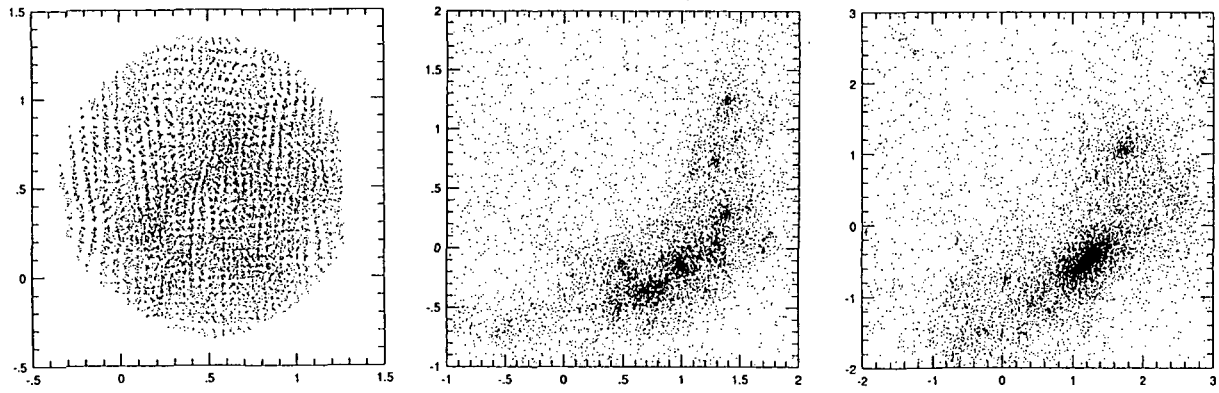

Fig. 2.–Result of N-body simulation. $n = -2$ case. $z_i = 20$, and $z_{nl} = 5$. Particle number is $N \simeq 2 \times 10^4$. From left to right, $z = 3.95$, $z = 1.70$, and $z = 0.70$.

References

Bertschinger, E. 1987, *Ap.J.(letters)*, **323**, L103.
Press, W.H., and Schechter, P. 1974, *Ap.J.*, **187**, 425.

The Spatial Correlation Properties of Dark Galaxy Halos in a CDM Universe

Tereasa G. Brainerd and Jens V. Villumsen
Department of Astronomy, The Ohio State University
174 West 18th Avenue, Columbus, OH 43210

We use the Hierarchical Particle Mesh (HPM) N-body code written by J. V. Villumsen (Villumsen, 1989) to investigate the two-point spatial correlation function, $\xi(r)$, of dark galaxy halos as a function of halo mass and local environment (*i.e.* high, low, or average mass density). We assume a standard cold dark matter (CDM) universe ($\Omega = 1$, $\Lambda = 0$, $H_0 = 50, \mathrm{km/sec/Mpc}$). Because of the large dynamic ranges in mass and length that can be obtained with the HPM code, it is well-suited to an investigation of this sort.

If we define σ_8 to be the mass fluctuation in a sphere of $8h^{-1}\mathrm{Mpc}$, then in a universe in which $1/\sigma_8 = 2.5$, high mass halos ($M_{\mathrm{halo}} \geq 9.8 \times 10^{12} M_{\odot}$) are more biased (relative to the mass) than low mass halos ($6.8 \times 10^{11} M_{\odot} \leq M_{\mathrm{halo}} \leq 3.3 \times 10^{12} M_{\odot}$) (Fig. 1). In a universe in which $1/\sigma_8 = 1.5$, high and low mass halos are biased to the same degree. If we define the epoch at which $1/\sigma_8 = 1.5$ to be "today", then from a redshift of ~ 0.7 to 0, $\xi(r)$ for low mass halos shows more evolution than $\xi(r)$ for high mass halos, but less than linear theory predicts (due to mergers of halos). If we assume that one luminous galaxy would reside in each of our dark matter halos and the mass to light ratio is a constant then, ignoring the possibility of luminosity evolution, we would expect $\xi(r)$ for faint galaxies to show more evolution with redshift than $\xi(r)$ for bright galaxies.

When compared to a fiducial correlation function that was computed without regard to environmental effects, $\xi(r)$ for halos in high density regions has a larger amplitude and is flatter than the fiducial correlation function, $\xi(r)$ for halos in average density regions is similar to the fiducial correlation function, and $\xi(r)$ for halos in low density regions has a smaller amplitude and steeper slope than the fiducial correlation function (Fig. 2). The fiducial correlation function of halos with overdensities ~ 2000 is completely dominated by halos in high density regions. This is not surprising because the formation of these objects is strongly biased toward high density regions (Brainerd and Villumsen, 1992). The fiducial correlation function of halos with overdensities ~ 200 and ~ 70 is dominated by halos in high density regions, but there is a contribution from halos in average density regions.

Ramella, Geller & Huchra (1992) have computed $\xi(r)$ for the galaxies in the "Great Wall" (Geller & Huchra, 1989) and find that $\xi(r)$ for the Great Wall galaxies is of the same form as that for the entire CfA survey, but has a correlation length roughly 3 times that of the entire survey ($r_{0,GW} \simeq 15h^{-1}\mathrm{Mpc}$). We find that $\xi(r)$ for halos with overdensities ~ 200 is well-fit by a power law, $\xi(r) = (r/r_0)^{-\gamma}$, with $\gamma = 1.86$ and $r_0 = 3.5h^{-1}\mathrm{Mpc}$, in rough agreement with the results of the CfA survey. The correlation length for the halos is short compared to the observed value for galaxies, which is likely due to an "overmerger" of halos in the simulations. Using the same normalization criteria as Ramella, Geller & Huchra, for $0.7h^{-1}\mathrm{Mpc} \lesssim r \lesssim 3.3h^{-1}\mathrm{Mpc}$ we find $\xi(r)$ for halos with overdensities ~ 200 that reside in high density regions to be similar to $\xi(r)$ computed without regard to environmental effects and has an extrapolated correlation length roughly twice as large, in qualitative agreement with the result for the Great Wall galaxies.

References

Brainerd, T. G. & Villumsen, J. V. 1992, ApJ, 394, 409
Geller, M. J. & Huchra, J. P. 1989, Science, 246, 897
Ramella, M., Geller, M., & Huchra, J. P. 1992, ApJ, 384, 396
Villumsen, J. V. 1989, ApJS, 71, 407

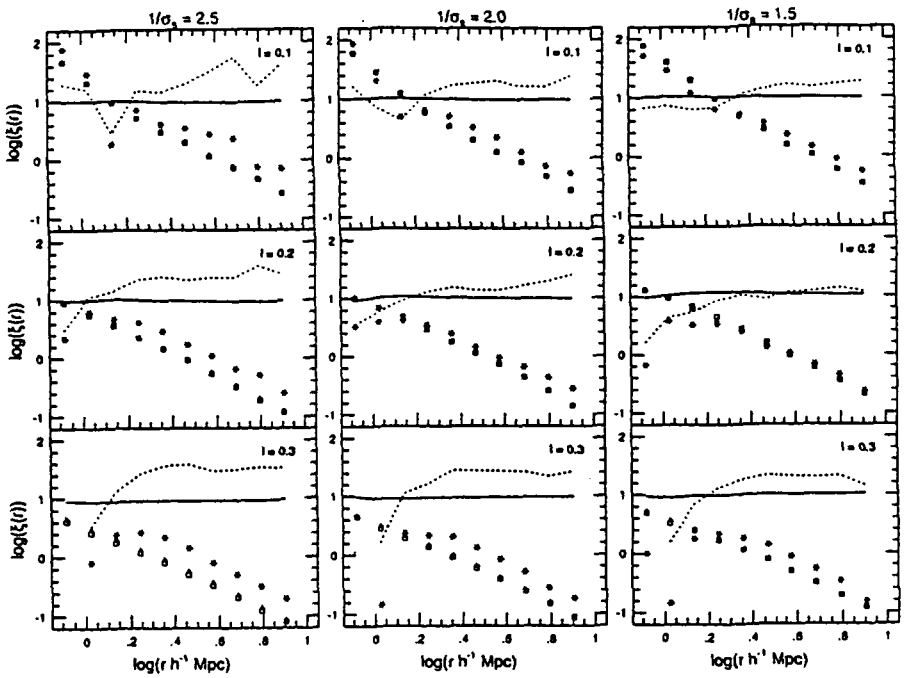

Figure 1: $\xi(r)$ for low mass halos (squares), high mass halos (asterisks), and all the halos (triangles) in the simulation at epochs corresponding to $1/\sigma_8 = 2.5, 2.0, 1.5$ for halos of overdensities ~ 2000 (l=0.1), ~ 200 (l=0.2) and ~ 70 (l=0.3). The square root of the ratio of $\xi(r)$ for the low (high) mass halos to that of $\xi(r)$ for all the halos is shown by a solid (dotted) line on a linear scale.

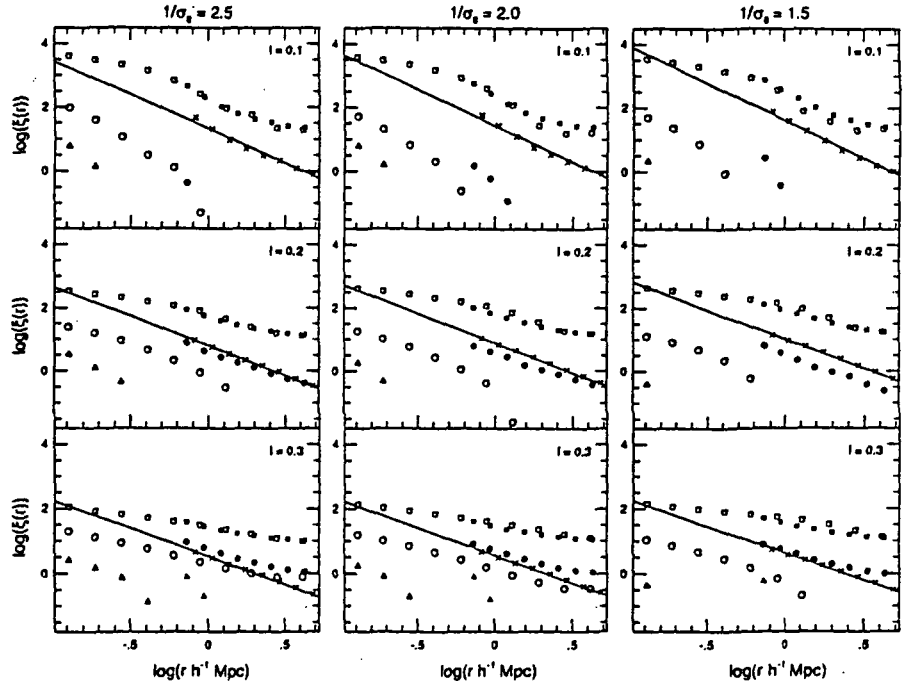

Figure 2: $\xi(r)$ for halos in high density regions (squares), average density regions (circles), and low density regions (triangles). Crosses show $\xi(r)$ for halos computed without regard to environmental effects, and the solid line is a power law fit to these "fiducial" correlation functions.

GAS DYNAMIC SIMULATIONS OF GALAXY FORMATION

August E. Evrard
Physics Department, University of Michigan

I will present results from a simulation modelling the formation of a group of galaxies in a "standard" cold, dark matter universe with $\Omega = 1$, $H_o = 50$ km s^{-1} Mpc^{-1}, baryon fraction $\Omega_b = 0.1$ and spectrum normalization $\sigma_8 = 0.6$ (bias parameter $b = 1.7$). This work is in collaboration with F. Summers and M. Davis of U.C., Berkeley (see F. Summers contribution to this meeting). Initial conditions are generated within a periodic box with comoving length 16 Mpc in a manner constrained to produce a small cluster of total mass $\sim 10^{14} M_\odot$. Two sets of 64^3 particles are used to model the dark matter and baryon fluids. Each gas particle represents $1.08 \times 10^8 M_\odot$, implying an L_* galaxy is resolved by ~ 1000 particles. The system is evolved self-consistently in three dimensions using the combined N-body/hydrodynamic scheme P3MSPH up to a final redshift $z = 1$. Evolving to the present is prohibited by the fact that the mean density in the simulated volume is above critical and the entire volume would be going non-linear beyond this point. We are currently analyzing another run with somewhat poorer mass resolution which was evolved to the present.

The baryons' thermal energy is subject to change due to adiabatic (PdV) work, shock heating and radiative cooling. The latter is assumed to be well described by a cooling function of a primordial plasma including line radiation and bremsstrahlung calculated assuming collisonal ionization. Star formation is not included. The baryons and dark matter are coupled gravitationally, the minimum scale resolved is ~ 10 kpc, roughly the optical size of a bright galaxy.

In collapsed regions, a two-phase structure develops in the baryons consisting a of cold, high density gas in rough pressure equilibrium with enveloping hot, tenuous halos at roughly the virial temperature of the dark matter halo. We identify a population of galaxy-like objects (*globs*) using a group finding algorithm designed to pick out concentrations of baryons above a fixed *physical* density of ~ 0.5 cm^{-3}. A minumum cutoff of 30 particles per galaxy, $3 \times 10^9 M_\odot$ in baryons, is imposed. The mass fraction of baryons in the galaxy population increases with time from roughly 5% at $z = 5.3$ to 18% at $z = 1.0$. During this time, the number of objects above the mass cutoff grows from 40 to 208.

A major result of this work is the formation of a significant population of rotationally supported baryonic disks. The accompanying figures show a prime example. Figure 1 shows face on (top row) and edge on (bottom row) views of the mass within 100 kpc of the center of the twelth largest glob found at the end of the simulation. The small bar in the panels denotes the 10 kpc resolution limit. Galaxies are clearly just barely resolved. The leftmost two panels, enlarged by a factor 3 compared to the rightmost two, show baryons in the cold phase $T < 3 \times 10^4$ K. The velocity field in the disk is regular, and an outer warp is apparent, most likely generated by interaction with a satellite just outside the region shown. Of the total baryonic mass of $1.2 \times 10^{11} M_\odot$ within 100 kpc, 65% is in the cold disk and 35% is in a hot halo with $T = 3 \times 10^6$ K shown in the right center panels. The dark matter halo is very nearly spherical and isothermal. The ratio of dark to baryonic mass is unity at 10 kpc, rising to 7.8 at 100 kpc.

Figure 2 shows the velocity field of the cold disk material in the principal component frame used in Figure 1. The solid line in 2a shows the mean tangential velocity as a function of radius while the dotted and dashed lines give the mean radial and z-components, respectively. The dispersion about the mean is shown in Figure 2b. The velocity field is very quiet, the major feature is a flat rotation curve of 200 km s^{-1} amplitude outside the resolution limit. Figure 3 shows the growth history of this disk. The only significant merger in its history involved a small satellite with mass $\lesssim 10\%$ of its own. Such quiet dynamical histories appear for the majority of galaxies identified in the simulation.

The poster will provide details on the formation and evolution of the galaxy population within the simulation.

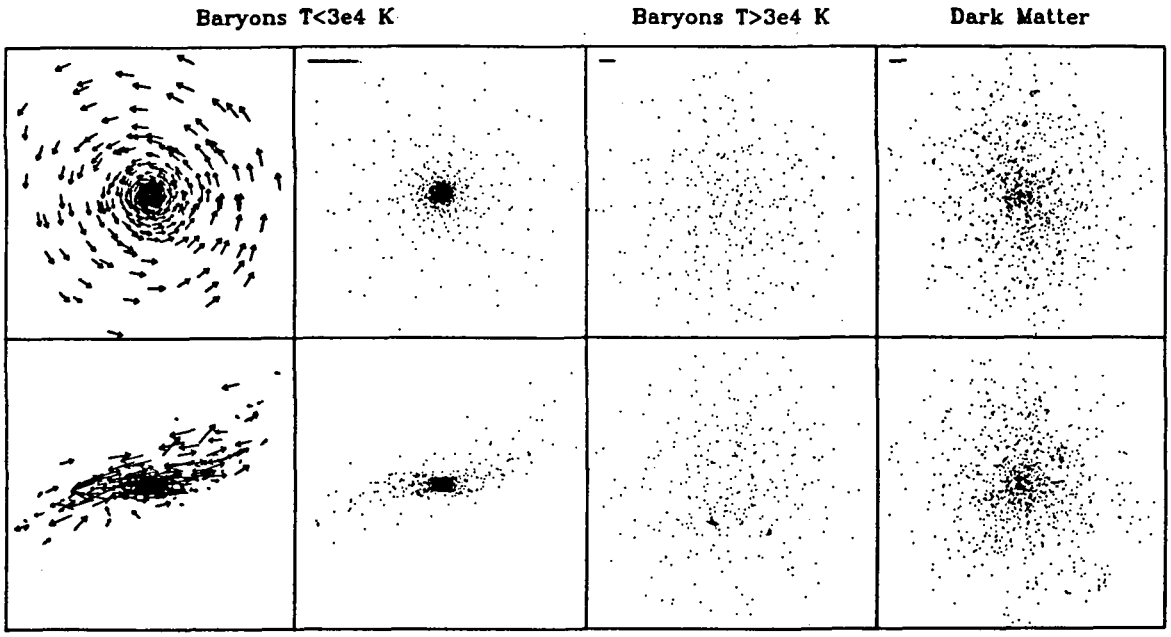

Fig. 1

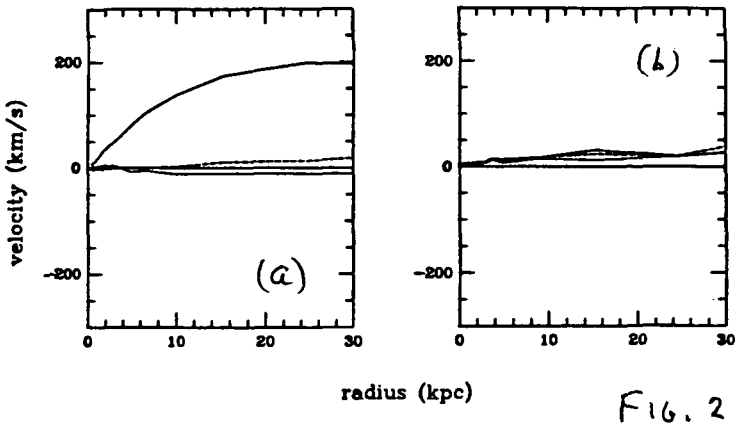

Fig. 2

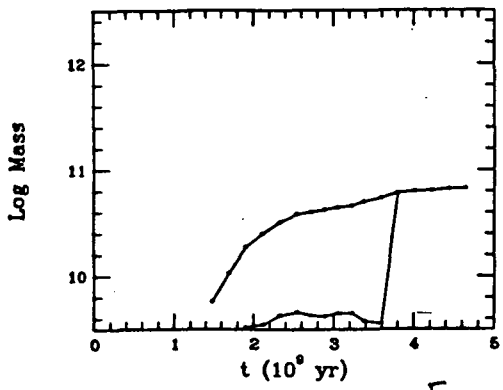

Fig. 3

THE GALAXY VELOCITY FIELD AND CDM MODELS

Giuseppe Tormen[1,3], Lauro Moscardini[1], Francesco Lucchin[1] and Sabino Matarrese[2]

[1] *Dipartimento di Astronomia, Università di Padova, vicolo dell'Osservatorio 5, 35122 Padova, Italy.*

[2] *Dipartimento di Fisica "Galileo Galilei", Università di Padova, via Marzolo 8, 35131 Padova, Italy.*

[3] *M.I.T. Physics Department, Cambridge, MA 02139*

It is generally accepted that some kind of non–baryonic dark matter accounts for most of the mass density of the universe. Considering such a component has become, in the last decade, a key ingredient in current theories of structure formation. In particular, the Cold Dark Matter (CDM) scenario has proven to be quite successfull in explaining most of the observed properties of galaxies and of their large–scale distribution. The standard CDM model is characterized by a primordial Zel'dovich spectrum ($\mathcal{P}(k) \propto k^n$, with spectral index $n = 1$) of random–phase adiabatic perturbations in a universe with density parameter $\Omega_0 = 1$ and vanishing cosmological constant.

This poster paper presents an analysis of observational data on peculiar motion of optical galaxies in comparison to the predictions of CDM models where the assumptions of the standard scenario: $\Omega_0 = 1$, $n = 1$ and bias parameter $b = 1$ are relaxed. In particular CDM models with $0 \leq n \leq 1$ and $0.4 \leq \Omega_0 \leq 1$ are considered.

The galaxy sample we used was compiled from the "Mark II" files kindly supplied by David Burstein; these are a collection of several data, including distances and peculiar velocities for different samples of elliptical and spiral galaxies. We put all these galaxies together and came out with a big sample of 1184 galaxies in 704 grouped objects.

We applied different statistics to this sample and to Monte Carlo simulations of the peculiar velocity field in the linear regime. The simulations were performed on 64^3 grid points. The velocity field was assumed to be Gaussian with a scale–free power spectrum. The box size of the simulations is 32,000 km s^{-1}. We considered the following values

for the model parameters: $\Omega_0 = 0.4, 1$, $n = 0, 0.5, 1$ and $b = 1, 1.5, 2$.

We constructed our simulated catalogs of radial peculiar velocities by locating the "observer" in a grid–point with features similar to those of the Local Group, and sampling the velocity field at the same position of the observed galaxies.

The observed velocity field is affected by sources of indetermination, mainly distance errors and sampling inhomogeneities. We tried to reproduce these effects on the simulated data, to better compare the real catalog with the mock ones. To take into account galaxy distance errors we perturbed each distance and radial peculiar velocity with Gaussian noise (e.g. Dekel, Bertschinger & Faber 1990, ApJ **364**, 349); we then extracted several catalogs from each simulation, by picking up different location of the Local Group, in order to reproduce the sparse sampling of the real data. This result in an overall number of 5,000 catalogs for each model.

Our study is carried out in the linear regime, both with *rms* values and with Monte Carlo simulations, in order to keep into account the different effects of statistical deviations from the mean, sparse sampling, distance errors and observational bounds. These effects will actually lead to remarkable differences between the simple *rms* theoretical prediction and the more realistic Monte Carlo simulations.

The first statistics we applied to our data sample is a velocity dipole analysis (bulk flow). The other relevent statistics is the velocity correlation function $\Psi_1(r)$ (Gorsky et al., 1989, ApJ **344**, 1). We applied these two statistics also to our simulated catalogs, together with a statistics based on the selection of the observers, i.e. the requirement that the spatial position from which each catalog is "seen" has features similar to those of the Local Group. The effect of these constraints proved to be strong; the statistical results for the models turn out to be quite different from simple unconstrained estimates.

As the statistics we used are independent, or almost independent, we could apply a Maximum Likelihood analysis to the theoretical results in the simplest way, $\mathcal{L}(\vec{\theta}) = \prod_{i=1}^{N} \mathcal{L}_i(\vec{\theta})$.

A discussion about the results of these analysis is presented.

The Hydrodynamics of Galaxy Formation on Kiloparsec Scales

Michael L. Norman and Wenbo Yuan Anninos
National Center for Supercomputing Applications

and

Joan Centrella, Drexel University

Two dimensional numerical simulations of Zeldovich pancake fragmentation in a dark matter dominated universe were carried out to study the hydrodynamical and gravitational effects on the formation of structures such as protogalaxies. Preliminary results were given in Yuan, Centrella and Norman (1991). Here we report a more exhaustive study to determine the sensitivity of protogalaxies to input parameters. The numerical code we used for the simulations combines the hydrodynamical code ZEUS-2D (Stone and Norman, 1992) which was modified to include the expansion of the universe and radiative cooling of the gas with a particle-mesh code which follows the motion of dark matter particles. The resulting hybrid code is able to handle highly nonuniform grids which we utilized to obtain a high resolution ($<<$ 1 kpc) in the dense region of the pancake.

In a universe with 10% of its mass composed of hydrogen and helium of cosmic abundances and 90% of its mass in the form of dark matter, we set up a sinusoidal density perturbation of λ=10 Mpc in the x1 direction and small density fluctuations in the x2 direction at z=50. The perturbation amplitude in the x1 direction is larger than the amplitudes of the fluctuations in the x2 direction so that the mass collapses in the x1 direction and a pancake forms at z=5.

We ran six runs of different resolutions and different amplitudes and types of initial density fluctuation in the x2 direction, and we find the following main results: (1) The gas density is about 10 times the dark matter density in the central region right after the pancake collapse at $z \approx 5$, but the gas and dark matter densities are about the same in the fragmented dense clump at $z \approx 0$. (2) The gas overdensity is larger than the dark matter overdensity only in the shocked region, so the gas is biased over the dark matter only on the

scale of equal or smaller than the size the shocked region. (3) The coupling of the cooling and gravitational instabilities causes the fragmentation of the gas pancake at the early time, the dark matter follows the gas fragmentation because the mass of the gas dominates the central region. The gravity dominates at later times causing the merging of the clumps. The scale of the initial fragmentation for all the runs fall in the range given by the critical wavelength of the cold pancake λ_{max} which is due to the gravitational instability and the distance sound wave travels in the pancake fragmentation time λ_f in the strong cooling region. (4) The time for the completion of the fragmentation and the amount of the cooled gas depend sensitively on the amplitude but not the type of the initial density power spectra.

References

Stone, J. M. and Norman, M. L. 1992. Ap. J. Suppl., 80, 000.
Yuan, W., Centrella, J. and Norman, M. L. 1991. Ap. J. Lett., 376, L29.

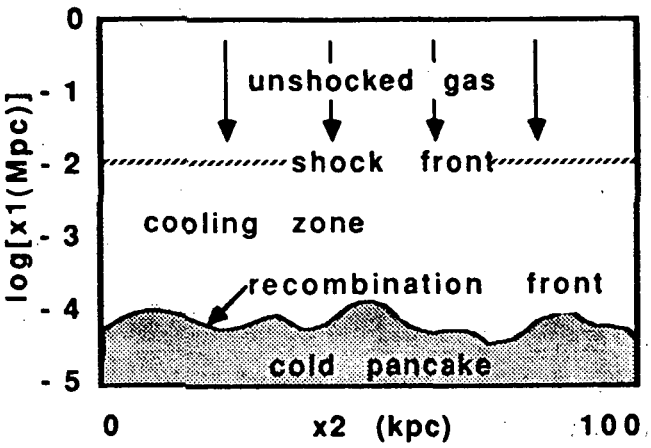

Fig. 1 Schematic of the pancake prior to fragmentation showing cold layer, cooling zone, and accretion shock.

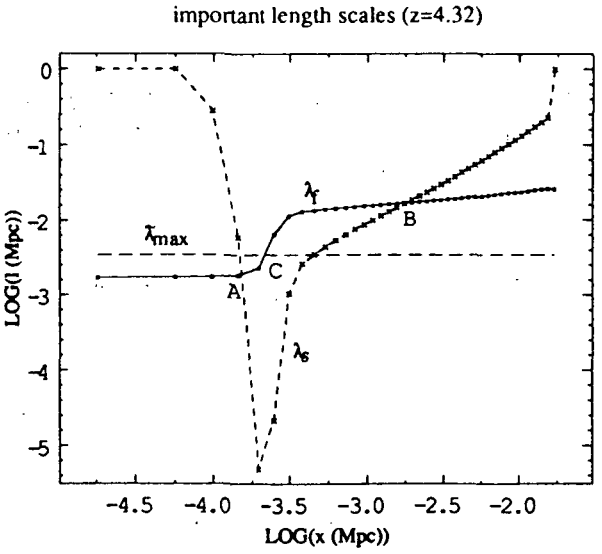

Fig. 2. The run of various length scales of interest as a function of x1: λ_f=fragmentation length in the cooling layer; λ_S=cooling length in the cooling layer; λ_{max}=wavelength of maximum perturbation growth due to gravitational instability in the cold pancake.

Do Galactic Potential Wells Depend on Their Environment?

H.J. MO and O. LAHAV

Institute of Astronomy, Madingley Road, Cambridge CB3 0HA, UK

Abstract Using galaxies in complete samples as tracers of the galaxy density field and about 1000 galaxies with measured circular velocities as targets, we examine the cross-correlation functions between the targets and tracers as a function of galaxy circular velocities. The correlation strength does not vary with the circular velocities except for elliptical galaxies with the highest velocity dispersions, where the effect may well be due to morphological segregations in clusters of galaxies. This is constrasted with the strong dependence of the correlation functions of dark halos on their circular velocities in some models of galaxy formation.

1. Introduction In order to study galaxy formation and matter distribution in the universe, we need to understand how the intrinsic properties of galaxies are correlated with the large-scale structure. The velocity dispersion (σ) of elliptical galaxies and the rotation velocity (v_c) of spiral galaxies (hereafter termed together as "circular velocities") are important intrinsic properties of galaxies. They are related not only to the process of galaxy formation, but, since they are used as the distance indicators (i.e. Tully-Fisher and D_n-σ relations), also to our study of the large-scale structures and motions in the universe. The dependence of galaxy clustering on galaxy circular velocities is predicted in some models of galaxy formation (e.g. White et al. 1987, hereafter WDEF). It is not yet known whether or not such a dependence exists in observations. In this paper, we examine the dependence of galaxy clustering on the circular velocities of galaxies, using galaxies in complete samples as tracers of the galaxy density field and the ~ 1000 galaxies with measured circular velocities (Mark II release, Burstein, private communication) as targets to study the segregation of the circular velocities by the large-scale structure. We calculate the two-point cross-correlation functions of target galaxies with trace galaxies, which enables us to make a maximum use of the available data and makes possible a direct comparison with theoretical models. Here is a brief report of our results.

2. **Results** To represent the galaxy density field, we use three complete samples of galaxies: the redshift survey of (2Jy) IRAS galaxies (Strauss et al. 1992), the CfA redshift survey of galaxies (Huchra et al. 1983) and the Southern Sky Redshift Survey of Galaxies (da Costa et al. 1991). For the targets representing the circular velocities of galaxies, we use the ~ 1000 galaxy sample of Burstein et al.

We define our problem as follows: Given a target galaxy with a certain intrinsic velocity, what is the expected correlation function of this galaxy with trace galaxies. In this case, we do not need a complete sample for the target galaxies. Fig.1 shows the ratios between the correlation functions for the target galaxies of different circular velocities. To minimize the peculiar-velocity effects, we actually calculated the cylindrical projections of the cross-correlation functions. The horizontal lines represent roughly the predictions given by WDEF for the dependence of the correlation functions of dark halos on circular velocities. There appears to be no trend for the correlation strength to vary with the circular velocities. This is true for both elliptical and spiral galaxies, except for elliptical galaxies with the highest velocity dispersions ($\sigma \gtrsim 280\,\mathrm{kms}^{-1}$), where the effect may well be due to morphological segregations in clusters of galaxies. The circular-velocity dependence in the observation is at a significantly lower level than the model predictions, if the observed circular velocities are correlated with the circular velocities of dark halos.

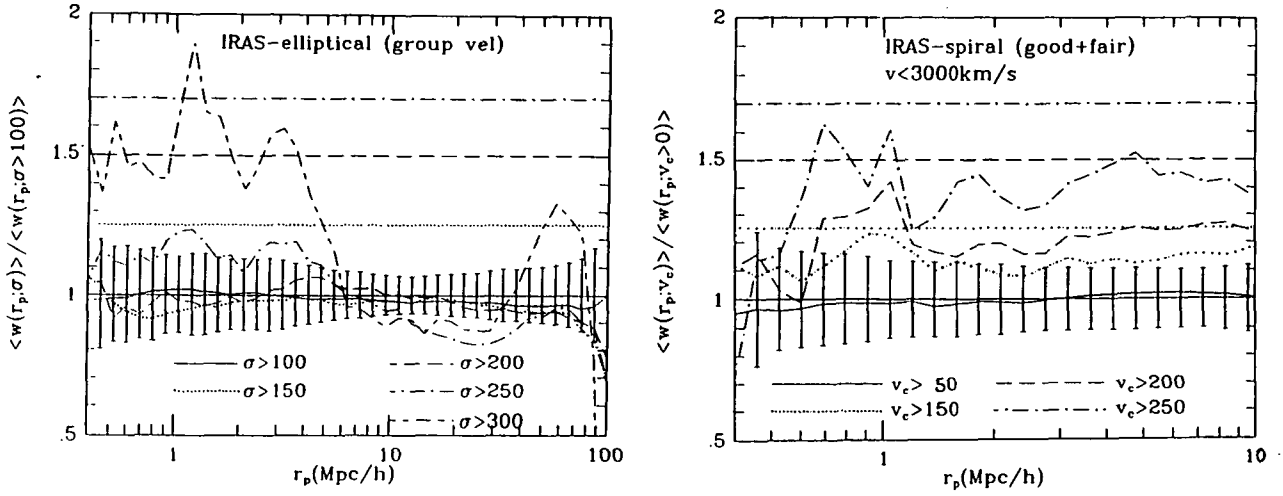

Fig.1. (a) The ratios between the projected correlation functions of different σ-samples of elliptical galaxies and that of the total sample. IRAS galaxies are used as tracers. The error bars represent 1σ bootstrap errors for the $\sigma > 250\,\mathrm{kms}^{-1}$ sample. They are about two times as large for the $\sigma > 300$ sample and slightly smaller for other samples. The horizontal lines represent the enhancements of the correlation functions of dark halos by circular velocites, predicted by the "natural" biasing model (WDEF). (b) The same as (a) but for spiral galaxies of different v_c. The error bars represent 1σ bootstrap errors for the $v_c > 200\,\mathrm{kms}^{-1}$ sample. They are about two times as large for the $v_c > 250$ sample and slightly smaller for other samples.

Following Kaiser (1989), we write the modulation of the circular velocity v_c of a dark halo by a long-wavelength density pertubation $\Delta_B(0)$ (at the present time) as

$$v_c'[z_f, \Delta_B(0)] = v_c(z_f)\left[1 + \frac{\Delta_B(0)}{1.68(1+z_f)}\right]^{\frac{(1-n)}{2(n+3)}} \approx v_c\left[1 + \frac{0.3(1-n)}{n+3}\frac{\Delta_g(0)}{b_g}\frac{1}{1+z_f}\right]$$

where z_f is the redshift at collapse, n is the power-spectrum index of the density fluctuations, and the large-wave-length *galaxy* density fluctuation Δ_g is assumed to be related to the matter density fluctuation by $\Delta_g = b_g\Delta_B$ (b_g is the biasing parameter). We estimate the density Δ_g around the target galaxies from our cross-correlation function. The weak variation of v_c with Δ_g in our analysis can be used to set the limit $(1-n)/[(n+3)(1+z_f)b_g] \lesssim 0.2$. To satisfy the Tully-Fisher relation $L \propto v_c^4$ and assuming that mass $M \propto L$, one gets $n = -2$. If $b_g = 1$ then $z_f \gtrsim 10$, which means that most halos were formed at a quite early epoch.

References

da Costa L.N., et al. 1991, ApJS, 75, 935.
Faber S.M. & Burstein D. 1988, in Large-scale Motions in the Universe, p116, eds. V. Rubin & G. Coyne, Princeton.
Huchra J., Davis M., Latham D. & Torry J. 1983,ApJS, 52, 89.
Kaiser N. 1989, in Large-scale structure and motions in the universe, p197, eds. M. Mezzetti et al. Kluwer.
Strauss M.A., Davis M., Yahil A. & Huchra J.P. 1992, ApJ, 385, 421.
White S., Davies M., Efstathiou G., Frenk C. S. 1987, Nature, 330, 451.

The Effect of Tidal Fields on the Shapes and Kinematics of Dark Halos

JOHN DUBINSKI
Harvard–Smithsonian Center for Astrophysics, 60 Garden St., Cambridge, MA 02138
e-mail: dubinski@cfa.harvard.edu

Dark halos form from the collapse of density perturbations layed down in the early universe. The collapse of a density perturbation to form a dark halo is strongly influenced by the tidal shear created by evolving structure in the local neighborhood. Tidal torques act during the collapse (Hoyle 1949; Peebles 1969; White 1984) since the tidal field couples very effectively to the perturbations which are filled with substructure and more generally triaxial (Bardeen et al. 1986). Tidal torques are the source of angular momentum in dark halos and galaxies as well as being influential in the development of the structure of dark halos.

We have carried out a series of N–body simulations to investigate the effect of tidal shear on the structure and kinematics of dark halos (Dubinski 1992). We simulate the collapse of density perturbations using a tree code as described in Dubinski & Carlberg (1991). Density peaks are selected from a random realization of a CDM density field and used as the initial conditions for N-body simulations. We use an experimental approach to examine the effects of tidal shear on collapse. The cosmological tidal field is treated as an external time dependent potential whose strength and orientation can be varied freely. We examine the effects of the tidal field with two experiments. In the first experiment we simulate a sample of 14 dark halos from the collapse of density peaks in the presence of a 1σ tidal field. In the second experiment, we use the same initial conditions though the tidal field is turned off allowing an experimental control for comparison to highlight the influence of tidal shear on the development of the structure and kinematics of the dark halos.

A comparison of the dark halos from the two experiments reveals the profound effect of tidal shear on the structure. The shape distribution of dark halos depends strongly on the strength and orientation of the tidal shear field. Dark halos which collapse without a tidal field are very flat ($c/a \sim 0.5$) and almost exclusively prolate. This tendency towards a prolate morphology probably results from the propensity of prolate density peaks in the initial conditions though may be partially due to the radial orbit instability (Merritt & Aguilar 1985). When we introduce a cosmological tidal field, the halos still are very flat though a variety of morphologies are apparent with roughly an even split between oblate and prolate forms. The shapes of the resulting dark halos are completely uncorrelated with the shapes of initial density peaks.

We also studied the kinematics in the two experiments using measurements of the angular momentum, the velocity ellipsoids, streaming motions and tumbling of the dark halos. Most of the angular momentum is in the form of streaming motions with tumbling motions having periods exceeding 4 Gyrs. The total angular momentum is coherently aligned and distributed roughly as $J(r) \propto r^2$. The angular momentum vector tends to align with the minor axis of the triaxial dark halos as observed previously by other investigators (Warren et al. 1991; Barnes & Efstathiou 1987). The alignment of the angular momentum vector probably has a primordial origin. During the expansion phase, the tidal torque vector tends to align with an axis perpendicular to the major axis of the given triaxial density peak. This effect apparently imprints a spin about the minor axis on dark halos. The origin of the tendency for the small misalignment angle between the rotation vector and the apparent minor axis in elliptical galaxies is probably due to the same effect (Franx et al. 1992) The tangential accelerations arising from tidal torques are comparable to the radial accelerations of the collapsing peaks. Orbits can acquire significant amounts of angular momentum from torques which produce isotropic velocity ellipsoids. In contrast, the velocity ellipsoids of the dark halos which collapse when neglecting the tidal field develop radially anisotropic velocity ellipsoids similar to those seen in cold collapse simulations (e.g., van Albada 1982).

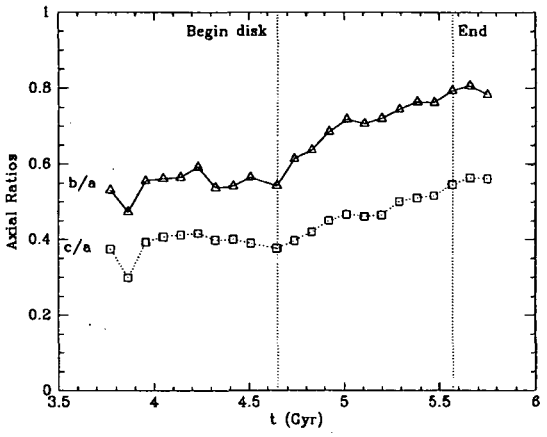

FIG. 1.–Axial ratio profiles for a dark halo. A disk potential scaled appropriately to represent a typical galaxy grows to it full mass in 1 Gyr. The halo transforms from a nearly prolate shape to an oblate one.

The dark halos produced in these simulations are extremely flat ($c/a \sim 0.5$) and often prolate especially in their centers. A disk embedded in a very flat prolate halo with its spin aligned with the minor axis should dramatically reflect the shape of the halo in its structure and kinematics. These extreme halos should result in disk galaxies which are ovally distorted with significant noncircular velocity deviations in their rotation curves (Franx and de Zeeuw 1991; Kuijken and Tremaine 1991) Some analyses suggest that such extremely flat dark halos (at least flat in the plane of disks) are not allowed by the observations (Franx and de Zeeuw 1991). A possible solution to this problem may come from the process of baryonic feedback on the evolution of the shape and density of the dark halo. As the baryons sink into the center of the dark halo to form a disk, the growing axisymmetric potential of a disk can modify the shape of the dark halo. Box orbits in the prolate potential (for example) may gradually be change into loop orbits in response to the oblate potential of the disk. We examined this process using a simulation of a dark halo with a growing potential. We grow a disk potential (Miyamoto–Nagai potential) in the center of an initially virialized dark halo which is nearly prolate. The shape of the dark halo changes slowly from an initially prolate object with $c/a = b/a = 0.5$ to a more oblate object. The halo remains flat with $c/a = 0.5$ but becomes considerably more oblate with $b/a = 0.8$ (Fig. 1). The dark halos surrounding disk galaxies are likely more oblate than dissipationless dark halo simulations would suggest.

REFERENCES

Bardeen, J.M., Bond, J. R., Kaiser, N., & Szalay, A. S. 1986, ApJ, 304, 15 [BBKS]
Barnes, J., & Efstathiou, G. 1987, ApJ, 319, 575
Dubinski, J. 1992, ApJ, in press.
Dubinski, J.& Carlberg, R. 1991, ApJ, 378, 496
Franx & de Zeeuw 1991, preprint
Franx, M., Illingworth, G., & de Zeeuw, T. 1992, ApJ, in press
Kuijken, K, & Tremaine, S. 1991, in Dynamics of Disc Galaxies, ed. B Sundelius, Goteborg, Sweden, p. 71.
Merritt, D., & Aguilar, L. A. 1985, MNRAS, 217, 787
van Albada, T. S. 1982, MNRAS, 201, 939
Warren, M.S., Zurek, W. H., Quinn, P. J., & Salmon, J. K. 1992, ApJ, in press
White, S. D. M., 1984, ApJ, 286, 38
Zurek, W. H., Quinn, P. J., & Salmon, J. K. 1988, ApJ, 330, 519

Near-IR Imaging of Moderate Redshift Galaxy Clusters

S.A. Stanford, M.E. Dickinson
University of California at Berkeley
P.R.M. Eisenhardt
JPL, Caltech

Spectroscopic studies of the "blue galaxy" cluster population which first appears at $z \sim 0.2$ – the Butcher-Oemler (BO) Effect (Butcher and Oemler 1984) – have uncovered several classes of objects suggesting a wide range of evolutionary histories for cluster galaxies: star forming spirals, AGNs, and post-starburst "E+A" objects resembling early-type galaxies with a strong A-star population superimposed (but no signs of ongoing star formation). At moderate redshifts, optical imaging samples the rest-frame near-UV and tells about the recent star formation histories of the cluster galaxies. Observations at IR wavelengths are necessary to measure the luminosity and colors of the underlying cool stellar population which should dominate the galaxies' mass. Optical-to-IR photometry will provide a broader understanding of the nature of BO activity and the galaxies it affects. For example, optically-red ellipticals and S0s, the "red envelope" galaxies which had been thought to define the track of quiescent galaxy evolution, also reveal signs of spectral evolution. Lilly (1987) analyzed near-infrared photometry of galaxies in several distant galaxy clusters, and found them to be ~0.1 mag redder in their $(V-H)$ colors than predicted by models.

We have obtained near-IR imaging of 3 moderate-z clusters on the 1.3m at KPNO with SQIID, a new camera offering wide-field (5.5 arcmin) simultaneous JHK band imaging. Our photometry on a sample of ~100 likely member galaxies in one of the clusters, Abell 370 at $z = 0.37$ (K band image shown in Fig. 1), shows that we can obtain magnitudes good to 20% down to $K = 18$, considerably below the estimated K_*=16.5 at this redshift. These data indicate that there are no systematic problems in obtaining photometry at faint levels with SQIID. With the development of larger arrays, the field is open to progress. Previous near-IR imaging work on moderate redshift clusters has been hampered by the small size of the first generation arrays. Aragon-Salamanca, Ellis, and Sharples (1991) recently published the first such work on Abell 370; they find that the longer wavelength colors are redder than supposed and indicate a strong contribution by AGB stars in a post-starburst phase. They were able to mosaic a field, in only the K band using IRCAM on UKIRT, on Abell 370 with only 1/10th the area of a single SQIID frame to the same depth that we reached in similar total integration time.

The resulting J, H and K data for the three clusters are combined with previously-obtained multiband optical photometry. We present an investigation of the spectral properties and evolution of the dominant cold stellar populations by comparing optical-to-IR colors and color-magnitude diagrams to predictions from population synthesis models and galaxy spectral evolution codes.

REFERENCES

Aragon-Salamanca, A., Ellis, R.S., and Sharples, R.M. 1991, MNRAS, 248, 128
Butcher, H. and Oemler, A., Jr. 1984, ApJ, 285, 426
Lilly, S.J. 1987, MNRAS, 229, 573

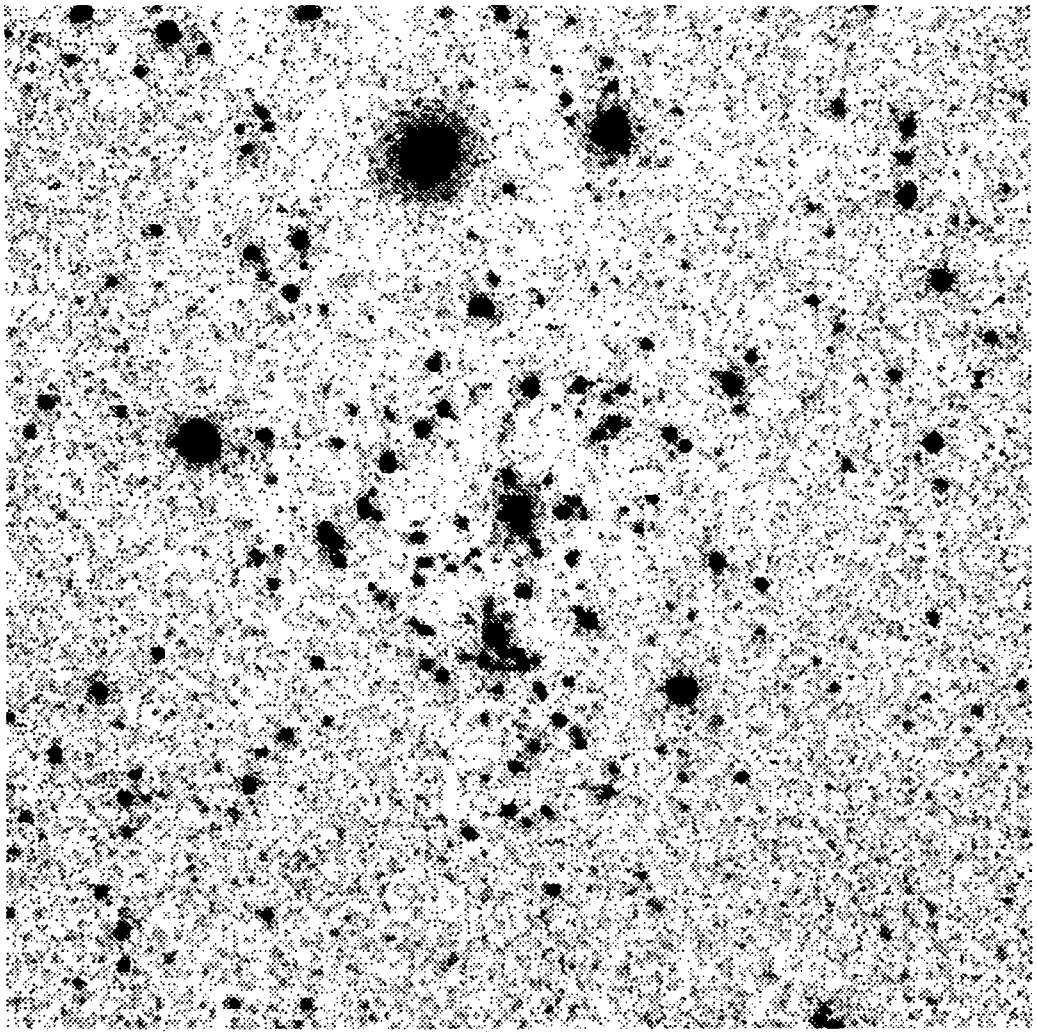

Fig. 1 – Abell 370, K band.

N93-26742

Distant Radio Galaxies in the Near IR

P. J. McCarthy, S. E. Persson, R. Elston
Carnegie Observatories
and
P. R. Eisenhardt
Jet Propulsion Laboratory

We are carrying out a program of near IR imaging and spectroscopy of radio galaxies with redshifts of 1.5 and greater. One of its principal goals is to constrain the ages and star formation histories of massive galaxies at early epochs.

The radio galaxies are drawn from the survey of 1Jy class sources by McCarthy et al (1989) and McCarthy (1990). The sample contains 18 radio galaxies with redshifts greater than 2 and an additional 10 objects with $1.5 < z < 2.0$. The redshifts were obtained from long slit spectra with the CTIO 4m. While the galaxies are quite faint ($r \sim 21 - 24.5$) all have Lyman α emission with rest frame equivalent widths of 100 - 1000Å. Multicolor photometry in the g,r,i and J,H,K bands has been obtained with the 2.5-m Du Pont Telescope on Las Campanas and with the Hale 5m telescope at Palomar. We have recently obtained near IR spectra, using the 4m telescopes at KPNO and CTIO, of a few objects with the goal of determining the Lyman α/Hα ratio and hence the reddening.

One of the key questions in the interpretation of the spectra of distant radio galaxies is whether they contain a single roughly coeval stellar population or a number of distinct populations. Presently, the only observational signature of two distinct components would be differences in the near IR (rest-frame visible) and rest-frame UV morphologies. The rest-frame UV morphologies of radio galaxies with $z > 1$ are highly irregular and are strongly aligned with the radio source axes. A crucial question is whether or not the near IR morphologies are also aligned with the radio axes. While observations of $z \sim 1$ galaxies from the 3CR catalog reveal a few cases of aligned morphologies in the K band (e.g. Chambers et al 1987; Eisenhardt et al 1989), many objects do not (Rigler et al 1990). Our high signal-to-noise ratio K images of Molonglo radio galaxies with $z > 2$ show very few cases of convincing K band alignments. Comparison with our optical images reveals a trend for the morphologies to become more compact at longer wavelengths, supporting the view that these systems contain two stellar populations with distinct star formation histories.

We use Bruzual's (1984) spectral synthesis code, as modified to include AGB stars by Chokshi and Eisenhardt to constrain the ages and star formation histories of our $z > 1.5$ sample. We adopt Lilly's 'Old galaxy + burst' paradigm for fitting the broad band spectral energy distributions. The old component is modeled as a single burst with a duration of 1 Gyr. The young component is taken as a zero age burst and has a nearly flat spectrum in F_ν units. The best fit is achieved by varying the time since the initial burst and the fractional contribution of the young component. The age of the old component is most sensitive to the colors longward of 4000Å rest, whereas the amplitude of the burst is constrained by the level of the far UV flux density. In figure 1 we show the fit to one of the reddest galaxies in our sample. These red objects are of the most interest from a cosmological standpoint as they provide the strongest constraints on the redshift of formation. For 0156-252, shown below, we derive a lower bound on the age for the compact red component of

2.8Gyr. The age required to fit the J, H and K colors of the compact core alone is well in excess of 3 Gyr. The implied redshift of formation is quite high even in the most conservative cosmologies. For $H_0 = 50$, $q_0 = 0.1$ the minimum formation redshift is 6, while for a $H_0 = 50$, $q_0 = 0.5$ universe, the implied redshift of formation is greater than 20. Roughly 15% of the $z > 2$ galaxies in our sample have extremely red colors. These galaxies, with r-K colors redder than 6.5 are also quite overluminous at K, the brightest object having K=16.8 at z=2.01.

Such extremely red spectral energy distributions and large luminosities suggest that highly obscured non-stellar sources may contribute to the light at long wavelengths. The only observational handle that we have on reddening comes from comparing emission lines arising from different levels of a single ionic species. The recent increase in sensitivity of near IR spectrographs has made it possible to measure Hα and the [NII]6548,6584 lines in the H and K windows at redshifts of ~ 1.5 and ~ 2.4. We have now detected Hα emission in four galaxies with redshifts of roughly 2.4. From these we determine the Lyα/Hα ratios. The observed ratios are typically $3 - 4.5$, while the case B ratio is 8.75. The implied spatially uniform reddening is rather small, E(B-V) $= 0.1 - 0.15$. The strong Hα emission contributes roughly 15% of the light at K, also making the galaxies appear redder than their true colors. The net result of the two effects is that the galaxies are roughly 0.7 magnitudes bluer in the rest-frame than observed. While this does reduce the implied ages slightly, it does not change the basic conclusion that these galaxies contain an old stellar population. Our near IR spectra fail to reveal a broad component to the Hα line, which must be present if an obscured quasar dominates the K band flux. Higher S/N Hα spectra will allow us to place a better constraint on the contribution of an AGN to the near IR colors. Based on the data that we have at the present it appears that the distant radio galaxies contain a population with an age of 1 Gyr or more at redshifts in excess of 2. These objects imply an early formation epoch for AGN host galaxies. Our approach, which is based on light from stellar photospheres leads us to essentially the same conclusions reached by Turner (1990) from fueling and collapse time scales in $z > 4$ quasars.

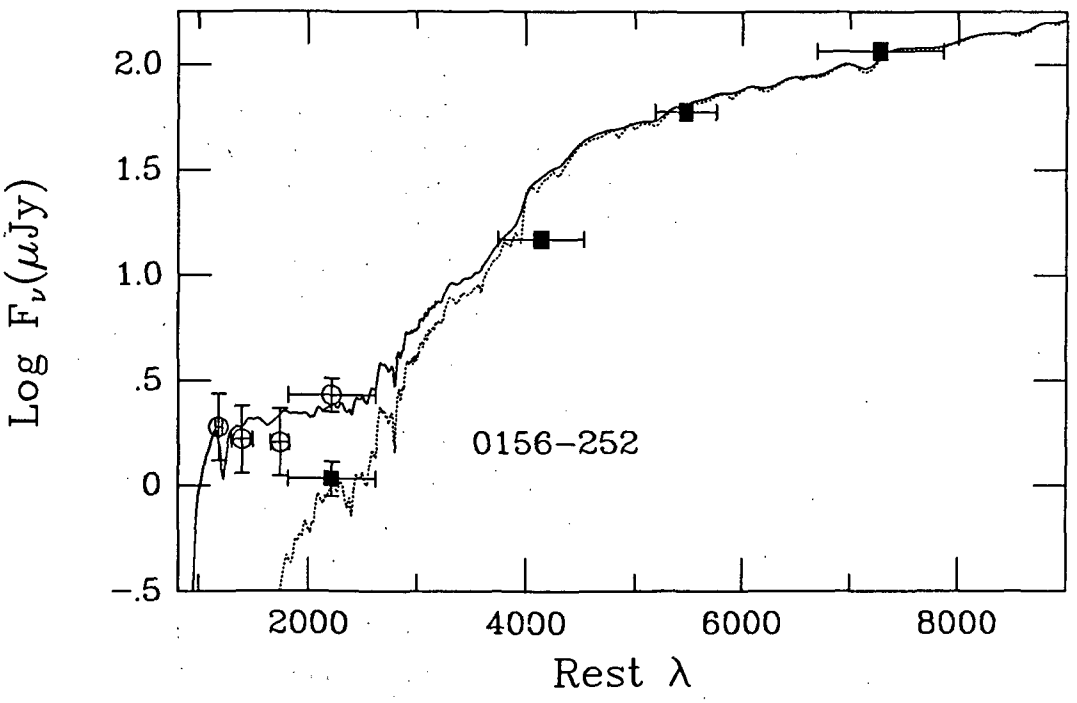

Figure 1. The SED of 0156-252 at a redshift of 2.02. The filled symbols refer to the compact near-IR core while the open symbols contain all of the light. The dotted line is a 2.8 Gyr old Bruzual C model. The solid line is the sum of this old galaxy SED and a zero age burst population.

Extremely Red Objects in the Fields of High Redshift Radio Galaxies

S. E. Persson, P. J. McCarthy, and Alan Dressler
Carnegie Observatories
and
Keith Matthews, Palomar Observatory

We are engaged in a program of infrared imaging photometry of high redshift radio galaxies (McCarthy, Persson, Elston, and Eisenhardt, this conference). The observations are being done using NICMOS2 and NICMOS3 arrays on the DuPont 100–inch telescope at Las Campanas Observatory. In addition, Persson and Matthews are measuring the spectral energy distributions of normal cluster galaxies in the redshift range 0 to 1. These measurements are being done with a 58x62 InSb array on the Palomar 5–m telescope. During the course of these observations we have imaged roughly 20 square arcminutes of sky to limiting magnitudes > 20 in the J, H, and K passbands (3 sigma in 3 square arcseconds). We have detected several relatively bright, extremely red, extended objects during the course of this work. Because the radio galaxy program requires Thuan–Gunn gri photometry, we are able to construct rough photometric energy distributions for many of the objects. Table 1 gives a sample of the galaxy magnitudes within 4 arcseconds diameter. All the detections are real; either the objects show up at several wavelengths, or in subsets of the data. The reddest object in the table, 9ab"B" was found in a field of galaxies in a rich cluster at z = 0.4; 9ab"A" lies 8 arcseconds from it.

TABLE 1 – RED "COMPANION" GALAXIES

Name	g	r	i	J	H	K	r-K	age (est)	z (est)	z (target)
0152-209	24.26	23.58	21.99	19.33	18.23	17.35	6.23	3 Gyr	0.8	1.89
+/-	0.45	0.24	0.10	0.06	0.04	0.05	0.25			
2139-292	23.34	23.34	21.93	19.91	18.78	18.18	5.16	2	1.0	2.55
	0.20	0.16	0.14	0.10	0.08	0.09	0.18			
9ab"A"	...	24.7	23.52	20.12	19.59	18.54	6.16	3	1.2	0.40
		0.3	0.15	0.20	0.20	0.10	0.25			
9ab"B"	...	>25.7	25.19	20.21	19.27	18.13	>7.5	3	1.8	0.40
		3σ	0.40	0.40	0.15	0.10				

Although there is insufficient information to show that these objects are galaxies at high redshift, such extreme IR-visible colors are difficult to reproduce without either a lot of reddening, or the large K-corrections associated with redshifts of order 1 or greater. The two extremely red objects in the 9ab field cannot be reproduced by an unreddened spectral energy distribution corresponding to present day galaxies of any Hubble type at the redshift of the 9ab cluster. The red objects found in the fields of the radio galaxies are as red, and often redder, than the radio galaxies themselves. Taking the K-correction explanation as a working hypothesis, we compare the spectral energy distributions with passively evolving single burst models from Bruzual (1985) to make a first estimate of their redshifts and star formation histories. The J-K and H-K colors alone constrain all four objects to have redshifts in excess of 0.5, even for very modest formation redshifts. Our objects fall quite close to the r-K vs. K relation derived for 3CR radio galaxies by Lilly *et al* (1985), suggesting redshifts between 1 and 2.5. Better redshift and age estimates can, in principle, be determined from fitting the entire SED with a Bruzual model, treating both z and the time since the burst (with a fixed 1 Gyr duration) as free parameters. Figure 1 shows a series of model energy distributions, for a burst lasting 1 Gyr, followed by passive evolution of the stellar population. The 4000 A break is the one feature that gives us some confidence in fitting the models to the data points. For both objects in the 9ab field the precipitous drop in the energy distribution between J and I provides a fairly robust lower limit to the redshifts. Lower bounds on z in the range of 0.8 - 1.2 are implied for all of the red companion galaxies.

While we are unable to determine if tne red companions to the radio galaxies are physically associated, and hence at the same redshift as the radio galaxies, their implied luminosities (of order 10L*) suggest that redshifts or order unity may be more likely. Thus our objects appear to be somewhat more extreme examples of the red field galaxies found by Cowie *et al* (1990) and Elston *et al* (1989). The statistics of our detection rate are uncertain, but are roughly consistent with those of the reddest objects of Cowie *et al.*

The combination of the redshift estimate and the stellar evolution timescale implied by the models leads, at face value, to fairly restrictive limits on either the formation redshift, the cosmology, or both. Even without allowing any time for gravitational accretion of material prior to the onset of the starburst, the formation redshifts implied for a a $q_o = 0.1$ and $H_o = 75$ cosmology are in the range 2 - 20. Formally, the onset of the burst responsible for 9ab"B" occurred at a z of 25. **Our basic result is that there do appear to be strong candidates for ordinary (non-radio) elliptical galaxies that have formed at very high redshifts.** This result supports the similar conclusion reached by Lilly (1989) for "1 Jansky" radio galaxies. In Lilly's (1989) K magnitude versus redshift diagram, our objects lie within the distribution, but systematically to the faint side of it. This is consistent with their being ordinary galaxies (i.e. not radio galaxies). Our estimates for z_f are consistent with those of Turner (1991), who argued from the existence of quasars at redshifts of four or greater that at least those quasars had to have formed at very high redshift. It is difficult to reconcile old stellar populations at high redshift with values of H_o near 100, or values of q_o near 0.5.

One possible way out of these conclusions is to invoke reddening to account for some part of the curvature of the SED, thereby lowering the passive evolution time estimates. To drop the age of 9ab"B" from 3 Gyr to 1 (2) Gyr, one would require a dereddening of 2.5 (1.0) magnitudes between rest frame wavelengths of 3000 and 4500 A, corresponding to an Av of 5 (2) magnitudes. For the latter value, and assuming the same redshift estimate, the formation redshift would be of order 5 and the luminosity would increase to 100 L*. Alternatively, the sharp drop in the energy distribution could be accounted for if the IMF of the stellar population were sharply bimodal, and that the galaxy was just old enough that all the high-mass stars have disappeared, leaving only a population of red giants and dwarfs.

With better SED data, it should be possible to further elucidate the nature of the red objects that have been found, and new ones that are certain to be found in the near future. Clearly, spectroscopic redshifts would remove much of the ambiguity in our constraints on z_f. However, on the basis of present data, the spectral energy distributions are consistent with the existence of high redshift quasars and radio galaxies, and provide evidence for galaxy formation at redshifts of order 10.

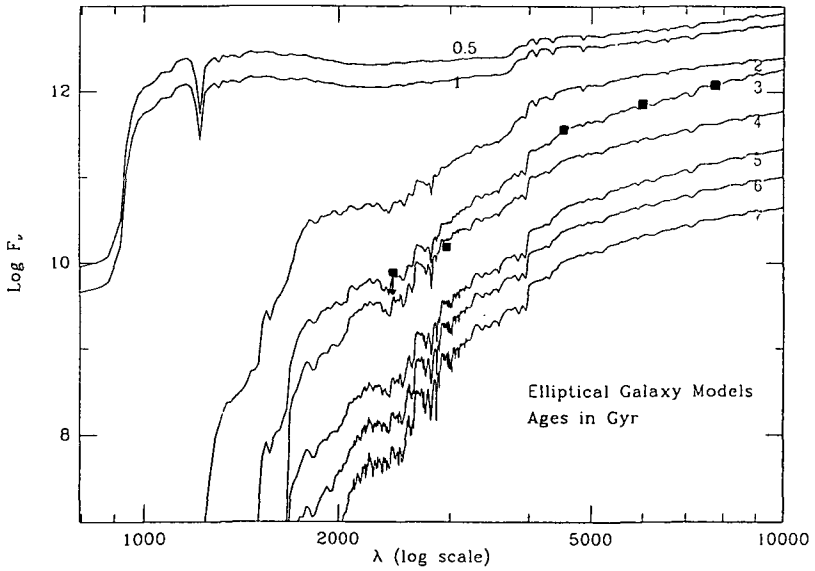

Figure 1. – Family of Bruzual C-model spectral energy distributions, with ages since the beginning of a 1 Gyr starburst indicated. The curves have been vertically shifted by arbitrary amounts for clarity. The data points refer to the reddest object in our sample – 9ab"B"; the data have been shifted horizontally and vertically to achieve a plausible fit to both the redshift and the age of the stellar population. Table 1 gives the resulting values.

Faint Blue Counts from Formation of Dwarf Galaxies at z≈1

ARIF BABUL[1] & MARTIN J. REES[2]
[1]*Canadian Institute for Theoretical Astrophysics, Toronto, Canada*
[2]*Institute of Astronomy, Madingley Road, Cambridge, UK*

1. Introduction.

The nature of faint blue objects (FBOs) has been a source of much speculation since their detection in deep CCD images of the sky (Cowie *et al.* 1988; Tyson 1988). Their high surface density argues against them being progenitors of present-day bright galaxies and since they are only weakly clustered on small scales (Efstathiou *et al.* 1992), they cannot be entities that merged together to form present-day galaxies. Babul & Rees (1992) have suggested that the observed faint blue counts may be due to dwarf elliptical galaxies undergoing their initial starburst at $z \approx 1$. In generic hierarchical clustering scenarios, however, dwarf galaxy haloes ($M \sim 10^9\,M_\odot$) are expected to form at an earlier epoch; for example, typical $10^9\,M_\odot$ haloes will virialize at $z \approx 2.3$ if the power-spectrum for the density fluctuations is that of the standard $b = 2$ cold dark matter (CDM) model. Under "ordinary conditions" the gas would rapidly cool, collect in the cores and undergo star-formation. Conditions at high redshifts are far from "ordinary". The intense UV background will prevent the gas in the dwarf haloes from cooling, the haloes being released from their suspended state only when the UV flux has diminished sufficiently.

2. Haloes in Stasis.

We begin by assuming that the redshift evolution and the spectrum (for frequencies greater than ν_L, the Lyman limit) of the intergalactic ionizing flux can be modeled as

$$J_{21}(z) = J_{21}\left(\frac{\nu_L}{\nu}\right)\left(\frac{1+z}{3}\right)^4 \times 10^{-21}\,(\nu_L/\nu)\ \mathrm{erg\,cm^{-2}\,Sr^{-1}\,Hz^{-1}\,s^{-1}}. \qquad (1)$$

Such a model is consistent with the limits for the UV flux derived from studies of the optical depth for the absorption of photons in a quasar spectrum shortward of $Ly\alpha$:

$J_{21} \gtrsim 1.6$ at $z \approx 2.6$ ($\tau \lesssim 0.05$, Steidel & Sargeant 1987)
$J_{21} \gtrsim 9$ at $z \approx 4.1$ ($\tau \lesssim 0.04$, Webb *et al.* 1992)

The UV background will photoionize the intergalactic medium, heating it to temperature $T \sim 3\times10^4$ K. Under such conditions, baryons in virialized dark haloes with $V_c \approx 30\,\mathrm{km\,s^{-1}}$ will be stably confined, neither able to escape not able to collapse.

Inside the halo, the gas will be in ionization equilibrium: $dn_R/dt = dn_I/dt$, where

$$\frac{dn_R}{dt} \approx 4.36\times10^{-13}\left(\frac{T}{10^4\,\mathrm{K}}\right)^{-3/4}\Omega_b^2\left[\frac{\rho_x(r)}{\mu_H m_p}\right]^2[1-\chi(r)]^2\,, \qquad (2a)$$

$$\frac{dn_I}{dt} \approx 4\pi\Omega_b\left[\frac{\rho_x(r)}{\mu_H m_p}\right]\chi(r)\int_{\nu_L}^{\infty}\frac{\sigma_\nu J_\nu e^{-\tau_\nu(r)}}{h\nu}\,d\nu. \qquad (2b)$$

In the above equations, $\chi(r)$ is the neutral fraction, $\sigma_\nu = 6.7\times10^{-18}(\nu_L/\nu)^3\,\mathrm{cm^{-2}}$ is the ionizing cross-section for hydrogen, and $\tau_\nu(r) = \int_r^R n_{HI}(r)\sigma_\nu\,dr$ is the optical depth for absorption for photons penetrating from the surface.

3. Epoch of Dwarf Galaxy Formation

As the background UV flux intensity decreases with redshift, the gas in the central regions of the haloes will become increasing neutral. To determine the corresponding epoch, we model the virialized dark haloes as a truncated isothermal sphere of radius R, with a core of radius r_c such that $r_c \approx 1\,\mathrm{kpc}$:

$$\rho_x(r) = \begin{cases} \rho_{xo}(R/r_c)^2, & \text{if } 0 \le r \le r_c \\ \rho_{xo}(R/r)^2, & \text{if } r_x \le r \le R, \end{cases} \tag{3}$$

where z_v is the redshift of virialization,

$$\rho_{xo} \approx 7.5\times10^{-27} h_{50}^2 \left(\frac{1+z_v}{3}\right)^3 \mathrm{g\,cm^{-3}}, \quad \text{and} \quad R \approx 12.2 h_{50}^{-1} \left(\frac{V_c}{30\,\mathrm{km\,s^{-1}}}\right)\left(\frac{1+z_v}{3}\right)^{-3/2} \mathrm{kpc},$$

The density distribution of the stably confined gas is $\Omega_b \rho_x(r)$.

Solving the equation for ionization equilibrium at each radii, we find that gas in a $V_c \approx 30\,\mathrm{km\,s^{-1}}$ halo that virialized at $z_v \approx 2$ (as in the standard $b = 2$ CDM model) will develop a warm ($T \sim 10^4$) neutral centre ($\chi \approx 0.95$) soon after virialization. Further cooling of a neutral metal-poor gas is only possible if H_2 molecules form. The declining intensity of the UV flux coupled with the increasing efficiency in shielding of the central regions suggests that by $z \approx 1.2$ the conditions for the formation of molecular hydrogen will be in place. As noted by Shapiro & Kang (1987), the gradual onset of shielding from the ionizing radiation will, in fact, enhance the formation of H_2 molecules. Cooling by H_2 molecules will cause the temperature to rapidly plummet down to to $\sim 10^2\,\mathrm{K}$, allowing the central regions to collapse.

Meanwhile, the hot gas in the ionized envelope will remain in hydrostatic equilibrium until an expansion wave signaling the loss of pressure-support due to the collapse of the neutral region propagates upstream. The response of the envelope under such conditions has been studied by Shu (1977). The envelope will collapse in $\Delta t \approx 8\times10^8\,\mathrm{yr}$. If the gas experience starburst upon collapse, the projected epoch of starburst is $z \approx 1$.

References

Babul, A. & Rees, M.J., (1992), *M.N.R.A.S*, **255**, 346.
Cowie, L.L., Lilly, S.J., Gardner, J.P. & McLean, I.S. (1988), *Astrophys. J.*, **332**, L29.
Efstathiou, G., Berstein, G., Katz, N., Tyson, J.A. & Guhathakurta, P. (1991) *preprint.*
Shapiro, P.R. & Kang, H., (1987), *Astrophys. J.*, **318**, 32.
Shu, F.H., (1977), *Astrophys. J.*, **214**, 488.
Steidel, C.C. & Sargeant, W.L.W., (1987), *Astrophys. J.*, **318**, L11.
Tyson, J.A. (1988), *Astron. J.*, **96**, 1.
Webb, J.K., Barcons, X., Carswell, R.F. & Parnell, H.C., (1992), *M.N.R.A.S*, **255**, 319.

Low Surface Brightness Galaxies and Tidally Triggered Star Formation

Dennis Zaritsky[1,2] and Stephen J. Lorrimer[3]

[1]The Observatories of the Carnegie Institution of Washington,
813 Santa Barbara St., Pasadena, CA 91101

[3] Dept. of Physics, South Road, Univ. of Durham, Durham, DH1 3LE, England

ABSTRACT

We present counts of companions to LSB galaxies and compare these to counts of companions to normal galaxies obtained with the same techniques and criteria. Our results are consistent with LSB's having no clustered companions and support the hypothesis that LSB galaxies have low star-formation rates because they lack external tidal triggering.

Despite the typically large distance between galaxies, interactions and collisions appear to be fairly frequent. The theorized effects of such interaction have been used to explain a wide variety of phenomena including the morphology-density relationship (Dressler 1980), the ultra-luminous IR galaxies (Sanders *et al.* 1986), and the formation of cD galaxies (Ostriker and Tremaine 1975). There is strong evidence that, if gas is present, interactions, especially direct collisions, enhance star-formation rates (cf. Sanders *et al*, and Solomon and Sage 1988). Such observations suggest that galaxies with low star-formation rates may be lacking tidal triggering.

Most galaxy surveys are strongly biased against finding low surface brightness (LSB) galaxies. However, there have been several attempts to conduct surveys specifically designed to find them (cf. Schombert and Bothun 1988, and Schneider *et al.* 1990). As a result, there now exist catalogs with significant numbers of galaxies with low lifetime-averaged star-formation rates. By comparing the number of nearby galaxies (companions) to low star-formation galaxies vs. the number of companions to normal galaxies we can test the interaction hypothesis. Our low star-formation rate sample will consist of selected galaxies from a LSB galaxy survey, while our control sample will consist of selected spirals and ellipticals from the CfA catalogue (Huchra 1991).

We have used photographic plates, scanned by the Automatic Plate Measuring machine at Cambridge, to measure the number of companions around galaxies. Since each galaxy, regardless of whether it is LSB or normal, has few companion galaxies, this study must be done statistically. Such an analysis was first conducted for normal spirals by Holmberg (1969) and more quantitatively by Lorrimer *et al.* 1992. For our study of LSB galaxies, we have used as our set of primary galaxies the LSB galaxy sample being developed by D. Sprayberry and C. Impey. The galaxies in this sample are unfortunately somewhat heterogeneous, but they are all brighter than $M_B = -16$ with a peak in the distribution near $M_B = -19$. The sample includes irregulars, some ellipticals, and a few extreme disk galaxies similar to Malin 1 (C. Impey, priv. comm.).

The analysis techniques are described fully by Lorrimer *et al.*, who also presented measurements on the number of companions per normal galaxy. Basically, the technique involves estimating the background level of galaxies from galaxy counts at a large distance from the primary and subtracting this background level from the counts obtained near the primary. The residual is attributed to companions. There are subtleties regarding possible fluctuations of the background level across the sky and the effects of vignetting and plate edges, which we have investigated by using several tests. The most powerful and elegant test involves random removal of certain plates from consideration. This test investigates whether specific plates are dominating the results. No peculiarities were found. A second test involves counting the "companions" around a set of randomly chosen centers. Since there is no primary at this position, the number of companions should be zero. Many such randomly positioned centers are investigated to evaluate uncertainties. These and other tests are fully described by Lorrimer *et al.*.

We present our results for the number of companions brighter than $M_B = -16$ per galaxy, for normal and LSB galaxies, and for random centers, outside 20 kpc and within either 250 kpc, 500 kpc, or 1 Mpc in Table 1. Note that the number of companions to LSB galaxies is consistent with zero within all three radii. In comparison, the numbers for the normal galaxies are all inconsistent with zero companions and are all

[2]Hubble Fellow.

Table 1: Number of Companions Within Projected Radius per Galaxy

Radius	Normal Galaxies	LSB Galaxies	Random Centers
250 kpc	1.66 ± 0.17	0.22 ± 0.38	-0.009 ± 0.046
500 kpc	3.67 ± 0.41	-0.1 ± 1.4	0.01 ± 0.17
1 Mpc	9.91 ± 0.77	2.4 ± 4.8	-0.14 ± 0.59

greater than the measurements for the LSB galaxies by more than 1σ. Finally, note that the results from the random-center simulations indicate that there are no systematic problems with background subtraction.

The effect of companions on star-formation has been discussed by Icke (1985) and by Lacey and Silk (1991). We recount a simple argument that suggests that companions can produce significant perturbations on the ISM of the primary galaxy. For an impulsive encounter, the magnitude of the typical velocity impulse given in the center-of-mass frame of the affected mass is estimated from a combination of the resulting acceleration and the time over which the force is applied:

$$\Delta v \sim \frac{2GM_p r}{R^2 v_p}$$

(cf. Binney and Tremaine §7.2), where M_p is the mass of the perturber, r is the radius of the primary, R is the pericenter distance, and v_p is the relative velocity of the encounter. For a plausible combination of parameters ($M_p = 10^{11} M_\odot$, $R = 100$ kpc, $r = 15$ kpc, and v_p =300 km s^{-1}) the resulting change in velocity is 5 km s^{-1}. Since such disturbances are of order the sound speed in the ISM, it is plausible to presume that they may affect star formation rates. Although not every companion will have significant impact on the primary (in fact small companions that are not on eccentric orbits will probably not have a noticeable effect), many of the companions identified could create velocity disturbances in the disk of order a few km s^{-1}.

We have shown that LSB galaxies have fewer nearby neighbors down to $M_B = -16$ than do normal surface brightness galaxies. An analogous conclusion regarding bright neighbors was reached by Knezek and Schneider (1992). We believe that this result supports the contention that interactions are an important agent for star-formation, although other interpretations cannot be ruled out. The sample of LSB's is still small and heterogeneous. The most interesting subsample is that of the Malin 1-type disks. A study of companions around those galaxies, once the sample is greatly enlarged, should be a strong test of the interaction hypothesis.

DZ acknowledges financial support from NASA through grant HF-1027.01-91A from STScI, which is operated by AURA, Inc., under NASA contract NAS5-26555. SJL acknowledges receipt of a SERC studentship. The authors also thank C. Impey and D. Sprayberry for access to their unpublished sample of LSB galaxies.

References

Binney, J. & Tremaine, S. 1987, Galactic Dynamics (Princeton: Princeton University Press).
Dressler, A. 1980, *Ap. J.*, **236**, 351.
Holmberg, E. 1969, *Ark. Astr.*, **5**, 305.
Huchra, J. 1991, *The CfA Redshift Catalogue.*
Icke, V. 1985, A&A, **144**, 115.
Impey, C. & Bothun, G. 1989, *Ap. J.*, **341**, 89.
Knezek, P. M, & Schneider, S. E. 1992, these proceedings.
Lacey, C. & Silk, J. 1991, *Ap. J*, **381**, 14.
Lorrimer, S., Frenk, C.S., Smith, R. M., White, S.D.M., & Zaritsky, D. 1992, in prep.
Ostriker, J.P., & Tremaine, S.D. 1975, *Ap. J. (Letters)*, **202**, L113.
Sanders, D.B., *et al.* 1988, *Ap. J.*, **325**, 74.
Schneider, S.E., Thuan, T.-X., Magri, C., & Wadiak, J.E. 1990, *Ap. J. Supp.*, **72**, 245.
Schombert, J.M, & Bothun, G.D. 1988, *A.J.*, **95**, 1389.
Solomon, P.M., & Sage, L.J. 1988, *Ap. J.*, **334**, 613.

MASSIVE LOW SURFACE BRIGHTNESS GALAXIES

by

Patricia M. Knezek and Stephen E. Schneider (UMass – Amherst)

We have completed a multi-wavelength study of an extreme type of galaxy which will assist us in our attempts to understand the formation and evolution of galaxies. In particular, we have observed a subset of low surface brightness ($\overline{\mu}_B \gtrsim 25\,\mathrm{mag\,arcsec^{-2}}$), giant galaxies (LSBGs) which contain large amounts of atomic gas ($\mathrm{M(H\,I)} \gtrsim 10^{10}\,\mathrm{M_\odot}$), have blue optical diameters similar to those of giant spiral galaxies ($\mathrm{D_{25}} \gtrsim 30\,\mathrm{kpc}$), but which do not seem to have prodigious amounts of ongoing star formation. Our sample was drawn from the first and second Palomar Sky Surveys. This population of galaxies has been largely ignored because of selection effects which make it difficult to detect optically. We address the question of how these massive systems differ from the higher surface brightness 'normal' spiral galaxies. Using B and R surface photometry, in conjunction with Hα, H I, ^{12}CO and far-infrared data, we attempt to determine if these galaxies had an early epoch of star formation that has since faded, have ongoing star formation with an unusual IMF, or are perhaps galaxies which have never efficiently formed stars due to a lack of molecular clouds.
Preliminary results of our observations indicate that:

- LSBGs show a variety of optical morphologies, ranging from well-ordered spiral systems to patchy irregulars with no obvious nuclei.

- LSBGs in general have very blue disks ($< B - R > \sim 0.8$) relative to higher surface brightness, actively star-forming systems.

- LSBGs have $B - R$ color gradients ~ 0.5 mag in their disks in the sense that the disks get bluer with distance from the nucleus.

- LSBGs have little Hα emission, and H II regions which are present are weak, and generally far out in the disk.

- LSBGs have low metallicites, $\sim 1/5$ solar, but there has been some chemical enrichment.

- LSBGs have H I linewidths, which along with their optical images, suggest they have dynamical masses similar to high surface brightness giant spirals (HSBGs).

- LSBGs have H I fluxes similar to HSBGs with the same optical size, and the H I does not appear to extend well beyond the optical disk. Thus, they have H I surface densities which are $\sim 10^{21}\,\mathrm{atoms\,cm^{-2}}$, similar to HSBGs.

- LSBGs have little FIR and ^{12}CO emission.

- LSBGs have a significantly lower fraction of massive neighbors than do HSBGs.

We conclude that the evidence collected to date is inconsistent with a scenario of LSBGs as faded disk remnants. We suggest that LSBGs represent a population of galaxies which have had inhibited star formation and slowly evolving disks, perhaps due to their relative isolation in the universe. Thus, in a global context, star formation in disks is partly an environmentally driven phenomena. The determination of the true frequency and distribution of these systems is of interest, since they could represent a significant fraction of the baryonic matter in the universe.

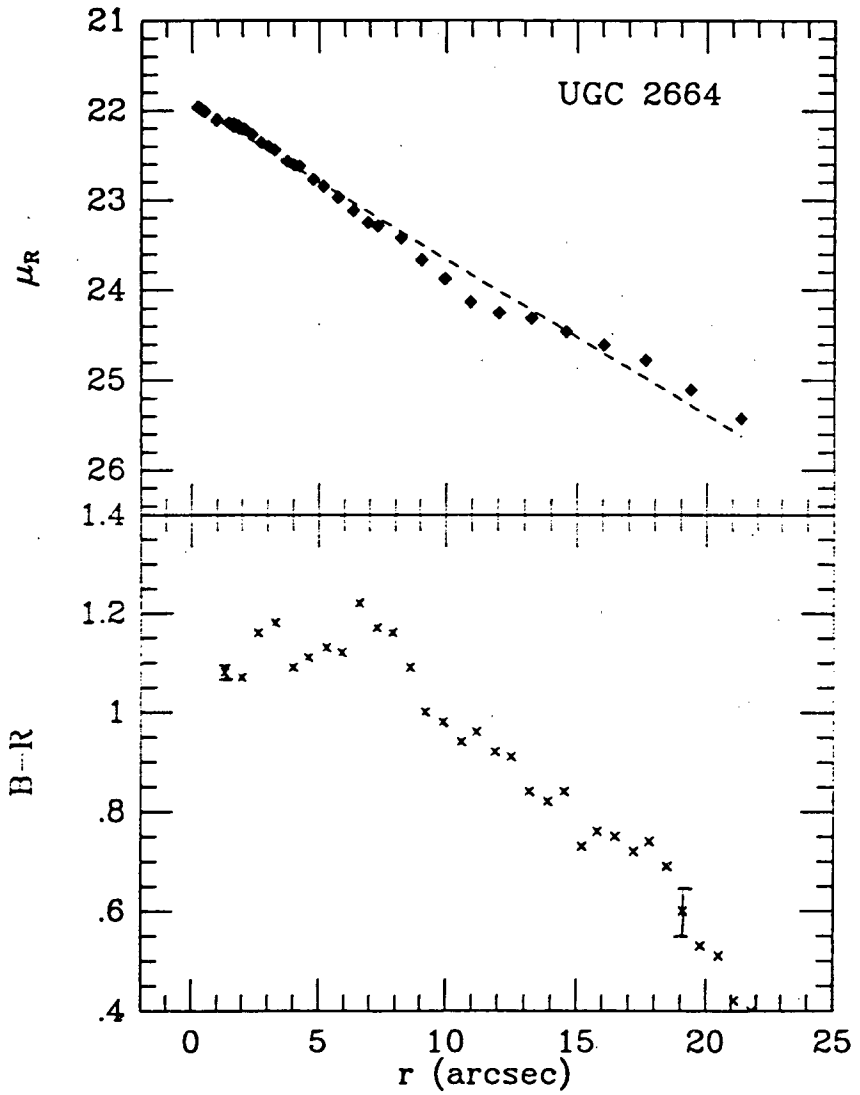

Figure 1 is the R surface brightness in mag/arcsec^{-2} vs. radius (top), and azimuthally averaged $B-R$ colors vs. radius (bottom) for the LSBG galaxy UGC 2664. The statistics for this galaxy are: $B_T = 18.0$:, $v_\odot = 6067\,km\,s^{-1}$, $w_{50} = 147\,km\,s^{-1}$, $M(HI) \sim 10^{10}\,M_\odot$, $\mu_B \sim 27\,mag\,arcsec^{-2}$, and $D_{25} \sim 50\,kpc$. All of these numbers assume $H_0 = 50\ km\,s^{-1}$ Mpc^{-1}.

OXYGEN ABUNDANCES IN LOW SURFACE-BRIGHTNESS GALAXIES*

Jari Rönnback, Astronomiska Observatoriet, Box 515, S-751 20 Uppsala, SWEDEN

INTRODUCTION

Recent theories[1,2] predict that some protogalaxies, in low-density environments of the field, are contracting and interacting so slowly that global star formation can be delayed until today. These systems should be gas rich and have low surface-brightness. Blue compact galaxies (BCGs), and other compact HII region galaxies currently experiencing a burst of star formation, are good candidates of truly young galaxies (in the sense that global star formation recently has been initiated). If they really are young, they ought to have a recent phase when their brightness was much lower than in the bursting phase. No claims of observations of such proto-BCGs exist. Observations of galaxies in their juvenile phases would undoubtedly be of great interest, e.g. the determination of the primordial helium abundance would improve. A proper place to search for young nearby galaxies could be among blue low surface-brightness galaxies (BLSBGs) in the local field.

The study of low surface-brightness galaxies (LSBGs) as a group began relatively recently. They are galaxies with extraordinary properties both as individuals[e.g.3,4] and as a group[e.g.5]. A few years ago we started an optical study of a sample of BLSBGs[6] (the sample galaxies have B-R < 0.5; typical B-R for normal E-Sdm types range from 1.7-0.9[7]) selected from the ESO/Uppsala catalogue. Here I report results of spectroscopic observations obtained on a subsample - 8 galaxies - of our selection. The HII region oxygen chemical abundances and its relation to the blue absolute magnitude and surface-brightness is investigated.

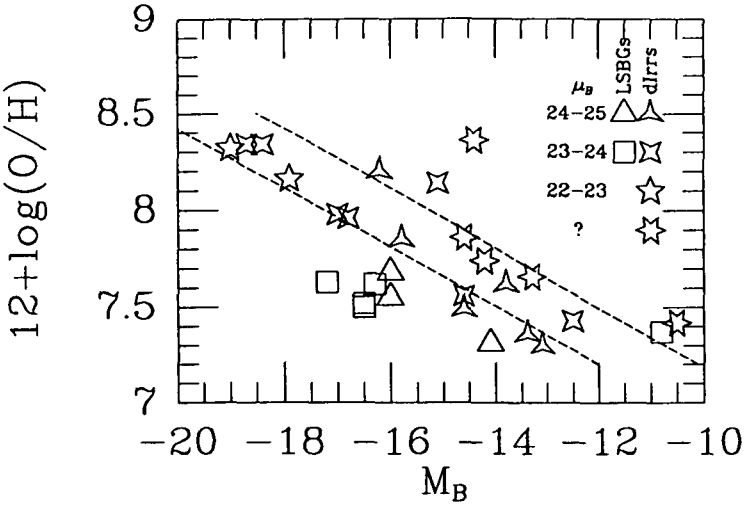

Figure 1. Absolute blue magnitude (M_B) - oxygen abundance (12+log(O/H)) plot, for nearby dwarf irregulars[11] (stars) and our data (triangles and squares). The uncertainties are 0.3-0.4 mag. at constant 12+log(O/H) and 0.2-0.3 dex at constant M_B. The dashed lines corresponds to the 1σ deviations of the nearby dwarf sample. Different symbols indicate the mean surface-brightness in mag. arcsec^{-2} (μ_B; the average surface-brightness inside the 25 mag. arcsec^{-2} B isophote).

OBSERVATIONS

We have obtained EFOSC spectra of 8 galaxies at the 3.6m telescope at ESO in 1989 and 1992. The wavelength region studied was 3700-7000 Å in low-dispersion mode. The resulting resolution using a slit $\sim$ 1.5 arcsecons wide is $\sim$ 13 Å. Integration times ranged from 900 to 10800 seconds.

* Based on observations collected at the European Southern Observatory, La Silla, Chile

The magnitudes[8] are from CCD imagery at the Danish 1.5m and the 2.2m telescopes at ESO in 1989 and 1991, and from the 2.5m Nordical Optical Telescope at La Palma in 1990.

The galaxies display low surface-luminosity nebular emission regions. They have distances of 2-40 Mpc and dimensions $\sim$ 1-30 kpc (however, $\sim$ 75 % of the galaxies have distances $\sim$ 20 Mpc and dimensions $\sim$ 10 kpc).

OXYGEN ABUNDANCES

The majority of the galaxies are to faint to show the [OIII]λ 4363 emission line, which is necessary for the derivation of the electron temperature (and subsequently the chemical abundances). Instead I use the empirical method[9,10], based on the $R_{23} = (\lambda 3727+\lambda 4959+\lambda 5007)/H\beta$ ratio, to estimate the oxygen abundance. This method should yield a 12+log(O/H) determination with an accuracy of 0.2 dex, for low abundance regions[10].

The global empirical HII region oxygen abundances of the eight galaxies thus derived (2, 3, 4, 4, 4, 5, 6 and 6 per cent of the solar) are very low for galaxies of their type. This becomes apparent if we compare them with nearby dwarf irregulars[11] in an absolute blue magnitude - oxygen abundance diagram (Fig 1.). Most of our objects lie well below the relation seen for the dwarfs (the dashed lines corresponds to the 1σ deviation for the dwarfs). One explanation for the observed M-Z relation is that the gas is expelled in dwarfs, due to supernova and stellar winds. The location of the BLSBGs in the diagram seems to speak against this scenario. It has been proposed[12] that a surface brightness - metallicity relation is more indicative of the chemical status of a galaxy than the M-Z relation is. As can be seen in Fig. 1 (where different symbols indicate the surface brightness) there is some tendency for higher surface-brightness galaxies to have a higher abundance. But such a relation is apparently insufficient to explain the large overall dispersion in the M-Z plane, it seems as if another parameter must be taken into account. Conditions rarely considered are the star formation history or the age of the stellar populations.

In two of the three galaxies where the [OIII]λ 4363 emission line could be measured we find that the abundance is a factor of $\sim$ 2 higher compared to the empirical values. This may be due to lower effective temperatures (T_{eff}), of the stars in the HII regions, than we assumed (the derived abundance, at constant R_{23}, in low abundance HII region models[10] depends on T_{eff}). A high mass cut off in the IMF would lower the T_{eff}. Low column densities of the gas, a condition expected in LSBGs, could make massive star formation inefficient[13].

CONCLUSIONS

The eight blue low surface-brightness galaxies studied all have empirical oxygen abundances below 7% of the solar value, in a few cases approaching the lowest values ever found for galaxies of their size. They break the tight M-Z relation for nearby dwarf irregulars. Their low abundances could be due to either galaxy youth or an anomalous star formation history. However, preliminary comparisons, for a few galaxies, of the BV*i* colours with spectral evolutionary models[14] result in ages > 2 Gyrs.

References

1. Lacey C., Silk J., 1991, ApJ 381, 14
2. Hoffman Y., Silk J., Wyse R., 1992, ApJ 388, L13
3. Bothun et al., 1987, AJ 94, 23
4. Salzer J. et al, 1991, AJ 101, 1258
5. Schombert J. et al., 1992, AJ 103, 1107
6. Bergvall N., Rönnback J., 1990, "A search for blue low surface-brightness galaxies" in Nordic-Baltic Astronomy Meeting, 71, eds Lagerkvist, Kiselman & Lindgren
7. Stevenson P., 1988, PhD thesis, university of Durham
8. Rönnback J., Bergvall N., 1992, in preparation
9. Pagel B. et al., 1979, MNRAS 189, 95
10. Skillman E., 1989, ApJ 347, 883
11. Skillman et al., 1989, ApJ 347, 875
12. Phillips et al., 1990, MNRAS 244, 168
13. Kennicutt R.C., 1989, ApJ 344, 685
14. Bergvall N., in preparation

CHEMICAL ABUNDANCES IN LOW SURFACE BRIGHTNESS GALAXIES: IMPLICATIONS FOR THEIR EVOLUTION

S. McGaugh and G. Bothun

Low Surface Brightness (LSB) galaxies are an important but often neglected part of the galaxy content of the universe. Their importance stems both from the selection effects which cause them to be under-represented in galaxy catalogs, and from what they can tell us about the physical processes of galaxy evolution that has resulted in something other than the traditional Hubble sequence of spirals. An important constraint for any evolutionary model is the present day chemical abundances of LSB disks. Towards this end, we have obtained spectra for a sample of 75 H II regions distributed in 20 LSB disks galaxies. Structurally, this sample is defined as having B(0) fainter than 23.0 mag arcsec^{-2} and scale lengths that cluster either around 3 kpc or 10 kpc. In fact, structurally, these galaxies are very similar to the high surface brightness spirals which define the Hubble sequence. Thus, our sample galaxies are not dwarf galaxies but instead have masses comparable to or in excess of the Milky Way. The basic results from these observations can be summarized as follows:

• Despite having disk masses similar to those galaxies which define the Hubble Sequence, LSB galaxies have substantially subsolar abundances. Specifically, 90% of the measured H II regions have $\log(O/H) < -3.6$.

• The LSB galaxies with the lowest metallicities are as low as any known extragalactic objects with the exception of I Zw 18 and SBS 0335 − 052. It is possible that objects with $\log(O/H) \leq -4.3$ are undergoing their first episode of star formation. The very blue continuum colors (particularly B-I) of these objects would support this.

• Although quite metal poor, these LSB disks do not cluster around any preferred value of O/H indicating a broad spectrum of enrichment timescales/star formation histories.

• Despite being quite deficient in molecular gas (e.g., CO) some star formation is occurring. The H II region luminosities/sizes indicate ionization by several stars with $M \geq 60\ M_{\odot}$. The distribution of the Balmer decrement indicates that some dust is present in these systems.

• Unlike the case for HSB galaxies, there is no correlation between the H II region ionization parameter (U) and the oxygen abundance. This argues that the observed correlation is a selection effect associated with only measuring the brightest (or most conspicuous) H II regions. Studies of more diffuse H II regions in normal galaxies would then remove the apparent correlation.

• Most H II regions in LSB galaxies have low values for the ionization parameter indicating that star formation is occurring in a more diffuse environment in these diffuse galaxies.

• The Nitrogen abundance in LSB galaxies is independent of the Oxygen abundance over an order of magnitude range in O/H. This unprecedented situation suggests an anamolous IMF as Nitrogen is mainly produced as a secondary product in the CNO cycles of 2-8 $M_\odot$ stars and oxygen is produced in more massive stars. This is the most curious aspect of the data which defies any current model.

• A well defined abundance floor exists for Sulfer and Neon, and, like Nitrogen, they exhibit an extremely weak dependence on O/H.

Selecting galaxies for low surface brightness obviously is an effective means for discovering low metallicity objects. Furthermore, the data indicate a substantially different element enrichment history that is adhered to by Hubble sequence spirals. In fact, the N,O,S,Ne abundance ratios which are observed practically demand a pre-enriched source of gas, which produced most of the N,S and Ne in order to keep their levels independent of O, despite the galaxies' best attempt to evolve. Alternatively, the IMF could be skewed in non-standard directions – a situation which generally will produce a LSB, high M/L galaxy. Finally, it seems clear that the low degree of chemical evolution shown by this sample confirms earlier speculation that LSB disks evolve rather slowly over a Hubble time. Indeed, the low abundances coupled with the very blue continuum disk colors argue that the mean ages of these systems must be rather young. Given the lack of CO emission, it would seem that the surface density of H I, at the time of formation, is the critical parameter which determines the evolutionary timescale. That LSB galaxies can remain relatively unevolved to the present epoch implies that selection effects may mask the true range of galaxy properties. Undoubtedly, there are more LSB galaxies awaiting discovery with even more extreme properties than those discussed here which may provide even more profound challanges of our understanding of galaxies and their evolution; hopefully this will require a future meeting near these mountains.

H II Regions in the Dwarf Galaxy UGC-A 86

Bryan W. Miller and Paul Hodge
University of Washington, Seattle, WA 98195

The uncertain nature of the dwarf irregular galaxy UGC-A 86 (VIIZw009) makes it a very interesting object for studying star formation at the low end of the galaxy luminosity function. Saha and Hoessel (1991) find that this object is composed of two main parts, one of which appears more resolved than the other. The more resolved component has an excess of blue stars, suggesting that it is currently undergoing star formation. Thus, they argue that UGC-A 86 could be either a superposition of unrelated galaxies, two interacting galaxies, or a single galaxy. However, surface photometry performed by Richter *et al.* (1991) indicates that it is a single galaxy with an exponential luminosity profile. Richter *et al.* also find UGC-A 86 to be extremely dusty and to be associated with the infrared source IRAS 3550+6657. The uncertainty is compounded by the large ambiguity in the distance, though a heliocentric H I velocity of 80 ± 7 km s^{-1} (Huchtmeier & Richter 1989) suggests that it is either a member of the Local Group or perhaps the IC 342 group. In this work we adopt a distance of 1.5 Mpc and a reddening of $E(B-V) = 0.65$.

We have observed UGC-A 86 in Hα in order to measure its current star formation rate. This is part of a larger project to study the star formation rates and histories of a complete sample of dwarf galaxies in the Local Group and other nearby groups. In this paper we present the H II region luminosity function and size distribution for UGC-A 86 and compare them with previous observations of similar dwarf galaxies.

Hα and continuum CCD images of UGC-A 86 were obtained with the KPNO 0.9-m telescope on December 13, 1991. The Hα image was taken through a 38 Å half-power bandwidth interference filter centered on 6569 Å while the continuum image was taken through a filter centered on 6092 Å. Observations of BD+28 4211 provided absolute flux calibration. We attempted to match the point-spread functions in the two images to get the optimum continuum subtraction. Also, to aid our identification of the H II regions we enhanced the calibrated Hα image using an unsharp masking technique developed by Drew Phillips.

We have identified a total of 114 H II regions in UGC-A 86. Fluxes for each region were measured inside the isophote corresponding to 2×10^{-17} erg cm^{-2} s^{-1} arcsec^{-2}. The effective diameter of an H II regions is defined by $D = 2\sqrt{Area/\pi}$. The cumulative diameter distribution is shown in Figure 1. We find that the diameter distribution is fairly well described by the exponential law $N(>D) = N_0 \exp(D/D_0)$. A least-squares fit to the binned data (for $D > 29$ pc) yields $D_0 = 19 \pm 1$ pc. Use of the maximum likelihood method (Ye 1992), for which the data does not need to be binned, gives $D_0 = 20 \pm 2$ pc, which is similar to D_0 for the irregular galaxies NGC 1569 and Ho II (Hodge 1983)

The Hα luminosity function is shown in Figure 2. The upper end of the luminosity function is consistent with a power law distribution $N(L) = AL^a dL$. A least-squares fit to the upper end of the luminosity function gives $a = -2.0 \pm 0.2$. This is slightly steeper than average for dwarf irregular galaxies but is not inconsistent with previous values of a between -1.5 and -1.8 (Strobel *et al.* 1991).

A complex of H II regions is found at each of the components identified by Saha and Hoessel. In fact, half of the total Hα luminosity, $L_{H\alpha} = 9 \times 10^{38}$ erg s^{-1}, comes from the southeast component. This supports their inference that UGC-A 86 is currently undergoing star formation. Our detection of Hα regions over the entire optical extent of the galaxy suggests that this is not a chance superposition of galaxies. Accurate optical or H I velocities should be able to distinguish whether this is one galaxy or an interacting pair. Future work should also include a search for Cepheids or planetary nebulae in order to resolve the uncertainty in the distance, and spectroscopy of the bright H II regions in order to determine the abundances.

REFERENCES

Hodge, P. W. 1983, AJ, 88, 1323

Huchtmeier, W. K. & Richter, O. G. 1989, A General Catalog of H I Observations of Galaxies (Springer, New York)

Richter, G. M., Schmidt, K.-H., Thänert, W., Stavrev, K. & Panov, K. 1991, Astron. Nach., 312, 309

Saha, A. & Hoessel, J. G. 1991, AJ, 101, 465

Strobel, N. V., Hodge, P. & Kennicutt, R. C. 1991, ApJ, 383, 148

Ye, T. 1992, MNRAS, 255, 32

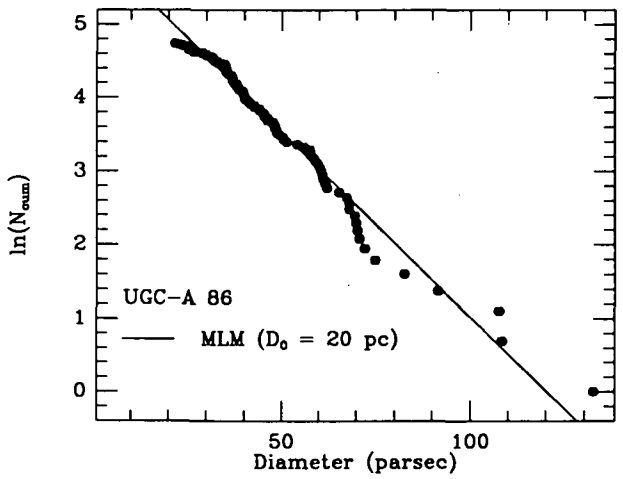

Fig. 1: Cumulative diameter distribution.

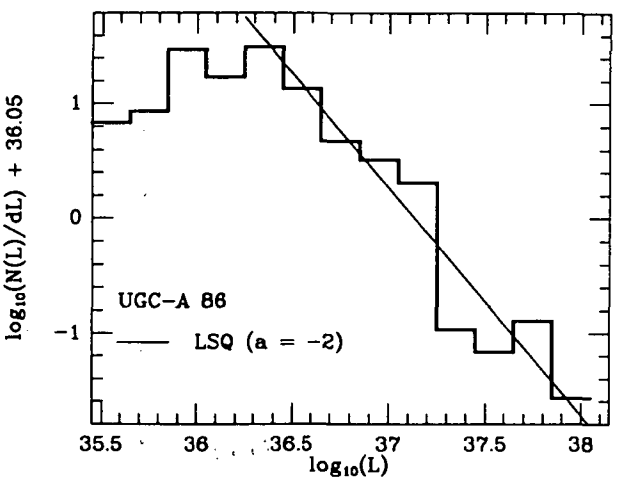

Fig. 2: HII region luminosity function.

Low Surface Brightness Galaxies

J. M. van der Hulst and W. J. G. de Blok

Kapteyn Astronomical Institute
Univ. of Groningen

S. S. McGaugh

Astronomy Department
Univ. of Michigan

G. D. Bothun

Astronomy Department
Univ. of Oregon

Abstract. A program to investigate the properties of low surface brightness galaxies involving surface photometry in U, B, V, R, I and Hα, HI imaging with the WSRT and the VLA and spectrophotometry of HII regions in LSB galaxies is underway. The goal is to verify the idea that LSB galaxies have low star formation rates because the local gas density falls below the critical density for star formation, and to study the stellar population and abundances in LSB galaxies. Such information should help understanding the evolutionary history of LSB galaxies. Here we report some preliminary results.

Introduction and Observations.

Low Surface Brightness (LSB) galaxies are galaxies whose light distribution is dominated by an exponential disk, which does not reach the canonical 21.6 mag arcsec $^{-2}$ central surface brightness that normal galaxies appear to exhibit (Freeman 1970, see also van der Kruit 1987). LSB galaxies have central surface brightnesses that are typically 1 - 2 mag arcsec $^{-2}$ fainter, and have a very low current star formation activity. Studies to date of a few LSB galaxies appear to favor the idea that after an initial phase of global star formation LSB galaxies have not been actively forming stars for the last few billion years and are just faded disks. The low gas densities found in a few cases (van der Hulst et al. 1987) and probably low metallicities (Webster et al. 1983, McGaugh 1992) support this idea.

In order to quantify more systematically the current gas content, star formation rate and stellar population we began a systematic program to observe a sample of about 20 galaxies in U, B, V, R, I and Hα at the 2.5-m Isaac Newton telescope at la Palma, and in the 21-cm HI line with the Westerbork Synthesis Radio Telescope (WSRT) and the Very large Array (VLA). In addition we recently obtained spectra of HII regions in about 10 LSB galaxies using the 4.3-m William Herschel Telescope at la Palma to estimate abundances. The 20 galaxies have been drawn from the new samples of Schombert and Bothun (1988) and Schombert et al. (1992).

Results and Discussion.

The HI distributions are fairly normal, but exhibit low peak column densities. Typical values are 4 - 8 $M_\odot$ pc^{-2}, systematically lower than what is found in normal galaxies

(Warmels 1989). The HI masses are, however, not abnormally low: the HI disks just are extended. A comparison with optical diameters determined from radial surface brightness profiles shows that the HI to optical diameter ratios are systematically larger than found for galaxies with normal surface brightnesses (see also McGaugh 1992)

From velocity - position cuts along the major axis of the galaxies we could make an estimate of the rotation curves and calculate epicyclic frequencies as a function of radius for a number of LSB galaxies. From these we can evaluate the critical density for star formation as a function of radius following the procedures developed by Kennicutt (1989). It appears that the observed HI surface densities are roughly similar or fall below the critical density throughout the entire disk of the galaxies studied. This suggests that the ISM does not fulfill the necessary conditions to sustain continuous, massive star formation, thus strengthening the idea that low surface brightness galaxies are objects in which active star formation ceased some few billion years ago, or is at most episodic and rare.

The colors of LSB galaxies on the other hand are rather blue, quite similar to the colors of late type high surface brightness galaxies. The colors show a large spread probably indicative for a large range in metallicities and star formation histories. A preliminary analysis of the spectroscopy indicates that the metallicities are below solar, about 1/5th to 1/3rd $Z_{\odot}$, similar to abundances in the outer regions of normal disk galaxies. This implies that part of the blue colors may be a result from metallicity effects. The bluest galaxies, however, can not be just faded disks and must have a complicated star formation history (Schombert et al. 1990, McGaugh 1992). A preliminary analysis of color distributions indicates that quite a few LSB galaxies show color gradients and become on average bluer in their outer parts.

These results indicate that LSB galaxies are in general unevolved, but do have a rather young population. The large range in colors and abundances imply that a single, simple scenario for the evolution is inadequate. The star formation history of LSB galaxies apparently is rather complex, perhaps episodec and may involve exotic IMS's

References

Freeman, K. C. 1970, ApJ, 160, 811.

Kennicutt, R. C. 1989, ApJ, 344, 685.

MgGaugh, S. S. 1992, Ph.D. Thesis, Univ. of Michigan, .

Schombert, J. M. & Bothun, G. D. 1988, AJ, 95, 1389.

Schombert, J. M., Bothun, G. D., Impey, C. D. & Mundy, L. G. 1990, AJ, 100, 1523.

Schombert, J. M., Bothun, G. D., Schneider, S. E. & McGaugh, S. S. 1992, AJ, 103, 1107.

van der Hulst, J. M., Skillman, E. D., Kennicutt, R. C. & Bothun, G. D. 1987, A&A, 117, 63.

van der Kruit, P. C. 1987, A&A, 173, 59.

Warmels, R. 1989, Ph.D. Thesis, Univ. of Groningen, .

Webster, B. L., Longmore, A. J., Hawarden, T. G. & Mebold, U. 1983, MNRAS, 205, 643.

A FAINT FIELD-GALAXY REDSHIFT SURVEY IN QUASAR FIELDS

H. K. C. Yee, University of Toronto

E. Ellingson, CASA, University of Colorado

Quasars serve as excellent markers for the identification of high-redshift galaxies and galaxy clusters. In our past surveys, (e.g., Ellingson et al. 1991), we have identified nearly 20 clusters of Abell richness class 1 or richer associated with quasars in the redshift range $0.2 < z < 0.8$. In order to study these galaxy clusters in detail, we are carrying out a major redshift survey of faint galaxies in these fields using the CFHT LAMA/MARLIN multi-object spectroscopy system. An equally important product in such a survey is the redshifts of the field galaxies not associated with the quasars. This paper presents some preliminary results on field galaxies from an interim set of data from our redshift survey in quasar fields.

Data from 7 fields centered on quasars are presented. The total defined area is ~130 sq' with each field covering an area of typically $6' \times 4'$. The observations were made with a minimum slit size of $2'' \times 11''$ giving a resolution of $\sim$ 20Å. A total of 16 masks were observed with typically 24 to 28 slitlets per mask. Exposure times were between 1 to 3 hours per mask. Absorption line redshifts were determined using cross-correlation techniques (Ellingson & Yee 1992). A total of 197 galaxy redshifts were obtained, of which 135 are considered field galaxies. Typical completeness fraction (of objects observed) is about 80 to 85% for galaxies of Gunn $r < 21.5$ mag. We can define a relatively complete sample of 94 galaxies for representing 57% of all galaxies brighter than $r < 21.5$ mag in the defined fields.

Preliminary result indicate that the absolute magnitude distributions (corrected for incompleteness) within fixed redshift bins are consistent with a slight luminosity evolution of the galaxies of about 0.5 mag at $z \sim 0.5$, similar to the value derived for galaxies around quasars at the same redshift range by Yee & Green (1987). Furthermore, comparison of the luminosities of galaxies associated with the quasars and field galaxies at similar redshifts indicates that they have similar luminosity function. However, the redshift distribution of the field galaxies as a function of apparent magnitude is consistent with a no-evolution model. This discrepancy may be due to the $\sim$ 15% incompleteness and selection effects in redshift determination. We also obtain a relatively low emission-line fraction of $\sim$ 50% for the field galaxies, compared to $\sim$ 80% for the Colless et al. (1989) sample. This presumably

reflects the dominance of early-type galaxies in a red-selected sample. However, there may also be a large field-to-field variation in the number of emission line galaxies. The colors of the galaxies are entirely consistent with their emission-line characteristics. Several fields show remarkable structures in redshift space, including one which shows at least 3 "sheets" of redshifts besides that of the quasar cluster.

References

Colless, M., Ellis, R., Taylor, K. & Hook, R. 1989, MNRAS, **244**, 408.

Ellingson, E. & Yee, H. K. C. 1992, preprint submitted to AJ.

Ellingson, E., Yee, H. K. C. & Green, R. F. 1991, ApJ, **371**, 49.

Page Intentionally Left Blank

Day 2: Tuesday, 7 July 1992

Page Intentionally Left Blank

Correlation Between Low Level Fluctuations in the X-ray Background and Faint Galaxies.

Eline Tolstoy & R.E. Griffiths

We are looking for a correlation between low-level X-ray fluctuations in the Cosmic X-ray Background flux and the large numbers of galaxies found in deep optical imaging, to $m_v \leq 24$ —26. We optically identified these (faint) galaxies by their morphology and colour in deep multi-colour CCD images and plate material. We then searched for statistically significant correlations between these galaxies and low-level X-ray fluctuations at the same positions in multiple deep Einstein HRI observations in PAVO and in a ROSAT PSPC field. Our aim is to test the hypothesis that faint "starburst" galaxies might contribute significantly to the cosmic X-ray Background (at $\sim$ 1keV).

We used two proven methods of correlating low-level X-ray fluctuations with optical sources: (1) For the Einstein data, we use the proven technique of "Stacking", or summing, the X-ray counts at the numerous positions of colour selected (flat-spectrum) galaxies in the field (Anderson 1985) to determine the mean X-ray flux for the class of optical sources which are stacked, as a whole; (2) For the more uniform sensitivity ROSAT data, the number of faint galaxies in a given cell area is cross-correlated at "zero lag" with the background X-ray fluctuations over the same area [following the general method of Jahoda et al. (1991)]. The errors on the net result are calculated with a Bootstrap analysis. Two probability distributions are created of the correlation coefficients resulting from 1000 tries, using the Bootstrap method to generate the the data samples from the original data set. One probability distribution is created from an uncorrelated sample, and one from the data. For a correlation to be meaningful, the two distributions must be significantly different from each other - not only must the mean values be displaced with respect to each other, but the samples must not have a sizeable over-lap, otherwise there is always a finite probability that all we are sampling is uncorrelated data. It has to be remembered when looking at these histograms that one is looking at two probability distributions, **not** two distributions of measured values.

We do not find any such correlation down to a (3σ) average source flux limit of 3×10^{-16}erg s^{-1}cm^{-2} using the stacking technique. This is the outcome of stacking 30 flat-spectrum galaxies ($m_v \leq 25$, V-I ≤ 1.0) galaxies over an $\sim 8'$ square field, corresponding to a source density of $\sim$1800 galaxies per square degree. The results from the zero-lag method are not so immeadiately clear. In Figure 1, we can see two distributions that have significantly different mean values, however, these are probability distributions and around half the points in each distribution lie within the same region as each other. Thus all we can say is that there is a mild trend towards a positive correlation, but it is not statistically significant. Also, when the

number of blue galaxies in a given cell is plotted against the number of X-ray counts in the same cell, there is poor evidence for a correlation, and certainly not one involving more than a small percentage of the data.

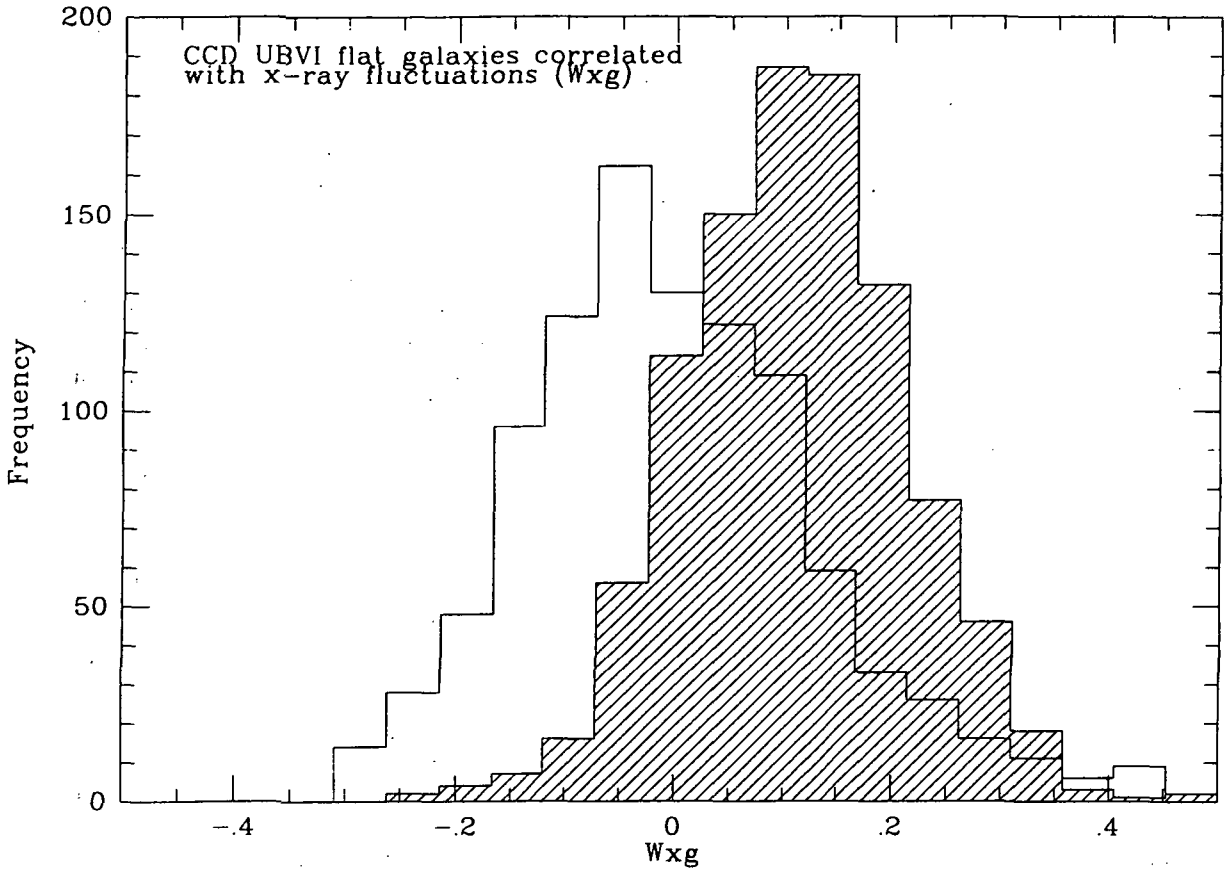

Figure 1: The bootstrap analysis distribution of the values of W_{xg}, the correlation coefficient calculated for samples of UBVI colour selected galaxies vs. low level X-ray fluctuations (shaded histogram), as well as the bootstrap distribution for two uncorrelated data samples W_{noise} (unshaded histogram). The mean value for the correlation distribution, $\overline{W}_{xg} = 0.110$, and for the uncorrelated distribution, $\overline{W}_{noise} = 1.616 \times 10^{-3}$.

References:

Anderson S.F. (1985) PhD thesis, University of Washington

Jahoda K., Lahav O., Mushotzky R.F., Boldt E. (1991) *Ap.J.* **378**, L37

THE HOT INTERSTELLAR MEDIUM IN NGC 1399

Michael Loewenstein, Peter J. Serlemitsos, and the *BBXRT* Science Team
NASA-GSFC/USRA

1. INTRODUCTION

The first two high signal-to-noise, broad bandpass x-ray spectra of elliptical galaxies were obtained with the *Broad Band X-ray Telescope* (*BBXRT*) as part of the December 1990 Astro mission. These observations provided unprecedented information on the thermal and metallicity structure of the hot interstellar media in two ellipticals: NGC 1399, the central galaxy in the Fornax cluster, and NGC 4472, the brightest galaxy in the Virgo cluster. Here I report on the finalized analysis and interpretation of the $\sim$ 4000 sec of *BBXRT* data on NGC 1399.

2. SPECTRA

The orientation of the five *BBXRT* pixels superposed on the *Einstein* Observatory IPC image is shown in Figure 1. The central pixel covers the inner $2'$ of NGC 1399 and the outer pixels extend from $3.5' - 8.6'$, allowing us to detect any strong spatial gradients in temperature, absorption, or abundances. The spectra in the central and in one of the outer pixels are shown in Figures 2 and 3, respectively. The best fitting thermal spectra obtained using all of our available data have the following characteristics (with 90% confidence levels in parentheses). For the central pixel, $kT = 1.07(1.03 - 1.11)$ keV, $N_H = 9.8(4.2 - 16.)\ 10^{20}$ cm^{-2}, $Z = 0.75(0.51 - 1.1)$ solar; for the outer pixels, $kT = 1.11(1.08 - 1.19)$ keV, $N_H = 5.7(.063 - 10.)\ 10^{20}$ cm^{-2}, $Z = 0.30(0.24 - 0.38)$ solar. Note that the temperature gradient is small or non-existent, but a clear negative abundance gradient is indicated as can be seen by the relative emission line strengths in the spectra shown in Figures 2 and 3. There is marginal evidence (at the 3 σ level) for an Fe K line in the central pixel that must come from a seperate emitting component of higher abundance and/or temperature.

3. IMPLICATIONS

a) temperatures and dark matter

Previous efforts to infer the total gravitating mass in elliptical galaxies have been significantly impeded by an absence of accurate gas temperature measurements. The *BBXRT* spectrum of NGC 1399 provides a temperature determination of sufficient accuracy – the uncertainties in temperature are more than an order of magnitude less than for the only previously published x-ray (*Einstein* IPC) spectrum of NGC 1399 – to enable secure constraints on the dark matter content in an elliptical galaxy to be placed for the first time.

The solid curve in Figure 4 shows the mass-to-light ratio, (M/L_B) in solar units divided by h, *vs.* radius in arcseconds ($1'' \approx 65h^{-1}$ pc) for NGC 1399. This is derived from the equation of hydrostatic equilibrium, where we have used the analytic fit of Killeen & Bicknell to the x-ray surface brightness profile to derive the gas density profile, and the *BBXRT*-derived temperature of 1.1 keV. We have assumed that the gas is isothermal, as indicated by the consistency in the inner and outer pixel best-fit temperatures. While the derived value of $(M/L_B)h^{-1}$ inside $\sim 30''$ is probably not reliable due to possible departures from hydrostatic equilibrium and isothermality in a cooling flow, the total M/L_B within the *BBXRT* field of view is well-determined. The mass density of the non-luminous component evidently $\propto r^{-2}$ from $r < 100''$ to $r > 500''$, and dominates the potential for $r > 200 - 300''$. The integrated dark-to-luminous mass ratio inside the *BBXRT* aperture lies in the range 1.8 - 3.3, with the uncertainty due to the uncertainty in the stellar mass-to-light ratio. This ratio will, of course, continue to rise with radius until the halo density distribution steepens or truncates. The dashed extension to the curve in Figure 4 shows the mass-to-light profile extrapolated to the maximum radius where x-rays were detected above background by the IPC, assuming that the temperature remains constant at 1.1 keV.

We have also constructed stellar dynamical models of NGC 1399 to investigate whether the observed projected velocity dispersion profile is consistent with the x-ray derived mass profile. We have solved the equations of stellar dynamics, considering a wide range of velocity dispersion anisotropy distributions, to derive velocity dispersion profiles for stars orbiting in the potential determined by the x-ray emitting gas. The solid curve in Figure 5 shows one particular well-fitting model as well as the observed velocity dispersions on the western side of NGC 1399 from Bicknell *et al.* 1989. The solid curve in Figure 5 shows a well-fitting model for an assumed constant M/L_B of $14h$ that also provides a good fit to the optical data. The two model curves start to diverge significantly at about the edge of the observed spectroscopy; based on the

x-ray derived dark matter distribution we would expect the velocity dispersion profile to remain flat as the optical observations are extended to greater radii.

b) absorption by cold gas

The hydrogen column density in the central pixel derived from spectral fitting is $\sim 3 - 15\ 10^{20}$ cm^{-2} above the Galactic value. This corresponds to $\sim 10^9 M_\odot$ of cold gas, comparable both to the total mass lost by stars in the inner 10 kpc of NGC 1399 over the past 10^9 yr, and also to the total amount of hot x-ray emitting gas in that region. This significant amount of cold gas may be analagous to the large quantities of optically thick cloudlets responsible for x-ray absorption in some intracluster media, and is strong evidence that the central ISM in NGC 1399 is best described as a multi-phase medium. The outer pixel spectra suffer from significantly higher uncertainties at low energies – the hydrogen column density could be comparable to that seen in the central pixel, but is also consistent with the Galactic value.

c) abundances

The iron abundance, relative to solar, in the hot gas derived from the *BBXRT* central pixel x-ray spectrum of NGC 1399 is $Z_{Fe} = 0.51 - 1.1$, while the iron abundance derived from the combined *BBXRT* outer pixels spectra is significantly lower, $Z_{Fe} = 0.24 - 0.38$. This is a reflection of an abundance gradient in the galactic distribution of mass-losing stars, *i. e.* in the galaxy itself during the period when these old stars formed. This is the first evidence that the abundance gradients inferred from optical line-strength measurements persist well beyond the half-light radius.

The central pixel iron abundance is in excellent agreement with the iron abundance of the stars in a similar field inferred from multicolor optical photometry. This places a severe constraint on the Type Ia supernova (SNIa) rate in NGC 1399 since the injection of SNIa debris into the hot gas provides $\sim 0.6 M_\odot$ of iron for every SNIa. In fact, adopting the most conservative SNIa parameters, the limits on the SNIa Fe contamination inferred from the *BBXRT* spectra imply a specific SNIa rate $< 0.88h^2$ SNIa per 1000 yr per $10^{10}\ L_\odot$. This rate is ten times less than the value usually assumed based on a handful of observed SNIa events, and implies that SNIa are energetically and dynamically unimportant for the evolution of the hot ISM in NGC 1399. Therefore, a mostly subsonic cooling inflow is likely to be the most appropriate description of the dynamical state of the hot gas.

4. CONCLUSIONS

Because, as in spiral galaxies, the mass, energy, and metals in elliptical galaxy interstellar media originate in stars and supernovae, X-ray spectra of these galaxies are reflections of their structure and even of their evolution. Stellar orbits and abundances, the distribution of dark and luminous matter, and the evolution of supernova-progenitor binary stars all play strong roles in determining the characteristics of the X-ray emission. A $\sim$ 1 hr observation of NGC 1399 with the *Broad Band X-ray Telescope* has provided us with unique data on temperatures and abundances in the hot interstellar medium in an elliptical galaxy. With this data, we have inferred the presence of significant intrinsic absorption by cold gas, placed powerful and surprisingly small upper limits on the supernvova rate, and derived the distribution of the significant amount of dark matter present in NGC 1399.

Figure 1.

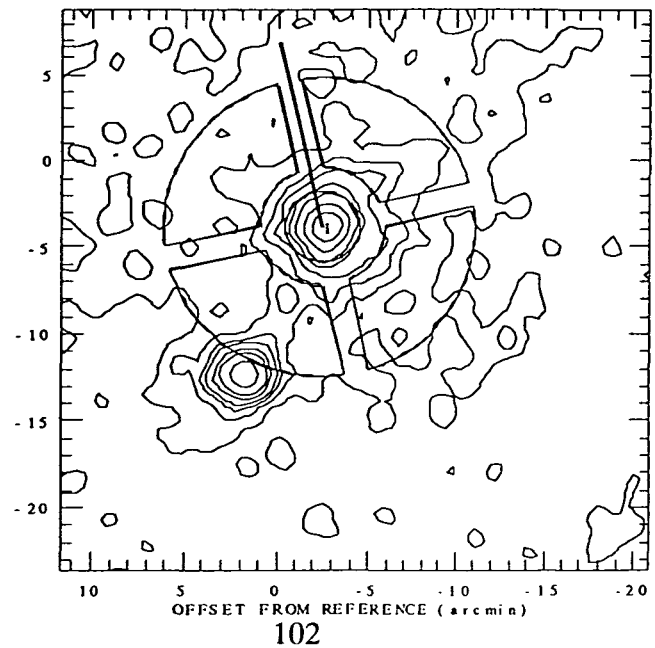

Figure 2.

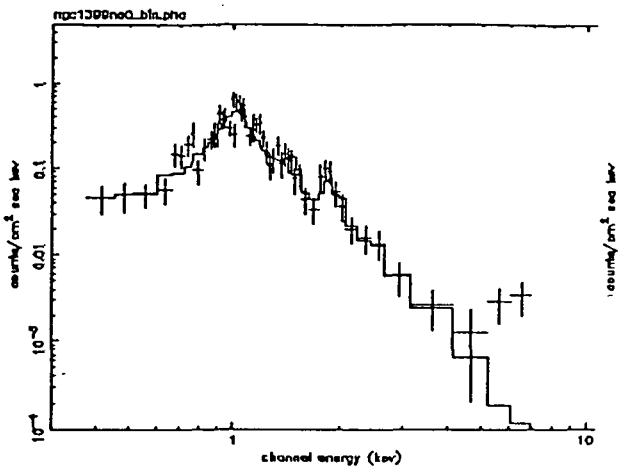

Night data from a0 det (2794 s)
fitted kT range 1.01-1.11 keV
fitted nH range 0.042-0.191 x 10^{22}

Figure 3.

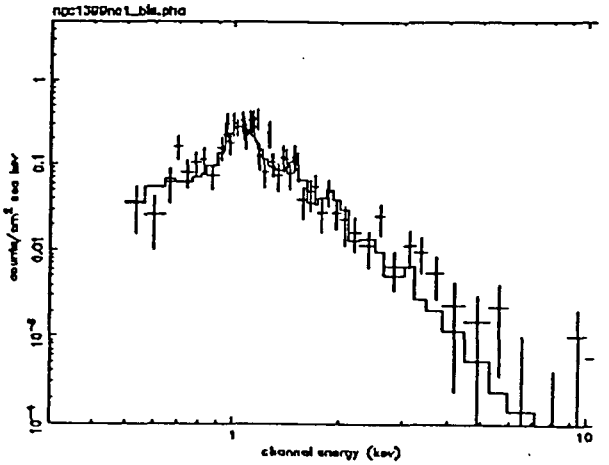

Night data from a1 det (2794 s)
fitted kT range 1.11 1.36 keV

Figure 4.

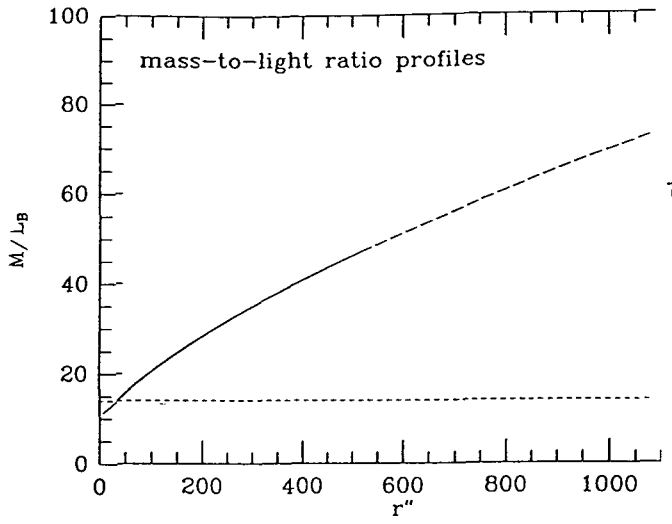

Figure 5.

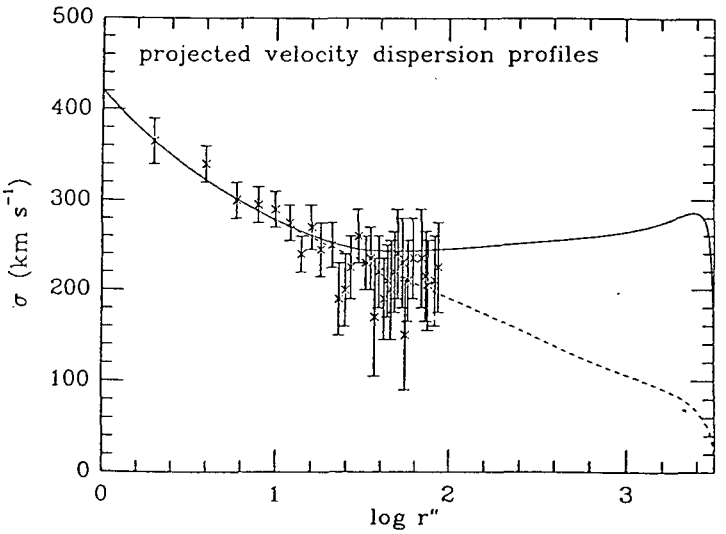

Analysis of the EINSTEIN Sample of Early-Type Galaxies

Paul B. Eskridge and Giuseppina Fabbiano

The EINSTEIN galaxy catalog (Fabbiano, *et al.* 1992, ApJSup. 80, 531) contains x-ray data for 148 early-type (E and S0) galaxies. We are engaged in a detailed analysis of the global properties of this sample. By comparing the x-ray properties with other tracers of the ISM, as well as with observables related to the stellar dynamics and populations of the sample, we expect to determine more clearly the physical relationships that determine the evolution of early-type galaxies.

Previous studies with smaller samples have explored the relationships between x-ray luminosity (L_X) and luminosities in other bands (see Fabbiano 1989, ARAA. 27, 87). Using our larger sample, and the statistical techniques of survival analysis (Schmitt 1985, ApJ. 293, 178; Isobe *et al.* 1986, ApJ. 306, 490), we have repeated a number of these earlier analyses. For our full sample, we find a strong statistical correlation between L_X and L_B (the probability that the null hypothesis is upheld is $P < 10^{-4}$ from a variety of rank correlation tests. Regressions with several algorithms yield consistent results. All give a relationship of the form

$$Log(L_X) = 1.80(\pm 0.15) Log(L_B) - 37.47(\pm 6.31). \quad (1)$$

Or, dropping the Local Group dwarf galaxies M32 and NGC 205,

$$Log(L_X) = 2.01(\pm 0.18) Log(L_B) - 46.49(\pm 7.93). \quad (2)$$

In all cases, luminosities are in ergs/sec. Both of these results are inconsistent with a simple slope–1 relationship to greater than 5σ. The relationship between L_X and L_{6cm} is also clearly steeper than slope–1: the best fit value for the full data set has a slope of $m = 1.62 \pm 0.09$.

Other strong correlations exist between L_X and $L_{12\mu m}$, and L_X/L_B. A weak correlation ($P \approx 0.03 - 0.06$, depending on the test) exists between L_X and $L_{100\mu m}$. This weak correlation vanishes when only E-type galaxies are considered ($P \approx 0.15$), but becomes stronger for the S0s ($P \approx 0.01 - 0.02$). As a rule, however, there do not tend to be significant differences between the Es and S0s in the luminosity-luminosity relations.

We are also examining relationships between the x-ray emission and structural parameters of the galaxies in our sample. Simple two-parameter correlation tests show that both L_X and L_X/L_B are strongly correlated with $Log(a/b)$, $Log(\sigma_v)$, and with the a_4 parameter as defined by Bender *et al.* (1989, AAp. 217, 35). Our a/b values come from the RC3, σ_v from Faber *et al.* (1989, ApJSup. 69, 763), and a_4 from Bender *et al.* and Peletier *et al.* (1990, AJ. 100, 1091). The relationships are such that more luminous x-ray galaxies tend to be rounder, have larger velocity dispersions, For the last, $P = 0.025$. While the last relationship was discussed by Bender *et al.* (1989), they did not test its significance. There is also a strong correlation between L_X and the Mg_2 parameter from Faber *et al.* ($P \approx 0.007$) in the sense that more luminous x-ray galaxies also tend to have higher values of Mg_2.

Because we are examining relationships among a large number of parameters, it is useful to ask if inter-relationships amongst multiple parameters will effect the results of simple two-parameter tests. One way of addressing this is the partial Spearman-rank method (Kendall and Stuart 1976, "Advanced Theory of Statistics, Vol. II). Kim *et al.* (1992, ApJ. Submitted) used this method to demonstrate relations between C_{21} and L_X, C_{21} and L_X/L_B, a/b and L_X, and a/b and L_X/L_B. C_{21} is the ratio of the mid- to soft-xray flux, defined by Kim *et al.* (1992, ApJSup. 80, 645), and effectively measures the line of sight absorption (N_H). These relations are in the sense that more luminous x-ray galaxies are rounder, and have larger N_H. The total N_H often exceeds the Galactic foreground value for the most luminous galaxies. With our current sample we have run tests on the combination (L_X, L_B, L_X/L_B, a/b, a_4), and confirmed the correlations ($P \leq 0.03$) between L_X and a_4 and L_X/L_B and a_4 that appeared in the two-parameter tests. Adding Mg_2 and σ_v, we confirm that L_X also correlates strongly with each of these parameters. We note, however, that our sample shows no evidence of correlation between a_4 and Mg_2.

Our analysis of these results is still somewhat preliminary. An overall picture has begun to emerge, however. Low-luminosity ellipticals and S0s have x-ray fluxes and spectra that are indistinguishable from spirals (Kim *et al.* 1992, ApJ. 393, 134). Above some limiting luminosity (ie., mass) the galaxy is able to retain some or all of its primordial and reprocessed ISM. The fraction of material retained appears to be a strongly increasing function of mass (σ_v). Thus more massive systems were also able to recycle their ISM, for a time, into new stars, leading to their higher metallicities (Mg_2). The high σ_v in these systems, plus energy input from SNe heats the gas up to x-ray temperatures, effectively preventing current large-scale star formation.

The steep correlation between L_X and L_{6cm} also indicates a physical interaction between the media generating these fluxes. The standard model (see Fabbiano 1989 for references) is that the x-ray gas acts as a confining medium for outflowing material from an active nuclear source. Our sample is large enough that we will be able to examine the details of this model. In particular, how the core and extended radio flux components relate to the x-ray emission. The lack of correlation between L_X and $L_{100\mu m}$ for ellipticals indicates that there is no relationship between the cool ISM traced by the 100μm emission and the x-ray gas. This supports the notion that the material responsible for the 100μm emission in ellipticals is either accreted or otherwise transitory. There does appear to be a correlation (at the $\sim 2.5\sigma$ level) between L_X and $L_{100\mu m}$ for the S0s. The slope of the regression is, however, consistent with 1, indicating that this is a 'bright-things-are-bright' correlation. This is in keeping with other work indicating that the FIR in S0s galaxies does not, as a rule, require appeals to accretion (Eskridge and Pogge 1991, AJ. 101, 2056).

The relationships between L_X, a/b, a_4, and C_{21} that the shape of the potential, as well as the total mass is important for determining the evolution of the ISM in ellipticals. For a given optical luminosity (or mass), rounder galaxies have larger L_X. These same galaxies also tend to have significant *intrinsic* N_H. It may be that the lack of rotation in these systems allows a significant amount of material to collect in their nuclei and cool to the neutral phase. The lack of rotation in these more massive ellipticals may be pointing toward differing evolutionary pathways for producing current elliptical galaxies. Brighter, rounder, boxier galaxies could be the products of mergers between rather sizable objects. Less luminous, more flattened, disky galaxies may be "primordial" ellipticals.

N93-26755

Searching for Lyman Alpha emission from a possible Zel'dovich "pancake"

CAROLINE COX, ERIC SCHULMAN AND JOEL N. BREGMAN
Department of Astronomy, University of Michigan
Ann Arbor, Michigan 48109-1090

Introduction

Uson, Bagri and Cornwell (1992) have reported the detection of 2×10^{14} $M_\odot$ of neutral hydrogen at a redshift of 3.397. Top-down theories of structure formation predict such a mass of hydrogen collapsing to form a protocluster of galaxies. We sought to observe this object in Lyman-α, which could be produced through ionization by the metagalactic ionizing radiation field or through internal ionization processes.

Observations

On April 29, 1992, we observed the region of the reported HI emission for 1800 seconds with the 1.3 meter McGraw-Hill reflector at Michigan-Dartmouth-M.I.T. Observatory. Because the HI emission reported by Uson *et al.* has a transverse scale of 300", we used a 1/3.06 reducing camera and a Thomson CCD to obtain a field of view of about 600" by 840". We used a filter 88 Å wide, centered at 5354 Å; Lyman-α emission at z=3.4 is redshifted to 5347 Å.

In order to avoid saturating the CCD with a bright star in the field, nine 200 second exposures were taken. The combination of these images shows no obvious extended Lyman-α emission at a level of about 28 magnitudes per square arcsecond.

The field we observed also shows a distant cluster of galaxies. In order to determine if the cluster could in any way be associated with the cloud of neutral hydrogen at z=3.4, we sought to estimate its redshift from the size and magnitude of the galaxies and of the cluster as a whole. We adopted Ω= 1 and H_0= 50 km s^{-1} Mpc^{-1}; our redshift estimates range from z=0.2 to z=0.6. The cluster is clearly not associated with the HI cloud at z=3.4

Analysis

We calculated the Lyman-α luminosity of the pancake assuming that there is no internal source of ionizing radiation but that it absorbs ionizing photons from the metagalactic radiation field (Donahue and Shull 1989). This resulting surface brightness is about 31 magnitudes per square arcsecond. Consequently, unless this object does have an internal source of ionizing radiation, it will be difficult to detect optically. There would be internal ionizing radiation if the pancake had collapsed sufficiently to produce star formation.

Uson *et al.* find that the HI cloud has a transverse scale of 300" but do not report the position angle; consequently we considered a circle 300" in diameter centered on the reported coordinates when we attempted to establish an upper limit to the flux reaching us from the HI cloud. We established 16 detection cells within the 300" circle and compared these cells with 16 cells from other parts of the frame. This is illustrated in Figure 1. We endeavored to avoid including stars or excessive noise (such as that due to the CCD bleeding in response to saturation by bright stars) in any of the cells. We find a nominal detection, but it is at a very low level; about 1.2 σ. This 1.2 σ detection corresponds to 18th magnitude, or 2.07×10^{-14} erg s^{-1} cm^{-2}, over the whole 16 cell detection region. In this region a 3 σ upper limit corresponds to about 17 magnitudes, or a flux of 5.16×10^{-14} erg s^{-1} cm^{-2}. This is equivalent to a luminosity at the source of 4.7×10^{45} erg s^{-1}. The Lyman-α flux expected to reach us from a Zel'dovich pancake at a redshift of z=3.4 is 3.2×10^{-15} erg s^{-1} cm^{-2}. Our calculations of the Lyman-α luminosity of an HI cloud with no internal source of radiation yield a Lyman-α luminosity of about 2.9×10^{44} erg s^{-1}.

There is a factor of three uncertainty in the strength of the metagalactic ionizing radiation field. If it were a factor of 3 more intense than the 10^{-21} erg s^{-1} cm^{-2} Hz^{-1} sr^{-1} assumed in our calculations, then a Zel'dovich pancake at z=3.4 could be detected in one night of observing at the MDM 1.3 m telescope. The observations reported here were limited to half an hour due to poor weather. We intend to dedicate more observing time to this object in the future.

References

Uson, J. M. , Bagri , D. S., and Cornwell, T. J. 1992, *Phys. Rev. Letters*, **67**, 3328.

Donahue, M. and Shull J. M. 1989, *Astrophys. J.*, **383**, 511.

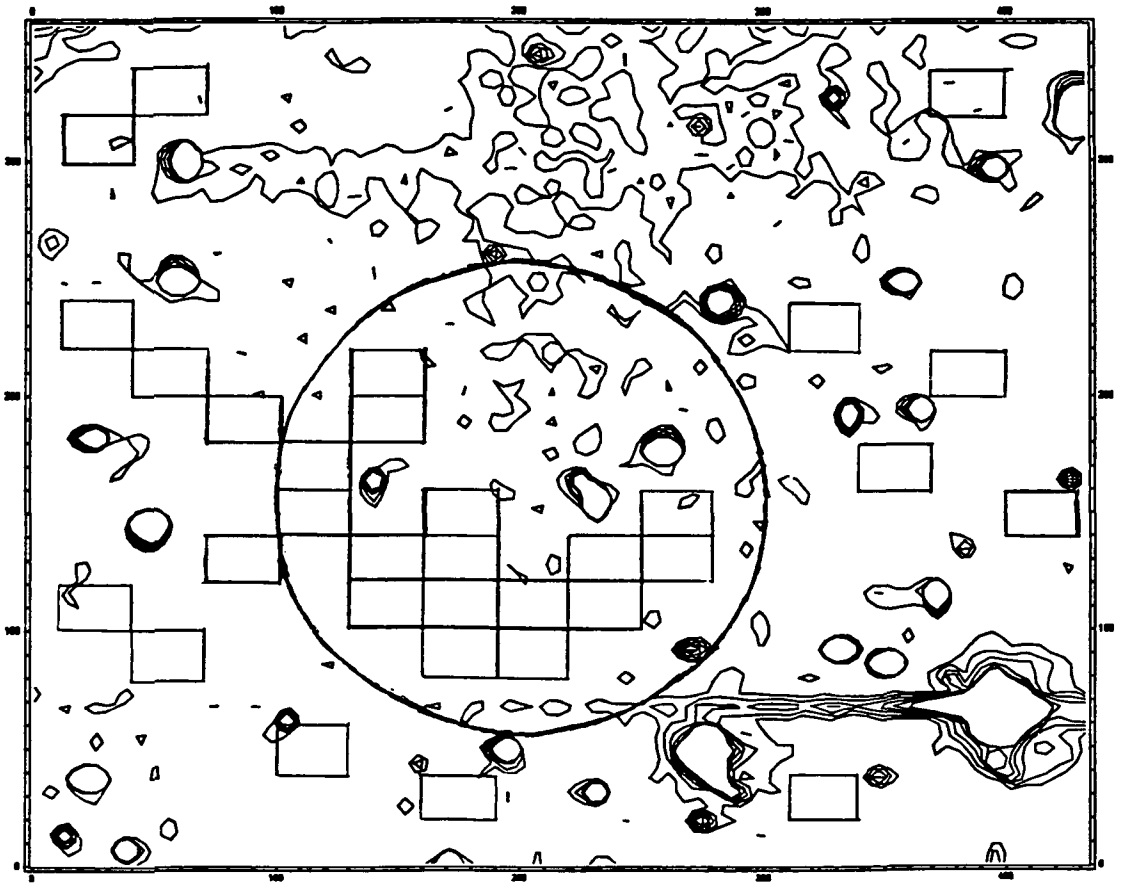

Figure 1

Contour plot showing 300" diameter circle centered on 0904+3352. The 16 detection cells within the circle were compared with the 16 detection cells outside the circle in order to determine the flux level.

CAN QUASARS PHOTOIONIZE THE INTERGALACTIC MEDIUM AT HIGH REDSHIFT?

AVERY MEIKSIN
Canadian Institute for Theoretical Astrophysics, University of Toronto

and

PIERO MADAU
The Johns Hopkins University and Space Telescope Science Institute

ABSTRACT

We discuss the reionization of the intergalactic medium (IGM) by quasar sources at high redshift. We compute the integrated UV background from observed QSOs, taking into account the hydrogen opacity associated with intervening Lyα clouds and Lyman limit systems. We note that the published data appear to indicate a significant underdensity of absorption systems in the Lyα forest with column densities $N_{HI} > 10^{15}\,\mathrm{cm}^{-2}$. This deficit results in a reduction of the opacity of the universe by a factor of 1.5–3 at $z = 3 - 5$ relative to previous estimates. The QSO contribution to the metagalactic flux at the Lyman edge may be as large as $J_{912}(z) \approx 6[(1+z)/4.5]^{0.5} \times 10^{-22}\,\mathrm{erg\,cm^{-2}\,s^{-1}\,Hz^{-1}\,sr^{-1}}$ for $q_0 = 0$, and slightly lower for $q_0 = 1/2$. For a density of the diffuse component of the IGM of $\Omega_D h_{50}^2 < 0.025$, QSOs could photoionize a smooth IGM sufficiently to satisfy the constraints imposed by the Gunn-Peterson effect. The epoch of reionization could be as recent as $z \gtrsim 5$. As a result, neutral patches of IGM would be detectable in the spectra of high redshift quasars. The patches would appear as absorption line systems with typical column densities of $10^{19} - 10^{20}\,\mathrm{cm}^{-2}$, and velocity widths of $100 - 1000\,\mathrm{km\,s}^{-1}$.

SUMMARY

In the past few years, the growing number of observed quasars with $z > 4$ (Schneider, Schmidt, & Gunn 1989) has promoted a renewed interest in the topic of the reionization of the universe. The absence of an absorption trough on the blue side of the Lyα emission line in the spectra of these high redshift QSOs requires the diffuse component of the IGM to have been highly ionized by $z \simeq 5$ (Schneider, Schmidt, & Gunn 1991a). We examine whether QSOs detected in optical surveys can supply the required metagalactic ionizing flux.

The key quantity here is J_{912}, the *mean* specific intensity of the diffuse radiation field at the observed wavelength $\lambda_{obs} = 912\mathrm{A}$, as seen by an observer at redshift z_{obs}:

$$J_{912}(z_{obs}) = \frac{c}{4\pi H_0}\int_{z_{obs}}^{z_{max}} \frac{(1+z_{obs})^3}{(1+z)^3}\frac{\epsilon(\nu,z)\exp\left[-\tau_{eff}(912,z_{obs},z)\right]}{(1+z)^2(1+2q_0z)^{1/2}}dz, \qquad (1)$$

where $\epsilon(\nu,z)$ is the proper volume emissivity (ergs $\mathrm{cm^{-3}\ s^{-1}\ Hz^{-1}}$) of QSOs at frequency $\nu = c(1+z)/[912\mathrm{A}(1+z_{obs})]$ and redshift z, $H_0 = 50h_{50}\,\mathrm{km\,s^{-1}\,Mpc^{-1}}$, and $\exp[-\tau_{eff}(912,z_{obs},z)]$ is the average transmission over all lines of sight of a clumpy medium. We assess the contribution of quasars to the ultraviolet extragalactic background at high redshift in light of the two major uncertainties: (1) the existence and degree of a controversial decline at the faint end of the QSO luminosity function for $z \gtrsim 3$ (Boyle 1991; Irwin, McMahon, & Hazard 1991; Schmidt, Schneider, & Gunn 1991; Warren, Hewett, & Osmer 1991); and (2) the continuum opacity of intervening absorption systems (e.g., Sargent, Steidel, & Boksenberg 1989; Lanzetta 1991). We use the QSO luminosity function of Boyle (1991), and consider two cases: (1) a population of QSOs with a constant comoving density for $z > 2$ and which turn on at a redshift $z_{on} = 6$ (case CC); (2) a QSO population which declines by a factor of 2 in comoving density per unit redshift for $z > 3$ (case ED). We estimate for the density of the diffuse intercloud medium which must be photoionized $0.02 < \Omega_D < 0.04$ for $H_0 = 50$ and $0.005 < \Omega_D < 0.01$ for $H_0 = 80$, after subtracting observed optically thick absorbers from the estimate of the baryonic density $\Omega_b h_{50}^2 = 0.05 \pm 0.01$ from Walker *et al.* (1991), based on nucleosynthesis constraints. A more complete discussion is presented by Meiksin & Madau (1992).

We evaluate the expected UV background from QSOs using two models for the amount of attenuation by intervening absorption systems. The model used by Madau (1992) gives a moderate amount of attenuation. After examining the H I column density distribution in the spectra of 4 QSOs observed at high resolution, however, we find a significant underdensity of Lyα systems with $\log N_{HI} > 15$ (Figure 1). A deficit by a factor of 3, significant at the 4σ level, occurs in the range $15 < \log N_{HI} < 16$. No Lyα forest lines were detected for $\log N_{HI} > 16$, with a significance of 3σ. We show the best fit line of slope $\beta = 1.7$ determined over the range $13.75 < \log N_{HI} < 14.8$ (*solid line*), and the same fit renormalized to systems in the range $14.8 < \log N_{HI} < 16$ (*dashed line*). The deficit, if real, would result in a decrease in the amount of attenuation by a factor of 1.5-3 from the moderate case. We note that the deficit may be a consequence of a Jeans instability in the Lyα clouds. Spherical clouds of diameter D would be gravitationally unstable for column densities greater than $N_{HI,max} = 3.0 \times 10^{16}(D/200\,\mathrm{kpc})^{-3} J_{-22}^{-1}\,\mathrm{cm}^{-2}$, where J_{-22} is the UV background intensity at the Lyman edge in units of $10^{-22}\,\mathrm{ergs\,cm^{-2}\,s^{-1}\,Hz^{-1}\,sr^{-1}}$.

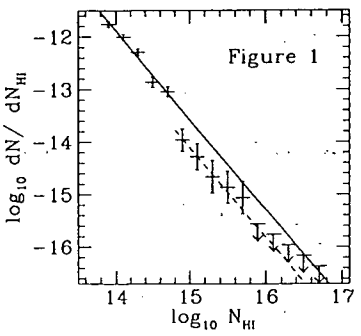

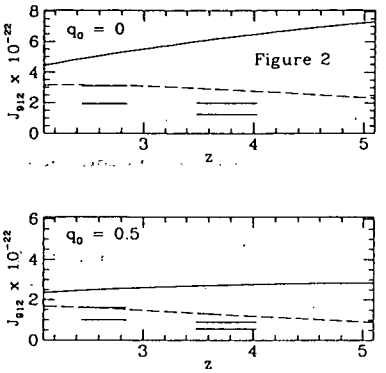

We show the resulting UV intensity for case CC in Figure 2. The intensity for both the low (*solid line*), and moderate (*dashed line*), attenuation models satisfies the Gunn-Peterson limits on the Lyα optical depth, τ_{GP}, for $\Omega_D h_{50}^2 < 0.025$. The horizontal bars are lower limits to the required intensity based on $\tau_{GP}(\langle z_{abs}\rangle = 2.6) < 0.05$ (Steidel & Sargent 1987), and $\tau_{GP}(\langle z_{abs}\rangle = 3.8) < 0.31$ (Jenkins & Ostriker 1991). In each pair, the upper (lower) bar corresponds to $H_0 = 50\,(80)\,\mathrm{km\,s^{-1}\,Mpc^{-1}}$. We assume $\Omega_D h_{50}^2 = 0.025$ and a temperature of 15,000 K. Case ED succeeds for the low attenuation model, but fails for a moderate amount of attenuation unless $H_0 > 80$.

The Gunn-Peterson limit places a direct constraint on the epoch of reionization, through the porosity parameter $Q(z)$ of the source H II regions, when radiative recombinations in the IGM can be neglected. For case CC, we obtain $\tau_{GP}(z)Q(z)/\Omega_D h_{50}^2 = 0.45 h_{50}^{-1} T_4^{-0.75}[(3+\alpha)/\alpha_S](1+q_0)^{-1}(1+z)^{4-2q_0}[1-(x/x_{on})^{1+q_0}]/\mathcal{J}_{912}(z)$, where $x = 1+z$, α and α_S are the spectral indices of the UV background and the sources, respectively, and T_4 is the IGM temperature in units of 10^4 K. The quantity $\mathcal{J}_{912}$ is a dimensionless integral given by dividing the integrand in eq.(1) by $\epsilon(c/912\mathrm{A}, z_{obs})$. To 15% accuracy, $\mathcal{J}_{912}(z) \simeq 0.65(1+z)^{0.5-q_0}$ for the low attenuation model, and $3.0(1+z)^{-(1+q_0)}$ for the moderate model. For case ED, we obtain, to 15% accuracy for $3 < z < 6$, $\tau_{GP}(z)Q(z)/\Omega_D h_{50}^2 \simeq 0.42 h_{50}^{-1} T_4^{-0.75}[(3+\alpha)/\alpha_S](1+z)^{3-2q_0}/\mathcal{J}_{912}(z)$, where $\mathcal{J}_{912}(z) \simeq 0.35(1+z)^{0.75-q_0}$ for low attenuation, and $1.2(1+z)^{-(0.5+q_0)}$ for moderate. The constraint $\tau_{GP} < 0.05$ at $z = 2.6$ requires $Q(z=2.6) > 54(25)$ for $q_0 = 0(0.5)$ ($\alpha = 0.5$, $\alpha_S = 0.7$, $T_4 = 1.5$) for case CC. The porosity evolves according to $Q(z) = Q(0)(1+z)^{-(1+q_0)}[1-(x/x_{on})^{1+q_0}]$. The limit on porosity constrains the reionization epoch z_I, when $Q = 1$, to $z_I > 5.9(5.7)$ for $q_0 = 0(0.5)$. For case ED, $Q(z=2.6) > 40(21)$ for $q_0 = 0(0.5)$. To 15% accuracy, $Q(z) = Q(0)(1+z)^{-(2+q_0)}\exp[-0.69(z-3)]$, for $3 < z < 6$. We then obtain $z_I > 6.2(5.2)$ for $q_0 = 0(0.5)$. Thus the reionization epoch may have been as recent as $z_I \lesssim 6$, and possibly more recent if radiative recombinations are significant. (Note that this conclusion generalizes to any class of radiation sources, depending only on their evolution and spectral shape.) For QSOs, we find $z_I = 5.8(5.6)$ for $q_0 = 0(0.5)$ for case CC. For case ED, we find $z_I = 6.2(5.2)$ for $q_0 = 0(0.5)$.

The epoch of reionization will first reveal itself as absorption lines arising from un-ionized patches of IGM. For $Q(z) \lesssim 1$, the patches will have neutral hydrogen column densities of $10^{19} - 10^{20}\,\mathrm{cm^{-2}}$ and black cores of velocity width $100 - 1000\,\mathrm{km\,s^{-1}}$, determined by the Hubble expansion across a patch. For model ED, the lines would persist over an extended range of $\Delta z \sim 0.5 - 1$, until Q falls below ~ 0.5 and the lines broaden into the Gunn-Peterson absorption trough shortward of the Lyα emission line.

N93-26757

Metal Abundances at z=3.4

Andrew Cooke
Institute of Astronomy, Cambridge, England CB3 0HA

Echelle spectroscopy data have been taken of the quasar 0000-263 on the 4m telescope at CTIO in Chile. Three nights of red and three nights of blue data were obtained (about four hours data per night). The resolution is typically 0.4 Å at 5000 Å ($\lambda/d\lambda$ = 12500) and has good signal-to-noise over the wavelength range 4600 Å to 8000 Å.

To keep the statistics manageable the data were not rebinned, although the instrument was stable enough for each night's data on the object to be co-added. Arc spectra taken between each exposure were also co-added within the nights. During profile fitting the model was convolved with a Gaussian whose width was equal to nearby arc lines, so any broadening generated by the co-adding of data will not affect the final results.

Since O I and H I have the same ionisation potential (13.6 eV),

$$[\,O\,/\,H\,] \sim [\,OI\,/\,HI\,].$$

Unfortunately, in this data only the 1302 Å O I transition is visible, and it is blended with H I in the Lyman Alpha forest. However, O I and N I coexist (the ionisation potential for N I is 14.5 eV) and so the N I triplet can constrain the redshift and turbulent width of the O I.

When a fit was made to the regions containing O I and N I absorption three systems were apparent with similar redshifts and velocity widths. These three systems were fitted with tied redshifts and turbulent widths, while the other lines in the region were fitted as Lyman-Alpha.

The saturated Lyman-Alpha profile was then fitted with three components at the same redshifts as these observed lines, with the line widths tied. (To do this the measured values and errors for O I and N I are taken into account: the difference between these and the fitted values contribute to the chi-squared statistic when fitting H I.)

Finally, metallicity ratios for the individual lines and their totals were calculated and compared to solar values.

The results for the separate clouds are (from low to high redshift):

$$-2.9 \pm 4.8$$
$$-0.4 \pm 5.6$$
$$-3.3 \pm 0.7$$

and for the total:

$$-2.5 \pm 4.2$$

where the values are dex relative to solar.

All of these results are consistent with the most accurate, and since the O I detection may be partly H I we obtain the limit:

$$[\,OI\,/\,HI\,] - [\,OI\,/\,HI\,]_{\odot} \lesssim -3$$

Since this poster was presented the metal lines have been re-fitted using Si II as an additional constraint. Further observations will cover O I, 1039 Å, and possibly Lyman–beta, giving more accurate results.

The following people have observed, donated telescope time, or helped reduce this data: Bob Carswell, Jack Baldwin, Gerry Williger, Dave Turnshek and Ken Lanzetta.

Enrichment and Heating of the Intracluster Medium by Ejection from Galaxies

Chris Metzler and August Evrard
Department of Physics, University of Michigan

We present results of N-body + hydrodynamic simulations designed to model the formation and evolution of clusters of galaxies and intracluster gas.

Clusters of galaxies are the largest bound, relaxed objects in the universe. They are strong x-ray emitters; this radiation originates through thermal bremsstrahlung from a diffuse plasma filling the space between cluster galaxies, the *intracluster medium* or ICM. From observations, one can infer that the mass of the ICM is comparable to or greater than the mass of all the galaxies in the cluster, and that the ratio of mass in hot gas to mass in galaxies, M_{ICM}/M_{stars}, increases with the richness of the cluster. If the ICM is predominantly gas left over from the galaxy formation process, why was galaxy formation more "inefficient" in rich clusters? Or, if the ICM came primarily from gas that fell into the cluster after it formed, why were rich clusters more efficient in collecting gas?

Spectroscopic studies of cluster x-ray emission show heavy element emission lines. While $M_{ICM}/M_{stars} \geq 1$ implies that most of the ICM is primordial in nature, the discovery of heavy elements indicates that some of the gas must have been processed through galaxies. Galaxy evolution thus directly impacts cluster evolution; can current theories of galaxy evolution account for the observed metallicities of galaxy clusters?

The current paradigm for evolution of the ICM involves infall of primordial gas into the cluster potential well. Gravitational collapse and shock heating then drives the gas up to observed temperatures. Recent analytical studies have examined enrichment of the ICM through supernova ejecta being blown out of galaxies as a wind, or ram-pressure stripped as galaxies plow through the ICM. We are integrating these studies with three dimensional N-body / gas dynamical evolutionary models of clusters. Our simulations follow three dynamically distinct components: cluster gas, galaxies, and dark matter. Shocks from gravitational collapse, along with mass, energy, and metal ejection from cluster galaxies, are incorporated into the models.

The initial conditions for our simulations were derived from a cold dark matter power spectrum, with a particle distribution at a redshift of 9 generated through linear theory. Galaxies are then placed in the initial conditions by-hand, using the gas mass associated with 2.5σ peaks in the density field. Our combined n-body / hydrodynamical simulation code then evolved these initial conditions to a final redshift of zero.

Radial profiles of cluster gas properties, including temperature, metallicity, and spatial distribution of ejecta were derived. Also, simulated x-ray surface brightness profiles were derived from the density and temperature data of the cluster. Despite the use of many

simplifying assumptions in these early runs, results have been obtained which roughly agree with observations. In particular, iron abundances of about half solar and nearly flat temperature profiles are found within an Abell radius. Future plans for the project include refinement of our ejection algorithm. We also plan to produce a cluster catalog of reasonable size by making many simulation runs, so that systematics of cluster properties - temperature profiles, metallicities, correlations of observables - can be explored, and so that more solid predictions can be made about the expected evolution of cluster properties. This project should provide important feedback on our theories of the evolution of cluster gas, when compared with observational results from BBXRT, ROSAT, ASTRO-D, and (hopefully) AXAF.

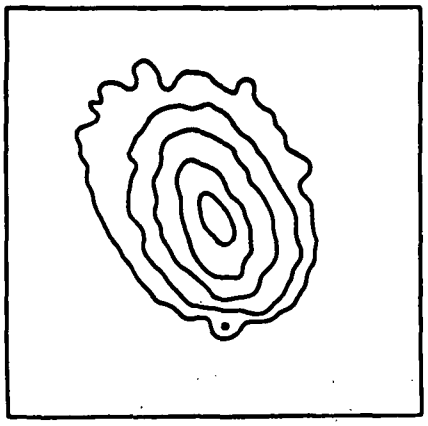

cl40r1c
z = 0.034.
f_{tot} = 6.713
L44 = 2.340
M14 = 0.720
1' = 0.055 Mpc
window = 38.40'

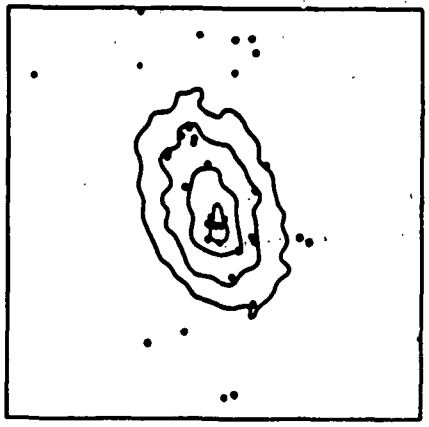

cl40r1c
z = 0.033.
f_{tot} = 2.808
L44 = 0.962
M14 = 0.525
1' = 0.055 Mpc
window = 38.40'

Simulated ROSAT PSPC images of clusters grown from same initial conditions; run above includes only gas and dark matter, while run below also includes galaxies and ejection of gas. Dots on lower plot show locations of bright galaxies. Outermost isophote at same level for both plots. z is redshift of cluster; f_{tot} is total counts per second in window, in the PSPC energy band; L44 is x-ray luminosity in window and in energy band, in units of 10^{44} ergs/s; M14 is total gas mass in the window, in units of $10^{14}M_{\odot}$.

The evolution of the intergalactic medium and the origin of the galaxy luminosity function

David Valls–Gabaud[1,2,3], Alain Blanchard[4] and Gary Mamon[4]

[1] Institut d'Astrophysique de Paris, France.
[2] Institute of Astronomy, Cambridge, UK.
[3] Physics Department, Queen's University, Canada.
[4] DAEC, Observatoire de Meudon, France.

ABSTRACT. The coupling of the Press and Schechter prescription, with the CDM scenario and the Hoyle-Rees-Ostriker cooling criterion leads to a galaxy formation scenario in which galaxies are overproduced by a large factor. Although star formation might be suppressed in the smaller haloes, a large amount of energy per galactic mass is needed to account for the present number density of galaxies. The evolution of the IGM provides a simple criterion to prevent galaxy formation without requiring feedback, since haloes with small virial temperatures are not able to retain the infalling hot gas of the IGM. If the ionising background has decreased since $z \sim 1-2$, then this criterion explains the slope of the luminosity function at the faint end. In addition, this scenario predicts two populations of dwarf galaxies, well differenciated in age, gas content, stellar populations and clustering properties, which can be identified with dE and dIm galaxies.

Evidence for a multiphase, inhomogeneous interstellar medium in damped Lyα systems.

David Valls-Gabaud[1,2,3]

[1] Institut d'Astrophysique de Paris, France.
[2] Institute of Astronomy, Cambridge, UK.
[3] Physics Department, Queen's University, Canada.

ABSTRACT. The large optical depth in absorption of the Lyα line in damped Lyα systems implies that the *emission* line produced by HII regions is very broad, since the number of diffusions is very large. The emission lines observed in DLyα systems are narrow, a fact that can only be explained if the emission comes from the outer layers alone, or if the interstellar medium is clumpy and multiphase. We show how discrete, cold HI clouds embedded in a hot, fully ionised phase, produce narrow lines. This might provide evidence for a SNR-dominated ISM at high redshift, in agreement with the observed metallicity and chemical evolution models. Other high redshift galaxies also offer evidence for such a multiphase, inhomogeneous ISM.

HST/FOS SPECTRA OF PG 1351+64: AN INTRINSIC ABSORBER at LOW REDSHIFT

Arno Granados, Elise Sachs, J. Michael Shull & John T. Stocke

CASA/University of Colorado

We present (Figures 1a-c) 1 Å resolution spectra of the nearby ($z = 0.08797$) Seyfert galaxy PG 1351+64 taken with the *Faint Object Spectrograph* onboard the *Hubble Space Telescope*. Spectral coverage runs from 1200-3200 Å in the observed frame and includes emission and absorption features due to Lyα, N V, Si IV, C IV, and Mg II. We have detected three distinct intrinsic absorption systems in Lyα, N V, Si IV, and C IV, and tentatively in Mg II, at velocities of 900 km s^{-1}, 1630 km s^{-1}, and 2900 km s^{-1} ($\pm$100 km s^{-1}) relative to the emission-line redshift of the QSO (absorption systems are marked on Figures 1a-c with an "A").

The maximum relative velocity of these absorbers is < 5000 km s^{-1} and therefore does not meet Weymann, Carswell, & Smith's (1981: see also Weymann *et al.* 1991) criteria for **B**road-**A**bsorption-**L**ine (BAL) QSOs at high-z. However, the absorptions are almost certainly intrinsic to the QSO given the low redshift of this object. In addition, PG 1351+64 is marginally radio-quiet, as are all BALQSOs, based on recent estimates of the radio-loud/radio-quiet dividing line (Kellerman *et al.* 1989; Stocke *et al.* 1992).

The narrow velocity width, ≤ 500 km s^{-1}, and low outflow velocities of the absorption systems are more similar to so called "associated absorbers" (Foltz *et al.* 1987) seen at high-z in radio-loud quasars, but whose absorptions are thought to arise in clouds much farther from the nucleus (≥ 1 kpc) than are BAL clouds (1-10 pc). Despite the qualitative resemblance to the associated absorbers, the absorption systems in PG 1351+64 appear to be the low-luminosity analogs of BALQSO absorption troughs. The lower observed outflow velocities in PG 1351+64 are due to the much lower luminosity of the nuclear source in comparison to the high-z, high-luminosity BALQSOs.

In addition, we have discovered "satellite" emission lines displaced 4000-5000 km s^{-1} blueward and redward of the Mg II emission (features marked with an "E" in Figure 1c). These satellite lines are much stronger than similar features observed near C IV in NGC 4151 (Clavel *et al.* 1987) and may also be present in our **HST/FOS** spectrum of Ton 951, a non-BAL Seyfert. These emission features may represent a direct detection of the heating and acceleration of broad line or narrow line clouds by the BAL outflow. Since observational selection effects may have precluded the detection of such features prior to **HST/FOS** spectra, these satellite emission features may be common in Seyfert galaxies.

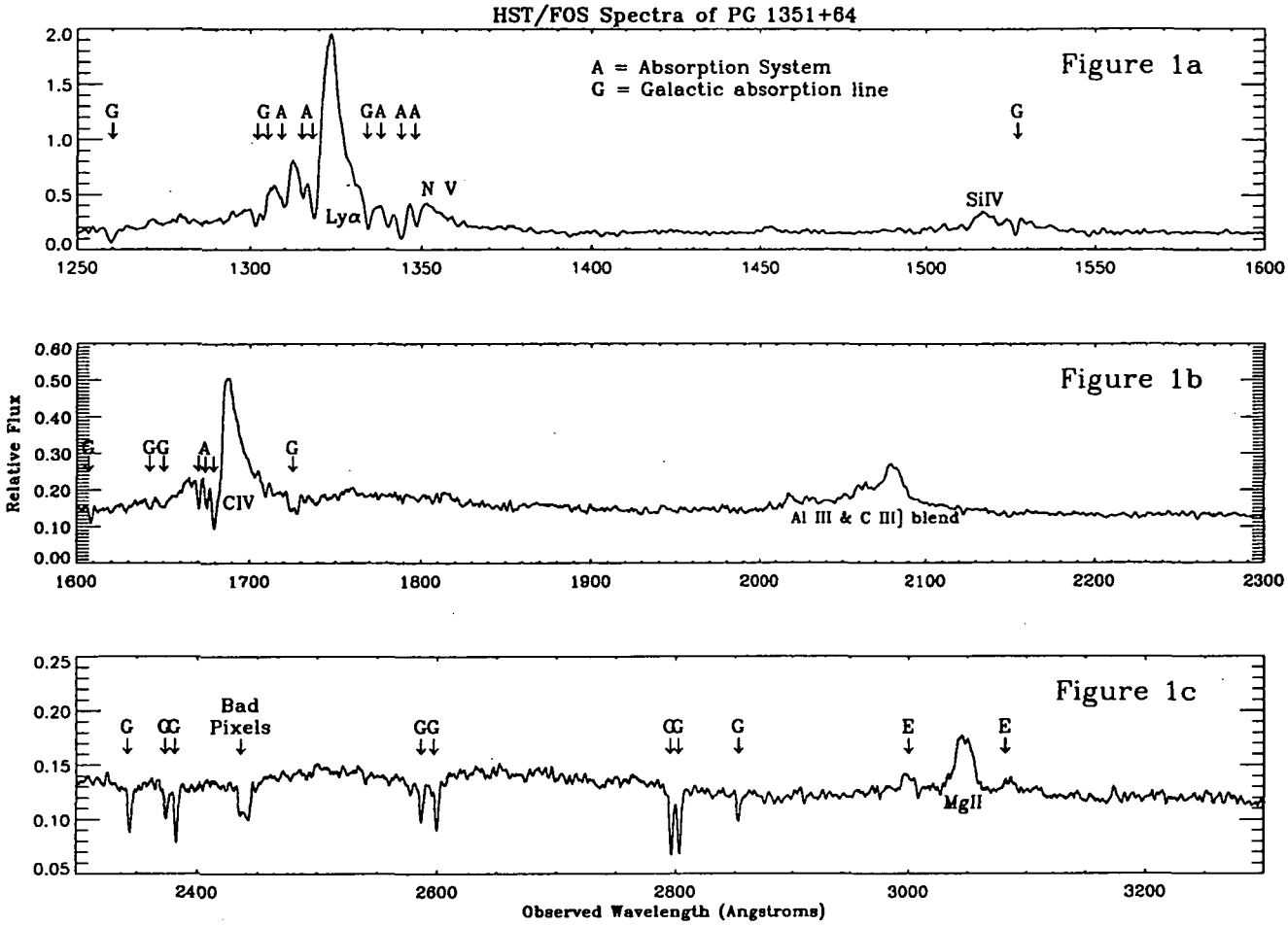

REFERENCES

Clavel, J., Altamore, A., Boksenberg, A., Bromage, G.E., Elvius, A., Pelat, D., Penston, M.V., Perola, G., Snijders, M.A.J., & Ulrich, M.H., 1987, *ApJ*, **321**, 251.

Foltz, C., Chaffee, F., Weymann, R., & Anderson, S., 1988 in QSO Absorption Lines, p. 53.

Kellerman, K., Sramek, R., Schmidt, M., Shaffer, D., & Green, R., 1989, *AJ*, **98**, 1195.

Pacholczyk, A., 1977, in Radio Galaxies, (Oxford, Pergamon), p. 197.

Stocke, J., Morris, S., Weymann, R., & Foltz, C. 1992 *ApJ*, in press

Weymann, R., Carswell, R., & Smith, M., 1981, *ARAA*, **19**, 41.

Weymann, R., Morris, S., Foltz, C. & Hewett, P., 1991, *ApJ*, **373**, 23.

Low Redshift Lyman Alpha Absorption Lines and the Dark Matter Halos of Disk Galaxies

Philip Maloney

NASA Ames Research Center, MS 245-6, Moffett Field, CA 94035

Introduction. Recent observations using the *Hubble Space Telescope* (Morris *et al.* 1991, ApJ 377, L21; Bahcall *et al.* 1991, ApJ 377, L5) of the $z = 0.156$ QSO 3C 273 have discovered a surprisingly large number of Lyα absorption lines. In particular, Morris *et al.* found 9 certain and 7 possible Lyα lines with equivalent widths above 25 mÅ. This is much larger (by a factor of 5–10) than the number expected from extrapolation of the high-redshift behavior of the Lyα forest. Within the context of pressure-confined models for the Lyα clouds, this behavior can be understood if the ionizing background declines sharply between $z \sim 2$ and $z \sim 0$ (Ikeuchi & Turner 1991, ApJ 381, L1). However, this requires that the ionizing photon flux drop as rapidly as the QSO volume emissivity; moreover, the absorbers must have a space density $n_0 \approx 2.6(N/10)h/(D/100\,\mathrm{kpc})^2\ \mathrm{Mpc}^{-3}$ where D is the present-day diameter of the absorbers. It is somewhat surprising that such necessarily fragile objects could have survived in such numbers to the present day.

Here I show that it is plausible that the atomic hydrogen extents of spiral and irregular galaxies are large enough to produce the observed number of Lyα absorption lines toward 3C 273, and that the neutral column densities and doppler b-values expected under these conditions fall in the range found by Morris *et al.* (1991).

Neutral Hydrogen in Low Column Density Gas Disks. Consider a gas disk in a galactic potential, exposed to an isotropic background radiation field. For neutral hydrogen column densities $N_{\mathrm{HI}} \lesssim 10^{16}\,\mathrm{cm}^{-2}$ the attenuation of the incident ionizing flux will be completely negligible. I assume that the radiation field is a power-law matched to the observed background at 1.5 keV; in terms of the photon flux $\phi_\nu = 4\pi J_\nu/h\nu$ this is $\phi_\nu = \phi_0 I_{\mathrm{Ly}}(\nu/\nu_H)^{-(\alpha+1)}$ where $\phi_0 = 2.3 \times 10^{-11}$ photons cm^{-2} s^{-1}, I_{Ly} is a scaling factor, and α is the spectral index; $\alpha = 1.45 + 0.490\log(I_{\mathrm{Ly}})$. A value of $I_{\mathrm{Ly}} = 1$ corresponds to a (4π sr) ionizing photon flux $\phi_i = 5.2 \times 10^4$ photons cm^{-2} s^{-1} and Lyman intensity $J_{\nu_H} = 4 \times 10^{-23}$ ergs cm^{-2} s^{-1} Hz^{-1} sr^{-1}. Solving for the neutral fraction gives

$$x_{H^0} \simeq \frac{1.2\alpha_A n_H}{\xi_H} = \frac{1.2\alpha_A n_H(\alpha+3)}{\phi_0 I_{\mathrm{Ly}} a_0 \nu_H} = n_H(\alpha+3)T_{e,4}^{-0.72} I_{\mathrm{Ly}}^{-1} \tag{1}$$

where n_H is the total hydrogen volume density and ξ_H the hydrogen ionization rate; I have assumed that $n_e = 1.2 n_{H^+}$ and $\alpha_A = 4.18 \times 10^{-13} T_{e,4}^{-0.72}$.

At the column densities of interest here, $N_H \lesssim 10^{19}\,\mathrm{cm}^{-2}$, the gas self-gravity is negligible, and the equilibrium gas vertical density distribution in the potential of a spheroidal halo will be a gaussian with dispersion (for gas vertical velocity dispersion σ_{zz})

$$\sigma_h(R) = \frac{(r_c^2 + R^2)^{1/2}\sigma_{zz}}{(4\pi G\rho_c r_c^2)^{1/2}} \simeq R\frac{\sigma_{zz}}{V_A} \tag{2}$$

where the approximation is true for $R^2 \gg r_c^2$; ρ_c and r_c are the core density and core radius of the halo. If the Z-motions of the gas are purely thermal, then $\sigma_{zz} = 12.9 T_{e,4}^{1/2}$ km s^{-1}. Combining equations (1) and (2) and integrating from $Z = 0$ to ∞, the neutral hydrogen column density is then

$$\begin{aligned} N_{\mathrm{HI}}(R) &= 2\int_0^\infty x_{H^0} n_H(R,Z)\,dZ \\ &= 1.4 \times 10^{13} \frac{N_{H,18}^2}{R_{50}} \frac{V_{A,100}}{T_{e,4}^{1.22}} \frac{(\alpha+3)}{I_{\mathrm{Ly}}}\ \mathrm{cm}^{-2} \end{aligned} \tag{3}$$

where R_{50} is $R/50$ kpc, $N_{H,18}$ is the total hydrogen column density $N_H/10^{18}\,\mathrm{cm}^{-2}$, and $V_{A,100}$ is the halo asymptotic velocity $V_A/100\,\mathrm{km\ s}^{-1}$ and I have assumed the gas is isothermal. Assuming that photoionization heating balances recombination and bremsstrahlung cooling, the temperature is

$$T_e = \frac{h\nu_H}{\overline{\beta}k}\left[\frac{(\alpha+3)}{(\alpha+2)} - 1\right]\ \mathrm{K} \tag{4}$$

where $\overline{\beta} \simeq 1.15$. Thus $T_e \simeq 46{,}000$ K for $\alpha = 1$ and $T_e \simeq 32{,}000$ K for $\alpha = 2$; the corresponding doppler parameters would be $b \simeq 28$ and 24 km s^{-1}.

Comparison with Observations. The number of galactic disks expected along a line of sight in a matter-dominated, $q_0 = 0$ universe is

$$N = \left(\frac{c}{H_0}\right)\frac{\sigma_0 n_0}{2}\left[(1+z)^2 - 1\right]\ . \tag{5}$$

where $\langle\sigma n\rangle_0$ is the luminosity function-averaged product of cross-section and density at the present epoch. Assuming a Schecter luminosity function, a Holmberg relation between cross-section and luminosity, $\sigma_{\mathrm{Ho}}(L) = \sigma_*(L/L_*)^\delta$, where σ_* is the cross-section of an L_* galaxy, and that the cross-section of the gaseous disk of a galaxy is related to the optical cross-section by $\sigma_{\mathrm{gas}}/\sigma_{\mathrm{Ho}} = f_{g*}(L/L_*)^\beta$, $\langle\sigma n\rangle_0 = \sigma_* f_{g*}\phi_* f_{\mathrm{sp}}\langle\cos i\rangle\Gamma(\delta+\beta-s+1)$ where f_{sp} is the fraction of galaxies which are spirals or irregulars, $\langle\cos i\rangle$ corrects for inclination effects, s is the slope of the luminosity function, and $\Gamma(x)$ is the complete gamma function. Taking $\phi_* = 1.6\times10^{-2}h^3\ \mathrm{Mpc}^{-3}$ (Efstathiou, Ellis & Peterson 1988, MNRAS 232, 431), $R_* = 11.5/h$ kpc (*cf.* Wolfe *et al.* 1986, ApJS 61, 249), $f_{\mathrm{sp}} \approx 0.7$, and $\langle\cos i\rangle = 0.5$ (for thin disks) the number of intercepted disks expected for $z = 0.15$ is $N(z=0.15) \approx 1.1\times10^{-3} f_{g*}\Gamma(\delta+\beta-s+1)$.

If we identify galaxies as the source of the absorption lines seen toward 3C 273, then the observed number of lines constrains f_{g*} and the variation of σ_{gas} with galaxy luminosity. At the $N_{\mathrm{HI}} \sim 10^{13}$ cm^{-2} level, galactic halos must satisfy $f_{g*}\Gamma(\delta+\beta-s+1) \sim 8\times10^3$. Thus, either L_* galaxies have huge ($R \sim$ several hundred kpc) halos ($f_{g*} \gg 1$) or low-luminosity (dwarf or low surface brightness) galaxies have large galos and are abundant. This second possibility is crucially dependent on whether there is a low-luminosity cutoff in the galaxy luminosity function, and on the faint-end slope relative to the variation of σ_{gas} with luminosity.

The nine certain Lyα lines detected by Morris *et al.* (1991) have equivalent widths between 57 and 302 mÅ and derived column densities between log $N_{\mathrm{HI}} = 13.04$ and 14.13 cm^{-2}; the latter is the only line with $\log N_{\mathrm{HI}} > 13.6\,\mathrm{cm}^{-2}$. The observed column density distribution will be area-weighted. For a $1/R$ distribution, the neutral column density will fall off as R^{-3}, and $N_L(N) \propto N^{-5/3}$. If the total gas distribution is an exponential, then $N_L \propto N^{-a}$, with $a \approx 1.2-1.3$. The nine certain Lyα lines have b-values ranging from 17–111 km s^{-1}; the latter is twice the next-highest value. The mean is 38 km s^{-1} (29 km s^{-1} if the 111 km s^{-1} point is discounted). The expected thermal b-values are $\sim 20-30$ km s^{-1}, depending only on the slope of the extragalactic radiation field. For thin disks, the contribution from rotation to the observed velocity dispersion will be small except for nearly edge-on geometries (Wolfe *et al.* 1986), less than 20 km s^{-1}. Thus the expected b-values for these thin disks are in reasonable agreement with the minimum observed b-values. Metal absorption lines such as C IV $\lambda\lambda$1548, 1551 may be detectable at the tens of mÅ level if the metallicity $Z \sim 0.1Z_\odot$ or greater.

Further studies of the low-redshift Lyα lines, especially observations of QSOs whose lines of sight intercept the halos of known low redshift galaxies, will constrain both the extragalactic radiation field and the gaseous and dynamical properties of galactic halos.

NEUTRAL HYDROGEN AT THE PRESENT EPOCH: A CONSTRAINT ON THE EVOLUTION OF HIGH REDSHIFT SYSTEMS

Sandhya Rao and Frank H. Briggs
University of Pittsburgh

Introduction

Damped Lyman α and metal absorption lines in the spectra of quasars indicate the presence of intervening gas-rich systems at high redshift ($z > 2$). These systems have characteristic size scales, velocity dispersions and neutral hydrogen column densities (N(HI)) similar to present day spirals and are thus thought to be their progenitors (cf. Wolfe 1988). Constraints on galaxy evolution can be derived by comparing the H I properties of high redshift systems to the present galaxy population.

Good observational statistics on high redshift absorbers specify the number of these systems along the line of sight as a function of N(H I), the column density of neutral hydrogen per absorber (cf. Lanzetta et al. 1991). Here, we derive similar statistics for nearby ($z = 0$) galaxies of which spirals are the only gas-rich systems that provide a significant cross-section for the interception of light from quasars.

The N(HI) distribution function at $z = 0$

A complete sample of spiral galaxies selected for optical diameters greater than $7'$ and by the range in declinations observable at Arecibo was used to determine absorption cross-sections as a function of N(HI). The probability distribution for interception specifies the number of systems intercepted per unit distance along the line of sight at a given column density, N. This can be determined from the integral over all magnitudes of the product of the luminosity function of spiral galaxies, $\phi(M)$, and the effective cross-sectional area of a galaxy, $A(M, N)\Delta N$, in a range of column densities ΔN centered on N. The results of this analysis are presented in Fig. 1 in a form comparable to the results of Lanzetta et al. (1991). For $z \sim 2.5$ they plot $f(N)$, a quantity described in the figure caption. Also plotted is the value of $f(N)$ at a column density of $10^{19.5}$ cm^{-2} as determined by Tytler (1987).

The conclusion is that the number of nearby absorbers per unit distance along the line of sight is at least a factor of 4 less than that at high redshifts. It thus appears that substantial evolution has taken place since a redshift of 2 or 3. The improved determination of the effective cross-sectional

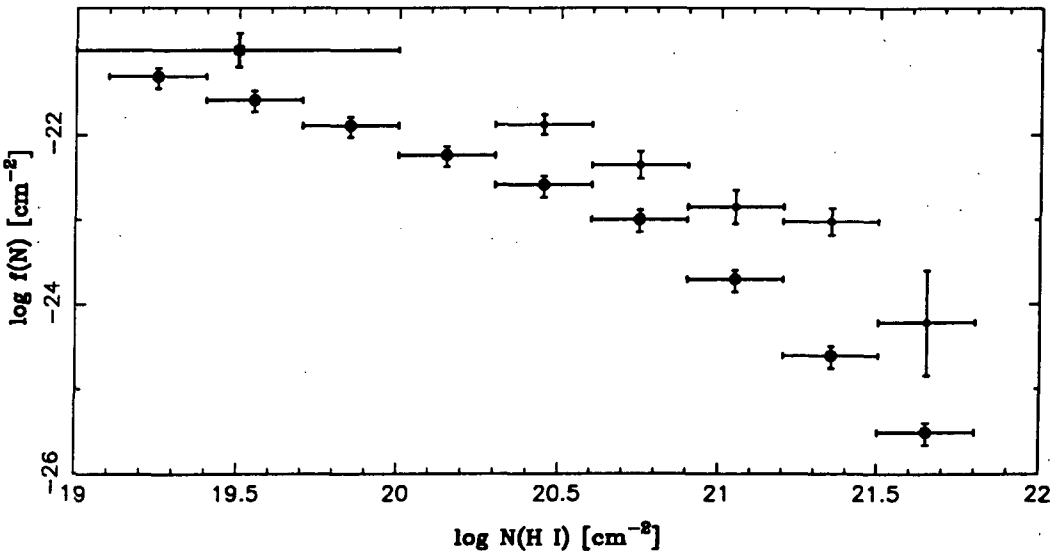

FIG 1. HI column density distribution function for high z systems and nearby galaxies.
• Lanzetta et al (1991), □ Tytler (1987): high z data. Horizontal bars indicate bin sizes and vertical bars indicate 1σ uncertainties.
○ This calculation: data from nearby galaxies. Horizontal bars indicate bin sizes and vertical bars are errors mainly due to the uncertainty in the mean density of nearby galaxies.
The product $f(N)dNdX$ specifies the number of absorbers in an absorption distance dX with HI column density in the interval between N and $N + dN$, where $dX = \frac{H_o}{c} dl$, with l in Mpc.

areas at the present epoch over previous estimates confirms the discrepancy in $f(N)$ and strengthens the implication that a) there were a greater number of them at high redshifts and/or b) they were larger. The discrepancy appears to increase with column density. This could be a result of poor sampling of high column density lumps due to inadequate resolution in the H I data (van Gorkom 1992, private communication). It could also be the effect of higher column density material forming stars more efficiently, thus depleting it faster than lower column density gas.

The cosmological mass density at $z = 0$

A comparison of the H I content and luminosity function of different galaxy types shows that over 90% of the neutral hydrogen cosmological mass density (Ω_{HI}) at the present epoch is associated with spiral galaxies (Rao and Briggs, in preparation). S0 galaxies, irregulars and ellipticals contribute the other 9%. Ω_{HI} at $z = 0$ is plotted in Fig. 2 along with $\Omega_D(z)$, the H I mass density at high redshifts derived by Lanzetta et al. (1991) from statistics of damped Ly α absorbers. It is reassuring that the local value of Ω_{HI} is consistent with the decreasing trend with time that is seen at high redshifts. The contribution of spirals to Ω_{HI} was computed using the isolated galaxy sample of Haynes and Giovanelli (1984). The mean M_{HI}/L_B ratio of their sample is larger than that of our sample of 27 nearby, large diameter spirals by about 30%. Preliminary calculations indicate that the value of Ω_{HI} determined from our sample is also smaller than that determined from the Haynes and Giovanelli galaxies. Thus in order to better determine an H I mass density that is representative of the local universe, larger samples that include a larger volume of space must be used.

Also plotted in Fig. 2 is the cosmological mass density of luminous matter, Ω_{lum}, at $z = 0$. It is determined by the sum of the luminous matter density in spirals and ellipticals. As galaxies evolve, neutral gas can disappear as a result of ionization or by being converted into stars. The sum of the present mass densities of luminous matter and of neutral hydrogen is ~ 3 times the HI mass density at the earliest epoch probed by the damped Lyman α surveys ($z \sim 3.5$).

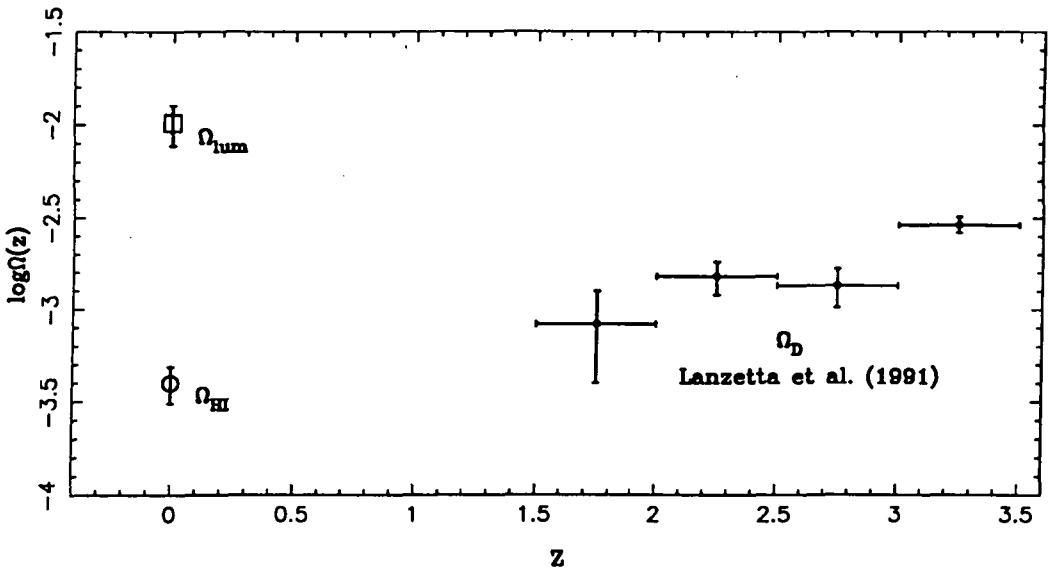

FIG 2. The cosmological mass density as a function of redshift.
• from the work of Lanzetta et al. (1991).
○ $\Omega_{HI}(z = 0)$, □ $\Omega_{lum}(z = 0)$

Acknowledgements: This work has been supported by grants AST 87-15070 and AST 91-19930 from the National Science Foundation.

REFERENCES

Haynes, M. P. & Giovanelli, R. 1984, *AJ*, **89**, 758

Lanzetta, K. M., Wolfe, A. M., Turnshek, D. A., Lu, L., McMahon, R. G., & Hazard, C. 1991, *ApJSS*, **77**, 1

Tytler, D. 1987, *ApJ*, **321**, 49

Wolfe, A. M. 1988, in QSO Absorption Lines: Probing the Universe, ed. J. C. Blades, D. A. Turnshek, & C. A. Norman (Cambridge University Press), p.297

Testing the Pressure-confined Lyα Cloud Model

ARIF BABUL[1] & GERARD M. WILLIGER[2]

[1] *Canadian Institute for Theoretical Astrophysics, Toronto, Canada*
[2] *Cerro Tololo Inter-American Observatory, La Serena, Chile*

Introduction: The Lyα absorption line forest, seen in quasar spectra, is generally interpreted as being due to cosmologically distributed "clouds" of primordial gas. Analyses of the observations (*e.g.* Rauch *et al.* 1992) reveal that the number distribution can be described by power laws: $d\mathcal{N}/dz \propto (1+z)^{\gamma}$ and $d\mathcal{N}/dN_{HI} \propto N_{HI}^{-\beta}$, where N_{HI} is the HI column density. The typical values for power law indices range between $2 \lesssim \gamma \lesssim 2.6$ and $1.7 \lesssim \beta \lesssim 1.9$. One model postulates that the Lyα clouds are optically thin entities, photoionized by the background UV flux, $J_\nu \propto (1+z)^j$, and confined by an adiabatically evolving intercloud medium (ICM): $P(z) \propto (1+z)^5$. Analytic studies of this model suggest that the ensuing Lyα line statistics can account for the observations (in particular, the $d\mathcal{N}/dz$ and the $d\mathcal{N}/dN_{HI}$ distributions) if the cloud mass spectrum is a power law $d\mathcal{N}/dM \propto M^{-\delta}$, $\delta \approx 1.9$, and $j \approx 4$ (*c.f.* Ikeuchi & Ostriker 1986, IO). One of the simplifying assumptions incorporated into these studies is the existence of a large mass range for the clouds at all epochs, the validity of which is questionable.

Simulations: We investigate the pressure-confined model using a 1-D spherically symmetric hydrodynamical code to simulate cloud evolution over the epoch $1.8 \leq z \leq 6$ This enables us to relax many of the assumptions incorporated in the analytic studies. We only consider clouds with masses $2.75 \leq \log(M/M_\odot) \leq 9.25$. Clouds with larger masses are Jeans unstable and tend to collapse; they are not "pressure-confined". The lower mass limit is chosen to ensure all clouds that can produce absorption features with equivalent widths $W_r \geq 0.2$Å over the epoch $1.8 \leq z \leq 3.6$ are considered. We calculate Voigt profiles from the model clouds at varying impact parameters and use the resulting absorption features to determine line-profile parameters (*e.g.* N_{HI}, the rest-frame equivalent width W_r, and the Doppler parameter b). We construct synthetic samples of lines subject to similar selection criteria used to define a sample of ~ 400 observed lines (*i.e.* $W_r \geq 0.2$Å). In this sense, the present study is unique: past theoretical studies have relied on column density thresholds. N_{HI}, however, is a fitted parameter and is sometimes subject to large uncertainties. Line widths have been traditionally used to define observational samples as they are directly measurable. We compare the synthetic $d\mathcal{N}/dW_r$, $d\mathcal{N}/dN_{HI}$ and $d\mathcal{N}/dz$ distributions against the observed trends. The synthetic results are normalized by demanding that the number of clouds with $W_r \geq 0.2$Å be the same as observed. Apart from studying the properties of clouds immersed in $j = 4$ UV background, we also consider the possibility that the UV background is constant at the epoch of interest. For more details, see Williger & Babul (1992; WB).

Results: The redshift-integrated $d\mathcal{N}/dW_r$ distributions for $j = 0$, 4 ($\delta = 1.90$) are shown in Figure 1. Clearly, there is a shortage of model lines with $W_r > 0.3$Å, in comparison with the observations. The result is partly due to the fact that $\langle b \rangle \approx 22\,\mathrm{km\,s^{-1}}$ for simulated pressure-confined clouds (with a dispersion of approx. $1\,\mathrm{km\,s^{-1}}$) — *i.e.* b is due to thermal velocities — while $\langle b \rangle \approx 35\,\mathrm{km\,s^{-1}}$ for the observed lines (with a dispersion of approx. $15\,\mathrm{km\,s^{-1}}$). The lower b for the simulated clouds implies that these clouds require larger column densities than those associated with the observed lines in order to account for the observed $d\mathcal{N}/dW_r$ distribution. The imposition of the upper mass limit for the pressure-confined clouds, however, restricts the column density range of the simulated clouds.

The $d\mathcal{N}/dN_{HI}$ distributions for the simulated and the observed clouds in the redshift range $2.6 \leq z \leq 2.8$ (Figure 2) shows that although the two are consistent with each other for $\log(N_{HI}) \lesssim 15.2$, there are fewer model clouds with N_{HI} larger than observed. Note that the shortage is more severe for the $j = 4$ case as the UV background at $z \approx 2.7$ is more intense than in the $j = 0$ case and therefore the clouds are more highly ionized. We also show the "analytic" $d\mathcal{N}/dN_{HI}$, computed using the simple homologously-expanding pressure-confined cloud model of IO and the prescription of WB (*e.g.* we explicitly take into account the upper mass limit). This distribution cuts off at even a lower N_{HI} than the synthetic distribution; the simulations reveal that the more massive clouds tend not to expand homogolously and, consequently, develop non-uniform density profiles. Self-gravity also retards their expansion.

In Figure 3, we show the observed and the synthetic $d\mathcal{N}/dz$ distributions for clouds with $W_r \geq 0.2$Å; the $d\mathcal{N}/dz$ distribution for a subset of clouds with $W_r \geq 0.3$Å is shown in Figure 4. For $W_r \geq 0.2$Å sample, the synthetic results match the observations well. Neither the normalization (reflecting the discrepancy in

the $d\mathcal{N}/dW_r$ distributions) nor the slope of the synthetic $d\mathcal{N}/dz$ (the number of pressure-confined clouds decreases much too rapidly at low redshifts) matches the observations for the subset with $W_r \geq 0.3$Å. The rapid decline in clouds with large equivalent widths towards lower redshifts is, once again, due to the upper mass limit for the clouds.

Conclusions: As a result of an upper limit to the mass of pressure-confined clouds and the "thermal" Doppler parameters, the equivalent width and column density distributions for spherical, pressure-confined clouds with a power-law mass spectrum fail to account for the observations. The upper mass limit is determined by nature of the evolution of both the ICM pressure and the UV background; in order to achieve an acceptable fit to the data, we require the ICM pressure to decrease as $P(z) \propto (1+z)^p$, $p \gtrsim 5.8$ (WB). This is difficult to justify physically. Aspherical clouds, on the other hand, may allow the pressure-confined model to remain viable.

References: Ikeuchi, S. & Ostriker, J.P. 1986, *Astrophys. J.*, **301**, 522.
Rauch, M., *et al.*. 1992 *Astrophys. J.*, **390**, 387.
Williger, G.M. & Babul, A., 1992. ***submitted to Astrophys. J.***

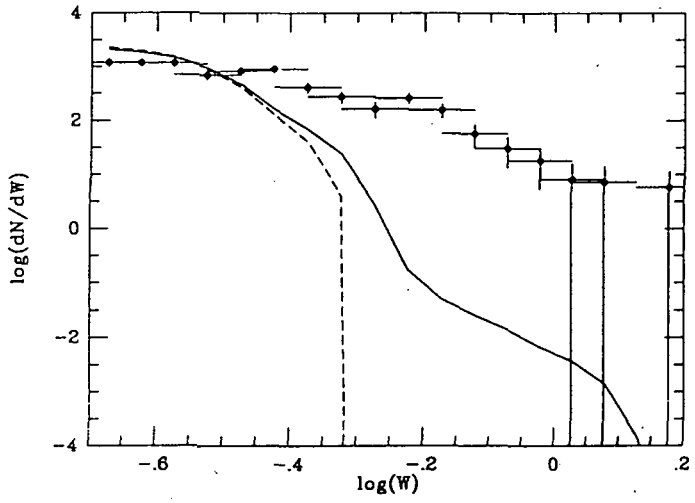

Fig. 1. $d\mathcal{N}/dW_r$ of the observed clouds *vs.* the $z-$integrated distribution of the model clouds. The $j = 0$, 4 cases for $\delta = 1.90$ are shown by solid, dashed lines respectively. The error bars indicate bin widths and 1σ errors for the observations.

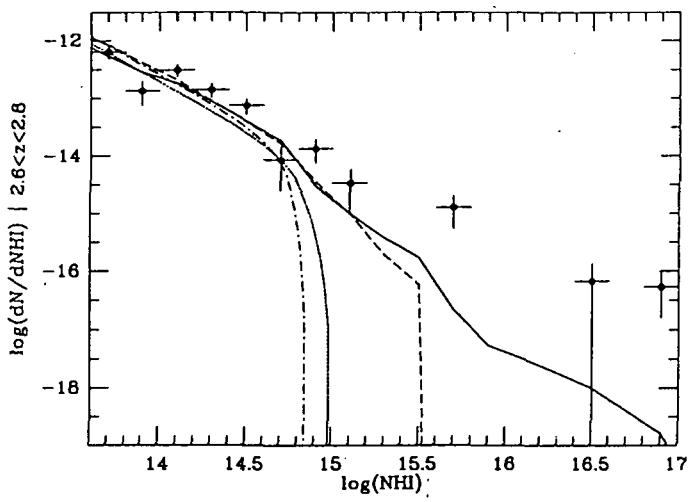

Fig. 2. Column density distribution of the observed clouds *vs.* models in the redshift range $2.6 < z < 2.8$. The various curves correspond to various analytic and synthetic results: $j = 0/j = 4$ synthetic (solid/dashed); $j = 0/j = 4$ analytic (dotted/dot-dashed). At high N_{HI}, the synthetic curves steepen before an abrupt cutoff. The cutoff is even lower for the analytic models.

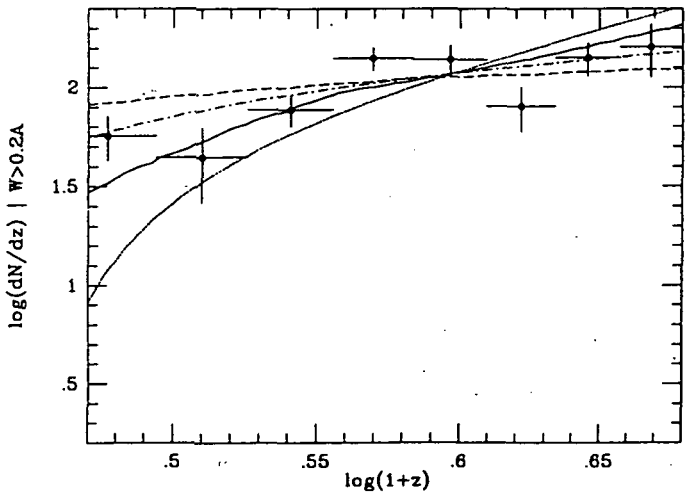

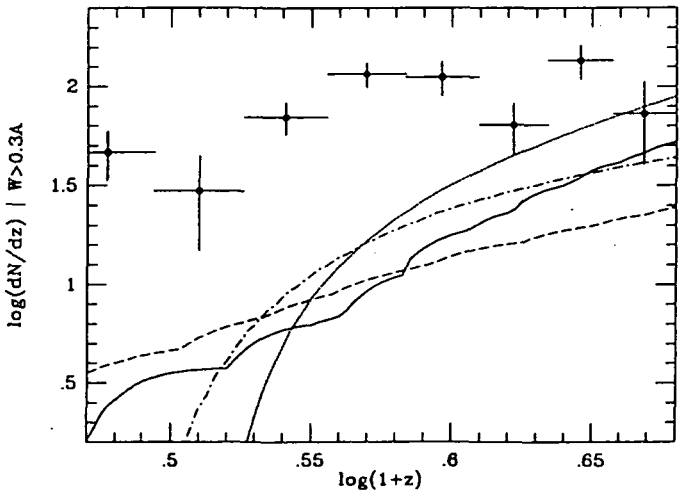

Figs. 3-4. The observed *vs.* model redshift distribution of Lyα clouds with $W_r \geq 0.2$Å (Fig. 3) and $W_r \geq 0.3$Å (Fig. 4). The various curves correspond to various analytic and synthetic results: $j = 0/j = 4$ synthetic (solid/dashed); $j = 0/j = 4$ analytic (dotted/dot-dashed). Although the synthetic curves fit the data for $W_r \geq 0.2$Å, there are significant discrepancies in the slope and the normalization for $W_r \geq 0.3$Å. The analytic fits are worse, except for $j = 4$, $W_r \geq 0.2$Å.

On the Evolution of Lyman α Clouds Based upon the Minihalo Model

N93-26765

Izumi MURAKAMI and Satoru IKEUCHI
Division of Theoretical Astrophysics, National Astronomical Observatory, Mitaka, Tokyo 181, Japan

ABSTRACT We consider intergalactic clouds confined by the gravity of cold dark matter (CDM), the so called minihalo. Assuming a simplified evolution law of UV flux and mass function of gas clouds, we can reproduce number density evolution and HI column density distribution by minihalo model. Considering interaction between supersonic flow and a minihalo, we can investigate no spatial correlation and the proximity effect of Ly α forest.

1. Introduction

Absorption line systems of QSOs prove the physical states at the high redshift universe which is hard to observe directly. Several observational properties are indicated for absorption systems of QSOs[1,2,3,4]. Minihalo model for Lyman α forest is proposed from CDM cosmogony[5,6,7]. In this model, a gas cloud is confined by the gravity of CDM and we calculate cloud evolution to reproduce observational properties of Ly α forest.

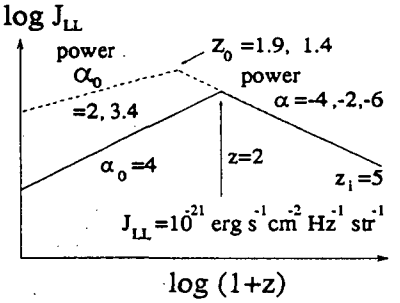

Fig.1 Assumed evolution of diffuse UV flux at Ly limit as a power-law function of $1+z$ with powers α and α_0.

2. Evolution caused by diffuse UV flux

We calculate the evolution of a spherical gas cloud, with primordial abundance, irradiated by the diffuse UV flux. we take into account heating by UV radiation and radiative cooling, and keep the CDM potential unchanged. Initially gas and CDM are in a gravitational equilibrium. We calculate ionization equilibrium. We assume the diffuse UV flux as $J_\nu(r;z) = J_{LL}(z)(\nu/\nu_{LL})^{-1}\exp(-\int_r^R n_{HI}dr/10^{17.5}\mathrm{cm}^{-2})$, and the evolution of $J_{LL}(z)$ at Ly limit, ν_{LL}, as Fig. 1. Here we take $\Omega = 1$, $q_0 = 0.5$, and $H_0 = 100\mathrm{km\ s^{-1}Mpc^{-1}}$. Parameters which characterize minihalos are: $D = \rho_d(r = 0)/\rho_{crit}(z = 10)$, and $X = \sigma_d^2/c_s^2(10^4\ \mathrm{K})$, where $\rho_{crit}(z)$ is the critical density at the epoch z, σ_d is the velocity dispersion of CDM, and $c_s(T)$ is the sound speed of gas.

We calculate HI column density as a function of an impact parameter, p. Setting comoving space density of minihalos to be constant with a power law mass function, we take 'observed' number as

$$\frac{d^2\tilde{\mathcal{N}}}{dzdN_{HI}} = \frac{c\pi}{H_0}n_*(0)\int\left(\frac{M_c}{M_*}\right)^{-\delta}d\left(\frac{M_c}{M_*}\right)\left|\frac{pdp}{dN_{HI}}\right|(1+z)^{1-q_0}. \quad (1)$$

This equation is valid only for $q_0 = 0$ or 0.5. In order to compare with observation, we calculate the z-integrated column density distribution averaged by absorption distance[1,8]. The number density evolution are obtained by integrating Eq.(1) with the column density[2,3]. We assume the continuum depression D_A comes from cumulative absorption of clouds[9].

For $\alpha > 0$ clouds gradually contract and neutral fraction of hydrogen increase due to the decrease of UV flux. When n_{HI}/n_H approaches unity at the center of cloud, the HI region, called neutral core, appears and grows up to be unstable and collapse. For $\alpha < 0$ clouds expand slowly. Since cross

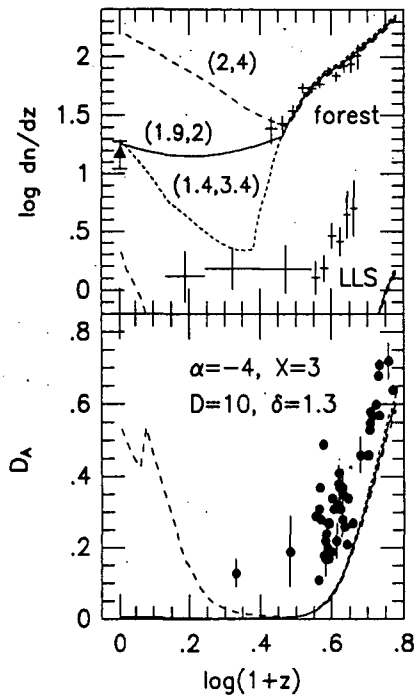

Fig.2 Number density evolution (upper panel) and continuum depression (lower) where lines are calculated results with (z_0, α_0). Crosses[2,3], triangle[4], and dots[9] are of ovserbations.

section for fixed HI column density becomes smaller with decreasing flux, observed number density and continuum depression decrease (Fig.2). HI column density distribution can be roughly approximated to a power-law form and fits observed one well.

Best fit model of UV flux is $\alpha = -4$ at $z \geq 1.9$ and $\alpha_0 = 2$ at $z \leq 1.9$ ($z_0 = 1.9$). Prefered values of other parameters to explain observations are: $\delta = 0.9 \sim 1.6$, $X \gtrsim 1$, and $D \sim 10$.

We propose a unified picture for HI absorption systems in this model. We can regard the Ly α forest as less massive ionized clouds and/or ionized envelopes of clouds with neutral cores, and high HI column density systems as neutral cores of massive clouds. Number of high column density components is smaller than observed one because the present model is restricted in the mass range of clouds. We must include massive collapsed systems and we may regard them as non-evolving components of LLSs. In our expanding minihalo model, gas clouds collapse at $z < 1$. These late collapse corresponds to formation of young dwarf galaxies[10].

3. Evolution caused by supersonic flow

We calculate the evolution of an initially spherical gas cloud exposed to supersonic gas flow in order to investigate the proximity effect and no spatial correlation for Ly α forest. Such flow seems to occur when a minihalo moves against ambient matter or a blast wave propagates from a QSO[11].

The gas cloud, of which central pressure is lower than the ram pressure of a supersonic flow, is blown out from the potential of minihalo. On the other hand, the gas cloud, of which central pressure is higher than the ram pressure, is stripped gradually by bow shock, if the escape velocity of gas is smaller than the velocity of gas flow. The timescale of this strip depends on the distribution of dark matter and the density and velocity of gas flow.

For the proximity effect, if we consider the blast wave ejected from a QSO with energy larger than 10^{63} erg, clouds are blown off from the potential of dark halos within $2 \sim 3$ Mpc from a QSO, which is its propagating distance by $z \sim 2$.

We consider the clustering of minihalos, which naturally occurs in the CDM cosmogony. In such a process, minihalos gain random velocity, which is about the virial velocity of the cluster, relative to surrounding matter. The moving gas clouds feel the ram pressure and are stripped. If we take mass and radius of such a cluster as ones of galaxies, the gas clouds can be stripped via their motion in a dense cluster and not be seen with time scale shorter than the Hubble time (Fig.3). As a result, the gas clouds which show high spatial correlation cannot be observed as absorption lines because their gas is almost stripped.

The minihalo model based on the CDM cosmogony can represent many characteristic properties of Lyman α forest and this result becomes one of indirect evidences supporting CDM scenario for the galaxy formation.

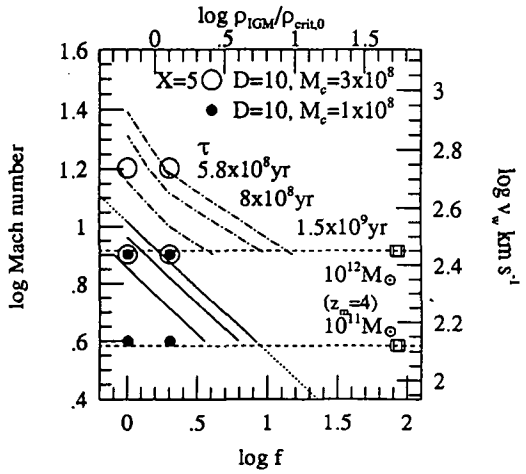

Fig.3 Contours of time scale losing gas for two clouds in flow density and velocity space. Squares are for clusters of minihalos.

References

1. W.L.W.Sargent, C.C.Steidel, and A.Boksenberg 1989, *Ap.J. Suppl.* **69**, 703.
2. L.Lu, A.M.Wolfe, and D.A.Turnshek, 1991, *Ap.J.*, **367**, 19.
3. K.M.Lanzetta 1991, *Ap.J.* **375**, 1.
4. J.N.Bahcall *et al.*, 1992, preprint.
5. M.J.Rees 1986, *M.N.R.A.S.* **218**, 25p.
6. S.Ikeuchi 1986, *Ap. Space Sci.* **118**, 509.
7. S.Ikeuchi, I.Murakami, and M.J.Rees 1988, *M.N.R.A.S.* **236**, 21p
8. D.Tytler 1987, *Ap.J.* **321**, 69.
9. D.P.Schneider, M.Schmidt, and J.E.Gunn 1989, *A.J.* **98**, 1951.
10. I.Murakami and S.Ikeuchi, 1991, submitted to *Ap.J.*
11. I.Murakami and S.Ikeuchi, 1992, in preparation.

Probing the Extent and Content of Low Ionization Gas in Galaxies: QSO Absorption and H I Emission

Donna S. Womble (CASS, U.C. San Diego)

The small projected separations of some QSOs and low-redshift galaxies provide unique opportunities to study the extent and content of gas in galaxies through observation of absorption in the QSO spectra. Observations of these systems provide valuable information on the connection between the absorbing gas and the galaxy, as well as detailed information on the morphology and environment of the galaxy itself. While there is direct evidence that galaxies can produce the intervening-type QSO absorption lines, over the past decade, the study of such "QSO-galaxy pairs" (at low redshift) has been considered unsuccessful because new detections of absorption were seldom made (Bothun, Margon, & Balick 1984, PASP, 96, 583; Morton, York, & Jenkins 1986, ApJ, 302, 272; Bowen, Pettini, Penston, & Blades 1991, MNRAS, 249, 145). A fundamental problem concerning the relation between these low-redshift systems and those seen at moderate to high redshift remains unresolved. Direct and indirect measures of galaxy absorption cross sections at moderate to high redshifts ($z \gtrsim 0.5$) are much larger than the optical and H I sizes of local galaxies. However, direct comparison of the low and moderate to high redshift systems is difficult since different ions are observed in different redshift regimes.

Observations are presented here for a new sample of QSO-galaxy pairs. We have observed 9 new QSOs which shine through nearby galaxies (on the sky-plane) to search for Ca II absorption in the QSO spectra at the foreground galaxy redshifts. These new pairs were selected to have QSO-galaxy impact parameters, b, less than $20\,h^{-1}$ kpc and less than 3.0 isophotal galaxy radii measured at 25 B-mag per square arcsec and spiral galaxies, only. This strict separation criterion was chosen to fill a crucial gap of impact parameters, $10 \lesssim b \lesssim 20\ h^{-1}$ kpc, left from previous studies of Ca II absorption in QSO-galaxy pairs (Bothun *et al.* 1984, Morton *et al.* 1986, Bowen *et al.* 1991). In conjunction with this optical spectroscopic data, we have obtained deep optical images and H I 21 cm spectral line maps of the galaxies to explore any global morphological trends which may significantly contribute to (or reduce) the cross sections of the galaxies and to quantify the Ca II absorption cross sections in terms of the H I column densities.

Observations

Optical spectroscopic observations of the background QSOs were obtained using the Lick 3-m and KPNO and CTIO 4-m telescopes at resolutions ranging from 0.8 to 3.0Å. These spectra were reduced in a standard manner. As most of the QSOs in this sample are moderately faint, a large number of individual spectra were obtained for each object; these were weighted and co-added to optimize the signal to noise in the resulting spectra. An automated line finding routine was used to locate all the narrow absorption lines in these final spectra in a unbiased manner; we adopted a 5σ equivalent width threshold for the detection of lines. This routine was also used to determine the observed equivalent width limits in cases where no galaxian absorption lines were detected. The identified lines were then individually measured to insure accurate determination of the values. Column densities and limits for the observed QSO-galaxy pair absorption systems were determined using curves of growth. However since many of the observed lines are saturated and are likely to consist of multiple, unresolved velocity components, these column densities are representative of the absorption system strengths but should be interpreted with caution.

H I 21 cm emission maps of a sub-sample of the pairs described above were obtained with the VLA in the D and C array configurations. The sub-sample was chosen based on the beam versus galaxy sizes for a given array configuration; it includes examples of both detections and non-detections of optical absorption lines. These data were calibrated and mapped in a standard

manner with some special steps taken in cases of severe interference and strong continuum source subtraction. The H I column densities at the QSO positions were determined by interpolating the spatial pixels of the spectral line cube and generating a one-dimensional spectrum at the precise background source position. Moment maps were also generated for the galaxies using a combination of velocity, flux and interactive blanking to reduce noise contributions.

Results

Of the nine new pairs, we have detected 4 new Ca II galaxian absorption systems and have possible detections in 2 additional objects. In the cases of possible systems and non-detections, the observed equivalent width limits are in the range 90 to 140 mÅ (3σ). These data are discussed here in conjunction with a "complete" compilation of all the QSO-galaxy pairs observed to date which have impact parameters less than 22 h^{-1} kpc. Two additional objects with larger impact parameters are also considered here since the QSOs show galaxian absorption systems; the many non-detections with $b \gtrsim 22\ h^{-1}$ kpc are analyzed in previous studies (Bothun *et al.* 1984, Morton *et al.* 1986, Bowen *et al.* 1991) and are not considered further here.

Considering both the new sample and the existing QSO-galaxy pair absorption systems, a number of conclusions can be reached. We see no correlation between the Ca II K-line strength with impact parameter measured in either kpc or iosophotal radii. This is unlike the correlation of Mg II absorption line strengths with impact parameters seen in moderate redshift QSO absorption systems (Lanzetta & Bowen 1990, ApJ, 357, 321). The existence of 2 Ca II absorption systems with unusually large impact parameters ($b \simeq 45$ & 60 h^{-1} kpc) indicates that there is no absolute maximum galaxy cross section for producing detectable Ca II absorption. Since non-detections are also seen over the entire range of b with 10 non-detections between 0 and $20\,h^{-1}$ kpc (4 of these between 0 and $5\,h^{-1}$ kpc), there is no minimum impact parameter below which Ca II absorption is always detected.

The H I column densities at the QSO positions are also not correlated with b as measured in h^{-1} kpc. The H I column densities are correlated with the optical extent of the galaxies; this is consistent with the Bosma (1981, AJ, 86, 1825) results but is somewhat misleading for the individual data points considered here. The spatial distribution of H I emission in many of the pairs shown here are highly non-uniform with respect to the optical extent in the QSO vicinity.

The measured Ca II line strengths are correlated with the H I column densities; this correlation is independent of the impact parameter. For high quality optical data with an equivalent width limit of 100 mÅ, Ca II absorption should be detectable for H I column densities greater than $10^{19.5}$ cm^{-2}. This is unlike the Mg II QSO-absorption selected sample which showed no correlation between the optical absorption properties and 21 cm optical depths (Briggs & Wolfe 1983, ApJ, 268, 76).

Of the 9 detections of QSO-galaxy pair absorption systems, most of the galaxies are tidally disrupted or in some way morphologically unusual. Many show a great deal of evidence for induced star formation. Some are classic starburst galaxies, and most are bright *IRAS* sources. The absorption non-detection galaxies with both H I and optical imaging data do not show the unusual morphological nature obviously evident in the detection-pairs. Ca II absorption appears to be a good tracer of large H I column densities. However, the large H I column densities seen in these systems do not imply disk-gas; tidal interactions and active star formation can have a very dramatic effect on the distribution of gas in in these galaxies. Finally, these data are not necessarily representative of all high redshift QSO absorption systems, but they probably form some subset of them.

This work has been supported in part by NASA, contract NAS 5-29293 and grant NAG 5-1630.

The Two-Point Correlation Function of Randomly Distributed Lyman-α clouds

Mark A. Fardal, J. Michael Shull, CASA and JILA/ University of Colorado

It is often assumed that Lyα forest clouds are randomly distributed, intergalactic objects that are highly ionized by the UV background produced by quasars. If these assumptions are true, fluctuations in the UV background should produce a nonzero two-point correlation function in the Lyα forest. This effect, which is really just a generalization of the proximity effect (Bajtlik et al. 1988), is more significant at high redshift ($z \approx 3-4$) because the mean free path for UV photons is smaller there, and the fluctuations correspondingly larger. We have studied this effect using both the semi-analytic techniques of Zuo's recent papers (1992a,b) and Monte Carlo simulations. The correlation function is expected to have a small yet potentially measurable amplitude that is consistent with current upper limits. Furthermore, the signature of this effect is distinctive because the nonzero correlation function extends over the photon mean free path, which is larger than the expected scale of large-scale structure. Observations or upper limits on this effect could provide information about the source of the ionizing background at high redshifts and the nature of the Lyα forest clouds.

The basic idea is the same as in the proximity effect. The neutral column density for a highly photoionized system is inversely proportional to the flux J_L at the Lyman limit, or more precisely to the photoionization rate; the distinction is important and is treated in a simplified manner. The distribution of H I column density N is proportional to $N^{-\beta}$, with $\beta \approx 1.7$. The observed density of Lyα clouds, which is assumed to be determined by a lower column density limit, is proportional to $J_L^{1-\beta}$. Then the two-point correlation function is

$$\xi(r) = \frac{\langle J_{L1}^{1-\beta} J_{L2}^{1-\beta} \rangle_r}{(\langle J_L^{1-\beta} \rangle)^2} - 1.$$

The average in the denominator is taken over all points in space, and the numerator is averaged over all pairs of points that are separated by a distance r. $\xi(r)$ depends on the point-source density, luminosity function, and distribution of the absorbers. The expected correlation function for redshift $z = 4.0$ is shown in Figure 1. The correlation function extrapolated to zero separation is shown as a function of redshift in Figure 2.

References

Bajtlik, S., Duncan, R. C., and Ostriker, J. P., 1988. Ap. J., **327**, 570.

Møller, P., and Warren, S., in *The Space Distribution of Quasars*, ed. D. Crampton (Astronomical Society of the Pacific).

Zuo., L., 1992a. M. N. R. A. S., submitted.

Zuo., L., 1992b. M. N. R. A. S., submitted.

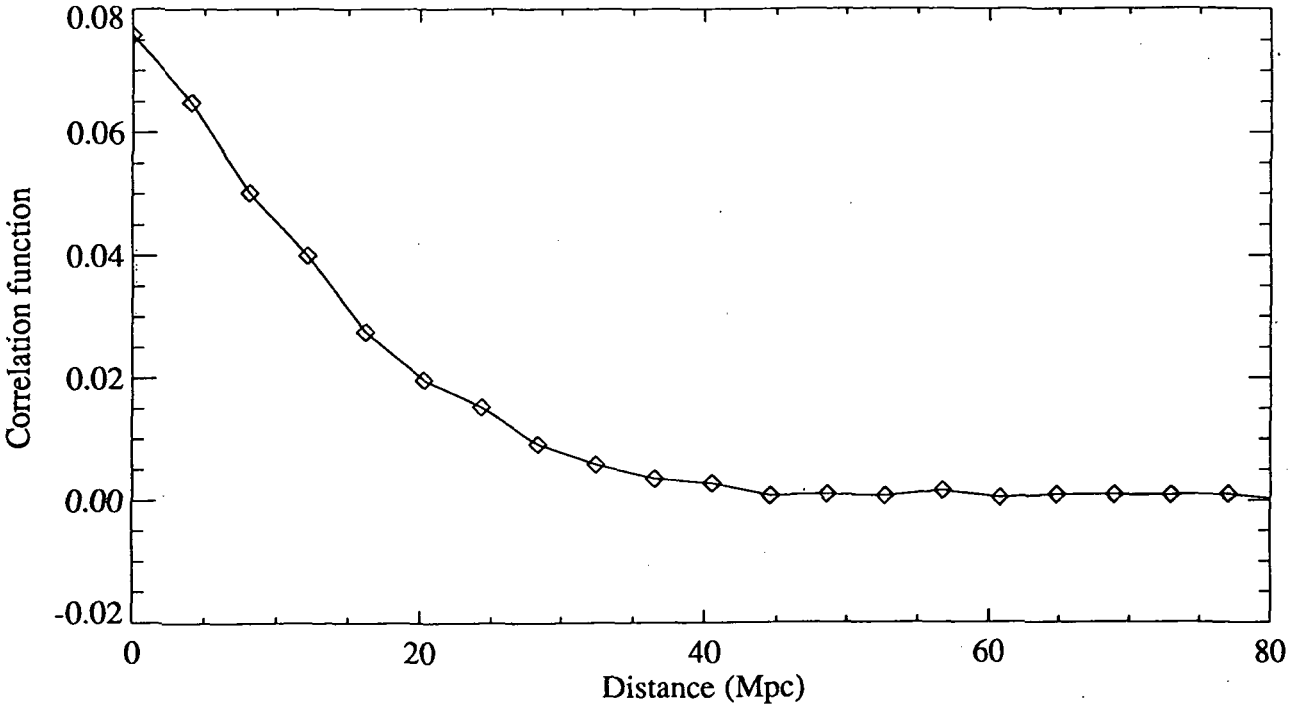

Figure 1. Expected correlation function at redshift $z = 4.0$, assuming exponential attenuation, UV power-law slope $p = -1$, constant comoving space density of quasars, and Møller and Jakobsen's (1991) model for the absorbers. Produced with truncated Monte Carlo technique. The absorption length here is 21.2 Mpc.

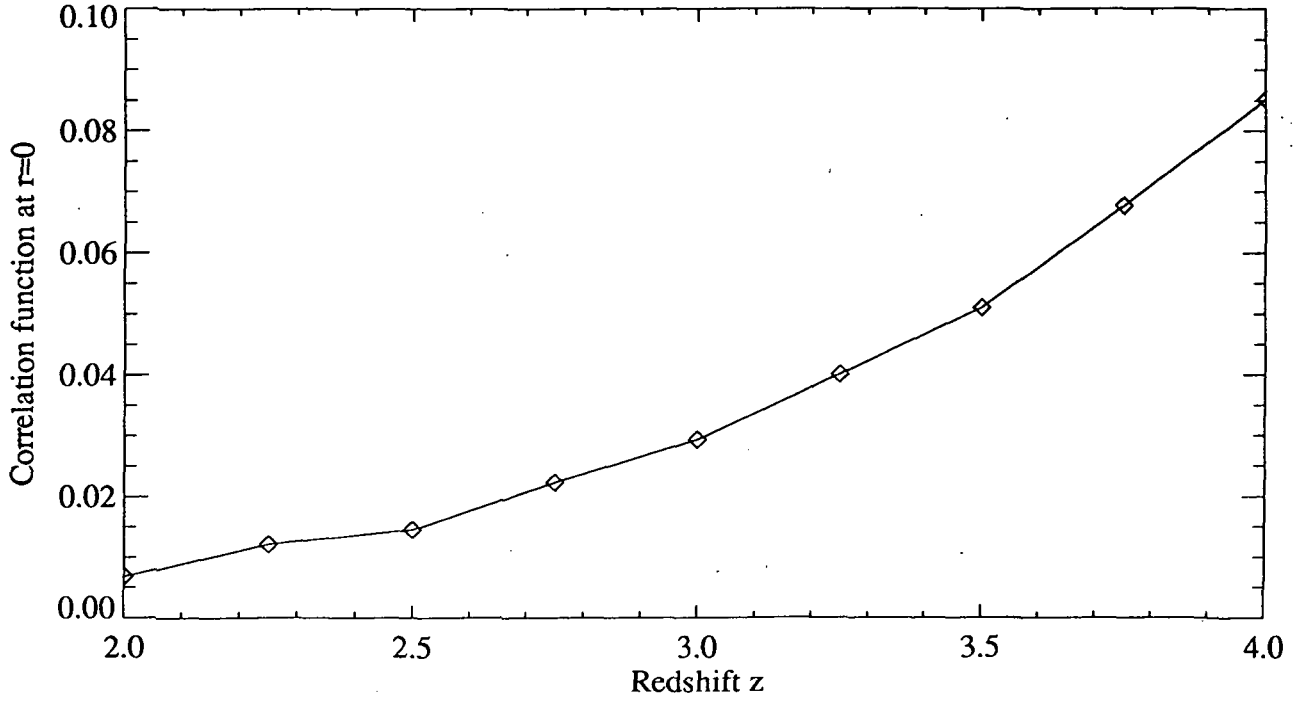

Figure 2. Maximum correlation function (correlation function extrapolated to zero separation) as a function of redshift; same assumptions as above but FT method used.

INTENSITY CORRELATION OF IONIZING BACKGROUND AT HIGH REDSHIFTS

Lin Zuo[1,2]
[1]Astronomy Department, Caltech, Pasadena, USA
[2]CITA, University of Toronto, Toronto, Canada

1. THE INTENSITY CORRELATION FUNCTION ξ_J

Suppose that in a Euclidean space there are uniformly (randomly) distributed discrete ionizing sources and absorbers.* In this case the effective optical depth is $\tau_{eff}(r) = r/r_0$, where r_0 is the absorption length scale at which $\tau_{eff} = 1$. Given two positions $\vec{r} = 0$ and $\vec{r_1}$ we have derived the joint probability $W(J_0, J_1)dJ_0dJ_1$ that the mean Lyman limit frequency intensity at $\vec{r} = 0$ is between $J_0 \rightarrow J_0 + dJ_0$ and at the same time the mean Lyman limit frequency intensity at $\vec{r_1}$ is between $J_1 \rightarrow J_1 + dJ_1$ (see Zuo 1992). In our derivation we have assumed that the total optical depths along two different lines of sight are not correlated. This is a good approximation if the sizes of the absorbers are small and if the space density of the ionizing sources is low. From $W(J_0, J_1)$ we can show that the Lyman limit frequency intensity correlation function $\xi_J(r_1)$ is given by (Zuo 1992)

$$\xi_J(r_1) \equiv \frac{\langle J_0 J_1 \rangle}{\langle J \rangle^2} - 1 = \frac{1}{8\pi r_0^3} \frac{1}{n} \frac{\langle L^2 \rangle}{\langle L \rangle^2} \frac{1}{u_1} I_J(u_1), \tag{1}$$

where $u_1 = r_1/r_0$ and

$$I_J(u_1) = 2 \int_0^\infty \frac{v}{\mathrm{sh}v} e^{-u_1 \frac{1+e^{-v}}{1-e^{-v}}} dv. \tag{2}$$

We assume that QSOs were the dominating ionizing sources at early epochs. We adopt $q_0 = 0.5$, $H_0 = 50\mathrm{km\ sec^{-1}Mpc^{-1}}$ and use the model B QSO luminosity function of Boyle, Shanks and Peterson (1988) for $z \leq 2.2$. At $z \geq 2.2$ we assume that quasars have a constant comoving space density and there was no luminosity evolution for individual sources. For the quasar spectrum we adopt $L_\nu \propto \nu^{-0.5}$ for $\lambda > 1216\AA$ and $L_\nu \propto \nu^{-1}$ for $\lambda < 1216\AA$. We then get, for $z \geq 2.2$, $\langle L^2 \rangle / (n \langle L \rangle^2) \simeq 0.3 \times 10^6 (1+z)^{-3} \mathrm{Mpc^3}$. We have calculated τ_{eff} and r_0 by using Miralda-Escudé and Ostriker (1990) Model A2 absorption.

The resulting intensity correlation ξ_J is large at small separations and at high redshifts. This is because the absorption by QSO absorption line systems reduces the total number of dominating ionizing sources involved in producing J and therefore enhances the fluctuations significantly.

2. ABSORPTION LINE EQUIVALENT WIDTH CORRELATION $\xi_{1/W}$

According to standard models the Lyα forest lines observed in quasar absorption spectra are produced by intervening clouds which are highly ionized by the ionizing background. Therefore these clouds may serve as intensity indicators and help us to constrain the

* Since the ionizing field at the Lyman limit frequency is a local phenomenon (see Zuo 1991), the Euclidean space approximation is good enough at high redshifts.

intensity correlation function and the space density of the dominating ionizing sources at high z. If the majority of Lyα forest lines are on the linear part of the curve of growth and the rest equivalent width W of an absorption line is proportional to J, we then have $W = A/J$, where A depends only on the intrinsic properties of an absorbing cloud, i.e., $A \propto \int \alpha_H n_H^2 dl$ for ionized clouds with α_H denoting the hydrogen recombination coefficient and n_H the total hydrogen number density. This suggests that we should study $1/W$ correlation of the Lyα forest lines.

For eight selected QSOs we have carried out the $\xi_{1/W}$ measurements (see Zuo 1992 for details). In four cases, i.e., Q0000–263, Q2000–330, Q0055–269 and Q1247+267, we have detected a positive correlation signal in the smallest separation bins, which seems to have been produced mainly by the lines near the QSO emission redshifts.

One explanation for the detected correlations is that the spectral signal-to-noise ratio (S/N) systematically declines towards the blue end because the detector quantum efficiency decreases at shorter wavelengths. Also when absorption lines are close enough to the quasar redshift to be superposed on the blue wing of the Lyα emission line, the S/N ratio is boosted significantly. Thus more weak lines near z_{em} may be included in the line list and this leads to the observed $1/W$ correlation. This explanation can be tested by measuring the simulated spectra with inhomogeneous continuum S/N. Another possibility is that the observed correlation signals may be produced by the enhanced ionizing field near the QSOs. If this is true then from the affected wavelength range and the estimated Lyman limit luminosity $L \approx 7 \times 10^{31}$ergs sec^{-1}Hz^{-1} of Q0000–263, we conclude $J_{-21} \lesssim 0.1$ at $z \simeq 4$, where $J = 10^{-21} J_{-21}$ergs s^{-1}cm^{-2}Hz^{-1}sr^{-1}.

How the measured $\xi_{1/W}$ results compare with our theoretical ξ_J? A straightforward comparison is difficult because of the equivalent width cut-off effect, i.e., observationally only those lines with an equivalent width larger than a certain threshold value can be positively detected. This effect depends on the intrinsic $f(A)$ distribution of the absorbing clouds and usually makes $\xi_{1/W}$ smaller than ξ_J (see Zuo 1992). If the observed $1/W$ correlation is produced by the proximity effect, then we know that the intrinsic $f(A)$ distribution is favorable enough for us to detect the general (not near a known QSO) J correlation. The sample 6 of Q0000–263, which excludes the lines within a distance 20Mpc from the QSO, does show a significant $\xi_{1/W}$ signal at the smallest separation. To check whether the magnitude is also consistent with our ξ_J calculation we need to know the exact shape of the $f(A)$ distribution. On the other hand if galaxies dominated J at high z then we don't expect to see any J correlation, except near a known powerful QSO (the proximity effect). The detected $1/W$ correlation may have to be explained by the non-uniform S/N ratio effect.

REFERENCES

Boyle, B. J., Shanks, T. & Peterson, B. A., 1988. *Mon. Not. R. astr. Soc.*, **235**, 935.
Miralda-Escudé, J. & Ostriker, J. P., 1990. *Astrophys. J.*, **350**, 1.
Zuo, L., 1991. *Ph.D. Thesis*, Ch. 2, California Institute of Technology.
Zuo, L., 1992. *Mon. Not. R. astr. Soc.*, in press.

Constraints on Chemical Evolution Models from QSOALS Abundances

J. T. Lauroesch

Department of Astronomy and Astrophysics, The University of Chicago, Chicago IL, 60637

1 Introduction

Models of the formation and early chemical evolution of our Galaxy are guided and constrained by our knowledge of abundances in globular cluster stars and halo field stars. The abundance patterns identified in halo and disk stars should be discernible in absorption lines of gas clouds in forming galaxies which are accidentally lying in front of background QSO's. Conversely, the ensemble of QSO absorption line systems (QSOALS) at each redshift may suggest a detailed model for the formation of our Galaxy that is testable using abundance patterns in halo stars.

2 Galactic Abundances

Over the past decade, high signal-to-noise ratio, spectroscopic studies of Population II stars have provided strong evidence that the oldest and most extremely metal deficient halo stars in our Galaxy are characterized by elemental abundance patterns which differ substantially from those characteristic of Solar System matter (Wheeler, Sneden, and Truran 1989, Gratton and Sneden 1991). In halo stars, it is found that oxygen and the other even-Z, alpha particle nuclei (neon, magnesium, silicon, sulphur, argon, calcium, and perhaps titanium), are enriched relative to iron and the other even-Z, iron peak nuclei (chromium, nickel, and zinc) by approximately a factor of 3, when [Fe/H]$\lesssim$-1.0. Aluminum, an odd-Z nucleus, is underabundant relative to the even-Z alpha particle nuclei for [Fe/H]$\lesssim$-1.0. While the even-Z iron peak nuclei (nickel, chromium, and zinc) have essentially solar abundance ratios compared to iron in metal-poor stars, Mn and Cu (both odd-Z nuclei) are relatively underabundant. These trends can be understood as a consequence of early formation of the bulk of the α nuclei in type II SNe, with the later buildup of the Fe-group by type I SNe (Wheeler, Sneden, and Truran 1989, Lauroesch *et al.* 1992).

Abundance determinations in Galactic gas clouds have shown that in the ISM there is selective depletion of some elements into dust grains. A review of elemental abundances in the ISM and of the inferred composition of interstellar dust is given by Jenkins (1987). It is important to note that S and Zn show little or no depletion, while Si and Mn are depleted by $\gtrsim$ 0.5 dex, and Al, Fe, Ni, and Cr are depleted by $\gtrsim$ 1 dex.

3 QSO Absorption Line Systems

Absorption lines appear in spectra of QSO's at $z_{abs} \lesssim z_{em}$. York *et al.* (1991) list ~900 absorption systems out to a redshift of z~4.5. Such absorption line systems, when studied at high redshifts, might be expected to show abundances similar to those in halo stars, as the halo stars are thought to represent the first low mass stars formed from Galactic interstellar clouds. Based upon depletion patterns in the local ISM, one should expect that abundances for S and Zn should be straightforward to interpret as indicators of overall metallicity if dust in QSOALS is like local interstellar dust, whereas the total abundances of other elements may be harder to determine depending on how much dust is present. However, by comparing specific gas-phase abundance ratios and assuming that dust depletion occurs in a similar manner to that in the local ISM, it is possible to set constraints on dust formation (Meyer, Welty, and York 1989). Additional constraints on the amount of dust depletion have been placed by Pei, Fall, and Bechtold (1991), who estimated that the typical dust-to-gas ratios in damped Ly-α sytems are 5%-20% of that in the Milky Way.

A number of studies of the heavy-element absorption line systems have found evidence that the metallicity in these systems is decreasing with increasing redshift. The number density of C IV absorption systems per unit z, M(z), decreases with increasing redshift, and the mean C IV doublet ratio systematically increases with increasing redshift (Sargent, Boksenberg, and Steidel 1988, Steidel 1990, York *et al.* 1991). In contrast the number of Lyman-limit systems per unit z is increasing (Steidel 1990, and references therein). Searches for C IV absorption in known Ly-α systems have found additional C IV absorption (Meyer and York 1987, Lu 1991). The number density of Si II, Si IV, and Fe II absorbers has also been found to decline with increasing redshift (York *et al.* 1991, Lauroesch *et al.* 1992), implying that the decline in density of systems is not due to an evolving radiation field.

Recent abundance determinations from high resolution and/or high signal-to-noise observations have been published for ~10 absorption systems at z~2. It is evident, at least for this sample, that typically [Fe/H]≃-2, and that nc species, including S and Zn, have abundances in excess of $\frac{1}{8}$ solar (Lauroesch *et al* 1992). Refractory elements such as Fe, Cr, and Ni are down by less than a a factor of 5 compared to Zn in QSO absorbers, whereas in the Galactic ISM they are depleted by factors of ~20-100. If dust is similar at all redshifts, the refractory elements are relatively more depleted today than in the available sample at z~2.

Is the gas in QSO absorbers the same type of gas from which the Milky Way halo stars formed? The gas is similar to halo stars in having low metallicities, however in only a few cases have abundances been measured for a number of species with different nucleosynthetic origins. In addition, for some systems, some abundances are derived from saturated lines, and may be underestimates. Finally, it is worth noting that these results are generally without any ionization correction, although the the corrections required appear small in some systems (Meyer, Welty, and York 1989). It remains to be seen whether any anomalies in relative abundances can be discerned and separated from dust depletion effects in a larger sample of absorbers. However, from the limited data available at present there are some suggestive results. The z_{abs}=2.140 system in 0528-250 shows Mn underabundant with respect to Cr and Ni (Meyer, Welty, and York 1989), Cr and Ni being among the more heavily depleted species in the local ISM. This is similar to the halo stars where Mn is underabundant compared to the even-Z iron peak nuclei, and suggests that type II SNe are the dominant source of the metals. The z_{abs}=1.766 system in 1331+170 (York *et al.* 1992) has a metallicity of $\sim \frac{1}{10}$ solar, but Si, S, and Mn appear to be in essentially solar ratios when compared to the Cr, Fe, Ni, and Zn. This may be a result of significant early type I SNe activity, which would explain the high Fe-group abundances and the high relative abundance of Mn.

4 Conclusions

Studies of abundances in QSO absorption line systems, determining the distribution of abundances at each redshift, should allow detailed modelling of the history of chemical evolution in the universe. Patterns in the relative abundances in the absorber systems can be used as probes of the history of chemical evolution in these systems, and can be compared both to the patterns observed in the Galactic halo and to chemical evolution models. If a large sample of relative abundance measurements can be made for a number of systems in different redshift intervals, it may be found that there are systems where the chemical evolution occurs in a manner quite different than in the Galactic disk and halo. This topic has been discussed in detail by Lauroesch *et al.* (1992). A program of high resolution measurements of a number of QSO lines-of-sight has begun using the 4-meter telscope at Kitt Peak National Observatory by J. T. Lauroesch, D. G. York, and R. F. Green.

REFERENCES

Gratton, R. G., and Sneden, C., 1991, A&A, 241, 501

Jenkins, E. B., 1987, in *Interstellar Processes* eds. D. J. Hollenbach and H. A. Thronson, Jr. (D. Reidel Publishing Company), p. 533

Lauroesch, J. T., Truran, J. W., Welty, D. E., and York, D. G. 1992, ApJ, submitted

Lu, L. 1991, ApJ, 3379, 99

D. M., and York, D. G., 1987, ApJ, 315, L5.

Meyer, D. M., Welty, D. E., and York, D. G., 1989, ApJ, 343, L37.

Pei, Y. C., Fall, S. M., and Bechtold, J. 1991, ApJ, 378, 6

Sargent, W. L., Boksenberg, A., and Steidel, C. C. 1988, ApJS, 68, 539

Steidel, C. C. 1990, ApJS, 72, 1

Wheeler, J. C., Sneden, C., and Truran, J. W. 1989, ARA&A, 27, 279

York, D. G., Yanny, B., Crotts, A., Carilli, C., Garrison, E., and Matheson, L. 1991, MNRAS, 250, 24

York, D. G., KeLiang, H., Green, R. F., Bechtold J., Welty, D. E., Carlson, M., and Khare, P. 1992, in preparation

---

This manuscript was prepared with the AAS WGAS LaTeX macros v2.2

Interstellar Mg II and C IV absorption by $1\frac{1}{2}$ galaxies along the sightline to Mrk 205

David V. Bowen & J. Chris Blades
(*Space Telescope Science Institute*)

We present the first results of our HST survey designed to search for Mg II and C IV absorption lines from the disks and haloes of low-redshift galaxies, using background QSOs and supernovae as probes. Our survey utilizes the high resolution of the *Goddard High Resolution Spectrograph* enabling us to calculate the column densities and doppler parameters of individual components within an absorption complex, and hence determine the physical conditions of the absorbing gas. Observing the complexity of the absorption line profiles i.e., the velocity distribution and total velocity extent of the constituent components, offers an important description of the kinematics of the absorbing gas, and hence an understanding of its origin.

We focus on one sightline in particular, that towards Mrk 205, which passes 3 – 5 kpc from the intervening galaxy NGC 4319. We detect Mg II and C IV absorption from both local Milky Way halo gas and from NGC 4319 (Fig. 1). The equivalent width (W) of the local C IV(λ1548) line is weak, $W(\lambda1548) = 159 \pm 29$ mÅ, but very similar to the extragalactic absorption, $W(\lambda1548) = 187 \pm 32$ mÅ. However, the disparity between the local Mg II absorption and that in NGC 4319 is severe: the lines arising in the Milky way gas are saturated [$W(\lambda2796) = 1.08 \pm 0.02$ Å], are composed of several components (≥ 5) covering a total velocity span of 100 km s^{-1}, and are flanked by weak high-velocity components at -215, -153. In contrast, the absorption by NGC 4319 is weak [$W(\lambda2796) = 234 \pm 17$ mÅ] and can be modelled with a single component.

Absorption by the local Milky Way

The line-of-sight towards Mrk 205 lies at Galactic co-ordinates $l = 125.4$, $b = 41.7$, passing through the outer spiral arm in the second quadrant and intercepting the edge of the HVC Complex C. Models which assume that a halo corotates with the disk demonstrate that the negative velocities of the Mg II components are entirely consistent with corotating gas. Only the two high velocity components (-215 & -153 km s^{-1}) show velocities which cannot be accounted for by corotation.

The 21 cm H I emission associated with the most negative velocity component is $N(\mathrm{H\ I}) = 1.93 \times 10^{19}$ cm^{-2} (Lockman & Savage 1992, in preparation), giving $N(\mathrm{Mg\ II})/N(\mathrm{H\ I}) = 3.1^{+2.0}_{-1.0} \times 10^{-7}$ for this HVC. However, the nearest 21 cm emission obviously associated with the second component at -153 km s^{-1} lies at -135 km s^{-1}. The feature is extremely weak, which may account for the discrepancy of 18 km s^{-1}, and is measured to have $N(\mathrm{H\ I}) = 1.4 \times 10^{18}$ cm^{-2}, with errors of a factor of 2. Whether of not this emission can be associated with the HVC, the number serves as a lower limit to N(H I), giving a ratio $N(\mathrm{Mg\ II})/N(\mathrm{H\ I})$ of $\lesssim 6.9 \pm 0.6 \times 10^{-5}$, over 200 times that in the higher velocity HVC!

For the C IV, the derived $N sin b$ is little different from the values seen towards the stars furthest away from the Galactic plane, demonstrating that there is no extra gas beyond the few kiloparces probed by halo stars. This uniformity is even more surprising considering that none of the sightlines previously investigated (Savage and Massa 1987) lay at positive declinations in the second quadrant. Assuming that the density of the gas $n(Z)$ is related to the height above the plane Z by $n_{\mathrm{C\ IV}}(Z) = n_{\mathrm{C\ IV}}(0) \exp(-Z/h)$, where h is the scale height above the plane, a formal fit to the line-of-sight towards Mrk 205 gives $h = 2.0$ kpc for $n_{\mathrm{C\ IV}}(0) = 8.0 \times 10^{-9}$ cm^{-2}.

Absorption by NGC 4319

The Mg II absorption seen in NGC 4319 characterizes a quiescent cool-phase of the ISM. Observations by Womble *et al.* (1992, in preparation) of 21 cm emission towards NGC 4319 show that the galaxy is completely anemic; at the position of Mrk 205, $N(\mathrm{H\ I}) < 2.8 \times 10^{19}$ cm^{-2}. Further, the existence of a single component means that the gas resides in a much less 'active' ISM than our own, that corotation, for example, does not serve to spread many components out over a wide velocity range. This is not simply an effect of inclination.

Though NGC 4319 appears face-on, the inclination of the galaxy ranges from $38° - 62°$ (where zero represents face-on inclinations), similar to the sightlines $(90 - b)$ latitude through our own Galaxy.

Though the local and extragalactic Mg II absorption and H I column densities are very different, N(C IV) in NGC 4319 and our own halo are surprisingly similar. However, the *lower limit* to the $\log N(\text{C IV})/N(\text{H I})$ ratio is quite different, $\gtrsim -5.4$, some 15 times the local value along the same sightline (which is already high compared to lines of sight to halo stars).

If Mg II and C IV absorption arise in the same gas, then we conclude that the gas in the inter-arm region of NGC 4319 is much more highly ionized than local, spiral arm gas. Alternatively, it could be that the C IV we see in the Galactic halo is in no way associated with the H I along the same sightline (for example, if the high-ionization species occur in cloud interfaces), in which case the quantities of C IV would be ambivalent towards the H I/Mg II columns, and no 'unusual' ionization mechanisms need be invoked. If so, however, any models of galactic halo production and support must allow that highly ionized species be produced specifically without the presence of large H I column densities.

Comparisons to higher-z absorption lines

The sightline towards Mrk 205 samples one and a half galaxy disks and haloes—half our own and all of NGC 4319's. Both sightlines demonstrate that galaxies can indeed produce the UV absorption lines seen at higher redshift, and both are examples of low-ionization systems, ones in which both Mg II and C IV are detected. At a mean redshift of $< z_{\rm abs} > = 1 - 2$ these two absorbers would be representative of $\approx 1/3$ of all absorption systems (Caulet 1989, Steidel & Sargent 1992, hereafter SS92). Further, the difference in the H I column densities between our galaxy and NGC 4319 means that we are observing the metal line properties of one damped, and one non-damped Lyα system at $z = 0$.

The equivalent width distribution of Mg II absorption lines at a mean redshift of $< z_{\rm abs} > = 1.12$ has been constructed by SS92. The observed absorption systems have equivalent widths which lie at the two extreme ends of this distribution. In NGC 4319, $W(\lambda 2796) = 0.23$ Å, which is less than the nominal 0.3 Å set by SS92 as the limit above which at least $\sim$ 80% of all Mg II absorbers are detected. In contrast, the total equivalent width observed through our own galaxy, including the HVC equivalent widths (but for only *half* a disk) is 1.40 ± 0.03 Å. Assuming, for example, that $n(W)dW \propto W^{-\delta}$, and that $\delta = 1.65$ (SS92), then only 18% of absorbers at $< z_{\rm abs} > = 1.12$ have $W(\lambda 2796)$ greater than that seen locally. This equivalent width distribution, however, is known to vary with redshift, in the sense that there are less strong lines at lower redshift (Petitjean & Bergeron 1990, SS92). This means that the type of absorption seen in our own Galaxy is predicted to be a rarity at zero-redshift. The redshift distribution of absorbers is usually expressed as $N(z) = N(0)(1+z)^{\gamma}$; given the values of γ and $N(z)$ found by SS92, and calculating $N(0)$, we expect systems with $W(\lambda 2796) \geq 0.3$ Å to be 14 times more common than systems with $W(\lambda 2796) \geq 1.0$ Å.

By analogy, the observed Galactic absorption—by gas whose kinematic behaviour we crudely understand—demonstrates that the velocity spread of individual components is completely consistent with absorption by galactic disks with scale heights of a few kiloparsecs at higher z, at least for the strongest Mg II systems. A similar conclusion was reached by Lanzetta & Bowen (1992) for the $z_{\rm abs} = 0.524$ system towards 0235+164, and the $z_{\rm abs} = 0.359$ system towards 1229−021. High resolution observations showed asymmetric line profiles with clouds clumped at velocities consistent with a model of rotating gas clouds intercepted at high inclination angles. The similarity between their profiles and the observed Galactic absorption is intriguing: one possible explanation for the HVCs seen locally is that they are simply distant spiral arms differentially rotating with the Galaxy. Are the weak components seen at the edges of the $z \sim 0.5$ complexes manifestations of corotating disks as predicted, or could they be the HVCs of external galaxies?

These results provide evidence that galaxies with kinematically ordered 'thick disks' have existed from redshifts of zero to at least 0.5. However, the evolution of the strong systems mentioned above offers the tantalizing possibility that either the disks of this population have collapsed and are, on average, smaller then they were at $z \sim 0.5 - 1.0$, or there are now fewer galaxies with such disks!

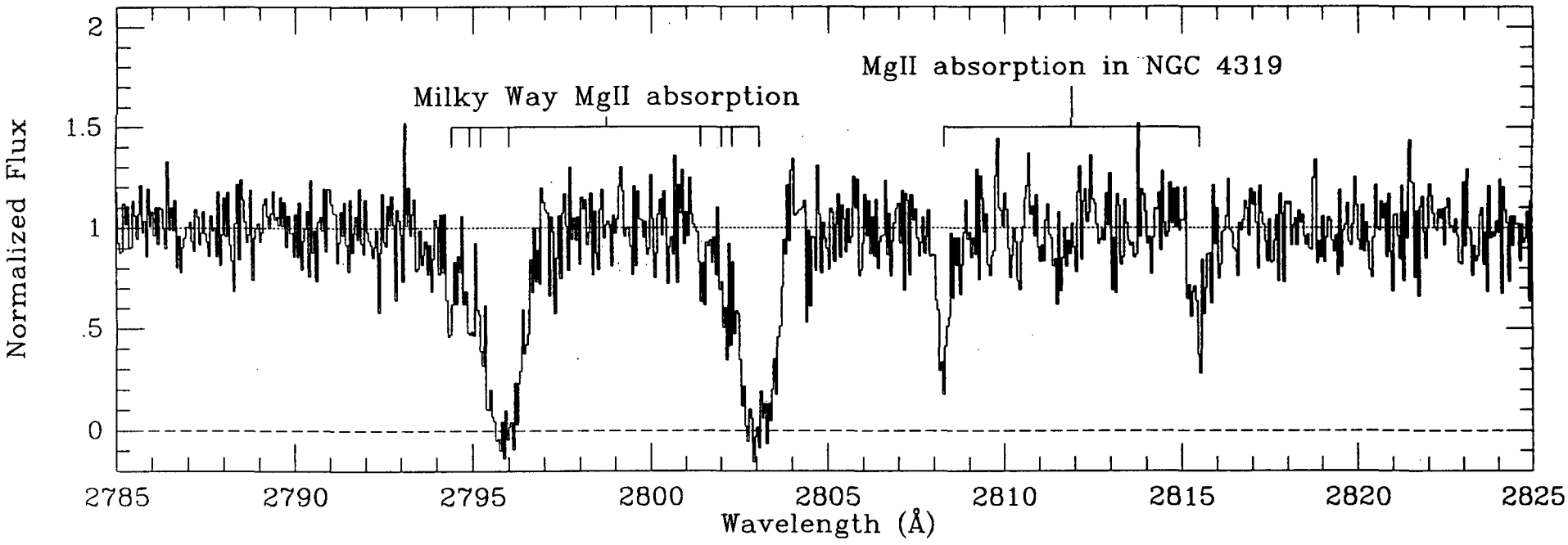
Milky Way MgII absorption
MgII absorption in NGC 4319
Normalized Flux
Wavelength (Å)
2785
2790
2795
2800
2805
2810
2815
2820
2825
0
.5
1
1.5
2

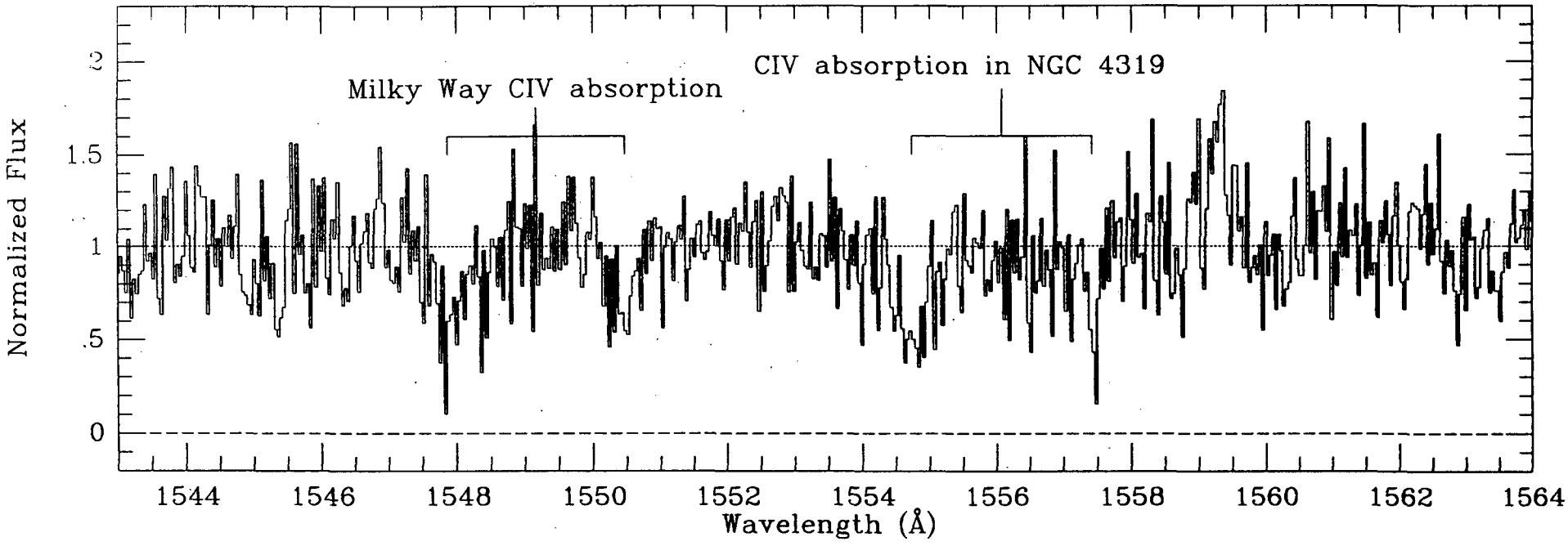
Milky Way CIV absorption
CIV absorption in NGC 4319
Normalized Flux
Wavelength (Å)
1544
1546
1548
1550
1552
1554
1556
1558
1560
1562
1564
0
.5
1
1.5

THE REIONIZATION OF THE UNIVERSE: THE FEEDBACK OF GALAXY FORMATION ON THE INTERGALACTIC MEDIUM

by
Paul R. Shapiro and Mark L. Giroux
University of Texas at Austin

I.

We have calculated in detail the thermal and ionization evolution of a uniform intergalactic medium (IGM) composed of H and He, undergoing "reionization," including the mean effect of gas clumps embedded in a smoothly distributed ambient gas. We have solved the rate equations for ionization and recombination, together with the equations of energy conservation, including the effects of cosmological expansion, radiative and Compton cooling, and the diffuse flux emitted by the gas, and radiative transfer. We have included the contribution to the continuum opacity of the universe due to the observed quasar absorption line clouds (QALC's). We have considered a variety of sources of photoionization, including quasars and primeval galaxies, as well as the possibility that hydrodynamical processes deposit thermal energy in the IGM. We shall describe applications of these calculations including the evolution of Ly α forest clouds.

II.

A self-consistent treatment of the thermal and ionization history of the intergalactic medium (IGM) must take account of the growth of structure in the universe, since the mean density of the IGM corresponds primarily to the time-varying *uncollapsed* fraction of the baryon-electron component of the matter, and the collapsed fraction, in turn, can have a "feedback" effect on this uncollapsed fraction by releasing ionizing radiation and thermal energy and by contributing to the opacity of the universe. We have begun to study this coupled evolution of the IGM and the emerging structure with a special focus on the reionization of the IGM, which is believed to have been completed by some redshift $z \gtrsim 4$, as inferred from the absence of the Gunn-Peterson effect in the spectra of high z quasars. We will describe the results and implications of detailed, numerical calculations of the thermal and ionization balance and radiative transfer in a uniform IGM of H and He, including the mean effect of an evolving distribution of gas clumps embedded in a smoothly distributed ambient gas.

Ionization States of Metallic Absorption-Line Systems in Continua of Quasars

KIYOMI DENDA and SATORU IKEUCHI

National Astronomical Observatory, Mitaka, Tokyo 181, Japan

ABSTRACT We study ionization states of metallic absorption - line systems in continua of quasars (QSOs), assuming that the metallic lines arise in gaseous halos of high-redshift galaxies in photoionization equilibrium under the background UV radiation, and obtain constraints on the intensity and spectral shape of the UV radiation. Then we discuss a structure of absorbers suitable for all of the metallic absorption - line systems.

1. INTRODUCTION

Metallic absorption - line systems in QSO spectra are generally supposed to be in photoionization equilibrium under the diffuse UV background, whose existence is supported by the Gunn-Peterson test (e.g., Gunn & Peterson 1965). These absorption systems can be classified into three groups, i.e., CIV system, Lyman limit system (LLS) and MgII system, according to the ionization state, in other words according to the column density of neutral hydrogen. However, we can study the ionization states of metallic absorption systems on the hypothesis that these difference in ionization states of three kinds of the absorption systems is caused by the difference in lines of sight through the absorbing halos. For example, Lanzetta, Turnshek & Wolfe(1987) suggested that MgII - absorbing clouds and CIV - absorbing clouds are grouped together and that the MgII clouds are concentrated toward the center of the group, on the other hand, the CIV clouds toward the edge. Furthermore, it is clear from observations at high spectral resolution that the metallic absorption - line systems consist of several subcomponents (e.g., Blades 1988). Their Doppler parameters are typically $b = 5 - 15\mathrm{km\ s^{-1}}$ and the total velocity spread of subcomponents ranges from $\sim 50\mathrm{km\ s^{-1}}$ to $\sim 800\mathrm{km\ s^{-1}}$. There have been a few analyses on the clumpy structure of absorbers (e.g., Lanzetta & Bowen 1990). Lanzetta & Bowen (1990) found that a radial profile of the spatial density of the clump roughly proportional to $r^{-\beta}$, with $\beta \simeq 2 - 3$.

In this paper, first, we assume a very simple model - absorber which has a density distribution $n_H \propto r^{-2}$ and examine probable contributions to ionizing radiation 1) from QSOs ; I_ν^d and/or 2) from early-type stars in the central high-z galaxy ; I_ν^s. Then we find constraints on the UV radiation to repoduce the observed ionization states of the metallic absorption-line systems. Second, we consider clumpy model - absorbers irradiated by the UV radiation obtained here and discuss a structure of these absorption - line systems.

2. Calculation

We calculate the ionization states of model - absorber under the conditions of photoionization equilibrium and thermal equilibrium. We assume an intensity of ionizing radiation including a correction for self-absorption due to halo gas: $I(\nu;r) = I_{\nu_{LL}}^d(\nu/\nu_{LL})^{-\alpha}\exp(-\tau_O) + I_\nu^s/(r/r_0)^2\exp(-\tau_I)$, where $\tau_O = \int_r^R n_{HI}dr/10^{17.5}\mathrm{cm^{-2}}$, $\tau_I = \int_{r_0}^r n_{HI}dr/10^{17.5}\mathrm{cm^{-2}}$ (R : radius of absorber, r_0 : inner radius). I_ν^s is adopted from Bregman & Harrington (1986) with upper cut-off at 500eV.

In order to compare with observations (summarized in Table 1 of Bergeron & Stasińska 1986), we calculate HI column density and column densities of several ions, e.g., CIV, MgII and SiIV. When we consider a clumpy model, we assume that an absorber consists of two components, with spatial density n^1 and n^2, respectively. The filling factor of subcomponent 2; $f(r) \equiv \Sigma V_{clump}/V_{total}$ is used to modify the column density of each ion on a line of sight at an impact parameter p, $N_{xi} = 2\int_p^R (n_{xi}^1(r)(1-f(r)) + n_{xi}^2(r)f(r))r/\sqrt{r^2-p^2}dr$. The optical depth is also modified according to the modification of N_{HI}. But for simplicity, we assume that $f(r)$ is constant in this paper. The chemical elements considered in our calculations are H, He, C, N, O, Mg, Si and Fe. We adopt the solar abundance from Allen (1972) and assume the metallicity of absorbing halos to be $Z/Z_\odot = 10^{-2}$.

3. Results and Discussions

In order to reproduce the observed ionization states, we find that the hydrogen Lyman - limit intensity of

the diffuse UV background should be $\log I_{\nu_{LL}}$(in ergs $cm^{-2}s^{-1}Hz^{-1}str^{-1}$) $= -21.0 \pm 0.5$ at $z \sim 2$ and its spectral shape should be $I_\nu \propto \nu^{-\alpha}$ with spectral index $1.5 \lesssim \alpha \leq 2$. It appears that quasars would be the dominant source of UV radiation at high redshifts and that the contributions from young galaxies should be negligible (See Figure 1 and Denda & Ikeuchi 1992). This result is consistent with previous studies (e.g., Steidel and Sargent 1989).

However, it is difficult to reproduce the observed ionization states of all of the three absorption systems at once, when we assume a spherical symmetric absorber with density distribution $n_H \propto r^{-2}$. Then we consider the cases of two - component models. The observed ionization states of all kinds of the metallic absorption systems are well reproduced by the clumpy model that has a smoothly distributed and thicker region, where $n_H \propto r^{-2}; r \lesssim 10$kpc, and a thin outer region with 'clumps', where a filling factor of 'clumps' is about 0.1 (See Figure 2). Moreover, the absorber may have an inner dense core which shields its gaseous halos from the stellar UV radiation of the central high-z (young) galaxy.

References

Bergeron, J., & Stasińska, G. 1986, A&A, 169, 1.

Blades, J.C. 1988, in *QSO Absorption Lines: Probing the Universe*, ed. Blades, J.C., Turnshek, D., & Norman, C.A. (Cambridge University Press: Cambridge), 147.

Bregman, J.N., & Harrington, J.P. 1986, ApJ, 309, 833.

Denda, K., & Ikeuchi, S. 1992, submitted to ApJL.

Gunn, J.E., & Peterson, B.A. 1965, ApJ, 142, 1633.

Lanzetta, K.M., & Bowen, D. 1990, ApJ, 357, 321.

Lanzetta, K.M., Turnshek, D.A., & Wolfe, A.M. 1987, ApJ, 322, 739.

Steidel, C.C., & Sargent, W.L.W. 1989, ApJ, 343, L33.

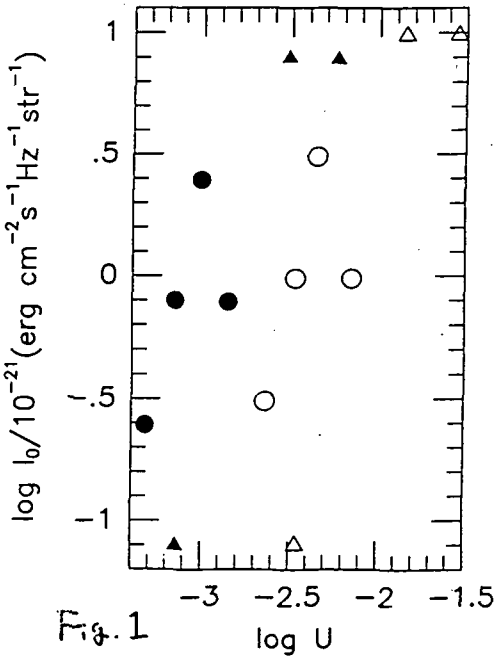

Fig. 1

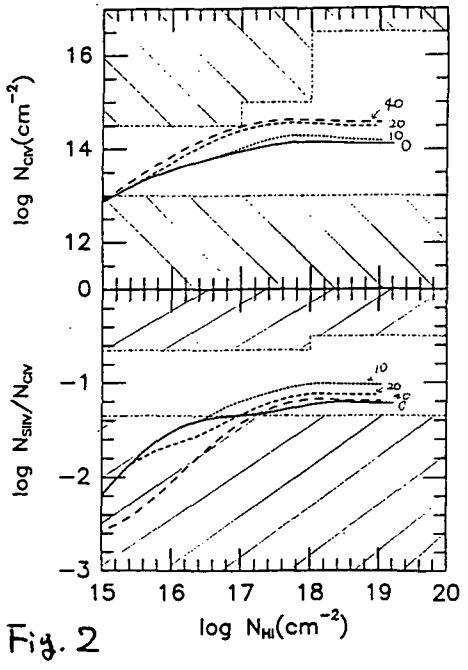

Fig. 2

Fig. 1 : log $I_{\nu_{LL}}$ versus log U for the suitable models to observations. The UV flux with spectral index $\alpha = 2$ is adopted here. Open circles and closed circles represent values, for which both the observations of the CIV systems and that of LLS can be well reproduced, respectively. Open triangles and closed triangles reprsent values, for which the CIV systems or LLS isn't reproduced, respectively. From this figure, it is seen that log $I_{\nu_{LL}}$(in ergs $cm^{-2}s^{-1}Hz^{-1}str^{-1}$) $= -21 \pm 0.5$ and log $U = -2.75 \pm 0.75$ are suitable for the ionization states of both the CIV systems and LLS.

Fig. 2 : The upper panel is the column density of CIV ion, N(CIV), versus the neutral hydrogen column density, N(HI), and the lower one is the ratio of column densities N(SiIV)/ N(CIV) versus N(HI) for clumpy models for $(n_H^1, n_H^2, f, n_H^c) = (0.1, 1.0, 0.1, 1.0)$, with different size of snoothly distributed region ; r_c and UV radiation with a spectral index $\alpha = 2$ and intensity log $I_{\nu_{LL}}$(in ergs $cm^{-2}s^{-1}Hz^{-1}str^{-1}$) = -21. The values of r_c is labeled on each curve and the hatched regions are excluded by the observational limits.

Absorption Spectra of Q 0000-263 and Q 1442+101

B. L. Frye, J. Bechtold, L. A. Moustakas,
Steward Observatory, University of Arizona

and A. Dobrzycki
Harvard-Smithsonian Center for Astrophysics
and Copernicus Astronomical Center

Studying the Lyman-α forest allows us to trace the cosmological distribution of matter through time, and may reveal insights into important questions such as the onset of galaxy formation. The number of Lyman-α absorption lines per redshift per rest equivalent in the Lyman-α forest can be written as

$$\frac{\partial^2 N}{\partial z \partial W} = \frac{A}{W^*}(1+z)^{\gamma} e^{-W/W^*} \qquad (1)$$

For a nonevolving population of clouds γ=1 for q_0=0, and γ=0.5 for q_0=0.5 (See Murdoch *et al.* 1986 and references therein).

By the inception of this project the evolution parameters γ and A_0 of Eq. (1) had been determined out to $z = 3.78$ (Hunstead *et al.* 1986). We present here a detailed study of the Lyman-α forests of Q 1442 +101 at z_{em}=3.54 and Q 0000–263 at z_{em}=4.11. The spectra were obtained at high signal-to-noise and moderate resolution rather than moderate signal-to-noise and high resolution to determine whether profile fitting yielded results consistent with high resolution data. Two different researchers de-blended the Lyman-α forest components by fitting Gaussian profiles of FWHM=2.0 pixels, or 1.1 Å, the results of which were very similar. The aim was to find the minimum number of components, as required by χ^2, to produce an acceptable fit. For Q 0000–263, the Lyman-β spectrum was used as a constraint for the Lyman-α data, assuming b=25.6 km/s.

In order to determine the parameters γ and W^* we include our two new Lyman-α line lists in a sample of echelle spectra compiled by Rauch *et al.* (1991; hereafter ECH). We determined $\gamma = 2.59 \pm 0.49$. The K–S probability that our fits for Q 0000–263 and Q 1442+101 are drawn from this redshift distribution is 0.30 and 0.93 respectively. The equivalent width distribution of the Lyman-α forest absorption lines is described by $p(W) \propto \frac{1}{W^*} e^{-W/W^*}$. The W^* from our two objects, $W^* = 0.084 \pm 0.008$Å, was lower than that derived for the whole ECH sample, $W^* = 0.179 \pm 0.010$ Å, and lower than that derived from equivalent width limited samples (see Figures 1 and 2). This indicated that line blending and the techniques used were affecting the equivalent width distributions.

The column density distribution derived from Voigt profile fitting of high resolution data is described by $p(N_{HI}) \propto N_{HI}^{-\beta}$. The characteristic equivalent width W^* from equivalent width limited samples is $W^* \approx 0.2 - 0.3$, corresponding to $\beta \approx 1.4 - 1.5$, is not consistent with the column density distribution samples with $\beta = 1.7$ (Barcons and Webb *et al.* 1991; Jenkins *et al.* 1992). However, our values $W^* = 0.179$ corresponds to $\beta = 1.7$ and $W^* = 0.084$ corresponds to $\beta = 1.9$ (all for b=25.6 km/s). We stress that the column density distribution expected of equivalent width-limited samples such as this one provides

a poor match to our observations. A steeper value of β is required, which is consistent with echelle results. Thus via profile fitting we find that our intermediate resolution but high signal-to-noise observations can be compared to high resolution data.

References.

Barcons, X., & Webb, J. K., 1991, MNRAS, 253, 207.

Hunstead, R. W., Murdock, H. S., Peterson, B. A., Blades, J. C., Jauncey, D. L., Wright, A. E., Pettini, M., & Savage, A. 1986, ApJ, 305, 496.

Jenkins, E. B., Bajtlik, S., & Dobrzycki, A. 1992, in prep..

Murdoch, H. S., Hunstead, R. W., Pettini, M., & Blades, J. C. 1986, ApJ, 309, 19.

Rauch, M., Carswell, R. F., Chaffee, F. H., Foltz, C. B., Webb, J. K., Weymann, R. J., Bechtold, J., & Green, R. F. 1992, ApJ, 390, 387.

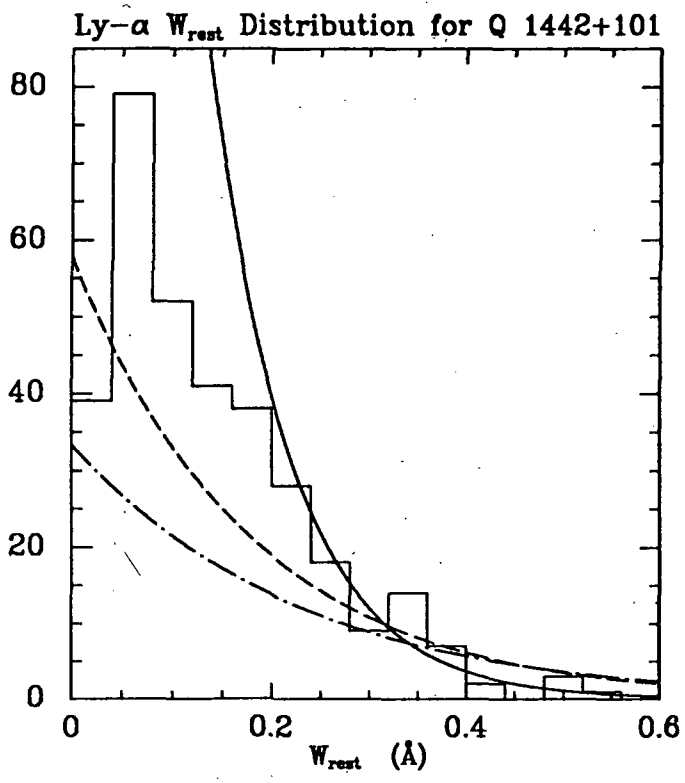

Figure 1.

The observed equivalent width distribution for Q 1442+101 with the normalized equivalent width distributions e^{-W/W^*} using $W^* = 0.114$ (solid line), $W^* = 0.179$ (dashed line) and $W^* = 0.227$ (dot-dashed line).

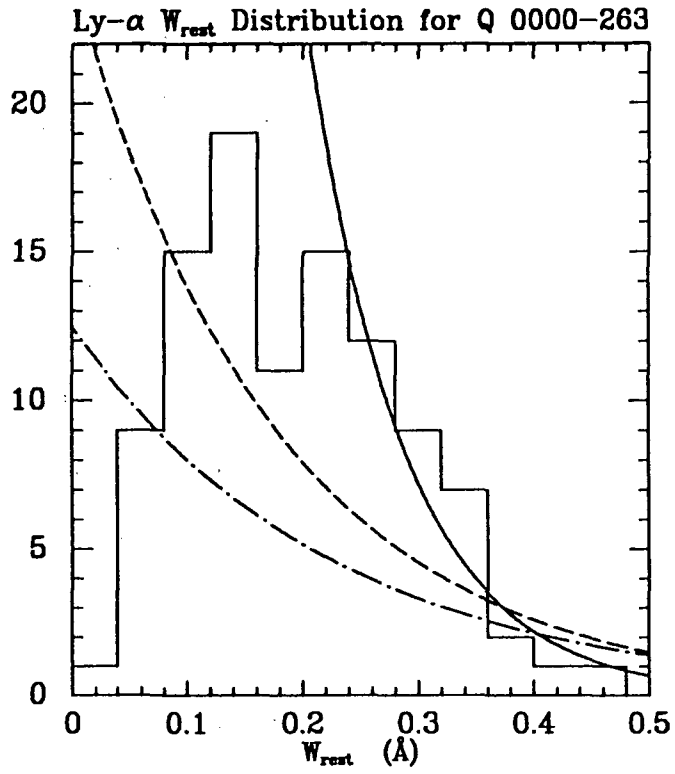

Figure 2.

The observed equivalent width distribution for Q 0000-263 with the normalized equivalent width distributions e^{-W/W^*} using $W^* = 0.131$ (solid line), $W^* = 0.179$ (dashed line), and $W^* = 0.227$ (dot-dashed line).

Pruning the Lyman-α forest of Q1331+170

Varsha P. Kulkarni and Donald G. York
Department of Astronomy and Astrophysics, The University of Chicago, Chicago IL, 60637

1 Introduction

A multitude of absorption lines seen shortward of QSO Ly-α emission, that cannot be traced to heavy element absorption systems, are assumed to be Ly-α lines arising in intervening clouds. Studies of these Ly-α clouds, typically done at 1 $\AA$ or lower resolution, have shown N(HI) $\sim 10^{13} - 10^{17} cm^{-2}$ and b $\sim$ 35 km/s. Sargent *et al* 1980, on the basis of a flat pair velocity correlation function (PVCF), argued that these clouds are intergalactic. But Crotts 1989 showed that the strong Ly-α lines are spatially clustered. High resolution studies of Webb 1987 and Rauch *et al* 1992 also report some evidence for weak clustering, but overall such high resolution studies have been rare. Here we report a study of the Ly-α forest of Q1331+170 over $z_{abs} = 1.60 - 2.19$ based on 18 km/s resolution data at $S/N \sim 15$, with metal-line deblending incorporated.

2 Observations and Sample Generation

The study of Q1331+170 ($z_{em} = 2.08$) made by York *et al* 1992 consisted of : (a) 18 km/s, mean S/N $\sim$ 15 Kitt Peak Echelle Spectra (over 3170-3970 $\AA$) (b) 1 $\AA$, S/N $\sim$ 40 MMT spectra (3900-9400 $\AA$) (c) limited 35 km/s resolution MMT scans over 6400-6820 $\AA$. Heavy element lines, including those in a previously known damped Ly-α system at $z_{abs} = 1.7765$, were identified and analyzed (York *et al* 1992). On the basis of analysis of heavy element lines from known systems longward of the emission Ly-α, we derive contributions of heavy element lines to lines in the Ly-α forest using profile fitting techniques. The remaining contribution is then the deblended Ly-α lines. The sample of lines thus derived is further searched for previously unknown metal line systems. Two samples are derived from the analysis of the resultant list of pure Ly-α lines : one consisting of single component profile fits (S1) and the other consisting of the minimum required number of multiple components (S2). Unidentified lines slightly longward of the presumed QSO redshift ($z_{em} = 2.08$) are also included. Sample S1 consists of 83 and sample S2 of 124 lines between $z_{abs} = 1.60 - 2.19$. Compared to a sample which would have ignored the metal-blended Ly-α lines completely, our procedure of metal line deblending adds $\sim$ 20% lines to each of the samples S1 and S2, and $\sim$ 23% and $\sim$ 29% lines to the sub-samples of strongest lines from S1 and S2, respectively.

3 Equivalent widths, Column densities, Doppler parameters

The highest S/N is achieved between $\sim 3500 - 3880 \AA$ resulting in rest equivalent width sensitivity of 20 m$\AA$ (4-5 σ) in the best parts of the spectrum. At this sensitivity, most Ly-α lines are found to be weak. Distributions of HI column densities for samples S1, S2 are shown in Fig. 1. Only a very small fraction of lines from sample S2 possess $N(HI) > 10^{14} cm^{-2}$. This is different from the power law distribution ($\sim N(HI)^{-1.7}$, $logN(HI) > 13$), which is common in the literature. (See for example, Carswell *et al* 1984.) According to this distribution, one would have expected about 9 lines with $N(HI) > 10^{14.5}$ in sample S2, whereas we see none. This is probably a result of the high resolution of our observations. High resolution studies of Ly-α lines in more sightlines would be needed to verify the generality of this. The b values range between 10 and 40 km/s for most of the lines, with a mean of $\sim$ 27 km/s. No obvious correlation is apparent between N(HI) and b. Lines within $\pm$ 10,000 km/s of the presumed QSO emission redshift, $z_{em} = 2.08$, are predominantly weaker than 100 m$\AA$, while lines 'outside' 10,000 km/s of the QSO are relatively stronger.

4 Velocity Correlations

Fig. 2 shows the inner 8000 km/s of the histogram of 'corrected' number of line pair separations for all lines in sample S2 with $W_{rest} > 30m\AA$, for $q_0 = 0.5$. Here, 'corrected' number means the number of pairs after correcting for the finite redshift range of the data by using a ramp-shaped function, as in Sargent *et al* 1980. Shown overlaid on the histogram are the mean and the $\pm 2\sigma$ levels expected in samples of randomly distributed Ly-α lines, computed as average of 100 simulated linelists, each having the observed number of lines with the observed set of equivalent widths, but distributed randomly between $z_{abs} = 1.6079$ and 2.1914. An excess in number of velocity pairs out to 100 km/s is apparent in the Ly-α lines toward Q1331+170. This result seems to differ from that of Rauch *et al* 1992, who, with observational setup almost identical to ours and data at 23 km/s resolution, did not report such a clustering. This could be a result of different methods of analyzing the data. However they do report clustering among the narrow Ly-α lines. We also find a marginal excess in the number of line pairs over $v <\sim 500$ km/s in the weakest ($30 < Wrest < 100m\AA$) lines, and the two findings could be related. An excess in number of velocity pairs out to ~ 200 km/s is also seen in the (admittedly small) sample of the strongest ($W_{rest} > 190m\AA$) lines. This excess comes entirely from a strong clump of Ly-α lines at $z_{abs} = 1.9637$.

5 Conclusions

We have pruned the Ly-α forest of Q1331+170 with metal line deblending and find that our sample of Ly-α clouds have low N(HI) and show an excess in the number of line pair separations on scales of $<\sim 200$ km/s. We have searched for CIV doublets and OI λ1302-SiII λ1304 pairs, since these have $\Delta v \approx 500$ km/s. We found only one, which has been taken out of the samples. The implied excess in the PVCF could be either due to clustering of the Ly-α clouds or due to complex structure in the clouds. The former conclusion is not expected in an intergalactic interpretation of the Ly-α clouds. This effect will have to be tested by more high resolution, high S/N studies of the Ly-α forest in other QSO's.

This work is part of a more detailed paper by Kulkarni *et al* 1992.

REFERENCES

Carswell, R., Morton, D., Smith, M., Stockton, A., Turnshek, D., and Weymann, R., 1984, ApJ, 278, 486

Crotts, A. 1989, ApJ, 336, 550

Kulkarni, V. P., Welty, D. E., York, D. G., Huang K.-L., Green, R. F., and Bechtold J., 1992, to be submitted

Rauch, M, Carswell, R., Chaffee, F., Foltz, C., Webb, J., Weymann, R., Bechtold, J., and Green, R. F., 1992, ApJ, 390, 387

Sargent, W., Young, P., Boksenberg, A., and Tytler, D. 1980, ApJS, 42, 41

Webb, J. 1987, in IAU Symposium 124, Observational Cosmology, eds. A. Hewitt, G. Burbidge, and L. Fang (Dordrecht: Reidel), p. 803

York, D. G., KeLiang Huang, Green, R. F., Bechtold, J., Welty, D. E., Carlson, M., and Khare, P. 1992, to be submitted

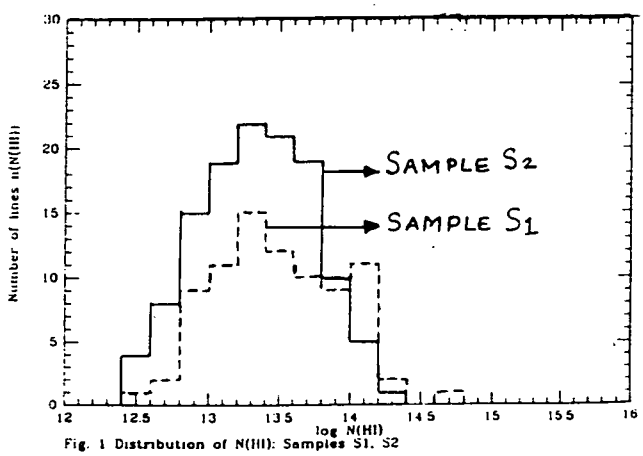

Fig. 1 Distribution of N(HI): Samples S1, S2

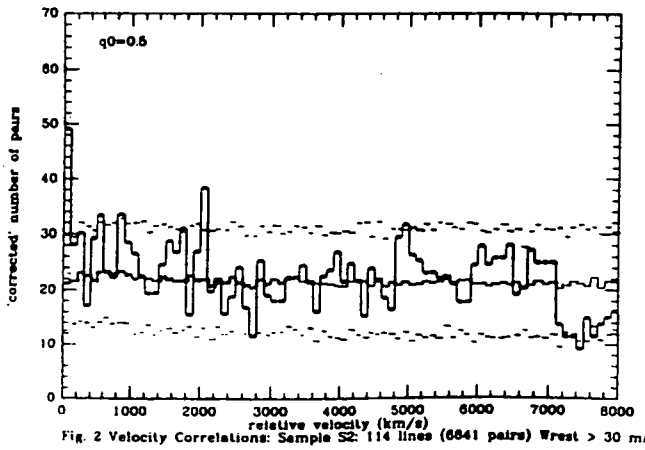

Fig. 2 Velocity Correlations: Sample S2: 114 lines (6641 pairs) Wrest > 30 mA

A re-analysis of the spectrum of 2206–199

M. Rauch & R.F. Carswell
Institute of Astronomy, Madingley Road,
Cambridge CB3 0HA, England
J. K. Webb
Dept of Physics, University of NSW,
Kensington NSW Australia
and
R.J. Weymann
Observatories of the Carnegie Institution of Washington,
813 Santa Barbara St, Pasadena CA 91101 USA

Recently Pettini, Hunstead, Smith and Mar (PHSM 1991) have performed an analysis of the Lyα forest of QSO 2206-199N at very high resolution (FWHM$\simeq 6 kms^{-1}$). On the basis of their observations they concluded that most Doppler parameters $b = \sqrt{2}\sigma$ of Lyα forest lines are below 22 km s^{-1} , with a range down to a few km s^{-1} and a median of 17 km s^{-1} . They also found a strong intrinsic correlation between Doppler parameter b and colum density N.

These results are in contrast to those of a similar study by Carswell, Lanzetta, Parnell and Webb (CLPW 1991) at comparable resolution with the same instruments, who find that most of the Lyα lines towards QSO 1100-264 have Doppler parameters above 15 km s^{-1} (median b=34 km s^{-1}), and that there is no significant correlation between b and N.

Whilst an intrinsic difference between the lines of sight to 2206-199 and to other QSOs can not be excluded a priori, previous disagreement between Doppler parameter estimates obtained by both groups (see the discussion in Blades et al., 1988 pp.100-105) pointed to a potential difference in estimation techniques and in the interpretation of the results. To investigate this possibility we have reanalysed the AAT/UCLES spectrum of 2206-199, obtained by PHSM. We extracted the spectrum from the raw data and determined the line parameters using the method described by CLPW.

Our main results can be summarized as follows:

• We agree with PHSM in finding at face value a substantial fraction of low Doppler parameters, and a strong b-N correlation, even after omitting a few additional metal lines which were previously misidentified as Lyα. It is unlikely that the sample of narrow lines is *dominated* by further unidentified metals, since in this case there would be too few real Lyα lines left.

• The bulk of the difference between the *median* Doppler parameters obtained for 2206-199 (PHSM) and 1100-264 (CLPW) arises because of the different sample selection criteria. PHSM selected for their sample only lines which appeared to be unblended and unsaturated. The second criterion restricts their sample to the low column density regime, whereas CLPW's sample of 1100-264 and our 2206-199 sample include *all* lines. Since there is a

strong positive correlation between the estimates for b and N restricting the sample to lower column densities yields a lower median Doppler parameter.

The median and mean Doppler parameters for the full Lyα sample of 2206-199 are b_{med}=26.5 km s^{-1} and $\bar{b}$=27.5$\pm$1.2 km s^{-1} , respectively. When we choose only lines above the column density completeness limit log$N$=13.3 these value become b_{med}=30.7 km s^{-1} and $\bar{b}$=33.9$\pm$1.3 km s^{-1} , in good agreement with $\bar{b}$=34 km s^{-1} for 1100-264.

• We have compared PHSM's parameter estimates to ours (obtained with the CLPW fitting method) for the individual lines we have in common. While our Doppler parameters for lines we estimate to be below 15 km s^{-1} agree well with PHSM's, their b values for lines above that value are systematically lower than ours by about 3 km s^{-1} . We identify differences in the size of the chosen fitting regions as possible causes of this discrepancy. It appears that PHSM's fitting regions are typically smaller than ours and do not always include both line wings. This amounts to a loss of information and results in a bigger scatter for the resulting Doppler parameter estimates.

• Extensive simulations were performed to study possible selection effects and the impact of finite signal-to-noise on the estimation of line parameters. We found that *the Doppler parameter estimates of low column density lines are systematically biassed towards lower values.* The bias appears to be due to the distortion of a weak line's Voigt profile by noise spikes, and its impact increases with decreasing signal-to-noise ratio and/or decreasing intrinsic column density of a line. The deviation of a Doppler parameter estimate from its intrinsic value can be so strong for low column density lines that error estimates (derived from χ^2 error contours in b-logN-z space and based on the assumption that the line is well-fitted by a Voigt-profile) may be too small by a factor of 2 or more.

The reality of the low Doppler parameters found by PHSM has to be assessed in view of this bias. Spuriously low Doppler parameter values and a strong artificial correlation between b and N, features reminiscent of the real line sample of 2206-199, can be produced in simulations where the underlying population of lines has $\bar{b}$=30 km s^{-1} at all column densities, and the signal-to-noise ratio of the spectrum is as in the real data of 2206-199. Although the presence of this effect *does not* disprove the existence of intrinsically narrow Lyα lines, the results of our simulations imply that an interpretation of the low b values towards 2206-199 as being intrinsic to the Lyα clouds might be premature on the basis of the data available.

We conclude that the present data of 2206-199 and in fact any data published to date provide little evidence for a significant population of cool clouds with Doppler parameters less than about 15 km s^{-1} .

References:

Blades,C., Turnshek, D., Norman, C.A., (eds.) "QSO Absorption lines: Probing the Universe", Cambridge 1988.

Carswell, R.F., Lanzetta, K.M., Parnell, H.C., and Webb, J.K., 1991, *Astrophys. J.*, **371**, 36.

Pettini, M., Hunstead, R.W., Smith, L., and Mar, D.P., 1990, *Mon. Not. R. astr. Soc.*, **246**, 545.

IRAS Studies of Galactic Supershells

Jon M. Saken (Univ. of Colorado, CASA), J. Michael Shull (Univ. of Colorado, CASA & JILA),
Robert A. Fesen (Dartmouth College)

Using IRAS Skyflux images and a new catalog of OB stars in the Cygnus region, we have identified a complete infrared supershell surrounding the Cyg OB1 Association (Saken *et al.* 1992). This supershell is seen as a conspicuous, well-defined $2° \times 5°$ region deficient of IR emission, with a limb-brightened edge and dimensions of about 50×130 pc at 1.5 kpc. The shell's elongated morphology is consistent with OB-star subclustering over the $\sim 10^6$ yr age of the bubble. With a parent star cluster still visible (10 O stars between 25 and 45 $M_\odot$, 3 – 4 Wolf-Rayet stars, and the possibility of 3 – 5 more massive stars that died as supernovae) the Cyg OB1 supershell is an excellent object for studying the formation and evolution of Galactic supershells. A discrepancy between the ≤ 1 Myr bubble age estimated from its size and the 5 Myr cluster turnoff age (45 $M_\odot$) may require non-coeval massive star formation to explain the number of post-main-sequence stars and limit the number of past supernovae.

The bubble appears too small for the 5 Myr age inferred from the main-sequence turnoff, particularly if 3 – 5 supernovae had occurred from stars of initial mass $45 - 80\ M_\odot$. If we assume that the cavity was produced by winds and supernovae from spatially distributed massive stars, we can model the dynamics as a set of ~ 3 overlapping bubbles, each of radius approximately equal to the minimum lateral size (25-30 pc). In spherical geometry, the radius and velocity of a bubble (Weaver et al. 1977) driven by a constant wind luminosity $L_o = (10^{38}\ \mathrm{ergs\ s^{-1}})L_{38}$ into a medium of constant ambient density $\rho_o = 1.4 m_H n_o$ yields a shell age of $t = (2.2 \times 10^5\ \mathrm{yrs})(n_o/L_{38})^{1/3} D_{1.5}^{5/3}$, for $R_s = R_{\min} = (26.2\ \mathrm{pc}) D_{1.5}$, far less than the association age of 5 Myr inferred from the main-sequence turnoff. Pushing all the scaling parameters to reasonable limits ($L_{38} = 0.2$, $n_o = 10$, and $D_{1.5} = 1.2$), one could arrive at a bubble age of 10^6 yrs – still a factor of 5 less than the inferred association age.

We favor a scenario involving non-coeval star formation. The evolved supergiants in the H-R diagram probably formed several Myr earlier than the 25 – 45 $M_\odot$ stars now on the main sequence. Non-coeval star formation has also been suggested to explain the H-R diagrams in three Magellanic Cloud clusters (Massey et al. 1989a,b). If we adopt an age for Cyg OB1 in the range 1 – 2 Myr, the initially most massive stars may now be Wolf-Rayet stars, and the superbubble could be driven entirely by stellar winds.

Thus the Cyg OB1 shell appears to be an example of a very young supershell, recently formed from the overlap of subassociation bubbles. The process may be continuing as the shell expands and encompasses new energy sources. The superbubble's nonspherical morphology is probably a result of the spatial distribution of the massive stars in this region.

Following the identification of the Cyg OB1 supershell, we have begun a search of the IRAS data for other supershell candidates using an updated catalog of OB stars (Garmany & Stencel 1992). We have found three examples that may illustrate the evolution of such shells.

IRAS data in the region of Cas OB6 shows two distinct IR bubbles around two sub-clusters of the association. The IR bubbles are coincident with the optical shells in Cas OB6 but differ substantially in morphology. These bubbles may represent an early stage in the development of shells like the one in Cyg OB1; over time they may expand and overlap to form a similar structure.

Another limb-brightened oval cavity can be seen in the IRAS images near Cyg OB8. Since no cluster members are found within the shell, it may be the relic of a previous episode of star formation. A different kind of shell can be seen near the OB association R103, not as a limb-brightened cavity, but as a "blow-out" of the Galactic plane with only a few well defined filaments along its edge. Shells that grow to sufficent size may eventually blowout in this manner, venting material to the Galactic halo.

References

Garmany, C. D., & Stencel, R. A. 1992, A&AS, in press
Maeder, A. 1990, A&AS, 84, 139
Maeder, A., & Meynet, G. 1989, A&A, 210, 155
Massey, P., Garmany, C. D., Silkey, M., & DeGioia-Eastwood, K. 1989a, AJ, 97, 107
Massey, P., Parker, J. L., & Garmany, C. D. 1989b, AJ 98, 1305
Saken, J. M., Shull, J. M., Garmany, C. D., Nichols-Bohlin, J., & Fesen, R. A. 1992, ApJ, 397, (in press).
Weaver, R., McCray, R., Castor, J., Shapiro, P., & Moore R. 1977, ApJ, 218, 377

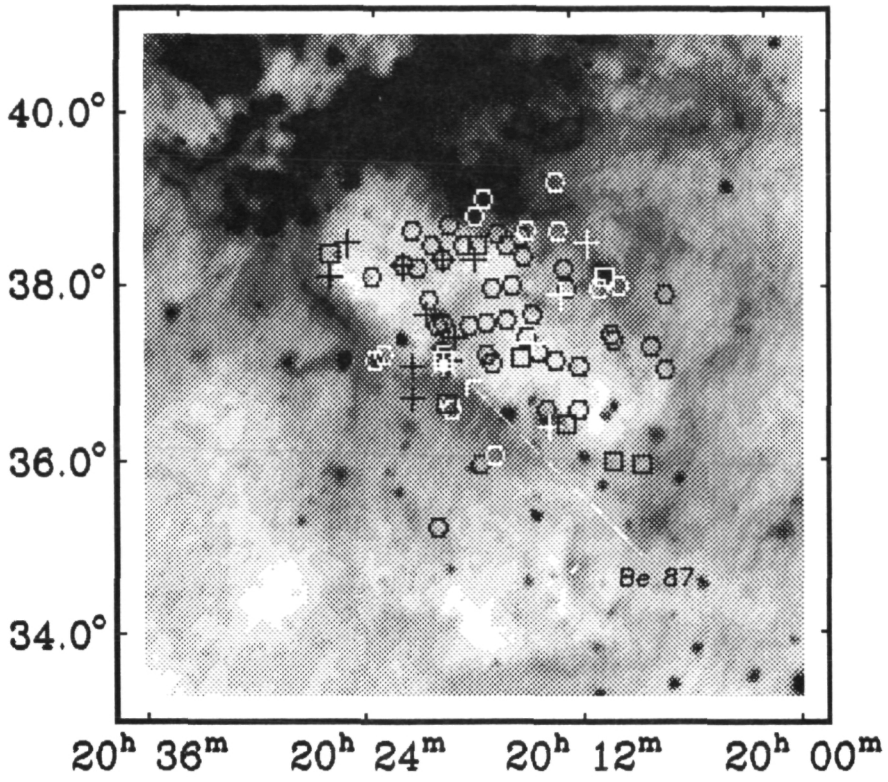

Closeup view of the IRAS supershell overlaid with 77 member OB stars (Garmany & Stencel 1992) and 9 Wolf-Rayet stars near the Cyg OB1 Association. For clarity, all symbols are black or white, depending on the background. Post-main-sequence OB stars are plotted with crosses and Wolf-Rayet stars with squares. Because of the IRAS pixel resolution, only 54 distinct OB stars are shown. The open cluster Be 87, which contains the Wolf-Rayet star WR 142, is shown as an asterisk near the center of the southern cavity boundary.

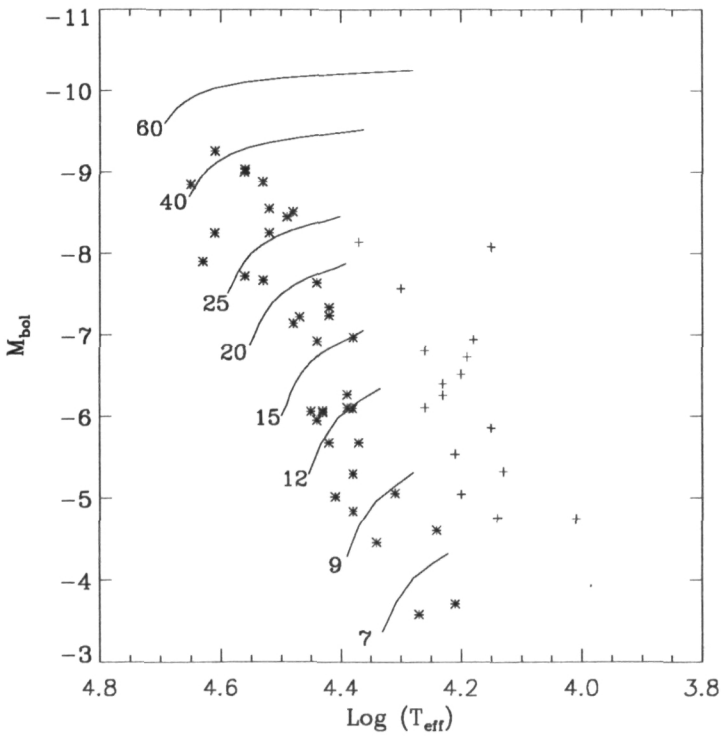

Hertzsprung - Russell diagram of 53 stars in Cyg OB1 for which estimates of bolometric magnitudes and effective temperatures are available (Garmany & Stencel 1992). Post-main-sequence stars are plotted with a cross. Mass tracks from Maeder & Meynet (1989).

Starburst Ages in HII Galaxies

N93-26777

Hans-Jörg Deeg

Institute for Astrophysics
University of New Mexico
Albuquerque, NM 87131

and

National Radio Astronomy Observatory
PO. Box O
Socorro, NM 87801

Introduction

The age of the starbursts of a few HII galaxies is derived from optical photometry and compared with previous results from radio continuum spectra. HII galaxies are gas rich and characterized by the dominance of giant HII regions, blue stellar colors, high surface brightness and narrow emission lines. The presently observed high abundances of bright young stars must be the result of a recent -or even ongoing- starburst. The question, whether the observed starburst is the first one or if it is a recurrent phenomenon, is still open. If the starburst is the first one, HII galaxies can be interpreted as being among the most unevolved galaxies known - their star formation characteristics possibly paralleling that of normal galaxies early in their evolution.

The optical data

A sample of five HII galaxies was observed with B,R and I broadband filters at the University of New Mexico's Capilla Peak observatory. They have been observed previously at several radio continuum frequencies (Deeg at al., 1992, submitted to ApJ). The photometric data are given in the Table. All colors given are corrected for galactic extinction. It should be noted, that II Zw 40 has an unusually large correction for galactic reddening of E(B-R) = 1.02, whereas this correction is 0.1 or less for all other galaxies.

Results of the photometry

B-R colors bluer than the color of the disk (which is assumed to be between 0.95 to 1.6) are indicators of star forming activity within time scales of 10^9 years. From the literature (e.g. Thuan and Martin 1981, ApJ, 247, 823, or the RC3) U-B color indices can be obtained. Color-color diagrams are frequently used to derive star formation histories in galaxies by comparison to colors obtained in stellar synthesis models. Using these two color indices, the stellar synthesis models by Krüger et al. (1991, A&A, 242, 343) allow estimates of the burst strengths, b, and the time *since* the star burst, T_b (see table). The burst strength b is defined as the ratio of the total mass of stars formed in the burst over the total mass of stars ever formed. The length of the burst itself, is relatively short and assumed to be $5 \cdot 10^6$ years. The models depend mostly on the low mass cut-off, which was taken as $\sim 4\ M_\odot$. The other, but not so crucial parameter, is the amount of starformation in the underlying disk, which is assumed to be exponentially decaying with a time scale of 10^9 years; the starburst is occuring after 15 Gyrs. The influence of possible earlier starforming episodes on the

colors of the current starburst is insignificant. It would be interesting to apply the generally bluer values of the cores ($B\text{-}R_{core}$) to the synthesis model; however, correspondingly detailed U-B colors are not yet known.

Comparison with radio-continuum spectra.

A majority of the objects in the sample have radio spectra which show a remarkable flattening at low frequencies (See Deeg et al., 1992). The flattening may be caused by several mechanisms, which are inherent to the special environment within these galaxies, such as high gas densities, large HII regions and the transient character of the peak starburst activity, after which the relativistic electrons are losing their energy within a few times 10^7 years. However, the two most likely mechanisms cannot be isolated with certainty, based on the radio spectra alone. They are free-free absorption of electromagnetic radiation in ionized HII regions and 'synchrotron aging', which describes the influence of the energy loss of relativistic electrons onto the radio-spectrum. Synchrotron aging allows an estimate of the age of the relativistic electrons, T_{syn} (see Table 2), i.e. of the time since the electrons were injected into the ISM . The ages T_{syn} are much less than those from the stellar synthesis, T_b (see the table below). T_{syn} depends on a galaxy' magnetic field as $B^{-3/2}$. Equipartition calculations lead to strong fields of typically 25 μG. If this were invalid, and assuming a field of 5 μG, then T_{syn} would be about 10 times larger. There are several possibilities to explain the discrepant ages derived from stellar colors and relativistic electrons. Radio spectra reflect the current or recent star forming activity in a few localized areas, whereas the integrated optical colors do not extract star forming regions. Or, the galaxies might undergo a bimodal star formation, where we currently observe a burst which is dominated by mass rich O stars, which follows a previous starburst which was dominated by lower mass stars. The radio-emission reflects the relativistic electrons which were injected by the very young O stars' supernovae, whereas the optical colors reflect the older starburst. Finally, the radio spectra would not indicate a starburst's age if they are not dominated by synchrotron aging but instead by free-free absorption at low frequencies. In conjunction with the optical data, the radio spectra can give quantities like the IMF, the abundances of O stars, the star formation rate and act as a guide towards a detailed picture of these galaxies' interstellar environment and their star formation history.

	Haro 15	II Zw 40	Mkn 297	Mkn 314	III Zw 102
$B\text{-}R_{25}$	0.67	0.73	0.92	0.86	0.60
$B\text{-}R_{core}$	0.47	-0.015	0.99	0.84	0.75
U-B	-0.41	-0.36	-0.45	-0.35	-0.14
b	0.006	0.005	0.001	0.004	0.02
$T_b[10^6$ yrs]	70	80	25	70	150
$T_{syn}[10^6$ yrs]	3	...	7	...	2

STARBURST MODELS OF MERGING GALAXIES

Andrea H. Prestwich,
Harvard-Smithsonian Center for Astrophysics,
60 Garden St.,
Cambridge, MA, 02138

1. INTRODUCTION

In the past decade, infrared observations have shown that interacting and merging galaxies have higher luminosities than isolated systems, with the luminosities in mergers as high as $10^{12} L_{\odot}$. However, the origin of the luminosity found in mergers is controversial, with two main competing theories. The first is the starburst scenario. As two gas rich galaxies start to merge, cloud-cloud collisions induce fast shocks in the molecular gas. This gas cools, collapses and fragments, producing a burst of star formation. The main rival to this theory is that the infrared luminosity is produced by a dust embedded active nucleus, the merger of two gas rich galaxies providing the 'fuel to feed the monster'. There has even been speculation that there is an evolutionary link between starbursts and active nuclei, and that possibly AGN's and QSO's were formed from a starburst. Assuming that the infrared luminosity in merging galaxies is due to star formation, there should be ionizing photons produced from the high mass stars, giving rise to recombination line emission. The objective of this study is to use a simple starburst model to test the hypothesis that the extreme infrared luminosity of merging galaxies is due to a starburst.

2. MODELLING THE BRACKETT LINE EMISSION

If the infrared luminosity of merging galaxies is indeed due to a burst of star formation, the infrared recombination lines arise in HII regions ionized by young stars. The number of ionizing photons from the burst can then be calculated assuming Case B recombination. We aim to determine whether the number of OB stars inferred from the flux of ionizing photons can produce the observed far infrared luminosity in a sample of merging galaxies. This is done by using a simple starburst (e.g. Telesco and Gatley 1984, Ap. J. 284 557) model to compare the star formation rate implied by the infrared luminosity measured by IRAS, to the star formation rate inferred from the number of ionizing photons measured by the Bγ flux. A starburst is a viable model for the luminosity generation if the ratio of the star formation rate implied by the infrared luminosity to that inferred from the ionizing flux (denoted Q) is ~ 1.

3. RESULTS AND DISCUSSION

Figure 1 shows the Bγ flux plotted aginst the integrated flux for all of the mergers in this sample. Also shown are lines of $Q = 1$ for several starburst models. Most of the mergers in this sample (6 out of a total of 8) have $L_{B\gamma}/L_{LIR}$ ratios that are consistent with a simple starburst model. The starbursts are either young or if they are evolved the lower mass cut off of the burst is $\sim 5M_{\odot}$, higher than seen in galactic star forming regions. These results lend quantitative support to the idea that mergers create a "super starburst", and that in some respects the star formation is very different from that in quiescent spiral galaxies. There are two infrared bright galaxies, Arp 220 and NGC 6240 that have a deficit of ionizing photons when compared to the other galaxies in this sample. In these galaxies an active nucleus may dominate the far infrared luminosity, but it is possible that extinction plus dust absorption of the Lyα photons results in a much decreased recombination line flux from a starburst. It is exciting to speculate that Arp 220 and NGC 6240 are evolved starbursts that have developed active nuclei.

Figure 1

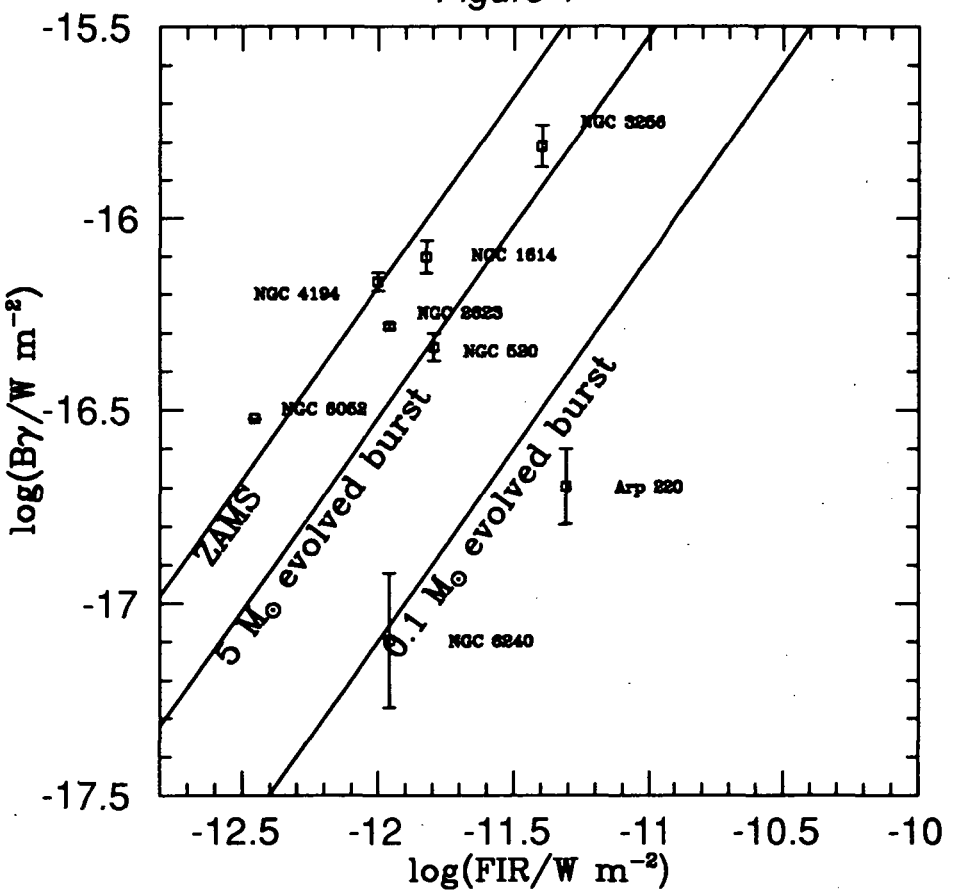

THE EFFECT OF MASSIVE STARS ON THE IONIZED MEDIUM OF EXTRAGALACTIC HII REGIONS

Héctor O. Castañeda

Instituto de Astrofísica de Canarias and Issac Newton Group of Telescopes, La Palma Observatory

E-38200 La Laguna, Tenerife, SPAIN

I. Introduction

Giant extragalactic HII regions (GEHR) are centers of active star formation, ionized by populous clusters of OB stars. These objects are characterized by their low electron density ($N_e \approx 10^2$ cm^{-3}), linear dimensions of order of 10^2 - 10^3 pc, varied morphology and inhomogenous distribution of the gas (Kennicutt 1984). They are ideal laboratories to study the processes of interaction between the gas and the stars, that could then be extended to the study of HII and starburst galaxies. In collaboration with C. Muñoz-Tuñon and J. Vilchez (IAC), R. Terlevich (RGO) and M.V.F. Copetti (U. Santa Maria, Brasil), we are conducting an observational program on a selected group of giant HII regions with the use of one- and two-dimensional spectroscopy. Our aim is two-fold: to understand the internal structure of the regions and to study the kinematics and dynamics of the ionized gas. In this paper I give a short report of our ongoing research.

II. The Kinematics of the Ionized Gas

Giant extragalactic HII regions show supersonic line widths in their emission lines (Smith and Weedman 1970). The normal dynamical evolution of an HII region can not provide the observed internal energy in the form of supersonic mass motions (10^{51} ergs for a typical region) and several solutions for the source of random motions have been suggested, as for example virial equilibrium between the gas and the stars and stellar winds (Terlevich and Melnick 1981; Rosa and Solf 1984). To understand the source of the turbulent motion in the gas new observations with high spatial and spectral resolution are required.

Two-dimensional imaging spectroscopy in the lines of Hα and [OIII]λ5007 were obtained for a sample of regions in the Local Group using TAURUS II, the Fabry-Perot imaging spectrograph at the Cassegrain Focus of the 4.2m William Herschel Telescope at the Roque de los Muchachos Observatory, with the Image Photon Counting System (IPCS) as detector. The two-dimensional imaging spectroscopy allows the mapping of the velocity field over the entire extent of the HII regions.

A preliminary analysis of the data reveals that systematic motions in the form of velocity gradients have been observed in our velocity maps, confirmed by comparison of velocity maps in different emission lines. An example is NGC 588, and "egg-shaped" nebula in M33. The velocity map in the [OIII]λ5007 line shows a gradient of the order of 25 km s^{-1} between the inner and the outer zones. This is also the area where the dispersion along the line of sight is larger. Most previous kinematical studies were based on line profiles integrated over the whole of the region. That could explain why large aperture spectra sometimes shows a non-gaussian profile (Arsenault and Roy 1986).

The effect of the massive stars on the kinematics of the regions is not only limited to the turbulent motions of the gas. Supernova remnants within the complexes and the stellar winds from massive stars should accelerate gas to high velocities. We have conducted a systematic survey for the

detection of high velocity gas at low intensity levels, with the use of CCD detectors, long slit spectroscopy, and high signal-to-noise ratio. Observations in the Hα line over ten regions associated with M101, M51, NGC6822 and NGC4861 only yielded one successful detection in NGC 5471: we detected a very broad (FWZI > 3000 km s^{-1}), low intensity ($\leq$ 2 % of line peak) for the Hα + [NII] doublet; a similar spectral feature has been reported recently in NGC 2363 (Roy *et al.* 1992). In both cases there is no conclusive evidence for the source of high velocity gas. The second part of this survey includes the regions of M33 and will be published in a forthcoming paper.

III. The Internal Structure of GEHR

To study the internal structure of the giant complexes, we have measured also the density gradient within HII regions (Castañeda, Vilchez, and Copetti 1992). The local density was obtained from the relative intensity of the [SII]$\lambda\lambda$6717,6731 doublet, measured with very high signal-to-noise ratio. In those regions where a density gradient has been found (as, for example, in NGC 5461), the measured density always peaks at the position of maximum surface brightness.

Theoretical models for the evolution of the insterstellar medium sourrounding massive stars predict that stellar winds and (sequential) SN explosions can blow a hot superbubble, and push out a large supershell of ionized gas. Since the gas in the superbubble will be too hot to emit in the optical range, a depression in the profile of the Hα flux should be expected to some extent but that is not observed in our data. There are several possible explanations for the discrepancy between our observations and the "superbubble" theory. The most likely situation is that the ionizing clusters are actually too young to reach the point of supernova explosions and develop the superstructures predicted by the models. For typical values of the mechanical luminosity L_w of order 10^{38} ergs s^{-1}, (where L_w is the total wind power of the whole association), the radius R of the corresponding wind-driven bubble can be written as $R = 269\ t_7^{0.6}\ n_o^{-0.2}$ pc, where t_7 is the time in units of 10^7 yr, and n_o is the density (cm^{-3}). The measured density in the brightest knots of NGC 5471, NGC 5461, NGC 5447 and NGC 5457 is of order 300 cm^{-3}. For this density value and time t_7 = 1 to 2, we would expect typical shell diameters of 5 to 10 arcsecs at the distance of M101. The presence of these structures in the regions is ruled out by the observations, and therefore, the most likely explanation of this fact should be that the ionizing clusters are very young and have not had time to develop large shells structures.

I want to gratefully acknowledge the CICYT (Spain) for a fellowship under which part of this work was carried out. The INT and WHT are operated on the island of La Palma by the Royal Greenwich Observatory at the Observatorio del Roque de los Muchachos of the Instituto de Astrofísica de Canarias.

Bibliography

Arsenault, R., and Roy, J.-R. 1986, *Astr. J.*, **92**, 567.
Castañeda, H.O. 1992, in *Proceedings of the P.A.S.P. Meeting "Massive Stars: Their Lives in the Interstellar Medium*, eds. J.P. Cassinelli and E.B. Churchwell, in press.
Castañeda, H.O., Vilchez, J.M., and Copetti, M.V.F. 1992, *Astr. Ap*, **260**, 370.
Kennicutt, R.C. 1984, *Ap. J.*, **287**, 116.
Rosa, M., and Solf, J. 1984, *Astr. Ap.*, **130**, 29.
Roy, J.-R, Aubé, M., McCall, M.L., and Dufour, R.J. 1992, *Ap. J.*, **386**, 498.
Smith, M.G., and Weedman D. 1970, *Ap. J.*, **161**, 33.
Tenorio–Tagle, G., and Bodenheimer, P. 1988, *Ann. Rev. Astron. Ap*, **26**, 145.
Terlevich, R., and Melnick J. 1981, *M.N.R.A.S.*, **195**, 839.

GAS DISTRIBUTION AND STARBURSTS IN SHELL GALAXIES

MELINDA L. WEIL & LARS HERNQUIST
Board of Studies in Astronomy & Astrophysics
University of California, Santa Cruz
Santa Cruz, California 95064

Detailed maps of most elliptical galaxies reveal that, whereas the greatest part of their luminous mass originates from a smooth distribution with a surface brightness approximated by a de Vaucouleurs law, a small percentage of their light is contributed by low surface brightness distortions termed "fine structures" (e.g. Seitzer and Schweizer 1990). The sharp-edged features called "shells" are successfully reproduced by merger and infall models involving accretion from less massive companions (e.g. Quinn 1984, Hernquist and Quinn 1988). In this context, dwarf spheroidal and compact disk galaxies are likely progenitors of these stellar phenomena. However, it is probable that the sources of shell-forming material also contain significant amounts of gas. This component may play an important role in constraining the formation and evolution of shell galaxies.

To investigate the effects of the gaseous component, we have performed numerical simulations to study the tidal disruption of dwarf galaxies containing both gas and stars by more massive primaries, and the evolution of the ensuing debris. The calculations were performed with a hybrid N-body/hydrodynamics code (Hernquist & Katz 1989). Collisionless matter is evolved using a conventional N-body technique and gas is treated using smoothed particle hydrodynamics in which self-gravitating fluid elements are represented as particles evolving according to Lagrangian hydrodynamic equations. An isothermal equation of state is employed so the gas remains at a temperature 10^4K. Owing to the large mass ratio between the primary and companion, the primary is modeled as a rigid potential and the self-gravity of both galaxies is neglected. The potentials of both the primary and companion are represented by an analytic model which mimics the mass distribution in elliptical galaxies (Hernquist 1990). The primary mass and scale length are both unity; the stellar component of the disk companion has a mass 0.1 and scale length 0.7 while the gas component has a mass 0.01 and the same scale length as the stars. Scaled to values appropriate for large ellipticals, a dimensionless time unit corresponds to a physical time $\sim 4 \times 10^6$ years. Initially, particles evolve in the time-varying field provided by solving the two-body problem consisting of the primary and secondary; after the the separation between the two galaxies is smaller than a prescribed radius, the companion is disrupted and particles evolve in the lone potential well of the primary.

The top row of Figure 1 shows an example of the evolution of a stellar disk accreted by a more massive spherical galaxy. In this simulation, the encounter was precisely radial and the plane of the disk coincided with the orbit plane. During its passage through the center of the primary the disk was destroyed by the tidal forces acting on it. The oscillations of particles with a range of binding energies through the primary potential leads to an enhancement in density at the turning points where the particle velocities are relatively low. After further evolution, a characteristic pattern of sharp-edged features develops, resembling those seen in shell galaxies.

The bottom row of Figure 1 shows the distribution of disk gas at the same times as the stars. Following the disruption of the companion, gas particles, like the stars, begin to oscillate back and forth in the potential of the primary. However, in addition to the gravitational forces which act on all particles, the gas is subject to local hydrodynamic accelerations arising from pressure gradients and shocks. Within a short time, the gaseous and stellar debris are effectively segregated. Because the gas is subject to self-interaction, shocks developed as oppositely-directed gas flows encounter one another and dissipate the orbital kinetic energy of the gas. Most of the gas still bound to the primary settles into a compact disk, which is somewhat smaller than the initial disk and spins in the same direction as it.

Additional models (not shown) demonstrate that the qualitative features of the results here are not altered by variations in orbital geometry (Weil & Hernquist 1992). If the orbit is not precisely radial, stars and gas are again segregated, but, instead of a nuclear disk, the gas forms a compact ring near the

center of the primary. If the disk is tilted with respect to the orbital plane, shells again form from stars and gas collects either into a disk or ring, but the gas structure is tilted with respect to the orbit plane.

The segregation and subsequent independent evolution of stars and gas has a number of implications for our understanding of fine structures in galaxies. As indicated by Figure 1, it is expected that little gas will be found near shells Thus, shells should not exhibit significant rates of star formation but should age as would an isolated stellar population and become redder with time. In contrast, it seems quite plausible that star formation will be boosted in the nuclear disks and rings formed during accretion events. This suggests that a population of stars will be produced near the center of the primary that will be distinct from that of its main body. Several recent observations support this contention. A significant fraction of shell galaxies ($\sim$ 20%) in the Malin & Carter (1983) catalog contain nuclear concentrations of A stars, indicative of recent star formation (Carter et al. 1988). The galaxy Markarian 717 displays a starburst nucleus and shells (Taniguchi et al. 1990). Our results may also be relevant to the interpretation of observations of NGC 1275, an elliptical which possesses shells and a central population of bright, blue point sources which have characteristics similar to those of young globular clusters (Holtzmann et al. 1992). These sources lie in a ring around the center of the elliptical, with a distribution and size comparable to that of the gaseous remnants in our non-radial encounter models.

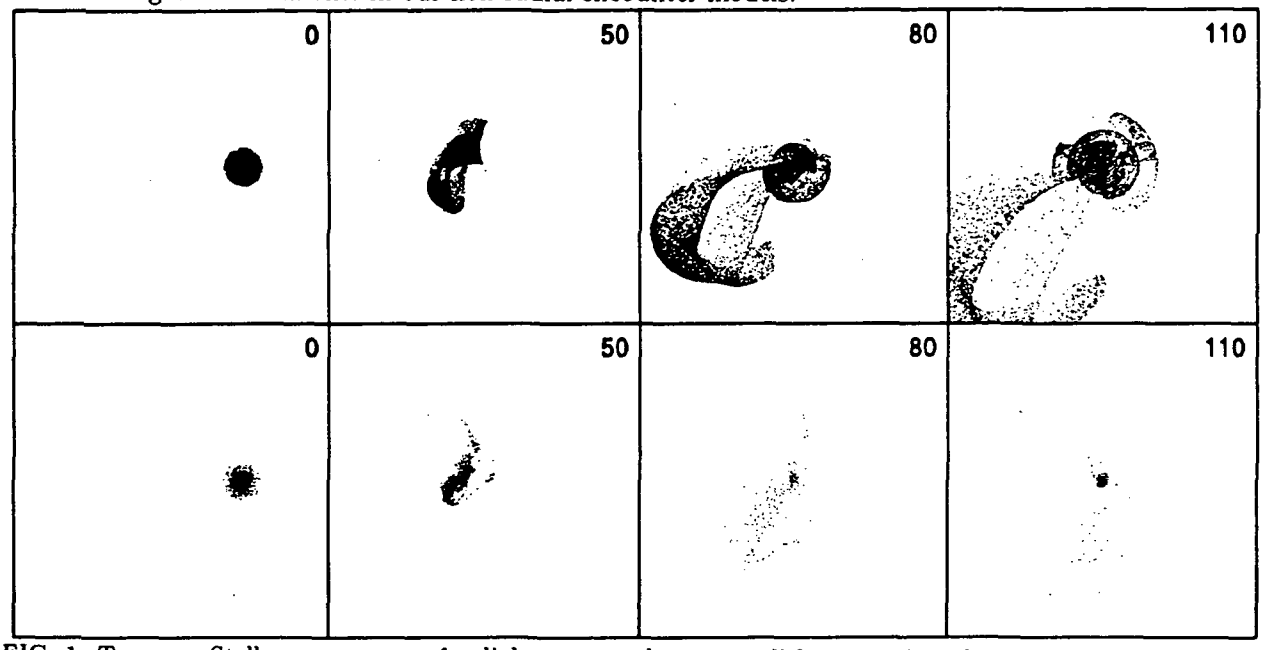

FIG. 1. Top row: Stellar component of radial encounter between a disk companion of mass 0.1 and scale length 0.7 and a spherical primary with mass and scale length equal to unity. Bottom row: Gas component with disk mass 0.01. Initial separation of the two galaxies is 10 primary scale lengths. All frames show x-y spatial projection, measure 40 length units per edge, and display dimensionless time in the upper right-hand corner.

REFERENCES

Carter, D., Prieur, J.L., Wilkinson, A., Sparks, W.B. & Malin, D.F. 1988, MNRaS 235, 813.

Hernquist, L. 1990, ApJ 356, 359.

Hernquist, L. & Katz, N. 1989, ApJS 70, 419.

Hernquist, L. & Quinn P.J. 1988, ApJ 331, 682.

Holtzmann, J.A., Faber, S.M., Shaya, E.J., Lauer, T.R., Groth, E.J., Hunter, D.A., Baum, W.A., Ewald, S.P., Hester, J.J.,Light, R.M., Lynds, C.R., O'Neil, E.J. & Westphal, J.A. 1992, Lowell Observatory preprint.

Malin, D.F. & Carter, D. 1983, ApJ 274, 534.

Quinn, P.J. 1984, ApJ 279, 596.

Seitzer, P. & Schweizer, F. 1990, in Dynamics and Interactions of Galaxies, ed. R. Wielen, Springer-Verlag, Berlin, 270.

Taniguchi, Y., Ichikawa, S., Hamabe, M., Yamagata, T. & Iye, M. 1990, A&A 233, 385.

Weil, M.L. & Hernquist, L. 1992, ApJ, submitted.

STARBURSTS TRIGGERED BY CENTRAL OVERPRESSURE IN INTERACTING GALAXIES

Chanda J. Jog and Mousumi Das,
Indian Institute of Science, Bangalore 560012, India.

Abstract :

We propose a triggering mechanism for the origin of enhanced, massive-star formation in the central regions of interacting spiral galaxy pairs. Our mechanism is based on the detailed evolution of a realistic interstellar medium in a galaxy following an encounter. As a disk giant molecular cloud (GMC) tumbles into the central region following a galaxy encounter, it undergoes a radiative shock compression via the pre-existing high pressure of the central inter-cloud medium. The shocked outer shell of a GMC becomes gravitationally unstable and begins to fragment thus resulting in a burst of star formation, when the growth time for the gravitational instabilities in the shell becomes smaller than the crossing time of the shock. The resulting values of typical infrared luminosity agree with observations. For details, see Jog & Das (1992).

Cloud Compression via Central Overpressure:

We consider a galaxy with pre-encounter gas parameters as in the Galaxy, and study its evolution as it undergoes an enounter. Our model starts with the well-established fact (e.g., Norman 1990) that galaxy interactions cause an inflow of gas into the central region from the disk region within a galaxy. Further, recent observations of the Galaxy have shown the existence of a fairly uniform, gaseous, inter-cloud medium (ICM) in the central 1 kpc region (Bally et al. 1988). We note that the average pressure within the ICM is about 25 times greater than the internal pressure within a disk GMC.

We show that as a disk GMC arrives into the central region, it undergoes a radiative shock compression via the pre-existing high pressure of the ICM. The compression continues until the growth time for the gravitational instabilities in the shocked shell of a GMC becomes smaller than the shock crossing time. This is shown to occur when the mass of the shocked shell is about 80 % of the cloud mass. Beyond this point, the shell becomes unstable and this results in a burst of star formation.

Enhanced Star Formation and Resulting IR Luminosity:

The star formation in the shocked, high-density gas in a GMC shell is characterized by a high star formation efficiency and a preferential formation of massive stars of a few $M_\odot$ each (Larson 1986). The resulting IR luminosity depends linearly on the gas infall rate, the cloud mass fraction that is shock-compressed, and the star formation efficiency. Our mechanism yields a lower limit to the central infrared luminosity of $\sim$ 2-6 $*10^9$ $L_\odot$, and the infrared luminosity-to-gas mass ratio of a few $L_\odot/M_\odot$, in reasonable agreement with observations of central starbursts in tidally interacting galaxies. The evolved mergers, with their higher central gas concentrations, yield higher values of $\sim 10^{11}$-10^{12} $L_\odot$, and $\lesssim$ 100 $L_\odot/M_\odot$ respectively, which agree with the observed values for the central regions of evolved mergers (e.g., Telesco 1988).

Not all interacting galaxies show starbursts. One reason for this may be that the galaxy may not have a high-pressure ICM , as we show to be the case in M33. We can thus explain why M33 does not show a central starburst despite a close interaction with M31.

Conversely, an isolated, barred galaxy may show a central starburst if the central ICM pressure is greater than the internal pressure in a disk GMC, as we show to be the case in IC 342.

The central ICM appears to be a common feature of spiral galaxies, and its energetics and evolution need to be studied further.

References:

Bally, J., Stark, A.A., Wilson, R.W., & Henkel, C. 1988, ApJ, 324, 223

Jog, C.J., & Das, M. 1992, ApJ, In Press.

Larson, R. B. 1986, in Stellar Populations, eds. C.A. Norman et al. (Cambridge: Cambridge Univ. Press), 101

Norman, C.A. 1990, in Massive Stars In Starbursts, eds. C. Leitherer and N. Walborn, In press.

Telesco, C.M. 1988, ARA&A, 26, 343

Feeding IC 342: The Nuclear Spiral of a Starburst Galaxy

D. Levine, J. Turner, R. Hurt

ABSTRACT

IC 342 is a large nearby (1.8 Mpc, Turner and Hurt, 1991, hereafter T&H) spiral galaxy undergoing a moderate nuclear starburst. T&H have previously mapped the inner arcminute in $^{13}CO_{(1-0)}$ using the Owens Valley Millimeter Interferometer and found evidence that the nuclear molecular gas takes the form of spiral arms in a density wave pattern. They suggest that radial streaming along the arms may channel gas from the exterior of the galaxy into the nucleus, feeding the starburst.

We have mapped the $^{12}CO_{(1-0)}$ emission of the inner 2 kpc of IC 342 at 2.8" resolution using the Owens Valley Radio Observatory (OVRO) Millimeter Interferometer. The greater sensitivity of ^{12}CO observations has allowed us to trace the spiral pattern out to a total extent of >1 kpc. The ^{12}CO observations extend considerably the structure observed at ^{13}CO and offer further evidence that a spiral density wave may extend from the disk into the nucleus of IC 342.

I. OBSERVATIONS

IC 342 was observed in the 2.6 mm ^{12}CO $(J=1->0)$ transition with 3" resolution at the OVRO Millimeter Interferometer. SSB system temperatures referred to above the atmosphere ranged from 300 to 900 K. Spectral line data were collected in two filterbanks, each with 32 channels, one at 5 MHz (13.6 km/s) resolution for an overall bandwidth of 160 MHz (435 km/s) and the other at 1 MHz (2.72 km/s) resolution with an overall bandwidth of 32 MHz (87 km/s).

Five overlapping fields were observed. The phase center of the central field was at $\alpha = 03^h41^m57^s.0$, $\delta = +67^\circ 56'30"$ with the other four offset by +/-30" and +/- 60" in declination. The central velocity at channel 17 corresponds to a V_{LSR} of 28.5 km/s. The individual 5 MHz channels were deconvolved using CLEAN and mosaicked. Natural weighting produced a synthesized beam of 2.9" x 2.9" in the central frame and the frames centered 30" north and south of the nucleus. Integrated intensity and intensity-weighted velocity moment maps were produced from the channel map mosaics.

II. RESULTS

The ^{12}CO integrated intensity maps extend the nuclear molecular structure observed at ^{13}CO (T&H) . The mosaic shows that the ^{12}CO emission takes the form of a kinked bar or very open 2-arm spiral which is fairly continuous out to a distance of 800 pc (90") from the optical center. Fainter, patchy emission out to the edges of the field, where the primary beam response is low, suggests that the spiral pattern continues out to >1 kpc. Also visible in the mosaic are symmetric spurs of molecular emission suggesting more tightly wound spiral arms to the concave side of the open arms. These spurs extend about 20" (175 pc) form the optical center of the nucleus.

Figure 1 is an overlay of the integrated intensity mosaic on a gray scale plot of the Hα emission (J.Young, private communication). T&H noted that the ^{13}CO emission traced the Hα arms, offset 50-100 pc (5-10"), as would be expected if the star formation is due to compression of the molecular gas by a trailing spiral density wave. The ^{12}CO emission clearly confirms this relationship, continuing to trace the

spiral structure, offset to the concave side of the arms, out to the edge of the field as overlaid. We also note that the molecular spur running from the southern arm towards the east traces the structure of the Hα emission at the edge of the innermost nuclear region. We have also compared the ^{12}CO emission to near-IR J,H,K-band SQUIID maps (I. Gatley, private communication). The K-band map also displays faint open spiral structure, parallel to the Hα at an offset slightly less than the ^{12}CO.

The distribution of the gas in the individual channel maps is consistent with a spiral density wave. The emission shifts from the north in the most positive velocity channels to the south, indicative of rotation, but maintains a bar-like morphology over many channels. This is consistent with the ^{13}CO work by T&H. The circular velocities as measured from ^{12}CO velocity moment map compare extremely well to those determined by T&H. They are consistent with the peak velocity measured in HI of 192 km/s (Rogstad, Shostock & Rots, 1973). The isovelocity contours of the molecular gas as traced by ^{12}CO become nearly parallel to the molecular bar to the extreme north, suggesting substantial radial motion.

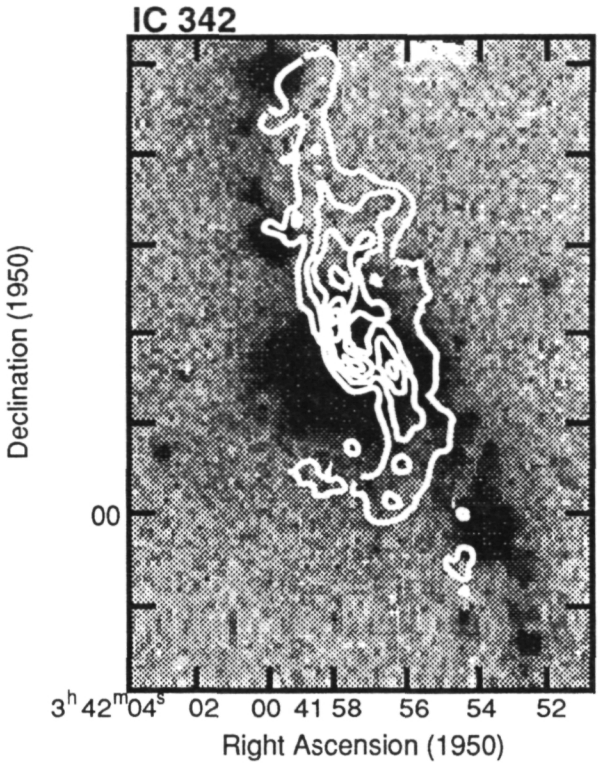

Overlay of the 12 CO mosaic on the Ha emission. Optical positions were determined from stellar positions on a POSS plate and are estimated to be accurate to 2"

REFERENCES

E.E. Becklin, *et al*, 1980 , *Ap J*, **236**, 441

D. H. Rogstad, G. S. Shostock & A. H. Rots, 1973, *A & A*, **22**, 111.

J. L. Turner & P.T. P. Ho, 1983, *Ap. J.*, **268**, L79.

J. L. Turner & R. L. Hurt, 1992, *Ap. J.* ,**384**,72 (T&H)

Observations of the CO J=6-5 Transition in Starburst Galaxies

A.I. Harris[1,6], R.E. Hills[2,6], J. Stutzki[1,3,6], U.U. Graf[1,4,6], A.P.G. Russell[1,5,6], L.J. Tacconi[1,6], and R. Genzel[1,6]

[1]Max-Planck-Institut für extraterrestrische Physik, W-8046 Garching, FRG.
[2]MRAO, Cambridge University, Cambridge CB3 0HE, United Kingdom.
[3]Now at Universiät zu Köln, Zulpicherstr. 77, W-5000 Köln 41, FRG.
[4]Now at Astronomy Department, University of Texas, Austin, TX 78712, USA.
[5]Now at Royal Observatory Edinburgh, Edinburgh EH9 3HJ, United Kingdom.
[6]Visiting Astronomer at the James Clerk Maxwell Telescope.

Over the past several years, short-submillimeter observations of carbon monoxide's (CO) mid-J rotational levels have revealed the presence of a large amount of excited molecular gas in luminous giant molecular clouds in our Galaxy. Submillimeter lines are specific probes of excited material: collisional excitation of the J=6 level requires gas temperatures approximately equal to the level energy of 116 K above ground, and the 6-5 transition's critical density is approximately 10^6 cm^{-3} in optically thin gas. Radiative trapping effects reduce the excitation requirements to some extent, but detection of the CO J=6-5 line is nearly indisputable proof of the existence of gas that is both warm and dense. The excitation conditions also imply that cool ($T <$ 20 K) molecular clouds within the beam neither emit nor absorb in the short-submillimeter lines; in our Galaxy, clouds with active massive star formation emit the strongest short-submillimeter CO rotational lines.

We used these properties to explore the distribution of excited molecular material and physical conditions within the star formation regions of several classical starburst nuclei: NGC253, M82, and IC342. We have used the 6-5 transition as a thermometer of warm molecular gas in starburst nuclei, unambiguously finding that the nuclear molecular gas in starburst galaxies is substantially warmer than in typical disk clouds.

A number of recent observations make it very plausible that the gas in the nuclei of galaxies is on average more excited than the gas in the disks. Low-J lines from CO and molecules with large dipole moments that trace density, radio and dust continuum, and far-IR line emission all tend to peak strongly toward nuclei. Detection of the CO 6-5 line toward relatively compact nuclear regions is in general agreement with this trend. The present data are consistent with either moderately excited widespread nuclear gas or highly excited gas in small regions. However many possible physical components the nuclear regions may have, detection of the 6-5 line is unambiguous evidence for molecular gas with temperatures of tens to hundreds of kelvins widely distributed in galactic nuclei, gas on average warmer than in typical disk clouds. Nuclear gas heating could be either large scale, for example turbulent motions or cloud-cloud collisions in noncircular bar orbits, more local effects of radiation from high mass star formation and supernovae, or some combination. High CO excitation temperatures can affect galactic nuclear mass estimates and consequently star formation efficiencies deduced from lower-J CO lines.

The first description of these results has been published in the Astrophysical Journal (Letters) 382, L75. We are presently mapping the extended 6-5 and lower-J lines in the nuclei of NGC253 and M82.

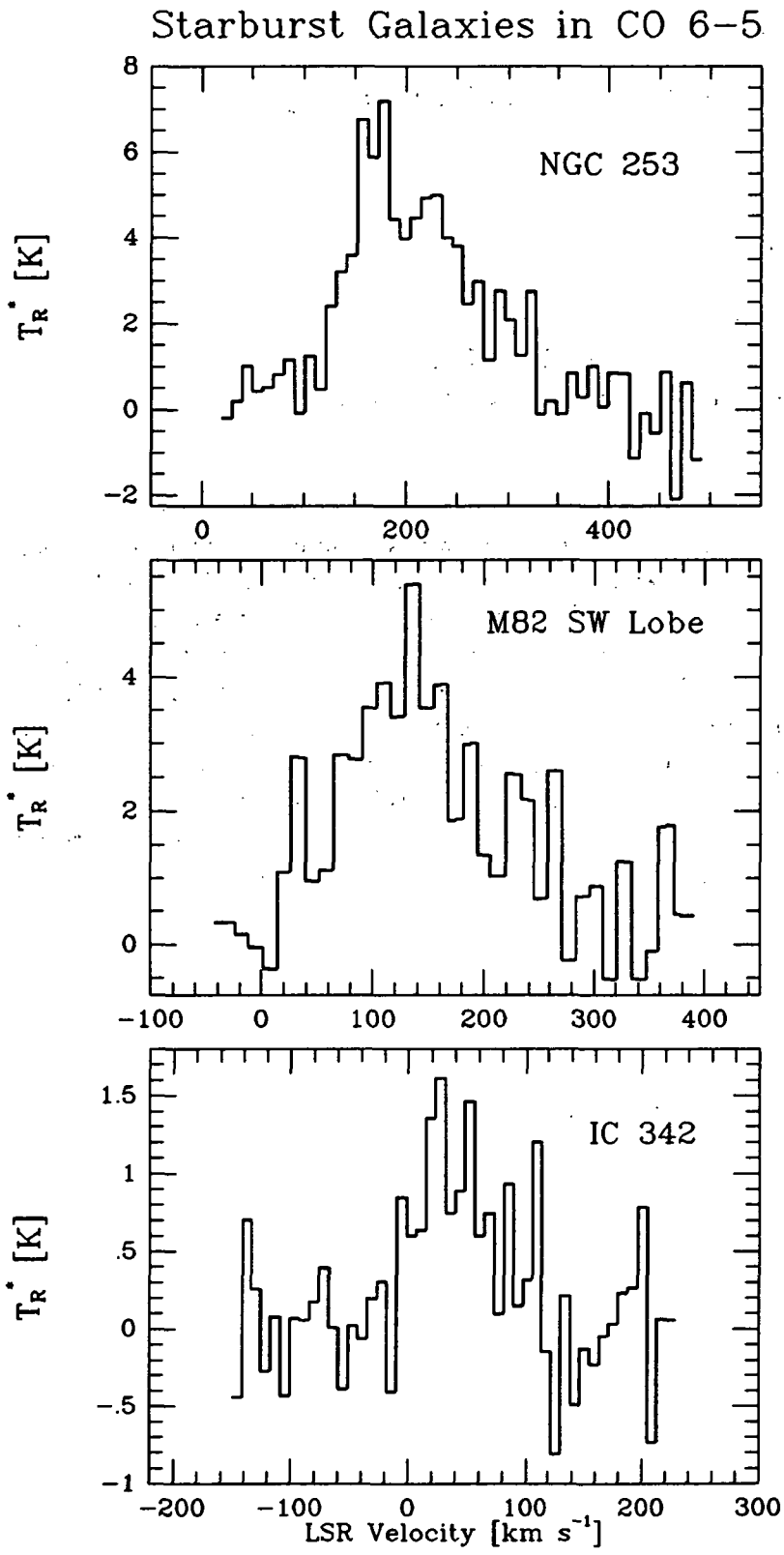
Starburst Galaxies in CO 6–5
NGC 253
M82 SW Lobe
IC 342
T_R^* [K]
LSR Velocity [km s^{-1}]

The Lyman α emission of starburst galaxies

David Valls-Gabaud[1,2,3]

[1] Institut d'Astrophysique de Paris, France.
[2] Institute of Astronomy, Cambridge, UK.
[3] Physics Department, Queen's University, Canada.

ABSTRACT. Nearby starburst galaxies have consistently shown anomalous Lyα/Hβ ratios. It has been suggested that dust, associated with resonant scattering, quenches the Lyα line by a large factor. However, the observed amount of dust can barely account for the large depletion factors. It is proposed here that a much more important effect is the age of the burst. Normal (ie, case B recombination) ratios are observed if the galaxy is currently undergoing the burst, while anomalous ratios appear when the galaxy is observed in the post-burst phase. Underlying stellar populations in the UV spectra should therefore be older in the latter case. This scenario explains the presence of Lyα in absorbtion. Implications for deep surveys are also discussed.

ULTRAVIOLET IMAGING TELESCOPE (UIT) OBSERVATIONS OF GALAXIES

S. G. Neff
(for the UIT team)
NASA Goddard Space Flight Center, Greenbelt, MD, U.S.A.

Ultraviolet images of several galaxies were obtained during the ASTRO-1 shuttle mission in December, 1990. The images have a FWHM angular resolution of $\sim$ 3 arcsecond and are of circular fields $\sim$ 40 arcminutes in diameter.

Most galaxies were observed in at least two and sometimes as many as four broad bands:

B6 (λ_{eff} = 1500 Å, $\Delta\lambda$ = 400 Å),
B1 (λ_{eff} = 1520 Å, $\Delta\lambda$ = 350 Å),
B5 (λ_{eff} = 1620 Å, $\Delta\lambda$ = 220 Å), and
A1 (λ_{eff} = 2490 Å, $\Delta\lambda$ = 1150 Å).

A very few fields were observed with narrower band filters.

The most basic result of these observations is that most systems *look* dramatically different in the UV from their well-known optical appearences. Preliminary results of these studies will be presented.

Information will be available on fields observed by the UIT during the ASTRO 1 mission; when that data becomes public it can be obtained from the NSSDC. The ASTRO observatory is expected to fly again in 1994 with approximately half of the observing time from that mission devoted to guest observers. The Ultraviolet Imaging telescope is extremely well suited for galaxy studies, and the UIT team is interested in encouraging a wide range of scientific studies by guest observers.

EVOLUTION OF LUMINOUS *IRAS* GALAXIES: RADIO IMAGING

S.G.Neff
NASA Goddard Space Flight Center, Greenbelt, MD, U.S.A.

J.B.Hutchings
Dominion Astrophysical Observatory, Victoria, B.C., Canada

In a recent study of IRAS galaxies' optical morphologies, we found that luminous IR sources lie in the IR color-luminosity plane in groups which separate out by optical spectroscopic type and also by degree of tidal disturbance. We found that the most luminous steep-IR-spectrum sources are generally galaxies in the initial stages of a major tidal interaction. Galaxies with active nuclei were generally found to have flatter IR spectra, to cover a range of IR luminosity, and to be in the later stages of a tidal interaction. We proposed a sequence of events by which luminous IR sources evolve: they start as interacting or merging galaxies, some develop active nuclei, and most undergo extensive star-formation in their central regions.

Another way to study these objects and their individual evolution is to study their radio morphologies. Radio emission may arise at a detectable level from supernovae in star-forming regions and/or the appearance of an active nucleus can be accompanied by a nuclear radio source (which may develop extended structure). Therefore, the compact radio structure may trace the evolution of the inner regions of IRAS-luminous sources. If the radio sources are triggered by the interactions, we would expect to find the radio morphology related to the optical 'interactivity' of the systems.

Here, we explore using the radio emission of IRAS galaxies as a possible tracer of galaxy evolution. We present and discuss observations of the compact radio morphology of 111 luminous IRAS-selected active galaxies covering a wide range of IR and optical properties.

We find that most IR-luminous sources are weak compact radio sources. Roughly three in four of those sources detected have a compact core source and at least one in five have ring-like structure characteristic of circumnuclear star-formation. The undetected sources tend to be dusty galaxies but are not clearly distinguished from the rest in their optical properties. The radio luminosity increases with IR spectral flatness, which may be a time sequence as dust is evaporated; this also corresponds to an increase in radio luminosity with optical blueness of the galaxy. The size of the radio source may increase with tidal interaction age, again suggesting a time sequence. The spread of the radio properties with optical and IR is large, and indicates that while the radio sources in most of these systems are fairly young, they do not all turn on at the start of the tidal event that we see in the optical and IR: there is a spread ranging over roughly half the characteristic timescale of the tidal event ($\sim 10^8$ years).

Overall, the radio data shows that both nuclear and circumnuclear radio activity is present, the latter being more noticeable in the optically identified LINER and "non-active" galaxy population. The radio flux correlates with both IR and optical fluxes, indicating a connection with the nuclear activity in both cases. The spread of properties, and the small fraction of undetected sources suggests that nuclear radio sources may be activated at stages later than the optical active nucleus in active galaxies.

Details of this work are presented in the *Astronomical Journal,* 1992.

Page Intentionally Left Blank

Day 3: Wednesday, 8 July 1992

Page Intentionally Left Blank

OB associations and Giant Molecular Clouds in the Galaxy

Jonathan Williams, Chris McKee
University of California, Berkeley

Giant molecular clouds (GMCs) are the sites of all OB star formation in the Galaxy. These OB stars typically form in large associations and photoionize the surrounding gas, eventually destroying the clouds from which they were born. CO surveys have revealed the distribution of GMCs in the Galaxy, and radio observations provide data on the distribution of associations. These results are extrapolated to determine Galactic mean distribution functions of each and then combined to determine how GMCs and OB associations are correlated.

The resulting probability distribution of luminosity given cloud mass inplies that although most of the molecular *mass* of the Galaxy is in massive star forming complexes, a large *number* of clouds are in a quiescent state, not forming massive stars. There is a threshold mass for molecular clouds above which massive star formation is extremely likely and abundant and below which it is almost certainly absent.

Hα observations of extra-galactic HII regions can be characterized in the same manner. Whilst we find that the form of the luminosity distribution of different Hubble types is similar to that of the Galaxy, we note that the maximum luminosity of OB associations in early type galaxies appears to be limited by some physical process absent in later type galaxies. However there is a definite limit to the mass of the largest GMCs for both types (otherwise the largest cloud would contain half the mass of the galaxy!), and we find that the basic conclusions drawn about the proportion of star forming GMC's is rather insensitive to the form of the GMC mass spectrum implying that the diagram below for the Galaxy may be qualitatively similar to what might be found for other spirals.

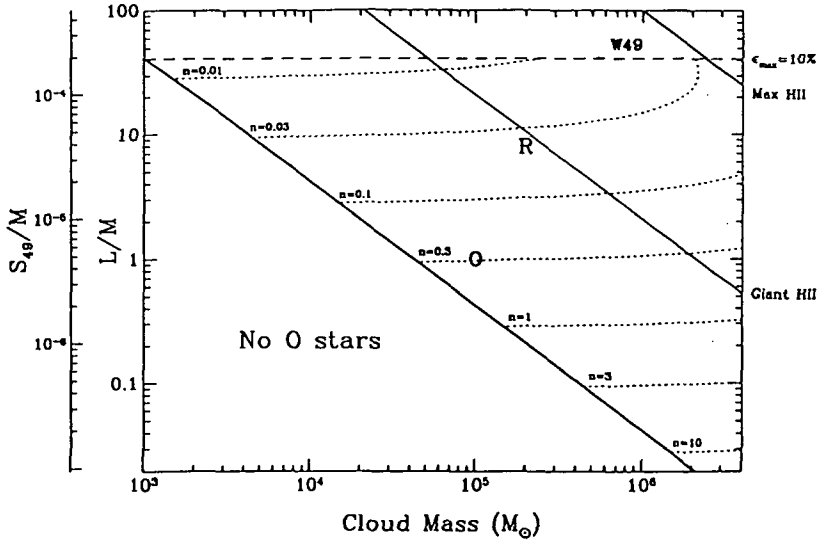

Luminosity per mass of O star associations against mass for the Galactic HII luminosity distribution and GMC mass spectrum. S_{49} is the ionizing photon luminosity in units of 10^{49} photons/sec. The solid diagonal lines are lines of constant luminosity and the dotted lines are contours of expected number of associations, as a function of luminosity and mass (if less than one it is interpreted as a probability). The Orion, Rosette and W49 HII regions are included on the diagram as examples.

N93-26788

Star-Dust Geometries in Galaxies: The Effect of Interstellar Matter Distributions on Optical and Infrared Properties of Late-Type Galaxies.

J.M. Capuano, Jr.,[1] H.A. Thronson, Jr.,[2] and A.N. Witt[1]

[1]Ritter Astrophysical Research Center, The University of Toledo, Toledo, OH 43606
[2]Wyoming Infrared Observatory, University of Wyoming, Laramie, WY 82071

The presence of substantial amounts of interstellar dust in late-type galaxies affects observable parameters such as the optical surface brightness, the color, and the ratio of far-infrared to optical luminosity of these galaxies.

We conducted radiative transfer calculations for late-type galaxy environments to examine two different scenarios: one, the effects of increasing amounts of dust in two fixed geometries with different star distributions; and two, the effects of an evolving dust-star geometry in which the total amount of dust is held constant, for three different star distributions. The calculations were done for ten photometric bands, ranging from the far-ultraviolet to the near-infrared (K), and scattered light was included in the galactic surface brightness at each wavelength. The energy absorbed throughout these ten photometric bands was assumed to re-emerge in the far-infrared as thermal dust emission.

Our principal result is that frequently invoked measures of dust mass, such as brightness reduction due to extinction, reddening, and the ratio of far-infrared to optical flux ratios are highly unreliable indicators of the actual amount of dust present in a given system. The residual surface brightness of a galaxy is largely determined by the stars not directly obscured by dust, and so is the color excess. The ratio of far-IR to optical flux depends mainly on the ratio of stellar luminosity deeply embedded in dust clouds to that only lightly affected by dust. Thus, the star luminosity distribution relative to the dust is far more important than the actual dust mass. Models differing solely in the relative distribution of stars relative to dust differ by more than one order of magnitude in the ratio of L(IR)/L(Opt). (See Fig. 1)

We also considered the evolutionary contraction of a constant amount of dust relative to pre-existing star distributions. In a spherical geometry, the optical depth increases with the inverse square of the length scale. Again, the star distribution is critical in determining whether in the process of dust contraction a greater fraction of sources is freed from the extinction effects or whether a greater fraction of the light of the sources still remaining in the dust is now absorbed due to the increasing optical depth. Thus, the contraction of a constant amount of dust can lead either to an increase in the optical surface brightness and a decline in the ratio L(IR)/L(Opt), in the case of a uniform star distribution, or to a decrease in surface brightness and a substantial increase in L(IR)/L(Opt), when the star distribution is strongly concentrated in the volume of space toward which the dust contraction occurs. (See Fig. 2)

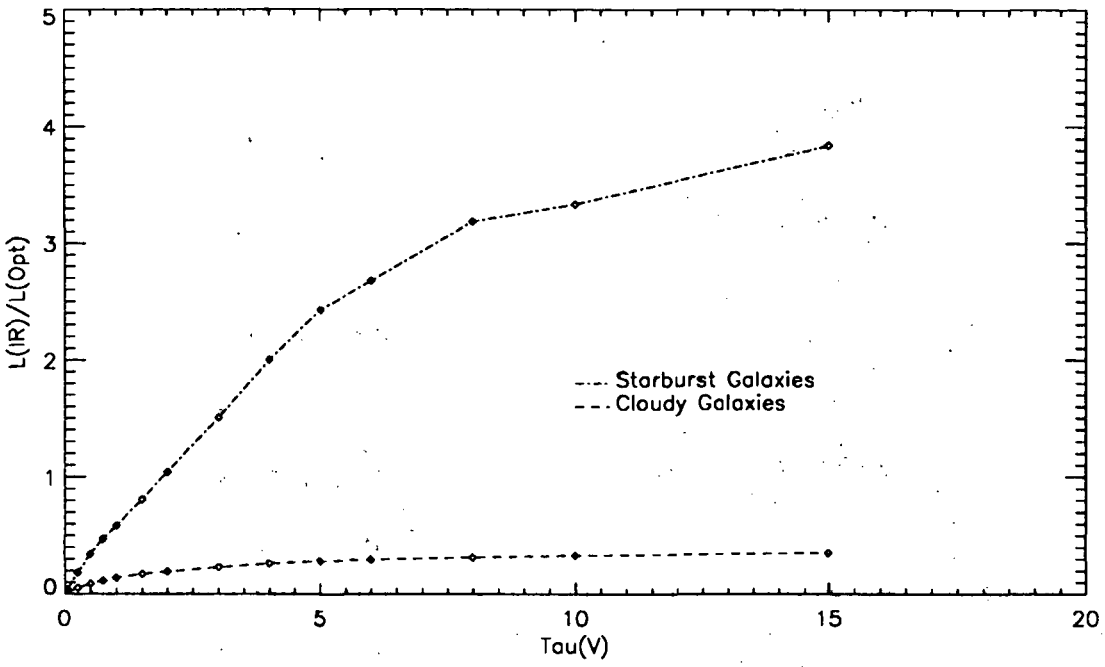

Fig. 1 – The ratio of infrared emission from heated dust grains, L(IR), to the total emitted starlight, L(Opt), for two environments as a function of V-band extinction optical depth, measured from the surface of the spherical geometry to the center. The dust occupies the inner one-third of the volume of these systems. The cloudy galaxy has a uniform star distribution, while the starburst galaxy has a radial luminosity distribution following a r^{-6} law.

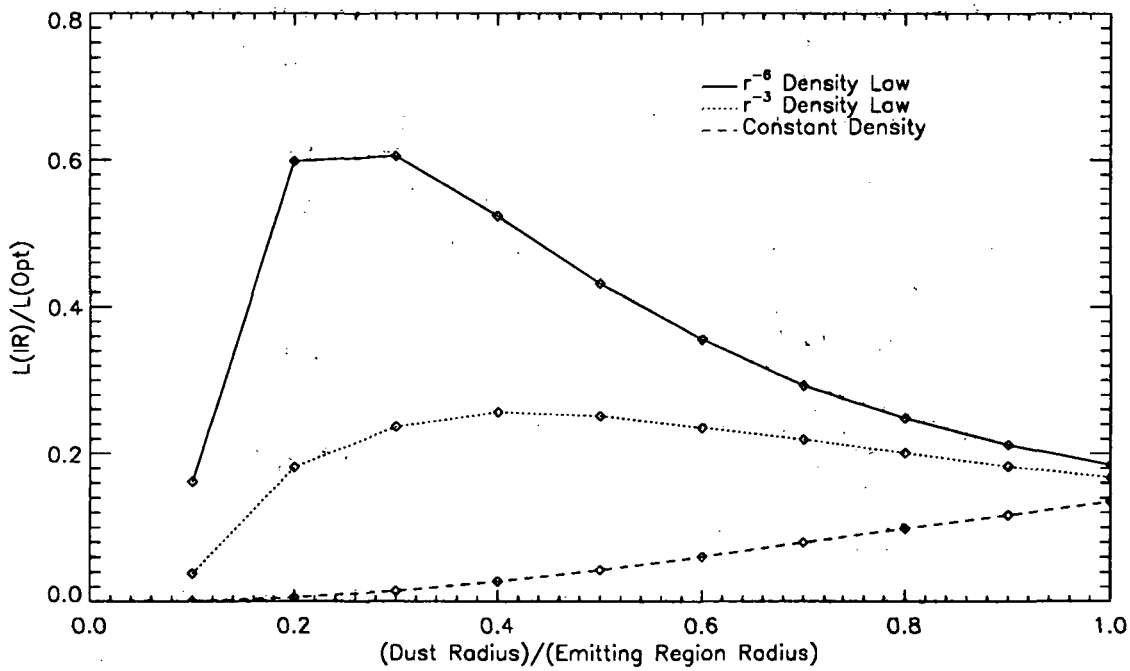

Fig. 2 – The ratio of L(IR)/L(Opt) for three different star distributions, in which a uniform dust distribution is allowed to contract from an initial V-optical depth radius of 0.25 (dust radius/radius of star distribution = 1.) to a final $\tau_v = 25$ (dust radius/radius of star distribution = 0.1). The three star distributions correspond to uniform density, a r^{-3} law, and a r^{-6} law.

The Environments of Seyfert and Markarian Galaxies

John W. MacKenty and Brian McLean (STScI)

The Third Teton Summer School -- July 1992

The environments of galaxies may affect both the presence and nature of the activity in their nuclei. We have undertaken a study of the environments of Seyfert and non-Seyfert Markarian galaxies to investigate the relationship between nuclear activity and external influences on the nucleus (MacKenty 1989; MacKenty, McLean, and Simpson 1990). Previous studies of the environments of Seyfert galaxies suggest a connection between the nature of the activity in the nuclear regions of the galaxy and its external environment. Petrosian (1982) finds Seyfert 2 galaxies to be located in regions of higher density than Seyfert 1 galaxies and Dahari (1984,1985) finds an excess of close companions to Seyfert galaxies compared to field galaxies. In a study of 102 Markarian galaxies, MacKenty (1989) confirms these results yet finds that non-Seyfert Markarian galaxies have the same frequency of companion galaxies as Seyfert Markarian galaxies and concludes from their IRAS colors that the companion galaxies tend to enhance star formation rather than directly influence the nuclear activity. Fuentes-Williams and Stocke (1988) reach conclusions quite different from Dahari's based on different control sample selection and background subtraction techniques.

Using the digitized images of the 20 minute V band Schmidt plates obtained for the construction of the Hubble Space Telescope Guide Star Catalog, we have investigated the morphologies and environments of the ~1500 galaxies in the Markarian catalog (Markarian 1967; Markarian *et al.* 1979) and ~600 galaxies from the published CfA 15.5 magnitude slice (Huchra *et al.* 1990) which lie outside of the Coma cluster. We have constructed an updated version of the Markarian catalog of galaxies with accurate positions measured in the HST Guide Star Selection System coordinate system, IRAS source identifications and fluxes, morphological classifications for the Markarian galaxies aimed at distinguishing those galaxies with possible signs of external influences on their nuclei, and number counts of neighboring galaxies. A COSMOS type algorithm was used to locate and classify (as stellar, nonstellar, or galaxy) all objects on the extracted images. All nonstellar and galaxy objects detected within a 50 kpc (H_0 = 75 km s^{-1} Mpc^{-1}) projected radius of each Markarian galaxy were counted as neighboring galaxies.

Figure 1: Number of Galaxies in Each Velocity Interval

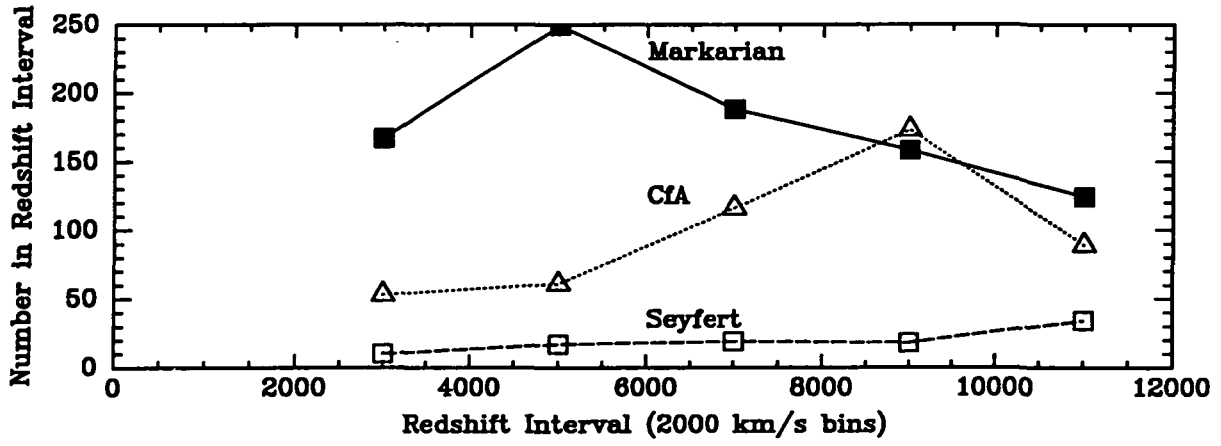

Figure 1 shows the differing redshift distributions of the galaxy populations. The incompleteness of the Markarian survey and the rather different distribution of the Seyfert galaxies subset are evident. This may have been a significant source of bias in prior studies. To control this bias, the sample was binned into 2000 km s^{-1} intervals. The fraction of the galaxies in each interval with neighbors within 50 kpc projected distance is shown in Figure 2.

Figure 2: Frequency of Neighbors within 50 kiloparsecs

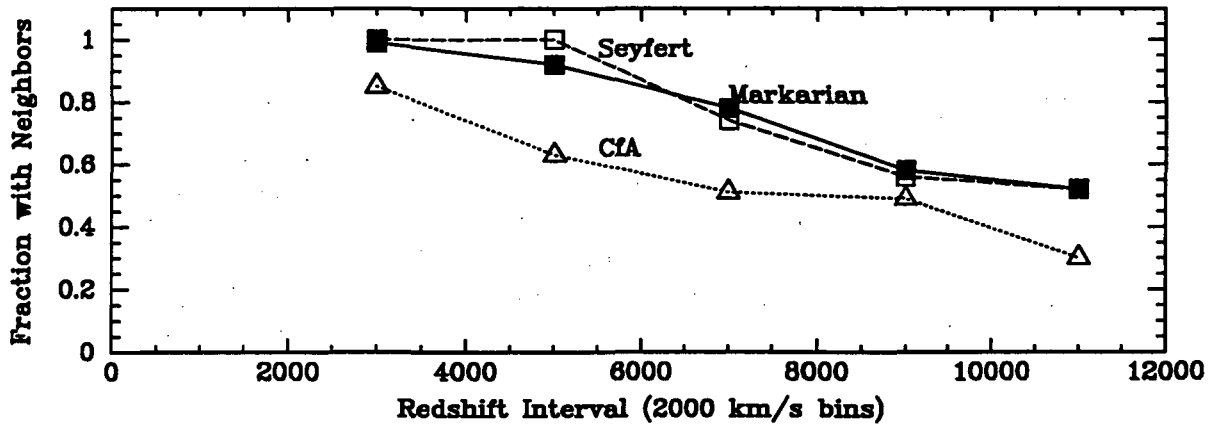

Conclusions

• We find an enhancement in the relative frequencies of companion galaxies about Markarian (and Seyfert) galaxies compared to the CfA galaxies but at a lower level than the enhancement found by Dahari (1984). This enhancement tends to decrease with the imposition of size constrains on potential companion galaxies supporting the suggestion of Fuentes-Williams and Stocke (1988) that small companions may be important.

• Within the Markarian sample, we find that the relative frequencies of Seyfert, Starburst, and UV excess nuclear activity are independent of their immediate environments in agreement with the conclusions of MacKenty (1989). This is not to imply that nuclear activity per se is not influenced by environment but rather that the type of nuclear activity (at least for Markarian galaxies) does not appear to be determined by the environment.

• Within the Markarian sample, there is no strong correlation between the type of nuclear activity and the morphology of the host galaxy although bar and ring morphologies are somewhat more common in Seyfert and Starburst galaxies.

Dahari, O. 1984, A.J. 89, 966.

Dahari, O. 1985, Ap.J. Suppl., 57, 643.

Fuentes-Williams, T. and Stocke, J.T. 1988, A.J. 96, 1235.

Huchra, Geller, DeLapparent, and Corwin 1990, Ap.J. Suppl., 72, 433.

MacKenty, J.W. 1989, Ap.J., 343, 125.

MacKenty, J.W., Mclean, B., and Simpson, C. 1990, in Paired and Interacting Galaxies (eds. Sulentic, J.W., Keel, W.C., and Telesco, C.M.; IAU Colloquium No. 124; NASA Conference Publication 3098), p. 165.

Markarian, B.E. 1967, Astrofizika, 3, 55.

Markarian, B.E., Lipovetskii, V.A., and Stepanian, D.A. 1979, Astrofizika, 15, 549.

Petrosian, A.R. 1982, Astrofizika, 18, 548.

A Radio Continuum Survey of Edge-On Spiral Galaxies at 90 cm

B. Heikkila, W.R. Webber, J.O. Burns, R.A.M. Walterbos
Dept. of Astronomy, New Mexico State University
Las Cruces, NM 88003
N. Duric
Dept. of Physics and Astronomy, University of New Mexico
Albuquerque, NM 87131

Abstract

Accurate spectral indices of the radio emission from both the thin disk and thick disk or halo components are critical to understand the propagation mechanisms of electrons within spiral galaxies. These spectral indices give information on the relative importance of diffusion and synchrotron energy loss in the propagation of electrons in the disk. Our goal of this survey is to locate a larger sample of spiral galaxies that exhibit halo phenomena so that a statistical analysis will be possible.

Introduction

Recent observations of the late type spiral galaxies NGC4631 (Hummel and Dettmar 1990; and references therein) and NGC 891 (Hummel et al. 1991; and references therein) have indicated that these two galaxies have extended radio halos. The spectral index of the radio emission from these galaxies also appears to increase with distance perpendicular to the disk. Do only late type spirals have radio halos or do all types exhibit this phenomena? Are the electrons responsible for the radio emission propagated primarily by diffusion related transport or does convection due to galactic winds play a role? In order to answer these questions in a statistical sense we have initiated a multi-frequency radio continuum study of a sample of twenty-seven edge-on ($i > 75°$) spiral galaxies that cover a wide range in morphological type (Sa - Sdm). The first phase of the observations at 90 cm has been completed, and analysis of the data is now in progress. The following two sections outline the selection criteria we used in chosing our sample of galaxies and our results at this stage in the analysis.

Selection Criteria

We selected a sample of galaxies from Tully's "Nearby Galaxies Catalog", which contains 2367 galaxies with systemic velocities less than 3000 km/s, using the following criteria:

- Inclination: Only those galaxies with inclinations greater than 75 degrees were selected. These inclinations facilitate the study of the spatial distribution of the radio halos perpendicular to the galactic plane.
- D25: The observed 25 mag/arcsecond^2 isophotal diameter range was limited to $3' \leq D25 \leq 15'$. Observationally, galaxies within this isophotal diameter range offer the best chance of showing resolved halos at the observing frequency of 90 cm.
- Morphology: All galaxies in the sample were required to be spirals (Revised Hubble Type: Sa - Sdm).
- Declination: To provide good *uv* coverage using the VLA "snapshot" mode, a lower limit of 18° was placed on the declinations of the sources.

The net result was a list of 47 galaxies. Due to limited telescope time, and the need to maximize our integration time on each source, only 27 of these galaxies were observed.

Observations and Data Analysis

The initial "snapshot" observations at 90 cm were completed on May 24/25, 1992 using the C-Configuration of the Very Large Array telescope (VLA) at Socorro, New Mexico. The approximate synthesized half-power beamwidth for this configuration at 90 cm is 56 arcseconds. In order to reach a theoretical sensitivity of 1 mJy/Beam using a bandwidth of 3.125 MHz we observed each of the twenty-seven galaxies for approximately twenty minutes split between two different hour angles. The 90 cm observations were calibrated and reduced with the AIPS processing software. Of the twenty-seven galaxies observed we have detected fifteen at the 4σ level and another five galaxies at the 2σ level. There appears to be no detections above the noise level in seven of the fields. Table I shows these results along with individual galaxy data tabulated from Tully's "Nearby Galaxy Catalog". Additional observations at 20 cm using the D-Configuration of the VLA are currently scheduled for each galaxy in our sample.

Table I: Results

GALAXY	RA	DEC	D25	INC	MORPH	BMAG	DIST	VEL(H)	PA
$\geq 4\ \sigma$ Detections									
NGC 2683	8 49 35.6	+33 36 32	9.1	79.	3A	9.82	5.7	415.	44
NGC 2820	9 17 43.7	+64 28 16	4.1	90.	5BP	12.46	26.0	1576.	59
NGC 3003	9 45 38.5	+33 39 19	6.0	90.	4B	11.48	24.4	1480.	79
NGC 3556	11 08 36.8	+55 56 33	7.8	81.	6B	9.97	14.1	697.	80
NGC 3735	11 33 04.8	+70 48 42	4.0	85.	5A	11.60	41.0	2696.	131
NGC 4013	11 55 56.6	+44 13 32	4.7	84.	4	11.60	17.0	835.	66
NGC 4096	12 03 28.4	+47 45 20	6.4	82.	5X	10.33	8.8	577.	20
NGC 4144	12 07 30.0	+46 44 00	6.3	81.	6X	11.20	4.1	267.	104
NGC 4157	12 08 34.6	+50 45 51	7.0	90.	3X	11.00	17.0	771.	66
NGC 4217	12 13 21.5	+47 22 17	5.1	78.	3	11.30	17.0	1028.	50
UGC 8246	13 07 44.3	+34 26 47	3.2	81.	6B	13.50	17.3	813.	83
NGC 5290	13 43 11.4	+41 57 46	3.4	81.	4BP	11.90	37.8	2579.	95
NGC 5529	14 13 27.7	+36 27 26	5.7	90.	5	11.90	43.9	2878.	115
NGC 5907	15 14 34.8	+56 30 33	11.2	90.	5A	10.31	14.9	666.	155
UGC 9858	15 24 52.4	+40 44 14	4.2	89.	4X	12.50	40.6	2619.	83
$2\ \sigma$ Detections									
NGC 3877	11 43 28.9	+47 46 21	5.1	85.	5A	10.90	17.0	894.	35
NGC 3972	11 53 10.0	+55 35 48	3.9	81.	4A	11.90	17.0	848.	120
NGC 4256	12 16 21.9	+66 10 37	4.2	89.	3A	11.70	39.1	2531.	42
UGC 7699	12 30 21.3	+37 53 49	3.7	79.	5B	12.20	6.2	503.	32
NGC 5297	13 44 18.4	+44 07 18	5.3	89.	3X	11.50	37.8	2404.	148
Null Detections									
NGC 2654	8 45 11.4	+60 24 21	3.9	90.	1	11.94	23.3	1382.	63
UGC 5459	10 04 54.0	+53 19 36	4.0	90.	5	12.80	20.3	1121.	132
NGC 3769	11 35 03.0	+48 10 05	3.2	76.	3B	11.20	17.0	714.	152
NGC 3917	11 48 07.7	+52 06 14	4.7	84.	6A	11.60	17.0	975.	77
NGC 4183	12 10 46.5	+43 58 33	5.1	90.	6A	12.30	17.0	934.	166
NGC 4359	12 21 41.8	+31 47 56	3.4	79.	5B	12.50	9.7	1253.	108
UGC 7941	12 44 00.0	+64 50 00	4.4	90.	7	13.20	36.2	2294.	8

References

Hummel, E., Dahlem, M., Van der Hulst, J.M., Sukumar, S.: 1991, *Astron. Astrophys.*, **246**, 10

Hummel, E., Dettmar, R.J.: 1990, *Astron. Astrophys.*, **236**, 33

Tully, R.B.: 1988, *Nearby Galaxies Catalog*

CO deficiency in galaxies of the Fornax cluster ?

Cathy Horellou[1], Fabienne Casoli[2,1], Christophe Dupraz[1,2]

[1] DEMIRM, Observatoire de Paris, Section de Meudon, F–92195 Meudon Cedex, France
[2] Ecole Normale Supérieure, 24 rue Lhomond, F–75231 Paris Cedex 05, France

There is ample observational evidence that cluster galaxies are different from those in the field. Interaction with the hot intracluster medium affects the morphology of the galaxies, their gaseous content and possibly their star-formation activity. Tidal encounters between galaxies also play an important role.

The atomic component has been investigated in detail for several clusters, among them our neighbour Virgo. A large fraction of the bright Virgo spirals have about one order of magnitude less HI than isolated counterparts of same optical size and type (Giovanelli & Haynes : 1983, AJ 88, 881). *What about the molecular phase of the interstellar medium in cluster galaxies ?* Molecular clouds are the raw material for star formation. CO surveys of Virgo bright galaxies (Stark et al. : 1986, ApJ 310, 660 ; Kenney & Young : 1989, ApJ 344, 171) do not show any evidence of H_2 deficiency : the mechanisms tearing out the low-density atomic gas leave intact the denser molecular clouds. A similar result has recently been found for the much denser and more distant Coma cluster (Casoli et al. : 1991, A&A 249, 359). To date, CO observations are available for those two rich clusters only.

With the Swedish-ESO 15 m telescope, we have observed in the ^{12}CO (1–0) transition the 23 brightest spirals and lenticulars of the Fornax cluster. Fornax is the nearest southern cluster of galaxies, at the same distance as Virgo (D = 17 Mpc adopted, consistent with $H_0 = 75$ km s^{-1} Mpc^{-1}). Fornax contains 7 times less galaxies than Virgo, but its central regions are 2.5 times denser. The spatial resolution of the CO observations is 44", corresponding to a linear distance of 3.6 kpc at 17 Mpc. Every galaxy with an optical diametre larger than 3' was mapped at half beamwidth along the major axis, even if no CO was detected towards the centre. Since every extended galaxy of the sample happens to have a high inclination, we expect not to miss any CO emission. With the Nançay radiotelescope, we also measured the HI emission of 11 galaxies of our sample. The resolution of the HI observations is 4' (E–W) by 21' (N–S).

Only 9 galaxies out of 23 were detected in CO, despite long integration times (typically 80 minutes) and the low noise level (we could detect H_2 masses as low as $5\ 10^7$ M_0). *The average CO emission of Fornax galaxies is 8 times lower than in a template sample* based on the FCRAO extragalactic survey. Figure 1 displays the $M(H_2)/D^2$ ratio for the Fornax (triangles) and template (circles) galaxies versus their morphological type.

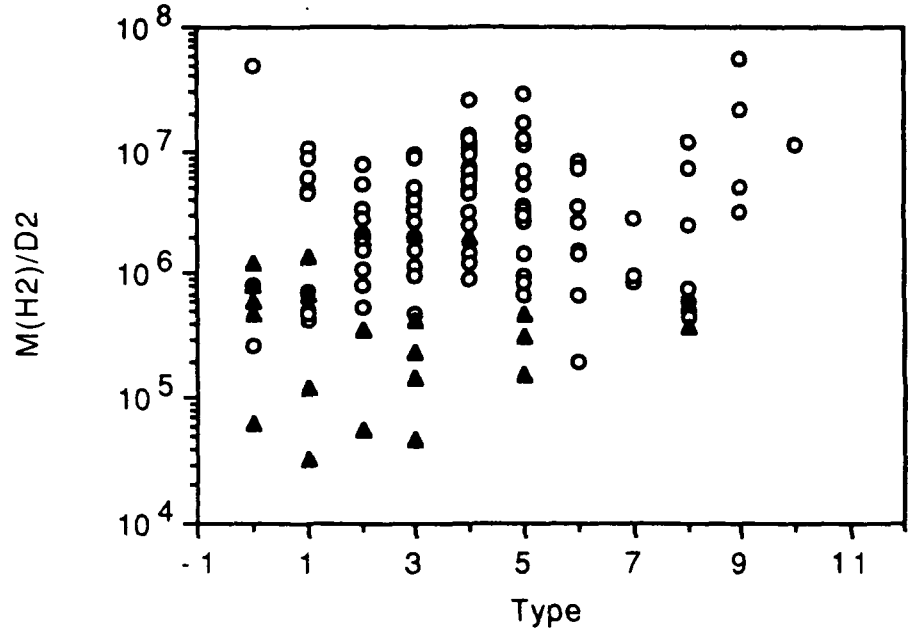

Figure 1 : Plot of the $M(H_2)/D^2$ ratio versus galaxy morphological type, for the Fornax sample galaxies (triangles) and the template FCRAO objects (circles).

In HI, we have detected 10 galaxies out of 11, and the HI masses of the other 12 objects were taken from the literature. Surprisingly, *the HI emission of the Fornax galaxies is normal* : this result is hard to explain, because all of the mechanisms which can be invoked (ram pressure stripping, evaporation, collisions between galaxies) affect the diffuse and extended atomic gas much more efficiently than the denser molecular gas.

Are the Fornax galaxies genuinely deficient in molecular gas, or must we suspect the conversion factor from CO emissivities to H_2 column densities ? As for the latter, we used the value $N(H_2)/I(CO) = 2.3\ 10^{20}\ cm^{-2}\ (K\ km\ s^{-1})^{-1}$ derived for the Milky Way by Strong et al. (1988, A&A 207, 1). The molecular masses may be underestimated if the Fornax galaxies have a low metallicity, but certainly not by a factor as large as 8. Indeed, even in the metal-poor Magellanic Clouds, the correction factor does not exceed 2 (Johansson : 1991, IAU 146, 1). Furthermore, our Fornax sample galaxies are more luminous than the LMC, thus more massive and metallic, and other indicators such as the color indices U–B and B–V or the FIR luminosity are consistent with a low star-formation activity.

The low CO emission can be partly due to the small size of the Fornax galaxies with respect to the template sample, but this effect alone cannot account for the observed deficiency.

In conclusion, we rather suggest that *the reference sample, as selected from the infrared, is strongly biased towards CO-rich galaxies*. Could the Fornax galaxies be more representative of "normal" galaxies ? Be what it may, our result stresses the need for CO observations of optically-selected isolated galaxies, in order to determine the molecular content of "normal" galaxies.

Presented at *The Evolution of Galaxies and their Environment*, July 6-10, 1992, Grand Teton, WY.

Molecular Gas Temperature and Density in Spiral Galaxies

W. F. Wall[1], D. T. Jaffe[2], F. N. Bash[2], F. P. Israel[3], P. R. Maloney[4], F. Baas[5]

[1] Code 685, NASA/GSFC, Greenbelt, MD 20771

[2] The University of Texas, Astronomy Dept., Austin, TX 78712-1083

[3] Sterrewacht, Postbus 9513, 2300RA, Leiden, Netherlands

[4] NASA-Ames Research Center, MS 245-6, Moffett Field, CA 94035

[5] Joint Astronomy Centre, 665 Komohana St., Hilo, HI 96720

ABSTRACT. We combine beam-matched ^{13}CO, ^{12}CO J = 3 → 2 and J = 2 → 1 line data to infer the molecular gas excitation conditions in the central 500 to 1600 pc diameters of a small sample of infrared-bright external galaxies: NGC 253, IC 342, M 83, Maffei 2, and NGC 6946. Additional observations of the J = 1 → 0 lines of $C^{18}O$ and ^{13}CO set limits on the opacity of the ^{13}CO J = 1 → 0 line averaged over the central kiloparsec of these spiral galaxies.

1. Introduction

The large-scale physical conditions of molecular gas can lead to understanding large-scale star formation in galaxies. To probe the molecular gas temperature and density on hundred or thousand parsec scales in a sample of 5 spiral galaxies (NGC 253, IC 342, M 83, Maffei 2, and NGC 6946), we compare the strengths of the J = 3 → 2 rotational lines of ^{13}CO and ^{12}CO with those of the corresponding J = 2 → 1 lines, observed at the Caltech Submillimeter Observatory, James Clerk Maxwell Telescope, and the Swedish ESO Submillimetre Telescope. All J = 3 → 2 and J = 2 → 1 observations had ∼ 20″ beamsizes, or ∼ 200-500 pc at the adopted distances (i.e. 1.8-5.5 Mpc). Larger beam (i.e. ∼ 60″) observations of the J = 1 → 0 lines of $C^{18}O$ and ^{13}CO were carried out at the National Radio Astronomy Observatory 12-meter telescope.

2. Results

The observed ratios of the integrated main-beam radiation temperature of the ^{13}CO J = 3 → 2 line to that of the ^{13}CO J = 2 → 1 line – abbreviated by $^{13}R_{32}$ – implies that the physical conditions of the molecular gas in the central 20″ (170-530 pc) diameter varies strongly from galaxy to galaxy. Figure 1 shows that the $^{13}R_{32}$ values range from 0.2 (in M 83) to 2.0 (in NGC 253), suggesting that the molecular gas density can change by at least an order of magnitude (from $n(H_2) \lesssim 10^4\,cm^{-3}$ to $n(H_2) \gtrsim 10^5\,cm^{-3}$) from galaxy to galaxy. The corresponding ^{12}CO line ratio, $^{12}R_{32}$, lies in the narrow range 1.1-1.3 (except in IC 342, see Wall & Jaffe 1990, Eckart *et al.* 1990), so that molecular gas temperature differences between galaxies cannot totally account for the $^{13}R_{32}$ variation.

Outside the central 20″, $^{13}R_{32}$ is small (i.e. $^{13}R_{32} \lesssim 0.1$) in M 83 and NGC 253, requiring low molecular gas densities ($n(H_2) \lesssim 10^4\,cm^{-3}$). The $^{12}R_{32}$ values imply molecular gas kinetic

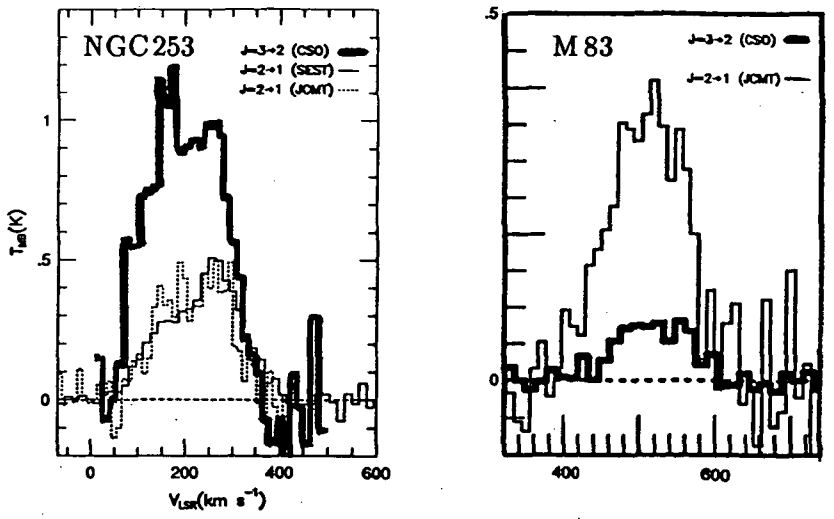

Figure 1 — The ^{13}CO J=3→2 (thick line) and ^{13}CO J=2→1 (thin and dashed lines) spectra are shown above in units of main-beam radiation temperature versus LSR velocity. Note the contrast between the NGC253 and M83 J=3→2/J=2→1 ratios.

temperatures at least as warm as that in our Galaxy (i.e. $T_K \simeq$ 5-20 K, Sanders *et al.* 1985).

The $C^{18}O$ J = 1 → 0 and ^{13}CO J = 1 → 0 data imply appreciable optical depth in the ^{13}CO J = 1 → 0 line (i.e. $\tau \simeq$ 1-5, assuming Galactic abundances, see Wannier 1989) over the central 60″ (720 pc) of NGC253. Similarly high optical depths have been inferred for ^{13}CO J = 1 → 0 in IC 342 (Wall & Jaffe 1990). It is possible that optically thick ^{13}CO J = 1 → 0 is common, even over 10^2-10^3 pc scales.

The total luminosity of CO over its entire rotational ladder from the central 60″ (∼ 0.5-1.6 kpc) of these galaxies is estimated from the ^{12}CO J = 3 → 2 line strength and radiative transfer models. The total CO luminosity is $\sim 10^5$-10^6 $L_\odot$, which is within an order of magnitude of that of the important [C II] 158 μm cooling line (Crawford *et al.* 1985, Wolfire *et al.* 1989, Stacey *et al.* 1991).

References

Crawford, M. K., Genzel, R., Townes, C. H., and Watson, D. M. 1985, ApJ, 291, 755.

Eckart, A., Downes, D., Genzel, R., Harris, A. I., Jaffe, D. T., and Wild, W. 1990, ApJ, 348, 434.

Sanders, D. B., Scoville, N. Z., and Solomon, P. M. 1985, ApJ, 289, 373.

Stacey, G. J., Geis, N., Genzel, R., Lugten, J. B., Poglitsch, A., Sternberg, A., and Townes, C. H. 1991, ApJ, 373, 423.

Wall, W. F. and Jaffe, D. T. 1990, ApJL, 361, L45.

Wannier, P. G. 1989, *IAU Symp.* **136**, *The Center of the Galaxy*, ed. M. Morris (Dordrecht: Kluwer Academic), p.107.

Wolfire, M. G., Hollenbach, D., Tielens, A. G. G. M. 1989, ApJ, 344, 770.

THE DEPENDENCE ON MORPHOLOGY OF THE GAS CONTENT IN GALACTIC DISKS

D. E. Hogg and M. S. Roberts
National Radio Astronomy Observatory[1]

Introduction

The classification S0 was introduced by Hubble to serve as a description of galaxies whose morphological characteristics seemed to lie between the disk-dominated spirals and the spheroidal elliptical systems. Since then there has been extensive discussion as to whether this classification sequence is also an evolutionary sequence. Many studies have focussed on a particular feature such as the luminosity profile, the bulge-to-disk ratio, or the nature of the interstellar matter, but the question of the evolution remains contentious.

Equally contentious is the question of the classification itself. For systems with well-developed disks there usually is no problem. Many spheroidal systems also are unambiguously classified as ellipticals in most catalogs. However, there are a number of early systems which have been reclassified following review using improved optical material. For example, Eder *et al.* (AJ, 102, 572, 1991) found that many of the S0 galaxies which are rich in neutral hydrogen have faint spiral features. The confusion about classification propagates into the discussion of the properties of early-type systems. Attempts to put the classification system on a quantitative basis have in general been unsuccessful.

Recently Sandage (private communication) has reviewed the classification of early systems and has defined a set of sub-classes for these objects. The S0 galaxies are divided into three groups, depending on the prominence of the disk. There are six subdivisions of Sa galaxies, depending upon the relative prominence of knots and other arm-like characteristics. We have explored the total gas content in these objects to see if there is a dependence on the galaxy morphology, as denoted by these new subclasses.

The Gas Content of Early Galaxies

We will use the estimates of mass that have been tabulated in the survey of Roberts *et al.* (ApJS, 75, 751, 1991). The hydrogen mass is derived from the observed flux in the usual way. The estimate of the mass of molecular hydrogen is obtained from the CO flux assuming the conversion factor obtaining in Galactic clouds. The dust mass is derived from IRAS fluxes at 60 and 100 micron wavelengths, but is sensitively dependent upon the value of the dust temperature which is assumed.

---

[1]Operated by Associated Universities, Inc., under Cooperative Agreement with the National Science Foundation.

Figure 1 shows the mean value of each of the quantities, and an estimate of the uncertainty, as a function of galaxy type. The values have been obtained from both detections and upper limits by the use of survival analysis techniques. In general the later galaxies have significantly greater mass of cold gas than do the earlier types. The masses of atomic and molecular hydrogen are comparable, although it must be emphasized that the CO data are severely limited. The dust mass is lower than the gas mass, by a factor of between 500 and 1000, as is expected from earlier work (cf. Thronson *et al.* ApJ, 344, 747, 1989).

The masses of the individual components have been combined to provide an estimate of the total amount of cold gas in these galaxies. As might be anticipated from Figure 1, the amount of material increases markedly in going from the earliest Sa galaxies to the latest Sa galaxies. The mass of cold gas in S0's is much less, but there is little evidence of a trend with subclass. A striking feature of the gas content of the most pronounced S0 galaxies is the large dispersion. There are galaxies for which the upper limit to the cold gas is 10^8 $M_\odot$, while there are galaxies of the same class having at least 3×10^{10} $M_\odot$ of matter.

Various tests lead to the conclusion that there is little current star formation, at least of luminous blue stars. The average surface density is less than 0.5 $M_\odot$/sq.pc for all but the latest Sa galaxies, a value too low to support vigorous star formation (cf. Kennicutt, ApJ, 344, 685, 1989). Very few of the objects have the ratio of infrared to radio luminosity characteristic of star-forming galaxies. Finally, the infrared luminosity is low in comparison to that of later spiral galaxies.

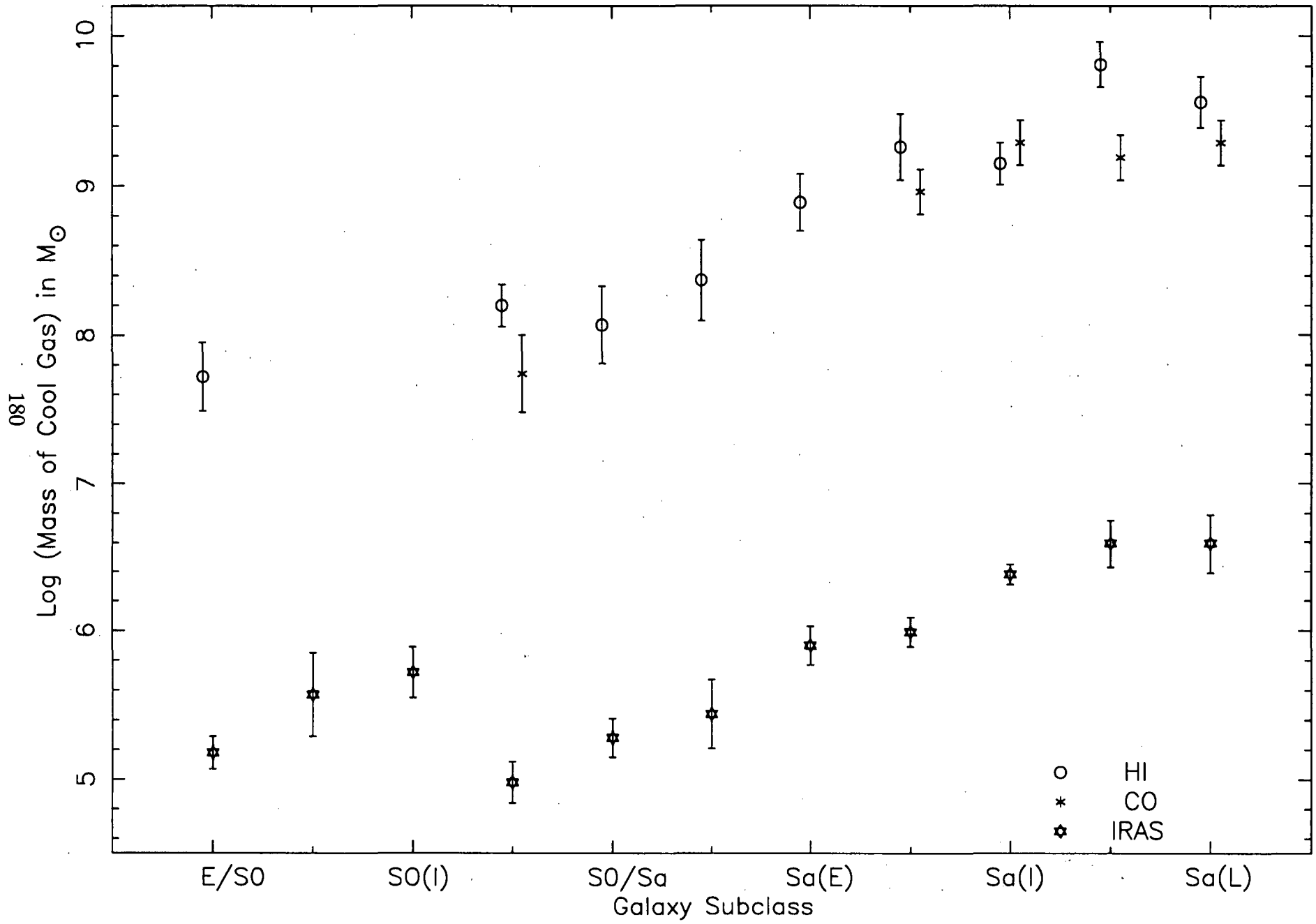
Log (Mass of Cool Gas) in $M_{\odot}$
10
9
8
7
6
5
HI
CO
IRAS
E/S0
S0(I)
S0/Sa
Sa(E)
Sa(I)
Sa(L)
Galaxy Subclass

HI Observations of Dwarf Galaxies Out to a Distance of 50 Mpc

Caroline Simpson and S. T. Gottesman

Department of Astronomy, University of Florida, Gainesville, Florida 32611

Abstract

Here we report our preliminary findings from an HI search for dwarf galaxies in three environmentally distinct regions of the sky: a galactic void, a galactic cluster, and an interaction field. This study is sensitive at the 5σ level to hydrogen masses as low as $5x10^5$ $M_\odot$. We have made three possible detections of previously uncatalogued objects: one in the void field, and two in the cluster field. Reduction of the interaction field is in progress.

Introduction

It is argued that most dwarf systems are in a dormant state during which star formation does not occur, and have therefore gone undetected in optical surveys. In 1988, Tyson and Scalo published a paper in which they modeled star formation bursts in dwarf galaxies (1988, ApJ **329**, 618). Their luminosity function shows an increase in galaxy number as galaxy brightness decreases, and their most conservative space density was determined to be 10 dwarf galaxies/Mpc^3.

We have made VLA observations of three fields out to 50 Mpc. Using the Tyson and Scalo luminosity function and mass-radius relation, we find that there should be 8 to 10 dwarf galaxies within our detection limits for a single field. We should see 6 systems with hydrogen masses on the order of 10^6 $M_\odot$, and 2 to 4 systems with M_{HI} on the order of 10^7 $M_\odot$.

If the theory of biased galaxy formation is correct, then dwarf galaxies should also be more evenly distributed than more massive (and brighter) galaxies. We have therefore chosen to observe three environmentally distinct fields to investigate whether the space density of dwarf galaxies is location dependent.

Each field is centered on a known dwarf galaxy in a different environment. The first galaxy, UGC 10805, is located near the edge of the local void. If dwarf systems are evenly distributed, then they should also be found in the void.

The second galaxy, UGC 2014, is located near a spiral galaxy at the edge of a cluster. If the spatial density of dwarfs is inhomogeneous, there should be more than the predicted number of dwarf galaxies in this field, and there may be an enhancement at distances comparable to that of the cluster.

The last galaxy, M81 dwarf B, is was chosen to determine whether there is an enhancement of dwarfs in an area near a spiral that isn't in a cluster. Arguments have been made that dwarf systems form out of material that has been stripped off of spiral galaxies. The well known interaction of the M81/M82 system may provide much material for the formation of dwarfs.

Observations

We have made 21 cm observations at the VLA using the D array, with a field of view (HPBW) of 30′. We used a 64 channel spectrometer with a 12.5 MHz bandwidth and a channel separation of 195 kHz (41 km/s). Each of the three fields was observed at 2 independent frequencies for approximately 4 hours per frequency. The central frequency for the first set of observations was 1413 MHz (corresponding to a velocity of 1500 km/s) and the central frequency for the second set was 1401 MHz (4100 km/s). Each set of data was Hanning smoothed in velocity to remove the effects of "ringing" caused by Gibbs' phenomenon.

Void Field (UGC 10805): We have completed preliminary reduction of the data from both frequencies for this field. The velocity range for the reduced data is from 380 – 5376 km/s; this is a distance range of 3.80 – 53.76 Mpc (H_0=100 km/s/Mpc.) The total volume surveyed is 3.0 Mpc^3.

Low Redshift Data: These observations have a resolution of 90″, with a measured single-channel r.m.s. of 0.43 mJy for an unresolved point source. The velocity range for the reduced data is from 380 – 2754 km/s; this is a distance range of 3.80 – 27.54 Mpc. The total volume surveyed for this field is 0.42 Mpc^3. The minimum hydrogen mass for a 5σ detection ranges from $5.3x10^5$ $M_\odot$ at a distance of 3.80 Mpc to $2.8x10^7$ $M_\odot$ at a distance of 27.54 Mpc.

We have detected only UGC 10805 in this field. It is at a distance of 15.4 Mpc, has an observed peak column density (N_{HI}) of $5.0x10^{20}$ atoms/cm^2, and a hydrogen mass (M_{HI}) of $4.5x10^8$ $M_\odot$. This result is in agreement with Weinberg *et al* (1990, preprint) as they did not find any galaxies (with $M_{HI} \geq 10^8 M_\odot$) within their void fields.

High Redshift Data: These observations have a resolution of 70″, with a single-channel r.m.s. of 0.38 mJy. The velocity range covered for this set of data is 2960.7 – 5376.0 Mpc; or a distance range of 29.61 – 53.76 Mpc. The total volume surveyed is 2.58 Mpc^3. The minimum hydrogen mass for a 5σ detection ranges from $2.9x10^7$ $M_\odot$ at 29.61 Mpc to $9.6x10^7$ $M_\odot$ at 53.76 Mpc.

There is one possible detection in this field. The object is at a distance of 49.1 Mpc, has an observed peak column density of $5.8x10^{19}$ atoms/cm^2, and a hydrogen mass of $2.9x10^8$ $M_\odot$. This is a 4.9σ detection in M_{HI}.

Cluster Field (UGC 2014): Only the low redshift data set is currently available.

Low Redshift Data: The resolution for this field is 60″, and the measured single-channel r.m.s. is 0.60 mJy. The velocity range for this data set is 256.0 – 2754.4 km/s; or 2.56 – 27.54 Mpc. The corresponding volume covered is 0.42 Mpc^3. The minimum detectable hydrogen mass therefore ranges from $3.4x10^5$ $M_\odot$ at the minimum distance of 2.56 Mpc to $3.9x10^7$ $M_\odot$ at the maximum distance of 27.54 Mpc that is available for this data set.

In addition to UGC 2014, we may have detected two uncatalogued objects. UGC 2014 is at a distance of 5.45 Mpc, has $N_{HI} = 9.0x10^{20}$ atoms/cm^2, and has $M_{HI} = 4.3x10^7$ $M_\odot$. Object 1 is at a distance of 4.21 Mpc, has $N_{HI} = 8.5x10^{19}$ atoms/cm^2, and has $M_{HI} = 1.6x10^6$ $M_\odot$. This is a 4.7σ detection in M_{HI}. Object 2 is at 2.56 Mpc, has $N_{HI} = 2.0x10^{20}$ atoms/cm^2, and $M_{HI} = 9.7x10^5$ $M_\odot$. This is a 9.2σ detection in M_{HI}, but as its peak signal is in an end channel where the data quality is poor, this should be regarded with caution.

Interaction Field (M81 Dwarf B): Analysis is in progress.

Discussion

This work indicates that the homogeneity of the spatial density of dwarf galaxies as well as the number density assumed by Tyson and Scalo may be incorrect. We have found only one possible object in the void field, and two in the incompletely analyzed cluster field. Other recent work (Weinberg *et al*, 1990; and Briggs, 1990, AJ **100**) also indicates that Tyson and Scalo's number density is incorrect: it predicts too many small galaxies. However, the preliminary results of work in progress by Tyson (1992, private communication) suggest that up to 50% of galaxies with masses $\leq 10^7$ $M_\odot$ will become depleted of gas due to winds driven by star formation bursts. This would reduce the number of gas-rich galaxies, and thus lower the number we would be able to detect in HI.

Gas-Rich Dwarf Galaxies in Dense and Sparse Environments

G. Lyle Hoffman
Dept. of Physics, Lafayette College, Easton, PA 18042-1782

I. INTRODUCTION

Dwarf irregular galaxies (generically labelled Im for the present purposes) pose an enigma to students of galaxy evolution. In nearby groups and the Virgo cluster, Im galaxies are at least as abundant as spiral galaxies, and their low surface brightnesses and high gas-to-stars ratios suggest that (at least in the stochastic self-propogating star formation scenario) there should be significant numbers of HI clouds with masses approaching 10^8 $M_\odot$ which have undergone very little or no star formation. To date, however, no clouds with so little star formation that they would not be recognized as Im galaxies on high-quality photographic plates have been identified. There have been suggestions (Dekel and Silk 1986) that such dwarfs may be tidally disrupted in regions of high galactic density, but may be prevalent in low density regions.

We offer data from three parallel programs relevant to this issue. (1) A large number of Im galaxies throughout the Local Supercluster have been mapped in the HI spectral line using the Arecibo Radiotelescope, and we can establish the frequency with which HI disks much more extended than their optically visible portions are found. (2) Our extensive mapping of spiral and dwarf galaxies in the Virgo cluster allows us to set stringent limits on the density of star-free HI clouds in that cluster. (3) We have conducted a sampling of the void in the distribution of galaxies toward the supergalactic pole, optimized for finding low-mass HI clouds at redshifts out to ~2000 km s^{-1}.

II. HI MAPPING OF DWARF GALAXIES

In several campaigns at Arecibo Observatory, we have mapped 70 dwarf galaxies with the 3.'2 Arecibo 21 cm beam. While this beam-size is too large for us to determine rotation curves accurately in many cases, it is almost optimal for detecting whether or not the galaxies (with optical radii ~1.' for the most part) have extended HI haloes. The overwhelming majority of these have HI extents no more than about twice their Holmberg radii, and we know of only four that have HI radii exceeding their Holmberg radii by a factor of 5 or more. Two of these (DDO 154 and HI 1225+01, the latter mapped by Giovanelli et al. 1991) are apparently isolated, but the other two (DDO 137 and VCC 2062) may be distended by tidal interaction with a larger galaxy at small separation. One (DDO 154) appears to be a rotating disk with the optical component at the center; the other three are more asymmetric, with an off-center peak column density and a small irregular patch of stars that sits squarely at the point of peak column density. In all cases the column density remains below a few$\times 10^{20}$ atoms cm^{-2} which is thought to be a threshold for star formation (Bothun et al. 1990 and references therein), except at the highly localized region occupied by stars.

The main point of our mapping campaigns is that such extended HI clouds are rare among dwarf galaxies. These four stand out graphically on a Tully-Fisher plot of HI profile width to HI diameter; however, on plots relating profile width to *optical* quantities these extended envelope galaxies do not appear extraordinary. It is clear that only a small fraction of dwarf irregular galaxies have a low density, extended, HI reservoir at this epoch, even if only dwarfs outside of known clusters and groups are considered. However, it is not clear whether other Im's evolved from such a cloud which was later stripped by tidal (or other) mechanisms.

III. LIMITS ON STAR-FREE HI CLOUDS IN VIRGO

In Hoffman et al. (1989) we established limits on the number of gas clouds in the Virgo cluster with HI masses comparable to those of the faintest Im galaxies, but no visible stars. Here, I will summarize those results briefly: We have acquired some 1640 ON/OFF pairs of spectra in our studies of the spiral and dwarf populations of the Virgo cluster. In the portions of those spectra outside the velocity range of the targetted galaxy, and in the accompanying reference beams, we detected no signal that could not be attributed to a known, optically visible, spiral or dwarf galaxy (or to the extended cloud around DDO 137 — Hoffman et al. 1992b). The effective surveyed volume is somewhat larger than 3% of the total volume spanned by the

Virgo cluster members in the *Virgo Cluster Catalog* (Binggeli et al. 1985), and our results limit the number of star-free clouds with HI masses $\gtrsim 3\times10^7$ $M_\odot$ to $\lesssim$100 for the entire volume.

IV. DWARF GALAXIES IN LOW-DENSITY REGIONS

To check the hypothesis that low-mass galaxies with low internal densities formed prolifically throughout the universe, but have been tidally disrupted within clusters and groups within superclusters, we sampled a region generally toward the supergalactic pole where the density of bright galaxies is quite low. Since the line-of-sight to any other void in the galaxy distribution must pass through some portion of the plane of the Local Supercluster, the supergalactic pole region should be the nearest void and therefore lends itself to the most sensitive limits on the number density of very low-mass HI clouds. Briggs (1990) has reviewed the various surveys for clouds of higher mass in a variety of environments.

Our pilot survey (Hoffman et al. 1992a) probed the environs of a small group of IRAS-detected spiral galaxies at redshift ~2500 km s^{-1} and galactic latitude $b^{II} \sim 15°$ and the redshift range in its foreground. We found two previously unknown dwarf galaxies in the group, but no signals in the foreground. Our sensitivity was such that we should have detected HI masses as low as 10^7 $M_\odot$ at the group redshift, down to ~5×10^5 $M_\odot$ at the near redshift limit (~250 km s^{-1}). Our limit translates to about 5% of closure density for HI masses as small as ~5×10^6 $M_\odot$ (assuming $H_o = 100$ km s^{-1}/Mpc) and is more stringent for larger masses ($\lesssim 10^8$ $M_\odot$). Weinberg et al. (1991) give even more stringent limits on the density for masses $\gtrsim 10^8$ $M_\odot$.

V. CONCLUSIONS

While a few dwarf galaxies ($\lesssim$ 10% or all mapped late-type dwarfs) with HI extents $\gtrsim$ 5 times the diameter of their star-forming regions have been found, we do not find the population of low-mass, optically faint, gas-rich dwarf galaxies that straight-forward applications of stochastic self-propogating star-formation models would seem to predict. This does not necessarily invalidate the scenario; refinements incorporating galactic winds and/or dependence of star formation efficiency on metal abundance may, as suggested by various authors, rapidly convert gas-rich proto-dwarfs to gas-poor dwarf ellipticals or spheroidals. The number density of gas-poor dwarfs at the present epoch is not constrained at all by our observations. One hypothesis that will be interesting to explore is whether all low-mass proto-dwarf galaxies disappeared (from our radio-telescopes at least) in the burst of "faint blue galaxies" at a redshift $z \sim 1$ (Broadhurst et al. 1988; Babul and Rees 1992), leaving only the much more massive (and relatively rare) systems like DDO 154, HI 1225+01 and the Malin-type spirals with arrested star formation in a persisting HI disk.

The research described here was conducted in collaboration with E.E. Salpeter and N.Y. Lu, and I thank them for the many insights they have contributed. C. Lamphier, T. Roos, B. Farhat, H.L. Williams, and G.T. Helou assisted with some of the observations. This work was supported in part by US National Science Foundation grants AST 84-06392, AST-8713394 and AST-9015181 at Lafayette College and by AST 84-15162 and AST-8714475 at Cornell, and in part by the National Astronomy and Ionosphere Center which is operated by Cornell University for the National Science Foundation.

References

Babul, A., and Rees, M.J. 1992, *MNRAS*, **255**, 346.
Binggeli, B., Sandage, A., and Tammann, G.A. 1985, *A.J.*, **90**, 1681.
Bothun, G.D., Schombert, J.M., Impey, C.D., and Schneider, S.E. 1990, *Ap.J.*, **360**, 427.
Briggs, F.H. 1990, *A.J.*, **100**, 999.
Broadhurst, T.J., Ellis, R.S., and Shanks, T. 1988, *MNRAS*, **235**, 827.
Dekel, A., and Silk, J. 1986, *Ap.J.*, **303**, 39.
Giovanelli, R., Williams, J.P., and Haynes, M.P. 1991, *AJ*, **101**, 1242.
Hoffman, G.L., Helou, G., Salpeter, E.E., and Lewis, B.M. 1989, *Ap.J.*, **339**, 812.
Hoffman, G.L., Lu, N.Y., and Salpeter, E.E. 1992a, submitted to *A.J.*
Hoffman, G.L., Salpeter, E.E., Lamphier, C., and Roos, T. 1992b, *Ap.J.Lett.*, **388**, L5.
Weinberg, D.H., Szomoru, A., Guhathakurta, P., and van Gorkom, J.H. 1991, *Ap.J.Lett.*, **372**, L13.

158μm [CII] Mapping of Galaxies: Probing The Atomic Medium

S.C. Madden[1], N. Geis[2], R. Genzel[1], F. Herrmann[1], J. Jackson[3], A. Poglitsch[1],
G.J. Stacey[4], and C.H. Townes[2]
[1]Max-Planck-Institut für Extraterrestrische Physik
[2]University of California, Berkeley
[3]Boston University [4]Cornell University

Previous observations of the 158 μm [CII] line toward the nuclear regions of external, gas rich spiral galaxies have shown that this far-infrared line alone contributes up to 1% of the total far-infrared luminosity, and that it arises from photodissociation regions (PDRs) formed on the surfaces of molecular clouds by the UV radiation from massive OB stars (Crawford *et al.*1985; Stacey *et al.* 1992).

Using the MPE/UCB Far-infrared Imaging Fabry-Perot Interferometer (FIFI) on the Kuiper Airborne Observatory (KAO), we have made large scale maps of [CII] in the spiral galaxies NGC 6946, NGC 891, M83 and the peculiar elliptical Cen A, thus allowing for the first time, detailed studies of the spatial distribution of the FIR line emission in external galaxies.

We find that the [CII] emission comes from a mixture of components of interstellar gas. The brightest emission is associated with the nuclear regions, a second component traces the spiral arms as seen in the nearly face on spiral galaxies NGC 6946 and M83 and the largest star forming/HII regions contained within them, and another extended component of low brightness can be detected in all of the galaxies far from the nucleus, beyond the extent of CO emission.

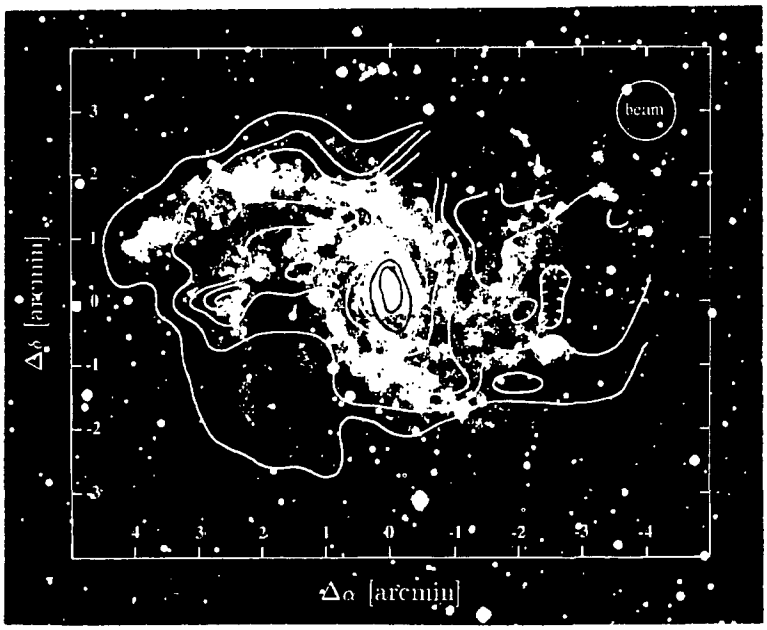

Figure 1. Integrated [CII] line intensity contours of NGC 6946 superposed on an optical image. The contour intervals are 1×10^{-5} erg $s^{-1}cm^{-2}sr^{-1}$ and the peak value is 7×10^{-5} erg $s^{-1}cm^{-2}sr^{-1}$. (Madden *et al* 1992).

C-4

The nuclear and spiral arm components are most likely associated with dense (n(H)$\geq$ $10^3 cm^{-3}$) photon-dominated regions (PDRs) at molecular cloud surfaces that are exposed to ultraviolet radiation produced by young massive stars. We interpret the extended component as originating in the diffuse atomic (HI) medium, representing the first detection of far-infrared line emission from atomic interstellar gas. The extended [CII] emission probably originates mainly in cold (T$\sim$100 K), neutral hydrogen clouds having a pressure between 6.0×10^3 and 1.0×10^4 cm^{-3} K, similar to HI clouds in our Galaxy. Low density HII regions also contribute about $\sim$25% of the extended [CII] emission. Hot (T$\sim$8000K) diffuse HI gas can only significantly contribute to the observed [CII] emission if it is clumped with a filling factor of about 10% or has a high ionization fraction (>10%).

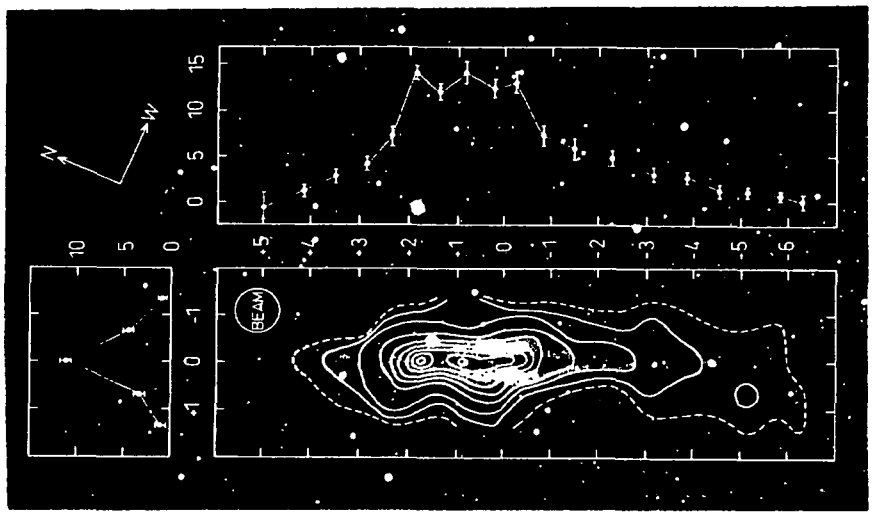

Figure 2. Integrated [CII] line intensity contours of NGC 891 shown on an optical image (lower right). The relative intensities of [CII] shown as a cuts along the plane of the galaxy (top) and along the z axis perpendicular to the plane (left) are shown. The peak [CII] line intensity is 1×10^{-4} erg $s^{-1}cm^{-2}sr^{-1}$ (Stacey *et al.* 1992).

References

Crawford, M. K., Genzel, R., Townes, C. H., and Watson, D. M. 1985, *Ap. J.*, 291, 755.

Geis, N., Genzel, R., Herrmann, F., Madden, S. C., Poglitsch, A., Stacey, G. J. and Townes, C. H. 1992, in preparation.

Madden, S. C., Genzel, R., Herrmann, F., Poglitsch, A., Geis, N. Stacey, G. J and Townes, C. H. 1992, submitted to *Ap. J.*

Stacey, G. J, Genzel, R., Herrmann, F., Madden, S. C., Poglitsch, A., Geis, N. and Townes, C. H. 1992, in preparation.

Far-Infrared Line Images of Dwarf Galaxies

A. Poglitsch[1], N. Geis[2], R. Genzel[1], F. Herrmann[1], S.C. Madden[1],
G.J. Stacey[3], and C.H. Townes[2]
[1]Max-Planck-Institut für Extraterrestrische Physik
[2]University of California at Berkeley [3]Cornell University

Irregular dwarf galaxies are about ten times more widespread in the universe than regular spiral galaxies. They are characterized by a relatively low metallicity, i.e. lower abundance of the heavier elements (metals) with respect to hydrogen than in the solar neighborhood. These heavier elements in the form of molecules, atoms, or ions, which have radiative transitions in the infrared, play a decisive role in the energy balance of the ISM and thereby for the formation of stars. Dwarf galaxies are thus model cases for the physical conditions in the early phase of the universe.

Large Magellanic Cloud: 30 Doradus. The two nearest dwarf galaxies are the Magellanic clouds at a distance $\sim$ 50 kpc. The LMC contains 30 Dor, a region with young, extremely massive stars which strongly interact with the surrounding ISM on account of their stellar winds and intense UV radiation. 30 Dor is the brightest object in the LMC at almost all wavelengths.

During two flight series on the Kuiper Airborne Observatory in March 1991 and March 1992 we mapped a 7'×6' area in the 158 μm [CII] line and in the 145 μm [OI] line. The [CII] line emission is shown in Fig. 1 , overlaid with the CO ($1 \rightarrow 0$) contour lines (Johannson *et al.* 1992). We find excellent spatial correlation between the two maps. [CII] radiation arises from photodissociation regions (PDRs), i.e. from the interface regions between fully ionized and molecular gas (Tielens and Hollenbach 1985). The [CII] line is bright (peak intensity 10^{-3} erg $s^{-1}cm^{-2}sr^{-1}$ (Poglitsch *et al.* 1992), and the [CII]/CO line intensity ratio is about ten times greater than in Galactic star formation regions (Stacey *et al* 1991). On the other hand, we find a [OI] to [CII] ratio $\sim$ 1/20 which suggests temperatures and densities comparable to that in Galactic PDRs. The enhanced [CII]/CO ratio can be understood by the effect of the low abundance of heavy elements: A low dust to gas ratio and reduced CO self-shielding lead to an increased penetration depth of UV photons into the molecular gas. A much greater fraction of the CO is dissociated which leads to a decreased filling factor of the CO line emitting regions. The C^+ column density will not be affected much since the lower carbon abundance is compensated by the greater depth of the photodissociated layer (Maloney and Black 1988). Therefore, in an ensemble of low metallicity clouds, one would expect an enhanced [CII] to CO ($1 \rightarrow 0$) line intensity ratio. We estimate that in the 30 Dor region more than half of the interstellar gas must be contained in PDRs compared to about 10% in molecular clouds in our Galaxy.

IC 10 is also a relatively nearby (1.3 Mpc) dwarf galaxy. Its metallicity of about 1/6 the solar value is even smaller than that of the LMC. As common with dwarf galaxies, this galaxy lacks a nucleus as generally thought of in spiral galaxies, but active star formation is concentrated in the central parts of the system. With our imaging far-infrared spectrometer FIFI we have mapped a $9' \times 5'$ area around the center of IC 10 in the [CII] fine structure line (Madden *et al* 1992). We find a [CII] peak intensity 8×10^{-5} erg $s^{-1}cm^{-2}sr^{-1}$ at the site of maximum HI (Shostak and Skillman 1989), CO (Becker 1990), and radio continuum emission. The [CII]/CO line intensity ratio ($\sim$ 15000) is not as extreme as in 30 Dor, but still 2.5 times greater than in Galactic star formation regions. Again we can conclude that a large fraction of the ISM (at least 1/4) is contained in photodissociation regions. Toward the local HI maximum west of the center where no CO emission has been detected we find [CII] emission. The line intensity is much greater than expected from standard atomic clouds. It is likely that a substantial fraction of the observed [CII] emission arises from molecular hydrogen gas not traced by CO emission. The low metallicity medium in IC 10 may allow molecular hydrogen clouds of substantial column density to exist which have no detectable CO.

HE2-10 is a more distant (5 to 10 Mpc) dwarf galaxy we have recently observed in [CII] and CO ($1 \rightarrow 0$). It is a blue compact dwarf (BCD) galaxy undergoing a recent burst of starformation, possibly triggered by the collision of 2 merging dwarf galaxies. Its high gas content and metallicity value 1/2 that of solar, higher than that of IC10 and 30 Dor, make it an interesting subject to add to the study of the effects of metallicity on star formation traced through [CII], CO and FIR. The [CII] intensity is estimated to be $7 \pm 2 \times 10^{-4}$ erg s^{-1} cm^{-2} sr^{-1} assuming a central 13" source. The ratio of I[CII] to I(CO) is $\sim 5 \times 10^3$, on the order of that seen in Galactic star formation regions, and a factor of 3 less than that in the lower metallicity dwarf IC10.

We conclude, at this stage in our study of low metallicity objects, that photodissociation regions consitute a larger fraction of the mass of these galaxies, as seen in the enhanced [CII] to CO ratio in the nearby galaxies IC10 and 30 Dor, compared to ratios observed in star formation regions in our Galaxy. In extreme cases with complete photodissociation of CO as possibly found in IC10 one could severely underestimate the amount of molecular gas when using CO as a tracer. The [CII] to CO ratio observed in more distant sources, such as HE2-10, is additionally affected by beam dillution. The PDR emission in the beam is then not dominated by the more prominent Orion-like sources (O-stars). Instead, we are likely seeing the affect of beam-averaging of the more common PDRs associated with B stars in the beam toward more distant sources, thereby reducing the effect of enhanced [CII] to CO ratio due to low metallicity.

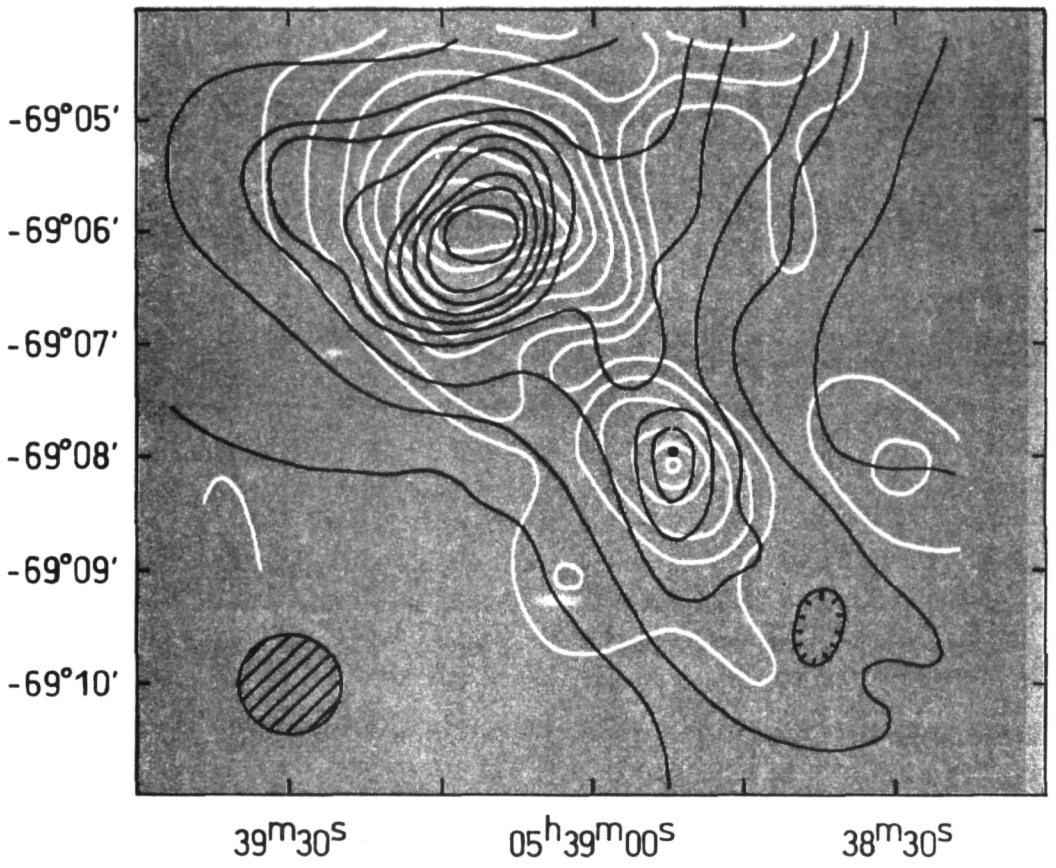

Fig 1.[CII] 158 μm emission (black) and CO (J=1-0) (white) in 30 Doradus.

References

Becker, R., 1990 Ph. D. Thesis, Bonn.

Madden S. C., Geis, N., Genzel, R., Herrmann, F., Poglitsch, A., Stacey, G. J., and Townes, C. H. 1992, submitted to *Ap. J.*

Maloney, P. and Black, J. 1899, *Ap. J.* 325, 389.

Shostak, G. S. and Skillman, E. D. 1989, *A & A* 214, 33.

Stacey, G. J., Geis, N., Genzel, R., Lugten, J. B., Poglitsch, A., Sternberg, A., and Townes, C. H. 1991, *Ap. J.* 373, 423.

Tielens, A.G.G.M. and Hollenbach, D. 1985, *Ap. J.* 291, 722.

The Fate of Captured Gas: NGC 3077 & Star Formation in the M81 System

Harley A. Thronson, Jr.
Wyoming Infrared Observatory
and
John Carlstrom
Owens Valley Radio Observatory

NGC 3077 is the third largest system in the M81 swarm of galaxies, after the giant spiral M81 itself and the dwarf oddity M82. As with most of the other dwarf companions in this system, NGC 3077 appears to have gravitationally stolen a significant amount of gas from the spiral — roughly 10^9 $M_\odot$ in this case — and is in the process of turning it into stars in its core. Thronson, Wilton, & Ksir (1991; MNRAS, 252, 543) note that the total gas mass in M82 and NGC 3077 is about the same, although the former is undergoing substantially greater star formation than is the latter. These authors suggest that while the efficiency of creating stars out of molecular material is similar in both objects, it is the preceding step — the creation of molecules out of the purloined atomic gas — which is less efficient in NGC 3077. Thronson, Wilton, & Ksir go on to argue that the higher kinematic "temperature" of this object relative to that of M82 played a major role in the low efficiency of atomic-to-molecular conversion.

We are interested in exploring the fate of molecular material in NGC 3077 further. For that reason we have mapped the distribution of $J = 1 \rightarrow 0$ CO emission in the central $\sim$ 1 arcmin (1 kpc) diameter region of the galaxy using the Owens Valley millimeter-array with an angular resolution of $6.''7 \times 5.''7$ (110 pc $\times$ 90 pc). The results are shown on the following page as a series of velocity channel maps with $\Delta v = 13$ km s^{-1}.

We find the gas concentrated to the central core of the galaxy, perhaps appropriate given the strong central gravitational potential well in dwarf elliptical systems (see also Becker, Schilke, & Henkel 1989; A&A, 211, L19). The conventional view is that star formation occurs most strongly in this region due either to an enhancement of cloud collisions or else an overpressure in the gas, which compresses H_2 clouds.

Our sensitivity and angular resolution have resolved three fairly distinct molecular complexes: two with v $\approx$ 0 km s^{-1} near the nucleus, with a third about 30″ to the west with v $\approx$ -20 km s^{-1}. Using standard techniques for estimating total H_2 masses, we estimate that the pair of central clouds have $M(H_2) \sim 10^7$ $M_\odot$, while the western cloud has $M(H_2) \sim 10^6$ $M_\odot$. The total molecular mass in this region of the galaxy is about 2×10^7 $M_\odot$, far less than the estimated HI mass over about the same region.

Comparing the distribution of CO with that of Hα (not shown) suggests that star formation is breaking out of the central condensation of molecular materials: molecular material forms a sort of basket partially surrounding the ionized gas. The appearance is reminiscent of the popular "blister" model for individual HII regions, although on a vastly larger scale in the galaxy. Of course, with a spatial resolution of only about 100 pc, it is almost certain that the actual structure of the H_2/HII clouds are far more complex than this simple description.

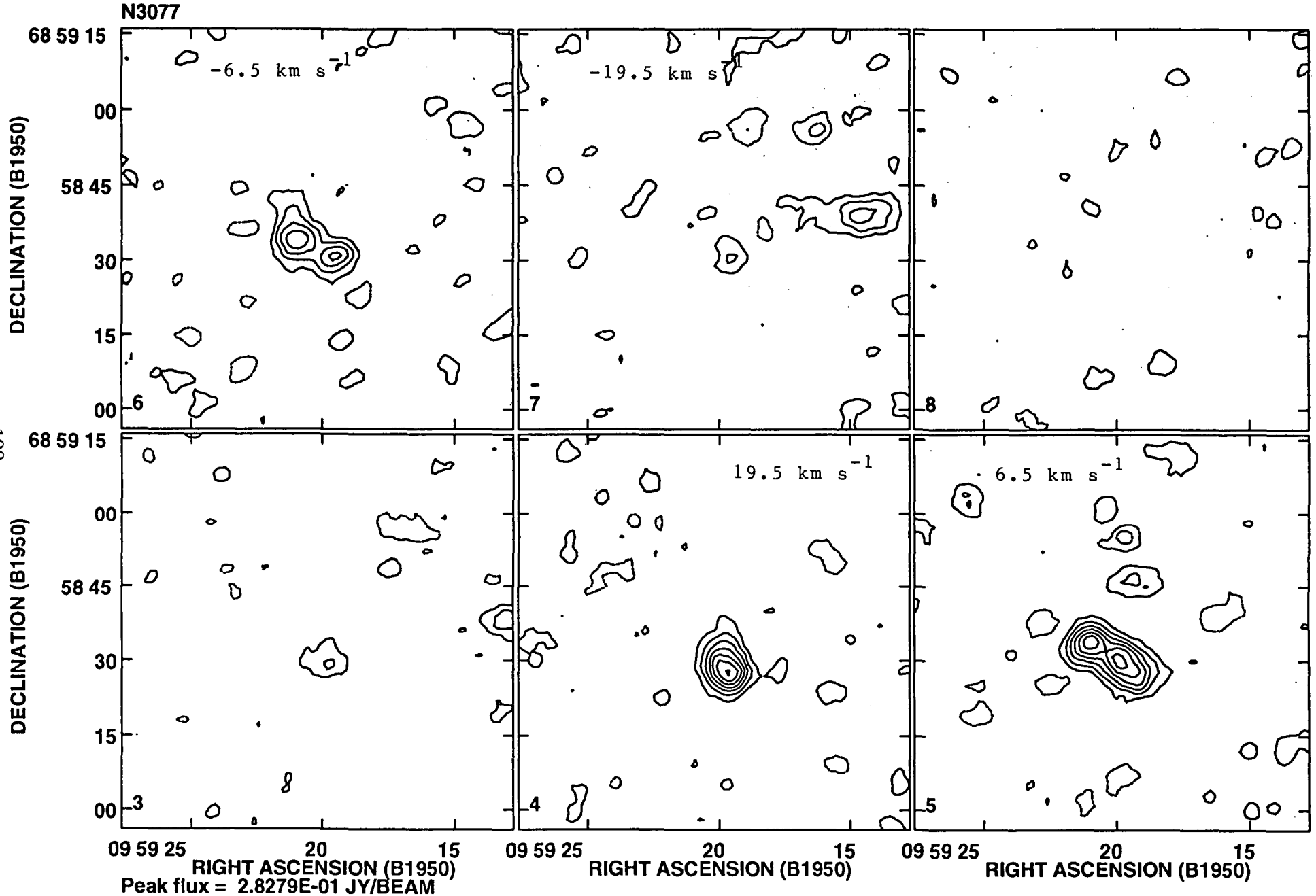
N3077
-6.5 km s-1
-19.5 km s-1
19.5 km s-1
6.5 km s-1
6
7
8
3
4
5
68 59 15
00
58 45
30
15
00
DECLINATION (B1950)
09 59 25
20
15
RIGHT ASCENSION (B1950)
Peak flux = 2.8279E-01 JY/BEAM

Dust and Ionized Gas in Elliptical Galaxies: Signatures of merging Collisions?

Paul Goudfrooij and Teije de Jong

Astronomical Institute "Anton Pannekoek", University of Amsterdam

Traditionally elliptical galaxies were thought to be essentially devoid of interstellar matter. However, recent advances in instrumental sensitivity have caused a renaissance of interest in dust and gas in – or associated with – elliptical galaxies. In particular, the technique of co-adding IRAS survey scans has led to the detection of more than half of all ellipticals with $B_T^0 < 11$ mag. in the Revised Shapley-Ames catalog, indicating the presence of $10^7 - 10^8$ $M_\odot$ of cold interstellar matter (Jura *et al.* 1987). In addition, CCD multi-colour surface photometry shows dust patches in about 30% of the cases studied to date (*e.g.*, Véron-Cetty & Véron 1988). Thorough study of the gas and dust in ellipticals is important to **(1)** determine its origin (mass-loss from late-type stars, merging collisions with other galaxies or accretion inflows from cooling X-ray gas), and **(2)** investigate the 3-D shape of ellipticals, as can be derived from the orientation of the dust lanes and the 2-D velocity field of the gas.

A major difficulty in studies of ISM in ellipticals has been the lack of a reliable, unbiased sample. For instance, our knowledge on X-ray emission of ellipticals is mainly-based upon serendipitous observations by the EINSTEIN satellite, and recent systematic searches for dust, CO and Hα emission have been performed mainly for galaxies with high IRAS flux densities (*e.g.*, Kim 1989, Lees *et al.* 1991, Huchtmeier & Tammann 1992). This obviously makes it difficult to give conclusive statements on the origin, global occurrence, and fate of ISM in elliptical galaxies *in general.* With this in mind, we have performed a systematic optical CCD survey of a complete, magnitude-limited sample of nearby giant elliptical galaxies. This survey comprises both multi-colour broad-band and narrow-band CCD imaging as well as long-slit spectroscopy. A more thorough description of the survey is given by Goudfrooij (1991).

An important result of our comprehensive CCD imaging program is that a relevant fraction ($\sim 40\%$) of the sample objects exhibits dust patches within *extended* Hα+[NII] line-emitting filaments. This common occurrence can be easily accounted for if the dust and gas have an external origin, *i.e.*, mergers or interactions with gas-rich galaxies. Evidence supporting this suggestion: **(a)** the ionized gas is usually dynamically decoupled from the stellar velocity field (see, *e.g.*, Sharples *et al.* 1983, Bertola & Bettoni 1988); **(b)** it is shown in a companion paper (Goudfrooij *et al.* 1992) that internal stellar mass loss alone can not account for the dust content of elliptical galaxies.

The extended line emission often has a peculiar distribution and is more sharply peaked at the nucleus than is the stellar continuum. Furthermore, these ellipticals exhibit a compact flat-spectrum radio source in their nucleus, suggesting that this nuclear activity also has an external origin. In this respect it would be interesting to know the excitation mechanism of the gas.

Studies of the excitation mechanism of gas in ellipticals are difficult due to the fact that the emission-line spectrum is superposed on a strong-lined stellar continuum, making the detection of *e.g.*, weak Balmer line emission a hard task. However, elliptical galaxies as a class have a very similar stellar population (see, *e.g.*, Bica 1988). A suitable template absorption spectrum has thus been built from ellipticals which do not show any evidence for ionized gas from our CCD images. Subtraction of this template effectively reveals the pure emission spectrum of the gas in ellipticals. Results of this method are examplified by the emission line spectrum of the merger candidate NGC 5044 in Fig. 1, together with the B–I and Hα+[NII] images of that galaxy. The size of the images is $1\farcm34 \times 1\farcm34$.

The nuclear spectra of *all* ellipticals with ionized gas in our sample are found to show emission-line ratios typical of the LINER class, which are well fitted by models of photoionization by a nonthermal power law spectrum with a low ionization parameter (see, *e.g.*, Ferland & Netzer 1983). This mechanism is also thought to be responsible for the nonthermal radio emission. We just might be witnessing the picture brought forward by Gunn (1979) where the central monster is being fueled by gas which has been brought in during a merger or interaction with a gas-rich galaxy.

Acknowledgements. A travel grant by Shell Nederland BV is gratefully acknowledged.

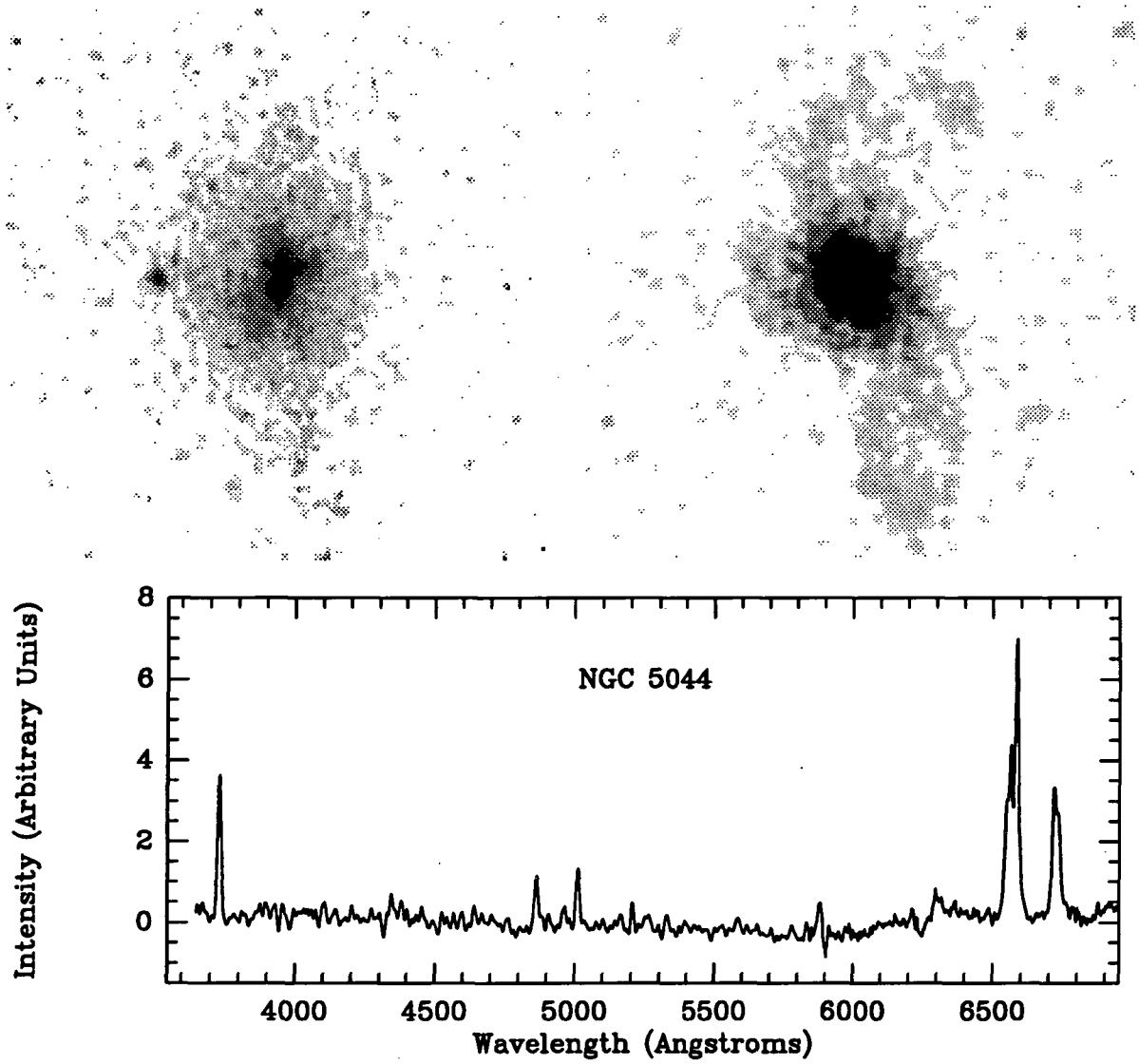

Figure 1. (Top) *The B−I colour index image (left) and the Hα+[NII] image (right) of NGC 5044. Note the spiral-like structure of the ionized gas which is associated with reddening by dust.* (Bottom) *Pure optical emission-line spectrum of the nucleus of NGC 5044, i.e., after subtraction of a suitable template absorption-line spectrum. Line ratios are typical of the LINER class.*

References

Bertola, F., Bettoni, D. 1988, ApJ, 329, 102

Bica, E. 1988, A&A, 195, 76

Ferland, G.J., Netzer, H. 1983, ApJ, 264, 105

Goudfrooij, P. 1991, The ESO Messenger, 63, 42

Goudfrooij, P., Nørgaard-Nielsen, H.-U., Hansen, L., Jørgensen, H.E., de Jong, T. 1990, A&A, 228, L9

Goudfrooij, P., de Jong, T., Nørgaard-Nielsen, H.-U., Hansen, L., Jørgensen, H.E. 1992, to be published in *ESO/EIPC Workshop on Structure, Dynamics and Chemical Evolution of Early-Type Galaxies*

Gunn, J.E. 1979, in *Active Galactic Nuclei*, eds. C. Hazard & S. Mitton, Cambridge Univ. Press, p. 213.

Huchtmeier, W.K., Tammann, G.A. 1992, A&A, 257, 455

Jura, M., Kim, D.W., Knapp, G.R., Guthathakurta, P. 1987, ApJ, 312, L11

Kim, D.-W. 1989, ApJ, 346, 653

Lees, J.F., Knapp, G.R., Rupen, M.P., Phillips, T.G. 1991, ApJ, 379, 177

Sharples, R.M., Carter, D., Hawarden, T.G., Longmore, A.J. 1983, MNRAS, 202, 37

Véron-Cetty, M.P., Véron, P. 1988, A&A, 204, 28

The multicomponent structure of bulges

Ralf-Jürgen Dettmar,[$] Thomas Krenz,[†] and Andreas Barteldrees
Radioastronomisches Institut der Universität Bonn, Bonn, FRG

Introduction

The morphology of disk galaxies is usually described by two major components, the centrally concentrated spheroidal component, called the bulge, and an oblate disk. The ratio of there contribution to the total luminosity – the bulge-to-disk ratio – is one of the parameters characterizing the Hubble sequence. Following de Vaucouleurs (1948), for most galaxies the radial distribution of the outer spheroid is fairly well described by the $r^{1/4}$ law: $I(r)=I_0 \cdot \exp(-\alpha r^{1/4})$, whereas the radial luminosity distribution of the disk follows an exponential law: $I(r)=I_0 \exp(-\alpha r)$ (Freeman 1970), with r the radial distance from the center. I_0 and α are characteristic constants for each individual galaxy.

Parameters for the structural properties of these components give important constraints for models of the formation and evolution of galaxies. Therefore we have tried to decompose disk and bulge components from high S/N CCD observations of a sample of edge-on disk galaxies.

A common procedure for the decomposition is to model one component in a region where it dominates and subtract it from the combined light distribution. This technique was successfully carried out e.g. by van der Kruit&Searl (1981, 1982) and Wakamatsu&Hamabe (1984, 1989).

Here we present two more examples of bulge-dominated edge-on S0 galaxies, namely ESO 506-G33 and NGC 7123, which show an additional small and concentrated central component besides disk and "bulge" .

Observations and reduction

We have investigated a sample of 10 bulge-dominated early-type disk galaxies (S0-Sa). The objects were selected by inspecting the ESO/SRC sky survey plates to insure that the inclination $i \approx 90°$. This "edge-on" geometry guarantees that the projected intensities of the components have the smallest overlap. The surface photometry observations were carried out with the 2.2m telescope at ESO/La Silla using a RCA CCD.

Preliminary results in the decomposition process indicated that in two cases, ESO 506-G33 and NGC 7123, there is a more complex structure. Plotting log(I) vs. $r^{1/4}$ for the minor axes of these galaxies clearly revealed a two component structure, resembling the minor axis profile of NGC 4565.

Results

While the outer spheroid of these two galaxies is successfully modelled with a de Vaucouleurs $r^{1/4}$ law, the remaining disks after subtracting the best-fit bulge models still show additional concentrated bulge-like central structures. With the bulge-to-disk of the residuum images, these galaxies could be classified as Sb/Sbc. The inner nuclear structure in NGC 7123 even resembles a box- or peanut-shaped bulge. The presence of these inner bulges is not very critically depend on the parameters chosen for the outer spheroids. This suggests that the additional structures are real and not just artifacts. However, our observations can not distinguish whether the remaining bulges are independent additional components or parts of more complex spheroids.

[$] present address: Space Telescope Science Institute, 3700 San Martin Dr., Baltimore, MD 21218, USA; affiliated to the Astrophysics Division in the Space Science Department of ESA

[†] present address: MPI für extraterrestrische Physik, Karl-Schwarzschild-Str., D-8046 Garching, FRG

A possible explanation for the presence of this additional structure is based on resent theoretical work e.g. by Combes et al. (1990). They found from N-body simulations that a bar can mimic the presence of a bulge. Depending on the projection direction of this "bulge" could be box-, or peanut-shaped, or round.

Conclusions

Our results corroborates the suggested relation between box- and peanut-shaped bulges and bars. This scenario has significant implications for any theory of galaxy evolution and formation: If (at least) some bulges, especially in later-type disk galaxies, developed as a resonance phenomenon or instability caused by a bar, they are an evolutionary structure rather than a relict of the galaxy formation process.

Acknowledgments. We wish to thank the Max-Planck-Institut für Astronomie in Heidelberg for the generous allocation of observing time. RJD gratefully acknowledges financial support by the Deutsche Forschungsgemeinschaft.

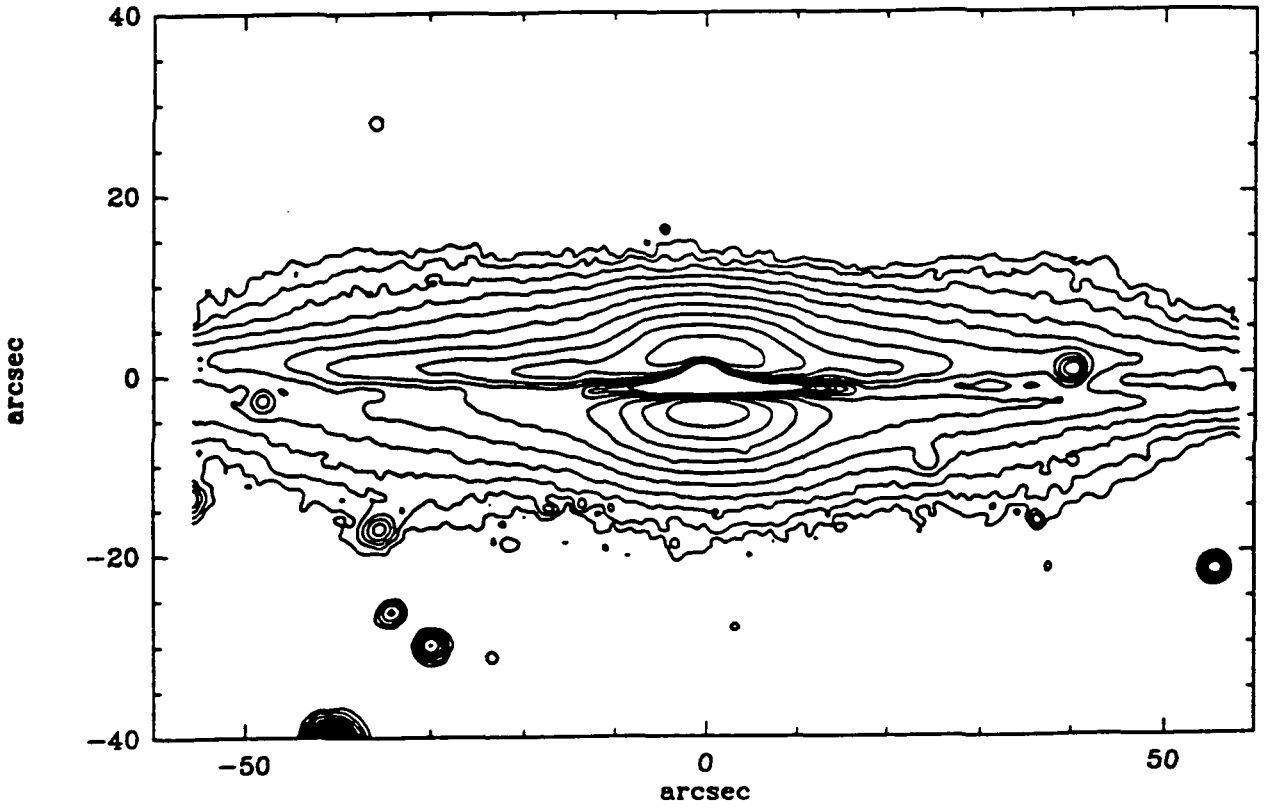

Figure 1: Resulting intensity distribution for NGC 7123 after subtraction of the dominant outer spheroid.

REFERENCES

Combes, F., Debbasch, F., Friedli, D., Pfenniger, D. 1990, *Astron. Astrophys.*, **232**, 87.

de Vaucouleurs, G. 1948, *J. de Obs.*, **31**, 113.

Freeman, K. 1970, *Astrophys. J.*, **160**, 811.

Hamabe, M., Wakamatsu, K. 1989, *Astrophys. J.*, **339**, 783.

Kruit, P. C. van der, Searle, L. 1981, *Astron. Astrophys.*, **95**, 105.

————————1982, *Astron. Astrophys.*, **110**, 61.

Wakamatsu, K., Hamabe, M. 1984, *Astrophys. J.*, **56**, 283.

VELOCITY RESOLVED SPECTROSCOPY OF MOLECULAR HYDROGEN EMISSION IN NGC6240

G.S. Wright, T.R. Geballe
Joint Astronomy Centre, 665 Komohana Street, Hilo, HI96720.

and

J. R. Graham
649 Campbell Hall, University of California, Berkeley, CA94720.

NGC6240 is a member of the class of luminous galaxies which emit a significant fraction of their total light in the infrared. Based on its highly disturbed morphology, Fosbury and Wall (1979) suggested that the system may be a merger of two gas rich galaxies. It has two nuclei separated by 2 arcsec which are visible in the near infrared and at radio wavelengths (Fried and Schultz 1983, Condon *et al.* 1982) and CO observations show that the galaxy contains a large mass (3×10^{10} $M_{\odot}$) of molecular gas (Young *et al.* 1984). Unusually strong H_2 emission lines dominate the near infrared spectrum of this galaxy (Joseph *et al.* 1984, Depoy *et al.* 1986). The galaxy emits $\sim 4 \times 10^7$ $L_{\odot}$ in the 2.12μm v=1-0 S(1) line alone, an order of magnitude more than other merging or starburst galaxies.

While it is clear that the H_2 emission must be related to the other copious activity displayed by NGC6240, the source of the excitation is poorly understood. The weakness of the hydrogen recombination lines indicates that there is insufficient UV to excite the H_2 fluorescently, irrespective of whether a model based on star formation or Seyfert type activity is used. The H_2 line ratios are consistent with most of the H_2 being collisionallly excited (Lester *et al.* 1988). It is frequently argued that since NGC6240 is the product of a recent merger of two galaxies, the H_2 emission is excited in global shocks arising from interaction driven cloud collisions. Given the starburst nature of NGC6240 inferred from the deep CO absorption bands which indicate the presence of a massive population of red supergiants, excitation in star formation regions or supernova remnants has also been proposed. Although global shocks are energetically feasible, explain the known characteristics of the H_2 emission and are attractive on account of their simplicity, other activity could equally well account for the observed emission.

Herbst *et al.* (1990) and Elston and Maloney (1990) have imaged the H_2 emission and shown that it is spatially extended on a scales > 1 kpc and does not follow the distribution of the continuum emission around the nucleus. The H_2 line is resolved with a FWHM $\sim 500 km/s$, which is consistent with the global shock model, but it is harder to explain in terms of the starburst model (the velocity dispersion in the quiescent CO lines is $\sim 300 km/s$).

To provide a better understanding of the physical processes responsible for the H_2 emission from NGC6240 we have begun a programme to obtain high spectral resolution observations using the echelle in CGS4 (Mountain *et al.* 1990) on the UKIRT. Preliminary data which were obtained in February 1991 are presented here. It is intended to obtain further observations with twice the spatial and spectral resolution in June of this year.

The spectrum presented in Figure 1 was obtained in a 3 arsec slit along the two nuclei with a resolution of 36 km/s. This spectrum confirms a $\sim 600 km/s$ FWHM but shows broad asymmetrical line wings extending up to at least 1200 km/s. The shock excited optical emission lines from the central 3-5 kpc which are believed to be generated by a superwind from the starburst have FWHM $\sim 1200 km/s$. This result may therefore be evidence linking the H_2 emission with the superwind. We speculate that the high velocity H_2 emission may be from molecular gas swept up and shocked by the superwind. In this case all the observational properties of NGC6240 could be explained in terms of a massive burst of star formation. It is difficult to produce these high velocities with global shocks from the merger of two galaxies. However a line width $\sim 1500 km/s$ is typical of that seen from Seyfert type active nuclei. Further observations to delineate the spatial extent of the broad line emission are planned. Such data should enable us to determine whether the emission is instead associated with obscured Seyfert activity in one of the nuclei.

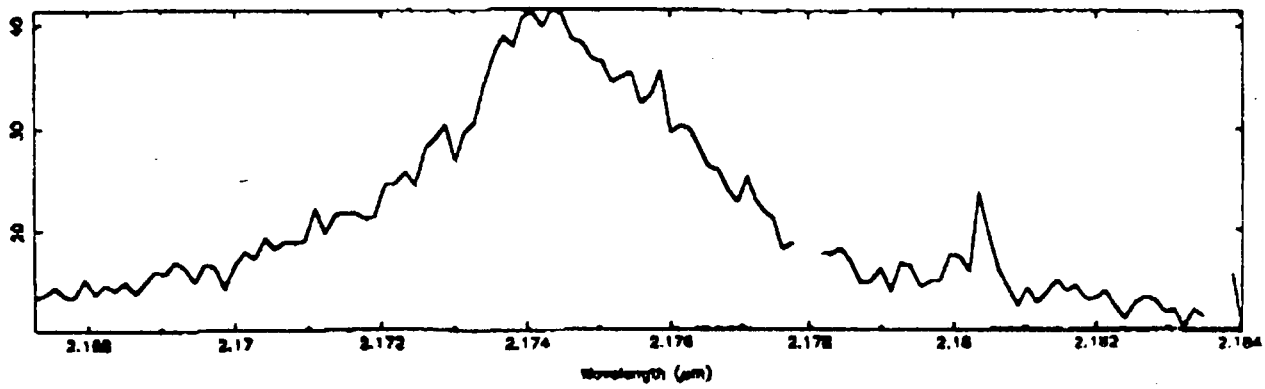

Figure 1. Infrared echelle spectrogram of H_2 1-0S(1) in NGC6240 at a resolution of 35 km/s

References

Condon, J. J., Condon, M. A., Gisler, G., & Puschell, J. J. 1982, *ApJ*, **252**, 102.
Depoy, D. L., Becklin, E. E., & Wynn-Williams, C. G. 1986, *ApJ*, **307**, 116.
Elston, R. & Maloney, P. 1990, *ApJ*, **357**, 91.
Fosbury, R. A. E., & Wall, J. V. 1978, *MNRAS*, **189**, 79.
Fried, J. W., & Schultz, H. 1983, *A&A*, **118**, 166.
Herbst, T. M., Graham, J. R., Beckwith, S., Tsutsui, K., Soifer, B. T., & Matthews, K. 1990, *AJ*, **99**, 1773.
Joseph, R. D., Wright, G. S., & Wade, R. 1984, *Nature*, **311**, 132.
Lester, D. F., Harvey, P. M., & Carr, J. S. 1988, *ApJ*, **329**, 641.
Mountain, C. M., Robertson, D. J., Lee T. J., & Wade, R. 1990, *Instrumentation in Astronomy VII SPIE* , **1235**, p25.
Young, J. S., Kenny, J. Lord, S. D., and Schloerb, F. P. 1984, *ApJ*, **287**, L65.

Observations of IRAS F10214+4724 at the Nobeyama Millimeter Array

Sakamoto K.[1,2], Ishizuki S.[1,2], Kawabe R.[2], and Ishiguro M.[2]

1. Dept. of Astronomy, Univ. of Tokyo, Bunkyo-Ku, Tokyo 113, Japan

2. Nobeyama Radio Observatory, Minamimaki, Minamisaku, Nagano 384-13, Japan

We have made CO(3-2) aperture synthesis observations of the z=2.286 IRAS source F10214+4724.

1. Introduction

F10214+4724 is an IRAS source at z=2.286 with $L_{FIR} \sim 10^{14} L_\odot$ (ref. *3*). The CO(3-2) emission was detected at the NRAO 12-m telescope (ref. *1*), and its molecular gas mass was estimated to be (1-3) $\times 10^{11} M_\odot$ (ref. 6). This object is unique and important because it is the first high-z object from which molecular line emission is detected and it enables us to investigate molecular gas content, star forming material, at an early stage of galactic evolution (the look back time is 17% of the present age of the universe. H_0=100 h km/s/Mpc and q_0 = 0.5 are assumed).

If IRAS F10214+4724 is a primeval galaxy at the formation process, it is possible the gas has not been collapsed yet to the galactic scale. On the other hand, it is also possible IRAS F10214+4724 is a merging or interacting system like the most of ultra-luminous infrared galaxies (ref. *5*). However, since the first detection was made with a medium size single-dish telescope (beam size ≈ 60" = 240 h^{-1} kpc), the precise position, extent, and distribution of the molecular gas had not been determined. The aim of our aperture synthesis observations is therefore to determine position and distribution of molecular gas.

2. Observations

Telescope : Nobeyama Millimeter Array (mm-wave interferometer with five 10-m antennas)

Date : January 21-25 and February 19-24, 1992, Array configuration : D, Integration : 32 hours

Line : CO(3-2), Center Frequency : 105.2 GHz, Bandwidth : 320 MHz = 910km/s, 1024ch

Phase tracking center : 10h21m31.14s, +47°24'22.9" (1950) , Calibrator : 0923+392 (4.5 Jy)

Field of view : 70"=280h^{-1}kpc (HPBW), Resolution : 8.9"× 6.0"=36× 24h^{-1}kpc (HPBW), PA=132°

3. Results and Discussion

Our main results are, (1)a compact emission is detected at the position of optical object (Fig.1, here we refer it as the *nuclear compact component*), (2)the nuclear compact component has about half the line width than previously reported as the first detection (Fig.2), (3)the beam deconvolved size, which gives an estimate of an upper limit size, of the nuclear compact component is about 3"=12 h^{-1} kpc, and (4)velocity gradient of the molecular gas was not detected.

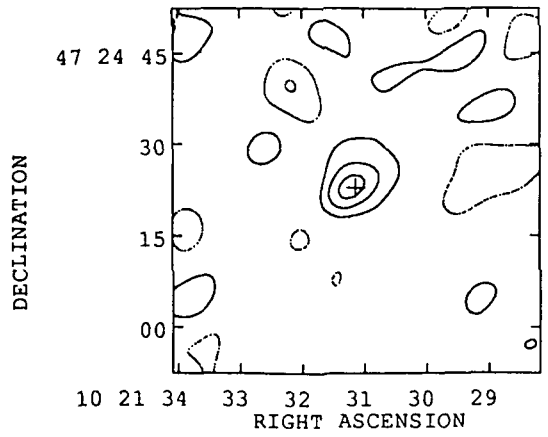

Fig.1 CO(3-2) map of IRAS F10214+4724 (ref. *4*)

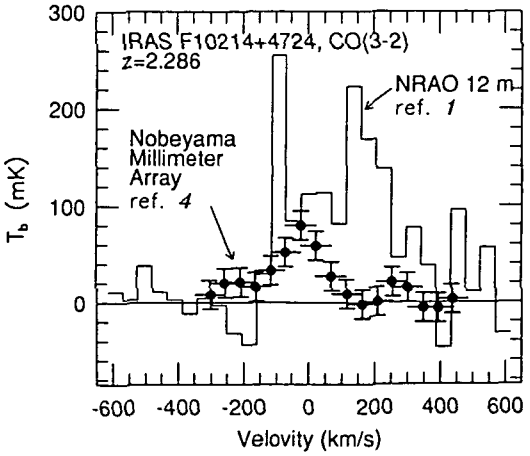

Fig.2 CO(3-2) spectrum (ref. *4*).

	our results	previous reports
position (1950)	10h21m31.2s,+47°24'23" (±1"),	10h21m31.12s,+47°24'23.9" (±0.5"), (ref.*3*)
CO(3-2) flux	7.5±1.9 Jy km/s	26 Jy km/s (ref.*1*)
line width	200 km/s	365 km/s (ref.*1*)
size	< 3"± 0.5" (CO(3-2))	4" (ref.*3*, optical)
$L_{CO(3-2)}$	$6.3 \times 10^{7}\ h^{-2}\ L_{\odot}$	
$M(H_2)$	$(2 - 11) \times 10^{11}\ h^{-2}\ M_{\odot}$ (the assumptions to derive the mass is discussed in ref. *4*)	
$\Sigma(H_2)$	$> (2 - 10) \times 10^{3}\ M_{\odot}\ /pc^{2}$	

Our observations served the following clues to the nature of IRAS F 10214+4724.

(1) A compact emission, the nuclear compact component, is associated to the optical object ('object F' in ref.*3*); thus the identification is confirmed.

(2) The nuclear compact component has already collapsed to the typical size of galaxies and its surface density of molecular gas is comparable to that of infrared luminous galaxies.

(3) From comparison of spectra obtained at the Nobeyama Millimeter Array and the NRAO 12-m telescope, it is suggested that there is some object which cannot be detected by interferometric high-resolution imaging, this suggest the extra object is extended or consists of a number of sub-components. It is necessary to confirm and determine the full linewidth with a medium size, i.e. field of view ~ 1', filled aperture telescope.

(4) If IRAS F 10214+4724 consists of a number of components, and taking account of the high concentration of molecular gas in the nuclear compact component, it is suggested that IRAS F 10214+4724 is a merging or interacting system.

(5) It is possible that intense star formation to occur because of the high concentration of molecular gas in the nuclear compact component. From the view point of infrared colors, however, an AGN is preferred as its dominant source of the huge luminosity of IRAS F 10214+4724 (see ref. *4*).

4. Future prospects

There are several bright sub-mm lines redshifted into millimeter atmospheric windows (Fig. 3).

CO(4-3), CI($^3P_1$-$^3P_0$) in 150GHz window

CO(7-6),(6-5), CI($^3P_2$-$^3P_1$) in 230GHz window

Observations of these lines and dust emission will determine physical condition of ISM in IRAS F102 14+4724. If there is a new class of objects similar to IRAS F10214+4724, or large mm-wave interferometers now in planning, such as the Large Millimeter Array (LMA) and the Millimeter Array (MMA), are constructed, it will be an interesting to prove the ISM in high-z objects with molecular and atomic lines. Such observations will affect the studies of formation and evolution of galaxies.

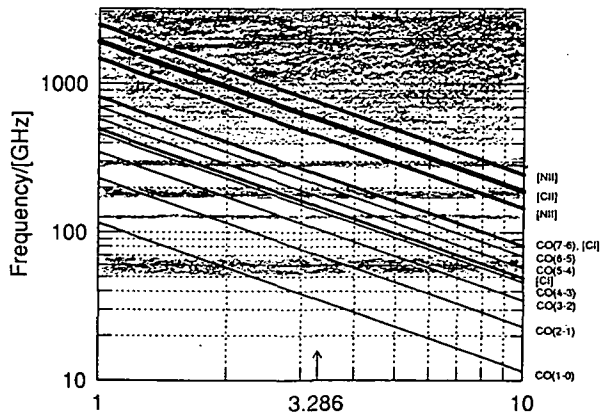

Fig. 3

5. References

1. Brown & Vanden Bout 1991, A.J., 102, 1956

2. Kawabe, Sakamoto, Ishizuki, Ishiguro 1992, Ap.J.L. in press

3. Rowan-Robinson et.al. 1991, Nature, 351, 719

4. Sakamoto, Ishizuki, Kawabe, Ishiguro 1992, Ap.J.L. in press

5. Sanders et.al. 1988, Ap.J., 325, 74

6. Solomon, Radford, Dowens 1992, Nature, 356, 318

AGES, CHEMISTRY AND TYPE IA SUPERNOVAE: CLUES TO THE FORMATION OF THE GALACTIC STELLAR HALO

Tammy A. Smecker-Hane & Rosemary F.G. Wyse
Dept. of Physics and Astronomy
Johns Hopkins University
Baltimore, MD USA 21218

ABSTRACT

We endeavor to resolve two confliciting constraints on the duration of the formation of the Galactic stellar halo – 2-3 Gyr age differences in halo stars, and the timescale inferred from the observed constant values of chemical element abundance ratios characteristic of enrichment by Type II supernovae – by investigating the timescale for the onset of Type Ia supernovae (SNIa) in the currently favored progenitor model – mergers of carbon and oxygen white dwarfs (CO WDs).

1. INTRODUCTION

Analysis of the kinematics, chemistry and spatial distributions of Galactic halo tracers have been the basis of differing estimates of the timescale of the collapse of the Galaxy (*cf.* Eggen, Lynden-Bell and Sandage 1962, Searle & Zinn 1978). More recently, two alternative methods again yield apparently conflicting answers. Recent isochrone-fitting to metal-poor globular clusters (*cf.* VandenBerg, Bolte & Stetson 1990) and field halo stars (Schuster & Nissen 1989) find 2-3 Gyr differences in their *relative* ages. In contrast, the observed constant chemical element ratios of halo stars (*e.g.*, [O/Fe] $\sim +0.5$) are in good agreement with theoretical yields of Type II supernovae (*cf.* Arnett, Schramm & Truran 1989). The onset of SNIa is identified with the decline in [O/Fe] at [Fe/H] $\simeq -1$, a metallicity higher than $\sim 80\%$ of the stellar halo and roughly in transition between halo and thick disk kinematics. Thus the abundance ratios suggest most of the halo formed before the explosion of numerous SNIa (*cf.* Wyse & Gilmore 1988, Matteucci *et al.* 1991), and the timescale for the onset of SNIa – ~ 0.1 Gyr in models of mergers of CO WD binaries – is an upper limit to the duration of the formation of the halo. Therefore, we explore the parameter space of SNIa models to determine the robustness of the derived timescale, and their ability to be consist with age differences.

2. THE SNIa MODEL

We adopt for the progenitors of SNIa the mergers of CO WD binaries with total degenerate mass $> 1.4\,M_\odot$ caused by orbital decay through the emission of gravitational wave radiation (*cf.* Iben & Tutukov 1987). Such catastrophic mergers occur in less than a Hubble time for WDs separated by $\lesssim 3\,R_\odot$. The initial separation, A, of the main sequence stars (M_1, M_2) is reduced during common-envelope (CE) phases of their evolution when a star overflows its Roche Lobe and its companion cannot accrete the material. The CE exerts tidal friction on the stars causing orbital energy and angular momentum to be transferred to the CE, expelling it and reducing the separation of the stars. The orbital energy lost by the binary is assumed to scale with the gravitational potential energy lost via α such that the reduced separation of the stars is proportional to αA. The value of α is poorly constrained *a priori*, and has usually been assumed to be unity which results in the timescale for the onset of the first SNIa, $\tau_{onset} = \tau_{\rm evoln,2} + \tau_{\rm gwr} \sim 0.1$ Gyr, where $\tau_{\rm evoln,2}$ is the timescale on which M_2 overflows its Roche Lobe, and $\tau_{\rm gwr}$ is the time for gravitational wave radiation to cause the WDs to merge. However, α has a strong, non-linear effect on $\tau_{\rm onset}$ as for two CE events characterized by α_1 and α_2,

$$\tau_{\rm gwr} = 0.15\ \alpha_1^4\alpha_2^4\left(\frac{M_{CO1}}{M_1}\right)^8\left(\frac{M_{CO2}}{M_2}\right)^4\left(\frac{A^4}{M_{CO1}M_{CO2}(M_{CO1}+M_{CO2})}\right)\rm Gyr$$

where M_{CO} are the masses of the CO WDs. Hydrodynamical calculations and analytic analysis (*cf.* Livio & Soker 1988, Taam & Bodenheimer 1991) suggest spin-up of the envelope and preferential mass loss in the orbital plane causes α to be a funtion of the evolutionary state of the Roche Lobe-filling star; $\alpha < 1$ for red giants leading to a rapid merger of two stars in the CE stage rather than SNIa, and $\alpha > 1$ for asymptotic-giant branch (AGB) stars leading to CO WD binaries and possible SNIa.

3. RESULTS ON TIMESCALE FOR ONSET OF SNIa

Below we present results assuming that a requirement for SNIa is the primary experiencing Roche Lobe (RLO) overflow on the AGB. We assume the mass of the resulting CO WD equals the CO core mass of the star at the time of RLO. For simplicity we assume $\alpha_1 = \alpha_2 \equiv \alpha$. We vary α and search all possible (M_1, M_2, A) to ascertain the predicted range of $\tau_{\rm onset}$. The size of the star and hence the evolutionary state of the primary when it experiences RLO depends sensitively on the initial metallicity of the star. Therefore, we adopt stellar models calculated for a range of initial metallicities with *solar* element ratios. Note the mean abundance of the stellar halo is [Fe/H] ~ -1.5 corresponding to Z = 6×10^{-6} for solar element ratios. Table 1 lists the adopted values of α, the initial chemical composition of the stellar models (Y and Z), the component masses of the binaries which are the first to explode, $\tau_{\rm onset}$, and the source of the stellar models (TC86 = Tornambé & Chieffi 1986, CCS90 = Castellani, Chieffi & Stranerio 1990).

Table 1. Timescales for the onset of SNIa

α	Y	Z	$M_1(M_\odot)$	$M_2(M_\odot)$	$\tau_{\rm onset}$ (Gyr)	Source for Stellar Models
0.5	0.20	10^{-6}	6	6	0.062	TC86
0.5	0.23	0.002	7	7	0.11	CCS90
0.5	0.27	0.02	9	4	0.24	CCS90
1	0.20	10^{-6}	6	6	0.063	TC86
1	0.23	0.002	9	9	0.58	CCS90
1	0.27	0.02	7	5	7.2	CCS90
2	0.20	10^{-6}	6	6	0.066	TC86
2	0.23	0.002	9	9	7.6	CCS90
2	0.27	0.02	9	4	27	CCS90

In the transition from solar to low initial metallicity, τ_{onset} decreases to $\lesssim 0.1$ Gyr due to a decrease in $\tau_{\rm gwr}$, regardless of α. The decrease results from a decrease in the minimum separation of the stars leading to a suitable pair of CO WDs as the maximum size of the star on the RGB decreases for lower metallicity stars because of a decrease in H^- opacity and density of free electrons donated by ionized metals. Hence, for low metallicity models, the minimum size of the star as it ascends the ABG sets the limit on τ_{onset}.

4. CONCLUSION

We find that for stars with metallicities typical of the Galactic stellar halo SNIa explode on timescales < 1 Gyr, in conflict with the derived 2-3 Gyr age differences if interpreted within context of a homogeneous collapse. However, both the observed chemical element ratios and few Gyr differences in the ages of halo stars could be obtained in some hierarchical models of galaxy formation, in which galaxies, and in particular stellar halos, are produced by the merger of proto-galactic fragments. The fact that the observed break in [O/Fe] is well-defined, with little scatter, means that if fragments have their own unique star formation history, so that time and [Fe/H] are related differently in each fragment, and the internal timescale for star formation in the fragments is ~few Gyr, then the timescale conflict is resolved. We are currently examining Galactic chemical evolution in CDM dominated cosmological models to determine the effect of the power spectrum of initial mass fluctuations on the age spread and chemical evolution of the halo stars, with emphasis on the elemental abundance ratios (Carlberg, Dubinski, Smecker & Wyse, in preparation).

TAS acknowledges support from an AAUW predoctoral fellowship, and an Amelia Earhart Fellowship from Zonta International. We also acknowledge support from the NSF (grant AST-90-16226).

References

Arnett, D., Schramm, D. & Truran, J.W. 1989, ApJ, 339, L25
Castellani, V., Chieffi, A. & Stranerio, O. 1990, ApJS, 74, 463
Eggen, O. J., Lynden-Bell, D. & Sandage, A.R. 1962, ApJ, 136, 748
Iben, I. & Tutukov, A.V. 1987, ApJ, 13, 727
Livio, M. & Soker, N. 1988, AJ, 329, 764
Ryan, S. & Norris, J. 1991, AJ, 101, 1865
Schuster, W.J. & Nissen, P.E. 1989, A&A, 222, 69
Searle, L. & Zinn, R. 1978, ApJ, 225, 357
Taam, R.E. & Bodenheimer, P. 1991, ApJ, 373, 246
Tornambé. A. & Chieffi, A. 1986, MNRAS, 220, 529
Wyse, R.F.G & Gilmore, G. 1988, AJ, 95, 1404
VandenBerg, D.A., Bolte, M. & Stetson, P. 1990 AJ, 100, 445

HIGH VELOCITY CLOUDS IN NEARBY DISK GALAXIES

ERIC SCHULMAN and JOEL N. BREGMAN
Department of Astronomy, University of Michigan

MORTON S. ROBERTS and ELIAS BRINKS
National Radio Astronomy Observatory

Introduction

Clouds of neutral hydrogen in our galaxy with $|v| > 100$ km s^{-1} cover approximately 10% of the sky to a limiting column density of 1×10^{18} cm^{-2} (Wakker 1990). These high velocity clouds (HVCs) may dominate the kinetic energy of neutral hydrogen in non-circular motion, and are an important though poorly understood component of galactic gas. It has been suggested that the HVCs can be reproduced by a combination of three phenomena: a galactic fountain driven by disk supernovae which would account for most of the HVCs (Bregman 1980), material tidally torn from the Magellanic Clouds (Giovanelli 1981), and an outer arm complex which is associated with the large scale structure of the warped galactic disk (Wakker 1990). We sought to detect HVCs in external galaxies in order to test the galactic fountain model.

Single-Dish Observations

We used the Arecibo 305 m telescope to observe 14 nearly face-on disk galaxies with no obvious companions and with HI profiles that are double-horned and well-behaved. Our goal was to determine whether the observational signature of HVCs, high velocity wings, is present in external galaxies. The observations were taken in April and September of 1991 with the dual-circular feed in a total-power mode, alternating five-minute ON-source scans with five-minute OFF scans. We obtained 40 ON-OFF pairs of NGC 5668 and reached an rms noise level of about 0.6 mJy per 2.1 km s^{-1} channel; 10-20 ON-OFF pairs were obtained for most of the other target galaxies.

We find high velocity wings, extending beyond the double-horned profiles, in 11 of 14 galaxies. The high velocity HI detected in the wings is from .5 to 3% of the total detected HI. Figure 1 shows the Arecibo profile of the Sd-galaxy NGC 5668, where the high velocity wings stretch from about 1470 to 1530 km s^{-1} on the blue side and from about 1660 to 1710 km s^{-1} on the red side. These features are confirmed in our Very Large Array (VLA) observations described below.

We developed simple disk galaxy models in order to better understand how high velocity gas from a warp or from HVCs produced by a galactic fountain affects the HI profiles. Galactic fountain HVCs were modeled as a component of galactic gas with a velocity dispersion of 50 km s^{-1}. The three galaxies without high velocity wings are well fit by models with neither a warp nor HVCs. Two of the galaxies with high velocity wings, NGC 765 and NGC 3344, are fit by models with moderate ($< 10°$) warps along the major axis and no HVCs. HVC models can produce the amount of high velocity gas but not the shape of the spectra. Models with HVCs and no warp are able to reproduce the spectra of the remaining nine galaxies. Models with just a warp are unable to reproduce the HI profiles of these galaxies. High velocity clouds make up 2 to 16% of the total HI in these models. The mass of *detected* high velocity material is a factor of 4 to 13 smaller because most of this high velocity material has the same line of sight velocity as quiescent disk HI (i.e., 1550 to 1610 km s^{-1} in Figure 1). In order to detect all the high velocity gas, we need observations with a synthesis telescope such as the VLA or the Westerbork Synthesis Radio Telescope (WSRT).

Synthesis Telescope Observations

We observed NGC 5668 with the VLA in D configuration for 24 hours in April of 1991 and obtained an rms noise level of 0.34 mJy beam^{-1} channel^{-1} for naturally weighted maps (FWHM= 1', channel width= 10.4 km s^{-1}). The highest velocity gas is not confined to an outer ring, as might be expected in a warped disk, but is distributed nonuniformly across the face of the galaxy. The VLA map reveals a much richer structure of HVCs not accessible to single-dish spectra (i.e., at velocities between the HI horns). From position-velocity diagrams, distinct HI complexes are evident at velocities considerably different from that of the underlying galaxy. Some HVCs extend 150 km s^{-1} away from the systemic velocity.

NGC 5668 does have a warp but the orientation of the warp is such that the affected material has a velocity *closer* to systemic over most of the face of the galaxy. The warp begins outside of the Arecibo beam and thus the warp material is at the wrong position and at the wrong velocity to be the high velocity gas that we detected with the Arecibo telescope. In addition, many of the HVCs seen in the position-velocity diagrams cannot be produced by a warp. We conclude that the high velocity material which we detect in NGC 5668 is not due to the warped disk.

Further VLA, WSRT, and optical observations will be used to test the galactic fountain model and will hopefully determine the nature, and mass, of the high velocity clouds in our own galaxy.

References

Bregman, J. N. 1980, *Astrophys. J.*, **236**, 577.
Giovanelli, G. 1981, *Astron. J.*, **86**, 1468.
Isobe, T., Feigelson, E. D., and Nelson, P. I. 1986, *Astrophys. J.*, 306, 490
Wakker, B. P. 1990, Ph.D. Thesis, Groningen.

Figure 1. Arecibo spectrum of NGC 5668.

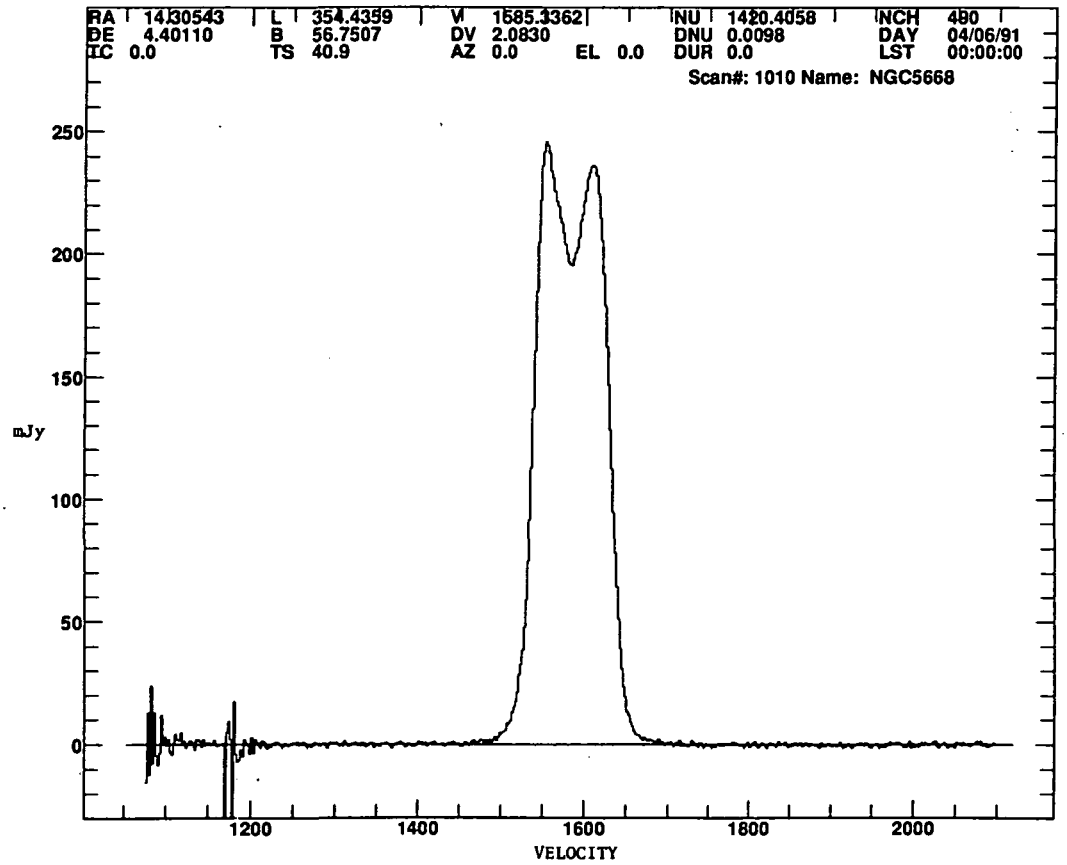

A COMPARISON OF EXTINCTION CURVES FOR DUST IN GALAXIES OF DIFFERENT HUBBLE TYPES

Leisa K. Townsley (University of Wyoming) and Jill S. Price (Bentley College)

A sample of 25 galaxies of various Hubble types has been observed in a variety of filters (Table 1). Extinction curves have been generated for absorption regions in these galaxies using a technique which previously had been used on just a few galaxies; for example, NGC 205 (Price and Grasdalen 1983), NGC 185 (Price 1985), NGC 3077 (Price and Gullixson 1989), and M31 (Walterbos 1986). The results from these studies suggested that there may be systematic trends in dust properties with Hubble type. This would not be surprising; dust properties should vary with metallicity, for example. It is well known that some galaxies (e.g. dwarfs) have lower metallicities than others (e.g. giant spirals or cD ellipticals) and their interstellar materials should reflect this difference.

In our own Galaxy, one can use the known properties of a certain spectral type to directly determine how much light is extinguished as a function of wavelength for a particular star. At the distances of most other galaxies, however, we cannot resolve individual stars so another method is needed. Therefore instead of looking at how much light is extinguished from an individual star, we look at how much galaxy light is extinguished, using the symmetry of the galaxy. This is accomplished in the following manner. The total amount of flux from a given point in a dust cloud (or an aperture) will be comprised of two parts: the flux from in front of the dust cloud, F, and the flux from behind the cloud, B, which has been extinguished by the dust, B[exp($-\tau$)]. The total amount of flux we see from that region of the galaxy, S, is the sum:

$$S = F + B[\exp(-\tau)] \qquad (1)$$

Suppose we could estimate how much flux, T, we should see from that portion of the galaxy if the dust were not present. If we assign a "luminosity distance" into the galaxy, x, so that the amount of flux F emanating from in front of the dust cloud is a fraction x of the amount of flux expected from that region of the galaxy, then:

$$F = xT \quad \text{and} \quad B = (1-x)T, \text{ since } T = F + B \qquad (2)$$

If we substitute the expressions in equation (2) into equation (1) and divide by T, we obtain:

$$F/T = x + (1-x)[\exp(-\tau)] \qquad (3)$$

This expression can be generated for data in different filters, and for n equations, we have n + 1 variables. This would appear to be a problem, except that we do get some help from galactic dust clouds, which have known ratios of optical depths. If we use one of these known ratios it reduces the number of unknowns to the same as the number of equations, allowing us to solve for x, and thus determine all the other optical depths. Alternatively, values of x may be assumed, and we can solve for the optical depths, generating extinction curves and comparing them to the average extinction curve for dust in our Galaxy. The ratio F/T is generated by observing how much flux is emanating from the dust cloud, F, and determining

the expected flux, T, from that region of the galaxy. This may be accomplished by either scanning across the dust on a line of galaxy symmetry or by doing spot photometry on the dust and comparing to a spot diametrically across the galaxy on a line of symmetry. Assumed values of x are restricted by the values of F/T, because since:

$$\tau = - \ln[(F - x)/(1 - x)], \qquad (4)$$

certain values of x are not allowed.

In practice this method allows us a way to see if dust is similar to galactic dust or not. If, for example, there is no value of x which gives a match with galactic optical depth ratios, then the dust in the galaxy differs from galactic dust in some quantitative way which can be probed with models of light scattering by dust grains. Caution is required, of course, because there is a wide range in dust properties even for dust within our own Galaxy. Careful thought must also be accorded to the error bars on our data points. Nonetheless in the past it has been possible to show that, at least in NGC 185, the dust was not like galactic dust (Price 1985), while in NGC 3077, the dust looked like galactic dust (Price and Gullixson 1989).

Results of this study may provide some clues, after modeling, to the structure and composition of dust in galaxies of various Hubble types. This should be helpful to theorists who wish to find out how star formation processes vary with Hubble type.

References

Price, J.S. 1985, Ap. J., 297, 652.
Price, J.S., and Grasdalen, G.L. 1983, Ap. J., 275, 559.
Price, J.S., and Gullixson, C.A. 1989, Ap. J., 337, 658.
Walterbos, R. 1986, Ph.D. thesis, University of Leiden.

TABLE 1

X = Observations Obtained (Filter Wavelengths in nm)

Galaxy/Type	550	633	805	425	500	600	700	800	900	485	535
NGC 128/$S0_2$(8)pec	X	X	X	X	X	X	X	X		X	X
NGC 520/IrrII	X	X	X	X	X	X	X	X		X	X
NGC 2685/$S0_3$(7)pec	X	X	X	X	X	X	X	X	X	X	X
NGC 4150/S0pec	X	X	X	X	X	X	X	X	X	X	X
NGC 4691/SBbpec	X	X	X	X	X	X	X	X	X	X	X
NGC 4753/S0pec	X	X	X	X	X	X	X	X	X	X	X
NGC 4826/Sab(s)	X	X	X	X	X	X	X	X	X	X	X
NGC 5195/IrrII	X	X	X	X	X	X	X	X	X	X	X
NGC 5273/S0/a	X	X	X	X	X	X	X	X	X	X	X
NGC 5614/Sa(s)	X	X	X	X	X	X	X	X	X	X	X
NGC 7331/Sb(rs)	X	X	X	X	X	X					
NGC 23/Sb	X	X	X	X	X	X					
NGC 157/Sc(s)	X	X	X	X	X	X					
NGC 210/Sb(rs)	X	X	X	X	X	X					
NGC 253/Sc(s)	X	X	X	X	X	X					
NGC 309/Sc(r)	X	X	X	X	X	X					
NGC 891/Sb	X	X	X	X	X	X					
NGC 972/Sbpec	X	X	X	X	X	X					
NGC 1068/Sb(rs)	X	X	X	X	X	X					
NGC 1084/Sc(s)	X	X	X	X	X	X					
NGC 1232/Sc(rs)	X	X	X	X	X	X					
NGC 1637/SBc(s)	X	X	X	X	X	X	X	X	X		
NGC 1832/SBb(r)	X	X	X	X	X	X	X	X	X		
NGC 1964/Sb	X	X	X	X	X	X	X	X	X		
NGC 2855/Sa(r)	X	X	X	X	X	X	X	X	X	X	X

Molecular Clouds in the Centers of Galaxies: Constraints from HCN and ^{13}CO Line Emission

S. Aalto[1], *J.H. Black*[2], *R.S. Booth*[1], *and L.E.B. Johansson*[1]

[1]Onsala Space Observatory, Chalmers University of Technology, S–439 00 Onsala, Sweden
[2]Steward Observatory, University of Arizona, Tucson, AZ 85721, USA

Summary. We have searched for HCN J=1–0 line emission in the centers of 12 galaxies and have detected it in 10 of them. We have obtained complementary data on J=1–0 and 2–1 transitions of ^{12}CO and ^{13}CO in these systems. The ratio of integrated intensities, $I(\mathrm{CO}\ 1-0)/I(\mathrm{HCN}\ 1-0) = 25 \pm 11$ for this sample. We find that HCN emission of this strength can be produced under conditions of subthermal excitation. In combination with the line ratios in CO and ^{13}CO, HCN puts constraints on the mean conditions of molecular clouds and on the mix of cloud types within the projected beam.

Observations and Results. We have observed HCN J=1–0 at 88.6 GHz in a sample of galaxies for which we have been obtaining data on several transitions of ^{12}CO and ^{13}CO with the 15m Swedish–ESO Submillimetre Telescope (SEST), the 20m Onsala telescope, and the 12m NRAO telescope. The sample includes isolated "normal" spiral galaxies, interacting systems, and luminous mergers. As found previously by Solomon, Downes, and Radford (1992) for a different sample, the HCN profiles typically resemble those of CO 1–0, which suggests that the clouds responsible for these emissions have similar kinematical distributions. The intensity in HCN 1–0 is detected at a level of 2 to 10 % of that in CO 1–0. Our previous result (Aalto *et al.* 1991) on the ^{12}CO/^{13}CO intensity ratio in J=1–0 has been extended to more systems: while there is a well defined mean value near 10 for nuclei of most galaxies, much higher ratios are observed in the most disturbed, luminous mergers. New results on the ^{12}CO/^{13}CO intensity ratio in J=2–1 show a range of values and help to clarify the interpretation in terms of optical depth in the dominant CO–emitting clouds.

Discussion. Line emission from polar molecules like HCN is conventionally taken to arise in a denser component ($n(\mathrm{H_2}) > 10^4$ cm^{-3}) of molecular gas than CO emission, which is more readily excited at low density ($n(\mathrm{H_2}) \approx 10^2 - 10^3$ cm^{-3}). We are developing techniques to model unresolved ensembles of molecular clouds with more than one population defined by density/temperature/size or with internal gradients of density and temperature. We also compare the line emission with the degree of central concentration of total mass, with the distribution of CO intensity, and with indicators of star–forming activity.

Preliminary conclusions include:

(1) Any population of dense ($n(H_2) \geq 10^4$ cm^{-3}) clouds, invoked to explain the HCN emission, must be consistent with the observed intensities and intensity ratios of ^{12}CO, ^{13}CO, and C^{18}O lines, which often require large quantities of more dilute molecular gas.

(2) The observed HCN 1–0 emission can sometimes be produced under conditions of subthermal excitation at relatively low densities, $n(H_2) < 10^4$ cm^{-3}.

(3) In some galaxies, with centrally concentrated 10 μm sources and molecular distributions, the excitation of HCN 1–0 may be enhanced by infrared pumping through a vibrational transition at 14 μm wavelength.

(4) We have not yet found a correlation between the intensity ratio, I(CO)/I(HCN), and disturbed morphology, far–infrared emission, or measures of star–forming activity in our sample of galaxies.

Future efforts will involve further observations of higher transitions of HCN and further refinements in the modeling of unresolved cloud distributions.

Acknowledgements. We are grateful for the support of the observatories at which the observations were made: SEST is a facility of the Swedish Natural Science Foundation (NFR) and the European Southern Observatory; the Onsala 20m is a facility of NFR; and the NRAO 12m is administered by Associated Unviversities, Inc. (AUI), under cooperative agreement with the US National Science Foundation.

References.

Aalto, S., Black, J.H., Johansson, L.E.B., & Booth, R.S. 1991, *A&A*, **249**, 323.

Solomon, P.M., Downes, D., & Radford, S.J.E. 1992, *ApJ*, **387**, L55.

MOLECULAR GAS CONTENT OF GALAXIES IN THE HYDRA-CENTAURUS SUPERCLUSTER

W.K. Huchtmeier

Max-Planck-Institut für Radioastronomie

Auf dem Hügel 69 , 5300 Bonn 1 , W. Germany

Abstract

A survey of bright spiral galaxies in the Hydra-Centaurus supercluster for the CO(1-0) transition at 115 GHz was performed with the 15m Swedish-ESO submillimeter telescope (SEST). A total of 30 galaxies have been detected in the CO(1-0) transition out of 47 observed, which is a detection rate over 60%. Global physical parameters of these galaxies derived from optical, CO, HI, and IR measurements compare very well with properties of galaxies in the Virgo cluster.

The Hydra I cluster (Abell 1060) is one of the nearest clusters and very similar to the Virgo cluster in many global parameters like type, population, size, and shape. Both clusters have comparable velocity dispersions (i.e. total mass) and are spiral rich. Hydra is well isolated in velocity space and appears more circular (Kwast 1966), and might be dynamically more relaxed, although the center may contain significant substructures (Fitchett and Meritt 1988) or projected foreground groups. Both clusters contain low luminosity central X-ray sources. We assume a distance of 68.4 Mpc for Hydra I in order to allow direct comparison with some (nearly) complete galaxy samples.

The Centaurus cluster provides a valuable contrast to Virgo and Coma. It is intermediate in distance and in galaxy population type with a relatively well defined S0-dominated core and an extensive S-rich halo. Its richness class in the Abell scale is 1 or 2 which is richer than Virgo and poorer than Coma. Centaurus is irregular in appearance like Virgo. Its complex structure in the radial velocity domain is interpreted as subclustering. We adopt a weighted average distance of 64 Mpc for Centaurus.

The comparison samples are:

a) the sample of nearby galaxies which includes 146 spiral and irregular galaxies with corrected redshifts $v_0 \leq 500 kms^{-1}$ (**KKT** the Kraan-Korteweg - Tammann sample), their global parameters as given by Huchtmeier and Richter 1988;

b) the sample of spiral and irregular galaxies in the Virgo cluster with HI observations available (252 galaxies, Huchtmeier and Richter 1989b);

c) the sample of bright spiral galaxies in Virgo with CO (J=1-0) observations available with good signal-to-noise ratio (57 galaxies, Stark et al. 1986, Kenney and Young 1988, Lees et al. 1991). This will be an ideal reference sample for comparisons with other clusters. The distance assumed for deriving global properties of Virgo cluster galaxies was 21.88 Mpc.

The observations were performed with the 15m Swedish-ESO submillimeter telescope (SEST) at La Silla in January 1990 and 1991 under favorable meteorological conditions. At a frequency of 115 GHz the half power beamwidth (HPBW) of this telescope is 43 arcsec. The cooled Schottky heterodyne receiver had a typical receiver temperature of 240K ; the system temperature was typically 350 to 500 K depending on elevation and humidity. An accousto-optic spectrometer with a bandwidth of 500 MHz yielded a channel width of 0.69 MHz or about 1.8 km/s. Nonlinearities in the frequency scale of the AOS were corrected by the computer software. For more details on telescope information and operation see Booth et al.(1989).

The CO line integral was used to derive the total mass of molecular hydrogen $M(H_2)$ assuming a conversion factor of $N(H_2)/I_{CO} = 2.810^{20} cm^{-2}(Kkms^{-1})$. The conversion factor derived in our galaxy is generally used for extragalactic systems. One should consider these H_2 masses as "nominal" masses. The IRAS fluxes at 60μ and 100μ are from Helou et al.(1988). In those cases where fluxes were not given we searched Roberts et al.(1991) and Lonsdale et al.(1985) in that order of priority. The infrared

luminosity L_{IR} and the amount of cool dust M_{dust} were derived from IRAS fluxes at 60μm and 100μm following Young et al. (1989).

The global H_2-to-HI mass ratio has been studied as a function of morphological type. The mean value of $M(H_2)/M(HI)$ decreases from 4.0 ± 1.9 for S0/Sa galaxies to 0.2 ± 0.1 for Sd/Sm galaxies. For a mixture of morphological types as in our samples we would expect the cold gas to be available in about equal amounts in mass as neutral and molecular hydrogen. The range of values occupied by the Virgo sample shows a good correlation. The Hydra galaxies fit quite well to the "bright end" of the Virgo range. Comparison of molecular gas masses with IRAS derived dust masses leads to mean gas-to-dust ratios of the order of $\sim$ 600 rather than a value of $\sim$ 150 (e.g.Spitzer 1978) as observed for our galaxy. Devereux and Young (1990b) find the mean inner disk gas to warm dust ratio to $\sim$ 1000 with no significant variation as a function of morphological type or dust temperature (e.g. Young and Scoville 1991). There is general agreement for the gas-to-dust ratios observed in field galaxies and the two cluster populations discussed in this paper. The ratio of infrared luminosity to the mass of molecular hydrogen L_{IR}/M_{H2} is considered as a measure for the formation of bright stars (e.g. Young and Scoville 1991). High star formation efficiences are present in interactive galaxies (Sanders and Mirabel 1985, Young et al. 1986, Solomon and Sage 1988).

It is interesting to see that elliptical galaxies which have been detected in CO (e.g. Roberts et al. 1991, Lees et al. 1991, Huchtmeier and Tammann 1992) populate the same range as spiral galaxies . But all those ellipticals are somewhat peculiar (for example: NGC7176 is an interacting system, NGC3928 is known as a Makarian galaxy) and are probably not representative for the class of elliptical galaxies (e.g. Bregman et al. 1992).

The small number of HI observations available for the Centaurus cluster does not permit any statement about HI deficiency. There are more observations available for the Hydra cluster; there is evidence for a mild HI deficiency in this cluster.

When comparing global parameters for the Virgo and Hydra-Centaurus galaxies we find a general agreement for both clusters which is not too surprising in view of the similarity of both clusters. Due to the greater distance of Hydra (sensitivity problem) only the bright end of the galaxy population of this cluster is accessible for CO observations presently.

References

Bregman, J.N., Hogg, D.E., Roberts, M.S. 1992 : ApJ 387,484

Booth, R.S., Delgardo, G., Hagström, M., Johannson, L.E.B., Murphy, D.C., Olberg, M., Whyborn, N.D., Greve, A., Hansson, B., Lindström, C.O., Rydberg, A. 1989 : A&A 260,350

Devereux, N., Young, J.S. 1990b : ApJ 359,42

Fitchett, M., Merritt, D. 1988 : ApJ 335,18

Helou, G., Khan, I.R., Malek, L., Boehmer, L. 1988 : ApJSS 68,151

Huchtmeier, W.K., Richter, O.-G. 1988 : A&A 203,337

Huchtmeier, W.K., Richter, O.-G. 1989b : A&A 210,1

Huchtmeier, W.K., Tammann, G.A. 1992 : A&A 257,455

Kenney, J.D., Young, J.S. 1988 : ApJSS 66,261

Kwast, T. 1966 : Acta Astr. 74,708

Lees, J.F., Knapp, G.R., Rupen, M.P., Phillips, T.G. 1991 ApJ 379,177

Londsdale, C.J., Helou, G., Good, J.R., Rice, W. 1985 : *Cataloged Galaxies and Quasars Observed in the IRAS Survey* NASA JPL D-1932

Roberts, M.S., Hogg, D.E., Forman, W.E., Jones, C. 1991 : ApJSS 75,757

Sanders, D.B., Mirabel, I.F. 1985 ApJ 298,L31

Solomon, P.M., Sage, L. 1988 : ApJ 334,613

Spitzer, L. 1978 *Physical Processes in the Interstellar Medium* Wiley,New York p.162

Stark, A.A., Knapp, G.R., Bally, J., Wilson, R.W., Penzias, A.A., Rowe, H.E., 1986 : ApJ 310,660

Young, J.S., Schloerb, F.P., Kenney, J., Lord, S.D. 1986a : ApJ 304,443

Young, J.S., Xie, S., Kenney, J.D.P., Rice, W.L., 1989 : ApJSS 70,699

Young, J.S., Scoville, N.Z., 1991 : Ann.Rev.Astron&Astrophys. 29,381

Galactic Oscillations

B. F. Smith (NASA/Ames) and R. H. Miller (U.Chicago)

Summary: Several oscillations have been identified in spherical galaxy models. These are normal mode oscillations in a stable galaxy. Each has its own distinct period and spatial form, and each rings without detectable damping through a Hubble time. The most important are: (1) a simple radial pulsation (fundamental mode), in which all parts of the galaxy move inward or outward with the same phase; (2) a second spherically symmetrical radial mode with one node, so material inside the node moves outward when material outside moves inward.

Numerical experiments suggest that normal mode oscillations may be present in nearly all galaxies at a considerably higher amplitude than has previously been thought. Amplitudes (variations in total KE, for example) typically run a few percent of equilibrium values, and periods are around $50 - 300$ Myrs in typical galaxies. These time scales are long enough that gas trapped near the center could cool during an oscillation cycle, allowing star formation activity. The second mode oscillations could cause bursts of star formation.

Disturbances: Fairly large systematic motions near the centers of galaxies reported earlier (Miller and Smith 1988, 1992) can produce effects often seen in the observations, such as the 50 km/sec velocity difference between galaxy and nucleus recently reported in *M*87 (Jarvis and Peletier 1991). Bajaja *et al.* (1984) reported that "the center of the HI distribution lies about 300 pc westward of the coincident optical and radio continuum nuclei" in the Sombrero galaxy, NGC 4594. They commented that this asymmetry is smaller than that which they usually find in spiral galaxies. The optical nucleus is 170 pc away from the rotational center in NGC 2903 (Simkin 1975). Other examples are given in Miller and Smith (1992). These center motions are local disturbances as the nucleus orbits around the galaxy's mass centroid. They naturally raise the question whether global motions that affect the galaxy as a whole are also present and whether these might be found experimentally. Galactic oscillations were found as we pursued that question.

Fundamental mode oscillations show up as continuing oscillations in the total kinetic energy. Peak-to-peak variations typically ran $2 - 5\%$ of the mean (time averaged) total kinetic energy, with periods around 300 Million years. They continued with large amplitude (22% peak-to-peak fractional variations in the kinetic energy) throughout 6 billion years without detectable damping in one experiment. A 5% decrease in amplitude could have been detected easily, but none was seen. This sets a lower limit to the damping time at around 100 billion years. This experiment allowed us to study oscillations with high signal-to-noise. Even so, study of these disturbances requires large numbers of particles and a stable experiment that extends over many crossing times because of severe signal-to-noise problems. The 22% peak-to-peak variation in kinetic energy corresponds to 8% RMS variation, about 80 times expected random fluctuations allowed by the virial theorem for the 400,000 particles of this experiment, and it is several thousand times the energy expected in a normal mode for a system that has undergone violent relaxation to a

steady state.

The second radial mode is spherically symmetrical with a radial node, and its period ranges from $100 - 150$ million years (it is *not* commensurate with the fundamental mode). It shows up clearly in plots of Lagrangian radii, and it is strongest in the inner parts of the galaxy. The radial node is about 6 kpc from the center, but we have seen it at radii as small as 2.5 kpc in other experiments. The central density varies by a factor three in this experiment, and the variation is due to the second radial mode. This mode was identified as an instability by Hénon (1973), but here it acts like a normal mode in a stable galaxy.

An $\ell = 2$, $m = 2$ mode was identified in plots showing the time dependence of elements of the virial tensors. An $\ell = 1$ mode has also been seen. Its amplitude is much smaller than either of the spherically symmetrical modes. Its period ranges from $140 - 190$ million years in various experiments, and it is not commensurate with either of the other modes. Other disturbances that act like global modes may be present in these galaxy models as well; the ones described here are those for which we have been able to design experimental probes. Searches would be facilitated by good predictions from analytic theory about frequencies and spatial forms of the disturbances, but these are not available.

Discussion: Several results emerge from this series of experiments.

1. Galaxy models support long-lived oscillations, which are normal modes of a stable system near equilibrium. They are not instabilities.

2. Four different patterns (or modes) have been identified, but others are likely to be present as well.

3. Periods of the oscillations are on the order of the galaxy's dynamical time scale (a crossing time, about 100 Million years).

References

Bajaja, E., van der Berg, G., Faber, S. M., Gallagher, J. S., Knapp, G. R., and Shane, W. W. 1984. *Astron.&Ap.* **141,** 309.

Hénon, M. 1973. *Astr. Ap.* **24**, 229.

Jarvis, B. J., and Peletier, R. F. 1991. *Astr. Ap.* **247**, 313.

Miller, R. H.. and Smith, B. F. 1988. In *Applied Mathematics, Fluid Mechanics, Astrophysics, a Symposium to Honor C. C. Lin.* D. J. Benney, F. H. Shu, & Chi Yuan, Eds., 366–372, World Scientific, Singapore.

Miller, R. H. and Smith, B. F. 1992. *Ap.J.*, **393**, 508, *Fiche* 122–B7 (includes a videotape).

Simkin, S. M. 1975. *Ap.J.*, **195**, 293, *Fiche* 5-C12.

A NEW METHOD TO SIMULATE VERTICAL AND HORIZONTAL STRUCTURE IN GALACTIC DISKS

JULIANNE J. DALCANTON & JAMES E. GUNN
Princeton University Observatory

ABSTRACT. We have modified the particles in an N-body treecode to have different softening lengths in the horizontal and vertical directions. This allows us to simultaneously have thin enough particles to resolve the vertical structure in galactic disks, and horizontally large enough particles to supress the vertical heating due to two-body effects.

1. Introduction

It has previously been difficult to use N-body techiniques to study the vertical structure in galactic disks. Because disk systems are usually at least 10 times larger horizontally than they are vertically, the height of the disk is only very sparsely sampled by particles. Furthermore, the large softening lengths that are needed to suppress two-body relaxation in the plane of the galaxy leave the vertical forces poorly resolved. By creating an N-body code that uses particles that have much larger effective softening lengths horizontally than they do vertically, we neutralize both of these problems.

2. Method

To create "flat" N-body particles, we modified the interparticle forces in Lars Hernquist's implementation of the Barnes and Hut tree code algorithm (Hernquist, 1990, Barnes & Hut, 1986). The modified forces are derived from an *ad hoc* potential and model approximately those of a flattened Plummer density distribution. Horizontally, the force between particles is the same as if the particles were simply spherically softened. Within the horizontal softening length, the vertical forces are roughly constant until a height above the plane on order of the horizontal softening length (as would be expected for a thin disk). Because the particles are extended horizontally, the vertical forces are effectively averaged over several particles, thus reducing vertical noise and two-body effects while maintaining vertical force resolution. The increase in relaxation time for N-body codes using flattened particles over standard N-body codes that have the same vertical scale as the flattened particles is roughly a factor of the ratio between the horizontal and vertical scale of the flattened particles, (about a factor of 10). The axis ratio of the flattened particles is adjustable.

To test the amount of vertical heating, we started with a horizontally very cold exponential disk (with constant Toomre's Q) embedded in a bulge and halo potential. The disk was designed to have the same scale length and surface density as the Galaxy, and bulge+halo system parameters were chosen to give a flat rotation curve of 220 km/sec. To suppress the firehose instability, to which such a vertically cold system is susceptible, we implemented a vertical force symmetrization routine. Preliminary runs were with 10^4 particles and ran for 2×10^9 years (about 8 disk rotations). All runs started with the same initial conditions. Larger simulations run for longer times are currently in progress.

3. Results

Figure 1 shows the initial conditions and the final states for two different simulations. One run used small spherically softened particles ($\epsilon = 75\,\mathrm{pc}$), and the other used flattened particles with a horizontal scale of 750 pc and a vertical scale of 75 pc. Clearly there is dramatically less vertical heating when the flattened particles are used. In the spherical case, the scale height increases from 15 pc to roughly 350pc, while in the flattened case, the scale height increases to not more than 17 pc. Likewise, the vertical velocity dispersion increases fivefold in the spherical case, and increases by at most 20% when using flattened particles, as can be seen in Figure 2.

4. Conclusions

With this new tool, we will be able to study numerically how the large scale horizontal structure of galactic disks (i.e. spiral structure) couples to the growth of vertical structure. The effects of gas infall and satellite infall can also be easily studied with this techinque.

REFERENCES

Barnes, J., Hut, P., 1986, Nature, 324, 4.

Hernquist, L., 1990, J. Comput. Phys., 87, 137.

Villumsen, J. V., Gunn, J. E., & Casertano S.,1987, preprint, Princeton Observatory.

White, Simon D. M., 1976, MNRAS, 174, 467.

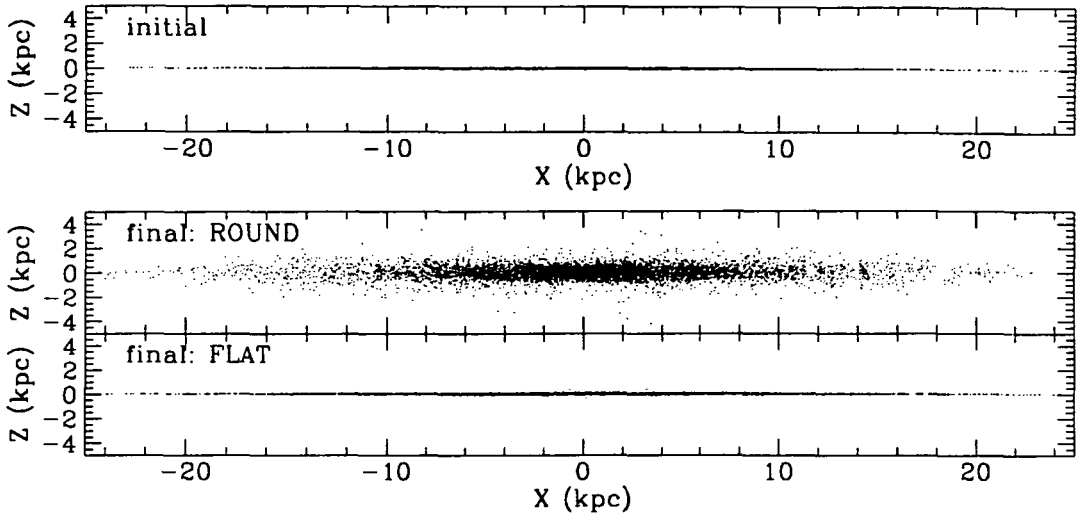

FIGURE 1. (top) Initial conditions, 10^4 particles. (bottom) Two simulations after 1.9×10^9 years, one using spherically softened particles and one using flattened ones.

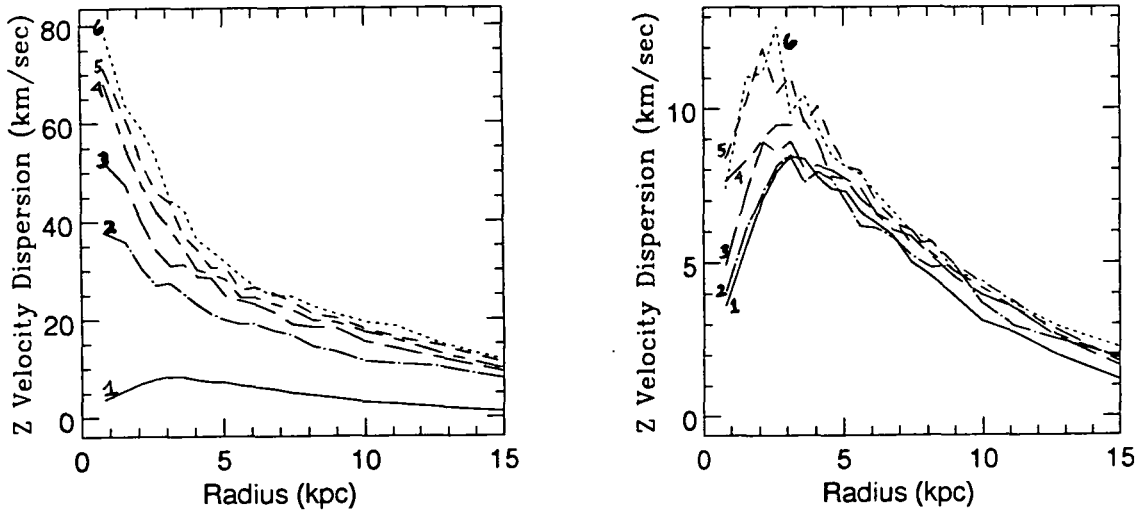

FIGURE 2. Growth of the vertical velocity dispersion with time, for the round particle and the flat particle simulations. Time steps are separated by 3.7×10^8 years. Note the different vertical scales.

THE VELOCITY FIELDS OF ELLIPTICAL GALAXIES: STEPS TOWARD A SOLUTION OF THE INTRINSIC SHAPE PROBLEM

Thomas S. Statler and Anne M. Fry
University of North Carolina at Chapel Hill

One of the few surviving signatures, at low redshift, of the process of galaxy formation should be the distribution of shapes of elliptical galaxies. Yet the problem of inferring this distribution from the observed ellipticals is still unsolved, because insufficient use has been made of kinematic information. The levels of "sophistication" of the theoretical models and of the observations have up to now been poorly matched. The kinematic data available for most ellipticals consists of only major and minor axis spectra; and Franx *et al.* (1991) find, using simple geometric models, that the addition of only one kinematic parameter (the ratio of minor axis to major axis rotation velocity) to the photometry is just not enough to finely constrain the intrinsic shape distribution. On the other hand, the more elaborate self-consistent models (*e.g.*, Levison and Richstone 1987, Statler 1987) have made only infrequent and model-dependent predictions of complicated velocity patterns, mostly at small radii, and have not discussed how they change with shape.

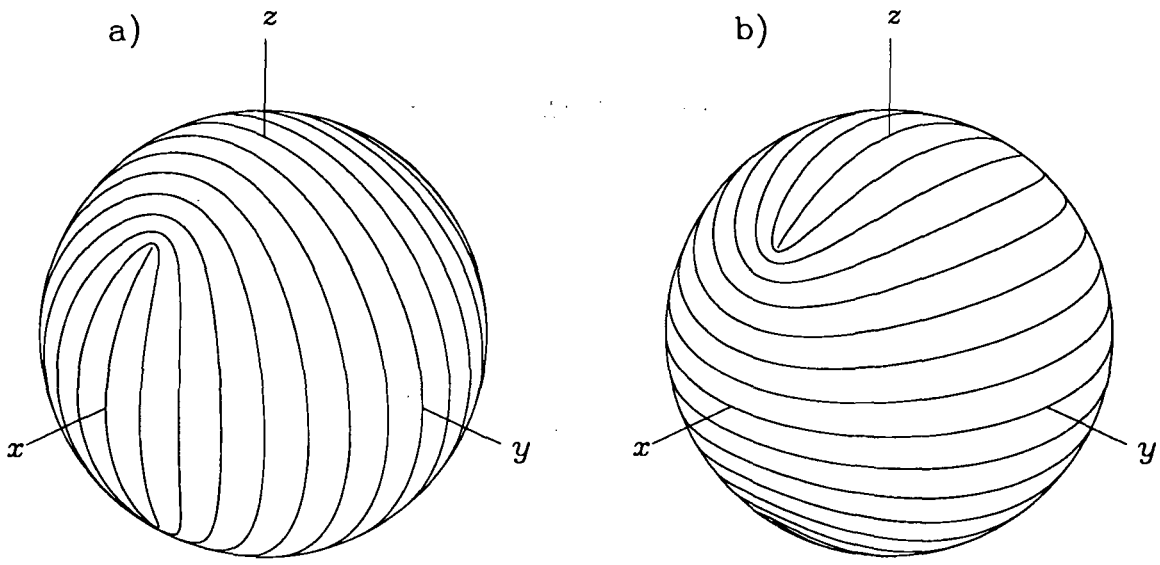

Figure 1. *Streamlines of the separate stellar flows around the (a) x axis and (b) z axis in the outer parts of a triaxial galaxy.*

Here we aim for an approximate but robust method of predicting the velocity field (hereafter VF) for a model elliptical of arbitrary shape. To avoid problems connected with strongly dissipative evolution in cores and the presence of central black holes, we take the view that the most useful VF features are to be found at large radii. We then assume (1) radial self-similarity at large r; (2) negligible rotation of the figure, which implies (3) intrinsic circulation (rotation) only around the long (x) and short (z) axes; (4) flow of the stellar "fluid" on spherical shells, on which (5) the streamlines of the x and z circulations are given by coordinate lines in a confocal ellipsoidal system (figure 1). This last assumption is suggested by the analytically tractable Stäckel potentials, in which the flow is exactly along those lines, but is *much less restrictive* than asserting the potential is separable. With the streamlines specified, each of the x and z flows is dictated by the equation of continuity, and the projected velocity follows with a little geometry.

Of course, a boundary condition is required to solve for the complete flow. An exact expression for the boundary condition for any one model would require knowing the complete distribution function for the tube orbits; however, we argue that models satisfying realistic requirements of smoothness (*e.g.*, that the

mean velocity is not spatially discontinuous) will all have very similar boundary conditions. (The details of this vague statement will be published elsewhere.) We are then able to calculate VFs at any intrinsic shape and projection for a small number of *distinguishable classes* of models — for instance, with intrinsic streaming about the long axis, about the short axis, or about both axes. These models are distinguishable from each other because we are able to look not merely at the apparent axis of rotation (*cf.* Franx *et al.* 1991), but at the *asymmetries* of the VF, which are the true signatures of triaxiality.

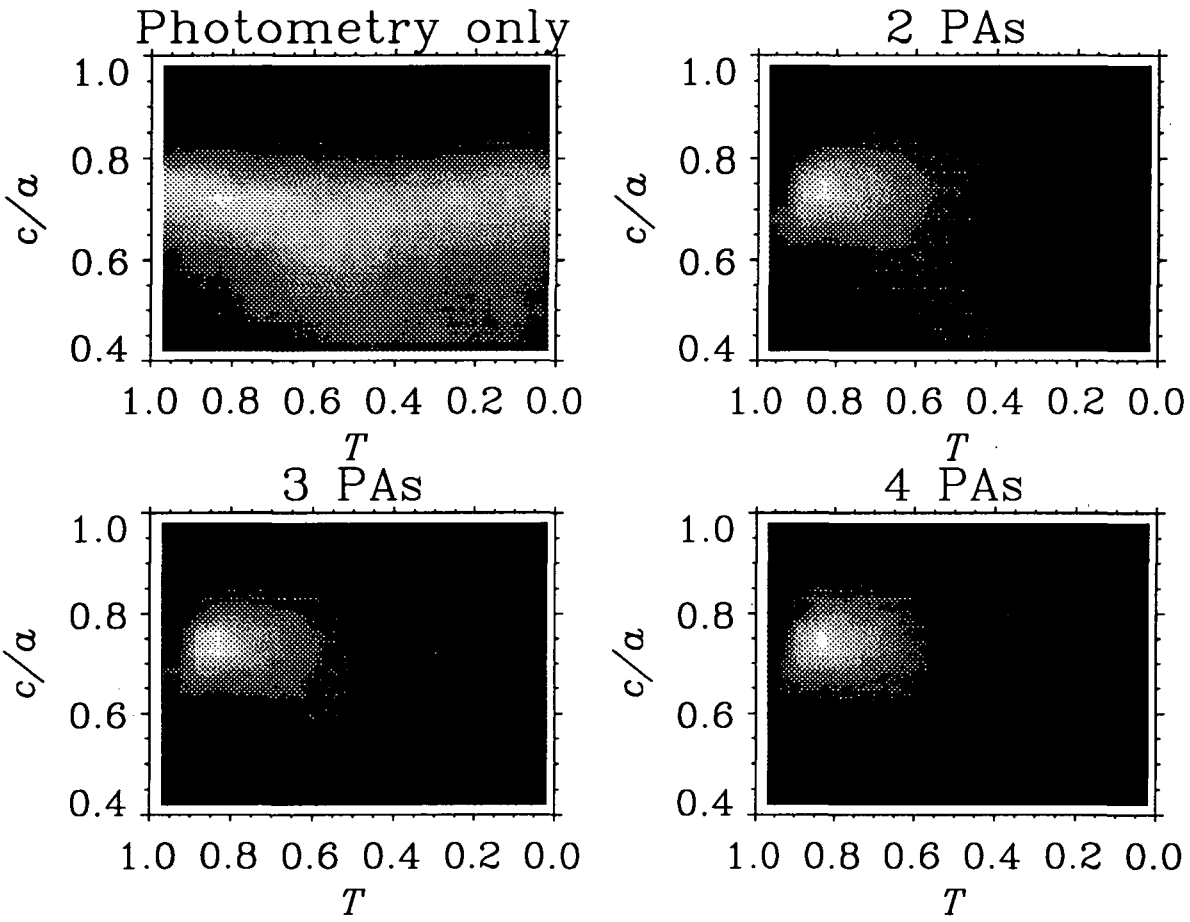

Figure 2. *Simulation showing the effect of adding kinematic constraints to the shape of a galaxy. The "observed galaxy" is E2, with large kinematic misalignment and velocity field asymmetry. Each frame shows likelihood density (goodness of fit) in the space of axis ratio c/a and triaxiality T. The benefit of of having spectra on four position angles is apparent from the two right-hand frames.*

The intrinsic shape distribution of the full population of ellipticals is likely to be formally consistent with most types of internal streaming models, though (we would hope) different for each type. Comparing with predictions from galaxy formation theories will be necessary to settle the problem decisively. Nonetheless, much can be learned immediately. Within the context of a *single* class of models, the intrinsic shape of any one galaxy can be well constrained with as few as four long-slit spectra (albeit of rather high signal-to-noise). This is shown in figure 2, where we have chosen intrinsic shapes at random and successively added constraints on the observable parameters. It is clear from frames (*b*) and (*d*) that there is much to be gained from spectra taken at $\pm 45^{\circ}$ from the major axis.

REFERENCES

Franx, M., Illingworth, G. D., and de Zeeuw, T. 1991, *Ap. J.*, **383**, 112.

Levison, H. F. and Richstone, D. O. 1987, *Ap. J.*, **314**, 476.

Statler, T. S. 1987, *Ap. J.*, **321**, 113.

Is a Local Bar a Good Place to Find a Companion? The Near Infrared Morphology of Maffei 2

Robert L. Hurt (UCLA), K. Michael Merrill (NOAO), Ian Gatley (NOAO), & Jean L. Turner (UCLA)

Maffei 2 is one of the closest large spiral galaxies lying just beyond the Local Group. It would probably be one of the most heavily studied galaxies in the sky were it not for the ~ 5 magnitudes of visual extinction resulting from its position behind the Galactic plane (l = 137°, b = -0°.3). It is the site of a burst of nuclear star formation indicated by strong infrared ($L_{FIR} \sim 4 \times 10^9 L_\odot$; Rickard & Harvey 1983; Ho *et al.* 1989), Brackett line (Ho, Beck, & Turner 1990) and radio continuum emission (Seaquist, Pfund, & Bignell 1976; Turner & Ho 1992). Interferometric maps of ^{12}CO (Ishiguro *et al.* 1989) and ^{13}CO (Hurt & Turner 1991) emission indicate that star formation is associated with a barlike structure consisting of arms of molecular gas that extend from within ~50 pc of the dynamical center out to a radius of at least 500 pc. HI maps have shown the galaxy to have an angular extent of ~15' and a neutral gas mass typical of a large spiral galaxy (Bottinelli *et al.* 1971; Shostak & Weilachew 1971; Love 1972; Hurt, Turner & Ho 1992).

Near infrared imaging of Maffei 2 using the Simultaneous Quad Infrared Imaging Detector (SQIID) at KPNO has proven a successful tool in determining the morphology of this optically obscured galaxy. It is a barred spiral galaxy with two distinct arms and a bright nucleus which are clearly visible in the K-band (Fig. 1). We find its Revised Hubble type to be SBb(s) pec. Its classification of "peculiar" is warranted by its asymmetric stellar distribution. The eastern spiral arm is more diffuse and about twice as long as the western arm, and the NE and SW halves of the bar are misaligned by ~ 10° when viewed in deprojection. There is also an anomalous arm in the north that appears to lead the end of the NE bar.

The infrared extinction traced in the J-band (Fig. 2a) and more clearly in the J-K image (Fig. 2b) matches the known distribution of molecular gas in this region. Within the inner arcminute of the nucleus mapped in ^{13}CO (Fig. 2c; Hurt & Turner 1991), the correlation between the density profile of the molecular gas component and the variations in the J-K image are striking (Fig 2d). The near infrared extinction appears to be an excellent tracer of molecular gas.

The presence of the disrupted morphology and nuclear starburst in Maffei 2 argues for some form of recent tidal perturbation. The first obvious candidate would be its companion Maffei 1, though the large distance between them (40'; 60 kpc) makes a dynamically recent interaction unlikely. The other alternative is that there is a closer companion which has remained undiscovered because of the high extinction in this region. The best shot at finding such a companion, which could easily have been stripped of gas from previous tidal encounters, would be in the near infrared. Indeed, there is a potential candidate in the SQIID images. The compact object at the end of the anomalous northern arm (Fig. 1) could well be a dwarf companion in the process of tidally disrupting the galaxy. In this scenario, the anomalous arm might then represent a streamer of material tidally drawn out by the encounter.

Bottinelli, L.*et al.* 1971, A&A, 12, 264
Ho, P. T. P., Beck, S. C., & Turner, J. T. 1990, ApJ, 349, 57
Ho, P. T. P., Turner, J. T., Fazio, G. G., & Willner, S. P. 1989, ApJ, 344, 135
Hurt, R. L. & Turner, J. T. 1991, ApJ, 377, 434
Hurt, R. L., Turner, J. T., & Ho, P., 1992, in preparation
Ishiguro, M. et al. 1989, ApJ, 344, 763
Love, R. 1972, Nature, 235, 53
Rickard, L. J, & Harvey, P. M. 1983, ApJ, 268, L7
Seaquist, E., Pfund, J., & Bignell, R. 1976, A&A, 48, 413
Shostak, G. & Weliachew, L. 1971, Ap. J., 169, L71
Turner, J. L. & Ho, P. T. P. 1992, in preparation

Figure 1

K-band Image

The contrast in this image has been adjusted to enhance the low surface brighness structures. Visible in this image are the bar and arms. The SW bar and western arm are compact and better-defined than the more diffuse NE bar and eastern arm. The eastern arm is about twice as long as the western one and has an anomalous extension directly to the north. This extension could be a small companion in the process of interacting with Maffei 2. The box indicates the area covered by Figure 2 (below).

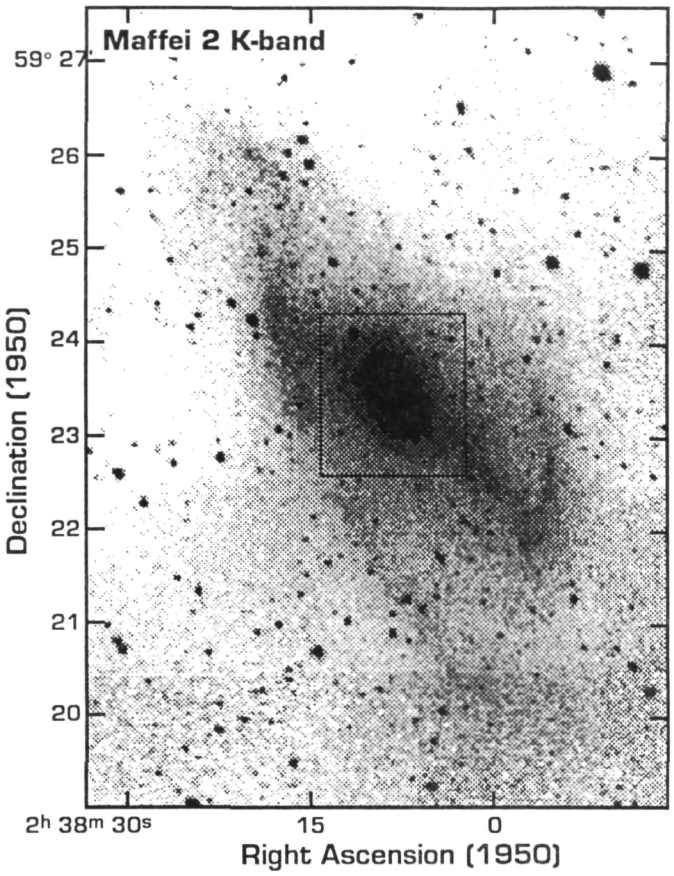

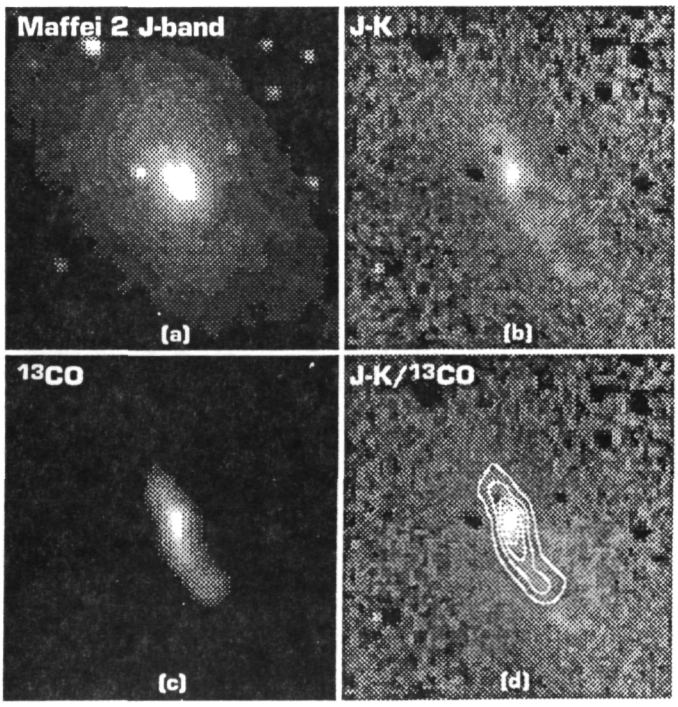

Figure 2

J-band, J-K, and ^{13}CO

Figures 2a-2d cover a 95" × 100" field, centered on the nucleus. Fig. 2a shows the J-band emission for this region, with clearly visible lanes of extinction. Fig. 2b is a J-K image constructed by taking a ratio of the individual J and K band images. The white to black greyscales represent ratios of 0.4 to 1.0. Fig. 2c is a greyscale representation of the ^{13}CO emission within a half-arcminute of the nucleus of the galaxy (Hurt & Turner 1991). The black to white greyscales represent integrated emission from 0.0 to 120 K km s^{-1}. Fig. 2d overlays contours of the ^{13}CO emission on the J-K map of Fig. 2b.

LUMINOSITIES OF Hα EMITTING REGIONS IN A PAIR OF INTERACTING GALAXIES IN THE BOOTES VOID

D. Weistrop, P. Hintzen, University of Nevada, Las Vegas, NV
R. Kennicutt, C. Liu, J. Lowenthal, University of Arizona, Tucson, AZ
K.-P. Cheng, R. Oliversen, B. Woodgate, NASA/Goddard Space Flight Center, Greenbelt, MD

Abstract: Luminosities of Hα emission from a pair of interacting galaxies in the low density environment of the Bootes void are presented. CG 692 (IRAS 1519+5050) has an Hα luminosity of 2 x 10^{42} ergs s^{-1}, indicating a star formation rate of 18.4 $M_\odot$ yr^{-1}. Individual extranuclear Hα regions have luminosities of approximately 10^{40} ergs s^{-1}. These luminosities are similar to those found for H II regions in bright, late-type galaxies in more densely populated parts of the Universe.

Based on spectroscopy and imaging data, we have recently identified a pair of interacting galaxies within the Bootes void (Weistrop *et al.* 1991, Weistrop *et al.* 1992). The brighter galaxy, CG 692 (IRAS 1519+5050) is a spiral undergoing large amounts of star formation, while its companion, CG 693, is a previously unidentified Seyfert 1 galaxy (Figure 1). The galaxies are at the same redshift within the uncertainties of the measurements, z = 0.0574, and have a projected separation of 34 kpc, (H_0=50 km $s^{-1}Mpc^{-1}$ assumed throughout). The galaxies are within the boundaries of the Bootes void as defined by Kirshner *et al.* (1987). We investigate the luminosity of the Hα emission in CG 692 and between the galaxies, to compare with galaxies in denser environments. Almost all the Hα emission from CG 693 arises in the nucleus, and is not considered further here.

Images were obtained at the redshifted Hα wavelength of the galaxies and a nearby continuum band, using the Goddard Fabry-Perot Imager on the University of Arizona's 90-inch telescope located at Kitt Peak (Weistrop *et al.* 1992). Flux calibration was obtained from observations of HZ 44. The total Hα flux for CG 692 is 1.38 x 10^{-13} ergs cm^{-2} s^{-1}, with an estimated $\pm$ 25% error due to the uncertainty in the conversion from count rate to flux. Since the galaxies are located at b = 53°, absorption within our galaxy is about 0.02 mag and has been ignored (Kennicutt & Kent 1983). For q_0 = 0, the total Hα luminosity of CG 692 is L = 2.06 x 10^{42} ergs s^{-1}, similar to the Hα + [NII] luminosities of the brightest interacting galaxies (Kennicutt *et al.* 1987). The star formation rate in CG 692 is 18.4 $M_\odot$ yr^{-1} using the conversion given by Kennicutt (1983).

We have determined the luminosity of several extranuclear Hα features in this system (Table 1). These regions are not spatially resolved. B and C, which are between the galaxies and may be the result of the interaction, have Hα luminosities similar to the luminosities of the brightest H II regions in field spiral and luminous irregular galaxies (Kennicutt 1988). (Values must be converted to H_0=75 km $s^{-1}Mpc^{-1}$ for comparison with Kennicutt's results.) J and K, the features beyond the end of CG 692's spiral arm, have luminosities similar to those of 'giant' or 'supergiant' H II regions found in late-type normal or peculiar galaxies. The knots within the

Table 1. Hα Luminosities[1]

Feature	log[L(Hα)]
B	39.78
C	39.86
J	40.47
K	40.55
	log[L(Hα) arcsec^{-2}]
D	39.74
F	39.69
G	39.57
H	39.75

[1] H_0=50 km s^{-1}Mpc^{-1}

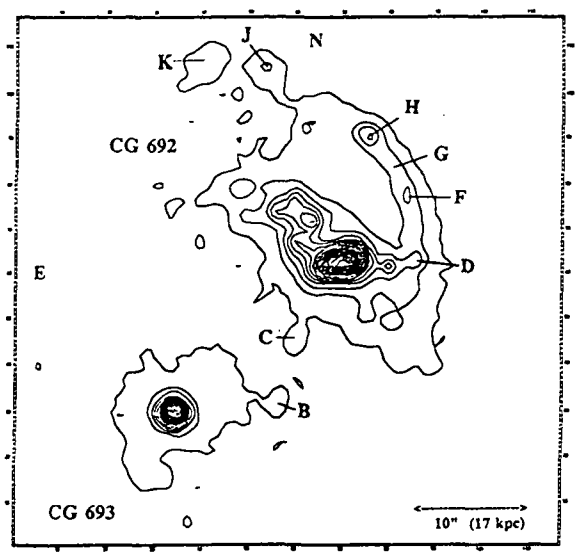

Fig. 1. Contour plot of the Hα image. The outermost contour represents a flux of 8.3x10^{-17}ergs cm^{-2} s^{-1}arcsec^{-2}. Successive contours increase in intervals of 2.76x10^{-16} ergs cm^{-2}s^{-1}arcsec^{-2}.

spiral arm are concentrations of emission embedded in an area of strong, extended Hα emission. In Table 1 we give the luminosities per square arcsec for several locations along the spiral arm. The total Hα emission from the strongest knot, H, is about 5.3 x 10^{40} ergs s^{-1}.

Kennicutt (1988) finds a relationship between the average luminosity of the brightest H II regions in a galaxy and that galaxy's absolute magnitude and Hubble type. M_B for CG 692 can be calculated from the apparent magnitude estimate given by Sanduleak & Pesch (1987). For CG 692, B = 15, giving M_B = -22.8. A discussion of the accuracy of the Case magnitudes is given by Weistrop & Downes (1991). Kennicutt's relationship predicts the mean luminosity of the brightest H II regions to be $\geq 10^{40}$ ergs s^{-1} for late type field or Virgo cluster spirals with M_B = -22 (H_0=75 km s^{-1}Mpc^{-1}). This is similar to the luminosity we obtain for the brightest extranuclear H II regions in CG 692.

This work was supported in part by NASA grant NAS5-31231.

References

Kennicutt, Jr., R.C. 1983, ApJ, 272, 54.
_____ 1988, ApJ, 344, 144.
Kennicutt, Jr., R.C., & Kent,S.M. 1983, AJ,88,1094.
Kennicutt, Jr., R.C., Keel,W.C., van der Hulst,J.M., Hummel, E., & Roettiger, K.A. 1987, AJ, 93, 1011.
Kirshner, R.P., Oemler, A.,Schechter,P.L., and Shectman, S.A. 1987, ApJ, 314, 493.
Sanduleak, N., & Pesch, P. 1987,ApJSS,63,809.
Weistrop, D., & Downes, R.A. 1991, AJ, 102, 1680.
Weistrop, D., *et al.* 1991, BAAS, 23,1428.
Weistrop, D., *et al.* 1992, ApJL (submitted).

Numerical Simulations of Bent, Disrupted Radio Jets

Chris Loken & Jack Burns
Dept. of Astronomy, New Mexico State University
Las Cruces, NM

Abstract

We present preliminary results from three-dimensional hydrodynamical simulations designed to investigate the physics of jet bending and disruption. The specific scenario considered here involves a mildly supersonic jet crossing a contact discontinuity at the interface between the interstellar medium (ISM) and the intercluster medium (ICM) and then encountering a cross-wind in the ICM. The resultant morphologies show many of the features observed in radio sources including jet flaring, bending and extended tails.

Introduction

WATs are generally the most luminous radio sources found in nearby rich clusters. Their morphological structure typically consists of two narrow, linear jets extending from the galaxy core for a distance of 10 - 50 kpc which symmetrically and suddenly transform into diffuse, edge-darkened tails up to a Mpc in length. The prototypical example is 3C 465 (e.g. Eilek *et al.* 1984) in A2634 but there is substantial variation in WAT morphologies (see e.g. O'Donoghue *et al.* 1990). Narrow-Angle Tailed (NAT) radio sources, such as 3C 83.1B in NGC 1265 (e.g. O'Dea and Owen, 1986), also exhibit bent jets. Clearly it is important to understand the processes involved in bending and disrupting jets but the inherent 3-D nature of the problem has severely limited numerical simulations until very recently.

Norman, Burns and Sulkanen (1988) carried out 2-D simulations which demonstrated that a jet could disrupt and flare upon passing through an external shock. Further 3-D investigation of this scenario was carried out by Balsara and Norman (1992) who passed a helically perturbed jet through an oblique shock in an effort to duplicate WAT behaviour. The same authors modelled the bending of narrow-angle tailed (NAT) radio sources in 3-D by propagating a jet through a cross-wind (with symmetry through the midplane of the jet enforced).

Jet Model

The atmosphere through which we propagate our jets consists of two uniform, static media separated by a contact discontinuity (a jump in density and temperature but not in pressure). A cross-wind blows parallel to the interface in the ICM (second medium). The jet travels first through the ISM and then encounters the ISM/ICM interface (oriented perpendicular to the jet axis). ZEUS-3D, a sophisticated Eulerian, finite-difference MHD code developed at NCSA was used for all our simulations (Clarke 1992, Stone and Norman 1992).

The simulation is completely characterized by 6 dimensionless numbers: the ratio of jet-to-ISM densities (η), the ratio of jet-to-ISM pressures (K), the internal Mach number of the jet ($M_j \equiv v_j/c_j$ where v_j is the jet velocity and c_j is the speed of sound in the jet), the ratio of ICM-to-ISM temperatures (ΔT), the Mach number of the wind ($M_w \equiv v_w/c_{icm}$ where v_w is the wind velocity and c_{icm} is the speed of sound in the ICM, $c_{icm} = \sqrt{\Delta T}\, c_{ism}$), and the distance from the jet origin to the ISM/ICM interface (X_{int}, in units of jet radii). We work in dimensionless units

with distances given in terms of jet radii (r_j) and the ISM density and sound-speed both set to unity.

The time evolution of one of our simulations is shown with logarithmic contours and velocity vectors in a slice through the symmetry plane of the jet in Fig. 1. The region shown is $60r_j \times 50r_j$ in size, spanned by 180×101 zones, and the jet radius is resolved laterally by 6 zones. A symmetry plane is assumed to reduce CPU time. Parameters are: $\eta = 0.02$, $K = 1.5$, $M_j = 3$, $\Delta T = 10$, $M_w = 0.5$, and $X_{int} = 10r_j$.

The cross-wind blows upwards in Fig. 1 and the resultant shear distorts the jet cocoon and drags it downstream of the jet. The wind sweeps away the cocoon on the upstream side of the jet, leaving it effectively naked. The jet is strongly bent at the contact discontinuity yet the flow remains continuous. In terms of jet radii, the radius of curvature of the jet is expected to be given by the ratio of the jet and crosswind ram pressures. For our model we get the expected radius of curvature to be $KM_j^2/M_w^2 = 54$ jet radii which is in rough agreement with the results of the simulation.

Fully three-dimensional simulations (no assumed symmetry plane) with a helical perturbation applied to the jet in order to break all symmetries have also been performed and yield similar results.

Conclusions

Our 3-D simulations reproduce many of the features seen in WATs and NATs including jet bending, flaring and the extended tails. We are currently investigating the results of projecting the fully 3-D model onto the sky in order to help identify features seen in radio maps.

This work was supported in part by a grant from the National Science Foundation (AST-9012353) to J.O.B.

References

Balsara, D. S., & Norman, M. L. 1992, *Ap. J.*, 393, 631.
Clarke, D. A. 1992, to appear in *Proceedings of the Ringberg Meeting on Extragalactic Radio Jets*, Springer-Verlag.
Eilek, J. A., Burns, J. O., O'Dea, C. P., & Owen, F. N. 1984 *Ap. J.*, 278, 37.
Norman, M. L., Burns, J. O., Sulkanen, M. E. 1988, *Nature*, **335**, 146.
O'Dea, C. P. & Owen, F. N. 1986, *Ap. J.*, 301, 841.
O'Donoghue, A. A., Owen, F. N., & Eilek, J. A. 1990, *Ap. J. Supp.*, 72, 75.
Stone, J. & Norman, M. L. 1992, *Ap. J. Supp.*, 80, 753.

Figure 1: Logarithmic density contours and velocity vectors for the 3-D simulation described in the text at scaled times t=3.5, 7.5 and 11.5. The crosswind velocity vectors are barely visible as they are so much smaller than the jet velocity.

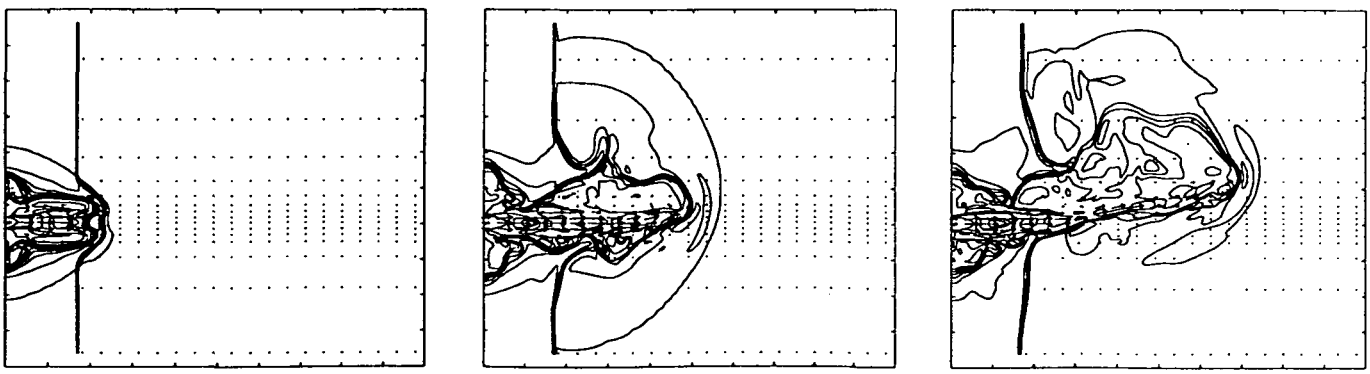

Numerical Models of Jet Disruption in Cluster Cooling Flows

N93-26814

Chris Loken, Jack Burns, Kurt Roettiger
Dept. of Astronomy, New Mexico State University
Las Cruces, NM 88003

Mike Norman
Dept. of Astronomy and National Center for Supercomputing Applications
University of Illinois, Urbana, IL 61801

Abstract

We present a coherent picture for the formation of the observed diverse radio morphological structures in dominant cluster galaxies based on the jet Mach number. Realistic, supersonic, steady-state cooling flow atmospheres are evolved numerically and then used as the ambient medium through which jets of various properties are propagated. Low Mach number jets effectively stagnate due to the ram pressure of the cooling flow atmosphere while medium Mach number jets become unstable and disrupt in the cooling flow to form amorphous structures. High Mach number jets manage to avoid disruption and are able to propagate through the cooling flow.

Introduction

X-ray observations have been used to infer the existence of cooling flows in a significant number of observed clusters (e.g. Jones and Forman 1984, Arnaud 1988). Burns (1990) found that $\approx 70\%$ of cDs with cooling inflows are radio-loud whereas $< 25\%$ of cDs in non-cooling flow rich clusters are radio-loud. Thus, cooling flow environs appear to be intimately linked with the existence of radio emission.

Many of the radio sources associated with dominant galaxies in cooling flow clusters are observed to have amorphous radio morphologies (Burns, 1990). Theses sources (e.g. 3C 317, Burns 1990) typically exhibit steep radio spectra, high rotation measures, small (50-100 kpc) diameters and small (< 1 kpc) or nonexistent jets. However, there are also good examples of extended, well-collimated jets in cooling flows - notably Cygnus A.

Since jet stability properties depend strongly on the internal jet Mach number, we propose that high Mach number jets manage to traverse cooling flows whereas their less powerful counterparts are disrupted and decollimated. In the latter case, the amorphous radio emission may then result from diffusion of the relativistic particles into the dense ICM or via a slow bulk flow of the poorly collimated radio plasma (Zhao 1990).

Cooling Flow Model

We have utilized ZEUS-3D, a sophisticated time-dependent hydrodynamics code (Clarke 1992, Stone and Norman 1992), to "relax" towards a steady-state cooling flow. We begin with an isothermal gas in hydrostatic equilibrium with the potential of a King model cluster and turn on radiative cooling. Mass drop-out is also included in these spherically-symmetric calculations.

Our "standard" cooling flow model assumes realistic cluster parameters with the gas initially in hydrostatic equilibrium at a temperature of 10^8 K. A steady-state cooling flow is established in a time just less than the initial cooling time of the central region with a sonic point at 0.73 kpc. The Mach number at the inner boundary (located at 0.4 kpc) is M=3 at this time.

Jet Stability

The cooling flow atmosphere derived above was used to initialize our 2-D hydrodynamical jet simulations performed with ZEUS-3D. Our geometry is the spherical coordinate analogue of the usual slab jet and

allows us to investigate non-axisymmetric instability modes. These modes are excited by means of a small perturbation, with frequency near the resonant frequency (e.g. Hardee and Norman 1988), applied to the θ-component of the jet velocity at the inlet.

The simulations discussed here have an inner boundary at 0.5 kpc and outer boundary at 20.5 kpc. Across this range, the density of the cooling flow atmosphere decreases monotonically by a factor of 10 while the temperature increases by a factor of 13. The Mach number of the cooling flow is M=1.8 at the inner boundary, corresponding to an inflow velocity of 280 km/s, and decreases to M=0.02 at the outer boundary. The jet radius at the inner boundary is fixed to be 0.1 kpc with an opening angle of 1^o.

In order for the jets to be able to propagate any significant distance through this particular atmosphere, we find that we need a relatively heavy ($\eta = 0.3$), overpressured ($K = 2$) jet. Mach numbers of 100, 25 and 6 were used in order to investigate the effect of jet Mach number upon the resultant morphology.

We scale the physical time as $t = t' r_j / M / c_a$ where r_j is the jet radius, M is the jet Mach number and c_a is the external soundspeed. Fig. 1 displays logarithmic density contours for the $M = 100, 25$ and 6 jets at $t' = 375, 375$ and 180, respectively. At this point the $M = 100$ jet is still propagating freely, the M=25 jet has begun flapping about and is hardly advancing and the M=6 jet has essentially been stagnant for half its lifetime. These results are in rough agreement with the linear stability analysis predictions of jet disruption occurring after $\sim (5-7) M r_j$ (e.g. Hardee and Norman, 1988).

Conclusions

We have begun to investigate the stability properties of radio jets propagating through realistic, cooling-flow atmospheres. We have demonstrated here that varying only the jet Mach number can result in a variety of possible radio morphologies. Low Mach number jets are not able to propagate through the cooling inflow resulting in compact structures; weak compact radio sources are commonly observed in association with dominant galaxies in clusters (Ball *et al.* 1992). Intermediate Mach number jets disrupt and can give rise to amorphous radio structures (e.g. 3C 317) whereas high Mach number jets can effectively blow through the cooling flow without being disrupted (e.g. Cygnus A).

This work was supported in part by a grant from the National Science Foundation (AST-9012353) to J.O.B. and M.L.N.

References

Arnaud, K. A. 1988, in *Cooling Flows in Clusters and Galaxies*, ed. A.C. Fabian (Dordrecht:Kluwer), p. 31.
Ball, R., Burns, J., & Loken, C. 1992, *Astron. J.*, in press.
Burns, J. O. 1990, *Astron. J.*, 99, 14.
Clarke, D. A. 1992, to appear in *Proceedings of the Ringberg Meeting on Extragalactic Radio Jets*, Springer-Verlag.
Hardee, P. E., & Norman, M. L. 1988, *Ap. J.*, 334, 70.
Jones, C.,& Forman, W. 1984, *Ap. J.*, 276, 38.
Stone, J. & Norman, M. L. 1992, *Ap. J. Supp.*, 80, 753.
Zhao, J.-H. 1990, thesis, University of New Mexico.

Fig. 1. Logarithmic density contours and velocity vectors for models with M=100, 25, and 6.

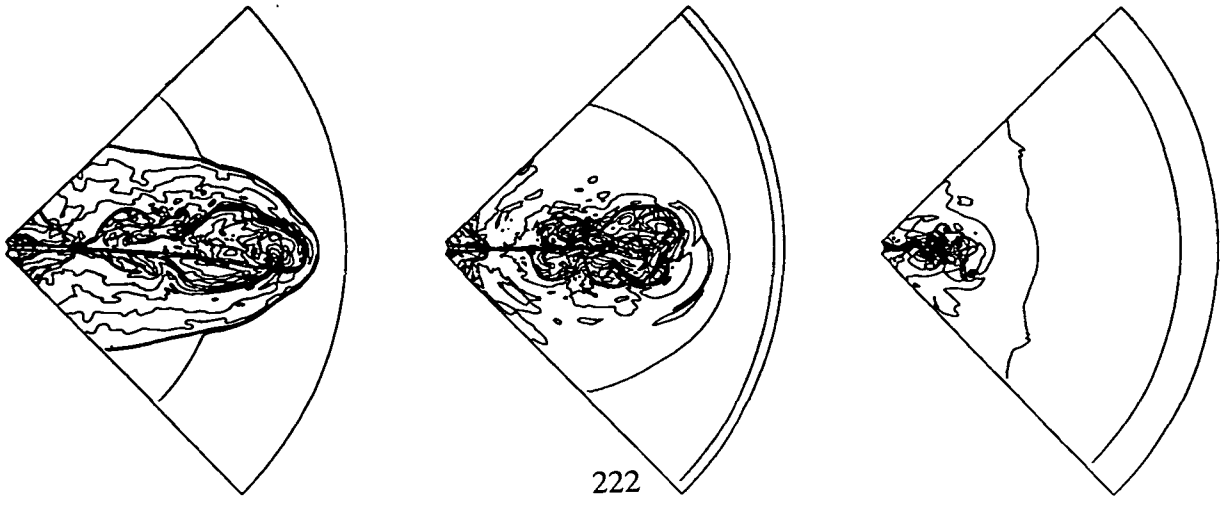

Atomic Hydrogen in the Disturbed Edge-on Galaxy NGC 4631

Richard J. Rand and J. M. van der Hulst

Kapteyn Astronomical Institute, Univ. of Groningen

Abstract. We present WSRT HI observations of the nearby, disturbed, edge-on galaxy NGC 4631. A low-resolution (45"x87") map shows previously unknown tidal debris at large distances from the plane, and two dwarf companions. A high-resolution (12"x22") map reveals a very disturbed gas layer in NGC 4631, with a wealth of small-scale structure. The most striking discovery is a supershell in the eastern half of the disk with a diameter of about 3 kpc, a mass of $\sim 10^8$ $M_\odot$ and a tentative expansion velocity of 45 km s^{-1}. If the expansion is real, the energy which must have been injected by supernovae to explain the shell's current parameters is roughly 4×10^{55} erg! Such a high energy requirement suggests an alternative formation mechanism, such as a collision with a small companion.

Introduction and Observations. NGC 4631 is a nearby (D=7.5 Mpc), nearly edge-on ($i = 85°$) galaxy which has a dwarf elliptical companion, NGC 4627, at about 3' NW of the nucleus, and an edge-on companion, NGC 4656, at about 30' to the SW. The system affords one of the best opportunities to see how interactions can disturb the gaseous layers of a galaxy. Previous WSRT observations (Weliachew, Sancisi & Guélin 1978), at a resolution of 48"x89", revealed a complex distribution of HI emission, with four long (20 to 50 kpc) spurs of gas protruding out of the warped main gas layer of the galaxy. Recent Hα observations by Rand, Kulkarni & Hester (1992) revealed a bright, thick, disturbed disk of ionized gas with much structure, patchy emission, and a few loops up to 1.5 kpc from the plane. There is also a 3–4 kpc diameter disturbance in the disk which, in projection, appears roughly circular. The interaction is presumably the cause of the strong star formation in NGC 4631 and the disturbances to its disk.

These results prompted several questions about the small-scale structure of the HI emission. How do the tidal features connect to the main disk? Do the disturbances in the ionized gas have HI counterparts? How disturbed is the gas layer in general? To address these issues, we mapped the system at the full resolution (12"x22") of the WSRT. A low-resolution (45"x87") map was also produced from this data set. Here we present some of the preliminary results.

Results and Discussion. The low-resolution map is not presented here but the results are briefly summarized. In addition to the four spurs found by Weliachew et al., very faint tidal debris can be seen extending in a large arc from Spur 3 (see Weliachew et al. for identifications), first to the north-east, then bending to the south. Also, two new compact sources have been detected. Both have optical counterparts on the Palomar Sky Survey, one catalogued (MCG+06-28-022), one not. The catalogued source lies about 30 kpc east-south-east of NGC 4631, has an HI mass of 2×10^7 $M_\odot$, and a velocity of $V_{hel} \approx 900$ km s^{-1}. The other source lies at about 50 kpc west-north-west of NGC 4631, has an HI mass of 5×10^7 $M_\odot$, and a velocity of $V_{hel} \approx 765$ km s^{-1}.

The high-resolution map reveals a wealth of substructure in the disk of NGC 4631, with many high-velocity and high-z features. Most striking is the discovery of a nearly complete supershell in the eastern half of the disk, with a diameter of 3 kpc and a mass of $\sim 10^8$ $M_\odot$, which is coincident with the circular feature in the *ionized* gas layer mentioned above (Figure 1). There is tentative kinematic evidence for expansion at 45 km s^{-1}. If the expansion is real, the kinetic energy is about 3×10^{54} erg, and the energy which must have been injected by supernovae to explain its current parameters is about 3×10^{55} erg, or the equivalent of 30,000 supernovae! The new ROSAT image of NGC 4631 (Walterbos, this volume) shows that there is an X-ray source near the center of the shell. The large energy requirement implies an unprecedentedly rich OB association for a galactic disk. Therefore, other formation mechanisms, such as a collision with a small companion, should not be ruled out. One clue as to its origin would be an association with the footprint of one of the four extraplanar spurs, but the evidence for such a connection is weak. How the shell formed therefore remains a matter of uncertainty.

References

Rand, R. J., Kulkarni, S. R., & Hester, J. J. 1992, ApJ, in press

Weliachew, L., Sancisi, R., & Guélin 1978, A&A, 65, 37

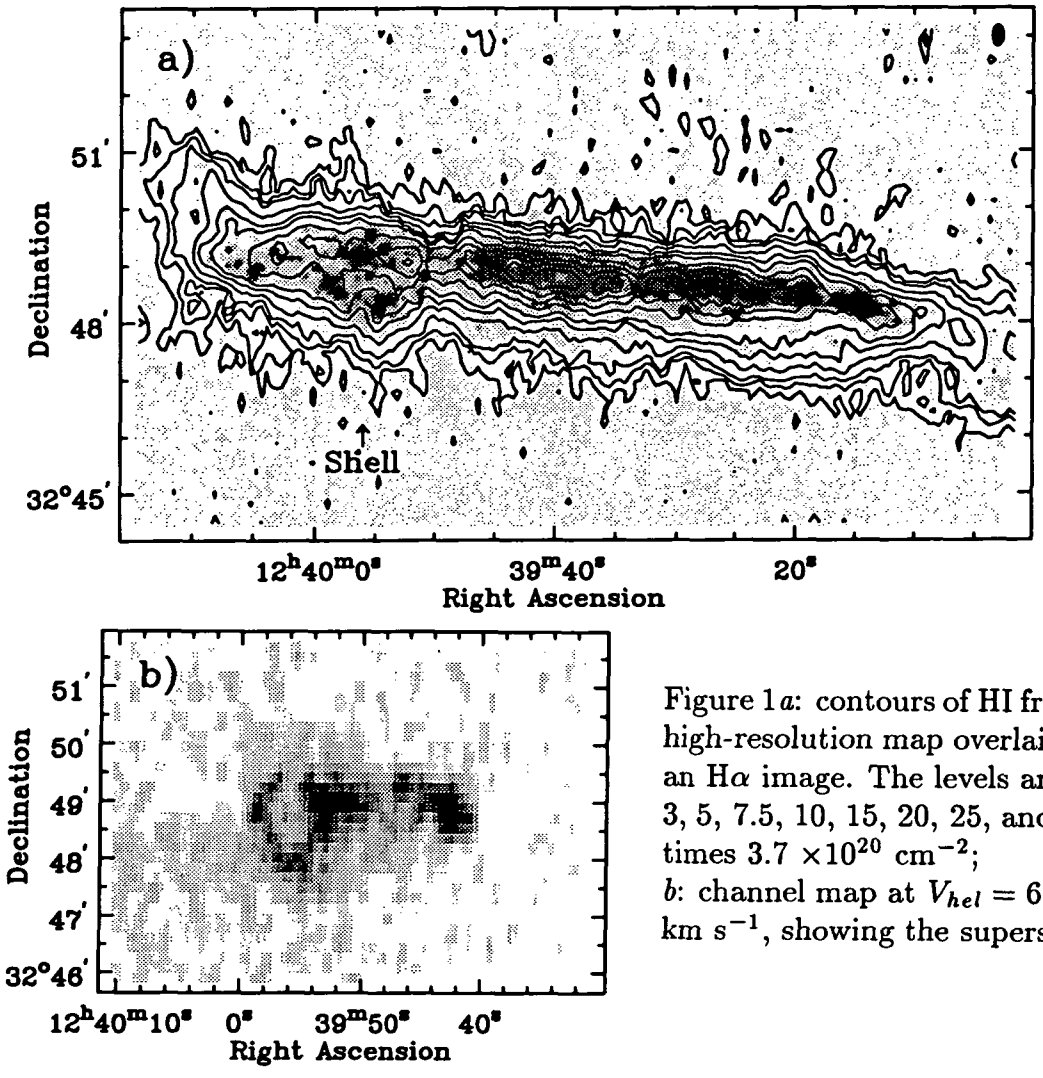

Figure 1*a*: contours of HI from the high-resolution map overlaid on an Hα image. The levels are 1, 2 3, 5, 7.5, 10, 15, 20, 25, and 30 times 3.7 $\times 10^{20}$ cm^{-2};
b: channel map at $V_{hel} = 675$ km s^{-1}, showing the supershell.

THE MORPHOLOGY OF AND LOCATIONS OF STAR FORMATION IN IMPACT INDUCED RING GALAXIES

by

Susan A. Lamb*†, Richard A. Gerber*, and Dinshaw S. Balsara†§

Observed ring galaxies appear to fall into two major types. The first tends to consist of isolated galaxies which display a smooth, apparently circular ring and a central nucleus. These have been variously classified as R(S) by de Vaucouleurs (1959) and as type O by Few and Madore (1986). The second class of ring galaxy nearly always has a close companion of comparable size (no less than about one tenth that of the ring galaxy). In these objects the ring is knotty in appearance, is usually elliptical, even when deprojected on the sky, and is often open on one side, having a 'horse shoe' or 'banana' shape. The nucleus does not usually appear at the center of the ring and is sometimes apparently absent, giving rise to an 'empty ring' galaxy. deVaucouleurs et al. (1976) designated this second type as RING, while Few and Madore (1986) have classified similar galaxies as P type. These galaxies have elevated far IR emission, bright HII regions, and blue spectral colors. The different environments of the two types or ring galaxy, together with their overall morphological and spectral differences suggest that the R(S)/O type are most probably the result of an instability that occurs in isolated galaxies, whereas the RING/P type appears to be the result of a recent collision between two roughly equal mass objects, at least one of which is a disk galaxy. Theys and Spiegel (1976) studied a sample of this latter type and identified three subclasses: RE: galaxies with crisp, empty rings; RN: galaxies like those of RE but with off-center nuclei; RK: galaxies having single dominant knots or condensations in the rings. A presentation of a preliminary understanding of the connections between these different observed forms in terms of parameters which are intrinsic to the galaxy system, such as time since collision and impact parameter, and in terms of our line of sight view is the purpose of this paper.

Here we report results we have obtained from three dimensional computer simulations of collisions between equal mass galaxies, one of which is a rotating, disk galaxy containing both gas and stars and the other is an elliptical containing stars only. We have used a combined n-body/SPH program (see Balsara,1990) to model fully self consistent models in which the halo mass is 2.5 times that of the disk and gas comprises ten percent of the disk mass.

In the experiments we have varied the impact parameter between zero (head on) and 0.9R (where R is the radius of the disk), for impacts perpendicular to the disk plane (see Gerber, Lamb, and Balsara, 1992b) and obtain a full ring (for head on collisions) or a partial ring (for off-center collisions), in both the stars and the gas. The results of our simulations, which cover a time period approximately equal to the dynamical time scale of the collision (typically a few times 10^8 years), when viewed from different lines of sight allow us to understand the gross connections between the different forms observed in RING/P type galaxies. For example, we find that:

1) The nucleus of the disk galaxy is always displaced out of the plane of the disk in the direction of travel of the elliptical and also that it will be offset from the center of the partial ring for off-center collisions. These two effects combine for off-center collisions to result in the nucleus appearing 'buried' in the ring for a non negligible range of viewing angles, thus leading to a natural explanation of the RE type of ring galaxy. In order to observe this effect, the disk plane must be tipped to the line of sight, and we expect that a viewing angle near 45°±15° would be optimal. A more face on view would reveal the nucleus to be distinct from the ring or arc and a more edge on view makes it hard to identify ring or arc structure in the galaxy. An example

* Department of Physics, University of Illinois at Urbana-Champaign.
† Department of Astronomy, University of Illinois at Urbana-Champaign.
§ Present address: Department of Astronomy, The Johns Hopkins University.

of a ring galaxy with an embedded nucleus is Arp 147. This object has been observed optically by, among others, Theys and Spiegel (1977) and more recently in the ultraviolet by Schultz *et al.* (1990) using the IUE satellite. In a recent paper, we were able to obtain a reasonable fit to the observed morphology and velocity data of this system (see Gerber, Lamb, and Balsara,1992a) using one of the off-center simulations discussed above.

2) The outwardly propagating ring or arc of excess density in the gas interacts with outer, infalling material to produce regions of shocks and dense gas, thus providing a region primed for star formation. In a head-on collision, the density wave moves outward as a ring; however, in off-center collisions the location of the densest regions has a more complicated history. In these latter cases, local maxima occur in the density of the disk at the impact point and at the nucleus at the time of impact. As the collision evolves the density at the nucleus diminishes somewhat due to the overall expansion of the disk galaxy subsequent to the impact; the density maxima at the impact point is spread into an arc by the differential rotation of the disk and develops several regions of high density within the arc structure. A typical configuration observed in several galaxies consists of two regions of high density in the arc, somewhat symmetrically situated on either side of the nucleus. Our numerical experiments show that this is a transient phenomena due to the combined effect of differential rotation in the disk, the expansion of the inner disk following the collision, and the continued infall of the outer disk. The one high density 'wing' is the remnant of the density enhancement produced at the impact point and the other is the result of strong collisions between infalling and expanding disk material.
3) As the ring or arc ages it becomes more diffuse and may tend to clump further.
4) More off-center collisions produce, among other things, more open arcs.
5) Regions of high volume gas densities do not necessarily coincide with regions of high surface gas densities. In many of our models the surface density, integrated along a given line of sight, peaks in the nucleus of the galaxy even though the volume gas density is greatest in the ring or arc. For this reason measured values of gas surface density alone may not be adequate for predicting the occurrence and quantity of star formation.

We conclude by stressing that those ring galaxies produced by collision provide a unique laboratory for the study of star formation in disturbed galaxies. The apparent sequential star formation identified by Appleton *et al.* (1991) and others can be understood in terms of the evolution of the high density structures produced by the collision. Thus, an experimental understanding of the evolution of the ring or arc structure for different collision parameters, together with an exploration of possible viewing angles, allows us to sequence observed galaxies and to thereby understand the star formation histories, not just for one system, but for galaxies of this general type.

REFERENCES

de Vaucouleurs, G., 1959, *Handbuch der Physik,* **53**, 275.

Few, J.M.A., and Madore, B.F., 1986, *M.N.R.A.S.*, **222**, 673.

de Vaucouleurs, G., de Vaucouleurs, A., and Corwin, H.,1976, *Second Reference Catalogue of Bright Galaxies*, University of Texas Press, Austin, Texas.

Theys, J.C., and Spiegel, E.A., 1976, *Ap.J.*, **208**, 650.

Balsara, D.S.,1990, *Ph.D. thesis. University of Illinois at Urbana-Champaign.*

Gerber, R.A., Lamb, S.A., and Balsara, D.S., 1992a, *submitted to Ap.J.Lett.*

Gerber, R.A., Lamb, S.A., and Balsara, D.S., 1992b, *in preparation.*

Schultz, A.B., Spight, L.D., Colegrove, P.T., and DiSanti, M.A., 1990, *in Massive Stars in Starbursts, STScI workshop.*

Appleton, P.N., Marston, A.P., Lysaght, M., and Struck-Marcell, C., 1991, *B.A.A.S.*, **23**, 1391.

The Critical Density for Star Formation in HII Galaxies

Christopher L. Taylor (N.R.A.O. and University of Minnesota)
Elias Brinks (N.R.A.O.)
Evan D. Skillman (University of Minnesota)

Introduction

The star formation rate (SFR) in galaxies is believed to obey a power law relation with local gas density, first proposed by Schmidt (1959). Kennicutt (1989) has shown that there is a threshold density above which star formation occurs, and for densities at or near the threshold density, the SFR is highly non-linear, leading to bursts of star formation. Skillman (1987) empirically determined this threshold for dwarf galaxies to be $\sim 1 \times 10^{21}$ cm^{-2}, at a linear resolution of 500 pc. During the course of our survey for HI companion clouds to HII galaxies (Taylor, Brinks & Skillman 1992, submitted) we obtained high resolution HI observations of five nearby HII galaxies. HII galaxies are low surface brightness, rich in HI, and contain one or a few high surface brightness knots whose optical spectra resemble those of HII regions. These knots are currently experiencing a burst of star formation. After Kennicutt (1989) we determine the critical density for star formation in the galaxies, and compare the predictions with radio and optical data.

Observations

We observed nine HII galaxies at the VLA with D-array in the 21-cm line in our survey for HI companion clouds. Each galaxy was observed for 70 minutes. The 4IF mode was used to simultaneously obtain low velocity resolution data (20 km s^{-1}) over a large velocity range, and high velocity resolution data (5 km s^{-1}) over the velocity range of each galaxy. The low resolution data cubes were searched, and four galaxies were found to have companions (Taylor *et al.* 1992). For those galaxies with companions, we made follow-up observations at the higher resolution C array, at high velocity resolution (5 km s^{-1}), which were combined with the D array data. The combined data have sufficient resolution for a detailed study of the HI distribution and kinematics of the HII galaxy/companion systems.

Some Theory

The instability condition for a thin isothermal gas disk is given by (Toomre 1964)

$$\Sigma_c \geq \left(\frac{\kappa \sigma}{\pi G m_p} \right) \tag{1}$$

where Σ_c is the critical surface density for instability, σ is the velocity dispersion of the gas, κ is the epicyclic frequency and m_p is the mass of a proton. As our galaxies are dominated by solid body rotation, $\kappa = 2\Omega$ is the appropriate choice, but even outside of regions of solid body rotation $\kappa \geq \Omega$ (Binney and Tremaine 1987). For σ we use 10 km s^{-1} (Gallagher and Hunter 1984), which is at most off by a factor of two.

Results

Using a position-velocity diagram to estimate each galaxy's rotation curve, we determined κ for the solid body region, with which we estimated the critical density for star formation for three of the four galaxies (the fourth was insufficiently resolved to obtain a reliable column density estimate). This value ranged between 4×10^{20} cm^{-2} to 3×10^{21} cm^{-2}, depending on the slope of the solid body rotation curves. It should be stressed that

the column densities are overestimates of surface densities, and that the rotation curve is underestimated, in both cases because no correction is made for galaxy inclination.

Comparing the HI distributions of the three galaxies with their blue POSS images, we find that the optical extent of each galaxy lies within its critical density contour. In two cases, the optical galaxy was within the $\kappa = 2\Omega$ contour, while in the third, that contour contained most of the optical image, but the $\kappa = \Omega$ contour contained it all. Apparently little or no star formation has occurred at densities under the predicted threshold densities. This must be considered cautiously, as star formation occurs on length scales an order of magnitude smaller than our beam size, which ranges from 2 to 6 kpc in size at the distance of the HII galaxies. Such a large beam size averages the column density over the area of the beam, effectively diluting it. Nevertheless, we find, as did Kennicutt, that a simple disk stability model agrees qualitatively with observations. It would be useful to increase the resolution of the observations to decrease the dilution and to get a better estimate of the inclination.

The Big Picture

This work is a follow up to a larger study, designed initially to search for extragalactic HI. Taylor, Brinks & Skillman (1992, submitted) pursued a new approach to search for extragalactic HI clouds, using HII galaxies as "pointers" to undetected companions. HII galaxies are believed to undergo bursts of star formation. One explanation of this bursting phenomenon is that they are triggered through gravitational interaction with nearby objects, such as another dwarf galaxy, a larger galaxy, or possibly an extragalactic HI cloud, as proposed by Brinks (1990). Taylor *et al.* (1992) reported the success of this approach in finding four companions in a sample of nine galaxies, and discuss the properties and implications of the companions. Of the four companions discovered, three have been identified with optical counterparts.

In the future, the high resolution data discussed here will allow for a more detailed study of the HI properties of the companions than in Taylor *et al.* . In addition we are undertaking a VLA D array survey of a complete, volume limited sample of HII galaxies. This sample will provide a statistical look at the properties of these interacting systems, both regarding the effects of interaction on star formation, and the frequency of companion occurrence.

REFERENCES

Binney, J. and Tremaine, S. 1987, Galactic Dynamics (Princeton: Princeton University Press).

Brinks, E. 1990, in Dynamics and Interactions of Galaxies, ed. R. Wielen (Springer-Verlag: Berlin), p.146.

Gallagher, J.S., and Hunter, D.A. 1984, ARAA, 22, 37.

Kennicutt, R.C. 1989, ApJ, 344, 685.

Schmidt, M. 1959, ApJ, 129, 243.

Skillman, E.D. 1987, in Star Formation in Galaxies, ed. C.J. Lonsdale Persson (NASA Conf. Pub. CP-2466:), p.263.

Toomre, A. 1964, ApJ, 139, 1217.

NUMERICAL SIMULATIONS OF GALACTIC WAKES

Eric A. Lufkin
Department of Physics and Astronomy
University of Alabama

It has long been supposed that the passage of a galaxy through a gaseous medium may produce an observable wake in the form of enhanced X-ray emission. This enhancement may be the result of a bow shock or, depending on the boundary conditions one assumes, a reflection shock downstream from the galaxy. The general problem of flow past a gravitating body has been studied previously by several authors. To simplify the calculations, one often assumes a point mass for the gravitating body (appropriate for accretion onto a compact object: e.g. numerical simulations by Fryxell et al., 1991 ApJ 371, 696 and references therein; Hunt 1971 MNRAS 154, 141) and either hypersonic or subsonic flow (e.g., analytic treatments by Ruderman & Spiegel 1971 ApJ 165, 1; Miller 1986 MNRAS 220, 713). A numerical calculation allows for arbitrary Mach number M as well as a nonsingular potential, which is more appropriate than a point mass when considering flow past a galaxy.

We have performed a series of numerical simulations which examine the simple but realistic case of a galaxy with a smooth potential corresponding to a King profile, and with no interstellar medium. This corresponds to the case of an early-type cluster galaxy that has previously been stripped of its gas. The simulations provide a numerical basis for future work involving galaxies with interstellar media. We use a time-explicit finite difference code (Lufkin & Hawley 1992, ApJ submitted) to obtain solutions to the nonlinear equations for adiabatic flow in axisymmetry. The computational grid covers a region extending 500 kpc from a stationary galaxy radially and along the symmetry axis. We use a graded mesh, allowing for full resolution near the galaxy. Because the assumed potential has a finite depth, no artificial inner boundary condition is necessary; reflection symmetry at the axis is assumed. With a total grid size of 64 radial $\times$ 128 vertical, each run requires approximately 5 minutes of cpu time on the NCSA Cray-2.

The initial configuration is that of uniform flow parallel to the axis throughout the computational domain. Gas enters at the $-z$ boundary, with velocity v_0 and temperature T_0. One can express the equations describing the flow in such a way that the gas density enters only through a logarithmic derivative. The flow is therefore insensitive to the value of the ambient density, provided the cooling time is long compared to a dynamical time. Hence, for a given perturbing potential, the flow properties are completely determined by the ambient temperature and velocity. However, because the X-ray emissivity is proportional to the square of the density, we choose ambient densities that are consistent with pressure equilibrium with a hot cluster atmopsphere.

The target galaxy has a potential well of finite depth corresponding to a velocity dispersion of about $250\,\mathrm{km\,s^{-1}}$ inside of 10 kpc. The highest velocities we consider here ($\sim 3000\,\mathrm{km\,s^{-1}}$) are probably rare in real clusters, but not impossible, as 3-D velocity dispersions exceed $2000\,\mathrm{km\,s^{-1}}$ in rich clusters. The mean free path is $l \sim 30\,T_8^2\,n^{-1}$ pc. Thus, shocks need be considered collisionless only at high temperature and low density (i.e., for a total number density $n \lesssim 10^{-2}$). Results are as follows:

- A bow shock develops quickly, within about one core radius of the center of the galaxy. The wings of the bow shock then stretch out along the Mach cone, with the flow asymptotically reaching a steady state. Full development of the shock takes less than about 5×10^8 yr. The shock arises solely from the gravitational perturbation caused by the galaxy's potential well, as there are no physical obstructions.
- The shock strength is sensitive to $\eta \equiv \frac{\text{local freefall time}}{\text{local crossing time}}$. That is, for a given impact parameter, a fluid particle is deflected most efficiently when the incident velocity is low, but not subsonic. We therefore see the strongest shocks at intermediate Mach numbers ($M \sim 2$) and low temperatures ($T \sim 10^7$ K).
- The Mach cone is a fair approximation to the shape of the wake, but is exact only in the weak-shock limit ($\eta \gg 1$). If the gas is heated significantly, the increased pressure buoys the shock out, so that the wake is slightly wider than one would expect from the Mach angle $\alpha = \sin^{-1}(1/M)$.
- The upstream flow is very nearly incompressible, as predicted analytically (references above).
- The perturbed velocity field shows no evidence of turbulence. This conclusion may change if 1) Axisymmetry is broken (full 3-D) or, 2) An obstruction is placed in the galaxy, either as a hard boundary or as a dense interstellar medium.
- The induced drag on the galaxy, calculated by direct summation, is within a factor of two of the value one would predict using analytic estimates for flow of a collisionless gas past a point mass. The drag rate is found to be inversely proportional to the gas velocity, also in agreement with the classical formula.
- The derived X-ray surface brightness profiles are neither limb-brightened nor limb-darkened. A mild density enhancement just at the shock is offset by the greater column through the interior.
- The wakes produced in low-temperature gas should be bright enough to observe with ROSAT. However, the low-temperature gas in clusters has been observed to have considerable filamentary structure on scales smaller than the size of the wakes (e.g., Sarazin et al. 1992 ApJ 389, L59).
- Wakes in hot gas ($T \sim 10^8$ K) are probably not observable. The simulated wake with $M = 2$ and $T = 10^7$ K is ten times brighter (bolometric luminosity, background subtracted) than the $M = 2, T = 8 \times 10^7$ run, assuming both have a total number density equal to 10^{-2} cm^{-3}. The former, with a conservative bolometric correction (25%), should be detectable by the proportional counter with S/N=5 in a five-minute integration. The low densities typical of hot, extended cluster atmospheres could make the latter very difficult to see, even if the hot gas is smoothly distributed.
- If wakes are seen in X-ray images, then they may provide direct measurements of galaxy velocities transverse to the line of sight. This assumes, however, that the temperature and the gas velocity with respect to the cluster mean are known. Wakes may also be illuminated by head-tail radio sources, where jets of relativistic particles are ejected transverse to the flow.

The Case of Missing ^{13}CO in Mergers

F. Casoli[1,2], C. Dupraz[2,1], F. Combes[2,1]

[1] Ecole Normale Supérieure, 24 rue Lhomond, F–75231 Paris Cedex 05, France
[2] DEMIRM, Observatoire de Paris, Section de Meudon, F–92195 Meudon Cedex, France

We present a comparison of the ^{13}CO and ^{12}CO emissions of six systems of merging galaxies : NGC 828, NGC 3256, NGC 4194, NGC 6240, Arp 220, and Arp 299. The observations were made in both J=1–0 and J=2–1 transitions with the IRAM 30 m and SEST 15 m telescopes. In all galaxies but NGC 828, the ^{13}CO is much weaker than in spiral galaxies. Figure 1 shows the ^{12}CO (1–0) and ^{13}CO (1–0) lines observed towards NGC 828, while Fig. 2 displays the same lines for NGC 4194. The average emissivity ratios measured at the few kiloparsec scale are :

$$^{12}CO\ (1–0) / {}^{13}CO\ (1–0) \approx 30,$$
$$^{12}CO\ (2–1) / {}^{13}CO\ (2–1) \approx 40.$$

These values are significantly larger than those usually measured in normal spiral galaxies, which are always between 5 and 15 for the J=1–0 line.

We show that such a peculiar behaviour cannot be interpreted as due to the dominant presence of diffuse gas and it cannot be attributed to optically thin CO emission either. The faint ^{13}CO emission of mergers must result from either an underabundance of ^{13}CO or an overabundance of ^{12}CO. They may be accounted for by different mechanisms :

• ^{13}CO molecules are more easily photodissociated than ^{12}CO ones – however our observations seem to rule out physical conditions characteristic of photodissociation regions ;

• in the course of the merging, large amounts of unprocessed gas, with a high [$^{12}CO/^{13}CO$] abundance ratio, are driven from the external regions of the progenitor galaxies to the new nucleus ; this could increase the [$^{12}CO/^{13}CO$] ratio by a factor of 2 ;

• the interstellar medium can also be quickly enriched in ^{12}C – thus in ^{12}CO – by a factor of 2, due to selective nucleosynthesis of this isotope (vs. ^{13}C) in the massive stars born during the starburst.

The last two processes can thus significantly contribute to the weakness of the ^{13}CO lines. The high ^{13}CO-to-^{12}CO line ratios that we have measured are due to the deep transformations that take place in the interstellar medium during the merging and the starburst : indeed, the only object with nearly normal line ratios, NGC 828, appears less perturbed and active in star formation than the other sources in the sample. In most mergers, the faintness of the ^{13}CO emission may indicate that the conversion factor from ^{12}CO emissivities to H_2 column densities could differ substantially from the standard galactic value.

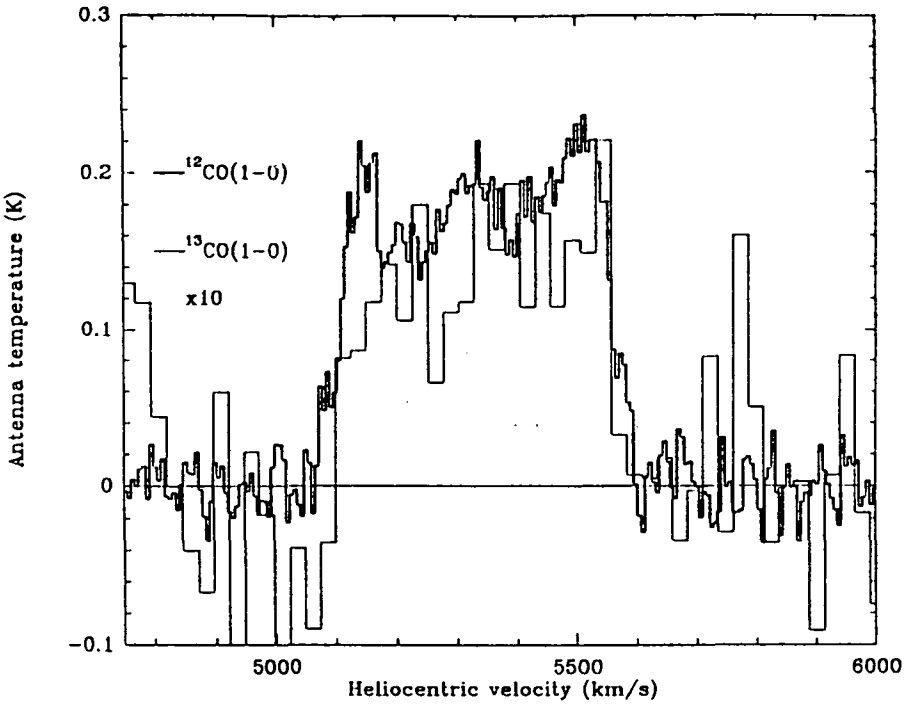

Figure 1 : The ^{13}CO emission of the merger NGC 828 is about 10 times weaker than its ^{12}CO emission, as found in normal galaxies (spirals).

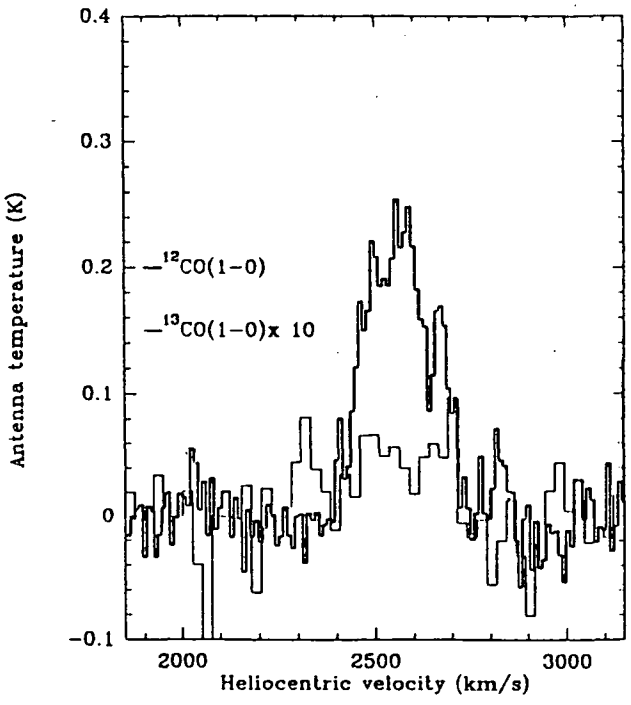

Figure 2 : The ^{13}CO line of the merger NGC 4194 is extremely weak : 55 ± 22 times weaker than the ^{12}CO line. This phenomenon is present in five mergers out of those six we have observed : NGC 3256, NGC 4194, NGC 6240, Arp 220, and Arp 299.

Density wave triggered star formation in grand design spirals

Cepa, J.; Beckman, J.E.; Knapen, J.H.
Instituto de Astrofísica de Canarias
E-3200 La Laguna
Tenerife
Spain

In normal spiral galaxies the arms are the main sites for star formation. This is the cause of their optical contrast compared with the rest of the disc. The spiral structure can be observed as a higher concentration of HII regions, neutral gas (both atomic and molecular via CO), dust and stars than in the interarm disc. It seems generally accepted that, at least in grand design spirals, there are density waves in the discs. However, several questions are not clear yet and still under discussion. An important question could be termed the *triggering dilemma* (by analogy with the "winding dilemma" raised in the forties): Is the enhanced star formation in the spiral arms triggered by the passage of a system of density waves or is it simply due to the presence of a higher column density of gas there?

In the present work, we use triggering in the same sense as the moderate to strong triggering defined by Elmegreen (1992), that is to say that star formation in the arms occurs at a rate faster than that in the interarm zone, relative to the available placental gas.

Our group has designed several tests to elucidate whether or not star formation is triggered in the arms with respect to the interam region and here we summarize one of them, that of the ratio of the star formation efficiency in the arms divided by that of the interarm zone at the same galactocentric distance which we may call the *relative massive star formation efficiency*, where the efficiency is defined using the ratio of the mass of stars (evaluated via the Hα flux) to the mass of neutral gas, atomic plus molecular (which must be measured with the adequate angular resolution). If the relative efficiency is of order unity, the star formation is proportional to the mass of gas, if some kind of induced star formation is present, the relative efficiency should be considerably larger than unity.

The relative star formation efficiency has been evaluated in great detail, up to now, in five spirals: NGC 628, NGC 3992 and M 33 (Cepa & Beckman 1990a), NGC 4321 (Cepa & Beckman 1990b) and M 51 (Knapen *et al* 1992). NGC 628, NGC 3992, NGC 4321 and M 51 are grand design spirals and M 33 is flocculent (Elmegreen 1987). The grand design spirals studied show relative efficiencies much larger than unity (of order 10–20) where all the arms of a given galaxy show a geometrically congruent pattern of peaks and dips (Figs. 1 and 2). The dips can be identified with resonances, the most conspicuous being the corotation radius (where the pattern speed and the velocity of the material of the disc are the same, and for this reason no triggering of star formation is to be expected). The region where the relative efficiencies are larger than unity is confined by the inner Lindblad resonance and the outer Lindblad resonance, the dominion of existence of a single mode of a density wave. These characteristics are in good agreement with the model of star formation triggering induced by a density wave, and would be difficult to account for by any of the alternative models which have been proposed to explain the presence of arms.

This situation of peaks and dips with relative efficiencies much larger than unity and coherent for all the arms is not present in the flocculent galaxy studied (M 33, as shown in Fig. 3) indicating that the star formation is not induced here by a resonant system, but could be a result of a self-propagating scenario (Seiden & Gerola 1982).

Cepa, J., Beckman, J.E. 1990a, ApJ, 349, 497
Cepa, J., Beckman, J.E. 1990b, ASS, 170, 209.
Elmegreen, D.M., Elmegreen, B.G. 1987, ApJ, 314, 3.
Elmegreen, B.G. 1992, in III Canary Islands Winter School, ed. G. Tenorio-Tagle, M. Prieto and F. Sánchez (Cambridge Univ. Press).
Elmegreen, B.G., Elmegreen, D.M., Seiden, P.E., 1989, ApJ, 343, 602
Knapen, J.H., Beckman, J.E., Cepa, J., van der Hulst, T., Rand, R.J. 1992, 385, L37.
Seiden, P.E., Gerola, H. 1982, Fund.Cosm.Phys., 7, 241.

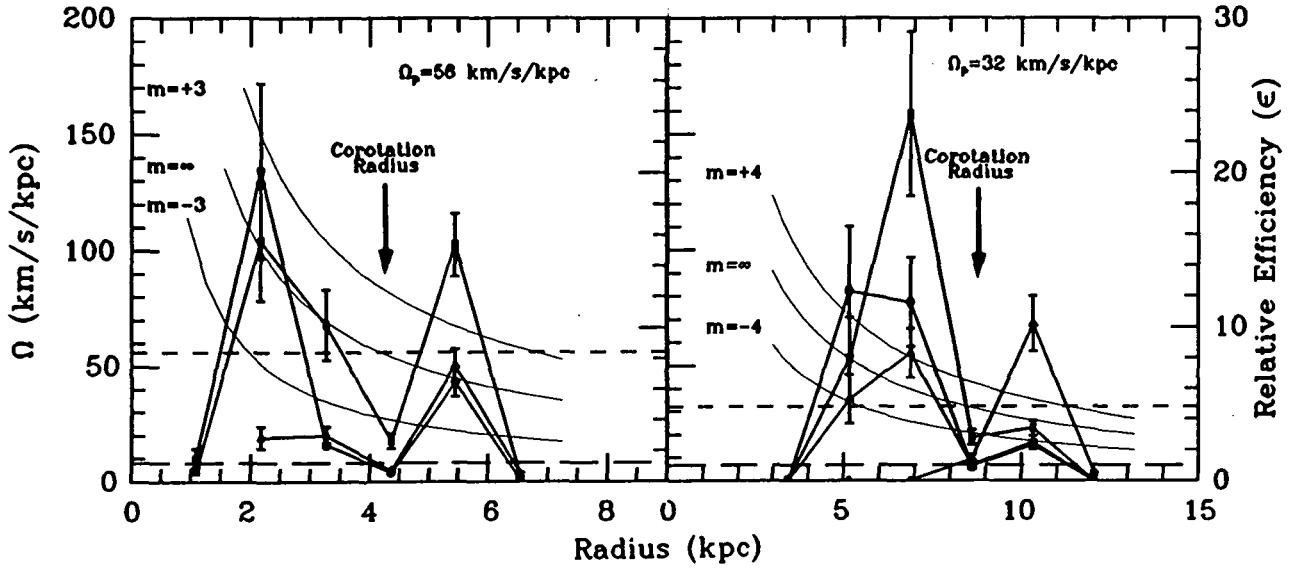

Figure 1.– Relative arm/interarm star formation efficiencies (scale on the right) for each arm of NGC 628 (left diagram) and NGC 3992 (right diagram) indicated by the continuous thick line. The continuous thin line shows the curves $\Omega + \kappa/m$ where Ω is the rotation curve, κ the epicyclic frequency and m the number of spiral arms (or mode). The corresponding scale is that on the left. The estimated values for the pattern speeds (Ω_p) are at the top of the diagrams and indicated by a dashed line. The intersections between the curves $\Omega + \kappa/m$ and Ω_p show the inner Lindblad resonance, the corotation radius and the outer Lindblad resonance, from lower to larger values of the radius. At resonances and corotation the efficiencies go down to unity peaking between them at values as high as 25, with the same qualitative behaviour with galactocentric radius in all arms of a given galaxy.

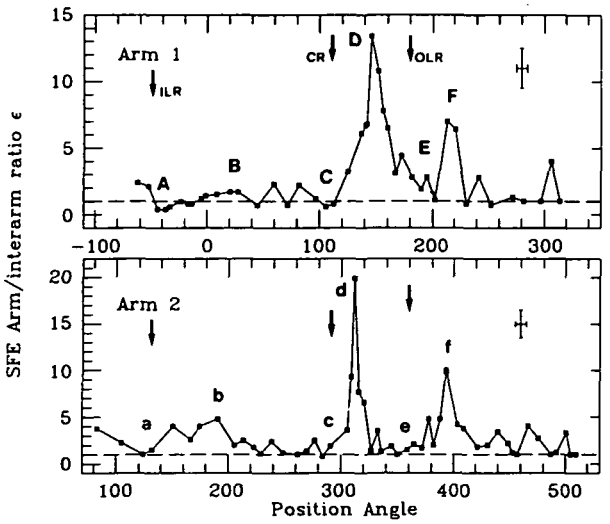

Figure 2.– Relative arm/interarm star formation efficiency for each arm of M 51 as a function of the position angle along the arms. Again, the same qualitative behaviour can be seen in both arms with relative efficiencies as high as 20 between the resonances identified by Elmegreen, Elmegreen and Seiden (1989) using broad band photometry.

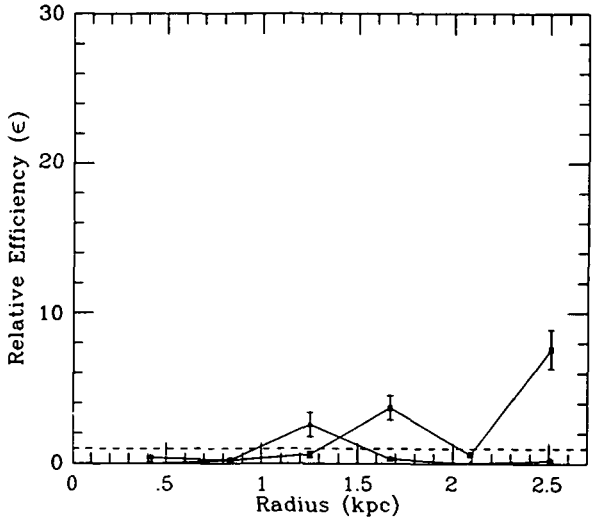

Figure 3.– Relative arm/interarm star formation efficiency for each arm of M 33 as a function of the radius. In this flocculent galaxy, the relative efficiencies are much lower than in the grand design spirals (Figs. 1 and 2), not rising to values above 4, except in the outermost point of one of the arms, which corresponds to NGC 604, a large and conspicuous HII region.

TIDAL INTERACTIONS AND THE FORMATION OF MAGELLANIC SPIRAL GALAXIES

S.C. Odewahn (U. Minnesota)
C.E. Woodward (Wyoming Infrared Observatory)
J.M. Bailey (Agnes Scott College)

The closest, brightest and best resolved galaxy in the sky, the Large Magellanic Cloud, is a prototype of the late-type disk systems referred to collectively as barred Magellanic spiral galaxies (SBm). These systems occupy a pivotal stage in the Hubble sequence since they represent the transition from spiral disk galaxies to chaotic, irregular galaxies and are characterized by an asymmetric spiral arm which emanates from one end of a high surface brightness bar. We present evidence that the formation of the one-armed spiral morphology involves the tidal interaction with a companion galaxy. In summary the major points of our observational investigation presented here are:

1. The vast majority of one-armed spiral galaxies possess bright nearby neighbors which appear to be physically associated.

2. The HI gas distribution and kinematics of one pair of SBm galaxies clearly reveal this system to be tidally interacting.

3. The infrared properties of the bars in two SBm galaxies support optical studies of bar luminosity profiles in late-type systems, and also suggest that the formation of compact star forming regions in these bars may not be uncommon.

Many of the classic cases of SBm morphology occur when a nearby neighbor galaxy is present. In some spectacular cases the neighbor galaxy also displays a one-armed spiral morphology. Could such a close match in galaxy types occur by accident, or could the formation of one-armed spirals be related to the mutual gravitational interaction of the two disks?

A search for neighbor galaxies in the vicinity of the largest ($\log D_{25} > 1.3$) Sm galaxies in the RC3 catalog was performed using the Palomar and UK Schmidt Sky Surveys. Statistical analysis of the data gathered in this survey revealed that among 75 galaxies with well classified asymmetric arms, only 4 were found to have no nearby neighbor within a separation of $5 \log D_{25}$. In fact, the classification of these 4 systems as Magellanic type galaxies is highly questionable (Corwin, private communication). In no case was a bright, dominant arm classified in a galaxy in which a clear neighbor galaxy was absent. The frequency distribution of apparent separations, which is strongly peaked at small separations, suggests that the observed galaxy pairs are not due to chance optical alignments, but are in fact the result of physical associations. Hence, scenarios invoking the formation of offset bars and/or dominant spiral arms through some tidal interaction mechanism might be attractive, since a common trait among the Sm galaxies appears to be the presence of a physical neighbor.

There is a high abundance of neighbor galaxies around SBm systems, and N body simulations of perturbed disks often produce one-armed spiral structures (Odewahn 1989). These facts support the idea that one-armed spiral features are produced through gravitational interaction. To identify signs of physical interaction in a paired SBm system, a HI kinematic study was undertaken using the VLA C and D array configurations. In Fig. 1, we present maps of the HI distribution, velocity field and velocity dispersion for the NGC4618-4625 system. Evidence that this is an interacting system can be seen in the bridge of HI extending from NGC 4625, and in the strong twisting of the kinematic line of nodes in the disk of NGC 4618. As explained by Bosma (1978), such nodal twisting in the outer regions of a disk is indicative of a strong warp which can be induced through tidal perturbations. A feature of additional interest is the degree of structure in the HI velocity dispersion map in NGC 4618. This is probably due to gas heating as a result of OB star formation in the arm region.

In conjunction with the kinematic observations, a systematic infrared study of the JHK properties of SBm systems has commenced using the new Simultaneous Quad Infrared Imaging Device (SQIID) at KPNO. In part, the objective of this imagery is to assess the role of dust absorption in determining the optical morphology and to deduce the stellar populations present in the bars. As discussed by Bothun (1990), combining high quality optical and infrared surface photometry will permit probing of the distribution of metallicity, age and rate of star formation throughout these systems.

In Fig. 2, we present an H-band image of NGC 4618. The IR morphology is very similar to the optical morphology derived from previous BVRI and Hα studies (Odewahn 1989). However, the bar light clearly dominates the total luminosity of the galaxy in the case of the IR, whereas the bar contributes only 10% to 15% of the total light in B. Elliptically averaged profiles in BVRHK (Fig. 3) have roughly the same form indicating very little change in exponential disk scale length from B to K. Of particular interest in the case of NGC 4618 was the structure of the bar. As predicted in Odewahn (1991) on the basis of optical photometry, the bar has a two lobed appearance in the IR. Linear profiles along the bar major axis (Fig. 4) reveal two peaks in the bar light from B to K. The northeastern peak appears to be due to a compact star forming region. The exponential decay in luminosity along the bar axis commonly observed in late-type barred galaxies (Elmegreen & Elmegreen 1985) is confirmed in the IR imaging of NGC 4618.

ACKNOWLEDGMENTS: This research was supported in part by the U. Wyoming Research Office and the Wyoming Faculty Grant-in-Aid Program. J.M.B. was supported by the NSF Research Experience for Undergraduates Grant AST91-00602.

References

Bosma A. 1979, Ph.D. Thesis, University of Groningen.
Bothun, G.D., 1991, *Astrophysics with Infrared Arrays*, ed. Richard Elston, 19.
Elmegreen, B. & Elmegreen, D. 1985, ApJ, **288**, 438.
Odewahn, S.C. 1991, AJ, **101**, 829.
Odewahn, S.C. 1989, Ph.D. Thesis, The University of Texas.

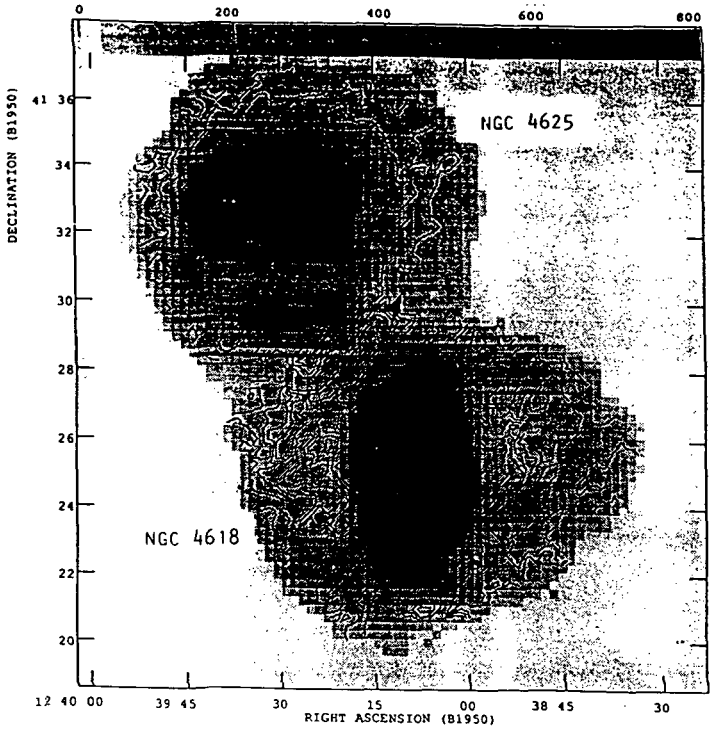
NGC 4625
NGC 4618
DECLINATION (B1950)
RIGHT ASCENSION (B1950)

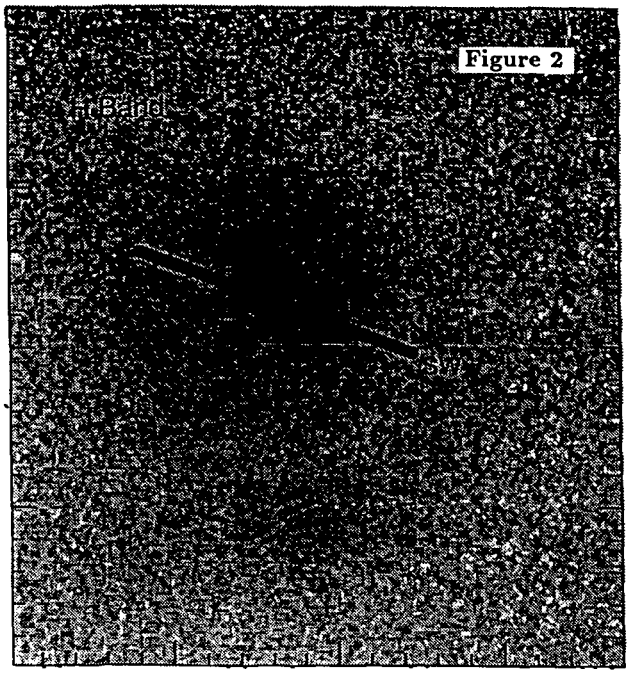
Figure 2
Bar

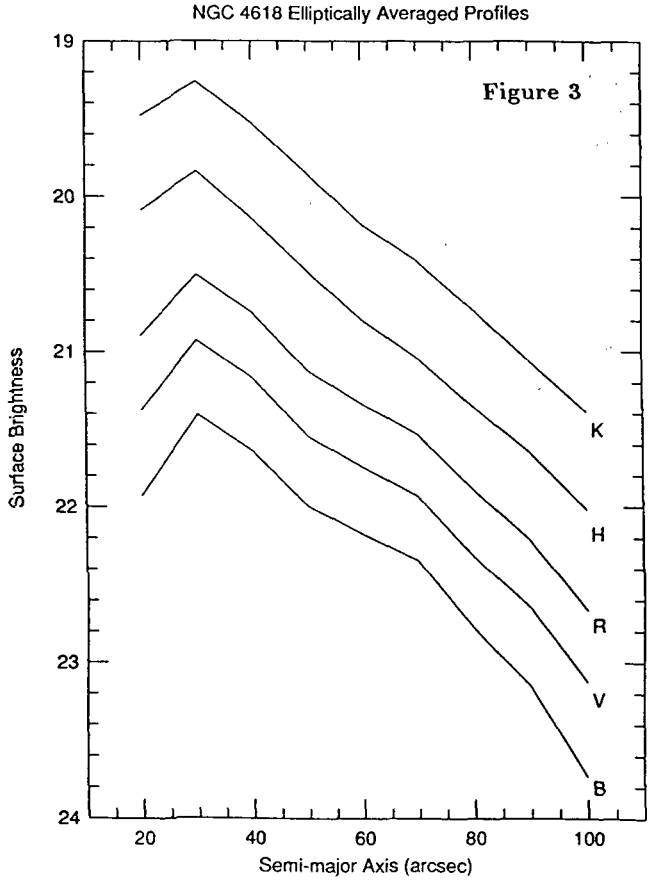
NGC 4618 Elliptically Averaged Profiles
Figure 3
Surface Brightness
Semi-major Axis (arcsec)
K
H
R
V
B

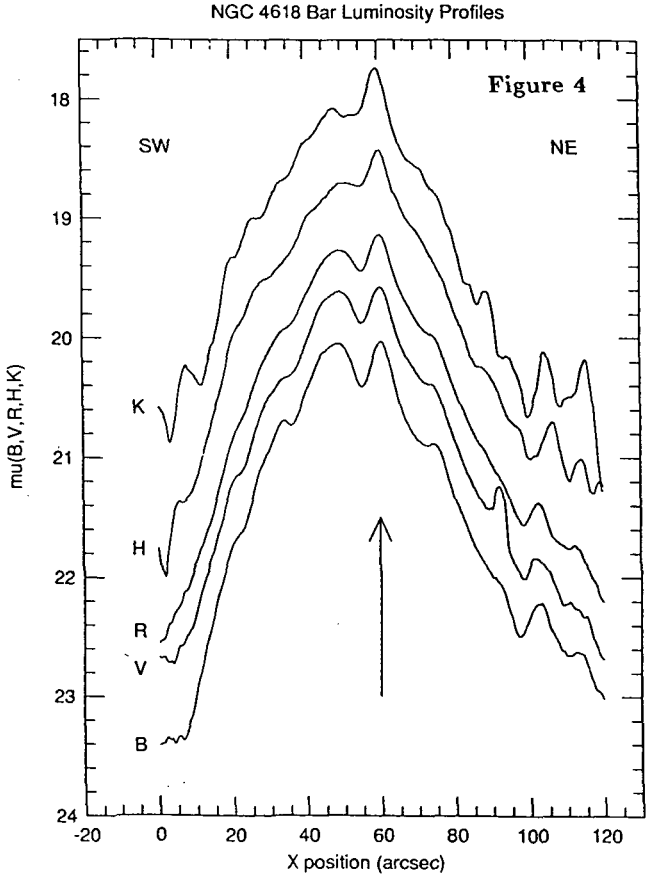
NGC 4618 Bar Luminosity Profiles
Figure 4
SW
NE
mu(B,V,R,H,K)
X position (arcsec)
K
H
R
V
B

FORMATION OF MASSIVE CLOUDS AND DWARF GALAXIES DURING TIDAL ENCOUNTERS

Michele Kaufman (Ohio St. U.), Bruce G. Elmegreen (IBM), Magnus Thomasson (Nordita), and Debra M. Elmegreen (Vassar)

Gerola et al. (1983) propose that isolated dwarf galaxies can form during galaxy interactions. As evidence of this process, Mirabel et al. (1991) find 10^9 $M_\odot$ clouds and star formation complexes at the outer ends of the tidal arms in the Antennae and Superantennae galaxies. We describe observations of HI clouds with mass $> 10^8$ $M_\odot$ in the interacting galaxy pair IC 2163/NGC 2207. This pair is important because we believe it represents an early stage in the formation of giant clouds during an encounter. We use a gravitational instability model to explain why the observed clouds are so massive and discuss a two-dimensional N-body simulation of an encounter that produces giant clouds. For more details see Elmegreen et al. (1992a).

VLA HI observations (Elmegreen et al. 1992b) reveal 10 giant clouds with HI mass in the range 1–5 $\times$ 10^8 $M_\odot$ in the outer parts and in the main disks of the galaxy pair IC 2163/NGC 2207 (see Fig. 1). One of the giant clouds in NGC 2207 lies between the optical spiral arms and shows no evidence of present star formation; this suggests it may be young. The measured velocity dispersion in each of these 10 clouds is typically about 40 km/s, the same as in much of the main disk of NGC 2207, but a factor of 4 times higher than for clouds in normal disk galaxies. The high velocity dispersion, which results from the agitation of the ISM by the galaxy interactions, appears to be the key to understanding why these giant clouds are at least 10 times more massive than the largest clouds in normal galaxies. In gravitational instability, the Jeans mass scales as the fourth power of the effective velocity dispersion. Giant clouds can form where the value of the Jeans mass is suitable and where the local value of the instability parameter Q for the gas is below threshold, e.g., in the outer regions and on the tidal arms. The time scale for these giant clouds to form by gravitational instability is 50–100 million years, and significant star formation should commence in about twice that time. This time scale is consistent with other evidence that IC 2163/NGC 2207 is a recent encounter.

We present results of an N-body gas + star simulation of an encounter between galaxies with extended gas disks and nearly equal mass. Giant complexes with a mass of about 10^8 $M_\odot$ and an internal velocity dispersion of about 25 km/s form in the tidal tail. The largest clumps in the simulations have a mass consistent with the Jeans mass and with the values observed in IC 2163/NGC 2207. In a simulation with a companion mass equal to 1.4 times the mass of the galaxy, giant complexes in the tidal tail escape to form independent dwarf galaxies.

This work was supported in part by NSF Grant AST-8914969 to M.K.

Elmegreen, B.G., Kaufman, M, Thomasson, M. 1992a, submitted to Ap. J.
Elmegreen, D.M., Kaufman, M., Brinks, E., Elmegreen, B.G. 1992b, in prep.
Gerola, H., Carnevali, P., Salpeter, E.E. 1983, Ap. J. **268**, L75.
Mirabel, I.F., Dottori, H., Lutz, D. 1991, Astr. Astrophys. **243**, 367.

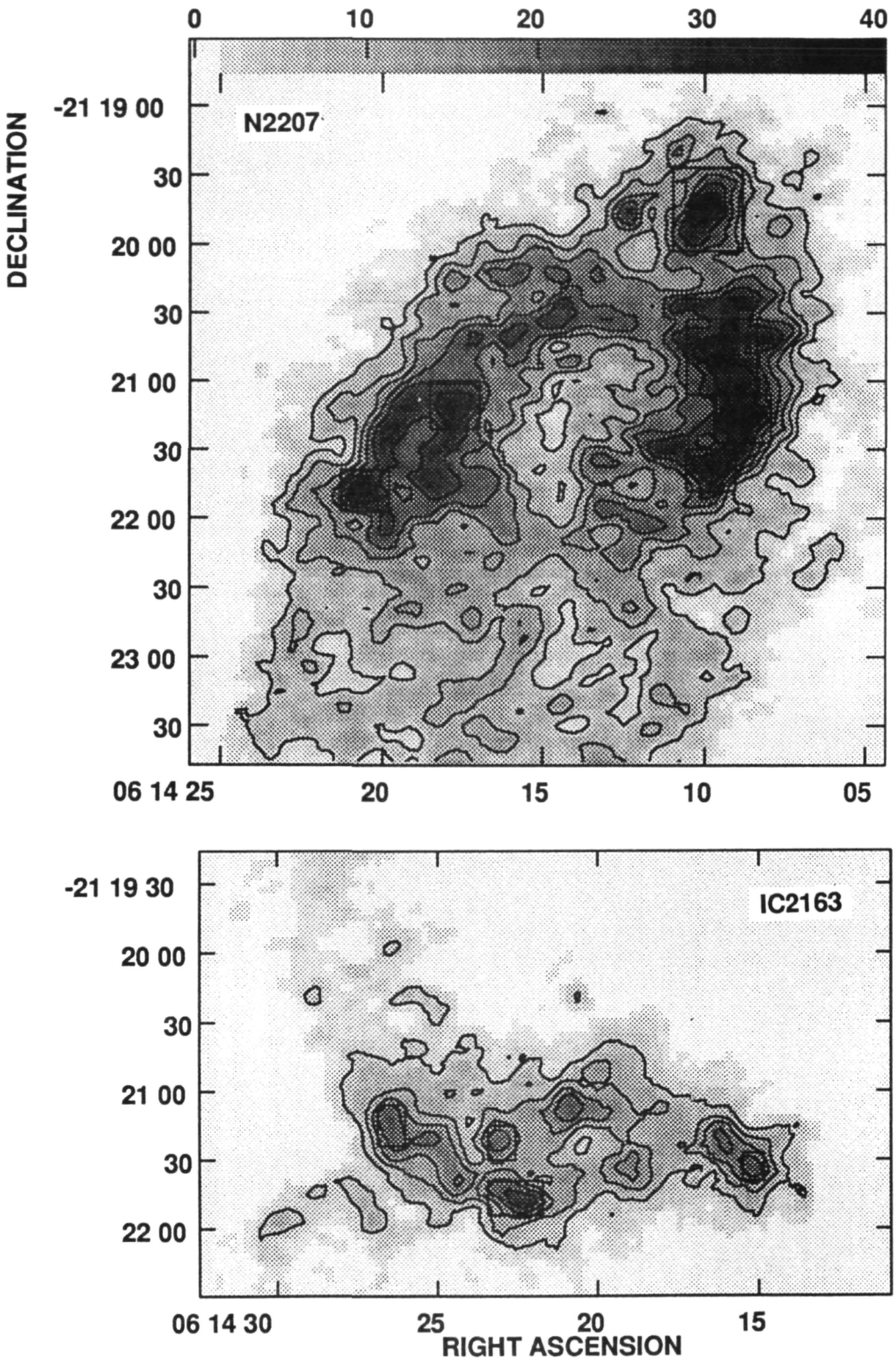

Figure 1. HI column density in IC 2163 and NGC 2207, presented as contours and as greyscale. The HI emission from the two galaxies was separated by using velocities and continuity. The greyscale wedge is labelled in units of $M_\odot$ pc^{-2}. Boxes are drawn around the 10 giant clouds.

MODELS OF THE CARTWHEEL RING GALAXY: SPOKES AND STARBURSTS

Curtis Struck-Marcell, Dept. of Phys. and Astron., Iowa State Univ., Ames, IA 50011

Recent observations of this famous ring galaxy, including optical and near-infrared CCD surface photometry (Higdon 1992a,c, in prep.; Marcum, Appleton and Higdon 1992, ApJ submitted), and VLA radio continuum and 21 cm. line mapping (Higdon 1992b, in prep.), have inspired a renewed modeling effort. Toomre's (1978, in The Large-scale Structure of the Universe, eds. Longair and Einasto) series of restricted three-body simulations demonstrated how the multiple rings could be produced in a nearly head-on galaxy collision. New models with a halo-dominated potential based on the 21 cm. rotation curve are able to reproduce such details as the spacing between rings, ring widths, offset of the nucleus, and several kinematical features, thus providing strong support for the collisional theory. (For details on these and the following results see Struck-Marcell and Higdon 1992, ApJ submitted).

The new observations have shown there are little or no old stars in Cartwheel; it may consist almost entirely of gas and stars produced as a result of compression in the ring wave. To model this process Smooth Particle Hydrodynamics (SPH) simulations of the Cartwheel disk have been performed. Fixed gravitational potentials were used to represent the Cartwheel and a roughly 30% mass collision partner. The interaction dynamics was treated treated as in the usual restricted three-body approximation, and the effects of local self-gravity between disk particles were calculated. We are particularly interested in testing the theory that enhanced star formation in waves is the result of gravitational instability in the compressed region (see e.g. Kennicutt 1989, ApJ 344, 685). The gas surface density in a number of simulations was initialized to a value slightly below the threshold for local gravitational instability throughout most of the disk. The first ring wave produces relatively modest compressions (a factor of order a few), triggering instability in a narrow range of wavelengths. Self-gravity in the disk is calculated over a comparable range of scales. Simulations were run with isothermal, adiabatic, and adiabatic with radiative cooling characterized by a relatively short timescale. The isothermal approximation is good except in the vicinity of the strong second (inner) ring, and several snapshots from one case are shown in the figure below.

Flocculent spiral segments are present before the collision, and these are compressed into dense knots in the ring wave. These knots are likely to be sites of vigorous star formation. In the strong rarefaction behind the outer ring most of the knots are radially stretched and sheared, giving rise to spoke-like features. A few dense knots are evidently very tightly bound, because they retain their coherence and are stretched relatively little through the rarefaction. This is in accord with evidence for continuing star formation in some spokes (Marcum, Appleton and Higdon 1992). The number and spacing of spokes is a direct function of the scale of the gravitational instability in the disk. Thus, the gravitational instability theory, together with the hypothesis that massive stars are only formed in dense knots of gas, can account for most of the distinct morphology of the Cartwheel. Some fine-tuning is required- the instability growth time must be less than the wave passage time. (In the Cartwheel models there are only a few growth times during the compressed phase.) But this helps explain why not all ring galaxies have multiple spokes. The simulations show that neither strong shocks, nor a greatly enhanced cloud collision rate, occur the outer ring, so evidently these processes are not the cause of the strong star formation in this galaxy.

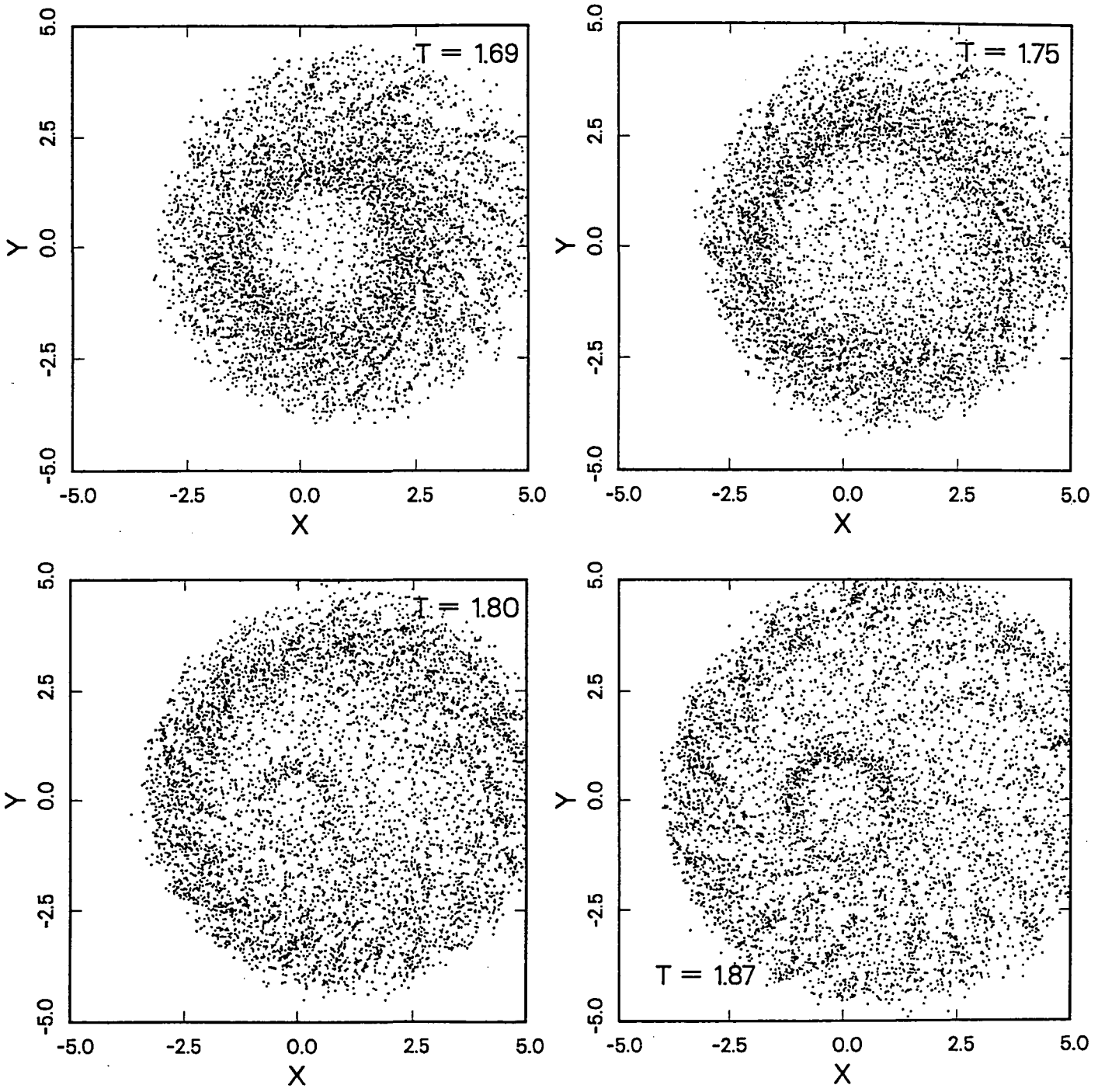

Snapshots of particle positions in a two-dimensional isothermal hydrodynamical simulation with local self-gravity computed over distances of $\Delta r = 0.4\gamma$, where γ is the scale-length of the gravitational potential. X and Y positions are also given in terms of this scale-length, see Struck-Marcell and Higdon (1992, ApJ submitted) for details.

CLUSTER TIDAL FIELDS: EFFECTS ON DISK GALAXIES

Monica Valluri
Department of Physics
Indian Institute of Science, Bangalore 560012, India.

Introduction

A variety of observations of galaxies in clusters indicate that the gas in these galaxies is strongly affected by the cluster environment. Here we present results of a study of the dynamical effects of the mean cluster tidal field on a disk galaxy as it falls into a cluster for the first time on a bound orbit with constant angular momentum (Valluri 1992). The problem is studied in the restricted 3-body framework. The cluster is modelled by a modified Hubble potential and the disk galaxy is modelled as a flattened, spheroid.

In the model adopted the galaxy experiences a mean tidal field which is strongest within 2 core radii of the cluster centre and is compressive within the core. The effect of the cluster tidal field on the disk galaxy resembles the phenomenon of compressive shocking of globular clusters by the Galactic disk (Ostriker, Spitzer & Chevalier 1972). Also since the time taken for the galaxy to cross the core (a few times 10^8 yrs) is comparable to the rotation time in the disk, the tidal perturbation may be considered to have a "pattern frequency" Ω_p, which is comparable to the rotation frequency in the disk $\Omega(R)$ and the epicyclic frequency κ. Thus resonances can enhance the tidal effects.

Thickening the Disks of Spiral Galaxies

The tidal effects on the disk are seen in the changes in the velocities of test particles. Gas clouds are represented by particles with low random velocities (5-10 $\mathrm{km\,s^{-1}}$) and stars are represented by particles with random velocities of 20-35 $\mathrm{km\,s^{-1}}$). The low velocity dispersion gas clouds experience a relatively larger increase in random velocity than the hotter stellar component. A strong tidal field increases the planar random velocities of all particles to between 50–60 $\mathrm{km\,s^{-1}}$. In most cases the vertical dispersion of particles is almost unaffected because the frequency of vertical oscillation is nearly an order of magnitude higher than the "pattern frequency" making the encounter adiabatic in the vertical direction.

The increase in planar random velocities results in a strong anisotropy between the planar and vertical velocity dispersions. Previous analytic (Kulsrud, Mark and Caruso 1971) and numerical (Raha *et. al.* 1991) work has shown that in such a situation the disk will become unstable to the "fire-hose instability" which leads

to bending modes normal to the disk. This helps to transfer planar kinetic energy to energy of vertical motion and results in an increase in disk thickness. Using energy conservation considerations we estimate that the disk thickness will increase typically be a factor of 1.5-2.0.

Gas Infall and Starburst

The spatial distribution of particles is also strongly perturbed by the tidal field. A disk parallel to its orbital plane in the cluster develops a spiral pattern primarily due to the bisymmetry in the tidal field. Circular orbits have resonaces at Ω and $\Omega \pm \kappa/2$, and these enhance the tidal perturbation producing a kinematic spiral pattern (Kalnajs 1973).

A disk which is perpendicular or inclined to the orbital plane, is transiently compressed as it passes through the cluster core. The originally circular disk is deformed into an oval or ellispe. The disk re-expands to 1.5 times its original size after it leaves the core region indicating a heating of the disk. Disks inclined to the orbital plane form transient warps which are fairly pronounced especially in the gas component.

These transient non-axisymmetric perturbations will transport angular momentum (Palmer & Papaloizou 1982). Simultaneously increasing the cloud velocity dispersion increases the frequency of cloud collisions leading to kinetic energy dissipation. These two processes can together lead to gas infall to the galaxy center and subsequently an enhanced rate of star formation. We also suggest that the mean tidal fields of rich clusters could have been stronger in the past particularly at the epoch of cluster formation and could have trigger activity in spiral galaxies in high red-shift clusters (the Butcher–Oemler clusters).

Acknowledgement: I am grateful to the Council of Scientific and Industrial Research, India, and Organisers of the 3rd Teton meeting for financial assistance. A special note of thanks to Harley Thronson for hospitality and for having made it all possible.

References

Kalnajs, A.J. 1973, Proc. Astr. Soc. Austr. 2, 174.
Kulsrud, R.M., Mark, W.-K. & Caruso, A. 1971, Astr. Sp. Sci, 14, 52.
Ostriker, J.P., Spitzer, L. & Chevalier, R.A. 1971, ApJ, 176, L51.
Palmer, P.L. & papaloizou, J. 1982, MNRAS, 199, 869.
Raha, N., Sellwood, J.A., James, J.A. & Kahn,F.D. 1991, Nature, 352, 411.
Valluri, M. 1992 ApJ, Preprint (Submitted)

HIGH CHEMICAL ABUNDANCES IN STRIPPED VIRGO SPIRAL GALAXIES

E. D. Skillman (U. Minnesota)
R. C. Kennicutt (U. Arizona)
G. A. Shields (U. Texas)

Based on a comparison of the oxygen abundances in H II regions in field and Virgo cluster late type spiral galaxies, Shields, Skillman, & Kennicutt (1991) suggested that the highly stripped spiral galaxies in the Virgo cluster have systematically higher abundances than comparable field galaxies.

In April 1991 and May 1992 we used the blue channel spectrograph on the MMT to obtain new observations of 30 H II regions in Virgo spiral galaxies. These spectra cover the wavelength range from [O II] λ3727 to [S II] λ6731. We now have observed at least 4 H II regions in 9 spiral galaxies in the Virgo cluster. Combining [O II] and [O III] line strengths, we calculate the H II region oxygen abundances based on the empirical calibration of Edmunds & Pagel (1984). Figure 1 shows a mosaic of empirical oxygen abundances versus galactic radius (normalized to effective radius) for the 9 Virgo spirals. Figure 2 compares the (HI diameter/optical diameter) ratios for the galaxies in Warmels (1986) field sample to those of our observed Virgo spirals as a function of RC3 morphological T-type. These observations show: 1) The stripped, low luminosity Virgo spirals (N4689, N4571) truly have abundances characteristic of much more luminous field spirals; 2) Virgo spirals which show no evidence of stripping (N4651, N4713) have abundances comparable to field galaxies; and 3) Evidence for transition galaxies (e.g., N4254, N4321), with marginally stripped disks and marginal abundance enhancements.

The new observations presented here confirm the validity of the oxygen overabundances in the stripped Virgo spirals. Shields et al. (1991) discussed two different mechanisms for producing the higher abundances in the disks of stripped galaxies in Virgo. The first is the suppression of infall of near-primordial material, the second is the suppression of radial inflow of metal-poor gas. Distinguishing between the two cases will require more observations of the Virgo cluster spirals and a better understanding of which parameters determine the variation of abundance with radius in field spirals (cf., Garnett & Shields 1987).

References

Edmunds, M.G., & Pagel, B.E.J. 1984, MNRAS, 211, 507.
Garnett, D.R., & Shields, G.A. 1987, ApJ, 317, 82.
Shields, Skillman, & Kennicutt 1991, ApJ, 371, 82.
Warmels, R.H. 1986, Ph.D. thesis, Groningen University.

Figure 1: Radial Oxygen Abundance Gradients for 9 Virgo Spirals

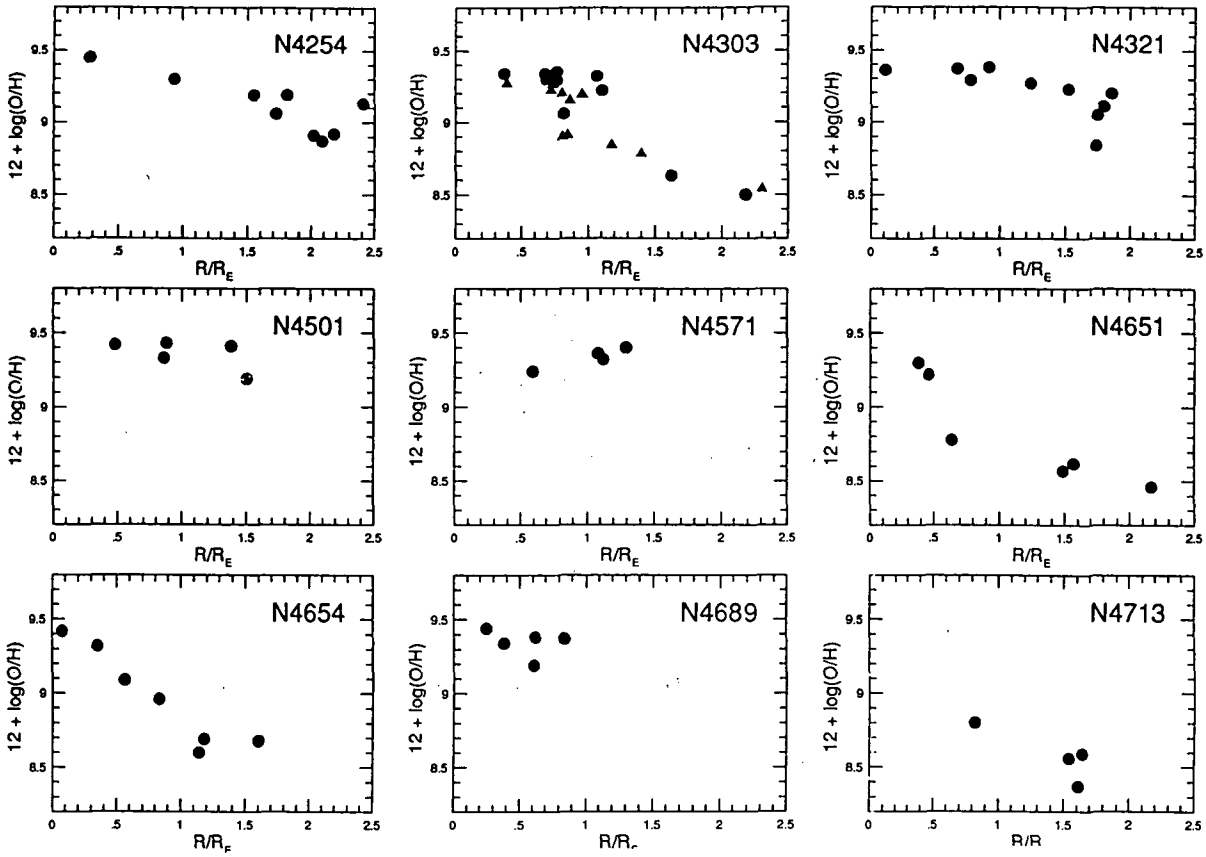

Figure 2: Virgo Galaxies vs. Warmels Field Sample

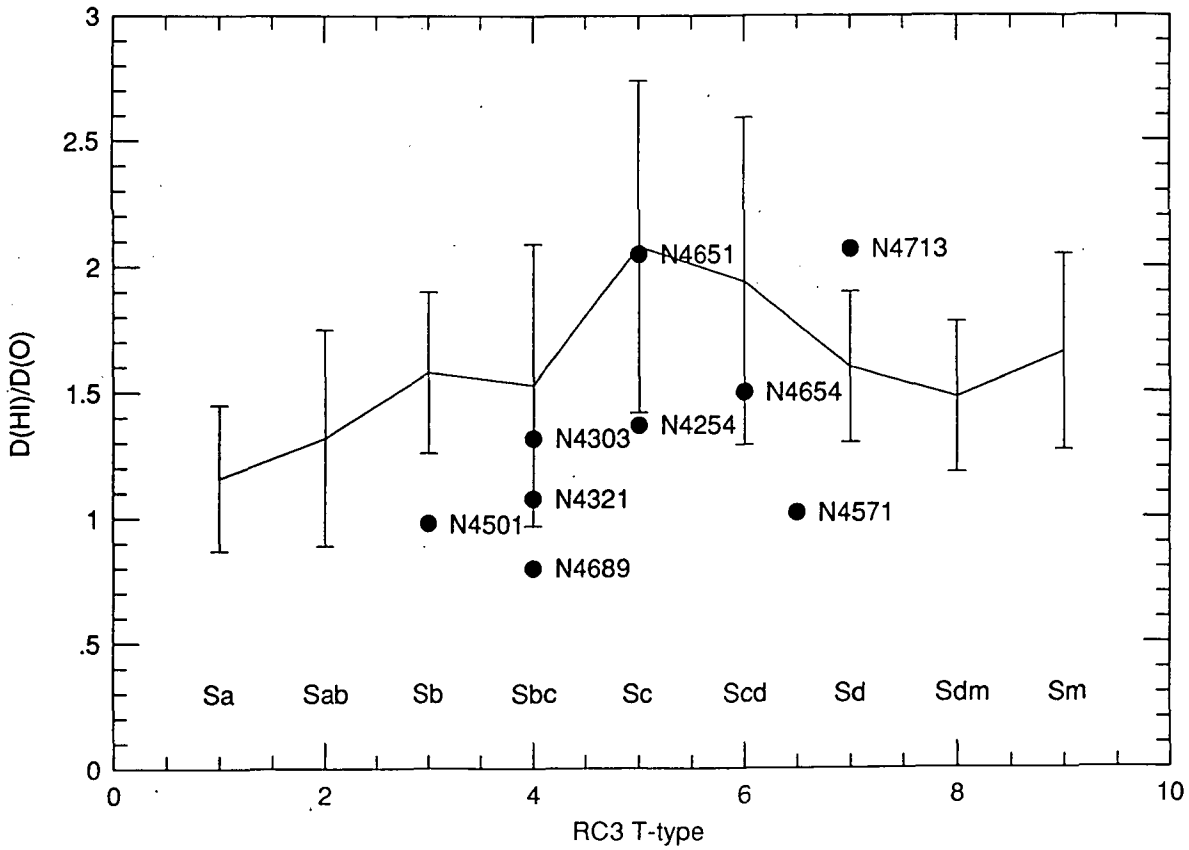

DEEP Hα IMAGES OF INTERACTING GALAXIES

S.C.Beck and O. Kovo
School of Physics and Astronomy, Tel Aviv University
Ramat Aviv, ISRAEL

I.Introduction and Motivation

Gravitational interactions between galaxies are believed to increase star formation activity dramatically, and most of the brightest starburst galaxies show clear signs of recent interactions. However, it is still not known how interaction triggers star formation, nor are there models to relate the type or strength of interaction to the location or amount of star formation. We report here on a series of deep Hα images of interacting and post-interaction galaxies which we took with the purpose of finding the young stars and ionized gas in these objects. We wre motivated in part by the hope that by studying the very recently formed stars we could see how the interaction process had affected the star formation.

II. The Sample

The galaxies selected show clear signs of having been through strong interactions. Most have HI plumes, filaments or tails, which are thought to be evidence for close interactions or actual mergers. We paid particular attention to the M81-M82-NGC3077 group because of Ho and Hun's detailed HI study which showed how HI is being transferred between the galaxies, to NGC 2782 because of its beautiful recently discovered HI plume, and to NGC 5253, although HI information is not available, because it is thought to be interacting with M83 and the two of them are candidates for the youngest starbursts known.

III. Observations and Results

We observed the galaxies through 50 Å-wide filters, one on the redshifted Hα line and one off, and a standard R filter. Depending on the galaxy and conditions, images in the B,V, and I filters were also obtained. The images were recorded with a 4x7' or 17' diameter CCD at the 1-meter telescope of the Wise Observatory in Mitzpe Ramon.

The Hα and continuum images are used, together with observations at other wavelengths, to put together as complete as picture as possible of star formation and interactions in each galaxies. The complete observation set is not yet available for all the galaxies but certain results are already clear. There do not seem to be any correlations between HI and Hα structures. In some HI plume galaxies Hα extensions were seen on the other side of the galaxy from the HI; in others extensive Hα filaments have been found but not HI. The preliminary results agree with the simplest model that interaction-induced star formation will be concentrated in the system center, since that is where the mass ends up.

DISSIPATIVE MERGING OF GALAXIES

M. UMEMURA
Princeton University Observatory /
National Astronomical Observatory of Japan

ABSTRACT. The galaxy merging is investigated with hydrodynamical processes taken into account. For this purpose, the 3D calculations are performed by the use of a smoothed particle hydrodynamics (SPH) scheme combined with an N-body sheme. In these calculations, we find a new merging criterion and the dependence of the central phase space density of merger remnants upon the gas fraction in progenitors. It is concluded that ellpticals can be formed just by merging of fairly gas rich primordial galaxies, not ordinary spiral galaxies.

1. Introduction

The calculations for galaxy interaction have been performed so far mainly by the N-body simulations of collisionless particles. They have succeeded in accounting for some properties of elliptical galaxies such as the $r^{1/4}$ law of surface density profiles. On the other hand, one physical problem has not been solved, that is, the problem of central phase space density. In purely collisionless merging, the phase space density should be perfectly conserved, while that in elliptical galaxies is by about two orders higher than in spirals.

Focusing on this problem, I've performed 3D hydrodynamical calculations of galaxy merger, using an SPH scheme combined with N-body scheme, and pursued the dynamical evolution of both collisionless stellar component and gaseous matter.

2. Model Galaxies

I assume exponential disks for progenitors: $I(r) = I_0 \exp(-r/r_d)$, $r_d = 5$kpc. The total mass of a progenitor is $10^{10} M_\odot$. And I consider the gaseous mass fraction of 0.01, 0.1, or 0.5. The gas is postulated to be isothermal with $T_g = 2 \times 10^4$K. At present the progenitors are composed just of stars and gas, not including dark halos. As for the kinematics inside a progenitor, the rotational velocities are decided so that the centrifugal force balances to the gravitational field at each point. These progenitors encounter each other in a parabolic orbit.

3. Numerical Results

i) Merging Criterion

It is a intuitive way to use the impulse approximation for a merging criterion taking into account dissipative effect. Then the change of total energy is

$$\frac{\Delta E}{E} = \frac{32 G^2 M^2 R_G^2}{3 r_p^4 v^4} + \beta \frac{M_g}{M}, \qquad (1)$$

where M, M_g, and R_G are the total mass, gaseous mass, and radius of a progenitor, respectively, r_p is the pericentric distance, and v is the relative velocity at r_p. When we adopt the condition

$\Delta E/E \geq 1$ as a conventional merging criterion, we get, using the virial theorem,

$$\alpha \gtrsim 1 - \beta \frac{M_g}{M}, \quad \alpha = \frac{32}{3}\left(\frac{R_G \sigma_*}{r_p v}\right)^4, \tag{2}$$

where σ_* is the stellar velocity dispersion or rotational velocity in a progenitor. The β is an unknown parameter which comes from dissipative effect, and should be determined in numerical simulations.

In numerical simulations, I adopted $r_p = 4.53$ kpc and $v = 200$ km s^{-1}, which corresponds to $\alpha = 0.75$. This means that this encounter doesn't satisfy the merging criterion without the dissipative effect. The simulations with 1% gas fraction have shown several clumps left after the collision. In the case of 10% gas fraction, there were two remnants left finally. And the progenitors with 50% gas fraction merge into one big remnant. Therefore, we obtain an empirical criterion for dissipative merging;

$$\alpha \gtrsim 1 - \frac{1}{2}\frac{M_g}{M}. \tag{3}$$

And also, progenitors with $M_g/M = 0.5$ merge three times faster than those with $M_g/M = 0.1$. The merging process is shown below for the case of $M_g/M = 0.5$.

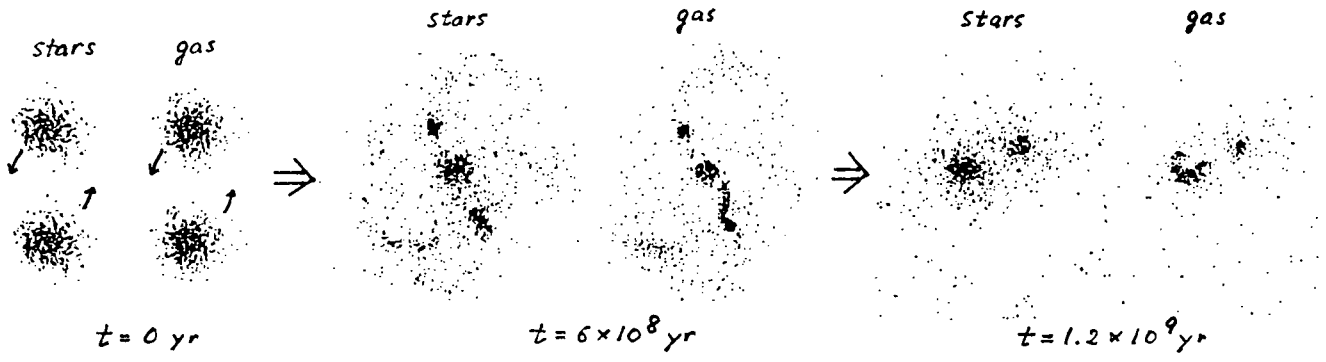

ii) Central Phase Space Density

The central phase space density is defined as

$$f_c = \frac{\rho_c}{(2\pi\sigma_c^2)^{3/2}}, \tag{4}$$

where ρ_c is the central density, and σ_c is the velocity dispersion. The f_c is significantly raised through the dissipative merging. The numerical results show that the amplification factor is 8, 14, and 90, respectively for $M_g/M = 0.01$, 0.1, and 0.5. These results can be compared to the observational ones in spiral or elliptical galaxies (see right). So, we can conclude that if there is as large an amount of gas in progenitor as 50% of total mass, the central phase space density can be accounted for by merging. This means that the merger remnant of ordinary spirals cannot be ellipticals, but gas rich primordial galaxies possiblly merge to form ellipticals.

Data: Carlberg (1987)

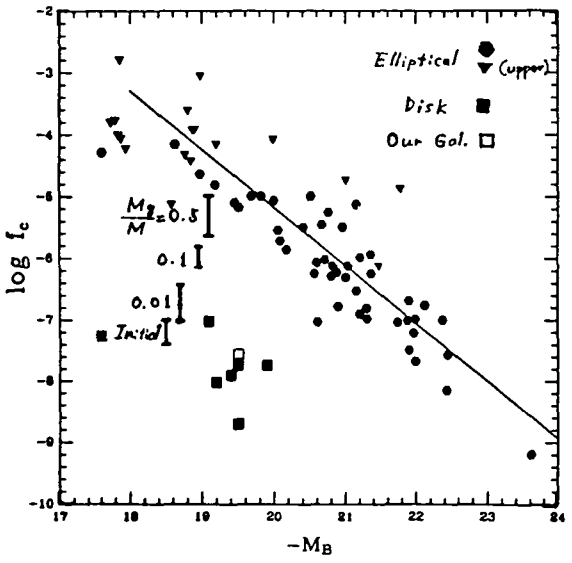

RADIO JETS IN COLLIDING GALAXIES: TESTING THE INTERACTION–ACTIVITY CONNECTION

Kirk D. Borne (Space Telescope Science Institute, Baltimore, Maryland)
and
Luis Colina (Universidad Autónoma de Madrid, Spain)

The idea that galaxy interactions and merging are related to the generation of starburst and AGN activity in galactic nuclei has been the subject of intensive investigations over the past several years and is still a matter of lively debate (for reviews, see: Hernquist 1989, Nature, 340, 687; Stockton 1990, in *Dynamics and Interactions of Galaxies*, p. 440; and Heckman 1990, in *Paired and Interacting Galaxies*, IAU Colloquium #124, p. 359). Peculiar morphologies, indicative of tidal interactions, have been detected in high–luminosity radio galaxies (Heckman *et al.* 1986, ApJ, 311, 526), in quasars (Hutchings 1987, ApJ, 320, 122), and in ultraluminous IRAS galaxies (Sanders *et al.* 1988, ApJ, 325, 74). In addition, low–luminosity radio and active galaxies show similar evidence for a recent merger or for nearby companions (MacKenty 1989, ApJ, 343, 125; Colina & Pérez–Fournon 1990*a*, ApJS, 72, 41; Colina & Pérez–Fournon 1990*b*, ApJ, 349, 45; Macchetto *et al.* 1990, ApJ, 356, 389; and Colina *et al.* 1991, ApJ, 370, 102).

In a recent CCD optical study of galaxies selected on the basis that they all contain well defined radio jets, it was found that almost half of the sample consists of pairs of elliptical galaxies (Colina & Pérez–Fournon 1990*a*,*b*). Many of these low–luminosity radio galaxies with companions (*e.g.*, 3C 31, 3C 278, 3C 449, and NGC 1044) show a well defined distorted radio jet structure at the VLA scale with an *S*– or *C*–shaped morphology.

We have developed a general numerical simulation algorithm for ballistic radio jets with the intention of applying this model to the study of the bent jets seen in colliding pairs of galaxies and with the hope of testing the well documented interaction–activity connection. In our model the morphological evolution of the jets is determined by their response to the simple mechanical forces (*i.e.*, gravity and ram pressure) imposed on them from both the host and the companion galaxies. Radiative losses, jet precession, magnetic effects, relativistic terms, and hydrodynamic instabilities have all been ignored.

Starting with a previously derived collision model for the interacting pair of elliptical galaxies NGC 4782/4783, we have used our algorithm to simulate the specific two–sided jet morphology seen in the radio source 3C 278, associated with NGC 4782. *This is the first time that such jet simulations have been produced for a galaxy pair whose relative orbit was determined independently from the jet modeling.* The masses of the galaxies and their relative orbit (including its 3–dimensional de–projection) were all derived from numerical simulations by Borne, Balcells, & Hoessel (1988, ApJ, 333, 567). Their best–fit collision model (as used here in the radio jet simulations) was constrained by a combination of optical morphological and kinematic data for this strongly disturbed pair of galaxies.

Our jet models constrain the initial jet parameters (*i.e.*, ejection speed, direction, and starting time), the properties of the hot (x–ray emitting) gaseous medium into which the jets are ejected, and the relative importance of gravitational deflection versus ram pressure bending in influencing the jet morphology. For 3C 278, *we find that the effects of ram*

pressure dominate the structural evolution of the jets. In our best–fit model the jet ejection speed is of order 10^4 km s^{-1}, the jets are ejected within $\sim 5°$ of the line–of–sight, the hot ISM in the non–jet galaxy (NGC 4783) has a much larger effect on the jet deflection than does that of the host galaxy (NGC 4782), and the jet activity began just over 70 million years ago, roughly 50 million years before the pericenter passage of the two galaxies (H_0 = 60 km s^{-1} Mpc^{-1}). *If there is a causal connection between the collision and the radio source generation, as indicated here, then it must become important early in the interaction.* This is not unreasonable since the derived collision model for the NGC 4782+4783 pair indicates that they have suffered a very strong tidal encounter, approaching one another on a deeply penetrating trajectory that had the cores of the galaxies separated by a little less than one galaxy diameter at the time that our model jet activity began. Therefore, *the onset of nuclear activity in 3C 278 appears to be related to the kinematically observed tidal shock* (*i.e.*, very large central stellar velocity dispersion, 392 km/sec [Tonry & Davis 1981, ApJ, 246, 666]) *and the very high central surface brightness* (Burbidge *et al.* 1964, ApJ, 140, 1462) *that have been induced in the core of NGC 4782 as a result of its deeply penetrating collision with NGC 4783.*

The general morphological features of the jets seen in 3C 278 (e.g., position angles, lengths, curvature, and deflection angles) are well matched by our simulations, indicating that our model for the mechanical forces acting on the jets can indeed reproduce most of the basic details of the jet morphology. High–resolution x–ray imaging (*e.g.*, from ROSAT) can be used to test our model by determining the true spatial distribution of the hot ISM within this system; it is this gas that is primarily responsible for the jet deflections observed here. Alternative jet–bending models have been investigated (*i.e.*, collisions with cold gas clouds, and flow against an external, intergalactic gaseous medium), but these produce jets that are not consistent with the observations. Other workers have found that the morphology of some bent radio jets could only be reproduced when some degree of artificiality was introduced into their models. Our simulations do not suffer the same defect, but they provide opportunities both to model a combination of detailed optical, radio, and x–ray data for a wide variety of interacting radio–jet galaxies and to investigate the causal connection between the interaction and activity seen in these systems.

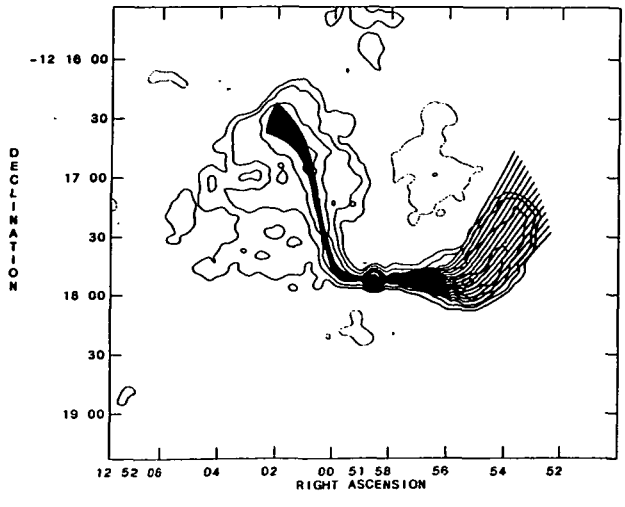

Figure — Comparison between the observed radio morphology and our best–fit jet model for 3C 278. The model is plotted over the VLA radio map (provided by Baum *et al.* 1988, ApJS, 68, 643), demonstrating the good match between the simulated and observed jet parameters: position angles, lengths, deflection locations, deflection angles, and curvature. The small open circle 40″ northeast of the jet nucleus, at position angle 15°, indicates the position of the center of NGC 4783. The broad, diffuse emission that is observed around the east jet probably resulted from the strong deceleration and deterioration of that jet induced by the ram pressure forces; that effect is not modeled here.

C-5

Declining rotation curves in interacting galaxies

Ralf-Jürgen Dettmar[$]
Radioastronomisches Institut der Universität Bonn, Bonn, FRG
and
Brian A. Skiff
Lowell Observatory, Flagstaff, AZ

Introduction

A declining rotation curve was recently found for the galaxy NGC 3521 by HI synthesis telescope observations (Casertano and van Gorkom 1991). From a comparison of the shapes of rotation curves for a larger sample of galaxies Casertano and van Gorkom argue that this is due to initial properties during the phase of galaxy formation.

In several studies of global properties of galaxies, NGC 3521 was always considered a "normal" unbarred, non-interacting, isolated spiral. However, here we present CCD surface photometry that shows at low surface brightness levels the typical signs of interaction or even merging.

Observations and reduction

A TI 800×800 chip with 15μm pixels was used with the 20 cm–aperture Takahashi ϵ200 telescope ("BBST", Gallagher et al. 1991) which is mounted on the side of the Lowell Observatory 1.1 m Hall-telescope. This set-up has a 51′ field of view at an image scale of 3.88″ /pixel. The Observations reported here were obtained with a broad band R filter.

Several Takahashi images were aligned and scaled as a function of exposure time. A plane was fitted to the sky background. The saturated inner parts of the long exposures were replaced by the short-exposure images.

Absolute calibration by simulated aperture-photometry was performed using photoelectric BVR measurements collected from the literature. The R-band calibration used here depends on a single aperture measure obtained in Kron-Cousin R at MSSSO.

Results

In Fig. 1 we present a contour plot of the surface brightness distribution in a 22 arcmin field for the calibrated R band data. This should be compared with the plates at different contrast settings given by Sandage and Bedke (1985).

Outside of the inner 5 arcmin NGC 3521 shows a pronounced asymmetry. In the north-west we can trace the galaxy out to ∼10 arcmin, while it ends at ∼6 arcmin in the south-east. At the fainter levels the spiral structure is disturbed too. A spiral spur connects the regular spiral arm in the north-west with the faint extended envelope. This spiral feature can be traced out to r=8 arcmin from the nucleus. The outer parts to the south-east are much brighter without any sign of sub-structure. The contour plot given shows a change in the slope of the brightness distribution at r=5 arcmin on the major axis. For r>5 arcmin the contours near the major axis become much wider spaced, indicating a larger scale length for the brightness distribution, and this outer disk also has a box-like structure. In the south-east this structure drops off in intensity very suddenly at r=6.5 arcmin, producing a sharp edge or shell with an opening angle of ∼15° at a position angle of PA=173°. The fainter but more extended northern part has an opening angle of 20° at a position angle of PA=175° with a brighter condensation at r=9 arcmin at PA=178°. The faint extensions are slightly twisted with respect to the inner disk which is at PA=168°.

[$] present address: Space Telescope Science Institute, 3700 San Martin Dr., Baltimore, MD 21218, USA; affiliated to the Astrophysics Division in the Space Science Department of ESA

Conclusions

With the evidence for a recent interacting event for NGC 3521 presented here, the declining rotation curve is best explained in an evolutionary scenario in which "soft" merging or interaction plays an important rôle. It it noteworthy that the spiral pattern of this galaxy is well behaved while the outer disk is heavily disturbed.

Acknowledgments. RJD gratefully acknowledges financial support by the Deutsche Forschungsgemeinschaft.

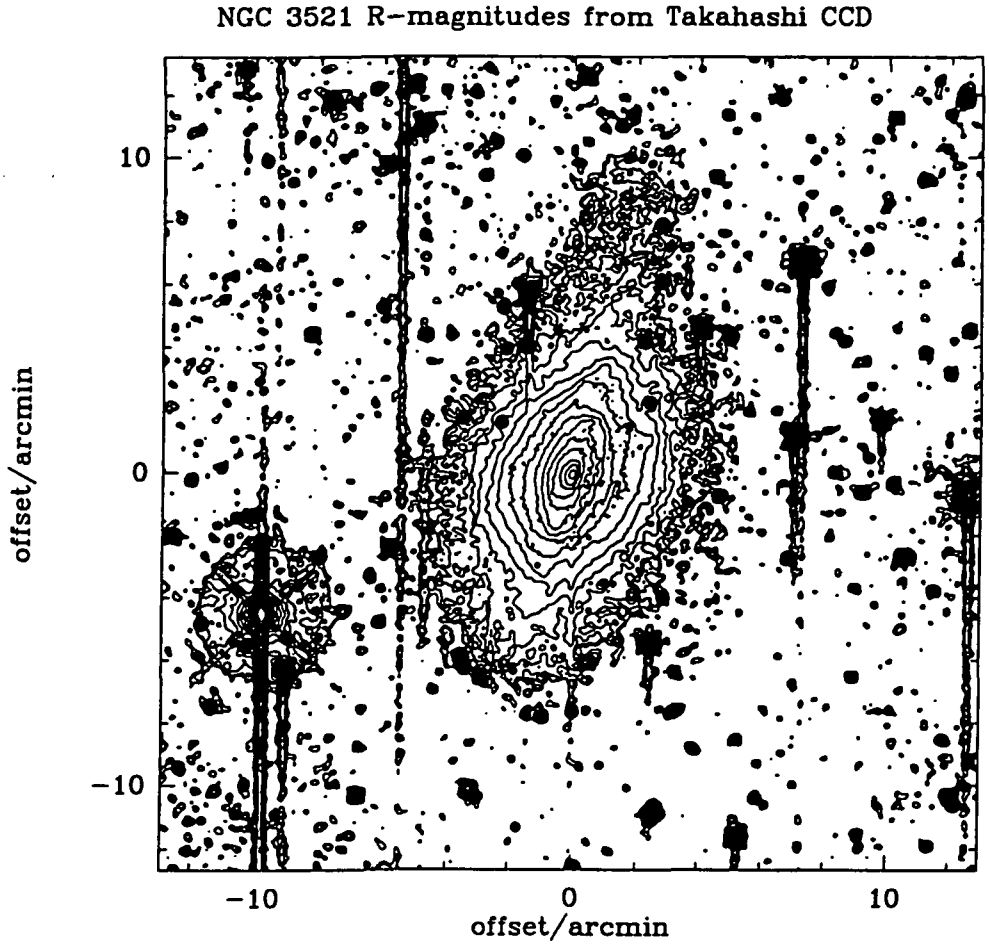

Figure 1: Contour plot of surface brightness distribution of NGC 3521 in the R band from Takahashi CCD photometry. The lowest contour is at μ_R=25.5. the step between contours is $\Delta\mu_R$=0.5.

REFERENCES

Casertano. S., van Gorkom, J. H. 1991. *Astronom. J.*. **191**. 1231.

Gallagher. J. S., Hunter, D. A., Gillet, F. C.. Rice. W. L. 1991. *Astrophys. J.*, **371**. 42.

Sandage. A., Bedke, J. 1985, *Astron. J.*. **90**. 1992.

A New Observational and Numerical Study of Tidal Interactions in M81-M82-NGC3077 system

M. S. Yun, P. T. P. Ho (Harvard-Smithsonian), N. Brouillet (Bordeaux), K. Y. Lo (Illinois)

A nearby system of interacting galaxies M81-M82-NGC3077 triplet (D=3.3 Mpc; Freeman & Madore 1988) has been studied using multi-wavelength observations and numerical simulations to obtain a comprehensive understanding on the dynamics and the consequences of tidal interactions in a group environment. The VLA 12-field mosaic HI observations of $2^\circ \times 1.^\circ5$ region have revealed a vast array of HI filaments which suggests that the severity and extent of tidal disruptions far exceed the previous estimates. A tidal remnant of the former HI disk of M82 extending up to 30 kpc (in projection) is identified for the first time, and the pervasive effects of the tidal disruption are traced into the inner disk by optical and CO observations, including a kinematic trace of a large scale bar potential (Yun, Ho, & Lo 1992). The HI disk of M81 is traced out to 40 kpc in radius, and a large scale ($l \sim 20$ kpc) velocity anomaly ("High Velocity Trough"), which may be a remnant of a gaseous collision, is found within the disk of M81. The large HI bridge between M81 and NGC 3077 (van der Hulst 1979) is also found to extend $\gtrsim 50$ kpc further, bending around NGC 3077, toward M82. The total HI detected in this experiment, $5.6 \times 10^9\ M_\odot$, represents the majority of the single-dish flux (Appleton, Davies, & Stephenson 1981) and suggests that the bulk of HI found in the region belongs to the three galaxies and the tidal filaments.

The impact and details of the tidal interactions have been further examined through the use of numerical techniques. The "restricted 3-body" approach was used to simulate the observed distribution of tidal HI streamers connecting the three galaxies, and the success of the simulation is further strengthened by the accurate predictions on the gas kinematics. As suspected from the observations, all of the HI bridges (or streamers) are found to be tidally produced. The majority of the HI gas surrounding M82 is identified to be the tidally disrupted HI disk of M82 itself, contrary to the previous suggestions of tidally captured gas from M81 (e.g., Cottrell 1977). The South Tidal Bridge between M81 and NGC 3077 is identified as a tidal arm originating from M81 while the North Tidal Bridge between NGC 3077 and M82 is found to be the tidally disrupted HI disk ($\sim 10^9\ M_\odot$) of NGC 3077. The latter conclusion is highly unusual since NGC 3077 is currently an apparent early type galaxy (Barbieri, Bertola, & di Tullio 1974; Price & Gullixson 1989), and additional studies are in progress to further explore this unusual discovery.

The high degree of success achieved by the restricted 3-body calculations is quite surprising since neither self-gravity nor hydrodynamics are included in the modeling, and this may suggest that the role of self-gravity and hydrodynamical effects in tidal interactions may not be so important. On the other hand, there are some curious details that seem improbable, such as the tidal disruption of NGC 3077 which appears to have occurred only during the most recent passage by M81 while they are modelled as a bound pair ($e = 0.7$). Our full N-body study of tidal orbit

decay suggests that NGC 3077 may have undergone a tidal capture by M81 from a more eccentric orbit, and the 3-body simulation may be interpreted as a short term tracing of the tidal interactions and the evolution of tidal remnants immediately following the capture. The shortness of the time scale involved in the simulation, 3×10^8 years, is consistent with this explanation and may also explain the apparently insignificant role of hydrodynamical effects in shaping the tidal remnants. The main difference of this simulation from the previous ones is that the masses of the galaxies and the sizes of the disks are larger at least by a factor of two. The use of numerical studies such as this may also be useful in determining the physical quantities of the systems under study. Since the mass, length (or distance), and velocity (or time) scales are linked by gravity in such tidal interactions, an independent determination of mass and velocity scales may lead to the determination of the distance to the system, for example.

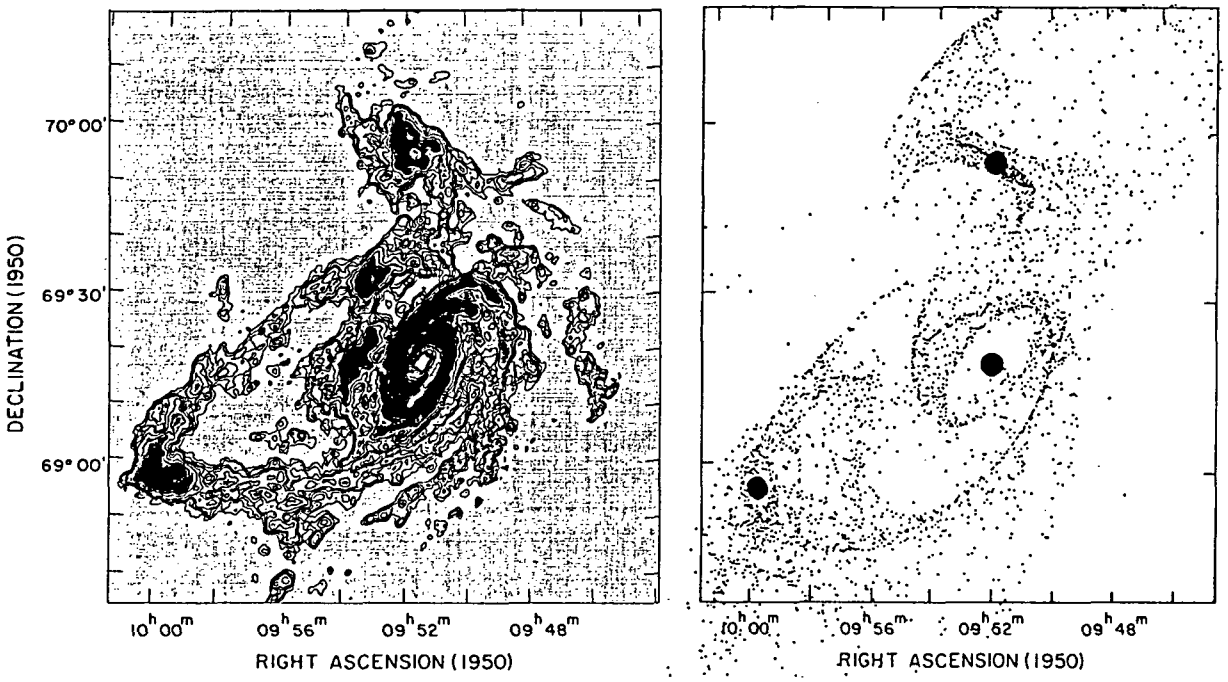

Figure 1. The 12-field VLA HI mosaic of the M81-M82-NGC3077 system (left) is compared with the result of the restricted 3-body simulation (right). The lowest contour for the HI map corresponds to the column density of 2.7×10^{19} cm^{-2}, and the contours increase in multiples of 1, 2, 3, 4, 6, 10, 15, 25, and 40.

References

Appleton, P. N., Davies, R. D., and Stenphenson, R. J. 1981, MNRAS, 195, 327
Barbieri, C., Bertola, F., and di Tullio, G. 1974, A&A, 35, 463
Cottrell, G. A. 1977, MNRAS, 178, 577
Freeman, W. L., and Madore, B. F. 1988, ApJL, 332, L63
Price, J. S., and Gullixson, C. A. 1989, ApJ, 337, 658
van der Hulst, J. M. 1979, A&A, 75, 97
Yun, M. S., Ho, P. T. P., and Lo, K. Y. 1992, ApJL, submitted

ABSTRACT

The Nature of the Evolution of Galaxies by Mergers

Tapan K.Chatterjee,Facultad de Ciencias,F.M.,Universidad A.Puebla, Puebla,Mexico.

The merger theory for the formation of elliptical galaxies is examined by conducting a dynamical study of the expected frequency of merging galaxies on the basis of the collisional theory,using galaxy models without halos.The expected merger rates obtained on the basis of the collisional theory fall about a magnitude below the observational value in the present epoch.In the light of current observational evidence and the results obtained,a marked regularity in the formation of ellipticals is indicated,followed by secular evolution by mergers.

Brief Summary of Material to be Covered

Using basically the impulsive approximation and a modification of the method used by Alladin,1965 (Astrophys.J.141,768) and described in detail in Chatterjee,1990 (I.A.U. Col. 124,519;"Paired and Interacting Galaxies";NASA Publ.No.3098),we study mergers between different types of progenitor pairs,each collision being characterized by the initial separation between the galaxies and the initial relative velocity therein.For each collision the change in relative velocity due to dynamical friction is taken into account.The merger takes place when the instantaneous relative velocity of the two galaxies equals the velocity of escape between the pair characterized at the instantaneous separation.

Results indicate that the expected frequency of merging galaxies, not considering the galaxies to be embedded in massive halos,is $\sim 10^{-2}$%,which falls short of the observed value in the present epoch ($\sim$0.3%) by an order of magnitude and falls short of the extrapolated past value ($\sim$ 5%) by two orders of magnitudes.The frequency of different types of proginator pairs in merger is of the same order of

magnitude.The majority of mergers are achieved in several orbital periods (2 to 3),and only about $\sim$10% of them are achieved in a single orbital period; and about 1% of them are due to central impacts.

There are bound to be many subtle kinamatical differences between the remnants owing their origin to different pairs of progenitors, and as the frequency of mergers with different pairs of progenitors is of the same order of magnitude,the frequency of these kinamatical differences should be observationally significant.These results are reinforced by current observational evidence,indicating the existance of racially different types of ellipticals.

The existance of the fundamental parameter plane(on which the global properties of elliptical galaxies lie),is indicative of a strong regularity in the process of elliptical galaxy formation,with fluctuations about the main process as a function of mainly the initial conditions,and of subsequent evolution as a function of mainly the local conditions,accounting for the observed diversity in ellipticals.It is this subsequent evolution where the mergers seem to a very prominent part.The virial theorm implies that any homologous family of self gravitating galaxies in dynamical equilibrium will define a plane,which will map into the fundamental plane if the mass to luminosity ratio is a unique function of the position of the plane; the mass to luminosity ratio for ellipticals seems to vary little.

The brightest cluster members and cDs even though sighted as evidence for the merger theory,have anomalous properties suggestive of an evolutionary history different from other ellipticals and modified by mergers.

This evidence is strongly indicative of the expected regularity in elliptical galaxy formation,and a secular evolution by mergers.

Mergers at z=1

Lancelot L. Kao
Department of Astronomy and Astrophysics
The University of Chicago
5640 South Ellis Avenue
Chicago, IL 60637, U.S.A.

ABSTRACT Multiband images of nearby interacting pairs of galaxies, mergers, and normal field galaxies are used to simulate images of high redshift mergers by identifying distinctive morphological features. Preliminary results indicate that it is feasible for the HST to detect these high redshift objects.

I. Introduction

The study of interacting galaxies may help us understanding of galactic evolution and galaxy formation. Observations of ellipticals with counter-rotating cores and ellipticals with multiple nuclei suggest their origins by the process of merging of spirals (Schweizer 1986, 1989; Kormendy 1989, & Wielen 1989). However, van den Bergh (1989) and others objected this idea based on the argument that the observed number of globular clusters per unit luminosity is higher than the sum of two spirals merging together. More recent studies of globular clusters in interacting systems by Ashman and Zepf (1992), and the HST detection of excess young blue globular clusters in NGC1275 support the interpretation that they were formed by merging (Holtzman *et al* 1992).

Moreover, the excess blue objects counts in deep sky surveys (e.g. Lilly *et al* 1991, Cowie *et al* 1991) suggests the possibility of merging plays an important role in the formation of galaxies. Overabundance of paired objects in deep sky survey have been reported by Zepf and Koo (1989), and most of the objects have been confirmed spectroscopically (Smetanka 1991). In order to evaluate the importance of merging events in the role of galaxy formation and to test the hypothesis that merging rate was higher at high redshift, it is crucial to find these objects in deep sky surveys.

The purpose of this paper is to illustrate the potential of using distinctive morphological signatures in nearby interacting systems as criteria to search for these candidates at high redshift with the HST.

II. Sample Selection and Observation

The selection criteria for the nearby merger candidates is similar to those of Karachentsev (1980) with additional restrictions:

(1) both members need to have accurate radial velocities measurements,
(2) the projected separation between the pairs is less than 200kpc,
(3) the angular separation is less than two arcminutes, and
(4) the candidate does not belong to a group or having a third member within 500kpc from their center.

The normal field galaxies come from two sources. One sample of field galaxies is from the sample used by Green, Anderson, and Ward (1992), and the other sample from a complete random selection from UGC catalogue.

All the observations were made from the Apache Point Observatory 1.8m reflector, using the High Resolution Imager (a TI800x800 CCD) with B, V, R, I, g, r, i filters . The average total exposure for an image is about an hour with the HRI; generally broken into 10 minutes segments, each a slightly different positions. These short images were aligned and median to produce the final image.

III. Data and Simulation

B, V, R broadband images of Arp243 have been obtained during February 24 to 26, 1992 (see figure 1a, 1c, 1e, respectively). The average seeings of those nights is about 1.6 arcsecond. The B and R band images are each 50 minutes exposure, and the V band image is only 10 minutes exposure. Morphological features, such as knot and bridge have been detected with size about 4kpc extended from the oval nucleus of the galaxy. We then use these images and simulate their appearances as if they are at z=1. For z=1, $q_0 = 0.5$, and $h = 0.75$ model, the angular size for structures of 4kpc is about 0.704 arcsecond, and it is feasible for the HST to resolve these

structures as it is demonstrated by figures 1b, 1d, and 1f. The data and simulation are generated by using the IRAF software packages.

The figures are in counts per pixel after sky-subtraction, the background is nominally zero. Figures 1a, 1c, 1e are Arp243 in B, V, and R band respectively. The size of the box is 130x130 arcsecond or 46x46kpc, and the pixel scale is 0.467arcsecond per pixel. Figures 1b, 1d, 1f are simulated HST images of Arp243 at z=1 with respect to the B, V, R band images. The size of the box is 8x8 arcsecond, and the pixel scale ranges from 0.045arcsecond per pixel for Planetary Camera to 0.1arcsecond per pixel for the Wide Field Camera of the HST.

IV. Discussion

Although the simulation did not include noise or the degraded point spread function of the HST, it did not affect our results. The crucial aspect of the simulation is whether we could identify disrupted morphologies at high redshift objects with the HST within reasonable observation time; and the simulated images do preserve the distinctive morphological signatures. Whether this can be done before the planned instrument upgrade is an item of further study.

Disrupted morphologies of interacting systems have been successfully accounted for by calculations of direct collision of galaxies (Toomre & Toomre 1972, etc). According to the model of Olson and Kwan (1990) enhanced star formation and morphological peculiarities are frequently found in or near the nuclei of the interacting pairs. Near-infrared images of peculiar galaxies from the Arp atlas have revealed a number of interesting morphological features that appear in theoretical calculation (Bushouse & Stanford 1992). Although the Arp sample is selected because of morphological peculiarities, it is pointed out by Madore (1985) that the majority of the sample is made up of interacting galaxies. Therefore, it is natural to assume that high redshift interacting systems will also show morphological peculiarities that are found in nearby interacting systems.

The major problem we need to resolve is the issue of completeness of the sample. The objects detected in this way are subject to bias towards strongly interacting systems. Systems that are not *active* may not be detectable in this way. We may assume that the distribution of interacting systems with different activity levels are invariant with time and only the rate of merging changes with time, then we could compare the rates of merging of similar systems in different epoch. Unfortunately, the above ad hoc assumption could not be tested.

The author would like to thank Don York for guidance and support in this project and Brian Yanny for helpful suggestions with computer problems.

REFERENCES.

Ashman, K. M. and Zepf, S. E. 1992, Ap. J., **384**, 50.
Bushouse, H. A. and Stanford, S. A. 1992, Ap. J. Suppl., **79**, 213.
Cowie, L. L., Songaila, A., and Hu, E. M. 1991, Nature, **354**, 460.
Green, P. J., Anderson, S. F., and Ward, J. M. 1992, M. N. R. A. S., **254**, 30.
Holtzman, J. A. *et al* 1992, A. J., **103** (3), 691.
Karaehentsev, I. D. 1980, Ap. J. Suppl., **44**, 137.
Kormendy, J. 1989, in *Dynamics and Interactions of Galaxies*, ed. R. Wielen (Springer-Verlag, New York), p.499.
Lilly, S. J., Cowie, L. L., and Gardener, J. P. 1991, Ap. J., **369**, 79.
Madore, B. F. 1985, in *Spectral Evolution of Galaxies*, eds. C. Chiosi and A. Renzini (Reidel, Dordrecht), p.97.
Olson, K. M. and Kwan, J. 1990, Ap. J., **361**, 426.
Schweizer, F. 1986, in *Nearly Normal Galaxies*, ed. S. M. Faber (Springer-Verlag, New York), p.19.
Schweizer, F. 1989, in *Dynamics and Interactions of Galaxies*, ed. R. Wielen (Springer-Verlag, New York), p.60.
Smetanka, J. 1991, private communication.
Toomre, A. and Toomre, J. 1972, Ap. J., **178**, 623.
van den Bergh, S. 1989, in *Dynamics and Interactions of Galaxies*, ed. R. Wielen (Springer-Verlag, New York), p.492.
Wielen, R. ed. 1989, *Dynamics and Interactions of Galaxies*, (Springer-Verlag, New York),
Zepf, S. E. and Koo, D. C. 1989, Ap. J., **337**, 34.

Figure 1a: The lowest contour corresponds roughly to a surface brightness of 25.8mag/arcecond^2 in B band.

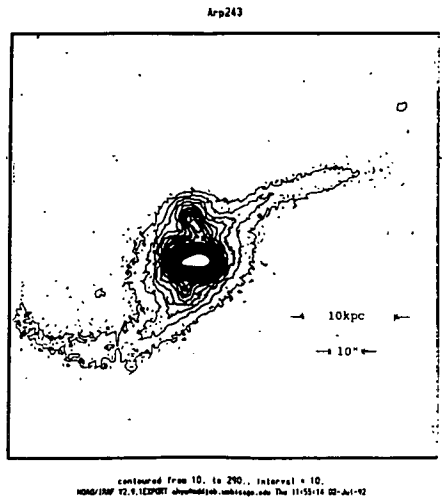

Figure 1b: The lowest contour corresponds roughly to a surface brightness of 28.8mag/arcecond^2.

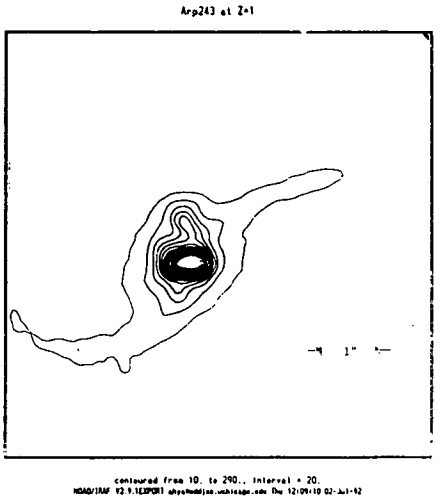

Figure 1c: The lowest contour corresponds roughly to a surface brightness of 24.2mag/arcecond^2 in V band.

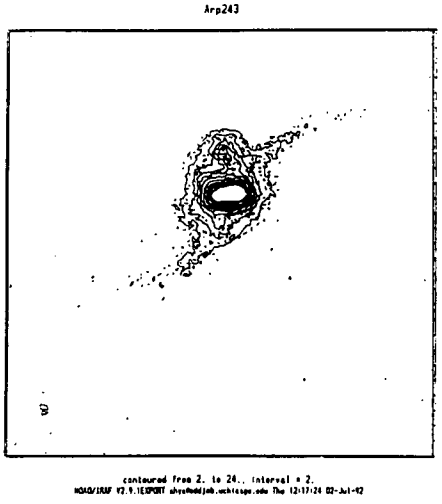

Figure 1d: The lowest contour corresponds roughly to a surface brightness of 27.2mag/arcecond^2.

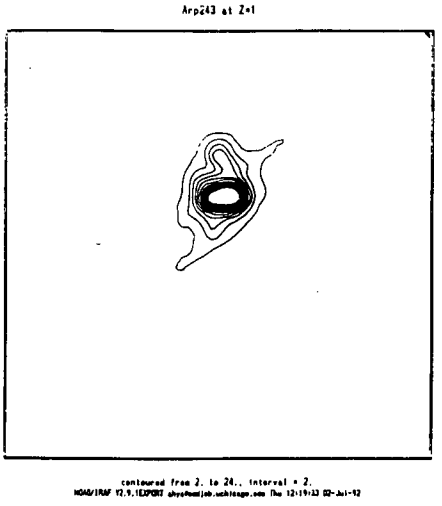

Figure 1e: The lowest contour corresponds roughly to a surface brightness of 24.8mag/arcecond^2 in R band.

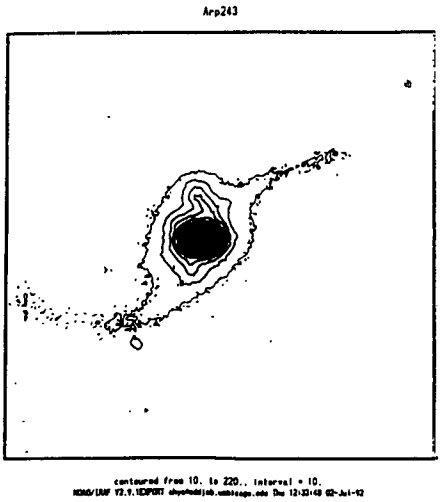

Figure 1f: The lowest contour corresponds roughly to a surface brightness of 27.8mag/arcecond^2.

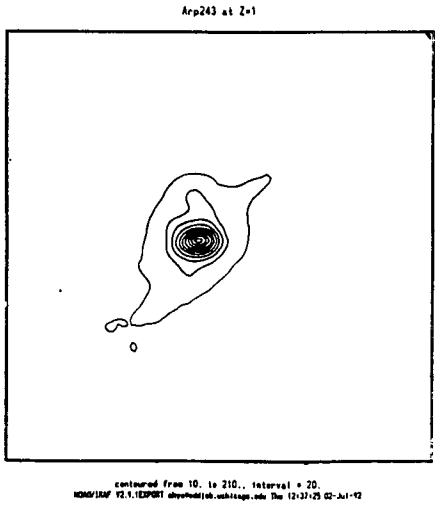

Page Intentionally Left Blank

Day 4: Thursday, 9 July 1992

Page Intentionally Left Blank

A Numerical Simulation of Galaxy Subcluster Mergers

Kurt Roettiger, Jack Burns & Chris Loken

Department of Astronomy
New Mexico State University
Las Cruces, NM 88003-0001

Abstract: We present preliminary results of a 3-D numerical simulation of two merging subclusters of galaxies. By self-consistently modelling the intracluster gas and dark matter dynamics, we hope to gain insight as to how the dynamics of both relate to such observables as the cluster X-ray emission, radio source morphology, and velocity dispersions.

1. Introduction

In recent years, both X-ray and optical surveys have revealed a significant level of substructure in both the gaseous ICM and galaxy components in clusters of galaxies (Forman and Jones 1982, Beers *et al.* 1991). One possible explanation for the origin of the observed substructure is subcluster mergers (McGlynn and Fabian 1984). This is an idea which could have significant implications for theories regarding the growth of large scale structure (LSS) in the Universe. Observationally, one may gauge the significance of subcluster mergers in building LSS though comparing the number of clusters with and without signatures of a merger event. Numerical simulations such as this one will aid in the identification and interpretation of merger signatures as well as their evolution. In addition, we will be able to study the post-merger cluster environment as it relates to radio source morphology.

This experiment is being performed in 3-D using a hybrid N-Body/MHD code. The hybrid code allows the study of the self-consistent evolution of a gas component, represented by the fluid equations of hydrodynamics, in a gravitational potential defined by self-gravitating dark matter, represented by the particles of the N-Body simulation. The MHD component of the code is ZEUS-3D, an Eulerian, finite difference code developed by D. Clarke and M. Norman (Stone and Norman 1992). The N-Body component of the code is the Hernquist Treecode (Hernquist 1987).

2. The Simulation

In this simulation, two galaxy subclusters are placed initially at rest with their cores separated by 6 Mpc. The dark matter in each cluster is represented by a virialized isothermal King model distribution of particles. The dominant of the two subclusters consists of 16,000 particles while the smaller cluster consists of 2000 particles. All particles are of equal mass. The dominant cluster is scaled to 1.0×10^{15} solar masses with a velocity dispersion of 1200 km/s. The dominant cluster core and tidal radii are 0.25 and 3 Mpc, respectively. The dimensions of the smaller cluster are one half of these. Each cluster is initialized with an isothermal gas distribution in hydrostatic equilibrium with the gravitational potential defined by the dark matter particles. The temperature of the gas is a free parameter which was chosen such that the sound speed in each cluster is equal to the velocity dispersion of that cluster. This implies a gas temperature of 1.0×10^8 K in the dominant cluster and 2.6×10^7 K in the small cluster. The gas distributions are not self-gravitating. However, the total gas mass is a small fraction of the total cluster mass, less than 15% in the small cluster and less than 5% in the dominant cluster.

The hydrodynamical calculations are performed on a grid with dimensions $190 \times 60 \times 60$ corresponding to a maximum resolution of 62.5 kpc.

3. Preliminary Results

The simulation reveals the formation of multiple shock fronts expanding both parallel and perpendicular to the merger axis resulting in a complex temperature structure. Gas behind the strongest shock front is heated to 3.0×10^8 K. In addition, a pocket of the cooler gas from the small cluster may remain for a considerable time after the merger. The density contours show an elongation of the gas distribution, initially perpendicular, and eventually parallel to the merger axis. Figure 1a is a 2-D slice in density and velocity parallel to the merger axis at 1.0×10^9 yrs after the time at which the cores are coincident. At this point, the smaller cluster, having entered from the top of the figure, has passed through the core of the dominant cluster (top/center) and can be seen in the lower half of the figure. Note the clumpiness and elongation of the density distribution. Figure 1b shows the corresponding shock structure as revealed by the gas Mach number. Three shocks are evident, the strongest of which is on the merger side of the dominant cluster core.

4. Future Work

We will explore the merger parameter space with significantly improved resolution. Simulated ROSAT and EINSTEIN imagery will be generated to assist in the analysis of the x-ray data. We will also examine the evolution of cooling flows within the merger environment.

This work was supported in part by a grant from the U.S. National Science Foundation (AST-9012353) to J.O.B.

References

Beers, T. *et al.* 1991, *A. J.*, **102**, 1581.
Forman, W. & Jones, C. 1982, *A. R. A. A.*, **20**, 547.
Hernquist, L 1987, *Ap. J. Suppl*, **64**, 715.
McGlynn, T. A. & Fabian, A. C. 1984, *M.N.R.A.S.*, **208**, 709.
Stone, J. & Norman, M. 1992, *Ap. J. Suppl.*, **80**, 791.

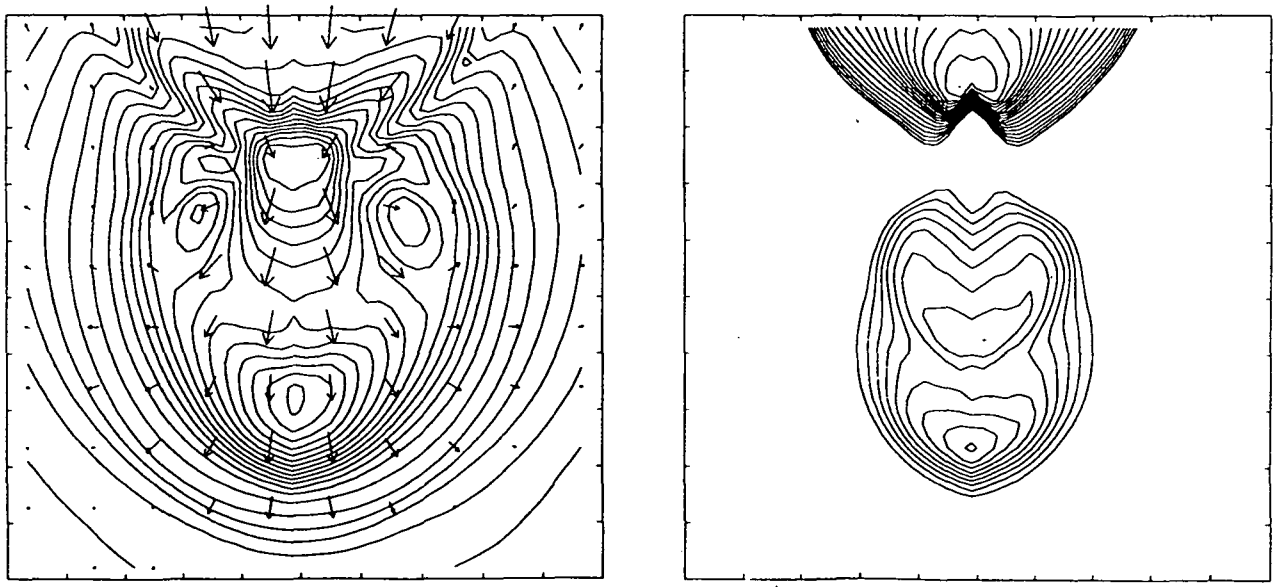

Figure 1. Density, velocity and Mach number shortly after the merger. The region depicted is nearly 3 Mpc on a side. The small cluster has entered from the top of the frame. a) Density contours with velocity vectors superimposed. Contours are logarithmic spaning 2 orders of magnitude. Note the clumpiness and elongation of the gas distribution. The maximum velocity corresponds to nearly 2300 km/s. b) Mach Number. Contours are linear ranging from 0.95 to 4.0.

LUMINOSITY SEGREGATION IN GALAXY CLUSTERS

as an indication of

DYNAMICAL EVOLUTION

F.W. Baier and K.–H. Schmidt, Potsdam-Babelsberg

Theoretical models describing the dynamical evolution of self–gravitating systems predict a spatial mass segregation for more evolved systems, with the more massive objects concentrated toward the centre of the configuration. From the observational point of view, however, the existence of mass segregation in galaxy clusters seems to be a matter of controversy.

A special problem in this connection is the formation of cD galaxies in the centres of galaxy clusters. The most promising scenarios of their formation are galaxy cannibalism (merger scenario) (Hausmann and Ostriker 1978, Ostriker and Tremaine 1975, White 1976) and growing by cooling flows (Mushotsky et al. 1981, Silk 1976).

It seems to be plausible to consider the swallowing of smaller systems by a dominant galaxy as an important process in the evolution of a cD galaxy. The stage of the evolution of the dominant galaxy should be reflected by the surrounding galaxy population, especially by possible mass segregation effects.

Assuming that mass segregation is tantamount to luminosity segregation we analyzed luminosity segregation in roughly 40 cD galaxy clusters. Obviously there are three different groups of clusters: (i) clusters with luminosity segregation, (ii) clusters without luminosity segregation, and (iii) such objects exhibiting a phenomenon which we call antisegregation in luminosity, i.e. a deficiency of bright galaxies in the central regions of clusters. This result is interpreted in the sense of different degrees of mass segregation and as an indication for different evolution stages of these clusters. The clusters are arranged in the three segregation classes 2, 1, and 0 (S2 = strong mass segregation, S1 = moderate mass segregation, S0 = weak or absent mass segregation).

We assume that a galaxy cluster starts its dynamical evolution after virialization without any radial mass segregation. Energy exchange during encounters of cluster members as well as merger processes between cluster galaxies lead to an increasing radial mass segregation in the cluster (S1). If a certain degree of segregation (S2) has been established, an essential number of slow–moving and relative massive cluster members in the centre will be cannibalized by the initial brightest cluster galaxy. This process should lead to the growing of the predominate galaxy, which is accompanied by a diminution of the mass segregation (transition to S1 and S0, respectively) in the neighbourhood of the central very massive galaxy. An increase of the areal density of brighter galaxies towards the outer cluster regions (antisegregation of luminosity), i.e. an extreme low degree of mass segregation was estimated for a substantial percentage of cD clusters. This result favours the cannibalism scenario for the formation of cD galaxies.

Obviously, some relations between the estimated segregation classes and the properties of the dominant galaxies seem to exist which may express the connection between evolving cD galaxies and their environment. Malumuth (1992) discussed the question if cD galaxies with large peculiar velocities can be formed by mergers in a virialized cluster. He compiled peculiar velocities of cD galaxies. There are galaxy clusters with large peculiar cD velocities (more than 100 km/s) in our sample (A 1146, A 1795, A 2029, A 2634, and A 2670). According to the calculations of

Malumuth the growing of the cD galaxies in these clusters by merging should have been occured not long ago. Four of them (A 1795, A 2029, A 2634, and A 2670) show low or absent central mass segregation, i.e. a hint at a diminution of the number of bright galaxies in the central cluster region, which can be explained by merging and a preceding stripping of the cluster galaxies. On the other side strong mass segregation is observed for the clusters A 779 and A 2199 with peculiar velocities of 20 km/s and 57 km/s, respectively. We may conclude that these both clusters are in an early stage of evolution without any perceptible cannibalism.

The cD galaxies of the clusters A 85, A 426, A 1060, A 1795, A 1991, A 2029, and A 2052 – which have a large peculiar velocity and/or show a relative strong cannibalism effect (segregation classes 1 and 0) – have relative blue central colours in comparison with their envelopes from radial u–b profiles (McNamara and O'Connel 1991).

On the other hand the cD galaxies in A 496, A 779, and A 2199 in segregation class 2 with low peculiar velocities show opposite radial u–b colour gradients, i.e. with slightly red centres and blue envelopes or at least "neutral" radial colour distributions without any pronounced gradient. We consider objects in class 2 as in a very early evolutionary stage before any stripping and cannibalism. Abell 1413 with weak mass segregation and a colour gradient from a red centre to blue outer regions – but with a pronounced red envelope – seems to be in a medium evolutionary stage before the onset of cannibalism and later than A 496, A 779, and A 2199.

We looked for any correlation between mass segregation and the envelope luminosity of dominant cluster galaxies using the envelope luminosities given by Schombert (1988).

Three of the objects in segregation class 2 (A 779 and A 400, and A 2199) show low envelope luminosities. Three further clusters (A 426, A 2634, and A 1904) in segregation class 1 show moderate luminosity of the cD envelope. There is a colour profile only for the cD galaxy of A 426 with a distinct blue central u–b excess. This excess as well as its strong radio emission favour activity due to the onset of cannibalism. We assume that the cannibalism process in this early phase did not have enough time in order to build up a pronounced envelope already.

On the opposite the clusters with high envelope luminosities (A 1795, A 2670, A 2029, and A 1413) belong to groups 1 and 0 (moderate and high cannibalism properties). Therefore, we conclude that there seems to be a correlation between envelope luminosity and cannibalism properties.

If these relations will be confirmed they may contribute to understand the late stages of evolution of clusters and the cD galaxies therein.

References

Hausman, M.A., and Ostriker, J.P.: 1978, Astrophys. J. **224**, 320
Malumuth, E. M.: 1992, Astrophys. J. **386**, 420
McNamara, B.R., and O'Connel, R.W.: 1991, Kapteyn Institute, Preprint, No 057
Mushotsky, R.F., Holt, S.S., Smith, B.W., Boldt, E.A., and Serlemitsos, P.J.: 1981, Astrophys. J. Lett., 244, L47
Ostriker, J.P. and Tremaine, S.D.: 1975, Astrophys. J. Lett. **202**, L113
Schombert, J. M.: 1988, Astrophys. J. **328**, 475
Silk, J.: 1976, Astrophys. J. **208**, 646
White, S.D.M.: 1976, MNRAS, **177**, 717.

F.W. Baier,
Working Group 'Galaxy Clusters' at the
University of Potsdam

K.–H. Schmidt
Astrophysical Institute Potsdam

An der Sternwarte 16
D–O 1591 Potsdam, Germany

Kinematics of compact groups and morphologies of the member galaxies

Claudia Mendes de Oliveira and Paul Hickson (UBC)

Abstract

We present the results of a kinematical and morphological study of galaxies in the Hickson compact groups. The redshift survey of 457 galaxies has been completed. The great majority of the galaxies have velocities within about 1000 km s^{-1} of the median velocity of the group. The velocities of the groups range from 1380 to 41731 km s^{-1} with a median of 8889 km s^{-1}, corresponding to a median distance of 89 h^{-1} Mpc. With the addition of the radial velocity selection criterion, a relatively large sample of physically dense compact groups was defined.

The nature of the velocity dispersion–morphology relation (Hickson, Kindl and Huchra 1989, hereafter HKH) is investigated. This is the tendency of groups with high velocity dispersions to contain fewer late–type galaxies. We find that this strong correlation is not due to any sample selection effects. The morphology concordance in compact groups (HKH), which is the trend for galaxies in a group to have similar morphological types, can be fully explained by the velocity dispersion–morphology correlation.

A significant correlation is found between crossing time and the fraction of gas–rich galaxies in the groups. Groups with short crossing times typically contain fewer late–type galaxies. This may be evidence that significant dynamical evolution has occurred in these groups.

Introduction

The Hickson Compact Groups (HCGs) are a sample that consists of 100 nearby groups of galaxies which typically contain four members. These were catalogued from a visual search of the Palomar Sky Survey red prints following a few criteria of magnitude concordance, isolation and surface brightness (Hickson 1982). For a large fraction of the groups, the spatial density of galaxies is as large as that in the cores of rich clusters of galaxies.

The conventional scenario for the history and fate of these compact groups is that their members will interact and merge into one single elliptical galaxy on time–scales comparable to their orbital periods (Barnes 1989). Therefore, compact groups may be ideal environments in which to study the formation of elliptical galaxies through mergers and the effects of collisions on the evolution of galaxies.

Results

We find that more than 84% of the galaxies have velocities within 1000 km s^{-1} of the median velocity of the group (hereafter, accordant members). 92 groups have at least three accordant members, and 69 groups have at least four. The median projected radial velocity dispersion of the groups is 200 km s^{-1}, comparable to values reported for loose groups. The median projected separation between galaxies within each group is 39 h^{-1} kpc and the median galactic crossing time is 0.016 Ho^{-1}. The details of the redshift survey are described in Hickson *et al.* 1992.

We have also studied the morphology of the galaxies in HCGs, and we have investigated correlations between dynamical parameters (velocity dispersion, crossing times) and morphological and structural parameters (fraction of late–type galaxies, brightness and size of the first–ranked galaxy, luminosity contrast of the first–ranked galaxy, degree of galactic asymmetry, interaction strength, intergalactic median separation). The only significant correlation, in addition to a velocity dispersion–morphology correlation (HKH) discussed below, was a crossing time–morphology correlation. Groups with short crossing times typically contain fewer late–type galaxies. This may be evidence for dynamical induced changes in the galaxy morphologies. Model collisions of two galaxies of comparable masses generally produce remnants that resemble elliptical galaxies (Barnes, 1989 and White, 1990). The correlation of crossing time with galaxy morphology is qualitatively consistent with this picture, assuming that the probability of an interaction increases as the crossing time decreases.

HKH analyzed a subsample of 60 HCGs and found that the group spiral fraction does not correlate strongly with the median projected galaxy separation. However, a strong correlation was found between the velocity dispersion and the fraction of late–type galaxies in the groups. Groups with high velocity dispersions contain fewer late–type galaxies. We find that this correlation is not caused by any selection effects in the sample and it must be real.

The HCGs are known to follow a morphological–type concordance (HKH). For the sample of 47 groups with redshifts $z \leq 0.03$, 28% have either only late–type galaxies or only early–type galaxies. The probability of this occurring from a random mix of morphological types is less than 10^{-3}. White (1990) pointed out that the probability calculation must take into account the morphology–velocity dispersion correlation. To test if the morphology–velocity dispersion correlation could explain the morphology concordance in the groups, we simulated quartets of galaxies with velocity dispersions drawn from a Gaussian distribution which matched the observed distribution for HCGs with $z \leq 0.03$ (mean = 2.2 and dispersion = 0.3, in the log). We then selected a sample of simulated groups which followed a morphology–velocity dispersion correlation as observed ($\sigma_v = -1.71 f_s + 3.21$, where σ_v is the velocity dispersion of the group and f_s the fraction of spiral galaxies). For 10000 runs of 47 groups we find that in 23% of the cases we are able to create a morphology concordance which is as strong or stronger than the one observed. This indicates that the morphology concordance in HCGs can be explained by the existence of the strong morphology–velocity dispersion correlation for compact groups.

References

Barnes 1989, Nature, 338, 123.

Hickson, P. 1982, Ap.J. 255, 382.

Hickson, P., Kindl, E. and Huchra, J.P. 1989, Ap.J., 331, 64.

Hickson, P., Mendes de Oliveira, C., Huchra, J.P., Palumbo, G.G.C., Ap.J., in press.

White , S.D.M. 1990, in *The Dynamics and Interactions of Galaxies*, Ed. R. Wielen (Berlin:Springer), p. 380.

The Dynamics of Abell 2634

J. Pinkney[1], G. Rhee[1], and J. O. Burns[1]
D. Batuski[2], J.M. Hill[3], P. Hintzen[4], W. Oegerle[5]
[1]Dept of Astronomy, New Mexico State University, Las Cruces, NM 88001
[2]Dept of Physics and Astronomy, University of Maine, Orono, ME 04469
[3]Steward Observatory, University of Arizona, Tucson, AZ 85721
[4]Physics Department, University of Nevada, Las Vegas, NV 89154
[5]Space Telescope Science Institute, Baltimore, MD 21218

Abstract

We have amassed a large sample of velocity data for the cluster of galaxies Abell 2634 which contains the wide-angle tail (WAT) radio source 3C 465. Robust indicators of location and scale and their confidence intervals are used to determine if the cD galaxy, containing the WAT, has a significant peculiar motion. We find a cD peculiar radial velocity of 219 ± 98 km s^{-1} . Further dynamical analyses, including substructure and normality tests, suggest that A2634 is an unrelaxed cluster whose radio source structure may be bent by the turbulent gas of a recent cluster-subcluster merger.

Introduction

Abell 2634 is a nearby rich cluster of galaxies which is an excellent setting for the study of environmental effects on galaxies. It contains a cD galaxy, NGC 7720, which is home to the prototypical wide-angle tail (WAT) radio source, 3C465. The bright radio core coincides with the optical nucleus and also the peak in the X-ray emission (Eilek et al. 1984). Diffuse X-ray emission asymmetrically surrounds the cD, which is roughly centered on the galaxy distribution. The cD also contains a companion projected about 12″ (7.2 h_{75}^{-1} kpc) away from the cD nucleus.

Most of the above features of A2634 can play a role in an underlying question of this project: what determines the structure and creation of the radio source 3C465? The WAT radio structure includes two straight jets eminating from the powerful core in opposite directions. The jets decollimate into tails at hot spots roughly equidistant from the core. The diffuse tails bend at or after these decollimation points and extend great distances (about 200 kpc in the case of 3C465). The tails of 3C465 are rather symmetrically bent forming an $\approx$ 90 degree angle with each other. This symmetry has suggested that the WATs are the slower analog of the NAT phenomenon, where motion of the galaxy through the intracluster medium (ICM) bends back the tails via ram pressure (Fanti 1984). Eilek et al. (1984) looked carefully at the physics involved in bending and disrupting the jets at the hot spots and found that galaxy velocities of $\approx$ 1000 km s^{-1} with respect to the ICM would be required for the ram pressure model. O'Donoghue et al. (1992) have recently reexamined the bending phenomenon and found that if another mechanism can be employed to disrupt the jets, lower velocities would be required to shape the tails. They found for tails that emit without *in situ* energization (the *adiabatic* model), the tails will bend by ram pressure even with low galaxy velocities (100 km s^{-1} was used). Their *kinetic* model, which is the opposite extreme where all energization occurs by *in situ* processes, did not allow the ram pressure bending. The true case is probably somewhere between these two models, so a lower limit on the required velocity is uncertain.

There are several reasons for opting for a bending mechanism which does not require the central dominant galaxies (CDGs) to move in WAT clusters. Few of the WATs in the O'Donoghue et al. sample (1990) show as symmetrically bent tails as 3C465, and one (Abell 690) even shows the two tails bending in opposite directions. Thus, it appears that more than simple galaxy motion through an ICM is required to create the structures. Moreover, observations of the central locations of CDGs (relative to both optical and X-ray centroids), as well their radial velocities (e.g. Quintana & Lawrie 1982) have set upper limits for their true velocities around 300 km s^{-1} . The lack of tidal truncation of extended cD envelopes puts even stricter limitations on the velocity of the CDG in their oscillations about the cluster center (Merritt

1984).. We thus became interested in carrying out a study of the dynamics of A2634. In particular, does the cD have a radial peculiar motion and is the cluster relaxed?

Results

We used the MX multifiber spectrometer and 90-inch telescope at Steward Observatory for redshift observations of 126 galaxies in Abell 2634 (i.e. $6000 < V < 14000$ km s^{-1}). This membership criterion reveals a central concentration of galaxies which is elongated with the same position angle as the cD galaxy and the asymmetric extension of X-ray gas. The companion galaxy to the cD is moving at 920 km s^{-1} with respect to the cD; it is not bound. The difference between the cD velocity and the cluster velocity centroid is -219 $\pm$ 98 km s^{-1} . The error for this peculiar motion suggests a 3% probability that the cD shares the radial velocity of the cluster. The velocity distribution can be rejected as Gaussian at the $\approx$ 93% level. It suffers from asymmetry and a long tail both due to high-velocity outliers. We looked for substructure using the δ-test (Dressler & Shectman 1988) and found that the East side of the cluster contained most of the velocity outliers. We did not find significant substructure in the sense of obvious spatial/velocity subgroups.

Discussion

A scenario which may explain the available observations is one of a progressed cluster-subcluster merger. Evrard (1990) has run an N-body, hydrodynamic simulation of cluster formation with a special emphasis on the appearance of the cluster in X-ray over time. The simulation includes a subcluster merger and he finds that the gas oscillates for a few crossing times (10^9 yr) before becoming blended into the general cluster distribution so that an elongation of gas along the direction of merger persists when the galaxies are fairly well mixed. This may explain the long X-ray extension in the core of A2634. The residual gas motion could also provide the ram pressure needed to shape the tails of a stationary WAT (since the infall velocity reaches 800 km s^{-1}).

We can account for the small peculiar motion of the cD using the merger idea in several ways. Our velocity sample may be contaminated and skewed by the presence of the subcluster so that the cluster velocity centroid no longer possesses the original cluster centroid. This contamination effect has been observed by Beers et al. (1991) in clusters with more pronounced substructure. More directly, the cD may have been given an impulse by a passing galaxy of the subcluster. We find that the net velocity change of the cD can be $\approx$ 170 km s^{-1} for a galaxy passing with an initial speed of $\approx$ 900 km s^{-1} , an impact parameter of 8 kpc and a mass of $.1M_{cD}$. It is also conceivable that the cD could have an induced oscillation in the cluster potential well due to the disturbance by the entire subcluster mass. For typical core radii and cluster potentials, however, the extent of the cD's oscillation is restricted by its lack of tidal stripping. Finally, the differences between our velocity distribution and a Gaussian, and the substructure results are both consistent with a progressed state of merger - where the galaxies may be dispersed but still do not have velocities characteristic of a relaxed cluster.

This work was supported in part by a grant from the U.S National Science Foundation (AST-9012353) to J.O.B.

References

Beers, T.C., Forman, W., Huchra, J.P., Jones, C., & Gebhardt, K. 1991, *Astron. J.* **102**, 1581.

Dressler, A., & Shectman, S.A. 1988, *Astron. J.* **95**, 985.

Eilek, J.A., Burns, J.O., O'Dea, C.P., & Owen, F.N. 1984, *Astrophys. J.* **278**, 37.

Evrard A.E., 1990, *Astrophys. J.* **363**, 349.

Fanti, R., 1984, in *Clusters and Groups of Galaxies*, ed. F. Mardirossian, G. Giuricin and M.Mezzetti (D. Reidel), p. 185.

Merritt, D., 1984, *Astrophys. J.* **276**, 26.

O'Donoghue, A., Owen, F.N., & Eilek, J., 1990, *Astrophys. J. Suppl.* **72**, 75.

O'Donoghue, A., Eilek, J., & Owen, F.N., 1992, preprint.

Quintana, H., & Lawrie, D.G. 1982, *Astron. J.* **87**, 1.

X–ray Opacity in Cluster Cooling Flows

Michael W. Wise (NOAO/KPNO) and Craig L. Sarazin (UVa)

ABSTRACT. We have calculated the emergent X–ray properties for a set of spherically symmetric, steady–state cluster cooling flow models including the effects of radiative transfer. Opacity due to resonant X–ray lines, photoelectric absorption, and electron scattering have been included in these calculations, and homogeneous and inhomogeneous gas distributions were considered. The effects of photoionization opacity are small for both types of models. In contrast, resonant line optical depths can be quite high in both homogeneous and inhomogeneous models. The presence of turbulence in the gas can significantly lower the line opacity. We find that integrated X–ray spectra for the whole cooling flow are only slightly affected by radiative transfer effects. However X–ray line surface brightness profiles can be dramatically affected by radiative transfer. Line profiles are also strongly affected by transfer effects. The combined effects of opacity and inflow cause many of the lines in optically thick models to be asymmetrical.

1. Introduction

Although the detailed hydrodynamics of the gas in cluster cooling flows is somewhat uncertain, the large X–ray surface brightnesses of these systems indicate large column densities of ionized gas are present. The opacity through these columns can be large, and can have a significant impact on the emission from these objects. The idea that resonant X–ray lines in clusters might have appreciable optical depths has been noted previously by several authors.[1,2,3] Significant levels of resonant scattering can redistribute line photons spatially in the cluster, reducing the surface brightness in the center of the cluster and increasing it at larger radii. Resonant line absorption can also affect the line profiles, producing distinctive double peaked profiles. In addition, there is a growing body of evidence that cooling flows may contain considerable continuum opacity as well.[4,5,6] Recently, White *et al.* have reported detection of significant amounts of excess absorption associated with 12 cluster cooling flows.[6] This absorption is apparently due to photoionization. Within the cooling flow regions of clusters, the gas column densities are significantly higher than those in the surrounding cluster. The increased optical depths which these conditions imply could significantly enhance these effects. In this work, we discuss the X–ray properties for a set of cooling flow models calculated including the effects of radiative transfer. We have examined the optically thin X–ray properties for these models previously.[7].

2. Continuum Opacity

In homogeneous models, the continuum opacity due to photoionization can be appreciable, reaching values of $\tau_{ph} \sim 0.7$ in the innermost regions of the cooling flow. The total X–ray emission from this model within a radius $r \leq 1\,\mathrm{kpc}$ is reduced by ∼15%. The effects of photoionization opacity are negligible, however, for strongly inhomogeneous models. For these models, the maximum photoionization optical depths are $\sim 3 \times 10^{-3}$. Neither class of model can produce the level of absorption implied by recent observations cluster cooling flows.[6] Although the opacity due to photoionization is appreciable in the homogeneous model, this absorption is spatially confined to a fairly small portion of the cooling flow region ($r < 1\,\mathrm{kpc}$). The results of White *et al.* indicate that the observed absorption must cover $\sim 2/3$ of the cooling flow region.[6] However, our assumption of steady-state cooling may be inaccurate for very cool gas.

3. Line Opacity

The optical depths due to resonant line opacity are also greatly enhanced in the homogeneous models as compared to inhomogeneous ones. These calculations include the emission from 566 X–ray lines of which 235 can lead to resonant absorptions.[8,9] For an inhomogeneous cooling flow model, maximum line optical depths are typically $\sim$ 1–3, with approximately 20 lines having optical depths greater than unity. In contrast, the homogeneous model can produce $\sim$ 100 lines with $\tau_l \geq 1$ and maximum optical depths which reach values of $\sim$ 1–100. The line optical depths depend inversely on the line widths. Consequently, for any given model, the inclusion of turbulent broadening will decrease the line optical depths.

4. Emergent X–ray Properties

Radiative transfer effects can have a significant impact on the X–ray emission from cluster cooling flows. These effects are most pronounced for models with homogeneous cooling. This is due to the shell of cooler, dense material which forms just inside the sonic radius in homogeneous cooling flow models. The temperature drops catastrophically within this shell (at $r \sim 0.7\,\mathrm{kpc}$), producing a large enhancement in the amount of absorbing material. For models with distributed, inhomogeneous cooling, radiative transfer will still affect the X–ray properties but to a lesser degree.

The integrated X–ray spectra are only slightly affected by the inclusion of radiative transfer in the gas. The largest optical depths are due to resonant line scattering, which merely redistributes the emission spatially and spectrally. Because the largest optical depths are confined to number of resonance lines which produce only a small fraction of the total X-ray luminosity, the total X-ray emission is not strongly affected by transfer effects. Within the central kpc, opacity effects remove $\sim$ 15% of the total X–ray luminosity in the homogeneous model assuming thermal line broadening. At larger radii, the change is less than a few percent.

More dramatic results of radiative transfer are seen in the X–ray line surface brightness profiles. The net effect of radiative transfer is to decrease the central values of the surface brightness, and increase the brightness at larger radii. The profiles for homogeneous models show the largest effect. The effect is reduced in inhomogeneous models, but is still appreciable. Turbulent broadening reduces the level of this effect, because of the dependence of the line opacity on the line width.

Line profiles are also strongly affected by transfer effects. In optically thin, spherically symmetric cooling flow models, the lines are always symmetrical (ignoring the effects of line blending). The combined effects of opacity and inflow cause many of the lines in optically thick models to be asymmetrical.

References

1. Shapiro, P. R., & Bahcall, J. N. 1980, ApJ, 241, 1.
2. Basko, M. M. Komberg, B. V., & Moskalenko, E. I. 1981, Sov Astr, 25, 402.
3. Gil'fanov, M. R., Sunyaev, R. A., & Churazov, E. M. 1987, Sov Astr, 13, L3.
4. Lea, S. M., Mushotzky, R. F., & Holt, S. S. 1982, ApJ, 262, 24.
5. Matilsky, T., Jones, C., & Forman, W. 1985, ApJ, 291, 621.
6. White, D. A., Fabian, A. C., Johnstone, R. M., Mushotzky, R. F., & Arnaud, K. A. 1991, MNRAS, 252, 72.
7. Wise, M. W., & Sarazin, C. L. 1992, ApJ, submitted.
8. Hamilton, A. J., Sarazin, C. L., & Chevalier 1983, ApJS, 51, 115.
9. Wise, M. W. 1992, Ph.D. thesis, University of Virginia.

On the Nature of Star Formation in Cooling Flow Ellipticals

Patricia C. Hanlan
Department of Astronomy, University of Michigan

James M. Schombert
Infrared Processing and Analysis Center, Jet Propulsion Laboratory
California Institute of Technology

and

Mary Barsony
Harvard-Smithsonian Center for Astrophysics

We present evidence based on narrow band optical and near-IR imaging that field and cluster cooling flow galaxies are enriched in low mass stars as a result of recent, truncated IMF star formation from accreting gas. We imaged 25 normal and 6 cooling flow ellipticals using a narrow blue band system. All galaxies have similar mean colors and color gradients. Near IR surface photometry was obtained for three normal ellipticals, three cooling flow ellipticals, and three cluster cooling flows.

Galaxies with low accretion rates ($\dot{M} < 5\,M_{\odot}$ yr^{-1}) have normal optical colors and color gradients, but red $V-K$ colors. The metallicity of these galaxies can be estimated using the narrow band $v-y$ color. The $v-y$ color is the same for all galaxies in the sample. The metallicity gradients derived from the $v-y$ radial color gradients can be converted to Mg_2 or [Fe/H] gradients to compare these new data to the literature. The $V-K$ color is also dependent on metallicity. For the galaxies studied, the [Fe/H] gradients derived from $v-y$ are the same as [Fe/H] gradients found using independent methods. (Thomsen and Baum, 1989). We then interpret the red $V-K$ colors of cooling flow galaxies as not a metallicity effect but an effect coming from star formation with an IMF enhanced in low mass main sequence stars.

Cluster cooling flow ellipticals ($\dot{M} > 50\,M_{\odot}$ yr^{-1}) display characteristics of weak bursts of star formation (i.e. blue optical colors - see Fig. 1). If one assumes a normal IMF, an upper limit on the total amount of star formation can be calculated because of the size of the blue color excess. The blue colors imply that only about 5% of the cooling flow mass turns into stars with a normal IMF. Red $V-K$ colors are also found in cluster cooling flow galaxies indicating that the remaining mass forms low mass stars.

The cooling flow galaxies in our sample have been plotted on a $V-K$, $U-V$ color-color diagram (Fig. 1). Also on this diagram, expected colors for given IMF's are plotted. For each IMF, the integrated colors are a function of $[Fe/H]$. The more metal rich, the stellar population, the redder the colors. For reference, two lines of constant $[Fe/H]$ are plotted in figure 1. The functional form of the IMF goes as mass$^{-(1+x)}$. The Salpeter IMF (x=1.35) is plotted, as well as an IMF dominated by low mass star formation (x=3.00). Normal ellipticals cluster about and x=2 IMF but the cooling flow ellipticals are consistent with an IMF of higher x.

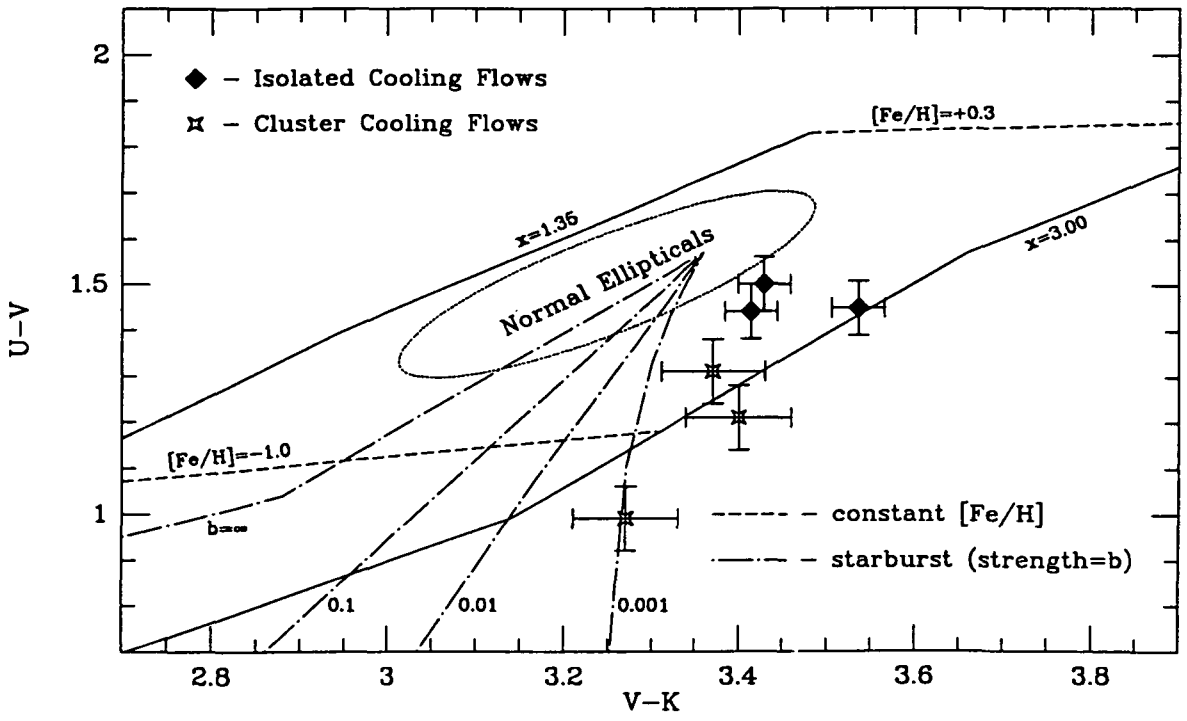

Figure 1. The optical to near-IR two color diagram. Solid and dashed lines show models for varying IMF and metallicity. Dash-dot lines show models of starbursts for various strengths (b = mass of new stars/mass of galaxy). Dotted ellipse is the region occupied by normal ellipticals.

STAR FORMATION IN COOLING FLOW GALAXIES

Nicolás Cardiel, Javier Gorgas

Departamento de Astrofísica, Facultad de Ciencias Físicas, Universidad Complutense de Madrid, 28040-Madrid, Spain

ABSTRACT

Spectroscopic observations of central dominant galaxies are reviewed. Through the analysis of absorption spectral features (mainly the strength of the Mg triplet at 5175 Å and the break in 4000 Å), both in the galaxy centers and along the radii, we will be able to impose limits on the ongoing star formation as the ultimate fate for the large amounst of acoreted gas. With the same aim we will carry out a dynamical study based on velocity dispersion measurements.

INTRODUCTION

X-ray observations have shown that some cluster dominant galaxies are accreting large amounts of gas (cooling flows) from the intracluster medium at typical rates of 100 $M_\odot$/yr. It is estimated that this gas accretion could have persisted for 1-10 Gyr. Therefore, such galaxies could have accreted a total mass of 10^{11}-10^{12} $M_\odot$, comparable with their estimated masses (Sarazin 1986, and O'Connell and McNamara 1989).

ABSORPTION FEATURES AND STELLAR FORMATION

Several studies have pointed out that the only plausible fate for the large amounts of gas accreted is the formation of new stars. However, the spectra of these galaxies are roughly similar to those of galaxies without accretion, and the studies devoted to detect such star formation have produced contradictory results so far. Whilst some galaxies exhibit evidences of ongbing star formation, in other objects with important cooling flows, no signs of an accretion population have been found.

A direct approach to this problem, almost not employed in previous works, is the study of spectral absorption features in cooling flow galaxies. In a preceding work (Gorgas, Efstathiou and Aragon, 1990), we have analyzed the line strengths in the central regions of a sample of cD galaxies. It should be noted that the Mg_2 index is very sensitive to changes in the stellar population and, therefore, to any possible recent star formation. Since both the velocity dispersion and Mg_2 decrease with radius in early-type galaxies (Gorgas and Efstathiou, 1987), these measurements must be corrected to the same lineal aperture. The corrected data show that there is no firm evidence that the Mg_2 indices for cooling flow galaxies differ from those of normal ellipticals at the same velocity dispersion (roughly same absolute magnitude). However, it should be remarked that the mean gradients for elliptical galaxies have been used to perform the aperture corrections. Using long slit observations of 3 cD galaxies, Carter *et al.* (1985) and Gorgas *et al.* (1990) found,

respectively, that the gradients in σ and Mg_2 are, in the mean, smaller than those found in ellipticals. Therefore such corrections could be overestimated and conclusive results can not be extracted until asystematic study with spatial resolution of cooling flow galaxies can be performed. Such study is essential to get information about the radial distribution of mass deposition. The comparison of the line-strength gradients in cooling flow galaxies with those found in giant ellipticals could help to determine whether the star formation is concentrated in the central regions (lower gradients for cooling flow galaxies) or whether the mass is deposited gradually along the galaxy radius (higher gradients). Our former results contrast with those found by Johnstone, Fabian and Nulsen (1987). These authors found evidences of star formation in cooling flow galaxies, showing a correlation between the depth of the break at 4000 Å, and the gas accretion rate. In order to compare these results with ours we have modelled, using an evolutionary synthesis technique, the expected changes in Mg_2 and D_{4000} for a range of ongoing star formation rates (Gorgas *et al.* 1990). The model predictions show that the changes in D_{4000} measured by Johnstone *et al* ($D_{4000} \approx 0.2$-1.2) should involve large variations in the Mg_2 index, not detected in our sample. It is important to note that the D_{4000} values from the correlation of Johnstone *et al.* are strongly correlated with the redshift of the objects, indicating the existence of an aperture effect analogous to that described for Mg_2. The measurement of radial gradients for both features in cooling flow galaxies is therefore hardly needed to confirm or not the existence of such a correlation.

Another information source is the analysis of emission lines frequentely found in these objects, which allow to know the possible ionization mechanisms (massive young stars, collisions) (Heckman *et al.* 1988), and the radial distribution of the accretion population.

REFERENCES

- Carter, D., Inglis, I., Ellis, R.S., Efstathiou, G., and Godwin, J., 1985, *Mon. Not. R. astr. Soc.*, **212**, 471
- Gorgas, J., and Efstathiou,G., 1987, *Structure and Dynamics of Elliptical Galaxies*, IAU Symp. 127, ed. Zeeuw, T., Reidel, Dordreoht, p. 189
- Gorgas, J., Efstathiou, G., and Aragón, A., 1990, *Mon. Not. R. astr. Soc*, **245** 217.
- Heckman, T.M., Baum, S.A., van Breugel, W., y McCarthy, P.J., 1988, *Cooling Flows in Clusters and Galaxies*, ed. Fabian A.C., Kluwer, p 2-5.
- Johnstone, R.M , Fabian, A.C., and Nulsen, P.E.J., 1987, *Mon. Not. R. astr. Soc.*, **224**, 75.
O'Connel, R.W., 1987, *Structure and Dynamics of Elliptical Galaxies*, IAU Symp. 127, ed. Zeeuw, T. Reidel, Dordrecht, p. 167.
- O'Connel, R.W. and McNamara, B.R., 1989, *Astron. J.*, **98**, 180.
- Sarazin, C.L., 1986, *Reviews of Mod. Physics*, **58**, 1.

JET INDUCED STAR FORMATION IN CENTRALLY DOMINANT GALAXIES?

Brian R. McNamara

Kapteyn Institute, Groningen, Netherlands

Using $U - I$ CCD color maps of two centrally dominant cluster galaxies, we find unusual color structures which may be due to star formation which has been induced by their radio sources. These objects, located in the clusters A1795 and A2597, have blue central colors to radii of $\sim$ 20 kpc, spatially extended emission-line structures, and powerful radio sources. They reside at the centers of cooling flows with mass-accretion rates which are estimated to be $\gtrsim$ 300 $M_\odot$ yr^{-1}. The regions of bluest local color are superposed on or along their radio-source structures (see Figure 1 for one example and McNamara & O'Connell 1992, AJ, Submitted). Our observations suggest that the radio sources associated with these objects may be inducing massive star formation in their central 20 kpc. The star formation may be the result of the radio plasma interacting with the warm emission-line gas and dense, X-ray-emitting filaments similar to those recently discovered in two other clusters with the *ROSAT* Observatory (Sarazin, O'Connell & McNamara 1992, ApJ, 389, L59; and in press). Since radio jets are likely to be transient, this may help to explain the scatter in the correlations between color and mass-accretion rate (*cf.* McNamara & O'Connell 1992 ApJ, 393,579), although other factors may also contribute. Alternatively, scattered radiation from a hidden active nucleus (Crawford & Fabian 1991, preprint; Sarazin & Wise 1992, preprint) or recent mergers may be responsible for the color structure. The color and radio properties of these objects are qualitatively similar but smaller in luminosity and spatial extent to those found in high redshift radio galaxies (McCarthy *et al.* 1987, ApJ 321, L29; Chambers *et al.* 1987, Nature, 329, 604.). Our observations of galaxies at $z \sim 0.06 - 0.1$ show that processes similar to "the alignment effect" found in high redshift radio galaxies occur at more recent epochs.

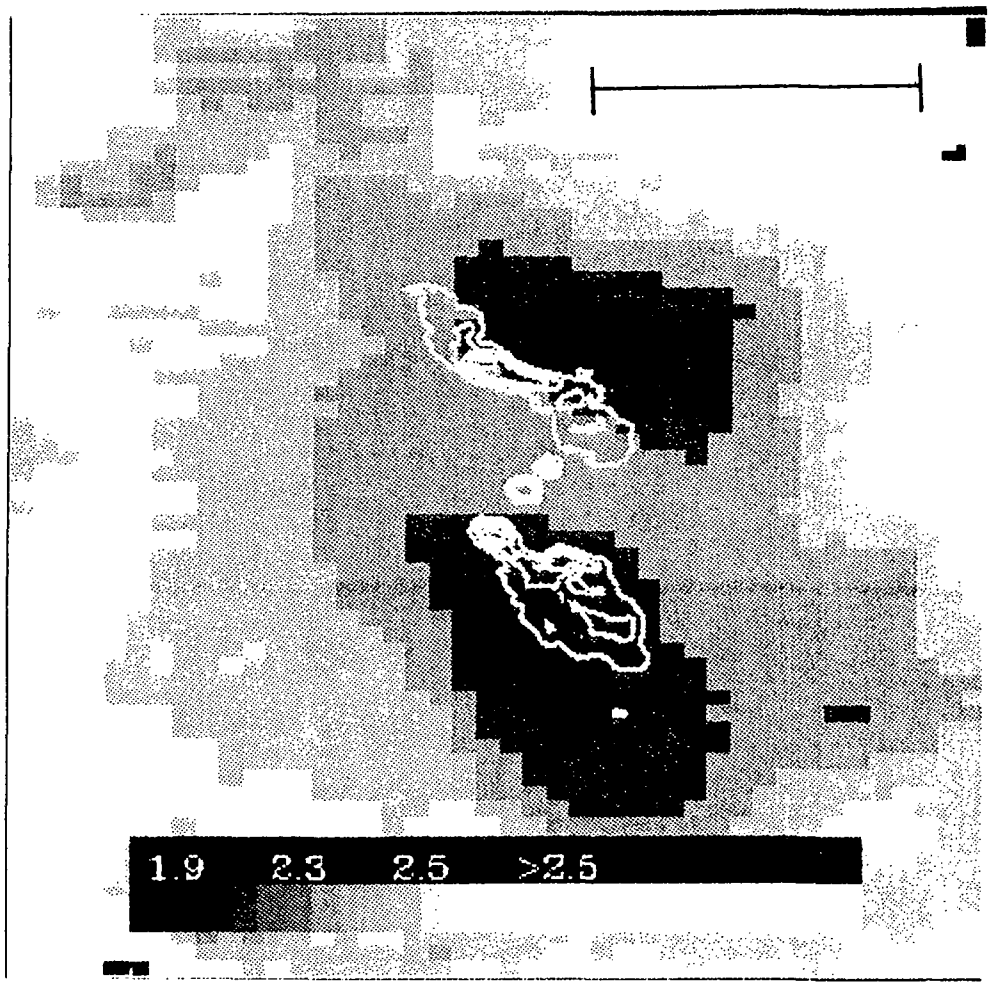

Figure 1 Gray scale version of a $U - I$ color map for the central region of the centrally dominant galaxy in the cluster Abell 1795. Superposed in white contours is a high resolution radio map at 3.6-cm (Ge 1991; PhD Thesis, New Mexico Tech). North is at the top, east is to the left; the scale bar to the upper right indicates 5 arcsec ($\sim$ 10 kpc; $H_0 = 50$ km/sec/Mpc). Both the U and I band images were smoothed with a 5×5 pixel sliding box before computing the color map. The white regions correspond roughly to old background population colors. The entire central $\sim$ 20 kpc is bluer than a normal centrally dominant galaxy. The blue lobes are $\sim$ 0.9 mag. bluer than normal. The region between and surrounding the blue lobes are 0.4–0.6 mag. bluer than normal. The radio and optical maps were aligned assuming the central radio source midway between the radio lobes is centered on the I-band nucleus. The blue lobes, primarily resulting from blue continuum light, are found along the edges of the radio lobes. The lobes are bluest in their centers. If the blue light is primarily due to massive star formation, the rate of star formation is $\sim 10 - 45$ $M_\odot$ yr^{-1} for ages between 5 Myr and 4 Gyr, assuming the Local IMF (McNamara & O'Connell 1992, AJ, submitted).

The Detection of Large Amounts of Cool, X-ray Absorbing Gas in Distant Clusters of Galaxies What Does This Mean?

Qingde Wang[1] and John T. Stocke

Center for Astrophysics and Space Astronomy,
University of Colorado, Boulder, CO 80309-0389

SUMMARY

We present an X-ray spectral study of 12 distant ($z = 0.17 - 0.54$) rich clusters of galaxies observed with the *Einstein* Observatory Imaging Proportional Counter. These X-ray spectral data show evidence for substantial excess absorptions beyond those expected in the Galaxy, indicating the presence of large amounts of X-ray absorbing cool gas in these distant clusters. The mean value of the excess absorptions corresponds to an absorbing gas column density $\gtrsim 10^{21}$ cm^{-2}. We calculate the X-ray luminosities of the clusters with observed fluxes only in the 0.8-3.5 keV band where the fluxes are less effected by the absorptions, and use the temperature-to-luminosity correlation (known only for nearby clusters) to estimate the temperatures of the hot intracluster medium (ICM) in the distant clusters. These temperature estimates, together with the spectral fits, provide further constraints on the column densities in the individual clusters. For the cluster CL 0016+16 (Fig. 1), the lower limit on the column density is found to be $\sim 8 \times 10^{20}$ cm^{-2} at the $\sim 99\%$ confidence limit. We also show that the ratio of the temperature obtained from the spectral fit to the temperature expected from the correlation tends to decrease with increasing look-back time, indicating possible temperature evolution of the hot ICM in the recent past. The inclusion of this evolutionary effect further increases the absorptions required in fitting the spectra. There are some important implications of these findings:

- ▷ The absorptions, together with temperature evolution, may explain why there are more high-luminosity clusters now than there were in the past.
- ▷ There might be a link between the excess absorption and the redness of some distant clusters. An apparent anti-correlation between the absorption and the percentage of blue cluster galaxies may be caused by dust extinction, likely associated with the cool gas.

[1] also at the Joint Institute for Laboratory Astrophysics, University of Colorado and National Institute of Standards and Technology

▷ The free-free emission from the X-ray absorbing gas, if existing in the $\sim 10^4$ K warm phase, could cause some serious confusion in the measurements of the Sunyaev-Zel'dovich effect of the hot ICM. Rim-brightened radio continuum emission features may be produced in the case that the gas is distributed primarily in shell-like regions surrounding the X-ray emitting central regions of the clusters. This could cause an overestimate of the S-Z effect in these clusters and an underestimate of H_o obtained by such studies.

A conceivable origin of the cool gas is the ram-pressure stripping of the gas from individual galaxies when they were falling into the clusters. This may connect the production of the cool gas to the high percentage of "post-starburst" galaxies seen in distant clusters.

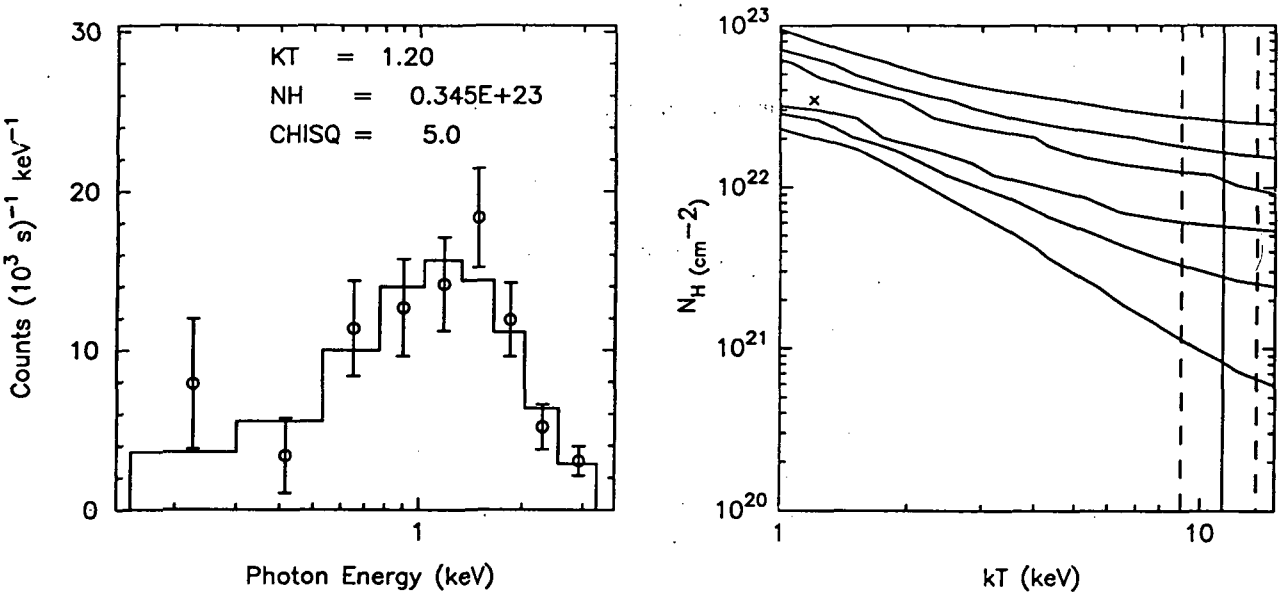

Fig. 1 The X-ray spectrum of the cluster CL0016+16 (z=0.54) and a model fit. The left side panel shows the best fit to the spectrum with a Raymond & Smith optically-thin thermal plasma model. The right side panel shows the 68%, 90%, and 99% confidence contours for T and N_H. The cluster temperature (solid line) and its uncertainties (dashed lines) are marked which are estimated from the cluster's luminosity using the $T - L_x$ correlation observed for nearby clusters.

MERGERS, COOLING FLOWS AND EVAPORATION

W.B. Sparks

Space Telescope Science Institute

1. Abstract

Mergers (the capture of cold gas, especially) can have a profound influence on the hot coronal gas of early-type galaxies and clusters, potentially inducing symptoms hitherto attributed to a cooling flow, if thermal conduction is operative in the coronal plasma. Heat can be conducted from the hot phase into the cold phase, simultaneously ionizing the cold gas to make optical filaments, while locally cooling the coronal gas to mimic a cooling-flow. If there is heat conduction, though, there is no standard cooling-flow since radiative losses are balanced by conduction and not mass deposition.

Amongst the strongest observational support for the existence of cooling-flows is the presence of intermediate temperature gas with X-ray emission-line strengths in agreement with cooling-flow models. Here, X-ray line strengths are calculated for this alternative model, in which mergers are responsible for the observed optical and X-ray properties.

Since gas around 10^4K is thermally stable, the cold cloud need not necessarily evaporate and hydrostatic solutions exist. Good agreement with the X-ray data is obtained. The relative strengths of intermediate temperature X-ray emission lines are in significantly *better* agreement with a simple conduction model than with published cooling-flow models. The good agreement of the conduction model with optical, infra-red and X-ray data indicates that significantly more theoretical effort into this type of solution would be profitable.

2. What can a merger do to pre-existing coronal gas?

Although optical emission filaments typically represent a trifling amount of mass, energetically they can be very important and can have radiated energy fluxes in excess of the X-ray excess. Sparks, Macchetto and Golombek (1989) favoured an accretion or merger origin for the optical emission filaments and dust-lane in NGC 4696 and showed that a conduction model, where the accreted cold gas is heated by the hot coronal plasma, works very well on energetic grounds. Sparks and Macchetto (1990) also showed that a conduction model correctly predicts optical line emission surface brightness *vs.* radius in M87. By contrast the cooling-flow model consistently fails to account for both the strength of optical line emission and the run of emission-line surface brightness with radius. Other reasons for inferring an accretion origin for cooler gas in general are reviewed by Macchetto and Sparks (1991).

If 10^4K is chosen as the cloud boundary, then clouds are highly radiative and do not need to evaporate. Models of static conduction interfaces can be constructed, with a wide range of conductive heat flux, q_0, across the inner boundary. The solution to the static, plane-parallel, isobaric heat-flow problem is:

$$q^2 = q_0^2 + 2\alpha g(y) \qquad (1)$$

where $y = (T/10^7\mathrm{K})^{7/2}$, $g(y) = \int_{y_0}^{y} \Lambda_{23} dy'/y'^{2/7}$, a dimensionless function derived from

the cooling function, Λ, q is the normalized heat flux, and $\alpha \propto n_0^2 T_0^2$. The solution expressed in this way contains the information needed to confront observations. It is a 'phase-space' solution with temperature gradient expressed as a function of temperature and changes in q indicative of radiative losses. The total emission from the cloud is the direct conductive heat input plus photons from the interface that travel inwards.

Using John Raymond's optically thin hot plasma emission code, this solution was used to calculate X–ray line fluxes for the example of M87, with parameters for the models obtained from optical observations of the filaments and X–ray observations of the corona. The resultant line ratios are given in the table, the conduction models representing extremes of entirely radiative and entirely conductive powering of the filaments. Observations are from Canizares *et al.* (1982) and the cooling-flow model from Stewart *et al.* (1984). Clearly the conduction models provide a statistically better fit. The absolute levels are also in good agreement with observation.

Table 1: Observed and Model X–Ray Line Ratios for M87

Line	Observed	$q_0 = 0$	$q_0 = 60$	Saturated limit	Cooling flow
OVIII Lyα	16.3 ± 5.4	23.1	21.2	19.2	9.5
OVIII Lyβ	< 2.3	4.0	3.8	3.6	
Blend 1	5.4 ± 1.0	3.9	3.9	3.8	4.2
Blend 1.5	< 1.5	1.1	1.1	1.0	
Blend 2	5.1 ± 1.1	5.3	5.2	5.1	5.4
Blend 3	4.3 ± 1.1	3.7	3.8	3.8	4.6
Blend 4	2.5 ± 1.1	3.3	3.4	3.7	4.8
Blend 5	3.2 ± 0.6	3.6	3.8	3.9	5.7
Blend 6	2.0 ± 1.0	1.7	1.7	1.8	1.3
FeXVII	2.5 ± 1.1	4.0	3.6	3.0	0.8
Continuum	100.0	100.0	100.0	100.0	
Reduced χ^2		0.89	0.75	0.76	3.28

3. Summary

Simple theoretical models of thermal interaction between hot and cold gas phases have been explored. Standard evaporation concepts have been questioned and solutions derived in the hydrostatic case, see Sparks (1992) for details. Detailed comparison of a simple conduction theory using reasonable, observationally derived parameters, with observations of M87 gives good agreement with the intermediate temperature X–ray properties, better in fact than the published 'cooling-flow' analysis of this galaxy. Observational results at X–ray, optical and infra-red wavelengths are readily understood within the framework of this description, including the strengths and ratios of X–ray lines, the strength of optical line emission, the spatial distribution of optical line emission and the presence of dust and infra-red emission associated with the optical filaments. Hence, it is possible that incorporation of heat conduction may provide the key to understanding inter-relationships between the different gaseous phases that have been observed in different wavelength regimes. Rather than treating systems as self-contained 'closed-boxes', it may be necessary to consider the environment in much more detail.

A Neutral Hydrogen Survey of the Hydra I Cluster

Pauline McMahon, Jacqueline van Gorkom (Columbia University)
Otto Richter (STScI), Henry Ferguson (Cambridge University)

Introduction

We are undertaking a project to image the entire volume of the Hydra I cluster of galaxies in neutral hydrogen using the VLA. This involves making a series of pointings spaced 30′ (the half power beam width) apart, each observed at three velocity settings in order to span the whole velocity range of the cluster. The purpose of this survey is to determine the true distribution, both in space and velocity, of gas-rich systems and hence, to deduce what effects a dense environment may have on the evolution of these systems. Most HI surveys of clusters to date have been performed on optically selected samples. However, optically selected samples may provide misleading views of the distribution of gas-rich systems, since many low surface brightness galaxies have an abundance of neutral gas (Bothun et al. 1987, Giovanelli & Haynes 1989). The Hydra project is providing the first unbiased view of the HI distribution in a cluster of galaxies.

Our 5σ sensitivity is 4.1×10^7 M$\odot$/beam, (assuming $H_o = 75$ km s^{-1} Mpc^{-1}) and our velocity resolution is 42 km s^{-1}. We have a spatial resolution of 45″, which means that only the largest galaxies are spatially resolved enough to determine HI disk size. Our coverage is about 50% of the central region plus eight other fields centered on bright spirals within about 2° of the center.

Results

The survey observations to date consist of four central fields having full velocity coverage and the eight other bright spiral fields. We have detected 41 galaxies in total. Using Richter's (1989) catalogue to determine the optical counterparts to these detections and counting only those late type galaxies with measured optical velocities, we find an overall detection rate of 75%, with no dependence on distance from cluster center. Many more spirals are catalogued with no measured optical velocities, of which we detect 10%.

HI images of the bright spirals reveal gas disks that in general show no evidence for severe stripping. Even the largest and central-most spiral, NGC 3312, displays a gas disk that is nearly as large as its optical. This is in contrast to images of central Virgo spirals, whose HI disks are as small as 25% of their optical disk diameters (Cayatte et al. 1990). In addition, the Virgo spirals show a decrease in stripping with distance from cluster center. Ram pressure stripping by the hot ICM is generally believed to be the cause of the effects seen in Virgo. It is then puzzling that spirals in Hydra, also an X-ray cluster, do not display these same effects.

The galaxies in Hydra are however systematically HI deficient. Taking only those galaxies for which we have photometric diameters, we determined the HI content using the parameter $\log(M_{HI}/D^2)$, and calculated the deficiency in units of the 1σ scatter of Haynes & Giovanelli (1984) field galaxies. The average deficiency is 1σ with a scatter of 1σ. We look for correlations between the deficiency and distance from the cluster center, relative velocity, and local surface density as defined by the ten nearest neighbors. We find a slight trend of increasing deficiency with local density only.

We have detected seven uncatalogued dwarf galaxies, five of which reside in the central fields. Careful examination of the ESO plates reveals small faint blue smudges at the locations of these detections. It is surprising to find gas-rich dwarfs in the central regions of an X-ray cluster and indeed the optical surveys of Virgo by Bingelli et al. (1987) and Fornax by Ferguson (1989) have shown that Im's tend to avoid cluster centers, while dE's are concentrated toward cluster centers. The usual reasoning used to explain centrally located dwarf galaxies is that they perhaps have circular orbits and never actually pass through the X-ray emitting hot gas. However, all the central dwarfs have large relative velocities (> 600 km s^{-1} both higher and lower) with respect to the cluster systemic.

The velocity histogram of all detections in the central fields, i.e., in the fields with full velocity coverage, reveals a bimodal distribution, one group centered at 3000 km s^{-1}, the other at 4500 km s^{-1} (see figure). This was also found by Fitchett & Merritt (1988) in their search for subclustering in Hydra. Plotting the velocity histrogram of all galaxies within 100′ of the center, they found a "hint of bimodality" for those

galaxies within 40′. and a gaussian distribution for those outside 40′. Although the number of galaxies with measured velocities is still quite small, we find that the bimodality is much more pronounced for the gas rich galaxies than for the ellipticals. This may be evidence that the ellipticals form a relaxed system while the spirals (and dwarfs) are more clumped and may be a clue to why the stripping is not very severe but is very constant.

Number of Central Gas-Rich Galaxies per Velocity Bin

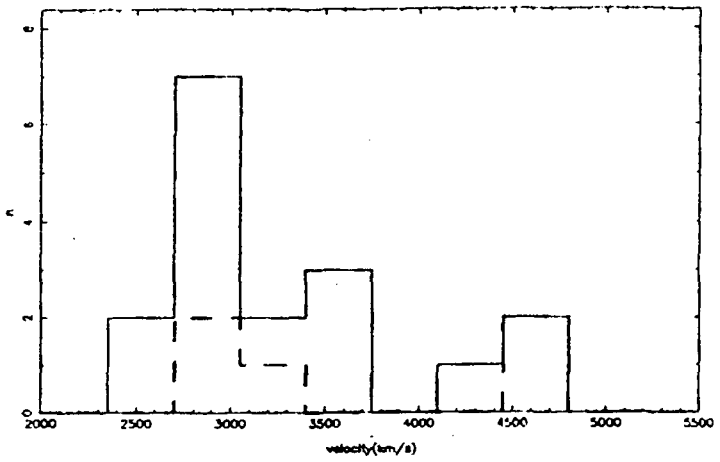

Number of Central Ellipticals and S0s per Velocity Bin

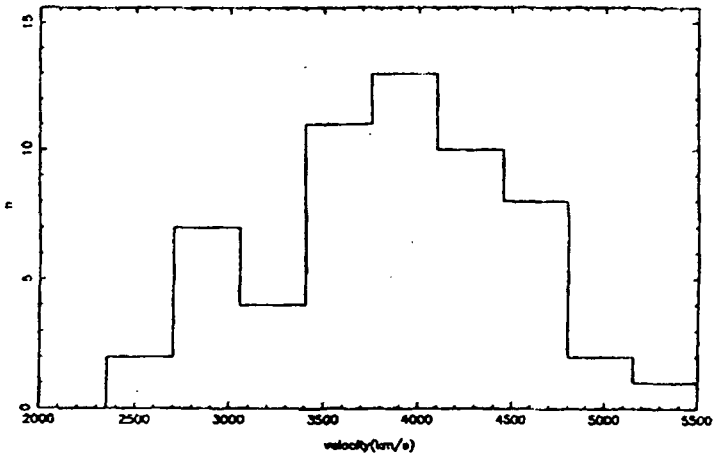

References

Binggeli, B., Tammann, G.A., and Sandage, A. 1987, AJ, 94, 251

Bothun, G.D., Impey, C.D., Malin, D.F., and Mould J.R. 1987, AJ, 94, 23

Cayatte, V., van Gorkom, J.H., Balkowski, C., and Kotanyi, C. 1990, AJ, 100, 604

Ferguson, H. 1989, AJ, 98, 367

Fitchett, M., and Merritt, D. 1988, ApJ, 335, 18

Giovanelli, R and Haynes, M.P. 1989, ApJ, 346, L5

Haynes, M.P., and Giovanelli, R. 1984, AJ, 89, 758

Richter, O.-G. 1989, A&AS, 77, 237

Using X-ray Images to Detect Substructure in a Sample of 40 Abell Clusters

J. J. Mohr, D. G. Fabricant, and M. J. Geller (Harvard-Smithsonian CfA)

Using a method for constraining the dynamical state of a galaxy cluster by examining the moments of its X-ray surface brightness distribution, we determine the statistics of cluster substructure for a sample of 40 Abell clusters. Space considerations preclude a detailed discussion of the method here, so we include a brief summary and refer the reader to Mohr *et al.* (1992). Using X-ray observations from the *Einstein* Observatory Imaging Proportional Counter (IPC), we measure the first moment $M_1(\bar{r})$, the ellipsoidal orientation angle $\theta_2(\bar{r})$, and the axial ratio $\eta(\bar{r})$ at several different radii in the cluster. We determine the effects of systematics such as X-ray point source emission, telescope vignetting, Poisson noise, and characteristics of the IPC by measuring the same parameters on an ensemble of simulated cluster images. Due to the small band-pass of the IPC, the ICM emissivity is nearly independent of temperature (for 2 keV $\leq$ kT $\leq$ 8 keV), so the intensity at each point in the IPC images is simply proportional to the emission measure ($EM = \int n_e n_p \, dl$) calculated along the line of sight through the cluster (e.g. Fabricant *et al.* 1980). Therefore, barring a chance superposition of two X-ray emitting clusters[1], a significant variation in the image centroid $M_1(\bar{r})$ as a function of radius indicates that the center of mass of the intra-cluster medium (ICM) varies with radius. We argue that such a configuration (essentially an $m = 1$ component in the ICM density distribution) is a non-equilibrium component; it results from an off-center subclump or a recent merger in the ICM.

Our sample of 40 Abell clusters is made up of all clusters at $\bar{z} \leq 0.06$ with *Einstein* IPC observations with enough collected photons to apply the method. We characterize the sample in a statistical sense by comparing the distribution in velocity dispersions with the distribution determined from a group of 65 Abell clusters (Zabludoff *et al.* 1990). Our sample has more high dispersion clusters (>1400 km s^{-1}) and fewer low dispersion clusters (<500 km s^{-1}), but the general shape of the distributions is similar. The median velocity dispersion in the Zabludoff *et al.* sample is 744 km s^{-1}, while in our sample it is 853 km s^{-1}. Given the velocity dispersion-X-ray luminosity correlation, the bias in our sample toward high velocity dispersion systems is not surprising; the low dispersion clusters tend to have low X-ray fluxes and only yield good images with extended observation.

As briefly discussed above we make measurements on simulated images in order to determine the significance of the measured variations in the IPC image centroid $M_1(\bar{r})$. For this sample we declare the variations to be significant (the cluster has substructure) if $\leq$1% of the simulated images have measured variations which are larger than the variations in the real IPC image. With this criterion, 27 of the 40 clusters (68%) exhibit measurable departures from dynamical equilibrium, while 13 do not. It is important to note that failure to find an $m = 1$ component in the ICM in no way guarantees that the cluster is a relaxed, equilibrium system. Mergers in which the symmetry axis lies close to the line of sight would produce very little signal. Systematic effects and poor signal-to-noise images decrease our sensitivity. This point is well illustrated by Figure 1. We plot the distribution in number of image photons (a measure of the quality of the

[1] Using the measured $\log N - \log S$ distribution for clusters, ignoring clustering or anti-clustering on 30′ scales, and taking the mean scale of X-ray emission from clusters to be 30′ in radius, we calculate the probability of a superposition for a middle flux-range cluster like Abell 2256 to be <1%.

Figure 1: Image Quality

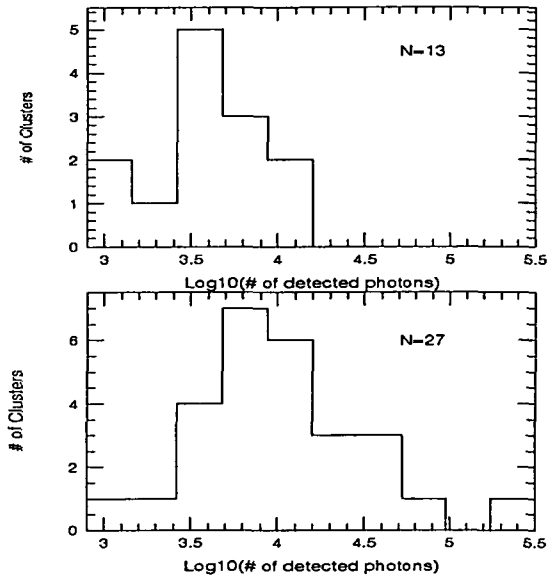

Figure 2: Velocity Dispersion

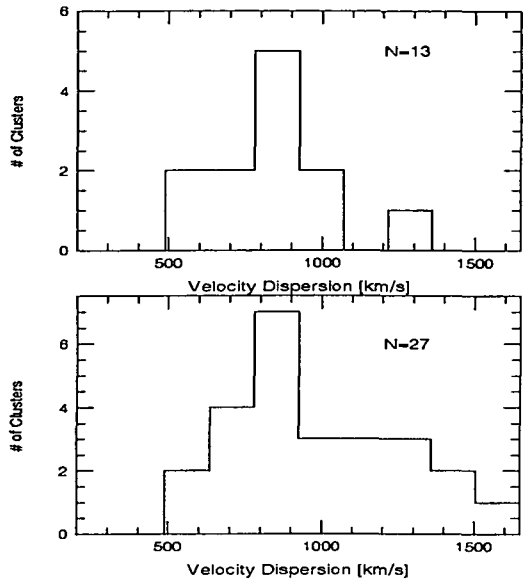

image) for the two cluster groups. The median number of counts in the group of 27 is 10,715, while the median number in the group of 13 is 4,046. Clearly, the clusters with the highest quality images tend to fall in the group of 27 with measured substructure. Therefore, we regard 68% as a lower limit to the actual fraction of clusters with measurable substructure. Further work on higher quality ROSAT images will allow a more sensitive examination of the clusters with poor *Einstein* images.

Although a full discussion of the characteristic differences between the two groups of clusters requires a longer paper, it is interesting to note (see Figure 2) that the clusters with high velocity dispersions (>1100 km s^{-1}) tend to be clusters with measurable substructure. One interpretation of this tendency is that the measured line of sight dispersions in these clusters are enhanced due to recent merger activities; if this is true, there may be considerable departures from an isotropic velocity dispersion in these systems which will complicate calculations of the cluster mass. Further investigation is required to substantiate this.

In summary, we present the results of a study of 40 Abell clusters using a method which examines the low order moments of the X-ray surface brightness profiles. We determine that $\geq$68% of the clusters in our sample have measureable substructure. This result is significant for several reasons: 1) the method is most sensitive to substructure in the core of clusters which are generally believed to be in virial equilibrium and 2) the higher sensitivity of the X-ray method yields a higher proportion of substructure than previous optical investigations.

References

Fabricant, D.G., Lecar, M., Gorenstein, P. 1980, *Ap. J.*, **336**, 77.
Mohr, J. J., Fabricant, D. G., and Geller, M. J. 1992, preprint.
Zabludoff, A., Huchra, J. and Geller, M., 1990, *Ap. J. Supp.*, **74**, 1.

A Study of the X-ray Environment of Radio Galaxies

George Rhee[1], Jack Burns[1] and Frazer Owen[2]

[1]Department of Astronomy, New Mexico State University, Las Cruces, NM 88003
[2]National Radio Astronomy Observatory, P.O. Box 0, Socorro, NM 87801

We are currently working on a program to use extensive X-ray and radio databases to investigate the relationship between extended radio emission and environment in clusters of galaxies. The radio galaxy morphology is determined using VLA imaging and the X-ray properties are determined from EINSTEIN IPC images.

This study is motivated by the hypothesis that the key to understanding radio galaxies lies in the local environment. This hypothesis is suggested by three observations;

1) The radio luminosity function for galaxies in the central 0.3 Abell radii is identical with functions derived for radio galaxies not selected on cluster membership.

2) The radio sources are not primarily identified with the brightest cluster member but seem to be associated with a range of galaxy luminosities.The number of sources detected as a function of richness class is proportional to Abell's number count of galaxies. The probability of radio emission from a galaxy does not depend directly on cluster galaxy density.

3) The distribution of projected distances from the cluster center is very peaked on Abell's position for the cluster. The cluster radio galaxies are more centrally condensed than either the optical or X-ray emission.

To test this hypothesis we have studied the detailed relationship between galaxy radio emission and the X-ray morphology of their parent clusters. In this pilot study we have used 35 radio sources found in 27 clusters. We have determined the position angle of the X-ray and radio emission, and X-ray and radio luminosities. The X-ray position was taken to be the position of peak flux of the subclump containing the radio galaxy. The radio position was taken to be the position of the optical galaxy.

We do not find a correlation between the X-ray and radio source position angle. This remains true when the sample is divided into subsamples according to radio morphology (wide angle tail, twin jet, narrow angle tail galaxies). We find a weak correlation between the radio source luminosity and the X-ray luminosity.

We have computed the distance from the radio galaxy position to the center of the X-ray clump. We find a mean distance from the X-ray clump center of 0.16 Mpc for the radio galaxies in this sample. The mean distance to the nearest clump of X-ray emission is typically half the distance to the optical cluster center. *We thus find strong evidence that radio galaxies are located very close to clumps of X-ray emission* (see Fig. 1). These subclumps are not always affiliated with the central cluster X-ray emission. This supports our hypothesis that X-ray emission may provide a key to understanding radio galaxy morphology. We find evidence that radio galaxies occur in clusters that contain prominent substructures. Radio galaxies may thus provide an added diagnostic of the cluster dynamical state.

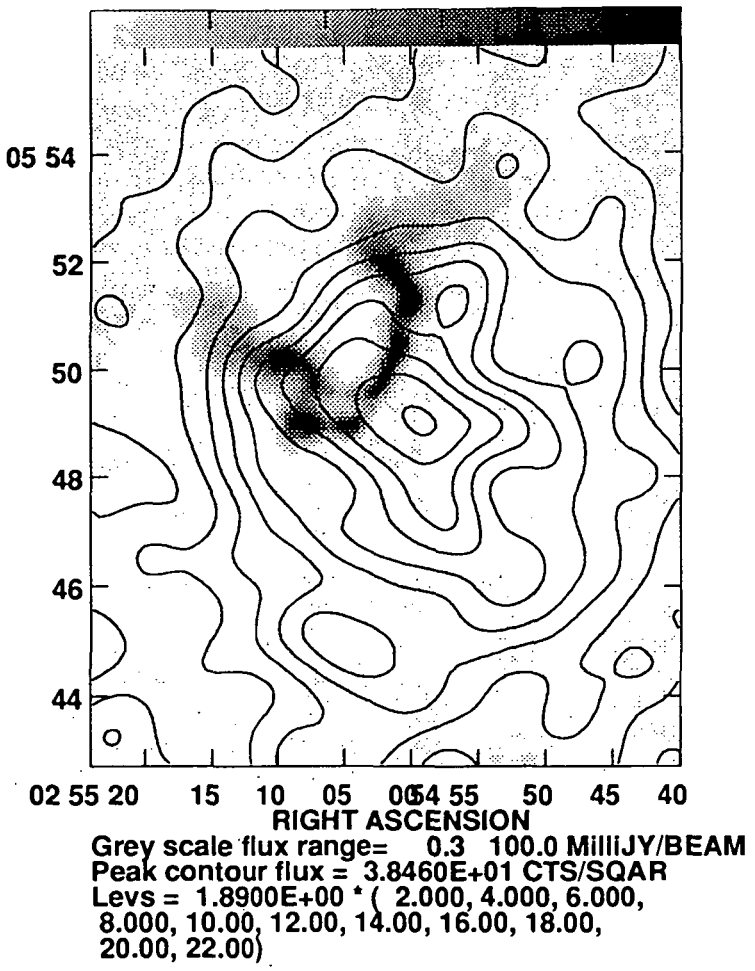

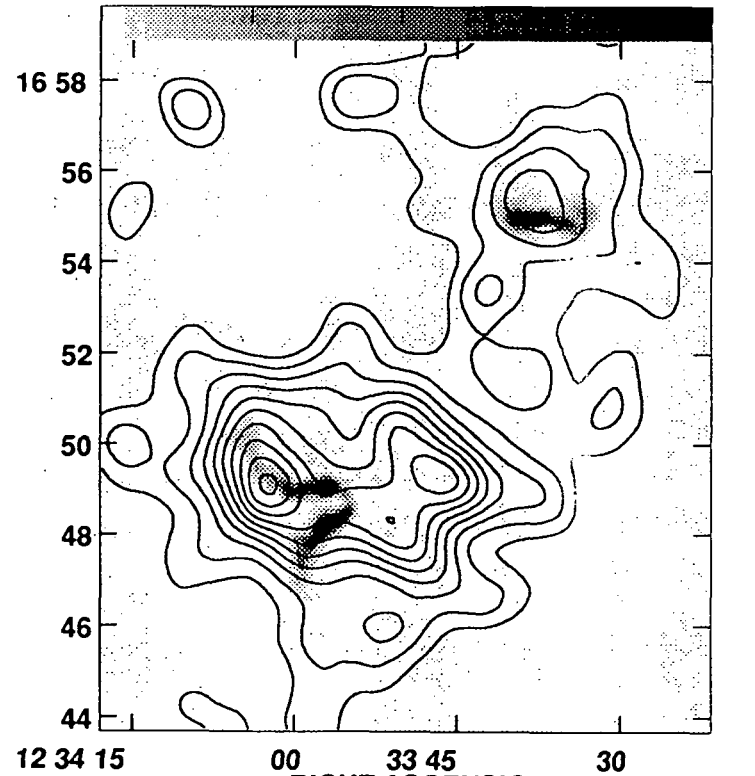

Figure 1. X-ray and radio emission for two clusters in our sample. The contours show the X-ray emission (EINSTEIN IPC), the greyscale shows the radio emission (VLA). The upper figure shows Abell 400 and the lower figure A1569.

MULTICOLOR PHOTOMETRY OF X-RAY SELECTED ABELL CLUSTERS

OMAR LOPEZ-CRUZ

Department of Astronomy, University of Toronto and INAOE-Tonantzintla

Strong evidence of evolution in cluster of galaxies at relatively low redshift has been indicated by recent X-ray studies (e.g. Forman W. and Jones C., 1982, *Ann. Rev. Astron. Astrophys.*, **20**, 547 and Edge *et al.*, 1990, *Mon. Not. R. Astron. Soc.*, **245**, 559).

We are conducting a comprehensive optical study of a sample of Abell clusters that are strong X-ray emitters in order to test the X-ray evolution scenarios that have been proposed. The initial observations consist of three-color (B, R, I) imaging of low-redshift ($0.025 < z < 0.25$) Abell clusters using the T2KA CCD on the 0.9m telescope at KPNO the large field ($23'X23'$, ~ 1 Mpc at $z = 0.025$ and ~ 7 Mpc at $z = 0.25$) gives the unprecedented ability to sample most of the extent of the field of low-redshift clusters using a CCD. Given the advantages of CCDs over photographic plates, we expect to improve on many of the previous studies. A list of X-ray selected cluster of galaxies (Jones C., 1992, *Private Communication*) provides a homogeneous sample of true clusters that cannot be mistaken from apparent over-densities due to projection effects of field galaxies.

Some optical indicators of cluster evolution are the population ratios of

cluster galaxies and their spatial distribution, a regular spiral-poor cluster is expected to be more evolved than an irregular spiral-rich cluster. Also regular spiral-poor clusters present high central concentrations while irregular spiral-rich are less concentrated. Variations in the Luminosity Function (LF) can indicate evolution (Dressler A, 1978, *Astrophys. J.*, **223**, 765). But in order to build reliable LFs is necessary to determine the Hubble types of the cluster galaxies (Binggeli *et al*, 1988, *Ann. Rev. Astron. Astrophys.*, **26**, 631)

In the past the classificactions of cluster galaxies have been done by visual inspection on photographic material, this technique is very limited and can lead to errors when the galaxies are faint. The Hubble types of cluster galaxies can be determined in an objective manner by comparing colors and profiles from surface photometry. To show that this approach is feasible, I have presented preliminary results from the photometric analysis of the Abell-cluster A1213. Colors and profiles of the surface brightness distribution were compared to determined the hubble types of the cluster galaxies.

This work is supported by an overseas scholarship from the *National Council of Science and Technology* (**CONACYT**) of Mexico. The travel funding has been provided by the *Carl Reinhardt Travel Award* and the *National Science and Engineering Research Council* (**NSERC**) of Canada through Dr. Howard K Yee's grant.

Optical and Near Infrared Photometry of Butcher-Oemler Clusters

Lisa M. Shier
Marcia J. Rieke
Steward Observatory
University of Arizona

Rich clusters of galaxies at moderate redshifts (z~.3) have a larger proportion of optically blue galaxies than their low redshift counterparts. Spectroscopic examination of the blue galaxies by various authors has shown that the blue galaxies are generally Seyferts, show evidence for recent star formation, or are foreground objects. Unfortunately, spectroscopy is too time consuming to be used on large samples. Thus, we have looked for a way to separate Seyferts, starbursts, ellipticals and nonmembers using photometry alone.

Five moderate redshift clusters, Abell numbers 777, 963, 1758, 1961 and 2218, have been observed in the V, R and K bands. We model the spectral energy distributions of various kinds of galaxies found in clusters and derive observed colors.

We have modeled the spectral energy distributions (SED) of several kinds of galaxies compute their colors as a function of redshift. We expect to see ellipticals, spirals, starbursts, post-starburst and Seyfert galaxies. The SED of elliptical and Sbc galaxies was observed by Rieke and Rieke (in prep.). The SEDs for the starburst galaxies was created by adding a reddened 10^8 year old burst to a spiral galaxy SED. The post-starburst (E+A) galaxy SEDs are composed of a slightly reddened 10^9 year old burst and elliptical galaxy SED. SEDs for the Seyferts were created by adding a $\nu^{-1.1}$ power law, and a hot dust thermal spectrum to the Sbc. From the SEDs the colors of galaxies at various redshifts with assorted filters were computed.

Lilly & Gunn (1985) have optical and infrared photometry for a sample of galaxies in CL0024+1654 observed spectroscopically by Dressler, Gunn and Schneider (1985). We have used this data to choose the most appropriate SEDs for our starburst and post-starburst models. Their data and our models are shown together in figure 1.

The most likely explanation for the optically blue colors in most cluster galaxies is star formation. Very few galaxies lie in the Seyfert locus. Abell 1758, shown in figure 2, has more Seyfert candidates than the other clusters, we observed.

It seems possible to roughly sort types of galaxies in clusters by color alone. The cluster population seems to vary considerably between clusters, but our K selected sample has few Seyferts in any cluster.

References

Lilly, S. J. and Gunn, J. E. *MNRAS*, **217**, 551.
Rieke, M. J. and Rieke, G. H., in preparation.
Dressler, A., Gunn, J. E., and Schneider, D. P., 1985 *Ap. J.*, **294**, 523.

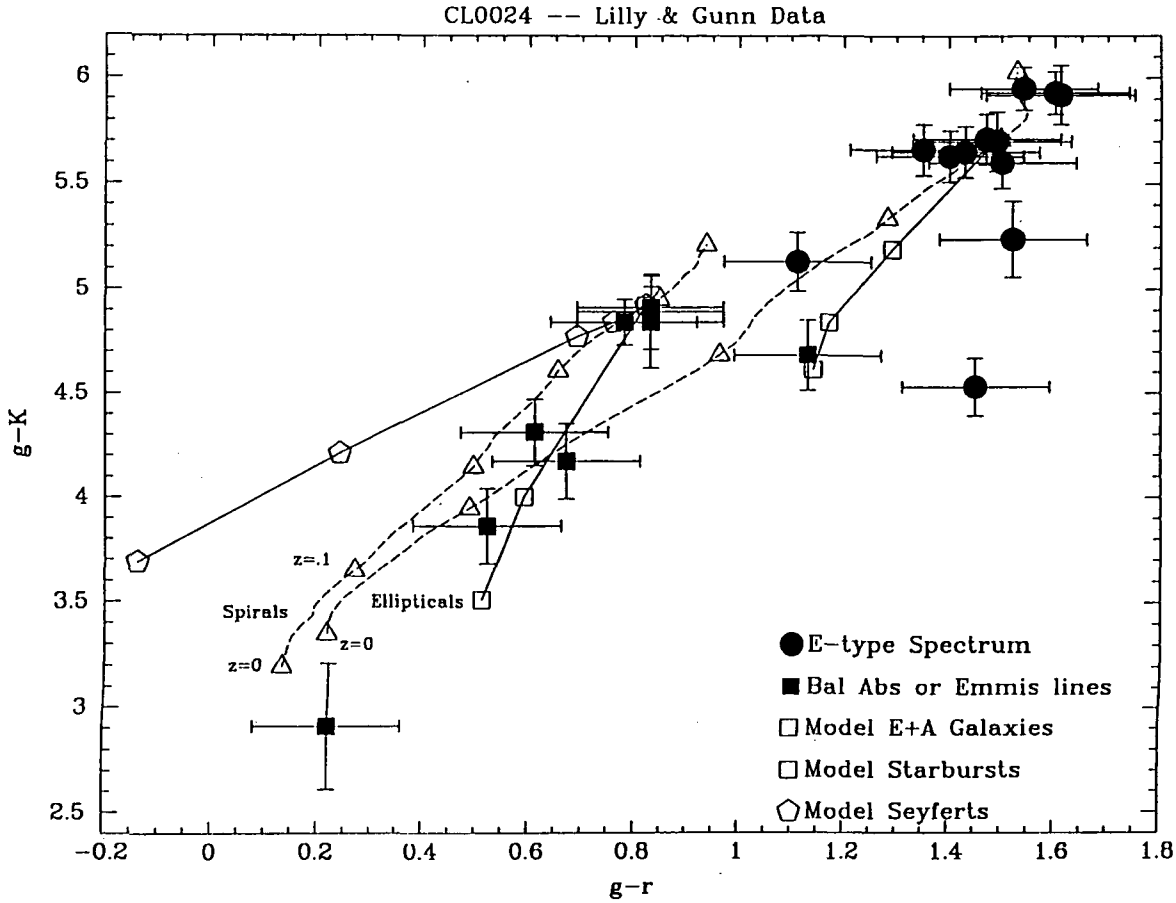

Figure 1. CL0024+17 photometry and models. Photometry taken from Lilly & Gunn (1985), spectroscopic information from Dressler, Gunn and Schneider (1985).

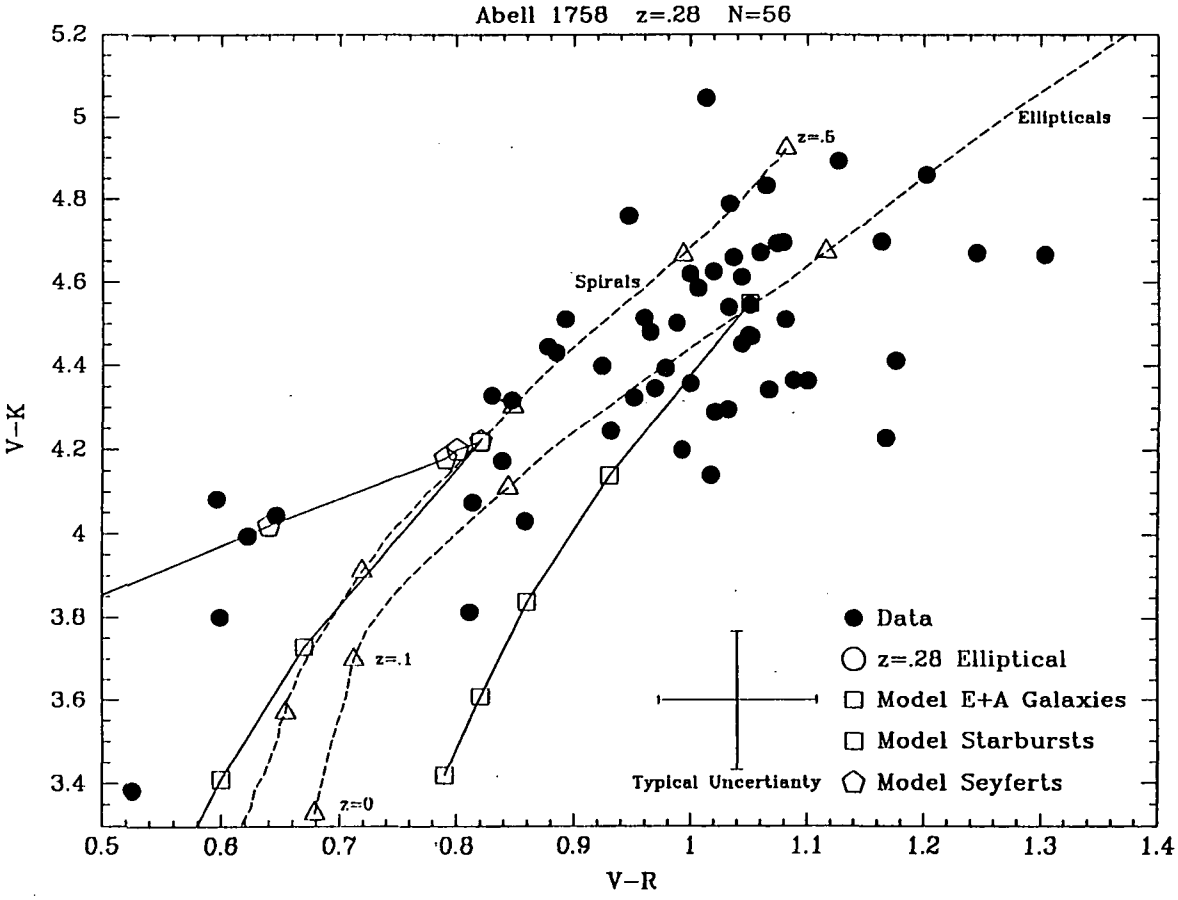

Figure 2. Abell 1758 and models at z=.28.

Deep, Wide-Field, Multi-Band Imaging of z ≈ 0.4 Clusters and Their Environs

David R. Silva and Michael J. Pierce (NOAO/KPNO)

The existence of an excess population of blue galaxies in the cores of distant, rich clusters of galaxies, commonly referred to as the "Butcher-Oemler" effect (Butcher and Oemler 1978,1984) is now well established. Spectroscopy of clusters at z = 0.2–0.4 has confirmed that the luminous blue populations comprise as much as 20% of these clusters (Dressler & Gunn 1983; Dressler, Gunn, & Schneider 1985; Lavery & Henry 1986,1988; Couch & Sharples 1987). This fraction is much higher that the 2% blue fraction found for nearby rich clusters, such as Coma, indicating that rapid galaxy evolution has occured on a relatively short time scale.

Spectroscopy has also shown that the "blue" galaxies can basically be divided into three classes: "starburst" galaxies with large [OII] equivalent widths, "post-starburst" E+A galaxies (i.e. galaxies with strong Balmer lines shortward of 4000Å but elliptical-like colors), and normal spiral/irregulars. Unfortunately, it is difficult to obtain enough spectra of individual galaxies in these intermediate redshift clusters to say anything statistically meaningful. Thus, limited information is available about the relative numbers of these three classes of "blue" galaxies and the associated E/SO population in these intermediate redshift clusters.

More statistically meaningful results can be derived from deep imaging of these clusters. However, the best published data to date (e.g. MacLaren *et al.* 1988; Dressler & Gunn 1992) are limited to the cluster cores and do not sample the galaxy luminosity functions very deeply at the bluest wavelengths. Furthermore, only limited spectro-energy distribution data is available below 4000Å in the observed cluster rest frame providing limited sensitivity to "recent" star formation activity.

To improve this situation, we are currently obtaining deep, wide-field UBRI images of all known rich clusters at z ≈ 0.4. Our main objective is to obtain the necessary color information to distinguish between the E+S0, "E+A", and spiral/irregular galaxy populations throughout the cluster/supercluster complex. At this redshift, UBRI correspond to rest-frame 2500Å/UVR bandpasses. The rest-frame UVR system provides a powerful "blue" galaxy discriminate given the expected color distribution. Moreover, since "hot" stars peak near 2500Å, that bandpass is a powerful probe of recent star formation activity in all classes of galaxies. In particular, it is sensitive to ellipticals with "UV excess" populations (MacLaren *et al.* 1988).

By going deep (S/N = 10 at B = 23.5), we are sampling the luminosity function of the elliptical, S0, and spiral galaxies well enough to investigate population differences within a class as a function of luminosity/mass. Given the extreme density contrast of these clusters and a 23 arcmin field-of-view, purely statistical arguments can be used to establish cluster membership. The large field-of-view also allows the investigation of the extended cluster/super-cluster associated with the observed cluster cores. These "field" data are directly relevant to issues regarding the evolution of faint blue galaxies.

Selected results for CL0939+4713 (z = 0.41) are presented on the next page. These data were acquired on 1992 Feb 28 UT at the KPNO 0.9m with a thinned Tektronix 2048^2 CCD (T2KA). The U, B, and R total integration times and 2.5σ detection limits were 7.5 hours/26 mag, 3 hours/25 mag, and 1.25 hours/26 mag, respectively. Only data from the central 12x12 arcmin (5x5 Mpc; $H_o = 100$, $q_o = 0.1$) field are discussed here. The central wavelengths of these U, B, and R data correspond to approximately 2550Å, 3070Å, and 4640Å, respectively, in the rest-frame of this cluster. The raw data was processed using standard IRAF reduction tasks. Galaxy/star discrimination and photometry were done with FOCAS.

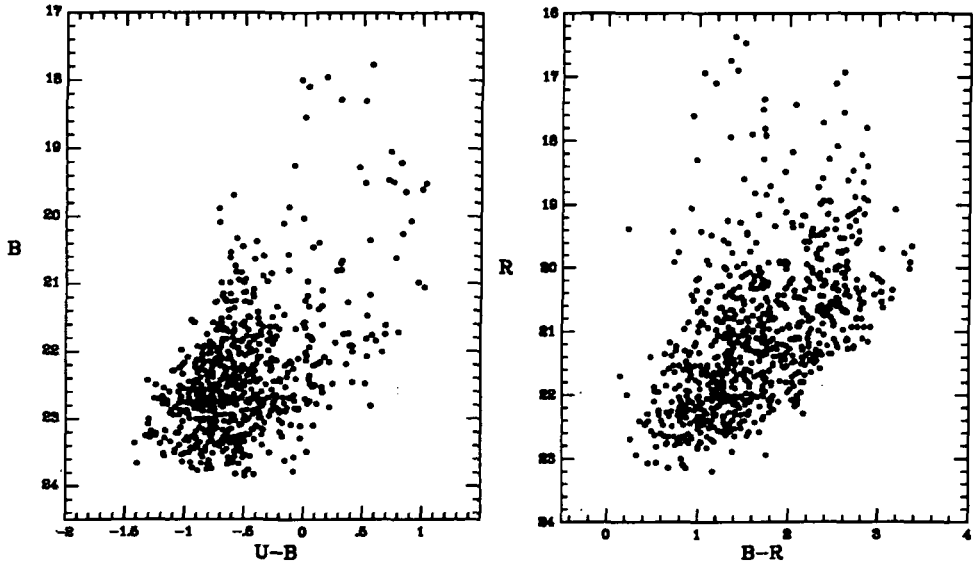

Figure 1 Color-Magnitude Diagrams. CMDs for all objects classified as galaxies by FOCAS with color uncertainties less than 0.2 mag. While some of the brighter galaxies are clearly foreground objects, the majority of the galaxies shown must be at the redshift of the cluster (see the radial distribution plot below). The galaxy colors are uncorrected for redshift or reddening. The "zones of avoidence" in the lower right corner are due to the adopted photometry cutoff in the bluer filter in each diagram. A large population of faint, blue galaxies is evident in both figures.

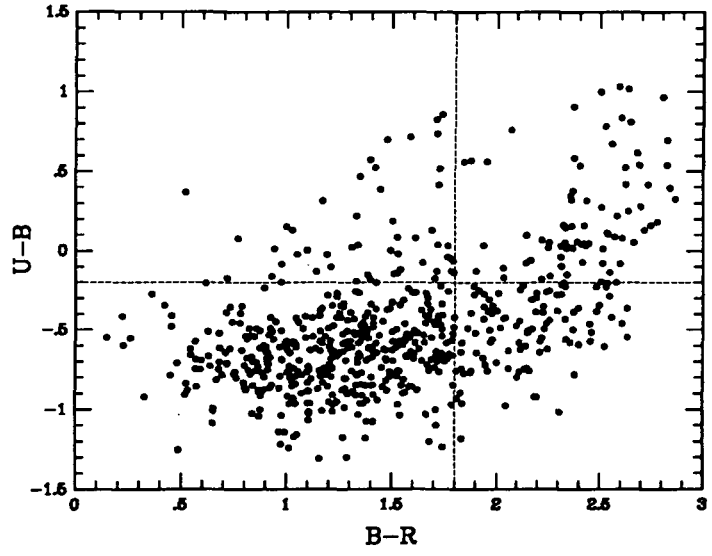

Figure 2 Two Color Diagram. U–B vs. B–R diagram of all galaxies with color uncertainties less than 0.2 mag. The dashed lines indicated the color criteria used to construct the radial density distribution plot below. Galaxies in the upper left "box" are likely to be in the foreground of the cluster. Galaxies in the lower right "box" are counted as both "blue" and "red" galaxies in the radial density distributions below. Note that the incompleteness obvious in the CMDs in Figure 1 is less obvious here but is a function of galaxy luminosity since only galaxies with S/N $\geq$ 5 in all three bands are shown.

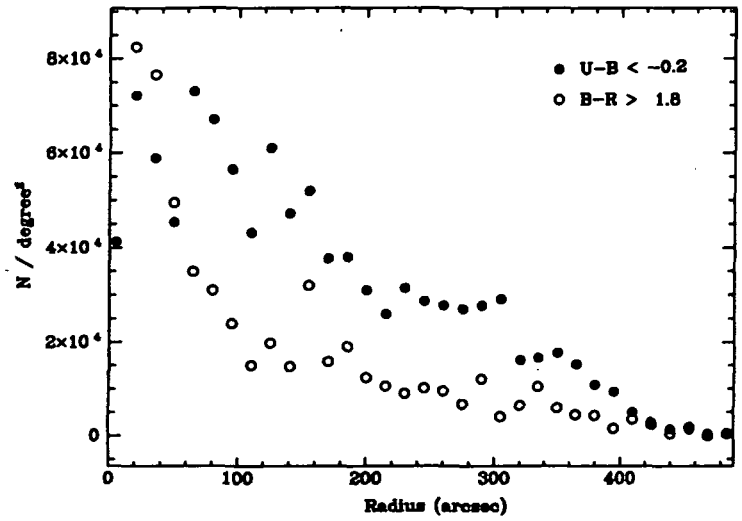

Figure 3 Radial Density Distributions. The radial density distributions of the bluest (U–B < –0.2) and reddest (B–R > 1.8) galaxies are shown here. Only galaxies with color uncertainties less than 0.2 mag were used. The "red" galaxies are significantly more centrally concentrated than the "blue" galaxies (cf. Thompson 1986). Furthermore, the extended nature of the blue galaxy density distribution suggests that the cluster blue galaxy distribution dominates the field blue galaxy distribution to the edge of the field analyzed. The smooth fall off in both distributions implies that most of the galaxies in the central 12 x 12 arcmin are associated with CL0939+4713.

N93-26849

SEARCHING FOR EMISSION-LINE GALAXIES: THE UCM SURVEY

J. Gallego[1], J. Zamorano[1], M. Rego[1], A. Vitores[1]

[1] Dpto Astrofisica, Universidad Complutense, Madrid, SPAIN

1. The UCM Survey.

We are carrying out a long-term project with the main purposes of finding and analysing low metallicity galaxies. A very small number of very low metallicity galaxies is known up to now. However these objects are particularly interesting since they are excellent candidates to "young galaxies" in evolutionary sense as POX186 (Kunth, Maurogordato & Vigroux, 1988). Since the interstellar matter in these objects is only weakly contaminated by stellar evolution, their study could provide valuable information about the primordial helium abundance and therefore it could place constraints on the different Big-Bang models.

The instrumental set up of our survey is an objective-prism used with the Schmidt telescope at Calar Alto Observatory. By using hypersensitized IIIaF emulsion and RG630 filter low resolution spectra in the Hα region of objects in a wide field is obtained (Rego et al. 1989, Zamorano et al. 1990).

Surveys carried out in the past two decades at optical blue wavelengths have also produced large samples of emission-line galaxies (ELGs), for example MacAlpine & Willians 1981 and references therein, Wasilewski 1983, Salzer and MacAlpine 1988, or Smith et al. 1976. Relying primarily on objective-prism plates taken in the blue, these surveys have found over 3000 blue/emission-line galaxies so far. A significant number of star-forming galaxies are missed by optical surveys in the blue because of their low-excitation spectra (MacAlpine and Willians 1981, Markarian et al. 1981 and references therein) or their low metallicity (Kunth and Sargent, 1986). This is identify that kind of galaxies.

2. General Objectives.

1. Identification and study of new young, low metallicity galaxies.
2. Clasification and determination of the overall properties and completeness of the sample.
3. Spatial distribution andluminosity function of the new galaxy population.
4. Comparison with other surveys. In particular, differences in the samples obtained with various objective-prism techniques.
5. Overall relation between the far infrared properties and the optical behaviour of the star-forming galaxies.
6. Determination of the evolutionary status and the different stellar subyacent population of the objects in order to detect any effect of evolution in the starburst fenomena.

3. Up-to-date main results.

- 18 plates have been visually scanned (648 square degrees of sky). So far the sample of ELGs obtained from our survey consists of 282 objects, i.e. 1 object per 2 square degrees. The detailed lists of the objects will be published this year (Zamorano et al. 1992, Rego et al. 1992).
- 136 candidates (the 48% of the sample) are galaxies which do not appear in any published catalogue. Only 36% of objects are Zwicky galaxies. Our survey recovers all the emission-line Markarian galaxies with z<0.04.
- Spectra at moderate resolution have been obtained for 113 candidates, i.e. 40% of the whole sample. A 85% are emission-line galaxies of different types.
- CCD images of 181 galaxies (64%) in the r band of Gunn-Thuan have been obtained with the 2.2 m telescope at Calar Alto.
- Far Infrared Data is also available for the whole sample after coadding the IRAS original data at Rutherford Appleton Lab. (Gallego, 1992). Preliminary analysis of IRAS colors (Rego et al. 1991) and luminosities shows different behaviour between our survey and other samples as Markarian.
- With the data available up to now, the completness of the UCM survey is assured up to r=17.3.

As an important result we have found that the F25 / F100 IRAS ratio is a good indicator of low metallicity and high excitation (Gallego, 1992). From the FIR data, we have selected a special subsample. These galaxies are candidates to genuine young galaxies which are experiencing the first burst of star formation because: 1) Previous spectroscopic observations, of low signal-to-noise, at low resolution, show galaxies with very high ionization and low abundance 2) CCD images with the 2.2 m telescope show compact, isolated and low-luminosity galaxies and 3) the far-infrared IRAS data point to the particular nature of these galaxies.

4. References

- Gallego, J., (1992) ISO/IRAS Newsletter (in press).
- Kunth, D., Sargent, W.L.W., (1986). Ap. J. 300, 496.
- Kunth, D., Maurogordato, S., Vigroux, L., (1988), Astron. Astrop. 204, 10.
- MacAlpine, G.M., Williams, G., (1981). Ap. J. S.S. 45, 113.
- Markarian, B.E., et al., (1981). Astrofizika 17, 619.
- Rego, M., Zamorano, J., González-Riestra, R. (1989). Astron. Astrop. S.S. 79, 443.
- Rego, M., Zamorano, J., Cordero, M., (1991). Active Galactic Nuclei simposium, Heidelberg, Springer-Verlag, in press.
- Salzer, J.J., MacAlpine, G.M., (1988). A. J. 96, 1192.
- Smith, M.G., Aguirre, C., Zemelman, M., (1976). Ap. J. S.S. 32, 217.
- Wasilewski, A.J. (1983). Ap.J. 272, 68.
- Zamorano, J., Rego, M., González-Riestra, R., Rodríguez, G., (1990). Astrophys. Space Science 170, 353.

MULTI-FILTER SPECTROPHOTOMETRY OF QUASAR ENVIRONMENTS

Sally E. Craven and Paul Hickson, University of British Columbia
Howard K.C. Yee, University of Toronto

Summary

A many-filter photometric technique for determining redshifts and morphological types, by fitting spectral templates to spectral energy distributions, has good potential for application in surveys. Despite success in studies performed on simulated data, the results have not been fully reliable when applied to real, low signal-to-noise data. We are investigating techniques to improve the fitting process.

Multi-filter spectrophotometry, in which photometry of images in many narrow-band filters produces a spectral energy distribution (SED), allows the redshift and type of many objects in a CCD field to be identified. Cross-correlation of spectral templates with real galaxy spectra has been successfully used to determine redshifts (e.g. Ellingson and Yee, in progress), but such methods depend on the presence of emission lines. The coarse resolution of the SEDs means that the presence of emission lines, if detected, will be poorly known. Here, we describe an alternative method by which galaxy spectral template are fit to the SEDs by minimization of errors.

The technique has immediate application in the planned survey by the University of British Columbia Liquid Mirror Telescope (LMT), a relatively inexpensive and easily constructed transit survey instrument with a set of forty narrow- and intermediate-band filters. Hogg, Hickson, and Gibson's paper in this volume describes the instrument in more detail.

Two fields were chosen for the experiment, each containing a quasar at the centre of a cluster of galaxies. The results presented in this paper are for the field around 3C 281, a quasar at z=0.602. The second cluster field in the study is that around the z=0.403 quasar PKS0812+020. Images 3.5×5 arcminutes in size were obtained at the Canada-France-Hawaii Telescope, two in each of twenty-four 100Å-wide filters. The aperture-photometry package PPP (Yee 1991, PASP 103, 396) was used to do the photometry in every filter, on each of the 247 objects in the 3C 281 field. The growth-curve algorithm assigns an appropriate aperture for photometry based on the shape of the magnitude-vs-aperture curve, and therefore the change in apparent size of the object imaged through different filters does not affect the fraction of light measured.

The morphological type and redshift for each object are estimated by finding the parameters of a model spectral energy distribution providing the best fit to the real SED. The object types are quantified in a series running from E (0.0) through Sab (1.0) and Sbc (2.0) to Im (3.0). Four real-galaxy templates were obtained from Coleman, Wu, and Weedman (1980, ApJS 43, 393). Intermediate-type templates (e.g. 1.1) are calculated by linearly interpolating between the known spectra.

Each model type, in increments of 0.1, is redshifted by amounts from 0.01 to 1.00, in steps of 0.01. At every point, the model (in log I–log ν space) has added to it a range of offsets, for each of which the fit is analyzed by calculating χ^2. The model type, redshift, and offset producing the lowest χ^2 value are assumed to correspond to the physical nature of the object. The χ^2 value is weighted according to the size of the uncertainties in the data : it is the sum over all the points in the SED of $(\log I_{model} - \log I_{data})^2/\sigma^2$. However, χ^2 would better represent the nature of the fit if calculated in the linear domain, rather than the log; this change will be instituted shortly. The solid lines drawn through the SEDs in the figure are the best-fit models. The uncertainties, indicated by the error bars, include contributions from possible missed light, zero-point uncertainty, Galactic and atmospheric extinction, and the PPP error which is due to sky noise in the photometry aperture.

At present, we cannot place much confidence in the redshifts and classifications obtained by this method. We compare our results with measured redshifts for twelve objects in this field, published by Ellingson, Yee, and Green (1991, ApJ 378, 476; hereafter EYG91), and find that only six of the redshifts derived by template-fitting correspond to the published values. Even then, some of the fits have poor χ^2 values, and their dubious appearance prompts caution!

Problems in the type/redshift identification arise from three sources: limited template range, the fitting technique, and the data quality. At this stage of the project only four galaxy template types, and models interpolated between them, are compared to the SEDs. Hence, active galaxies, QSOs, and stars are not represented by the template set, and are forced to fit a galaxy model. A priority in the near future is to incorporate a more physically complete range of galaxy templates into the fitting program.

The χ^2-minimizing technique used to fit the templates to the SEDs can take into account the uncertainties in the data points, but does not exclude (or otherwise acknowledge) sporadic data points. Especially in the fainter objects, significant errors in the flux values are common due to low signal-to-noise and a lack of compensation for cosmetic flaws in the CCD. We intend to develop a fit-independent means of identifying these outliers; if this is unsuccessful, we will replace the χ^2 algorithm with a more robust statistical fitting technique.

The data quality is the limiting factor in the accuracy of the classification technique. The outliers and scatter typical of most of the SEDs may be a result of the low brightnesses of many of the objects, which cause them to be easily contaminated by sky noise. (Typical signal-to-noise values range from 0.1 to 10 in blue-end filters, 1.0 to 15 in the red end, with a few higher values for bright objects.) In addition, the photometry package does not compensate for CCD defects and cosmic rays, which will affect the flux in some objects.

In a modelling analysis, the problems described above can be avoided. Callaghan, Gibson, and Hickson (in this volume) present a discussion of the accuracy of the technique. They use idealized Gaussian filters with the same central wavelengths as the filter set used here.

This technique will be used in analysing the data acquired by the Liquid Mirror Telescope. However, that survey has both wider and better- sampled wavelength coverage, and a higher-quality filter set. SEDs from the survey should be of much better quality than the ones shown here, and the classification results will be correspondingly better.

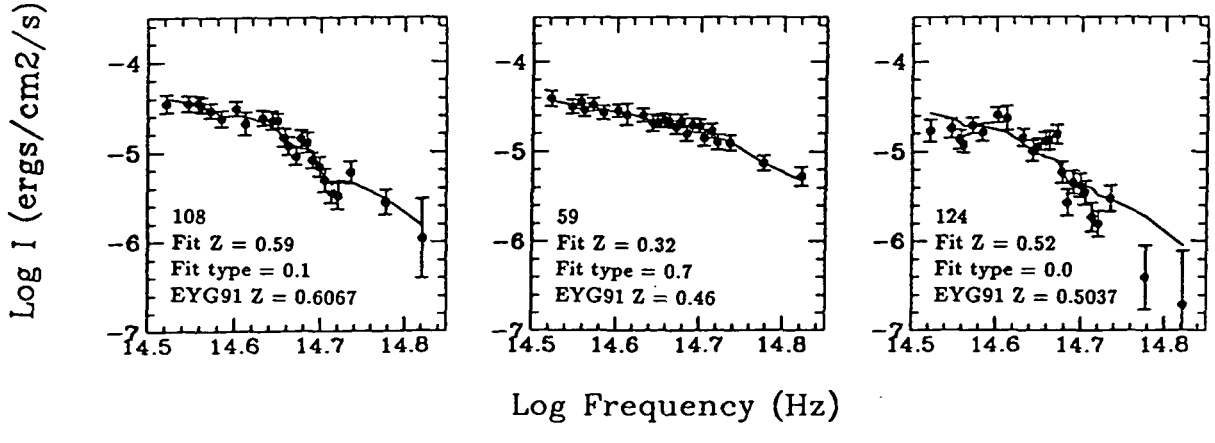

Figure: Examples of spectral energy distributions with their best-fitting templates overplotted. The vertical axis is log intensity (in ergs $cm^{-2}s^{-1}Hz^{-1}$) and the horizontal axis is log frequency (in Hz). Notice that the fit to object 59 seems clean, but the redshift is wrong, while 108 has the right redshift but a poor fit.

THE ENVIRONMENT OF X-RAY SELECTED BL LACS: HOST GALAXIES AND GALAXY CLUSTERING

Ron Wurtz, John T. Stocke, and Erica Ellingson

Center for Astrophysics and Space Astronomy, University of Colorado

Howard K. C. Yee

University of Toronto

ABSTRACT

Using the Canada-France-Hawaii Telescope, we have imaged a complete, flux-limited sample of Einstein Medium Sensitivity Survey (EMSS; Gioia, *et al.* 1990, Stocke, *et al.* 1991) BL Lacertae objects in order to study the properties of BL Lac host galaxies and to use quantitative methods to determine the richness of their galaxy cluster environments.

INTRODUCTION

The extreme characteristics of BL Lacs have been suggested to be due either to Doppler-boosted beaming from a relativistically moving jet aimed almost exactly in our direction (*e.g.* Blandford and Rees, 1978; Browne, 1989) or gravitational lensing of a background QSO (Ostriker and Vietri, 1985). In this case the apparent host galaxy is actually the foreground lensing galaxy.

These two theories for BL Lacs make very different predictions about the host galaxy morphologies that we have begun to test with our imaging surveys:

1. Host galaxy morphology: the jet hypothesis requires all BL Lacs to have giant elliptical hosts since these are the hosts of the FR1 radio galaxies which are the proposed parent population for BL Lacs (*e.g.* Padovani and Urry, 1991). The lensing hypothesis prefers giant ellipticals since they have the deepest potential wells, but spirals and lower luminosity galaxies of any type can also be the lensing galaxies.

2. Point-source position: the jet hypothesis requires the point sources to be well-center in the host galaxy like they are for radio galaxies. The lensing hypothesis often requires off-centered point sources if most BL Lacs are lensed.

3. Clustering: the jet hypothesis suggests that many BL Lacs should be found in rich clusters since many FR1s are in rich clusters (*e.g.* Prestage and Peacock, 1988). The lensing hypothesis makes no specific clustering predictions.

CLUSTERING PROPERTIES AND HOST GALAXIES OF MS1207+39 AND MS1407+59

By measuring the amplitude of the galaxy-BL Lac spatial covariance function, B_{gb} (Yee and Green 1987), we have discovered rich clusters around two EMSS BL Lacs (see table below). For comparison, B_{gb} for clusters of Abell richness class 1 $\sim$ 650 and B_{gb} for Abell richness class 2 $\sim$ 945.

Both these objects are in well-resolved host galaxies consistent with FR1 hosts. A three-parameter fit of the isophotal profiles to a de-Vaucouleurs model elliptical galaxy plus point source gives an absolute Gunn-r magnitude for the host galaxies of -22.9 for MS1207+39 and -23.2 for MS1402+59 ($H_0 = 50, q_0 = \frac{1}{2}$). These absolute magnitudes are consistent with $\langle M_r \rangle = -23.3$ for brightest cluster galaxies (BCGs) (Hoessel *et al.* 1980).

This evidence leads us to the conclusion that these two BL Lac objects are in the nuclei of cD galaxies in rich clusters.

SPATIAL COVARIANCE AMPLITUDES B_{gb}

name	z	B_{gb}
1207+39	0.615	1092±228
1407+59	0.495	845±173

THE REMAINING EMSS BL LAC HOST GALAXIES

Of the remaining host galaxies, nearly all are resolved and their fitted profiles are consistent with BGCs as well (Figures 1 and 2). However, a small subsample demonstrates properties that may be inconsistent with the beamed FR1 hypothesis. In one case, MS 0205+35, the resolved host is clearly decentered (Figure 3), and the absolute Gunn r-magnitude of the galaxy at the measured redshift of 0.318 is <-21, too small for a BCG and also an unlikely FR1 host. In two other cases, MS0950+49 and MS1402+04 (z =0.200:), we were unable to resolve an underlying host. Consequently as many as 3 of 22 EMSS BL Lacs may be due to gravitational lensing, the remainder are consistent with being beamed FR1s.

REFERENCES

Blandford, R. and Rees, M. 1978, in **Pittsburgh Conf. on BL Lacs**, p. 328

Browne, I. 1989 in **BL Lac Objects**, p. 401

Gioia, I., *et al.* 1990, ApJS, 72, 567

Hoessel, J. G., Gunn, J. E., and Thuan, T. X. 1980, ApJ, 241, 486

Ostriker, J. and Vietri, M. 1985, Nature, 318 446

Padovani, P. and Urry, M. 1991 ApJ, 368, 373

Prestage, R. M. and Peacock, J. A. 1988, MNRAS, 230, 131

Stocke, J. T., *et al.* 1991, ApJS, 76, 813

Yee, H. K. C. and Green, R. F. 1987, ApJ, 319, 28

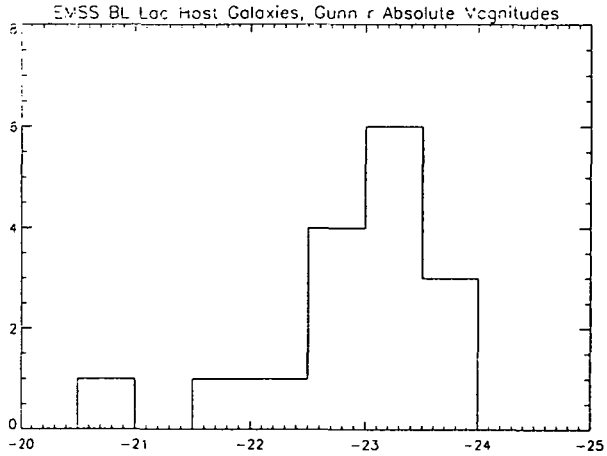

Figure 1. Absolute magnitude of host galaxies, determined from total magnitude of the profile fit. Where the fit was unsuccessful, we have plotted the lower limit on M_r given by subtracting a point spread function (PSF) fit to the central source and determining the magnitude of the remainder. $\langle M_r \rangle$ is -23.3 for brightest cluster galaxies (Hoessel *et al.* 1980).

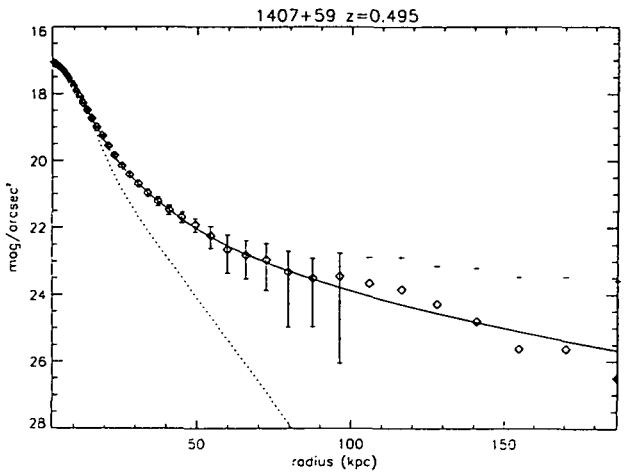

Figure 2. An example of a profile fit. The solid line is the fit to a point source + deVaucouleurs profile for 1407+59. The dotted line is the best fit PSF.

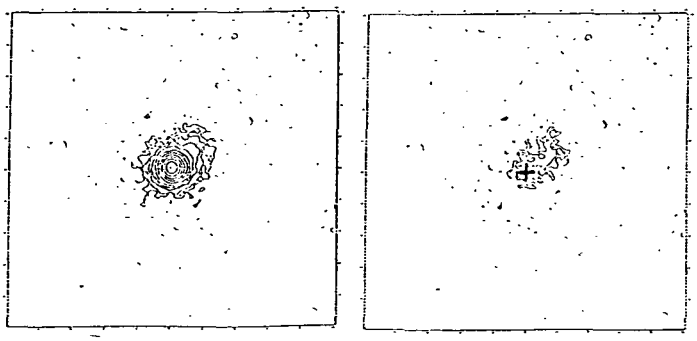

Figure 3. The image on the left is MS0205+35 before PSF subtraction. The image on the right is the same frame after subtracting a point source centered on the position of the cross. Each frame is 25 arcsec on a side.

NUCLEAR ACTIVITY AND THE ENVIRONMENTS OF NEARBY RADIO GALAXIES

Arjun Dey[1] and Wil van Breugel[2]

Much of our present understanding of galaxy evolution over a large redshift range is based on the study of samples selected on the basis of non-thermal radio emission. It is therefore necessary to understand the relationship between radio source activity and the host galaxy. Recent observations suggest that there is a connection between radio galaxy (RG) activity and radio galaxy evolution. For example, high-redshift RGs ($z \gtrsim 0.7$) show evidence for significant populations of young stars, and have optical continuum morphologies nearly always aligned with the radio axis (McCarthy *et al.* 1987; Chambers *et al.* 1987). This phenomenon is generally attributed to radio jet induced star formation (DeYoung 1989), but the lack of high S/N spectra of the galaxy continua, and recent detections of polarized light in a few objects make it hard to rule out other processes such as scattering or synchrotron radiation. A detailed study of the continuum light in the distant RGs is difficult as they are optically very faint. However, nearby RGs ($z \lesssim 0.1$) have bluer *B-V* colours than radio-quiet ellipticals, presumably due to the presence of young stellar populations (Smith and Heckman 1989) and several have extended UV continuum emitting regions along their radio axes (van Breugel *et al.* 1985*a*, *b*, di Serego Alighieri *et al.* 1989), reminiscent of the alignment effect seen in the high redshift RGs.

We have almost completed a continuum imaging survey of *nearby* (and therefore optically brighter), powerful RGs to study any possible relationships between the optical continuum light and radio source activity. In particular we are interested in (1) whether these lower redshift RGs show any evidence for the alignment effect (in their rest-frame UV light) that is seen in the distant RGs, and (2) the effects that the radio source has on the environment of the host galaxy.

Our sample is comprised of 45 nearby ($0.08 < z < 0.2$), powerful (FR II, $P_{408MHz} > 10^{33}$ ergs/s/Hz) RGs selected from the 3CR, B2 and PKS catalogues. We are imaging these galaxies through *U* (liq. $CuSO_4$+UG2) and r' (6500/750) filters which sample the galaxian continuum at $\lambda_{rest} < 3700$Å and $\lambda_{rest} \sim 5700$Å respectively; the filters are uncontaminated by strong emission lines in the redshift range chosen, and the survey is therefore extremely sensitive to the distribution of UV *continuum* light in these galaxies. The main goal of our imaging survey is to search for extended UV excess regions that are associated with the radio source structure, and to determine whether any correlation that may exist between the spatial distribution of these objects and the radio source is statistically significant. The optically brightest cases are then followed-up spectroscopically. High S/N spectroscopy of the blue light will allow us to determine whether or not it is due to stars. If the continuum light is primarily stellar, then modelling of the absorption line spectrum will allow us to study the stellar populations and any possible relations with the radio source. If the continuum light is *not* stellar, modelling the emission-line and continuum spectrum may help us distinguish between various ionization mechanisms.

We present preliminary results of our imaging survey and discuss a few specific cases of interest. Thus far, more than 30% of the galaxies imaged show evidence of patchy,

[1] Astronomy Dept., University of California at Berkeley

[2] Inst. of Geophysics and Planetary Physics, Lawrence Livermore National Lab.

extended UV continuum emission along the radio axes both internal and external to the host galaxy. Although *most* of the galaxies in the sample *do* show evidence for extended blue continua, most of these are at very low surface brightness levels ($\sim$ 24 AB mag/sq. arcsec.). Our U-band imaging survey has demonstrated that the alignment effect is also seen in a significant fraction of nearby RGs.

Spectroscopy of the brightest cases shows that there is a variety of processes at work. In most cases the UV continuum emission has associated line emission; in some of these cases the emission line ratios are similar to those seen in HII regions, suggesting that induced star formation may not be an uncommon phenomenon, and in others they resemble those seen in LINERs. In at least one case, 3C346, there is no associated line emission and the UV light is associated with a bright knot in a radio jet implying that it is due to optical synchrotron radiation. Figure 1 shows our data on PKS 1414-212, where we have discovered a very blue continuum object associated with a radio knot. The brightest radio emission straddles the knot rather than being coincident with it. Our spectrum of the knot shows strong line emission, with line ratios typical of those seen in Seyfert 2 galaxies. It is possible that the knot is being photoionized by beamed radiation from the host galaxy nucleus.

References:

Chambers, K. C. *et al.* 1987, *Nature*, **329**, 604.
DeYoung, D. S. 1989, *Ap.J.Lett.*, **342**, L59.
di Serego Alighieri, S. *et al.* 1989, *Nature*, **334**, 591.
McCarthy, P. J. *et al.* 1987, *Ap.J.Lett.*, **321**, L29.
van Breugel, W. *et al.* 1985*a*, *Ap.J.*, **290**, 496.
van Breugel, W. *et al.* 1985*b*, *Ap.J.*, **293**, 83.
Smith, E. and Heckman, T. 1989, *Ap.J.*, **341**, 658.

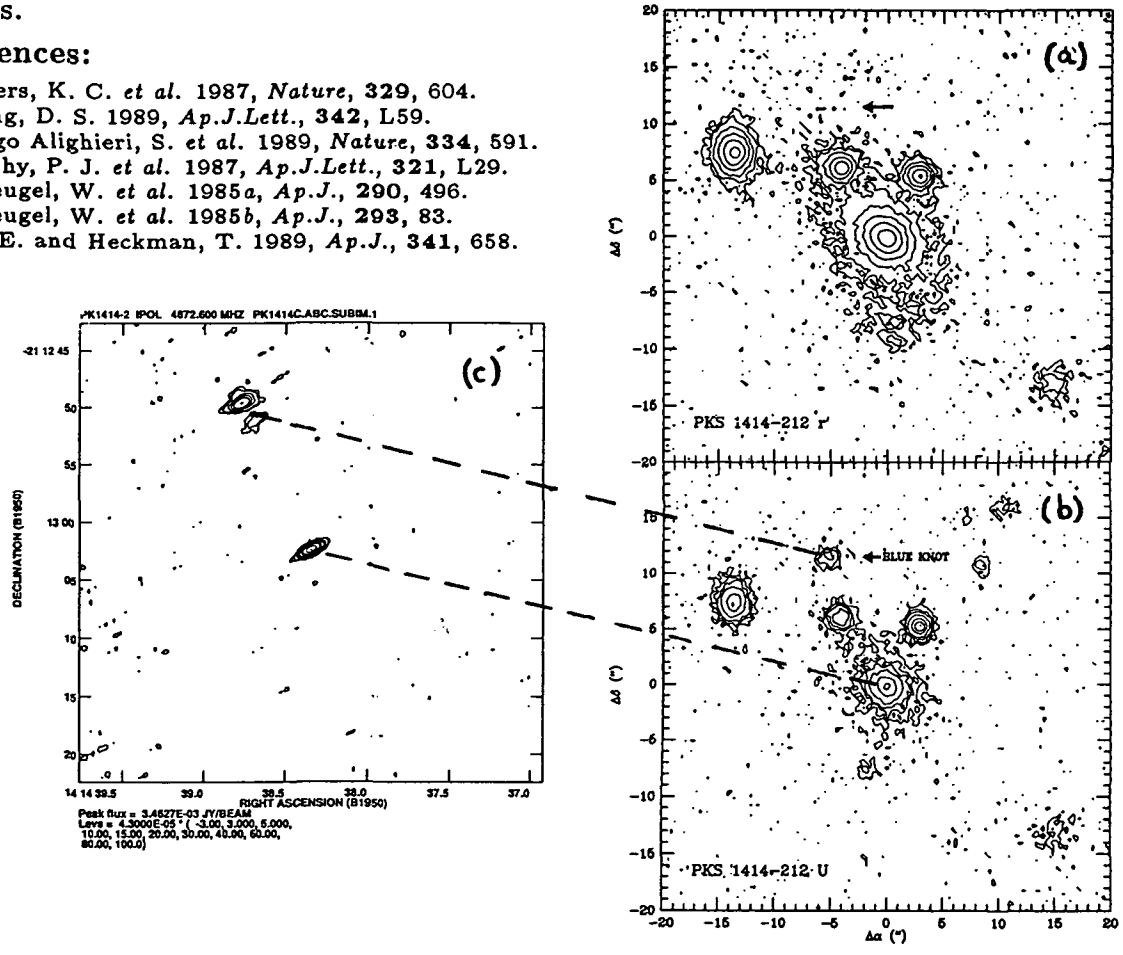

Figure 1: PKS 1414-212. (a) Intermediate-band r' image, and (b) U-band image of PKS 1414-212 obtained using the 4-m PFCCD at CTIO. Note that the feature marked 'BLUE KNOT' in the U-band image is *absent* in the r'-band image. The UV emitting knot lies inbetween the two components of the radio knot seen in the 6cm VLA map (c). The large scale structure of the radio source (not shown) has an FRII morphology.

Infrared Coronal Emission Lines and the Possibility of Their Maser Emission In Seyfert Nuclei

Matthew A. Greenhouse[1], Uri Feldman[2], Howard A. Smith[1],
Marcel Klapisch[3], Anand K. Bhatia[4], and Abi Bar-Shalom[5]

ABSTRACT

Energetic emitting regions have traditionally been studied via x-ray, UV and optical emission lines of highly ionized intermediate mass elements. Such lines are often referred to as "coronal lines" since the ions, when produced by collisional ionization, reach maximum abundance at electron temperatures of $\sim 10^5 - 10^6$ K typical of the sun's upper atmosphere. However, optical and UV coronal lines are also observed in a wide variety of Galactic and extragalactic sources including the Galactic interstellar medium, nova shells, supernova remnants, galaxies and QSOs.

Infrared forbidden lines typically result from fine structure transitions within the ground electron configuration and are excited predominantly by electron impact. Although these relatively low energy transitions are easily excited, the coronal ionization states are only produced in energetic environments by collisional ionization in a kinetically hot gas or by photoionization in power law continuum radiation fields. In the latter case, coronal emission lines can be produced in relatively low kinetic temperature ($T_e \sim 10^4$ K) or low density ($n_e < 10^5$) plasmas due to their low excitation temperature. As a result of their relatively high critical density ($n_e > 10^6$ cm^{-3}) for collisional de-excitation, coronal fine structure lines are also important coolants of higher density collisionally ionized plasmas. They are produced in a wide variety of environments found in AGN and many Galactic sources

Infrared coronal lines are providing a new window for observation of energetic emitting regions in heavily dust obscured sources such as infrared bright merging galaxies and Seyfert nuclei and new opportunities for model constraints on physical conditions in these sources. Unlike their UV and optical counterparts, infrared coronal lines can be primary coolants of collisionally ionized plasmas with $10^4 < T_e\,(K) < 10^6$ which produce little or no optical or shorter wavelength coronal line emission. In addition, they provide a means to probe heavily dust obscured emitting regions which are often inaccessible to optical or UV line studies. The wide range of critical densities spanned by infrared coronal lines ($5 < \log n_e$ (cm^{-3}) < 10) combined with their reduced extinction make them ideal probes of Seyfert broad line region cloud kinematics. Finally, they are useful for abundance studies in AGN and Galactic sources, and are modeled to be bright in colliding galaxies and galaxy cluster cooling flows.

In this poster, we provide results from new model calculations designed to support upcoming Infrared Space Observatory (ISO) and current ground-based observing programs involving infrared coronal emission lines in AGN. We present a complete list of infrared ($\lambda > 1$ μm) lines due to transitions within the ground configurations $2s^2 2p^k$ and $3s^2 3p^k$ ($k = 1$ to 5) or the first excited configurations $2s2p$ and $3s3p$ of highly ionized ($\chi \geq 100$ eV) astrophysically abundant ($n(X)/n(H) \geq 10^{-6}$) elements. Included are approximately 74 lines in ions of O, Ne, Na, Mg, Al, Si, S, Ar, Ca, Fe, and Ni spanning a wavelength range of approximately $1 - 280$ μm. We present new results from detailed balance calculations, new critical densities for collisional de-excitation, intrinsic photon rates, branching ratios, and excitation temperatures for the majority of the compiled transitions. The temperature and density parameter space for dominant cooling via infrared coronal lines is presented, and the relationship of infrared to optical coronal lines is discussed.

We find that roughly half of the infrared coronal line transitions examined are potentially bright. These relatively bright lines span a wavelength range of $1 < \lambda$ (μm) < 25 with the majority of the transitions accessible only to space-based and suborbital spectrometers. Several bright transitions can be observed from the ground at sites affording exceptional infrared transmission. For example, recent ground-based observations have revealed that emission lines due to [Si VI] and [Si VII] in NGC 1068 and [Al VI] on NGC 4151 are among the brightest infrared lines in these archetypal galaxies. Critical densities for collisional de-excitation of the brighter transitions span a range of $4.8 \leq \log n_e$ (cm^{-3}) ≤ 9.8 with excitation temperatures spanning

[1] Laboratory for Astrophysics, National Air & Space Museum, Smithsonian Institution, Washington, DC 20560.
[2] Solar Terrestrial Relationships Branch, Naval Research Laboratory, Washington, DC 20560.
[3] Artep Inc., Naval Research Laboratory, Code 4694, Washington, DC 20375.
[4] NASA Goddard Space Flight Center, Greenbelt, MD 20771.
[5] Nuclear Research Center of the Negev, P.O. Box 9001, Beer Sheva, Israel.

$3.2 \leq \log\,(E_j/k)\ (\mathrm{K}) \leq 5.6$. The ions themselves reach maximum abundance in collisionally ionized regions at $5.2 \leq logT_e\ (\mathrm{K}) \leq 6.4$, but their infrared forbidden lines can also probe cooler (10^4 K) photoionized regions due to their relatively low excitation temperature.

Relatively Bright (log $[A_{ji}n_j/n_e] \geq -10$) Infrared Coronal Lines of Astrophysically Abundant Elements

Species	Transition	λ (μm)	Species	Transition	λ (μm)
Ar XIII	$^3P_0 - ^3P_1$	c 1.0159(40)	S IX	$^3P_1 - ^3P_0$	c 3.75(3)
S XIII	$^3P_1 - ^3P_2$	c 1.0264(30)	Si IX	$^3P_0 - ^3P_1$	m 3.92(2)
Fe XIII	$^3P_0 - ^3P_1$	m 1.07468(4)	Mg IX	$^3P_1 - ^3P_2$	c 4.06(4)
Fe XIII	$^3P_1 - ^3P_2$	m 1.07979(4)	Ca VII	$^3P_1 - ^3P_2$	c 4.086(5)
S IX	$^3P_2 - ^3P_1$	c 1.2520(20)	Mg IV	$^2P_{1/2} - ^2P_{3/2}$	c 4.487(4)
Ni XIV	$^2D_{3/2} - ^2D_{5/2}$	c 1.28150(12)	Na VII	$^2P_{1/2} - ^2P_{3/2}$	c 4.675(22)
S XI	$^3P_1 - ^3P_2$	c 1.3924(50)	Mg VII	$^3P_1 - ^3P_2$	c 5.50(3)
Si X	$^2P_{1/2} - ^2P_{3/2}$	m 1.4301(4)	Mg V	$^3P_2 - ^3P_1$	m 5.60(2)
S XI	$^3P_0 - ^3P_1$	c 1.9200(70)	Al VIII	$^3P_0 - ^3P_1$	c 5.85(10)
Si XI	$^3P_1 - ^3P_2$	c 1.932(50)	Ar VII	$^3P_1 - ^3P_2$	c 5.95(5)
Si VI	$^2P_{3/2} - ^2P_{1/2}$	m 1.9590(70)	Fe XI	$^3P_1 - ^3P_0$	c 6.082(19)
Al IX	$^2P_{1/2} - ^2P_{3/2}$	m 2.040(7)	Ca VII	$^3P_0 - ^3P_1$	c 6.154(8)
Fe XII	$^2D_{3/2} - ^2D_{5/2}$	c 2.2170(3)†	Na VIII	$^3P_1 - ^3P_2$	c 6.23(3)
Ca XIII	$^3P_1 - ^3P_0$	c 2.258(15)	Si VII	$^3P_1 - ^3P_0$	c 6.515(18)
Ca VIII	$^2P_{1/2} - ^2P_{3/2}$	m 2.32(2)	Ne VI	$^2P_{1/2} - ^2P_{3/2}$	m 7.642(6)
Si VII	$^3P_2 - ^3P_1$	m 2.474(7)	Na VI	$^3P_1 - ^3P_2$	c 8.61(9)
Si IX	$^3P_1 - ^3P_2$	c 2.5839(5)	Mg VII	$^3P_0 - ^3P_1$	c 9.03(9)
Ar XI	$^3P_1 - ^3P_0$	c 2.60(5)	Al VI	$^3P_1 - ^3P_0$	c 9.116(6)
Al X	$^3P_1 - ^3P_2$	c 2.753(20)	Ne VII	$^3P_1 - ^3P_2$	c 10.6(7)
Al V	$^2P_{3/2} - ^2P_{1/2}$	m 2.879(14)	Mg V	$^3P_1 - ^3P_0$	c 13.54(5)
Mg VIII	$^2P_{1/2} - ^2P_{3/2}$	m 3.0275(20)	Na VI	$^3P_0 - ^3P_1$	c 14.3(3)
Ca IX	$^3P_0 - ^3P_1$	c 3.088(13)	Ne V	$^3P_1 - ^3P_2$	m 14.32(3)
Al VI	$^3P_2 - ^3P_1$	m 3.661(14)	Ni XIII	$^3P_1 - ^3P_0$	c 19.3(4)†
Al VIII	$^3P_1 - ^3P_2$	m 3.72(2)	Ne V	$^3P_0 - ^3P_1$	m 24.28(2)
			Ca VI	$^2D_{3/2} - ^2D_{5/2}$	c 24.30(17)

measured or calculated wavelength denoted by m and c respectively.

We find that under physical conditions found in Seyfert nuclei, 14 of 70 transitions examined have significant population inversions in levels that give rise to infrared coronal lines. Maser gain lengths in these transitions are presented for dense ($10^6 \leq n_e\ (\mathrm{cm}^{-3}) \leq 10^9$) collisionally ionized plasmas. We find that significant maser gains are possible in conditions expected in the intermediate zone of Seyfert nuclei. Application of these results to cooler plasmas photoionized by power law continuum radiation fields is also presented.

Coronal line maser gain lengths for Seyfert nuclei

1	2	3	4	5	6
Species	λ μm	$-log\left[\frac{n(ion)}{n(element)}\right]_{coll}$	$12 + log\left[\frac{n(X)}{n(H)}\right]$	$[l_6]_{coll}$ pc	$[l_9]_{coll}$ pc
Ne V	24.28	0.21	8.09	a	$1.7e-3$
Mg V	13.54	0.22	7.58	$1.2e+0$	a
Mg VII	9.03	0.30	...	a	$3.8e-3$
Al VI	9.12	0.28	6.47	$7.1e+1$	a
Al VIII	5.85	0.38	...	a	$4.5e-2$
Si VII	6.52	0.30	7.55	$1.9e+1$	$1.6e-2$
S IX	3.75	0.35	7.21	$3.4e+2$	$1.9e-3$
S X	8.68	0.35	....	$9.8e+2$	$5.6e-3$
Ar XI	2.60	0.39	6.56	$7.7e+3$	$1.3e-2$
Ca VII	6.15	0.35	6.36	a	$1.0e-3$
Ca XIII	2.26	0.41	...	$3.3e+4$	$4.2e-2$
Ca XIV	1.31	0.41	...	$1.3e+6$	$1.3e+0$
Fe XI	6.08	0.57	7.67	a	$3.3e-3$
Fe XII	2.22†	0.53	...	$7.9e+2$	$3.9e-3$

5, 6 – column length for maser gain of e^1 evaluated at $n_e = 10^6$ and 10^9 cm^{-3}
a – no inversion at this density

Influence of the Active Nucleus on the Multiphase Interstellar Medium in NGC 1068

Jonathan Bland-Hawthorn and Jon Weisheit
Rice University, Houston, TX 77251

Gerald Cecil
University of North Carolina, Chapel Hill, NC 27599

James Sokolowski
Space Telescope Science Institute, Baltimore, MD 21218

The luminous spiral NGC 1068 (14.1 Mpc; $1'' \approx 68$ pc) has now been imaged from x-ray to radio wavelengths at comparably high resolution ($\lesssim 5''$ FWHM). The bolometric luminosity of this well-known Seyfert ($\sim 2 \times 10^{11} L_\odot$) is shared almost equally between the active nucleus and an extended 'starburst' disk[1]. In an ongoing study, we are investigating the relative importance of the nucleus and the disk in powering the wide range of energetic activity observed throughout the galaxy. Our detailed analysis brings together a wealth of data: ROSAT HRI observations[2], VLA $\lambda\lambda 6-20$cm[3] and OVRO interferometry[4], $\lambda\lambda 0.4-10.8\mu$m imaging, and Fabry-Perot (Hα, [NII], [OIII]) spectrophotometry.

In earlier papers[5,6], we have shown that a 'diffuse ionized medium' (DIM) pervades the inner 10 kpc disk of NGC 1068. Throughout this warm phase, the strengths of low ionization lines (N^+, O^+, S^+) with respect to Hα, the line dispersions (150–250 km s^{-1} FWHM) and the inferred scale height ($\sim$400 pc) are all considerably enhanced with respect to the adjacent HII region population, while the O^{++} emission is much weakened (see Fig. 1). After removing the influence of HII regions, the [NII] surface brightness profile is well described by an inverse square law. Others have shown

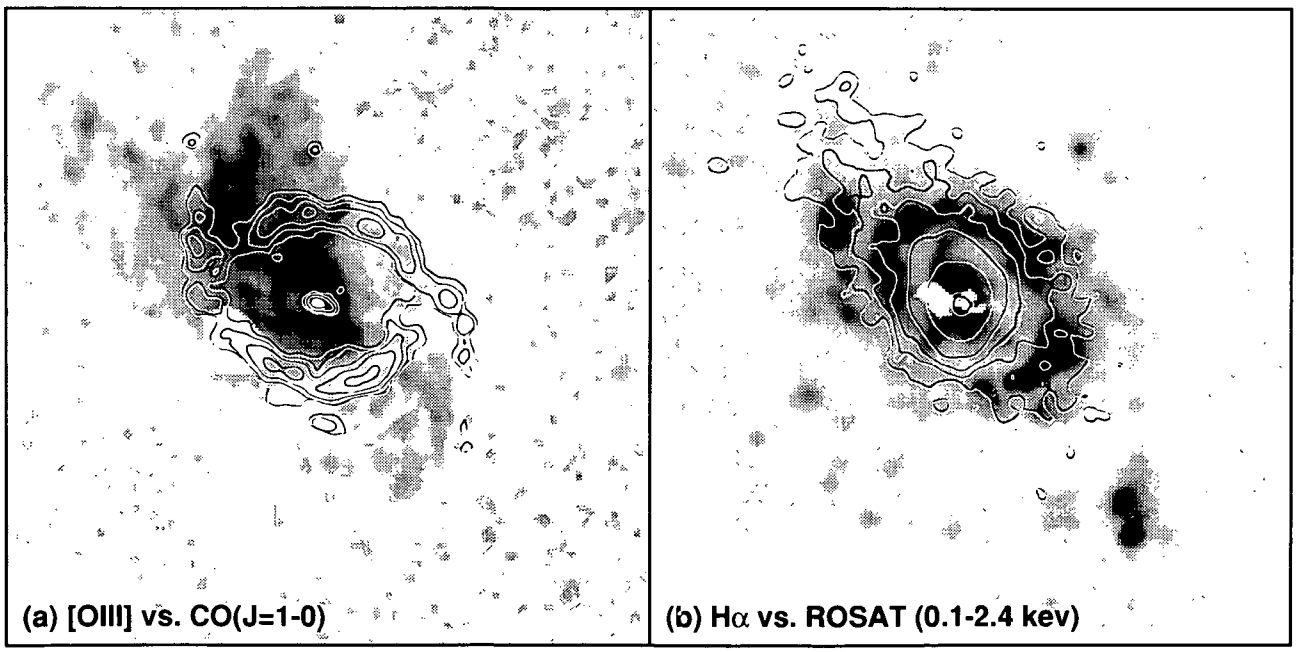

Fig. 1*a*.– Contours of OVRO CO (J=1–0) data (beam $\approx 3''$ FWHM) overlaid on new CTIO Fabry-Perot [OIII] observations ($\approx 1''$ FWHM). The horizontal E–W axis is 100″ in length. The hole 15″E of center arises from an internal reflection. *b*.– Contours of ROSAT (0.1–2.4 kev) HRI data ($\approx 4.5''$ FWHM) overlaid on HIFI Fabry-Perot Hα observations ($\approx 1''$ FWHM).

that the brightest O^{++} emission[7,8] and higher ionization species[9] (Ne^{++}, Ne^{4+}, He^{+}, etc.) are confined to a narrow sector aligned with the radio[10]/optical[11] jet axis (PA $\approx 45°$; see Fig. 1*a*).

Two distinct mechanisms have been proposed to explain the DIM phase. While both models suppose that the enhanced line widths reflect turbulent motion in the large-scale ISM, they differ in the source of excitation for the low ionization emission. Sokolowski *et al.*[6] contend that the same electron-scattering medium that gives rise to the observed x-ray spectrum and the polarized broad-line spectrum can produce a dilute, hard ionizing continuum that is sufficiently energetic to power the low ionization emission. Slavin *et al.*[12] have considered the coronal emission arising from the turbulent 'mixing layers' in the multiphase ISM which naturally produces a slew of strong, low ionization lines. Both ideas are highly model dependent: in particular, the former depends on the scattering geometry while the latter requires a high rate of mass injection to provide sufficient enthalpy flux. Halpern[13] has suggested that the extended x-ray disk observed by ROSAT[2] may not be sufficient to balance the implied cooling rate of the DIM ($\sim 10^{42}$ erg s^{-1}).

Under the assumption that the DIM is photoexcited by the active nucleus, the [OIII]/[NII] line ratio and the observed x-ray spectrum can be used to predict the local ionization parameter, U, throughout the disk. The computed map demonstrates that the general disk is characterized by a value of U one or two orders of magnitude smaller ($\sim 10^{-4}$) than along the radio axis, consistent with the very different distributions of high and low ionization species. Figures 1*a*,*b* illustrate that the bipolar anisotropy in the radiation field is oriented so as to illuminate the near side of the ISM to the NE and the far side to the SW, as deduced from the optical jet[11]. In particular, *notice how the [OIII] emission to the SW is evidently blocked by the CO ring.* There is a clear association between the [OIII]/CO distributions and kinematics. This has led us to consider a model in which the hot wind detected by ROSAT (Fig. 1*b*) is irradiating and driving shocks into giant molecular clouds within the disk. Such a model may explain the hot dust[14] and high CO(J=2–1)/CO(J=1–0) excitation temperatures[4] associated with clouds along the radio axis.

In Fig. 1*a*, we find bisymmetric counterparts in the SW to the brightest [OIII] 'plumes' to the NE. The SW filaments are systematically fainter by $A_V \approx 2$–3 mag indicating a column depth of $\sim 5\times 10^{21}$ cm^{-2} in the general disk away from the CO ring. In this case, with due attention to the sharp oxygen edge within the ROSAT (0.1–2.4 kev) bandpass, we determine that the optical depth to x-ray absorption is close to A_V. Therefore, we conclude that *the one-sided distributions of both the [OIII] and the x-ray emission arise from intervening absorption by the large-scale disk to the south west.* In contrast to the [OIII] emission, the 10.8μm emission is symmetric about the nucleus. This is consistent with our picture since the molecular clouds are optically thin to mid-infrared radiation since, from the OVRO observations, we determine the cloud column density in the CO ring to be $\approx 1.2\times 10^{23}$ cm^{-2} for which $A_V \approx 62$ mag and $A_{10.8\mu m} \sim 0.5$ mag.

1. Telesco, C.M. *et al.* 1984, ApJ, 282, 427.
2. Wilson, A.S. *et al.* 1992, ApJ, 391, L75.
3. Wynn-Williams, C.G., Becklin, E.E., and Scoville, N. 1985, ApJ, 297, 607.
4. Planesas, P., Scoville, N., and Myers, S.T. 1991, ApJ, 369, 364.
5. Bland-Hawthorn, J., Sokolowski, J., and Cecil, G. 1991, ApJ, 375, 78.
6. Sokolowski, J., Bland-Hawthorn, J., and Cecil, G. 1991, ApJ, 375, 583.
7. Balick, B. and Heckman, T.M. 1979, AJ, 90, 197.
8. Pogge, R.W. 1988, ApJ, 328, 519.
9. Bergeron, J., Petitjean, P. and Durret, F. 1989, A&A, 213, 61.
10. Wilson, A.S. and Ulvestad, J. 1983, ApJ, 275, 8.
11. Cecil, G., Bland, J. and Tully, R.B. 1990, ApJ, 355, 70.
12. Slavin, J.D., Shull, M. and Begelman, M.C. 1992, ApJ, submitted.
13. Halpern, J. 1991, In Testing the AGN Paradigm, eds. S. Holt, S. Neff, and M. Urry, p. 524.
14. Telesco, C.M. and Decher, R. 1988, ApJ, 334, 573.

Reduction and Analysis of VLA Maps for 281 Radio-Loud Quasars Using the UNLV Cray Y-MP Supercomputer

Ailian Ding, Paul Hintzen, Donna Weistrop
Department of Physics, University of Nevada, Las Vegas
and **Frazer Owen**
National Radio Astronomy Observatory

Introduction

The identification of distorted radio-loud quasars provides a potentially very powerful tool for basic cosmological studies. If large morphological distortions are correlated with membership of the quasars in rich clusters of galaxies, optical observations can be used to identify rich clusters of galaxies at large redshifts. Hintzen, Ulvestad, and Owen (1983, HUO) undertook a VLA A array snapshot survey at 20 cm of 123 radio-loud quasars, and they found that among triple sources in their sample, 17% had radio axes which were bent more than 20° and 5% were bent more than 40°. Their subsequent optical observations showed that excess galaxy densities within 30 arcsec of 6 low-redshift distorted quasars were on average 3 times as great as those around undistorted quasars (Hintzen 1984). At least one of the distorted quasars observed, 3C275.1, apparently lies in the first-ranked galaxy at the center of a rich cluster of galaxies (Hintzen and Romanishin, 1986). Although their sample was small, these results indicated that observations of distorted quasars could be used to identify clusters of galaxies at large redshifts. The purpose of this project is to increase the available sample of distorted quasars to allow optical detection of a significant sample of quasar-associated clusters of galaxies at large redshifts.

Sample and Observations

The sample includes all the candidates for the complete samples of radio-loud quasars discussed by Wills and Lynds (1978). The criteria defining the initial complete samples included limits on right ascension, declination, and flux densities at 178 MHz and 2700 MHz. Wills and Lynds also required a minimum luminosity at 2500 Angstroms. The redshifts of the 192 sources in the resultant sample range from 0.104 to 2.877 with the great majority between 0.5 and 1.5.

VLA "snapshot" observations for the 192 sources were obtained in the A array at 6 cm in order to achieve high resolution. In order to obtain large scale information, VLA "snapshots" in the C array at 6 cm were also obtained. Eighty-nine additional sources were observed in the C array because extra observation time was available. These 89 sources were selected from previously unmapped 4C, Molonglo, Parkes, and B2 quasars in the Hewitt and Burbidge (1980) catalog.

Data Reduction

The data were edited and calibrated at the VLA site. Subsequent mapping and analysis were done by using the AIPS (Astronomical Image Processing System) software installed on the Cray Y-MP 2/216 at the UNLV Supercomputer Center. Because image construction and deconvolution make extensive use of 2D Fourier transforms, the speed provided by the Cray Y-MP 2/216 supercomputer allowed more iterations of "clean" and self-calibration than is possible with slower computers.

The routine reduction included two passes of phase self-calibration, sometimes followed by one pass of amplitude and phase self-calibration. The resulting maps were 512 or 1024 pixels square with each pixel subtending 0.1 arcsec for A array data and 1.3 arcsec for C array data. The clean

beams are generally between 0.4 and 1.0 arcsec for A array data and between 4.0 and 8.0 arcsec for C array data. The rms noise ranges from 0.1 to 0.2 mJy/Beam for A array data and from 0.2 to 0.4 mJy/Beam for C array data (measured near the tracking center after primary beam correction). The dynamic ranges, defined as the ratio of the peak to the rms noise, are generally over a thousand for both A and C array data.

Measurements and Analysis

Positions and flux densities were measured for each source component. Positions for associated optical objects were obtained from HUO, Wills (1979) and Hewitt and Burbidge (1989). Contour maps were plotted for sources with significant structures.

The "bending angle" θ is defined as the angle of intersection of the two lines connecting the flux peaks of each outer lobe with the central component of the triple source, such that $\theta = 0$ for straight sources. About half the sources have bending angles $\theta \geq 10°$, 14/70 (20%) of the sources have $\theta \geq 20°$, and 5/70 (7%) have $\theta \geq 40°$.

If an appreciable fraction of the observed distortions is caused by interactions between the radio sources and surrounding media, such as ICM, the distorted sources should tend to have relatively small overall physical sizes, since the distorting medium would also slow the outward flight of the radio components. In addition, small distortions may be magnified by projection effects if the radio source axis lies close to our line of sight, in which case the apparent overall size of the radio source would also be reduced (Kapahi and Saikia 1982). In light of these considerations, it is expected that the radio source bending angles and physical sizes would show an inverse correlation. In order to test this expectation, the bending angle θ as a function of relative physical size(R) was plotted and an anticorrelation is apparent. All sources with $\theta \geq 20°$ are smaller than $R = 14.1$ arcsec. Further, all sources with $R > 14.1$ arcsec have $\theta \leq 12.2°$.

Conclusion

We found that among 192 sources observed in the A array, 70 are triples. About half of these triples have bending angles $\theta \geq 10°$. 20% of these sources have $\theta \geq 20°$, and 7% have $\theta \geq 40°$. If quasars showing large distortions ($\theta \geq 20°$) are associated with rich clusters of galaxies, about 20% of quasars associated with triple radio sources can be used to identify clusters of galaxies. An apparent anticorrelation was also found between bending angle and relative physical size and it is consistent with the hypothesis that quasars are distorted by interactions with dense intracluster media.

The flux densities, positions, and contour maps for both A and C array data are being prepared for publication.

References

Hewitt, A. and Burbidge,G. (1980). *ApJ. Suppl.*,43, 57.

Hewitt, A. and Burbidge,G. (1989). *ApJ. Suppl.*, 69, 1.

Hintzen, P. (1984). *ApJ. Suppl.*, 55, 533.

Hintzen, P., and Romanishin, W. (1986). *ApJ. Letters*, 311, L1.

Hintzen, P.,Ulvestad,J., and Owen, F. (1983). *Astro. J.*, 88, 709.

Kapahi,V. and Saikia,D. (1982). *J. Astrophys. Astron.*, 3, 161.

Wills, D. and Lynds, R. (1978). *ApJ. Suppl.*, 36, 317.

Wills, D. (1979). *ApJ. Suppl.*, 39, 291.

QUASARS IN RICH GALAXY CLUSTERS

E. Ellingson, *CASA, U. Colorado*

H. K. C. Yee, *U. Toronto*

N93-26856

ABSTRACT

The evolution of AGN activity in rich clusters of galaxies is found to be approximately 5 times more rapid than that in poor clusters. This rapid evolution may be driven by evolution in the dynamics of galaxy cluster cores. Results from our spectroscopic studies of galaxies associated with quasars are consistent with this scenario, in that bright AGN are preferentially found in regions of lower velocity dispersion. Alternately, the evolution may be driven by formation of a dense intra-cluster medium (ICM). Galaxies close to quasars in rich clusters cores are much bluer (presumably gas rich) than galaxies in the cores of other rich clusters, in support of this this model.

Rapid Evolution of AGN in Rich Galaxy Clusters

Figure 1 shows the absolute nuclear B magnitudes versus redshift for samples of quasars and radio galaxies ($z < 0.1$) from the 3C, 4C and Parkes radio samples. Nuclear magnitudes for the latter were determined spectroscopically (e.g. DeRobertis and Yee 1990). The quasar-galaxy spatial covariance amplitude, B_{gq}, was determined for many objects in order to quantify the richness of the galaxy cluster environment. Objects with environments richer than Abell class 0 clusters ($B_{gq} > 500$ Mpc$^{1.77}$) and are denoted by closed dots, and objects in poorer environments with open dots, and those without information as crosses.

Assuming a luminosity function (LF) for AGN and its evolution, we construct models predict the brightest that will be included in our samples, as a function of redshift. The dotted line in Figure 1 represents a model using the standard quasar LF and evolution determined by Boyle *et al.* (1989). This model matches the upper envelope for objects in poor environments well. The dashed line represents a model using the same LF form, but which requires evolution 5 times faster in order to match the behavior of AGN in rich clusters of galaxies. The e-folding timescale for this evolution are approximately 1 Gyr, similar to dynamical timescales in these environments.

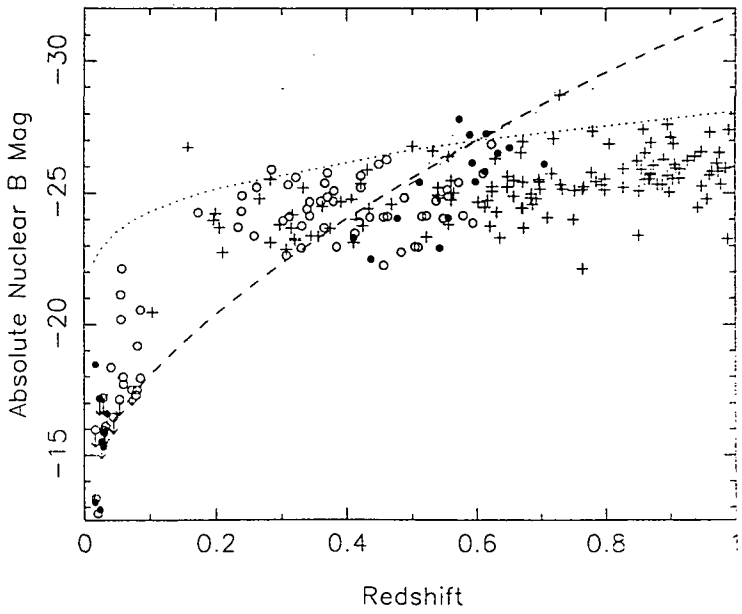

The model describing the evolution of AGN activity in rich clusters, drastically overpredicts the density of quasars for $z > 0.7$. A possible explanation for this abrupt change in the evolution of AGN in rich environments is that the formation rate of galaxy clusters declines at $z \sim 0.7$. In this scenario, AGN activity is primarily associated with young, unevolved clusters (see below for evidence supporting this possibility). At $z \sim 0.7$, however, a decline in the supply of new rich sites means that the AGN activity in rich environments would decline on timescales similar to evolutionary timescales of the cores of rich galaxy clusters, as is seen.

Dynamics of AGN Environments

Dynamical evolution in the cluster core may be responsible for this rapid evolution of AGN activity in rich clusters. Much evidence suggests that quasar activity is linked with galaxy–galaxy interactions and that these interactions are most efficient at low relative velocities (DeRobertis 1985, Roos 1985). In this scenario, young, unevolved clusters might also have low velocity dispersions, but as they virialize, the velocities in their cores increase, causing the observed AGN activity to decline.

Multi-object spectroscopic observations of faint galaxies in quasar fields with $0.4 < z < 0.6$ have been taken at KPNO and the CFHT in order to examine the dynamics of quasar environments. A large sdample of galaxies associated with quasars have now been identified (Ellingson, Green and Yee 1991, Ellingson and Yee 1992). For a sample of high-redshift quasars in rich clusters, 59 galaxies yield a composite velocity dispersion of 580 (+50 -70) km/sec. For comparison, the velocity dispersions of clusters of similar richness which are associated with the radio galaxies at low redshift are usually 700-900 km/sec (Zabludoff *et al.* 1990), significantly higher. These results are consistent with the scenario where increasing velocity dispersions are linked with decreasing AGN activity in the cores of rich clusters.

The ICM in Clusters Associated with Quasars

A second possible mechanism responsible for the rapid evolution of AGN activity in rich galaxy clusters, may be that it is in response to evolution in the intra-cluster medium (ICM). The presence of a dense ICM may be able to strip gas from either the AGN host galaxy or from companion galaxies, depriving the central engine of a necessary fuel source (Stocke and Perrenod 1981). Recent results of X–ray observations of distant galaxy clusters (Gioia *et al.* 1990, Edge *et al.* 1990) do indeed suggest that the ICM has evolved significantly since $z \sim 0.5$, in agreement with this scenario.

Observed g–r colors of galaxies in the cores of clusters associated with quasars at $z \sim 0.5$ indicate a very high fraction of blue galaxies located within only 10–15 " of the centers of rich galaxy clusters. A lower limit of 60% is found, in comparison with ~20% found in other clusters at similar redshifts (e.g. Butcher and Oemler 1984). This result implies that the near environments of quasars contain many gas-rich galaxies, despite their location in the cores of rich galaxy clusters. This results is therefore consistent with, but not necessarily indicative of the evolving ICM model.

REFERENCES

Boyle, B. J., Shanks, T., & Peterson B. A. 1988, *MNRAS*, **235**, 935.

Butcher, H. R. and Oemler, A. 1984, *Ap. J.***285**, 426.

DeRobertis, M. M. 1985 *A. J.*, **235**, 351.

DeRobertis, M & Yee, H. K. C. 1990 *A. J.*, **100**, 84.

Edge, A. C., Stewart, G. C., Fabian, A. C., & Arnaud, K. A. 1991, *MNRAS*, **245**, 559.

Ellingson E., Green, R. F., & Yee H. K. C. 1991, *Ap. J.*, **378**, 476.

Ellingson, E., Yee, H. K. C., & Green, R. F. 1991, *Ap. J.*, **371**, 36.

Ellingson, E. and Yee, H. K. C. 1992, in preparation

Gioia I. M., Henry, J. P., Maccacaro, T., Morris, S. L., Stocke, J. T., & Wolter, A. 1991, *Ap. J.*, **356**, L35.

Roos, N. 1985 *A. & A.*, **104**, 218.

Stocke, J. T. & Perrenod, S. C. 1981, *Ap. J.*, **245**, 375.

Yee, H. K. C. & Green, R. F. 1987, *Ap. J.*, **319**, 28.

Zabludoff A., Huchra, J. P. & Geller, M. J. 1990, *Ap. J. Suppl.*, **74**, 1.

FINDING THE RAREST OBJECTS IN THE UNIVERSE:

A New, Efficient Method for Discovering BL Lacertae Objects

John Stocke, Eric Perlman and Arno Granados
CASA, University of Colorado, Boulder

Jonathan Schachter and Martin Elvis
X-ray Division, CfA

Meg Urry
Space Telescope Science Institute

Chris Impey and Paul Smith
Steward Observatory, University of Arizona

Introduction

While recent objective prism, UVX, radio and X-ray surveys have dramatically increased the number of known QSOs (typical discovery rate now averages one per day), the number of BL Lac Objects known has increased only very slowly (average rate about 5 per year) over the last twenty years. And while recent X-ray surveys (*Einstein*, EXOSAT and ROSAT) are dramatically increasing the number of known BL Lacs, the rarity of these objects (BL Lacs account for only $\sim 5 - -10\%$ of all faint X-ray sources) still requires a substantial commitment of optical observing time to find them. For example, the 36 new BL Lacs found in the *Einstein* Extended Medium Sensitivity Survey (EMSS; Gioia *et al.* 1990; Stocke *et al.* 1991) required $\sim$ 8 years of optical spectroscopy to identify. Other methods for finding BL Lacs (high frequency radio surveys or optical polarization or color surveys) have similarly low success rates for finding new BL Lacs; e.g. $0 - 10\%$.

We present a new, efficient method for discovering new BL Lac Objects based upon the results of the EMSS. We have found that all X-ray selected BL Lacs are radio emitters (Stocke *et al.* 1990) and further that in a "color-color" diagram (radio/optical and optical/X-ray) the BL Lac Objects occupy an area distinct from both radio loud quasars and the radio quiet QSOs and Seyferts which dominate X-ray selected samples. After obtaining radio counterparts via VLA "snapshot" observations of a large sample of unidentified X-ray sources, the list of candidates is reduced to those which fall in the correct area of Figure 1. These candidates then can be confirmed with optical spectroscopy and/or polarimetry. Since $> 70\%$ of these sources are expected to be BL Lacs, the optical observations are very efficient.

We have tested this method using unidentified sources found in the *Einstein* Slew Survey (Elvis *et al.* 1992). 162 Slew Survey X-ray source positions were observed with the VLA in a mixed B/C configuration at 6 cm resulting in $\sim$ 60 detections within 1.5 position error circle radii. These X-ray/optical/radio sources were then plotted on Figure 1 and $\sim$ 40 BL Lac candidates were identified.

To date **10** candidates have been spectroscopically observed resulting in **10** new BL Lac objects! Radio flux, optical magnitude, and polarization statistics (obtained in white light with the Steward Observatory 2.3 m CCD polarimeter) for each is given in Table 1.

The Method

The key to finding BL Lacs is to exploit three facts:

1. All BL Lacs are radio loud;
2. BL Lacs have distinctive radio/optical/X-ray colors (Figure 1, also Stocke *et al.* 1991); and
3. The surface density of X-ray-selected BL Lacs flattens at fluxes below $10^{-12} ergs\ s^{-1}\ cm^{-2}$ (Wolter *et al.* 1991).

Therefore wide-angle, high-flux surveys are better for detecting BL Lacs than deeper, narrow-beam surveys.

Together these properties allow us to define a multi-step approach to identify new X-ray selected BL Lacs in the Slew Survey:

1. Choose sources at high galactic latitudes ($|b| > 15°$) with moderate positional uncertainties ($\sim 1'$ at 90% certainty for the Slew Survey).
2. Observe them with the VLA, giving an accurate radio flux and position ($1 - 2$" is sufficient).
3. Use the radio positions to find optical counterparts and magnitudes from digitized sky survey plates.
4. Place objects in the radio/optical/X-ray color-color plot (Figure 1).
5. Obtain optical spectra only for candidates with correct colors.

Results

Approximately 40 Slew Survey BL Lac candidates have been selected using the above method. Of these, **10** have been observed spectroscopically, resulting in the confirmation of **10** new BL Lacs — already an increase in the known number of BL Lacs by 10%! The identification program will continue this September at the Kitt Peak 2.1 meter telescope. Based on these results, we expect approximately 30 more BL Lacs to be discovered in the Slew Survey. If this method is applied to the bright sources in the ROSAT all-sky survey, nearly 1000 BL Lacs should be discovered!

Table 1. New Slew Survey BL Lac Objects

Object Name	$f(6cm)$,mJy	V	P(%)	θ
1. 1ES0229 + 200	41.5	18.0	—	—
2. 1ES0347 − 121:	7.6	19.1	—	—
3. 1ES0502 + 675	31.3	16.5	3.89 ± 0.45	$124.3° \pm 3.3$
4. 1ES0647 + 250	61.0	15.3	—	—
5. 1ES0806 + 524	169	15.3	1.68 ± 0.50:	—
6. 1ES1028 + 511	42.5	17.0	8.13 ± 0.39	$17.3° \pm 1.4$
7. 1ES1440 + 122	40.2	15.3	≤ 1.8	—
8. 1ES1544 + 820	45.1	15.3	1.81 ± 0.41:	—
9. 1ES1959 + 650	241	14.6	2.76 ± 0.25	$147.1° \pm 2.6$
10. 1ES2343 − 151:	7.7	19.2	—	—

A colon after the name indicates either that the identification as a BL Lac is not certain due to low SNR spectra at present (objects 2 and 10); a colon after the polarization percentage indicates that the polarization detection is only possible (objects 5 and 8).

References

Elvis, M., Plummer, D., Schachter, J., and Fabbiano, G., 1992, *Ap. J. Supp.* **80**, 227.

Gioia, I., *et al.*, 1990, *Ap. J. Supp.* **72**, 567.

Stocke, J., *et al.*, 1991, *Ap. J. Supp.* **76**, 813.

Stocke, J., *et al.*, 1990, *Ap. J.* **348**, 141.

Stocke, J., *et al.*, 1989, in *BL Lac Objects*, ed. L. Maraschi, T. Maccacaro, and M.-H. Ulrich (Springer-Verlag), p.242.

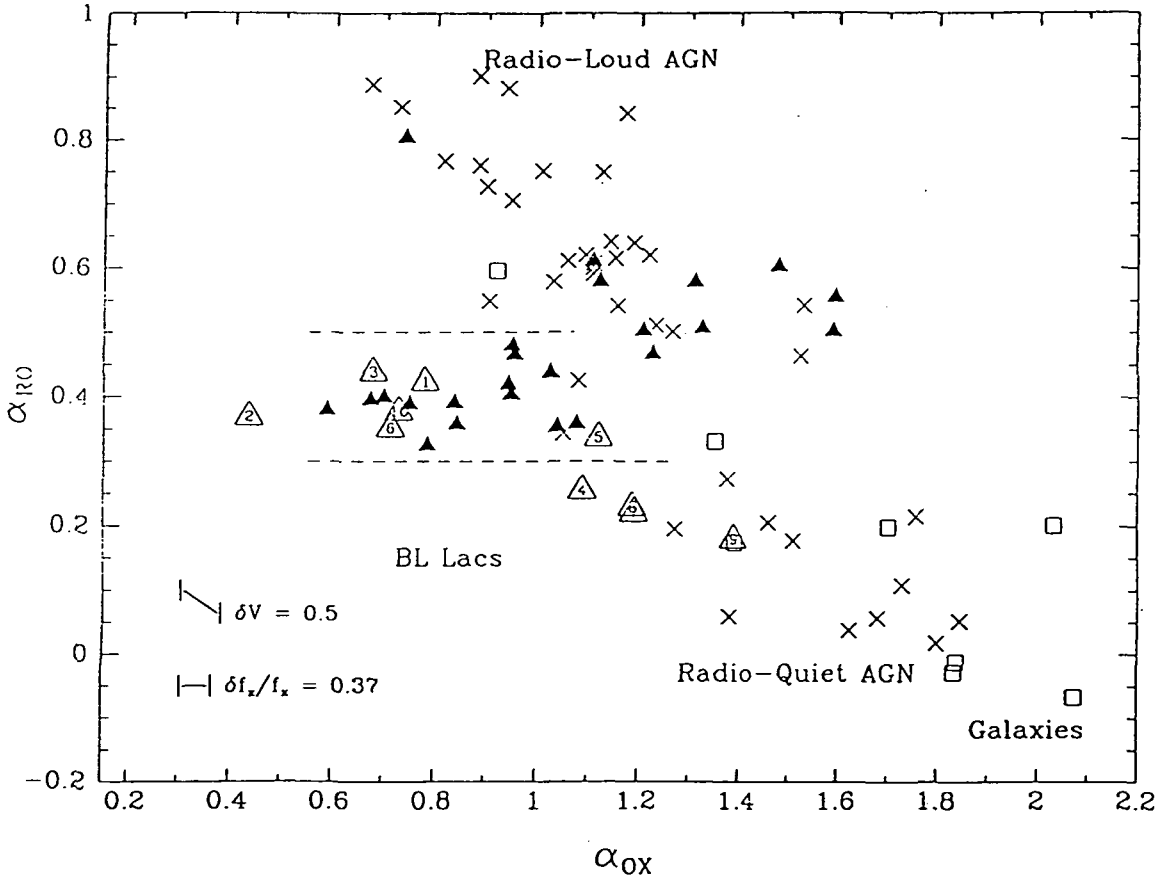

IUEAGN: A Database of Ultraviolet Spectra of Active Galactic Nuclei

G. Pike, R. Edelson, NASA/GSFC
J. M. Shull, J. Saken, CASA/ University of Colorado

In 13 years of operation, *IUE* has gathered ~5000 spectra of almost 600 Active Galactic Nuclei (AGN). In order to undertake AGN studies which require large amounts of data, we are consistently reducing this entire archive and creating a homogeneous, easy-to-use database. First, the spectra are extracted using the Optimal extraction algorithm (Kinney, Bohlin & Neill, 1991, *P.A.S.P.*, 103, 694). Continuum fluxes are then measured across pre-defined bands, and line fluxes are measured with a multi-component fit (see Figure 1). These results, along with source information such as redshifts and positions, are placed in the IUEAGN relational database. Analysis algorithms, statistical tests and plotting packages run within the structure, and this flexible database can accommodate future data when they are released.

This archival approach has already been used to survey line and continuum variability in six bright Seyfert 1s (Edelson, Krolik, & Pike, 1990, *Ap. J.*, 359, 86). and rapid continuum variability in 14 blazars (Edelson, Saken, Pike, Kinney, & Shull 1992, *Ap. J.*, in press) (see Figure 2). Among the results that could only be obtained using a large archival study is evidence that blazars show a positive correlation between degree of variability and apparent luminosity, while Seyfert 1s show an anti-correlation. This suggests that beaming dominates the ultraviolet properties for blazars, while thermal emission from an accretion disk dominates for Seyfert 1s. Our Future plans include a survey of line ratios in Seyfert 1s, to be fitted with photoionization models to test the models and determine the range of temperatures, densities and ionization parameters. We will also include data from *IRAS*, *Einstein*, *EXOSAT*, and ground-based telescopes to measure multi-wavelength correlations and broadband spectral energy distributions.

Figure 1a

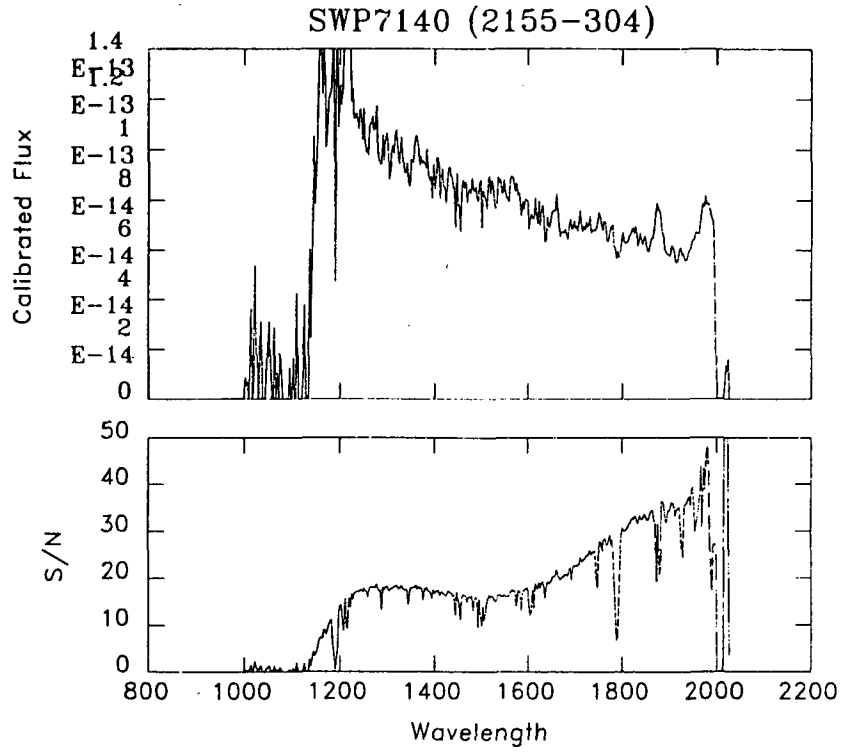

Figure 1b

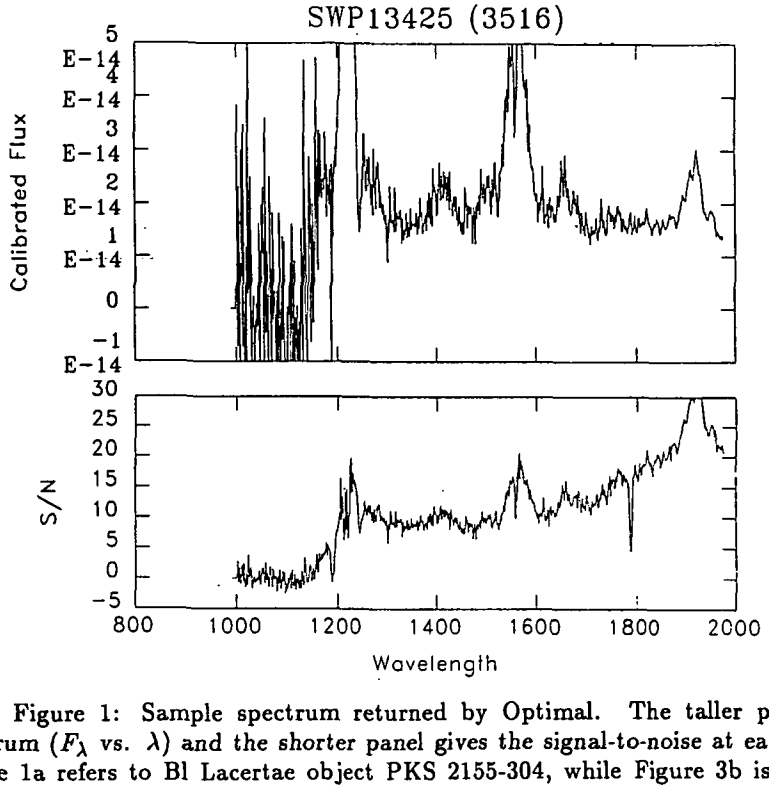

Figure 1: Sample spectrum returned by Optimal. The taller panel gives the spectrum (F_λ vs. λ) and the shorter panel gives the signal-to-noise at each wavelength. Figure 1a refers to Bl Lacertae object PKS 2155-304, while Figure 3b is NGC 3516, a Seyfert 1.

Figure 2

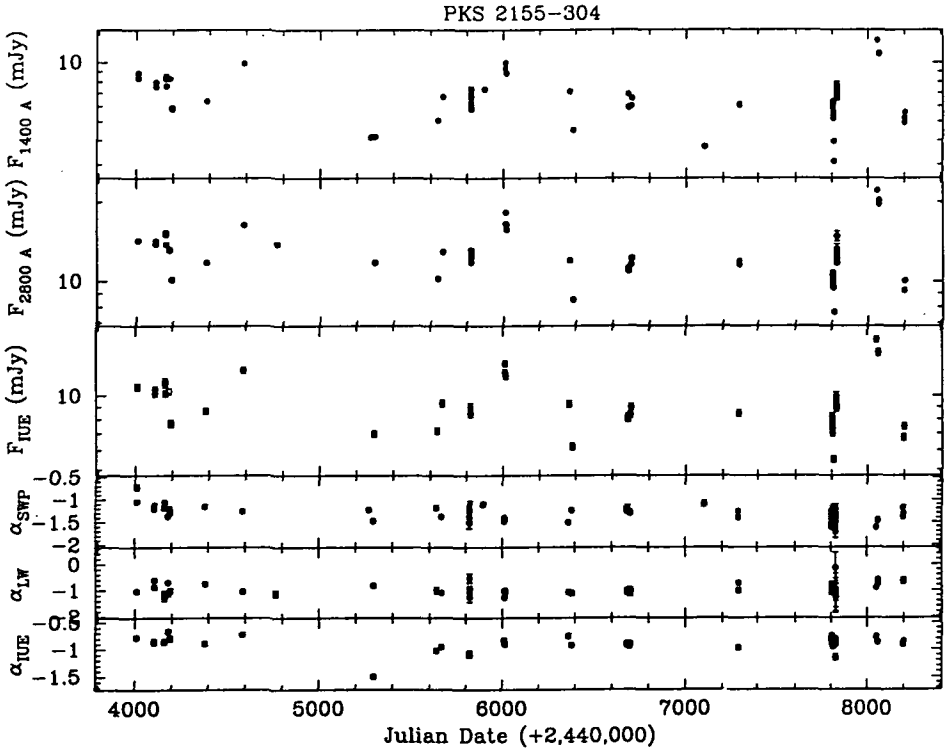

Figure 2: Light curve for the BL Lacertae object PKS 2155-304 during the period 1978-1990 (Edelson, Krolik & Pike, 1990, *Ap. J.*,359, 86).

High Resolution 1-20μm Imaging of the Nuclear Environment of NGC 1068

M. Cameron[1], J.W.V. Storey[2], V. Rotaciuc[1], M. Blietz[1], R. Genzel[1], A. Krabbe[1], L. Verstraete[1], P. van der Werf[1], S. Drapatz[1] & T. Lee[3]

[1]*Max-Planck-Institut für extraterrestrische Physik, Garching, Germany*
[2]*University of New South Wales, Sydney, Australia*
[3]*Royal Observatory, Edinburgh, Scotland*

We present new mid-infrared continuum and near-IR line images of the nuclear environment of the nearby (14 Mpc) Seyfert 2 galaxy NGC 1068. The 8, 10 & 19 micron data were measured with our new mid-IR array camera, MIRACLE (Cameron *et al.* 1992a), at UKIRT in November 1991 while our images of the H_2 2.121μm and [Fe II] 1.64μm lines were obtained with FAST, the MPE imaging spectrometer, at the 4.2m William Herschel Telescope in August 1991. The MIRACLE data were imaged through narrow band ($\frac{\lambda}{\Delta\lambda} \geq 50$) filters whereas FAST incorporates a Fabry-Perot etalon ($\frac{\lambda}{\Delta\lambda} \geq 950$).

The 8 & 10 micron emission is resolved with respect to our $\sim$1″ point spread function (PSF) and, as such, these data represent the highest spatial resolution mid-IR images of NGC 1068 hitherto obtained. In addition, MIRACLE's good spatial sampling (0.17″/pixel) and the high signal-to-noise quality of our 10μm data has allowed us to effectively deconvolve the raw images. These deconvolved data, which have a resulting spatial resolution of 0.5″, are presented in Figure 1 (inset) superimposed on a map of the narrow line emission clouds obtained with the HST. It is apparent that the mid-infrared emission, which arises from dust heated to several hundred Kelvin, is extended on angular scales of $\sim$2″, corresponding to $\sim$140 pc at the distance of NGC 1068, along the direction of the outflow from the nucleus which is observed at radio wavelengths. The spatial distribution of the 10μm emission bears a striking resemblance to that of the optical [O III] emission. Such a spatial coincidence suggests an intimate link between the warm dust and narrow line clouds (Genzel, Cameron & Krabbe 1992; Cameron *et al.* 1992b).

The 2.121μm H_2 v=1-0 S(1) line data is shown in figure 1 superimposed on a map of the radio continuum emission. The warm circumnuclear molecular gas is extended $\sim$5″ (340 pc) east-west and consists of several embedded knots which represent concentrations of dense, massive molecular clouds. The brightest H_2 knot, centred 0.3″ south-west of the near-IR continuum peak, has a molecular hydrogen column density in excess of 10^{23} cm^{-2} and may contribute significantly to the large obscuration of the nucleus that is inferred from optical polarisation measurements. In contrast, the [Fe II] emission is extended over $\sim$7″, is elongated at position angle $\sim$35° and closely traces the narrow line region and the central collimated part of the radio jet (Blietz *et al.* 1992).

Based on these observations we propose a model of NGC 1068 in which the H_2 emission arises in warm gas heated by X-ray and UV radiation from the central source (Rotaciuc *et al.* 1991). The extended mid-IR emission may be explained as dust, located in clouds at the interface between the conical outflow channel and the circumnuclear ISM, which is *directly* heated by radiation from the active nucleus. In particular, our model does not require the presence of a thick, dusty, few parsec scale torus surrounding the nucleus but, rather, we pro-

pose that the bulk of the molecular material in the inner ~150 pc is actually located at large distances from the nucleus. In the absence of a compact dusty torus, our direct view of the nucleus is probably blocked by one or more molecular clouds located a few 10 pc from the AGN (Cameron *et al.* 1992b).

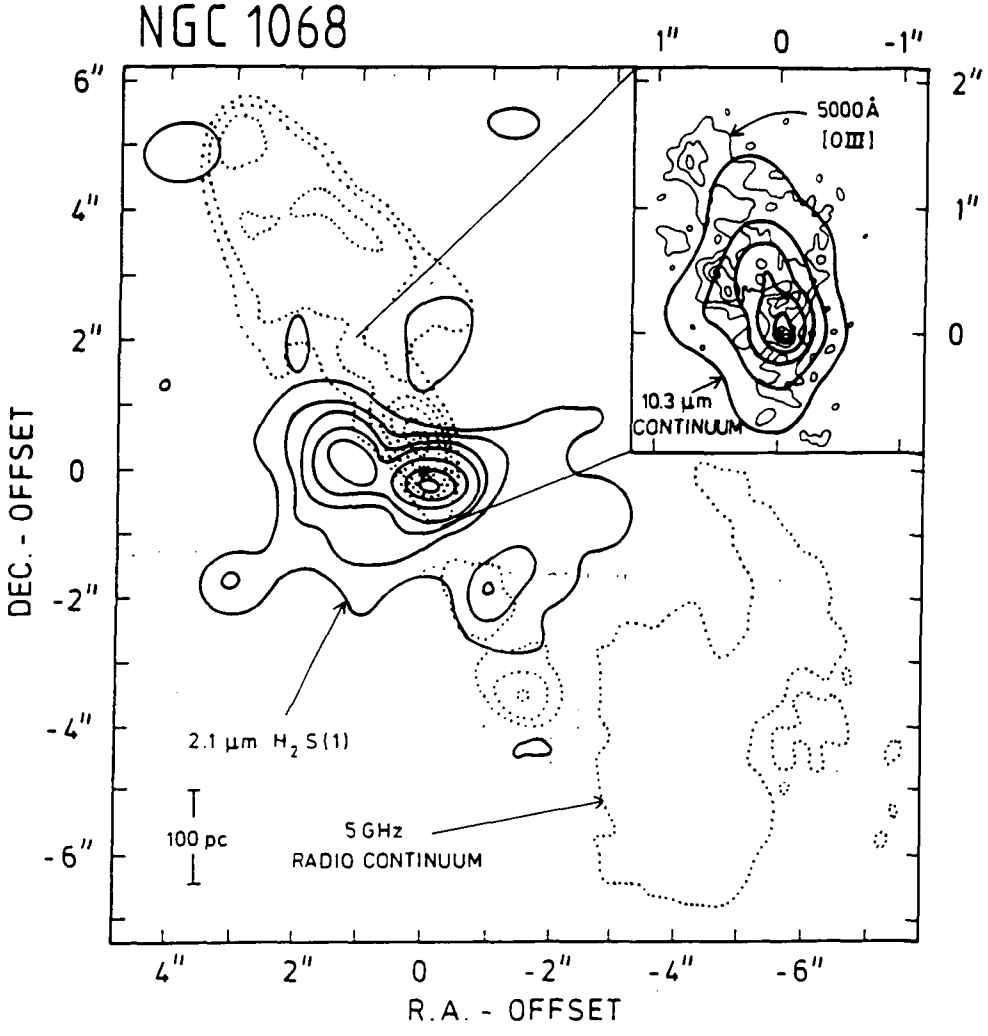

Figure 1: Image of the 2.121μm H_2 v=1-0 S(1) line obtained with the MPE imaging spectrometer (FAST) towards the nuclear region of NGC 1068 (solid lines) superimposed on the 5 GHz radio continuum map (dotted lines). The spatial resolution of the near-IR data is ~1". The inset shows the map of the deconvolved 10.3μm emission obtained with MIRACLE (thick lines) superimposed on an image of the narrow line clouds measured by the HST (thin lines). The effective spatial resolution of the mid-IR data is 0.5".

References

Blietz M. *et al.*, 1992, in preparation.

Cameron M. *et al.*, 1992a, in proceedings of the ESO Garching Conference on *Progress in Telescope and Instrumentation Technologies*, ed: Ulrich M-H.

Cameron M. *et al.*, 1992b, in preparation.

Genzel R., Cameron M. & Krabbe A., 1992, in proceedings of the Madrid symposium on *The Nearest Active Galaxies*, eds: Beckman J. & Colina L.

Rotaciuc V. *et al.*, 1991, *Ap. J.*, **370**, L23.

NARROW BAND IMAGING AND LONG SLIT SPECTROSCOPY OF UGC 5101

R. M. STANGA and F. MANNUCCI
Dipartimento di Astronomia e Scienza dello spazio dell' Università, Firenze.

J. M. RODRIGUEZ ESPINOSA
I.A.C., La Laguna, Spain.

ABSTRACT

UGC 5101 ($z = 0.04$; D $\simeq$ 240 Mpc) is one of the so called *Ultraluminous* IRAS sources. Two important properties of the members of this group are 1) their $L_{IR} \geq 10^{12}$ $L_{\odot}$, and 2) their space density in the universe up to $z \leq 0.1$ is equal or even larger than the space density of the quasars. Further noteworthy features of the *Ultraluminous* IRAS sources are their being morphologically peculiar, and the fact that they all seem to host active nuclei in their center.

We have observed UGC 5101 in an effort to study the interplay between the gas ionized by the central active nucleus and that gas ionized by other processes which may hold important clues to the understanding of the entire picture of this object. In particular these other ionizing processes could well be massive stars formed recently after the galactic encounter, and shocks possibly also related to the galaxy collision.

The data that we discuss were obtained between December 1989 and January, 1992 with the WHT 4.2m telescope on the island of La Palma, using the two-arm spectrograph ISIS. Several spectral frames were obtained at three different position angles: P.A. 84, along the tail of the galaxy; P.A. 32, along the dust lane; and P.A. 110. The blue spectra are centered on the Hβ line, while the red spectra are centered on the Hα line. In the configuration we used for the long slit spectra, the spectral scale was 0.74 A per pixel, and the spatial scale was .37 arcsec per pixel; we also observed the Hα region with a spectral scale of .37 A per pixel, at position angle 84.

The narrow band images were obtained at the auxiliary port of ISIS, with a scale of .2 arcsec per pixel, and were centered at the Hα wavelength, and on the adjacent continuum.

The Hα images and the spectra support the following model.

UGC 5101 hosts an active nucleus; the NLR extends up to about 1.5 kpc and shows a complex velocity field, superimposed on the rotation curve of the galaxy. Besides the NLR, in the Hα image are visible two bright cones that

extend up to 3 kpc along P.A. 32. The long slit spectra at P.A. 32 show that the velocity field of the gas in these regions is peculiar, while the ionization structure of the gas is similar to that of the NLR.

Around the nucleus, at a distance of about 3 kpc there is a ring-like structure made up by giant HII regions. In this ring an intense activity of star formation is taking place, as is testified by the estimated large number of O stars required to keep the HII region ionized.

The simultaneous presence of the GEHR's, that cannot be older than a few generations of O stars, opens the question whether a single event triggered the onset of all of them. Still uncertain is the answer to the question whether there is any relation between the GEHR's and the active nucleus. The presence of the central disk of clouds of ionized gas with a complex velocity field might be a hint that gas is flowing from the HII region ring to the center of the galaxy.

LONG SLIT SPECTROSCOPY OF NGC 5506

R. M. STANGA and R. MAIOLINO
Dipartimento di Astronomia e Scienza dello spazio dell' Università, Firenze.

J. M. RODRIGUEZ ESPINOSA
I.A.C., La Laguna, Spain.

ABSTRACT

The galaxy NGC5506 hosts an active nucleus, that presents characteristics that are intermediate between Syl and Sy2.

We discuss long slit spectra of NGC 5506 in the ranges 4675-5475 A and 6300-7125 A, that were obtained at three different position angles, in April 1991 at the WHT 4.2 m telescope on the island of La Palma.

The peculiar kinematics of the emitting gas has already been observed by Wilson et al. (1985); following the model proposed by Wilson et al., that the emitting gas is located in two cones, we determined the aperture of the cones. Our data, moreover, support the hypothesis that the gas is receeding from the nucleus.

We modelled the intensity and the ratios of the emission lines, and verified that the active nucleus of NGC 5506 can be described as a Syl nucleus, with the UV-X source that is partially obscured to our line of sight. On the contrary, a good fraction of the interstellar gas of the galaxy is directly illuminated and photoionized by the central source.

Our data also show evidence of star formation close to the nucleus; we estimated the star formation rate, that is high with respect to "normal" spirals, but not high enough to be comparable to star formation rates in a starburst galaxy.

STATIC GALACTIC HALO AND GALACTIC WIND

CHUNG-MING KO
Department of Physics and Institute of Astronomy
National Central University, Chung-Li, Taiwan, R.O.C.

1. INTRODUCTION

Although the exact state of the interstellar medium (ISM) in our Galaxy (other galaxies as well) is not clear at all, the "common consensus" is a rough pressure balance (or equipartition of energy) exists between different components and phases, say, cold, warm, hot phases of the ISM, magnetic field, cosmic rays, etc. If the halo of a galaxy is taken to be an extension of the ISM, then its structure is influenced by various ISM components. A "complete" description of the halo is evidently very complicated. This contributed paper gives a brief account on cosmic ray halo, which emphasizes the role played by cosmic rays. The interaction between cosmic rays and thermal plasma is facilitated by magnetic field. The cosmic rays are scattered by hydromagnetic waves (e.g., Alfvén waves) which in turn can be generated by cosmic ray streaming instability. This constitutes a self-consistent picture. Since we are interested in the structure of the halo, we adopted a hydrodynamic model in which the cosmic rays and waves are described by their pressures (see e.g. Ko 1992). In general there are two classes of halos: static and dynamic.

2. STATIC GALACTIC HALO

The basic model includes magnetohydrostatic equilibrium and energy exchange between cosmic rays and Alfvén waves. Magnetohydrostatic equilibrium is achieved when the total pressure gradient (which includes thermal plasma, cosmic rays and Alfvén waves) is balanced by the Lorentz force and the gravitational force. Cosmic rays and Alfvén waves are described by their energy flux equations. Energy exchange is simply the work done on the waves by the cosmic rays. To further simplify the model, we consider the so called *flux-tube formulation* (see e.g., Ko 1991). In this formulation, the background magnetic field is assumed to be a nice smooth vector field without any singularities so that we can form a flux tube. Moreover, assume that the Alfvén waves travel along the field line and there are no cross field line diffusion of cosmic rays. Under this formulation the model is essentially one dimension (along the flux tube).

Take our Galaxy as an example. The "base" of the halo is taken to be at 1 kpc above the mid-plane. At this level, the thermal plasma density and pressure are about 10^{-3} cm^{-3} and 0.25 eV cm^{-3}, respectively. The cosmic ray pressure is about 0.16 eV cm^{-3} and the pre-existing wave pressure is negligible. The density (and pressure) of the halo exhibits two scale heights. Close to the disk, the thermal

plasma pressure (small scale height) dominates. At large distances the halo is supported by cosmic rays and self-generated waves (large scale height). In the case of our Galaxy, the coupling between the cosmic rays and background plasma is strong. The cosmic rays lift the halo to large distances and give rise to a pressure (about 6×10^{-3} eV cm^{-3}) too large to match the intergalactic medium (IGM) pressure. In addition, stability analysis on this kind of static halo shows that the halo is very susceptible to overturning instability. In the case of our Galaxy the growth time is of the order of 2×10^7 yr (see e.g., Ko et al. 1991; Ko 1991). As a result, at least in the case of our Galaxy, a dynamic model is needed.

GALACTIC WIND

The large pressure difference between the static halo and IGM at large distances initiates an outflow, namely, galactic wind (if the material falls back to the disk afterwards, it is called a fountain then). A cosmic ray driven wind model can be constructed from the above static cosmic ray halo model by simply replacing the magnetostatic equilibrium condition by the mass, momentum and energy fluxes equations. The model can also be formulated along the flux tube provided that the flow and Alfvén waves follow the field line and no cross field line diffusion of cosmic rays. For steady state, the problem reduces to analysing a wind equation. To match the small IGM pressure, a transonic solution (from subsonic near the disk to supersonic far away) is required. In our Galaxy, the cosmic ray is able to push the plasma through the critical point and forms a supersonic cosmic ray driven galactic wind (see Breitschwerdt et al. 1991).

Finally, a few words about galactic rotation. When galaxy rotates, the magnetic field line forms Parker's spiral type helix (assume the flow dominates the field at large distances). Suppose the wind speed is about $250 \sim 500$ km s^{-1}. In our Galaxy the helical structure is important when we are interested in distances larger than $50 \sim 100$ kpc. Helical field line complicates the above formulation. Of course, there is no problem if we consider an isolated rigid thin flux tube. If we consider an extended region, then we must modified the above formulation simply because we can't use a helical curve as one of the coordinate curves. When axisymmetry is assumed, a formulation closely resemble the above one can be constructed and is called *projected flux-tube formulation* (c.f. Ko 1991).

REFERENCES

Breitschwerdt, D., McKenzie, J.F., Völk, H.J., 1991, *Astron. Astrophys.*, **245**, 79.
Ko, C.M., 1991, *Astron. Astrophys.*, **242**, 85.
Ko, C.M., 1992, *Astron. Astrophys.*, in press.
Ko, C.M., Dougherty, M.K., McKenzie, J.F., 1991, *Astron. Astrophys.*, **241**, 62.

Turbulent Mixing Layers in the Interstellar Medium of Galaxies

J. D. Slavin, J. M. Shull, M. C. Begelman (University of Colorado, JILA)

We propose that turbulent mixing layers are common in the interstellar medium (ISM). Injection of kinetic energy into the ISM by supernovae and stellar winds, in combination with density and temperature inhomogeneities, results in shear flows. Such flows will become turbulent due to the high Reynolds number (low viscosity) of the ISM plasma. These turbulent boundary layers will be particularly interesting where the shear flow occurs at boundaries of hot ($\sim 10^6$K) and cold or warm (10^2– 10^4K) gas. Mixing will occur in such layers producing intermediate-temperature gas at $T \approx 10^{5.0-5.5}$ that radiates strongly in the optical, ultraviolet, and EUV.

Expanding on the ideas of Begelman & Fabian (1990), we have modeled these layers under the assumptions of rapid mixing down to the atomic level and steady flow. By including the effects of non-equilibrium ionization and self-photoionization of the gas as it cools after mixing, we predict the intensities of numerous optical, infrared, and ultraviolet emission lines, as well as absorption column densities of C IV, N V, Si IV, and O VI.

We obtain the following results:

1) All of the C IV λ1550 emission observed by Martin & Bowyer (1990) could be explained by mixing layers in the thick disk/low halo. To match the emission/absorption ratio, a pressure, $p/k_B \approx$ 2000–3000 cm^{-3} K, is required. If $\log \bar{T} = 5.3$ the models match the observed emission line ratio C IV/O III] λ1663 $\sim$ 2.

2) The observed absorption-line column densities of C IV, N V, Si IV and O VI can all be matched by mixing layer models with $\log \bar{T} =$ 5.0–5.3 if there is some grain depletion.

3) A significant contribution to the Hα background in the Galaxy could come from mixing layers between gas at 10^6 K and cold clouds at 10^2 K. The calculated optical line ratios of [N I] λ5201, [N II] λ6583, [O I] λ6300, [O III] λ5007 and [S II] λ6716 relative to Hα are close to the observed values.

4) Mixing layers with warm (10^4K) gas produce [S II] λ6716/H$\alpha \approx$ 0.3, in good agreement with observations of diffuse ionized gas in "interstellar froth" in Magellanic irregulars and some edge-on spirals and with the extended component of diffuse ionized gas in the Seyfert NGC 1068. Both the [N II] λ6583/Hα and the [O II] λ3727/[O III] are close to observed values as well.

5) The cooling time for hot gas is decreased by factors of 10–100 in mixing layers over quiescent cooling. This could be important for regulating the hot gas filling factor and could serve to quench galactic fountain activity. Some 20% of the supernova power in the Galaxy and 75 $M_\odot$ yr^{-1} may be processed through mixing layers.

Further observations of the emission lines O III] λ1663, [O III] λ5007 and O VI λ1032,1038 at high latitude are important to test our models and to understand the nature of "frothy" diffuse ionized gas in the ISM.

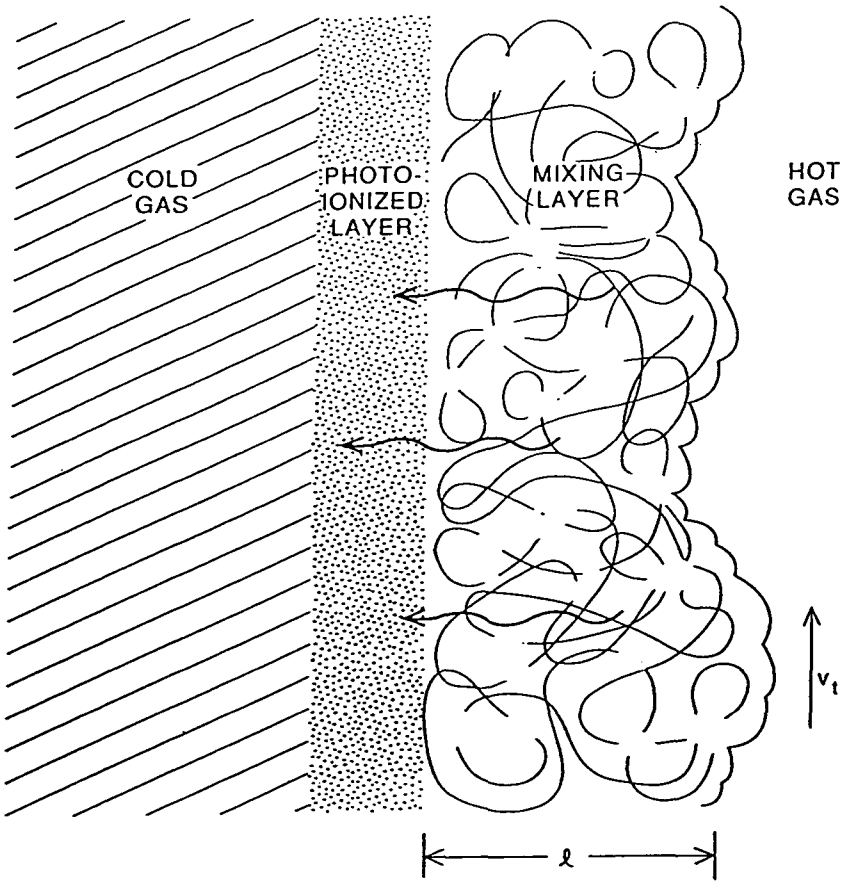

Fig. 1.—Schematic drawing of mixing-layer geometry, showing hot and cold gas and a photoionized layer abutting the mixing layer.

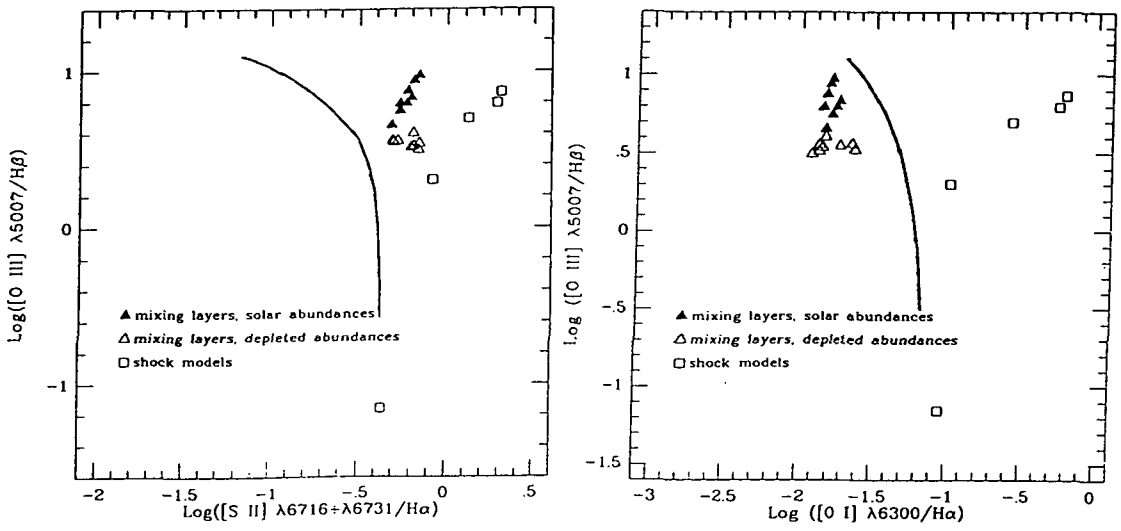

Fig. 2.—Emission line ratios in turbulent mixing layers with $\log \bar{T} = 5.5$ *and 5.7 and in the shock models of* Shull & McKee (1979, ApJ 227, 131) for shock velocities ranging from 80 to 130 km s^{-1}. The curve, from Osterbrock & Viellieux (1987, ApJS 63, 295), seperates AGN (upper right) from H II regions (lower left).

The Formation of Low-Ionization Emission in the Halo of NGC 891

James Sokolowski† and Jonathan Bland-Hawthorn‡

INTRODUCTION:

Imaging and Spectroscopic study first revealed the presence of a *diffuse ionized medium* (DIM), having unusual excitation, pervading the lower halo of the edge-on spiral galaxy NGC 891.[1,2] Emission from this DIM is strongest northeast of the nucleus,[3] at radii between 2 and 8 kpc (hereafter region 1), where Hα emission can be traced out to $|z| \simeq 2$ kpc and the electron density is $n_e \simeq \frac{1}{2}\ \phi^{-1/2} e^{-|z|/z_0}$ cm^{-3} for a DIM filling factor ϕ. The [NII]λ6583/Hα and [SII]$\lambda\lambda$6716,6731/Hα ratios increase dramatically with $|z|$ in region 1, from 0.6 and 0.5 respectively at $|z| \simeq 500$ pc to 1.1 and 1.0 at $|z| \simeq 1$ kpc,[4] while nondetections of [OI]λ6300 and [OIII]λ5007 emission yield upper limits of [OI]λ6300/Hα $\lesssim 0.05$ and [OIII]λ5007/Hα $\lesssim 0.15$ for $|z| \lesssim 1$ kpc.[3] Previous photoionization models,[5] using the radiation field from disk O and B stars, have been successful in reproducing the elevated [NII]λ6583/Hα and [SII]$\lambda\lambda$6716.6731/Hα ratios observed. However, these radiation bounded models also produce significant [OIII]λ5007 emission, in conflict with the observed upper limit. Here, we report the results of new, matter bounded models for the photoionization of the DIM in region 1 of NGC 891.

PHOTOIONIZATION MODELING:

We use the photoionization code CLOUDY[6] to examine the parameter space available to individual photoionized DIM elements (clouds, filaments, sheets) using plane-parallel, constant (low) density, matter bounded models. All models include the optical and thermal (heating and cooling) properties of standard interstellar dust grains,[6] and use the hardened radiation field of a Salpeter IMF stellar population detailed elsewhere.[5] Depleted elemental abundances, calculated using standard interstellar depletion parameters[7] for an average density of $\frac{1}{2}$ cm^{-3} are used throughout. Acceptable reproduction of the observational constraints can be obtained for ionization parameters of order 10^{-4} and hydrogen columns in the range $5 \times 10^{18} \lesssim N_H\ (\mathrm{cm}^{-2}) \lesssim 2 \times 10^{19}$. We compare model results with observations in Table 1 and present the $N_H = 10^{19}$ cm^{-2} line ratios Figure 1.

We can estimate the ionization parameter throughout the DIM of NGC 891 by using the electron density distribution given above and appealing to its ionization equilibrium. Specifically we find; $U(|z|) \simeq \alpha_{rec} (\int_{|z|}^{\infty} \phi\, n_e^2(z')\, dz') / (n_e(|z|)\, c)$, where α_{rec} is the hydrogen recombination coefficient (2.6×10^{-13} cm^3 sec^{-1} at 10^4 K) and c is the speed of light. This yields $U(|z|) \simeq 5 \times 10^{-3}\, \phi^{1/2}\ e^{-|z|/1\mathrm{kpc}}$ throughout region 1. Therefore, the ionization parameter falls by a factor of 5 out to $|z| \simeq 2$ kpc, and by a factor of $\sim$1.5 over 500 pc $\leq |z| \leq 1$ kpc. Successful reproduction of the full range of [NII]λ6583/Hα ratios observed and the strong emission gradients with $|z|$ requires $U \simeq 10^{-4}$ at $|z| = 1$kpc. This suggests that the DIM filling factor is $\sim$0.003, significantly lower than previous estimates.[5]

† Space Telescope Science Institute. 3700 San Martin Drive, Baltimore, MD 21218
‡ Dept. of Space Physics and Astronomy. Rice University, Houston, TX 77251-1892

Table 1: Model Results

Emission Property	Observed	Model		
		5×10^{18}	1×10^{19}	2×10^{19}
[SII] $\lambda\lambda$ 6716,6731/Hα	0.5 - 1.0	0.3 - 1.0	0.3 - 1.0	0.2 - 0.9
[NII] λ 6583/Hα	0.5 - 1.1	0.6 - 1.0	0.5 - 1.1	0.5 - 1.1
[OI] λ 6300/Hα	$\lesssim$0.05	$\lesssim$0.02	$\lesssim$0.05	$\lesssim$0.08
[OII] λ 3727/Hα	Unknown	1.2 - 1.6	1.2 - 1.8	1.0 - 1.9
[OIII] λ 5007/Hα	$\lesssim$0.15	$\lesssim$0.1	$\lesssim$0.2	$\lesssim$0.3

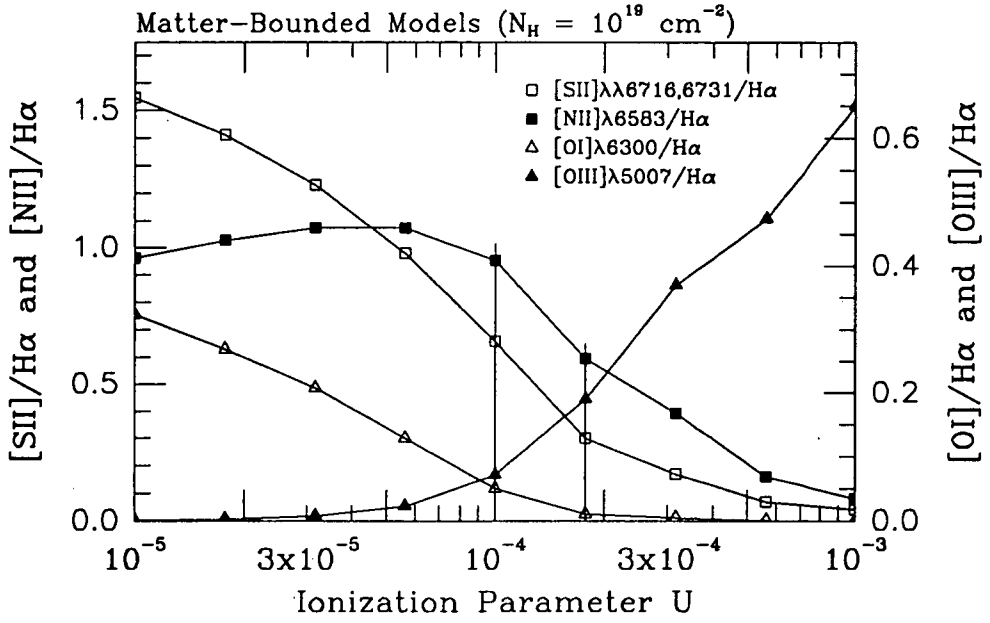

Figure 1: Results of matter bounded photoionization models having $N_H = 10^{19}$ cm^{-2}. The solid vertical lines delimit the ionization parameter range estimated to exist over 500 pc $\lesssim |z| \lesssim$ 1kpc, for $\phi \simeq 0.003$.

REFERENCES:

(1) Dettmar, R.J. 1990, A&A, 232, L15

(2) Rand, R.J., Kulkarni, S.R., & Hester, J.J. 1990, ApJ, 352, L1

(3) Dettmar, R.J., 1992, Fund. of Cosmic Physics, in Press

(4) Dettmar, R.J. & Schultz, 1992, A&A, 254, L25

(5) Sokolowski, J. 1992, in Massive Stars: Their Lives in the Interstellar Medium, in Press

(6) Ferland, G.J. 1991, OSU Internal Report 91-01

(7) Jenkins, E.B. 1987, Interstellar Processes, ed. D.J. Hollenbach and H.A. Thronson, 533

The Disk-Halo Interface in Edge-on Spirals

René Walterbos, New Mexico State University, Las Cruces

Robert Braun, Netherlands Foundation for Radio Astronomy, Dwingeloo

Colin Norman, Space Telescope Science Institute and John's Hopkins University, Baltimore

We are studying the disk-halo interface in several edge-on spiral galaxies through extensive imagery in Hα and other emission lines from Diffuse Ionized Gas (DIG), also referred to as the Warm Ionized Medium (WIM). In addition, for the nearby Sc galaxy NGC4631 we have obtained X-ray observations with ROSAT, to map the distribution of hot (10^{6-7}K) gas in the disk and halo. Here we present initial results for two late-type spirals, NGC4244 and NGC4631.

It has been realized for some time now that the WIM in the Galaxy is an important component of the interstellar medium, with a volume filling factor $\sim$ 20% and a large vertical scale height, $\sim$ 1 kpc (Kulkarni and Heiles 1988, and Reynolds 1991). The widespread nature of the WIM is also confirmed in observations of the spiral M31, where we detect the WIM all along the spiral arms (Walterbos and Braun 1992). The large vertical scale height and the high spatial resolution attainable in the optical make this gas an ideal probe of the disk-halo interface. Energy and mass exchange between galactic disks and halos, due to the combined effects of supernovae and stellar winds from massive stars, either in the form of galactic fountains (Bregman 1980) or chimneys (Norman and Ikeuchi 1989) is thought to be an important process. Surprisingly few concrete data exist so far, however, to determine how common this process is, and under which conditions it occurs. Rand *et al.* (1990) and Dettmar (1990) mapped the WIM in the edge-on spiral NGC891 and found a thick Hα emitting gas layer, with structures reminiscent of those predicted in the chimney model from Norman and Ikeuchi. Walterbos (1991) did not find a similarly thick disk in NGC4244, an Sc galaxy with a much lower star formation rate than NGC891.

We have obtained new, deep Hα imagery of NGC4244 and NGC4631 with the 36" at KPNO in the spring of 1991 and 1992. The new data confirm the lack of a thick WIM layer in NGC4244. The z-distribution of the Hα emission has an exponential scale height of 200 pc, similar to that of the stellar light (Van der Kruit 1979). There is no evidence for a more extended distribution of WIM superposed on that. In NGC4631, on the other hand, the scale height of the ionized gas distribution is of order 1 kpc. The irregular shape of this galaxy and its inclination, 85°, make it difficult to directly interpret this number as an actual vertical scale height. Nevertheless, there is widespread diffuse gas, with various Hα kpc-scale filaments or chimneys, in the central region (Fig. 1). [SII] images of this galaxy show the typical increase in [SII] over Hα intensity ratio for the DIG above the plane with respect to the discreet HII regions. A full report of the results for these two galaxies will be presented elsewhere.

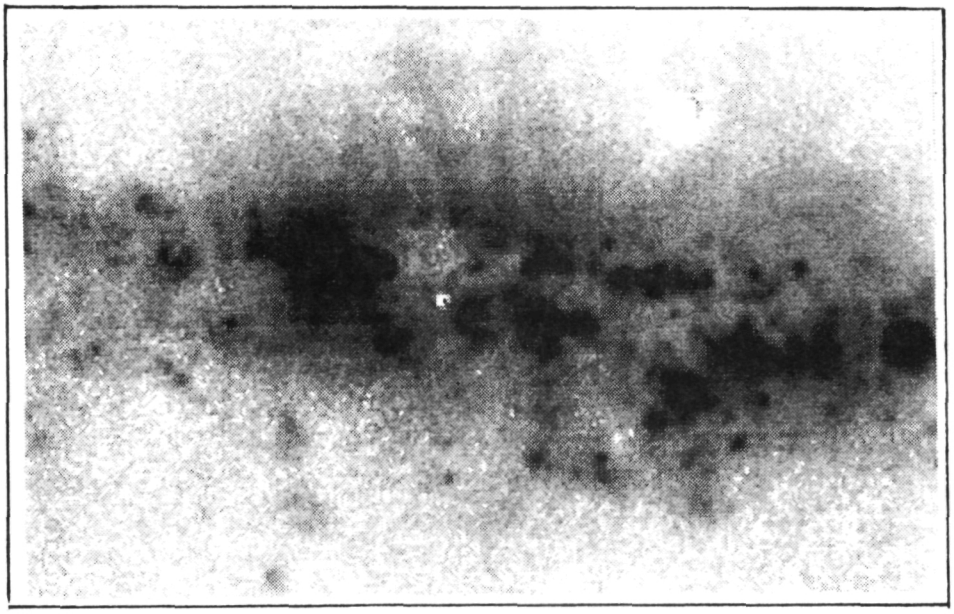

Fig. 1. The distribution of Hα emission in the central 6.9×4.3 kpc^2 region of NGC4631.

With its vigorous star formation activity, and its large radio halo (Hummel and Dettmar 1990) NGC4631 is one of the most likely nearby galaxies to show a halo of hot, X-ray emitting gas. We obtained deep ROSAT images of this galaxy and reproduce an initial image (based on a part of the total exposure) in Fig. 2. The X-ray emission from the disk of spiral galaxies is mostly contributed by (massive) binary systems. The strong point source in the disk of NGC4631 was already apparent in Einstein data (Fabbiano and Trinchieri 1987). The concentration of X-ray emission in the East part of the disk, however, may well coincide with the giant HI shell discussed by Rand *et al.* (these proceedings). Emission above the disk is not likely due to discrete sources. There appear to be three filaments perpendicular to the disk suggestive of outflow of hot gas from the disk into the halo. At lower levels there is also a strong suggestion in the data for a more extended diffuse X-ray halo, roughly of similar size as the optical disk of the galaxy, providing direct evidence for the elusive hot component of the ISM.

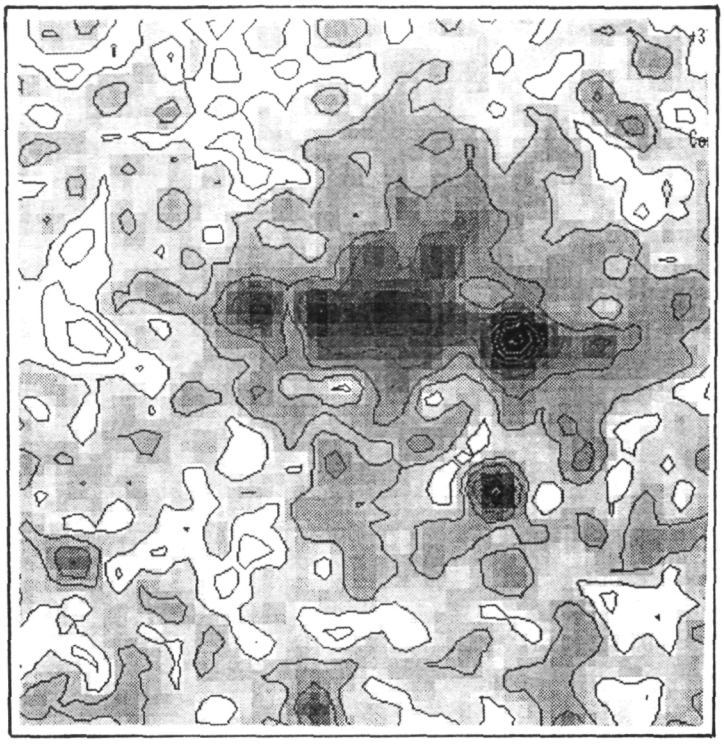

Fig. 2. ROSAT PSPC image of NGC4631, smoothed to a resolution of about 45″. The frame measures about 15′ (or 32 kpc) on the side. The exposure time was about 20,000 sec.

Acknowledgements. The ROSAT observations of NGC4631 are being analyzed with support from NASA, through grant NAG 5-1924 to NMSU. RAMW acknowledges support from NASA through grant HF-1010.01-90A, awarded by the Space Telescope Science Institute, which is operated by the AURA, for NASA under contract NAS5-25555, during the initial states of this project.

References

Bregman, J.N.: 1989, ApJ 236, 577.
Dettmar, R.-J.: 1990, A&AL 232, L15.
Fabbiano, G., Trinchieri, G.: 1987, ApJ 315, 46.
Hummel, E., Dettmar, R.-J.: 1990, A&A 236, 33.
Kulkarni, S.R., Heiles, C.: 1988, in *Galactic and Extragalactic Radio Astronomy*, eds. G. Verschuur and K.I. Kellermann, 2nd Ed., Springer Verlag, p95.
Rand, R.J., Kulkarni, S.R., Hester, J.J.: 1990, ApJL 352, L1.
Norman, C.A., Ikeuchi, S.: 1989, ApJ 345, 372
Reynolds, R.J.: 1991, in The Interstellar Disk-Halo Connection, IAU Symp. 144, ed. J.B.G.M. Bloemen, (Dordrecht: Kluwer), p 67
Van der Kruit, P.C.: 1979, A&AS 38, 15.
Walterbos, R.A.M.: 1991, in The Interstellar Disk-Halo Connection, IAU Symp. 144, ed. J.B.G.M. Bloemen, (Dordrecht: Kluwer), p 223
Walterbos, R.A.M., Braun, R.: 1992a, A&AS 92, 625

N93-26866

Numerical Modeling of the Interstellar Medium in Galactic Disks

A. Rosen, J.N. Bregman (U. Michigan), M.L. Norman (NCSA, U. Illinois)

We have been developing detailed hydrodynamic models of the global interstellar medium in the hope of understanding the mass and volume occupied by various phases, as well as their structure and kinematics. In our model, the gas is modeled by one fluid while representative Pop I stars are modeled by a second fluid. The two fluids are coupled in that the gas forms into stars at a rate given by a Schmidt law while stellar mass loss returns matter into the gas phase (on a time scale of 100 Myr). Also, the stars heat the gas through stellar winds and the gas cools through optically thin radiation. The time behavior of these two fluids is studied in two spatial dimensions with the Eulerian finite difference numerical hydrodynamic code *Zeus*. The two spatial dimensions are along the plane of a disk (x, total length of 2 kpc) and perpendicular to the disk (z, total height of $\pm$ 15 kpc) and a galactic gravitational field in the z direction, typical of that at the solar circle, is imposed upon the simulation; self-gravity and rotation are absent. For the boundary conditions, outflow is permitted at the top and bottom of the grid ($z = \pm$ 15 kpc) while periodic boundary conditions are imposed upon left and right sides of the grid. As initial conditions, we assumed a gaseous distribution like that seen for the HI by Dickey and Lockman (1990), although the results are insensitive to the initial conditions.

We have run simulations in which the heating due to stars, parameterized as a stellar wind velocity, a, is varied from low (a = 150 km/s), to intermediate (a = 300 km/s), to high (a = 600 km/s). Since the intermediate case is roughly equivalent to the Galactic energy injection rate from supernovae, this summary will concentrate on results from this simulation. Initially hot gas (T > 100,000 K) is buoyant and rises up before cooling into neutral material. Eventually, the cold gas (T < 4000 K) becomes filamentary and occupies a small volume compared to the warm (4000 K < T < 100,000 K) and hot gas (see figure 1). This filamentary structure of cold gas is elongated parallel to gravitational acceleration. Within a few hundred parsecs of the midplane (within 30–50 zones), the volume filling factors for the cold, warm, and hot gas are 10%, 20% and 70%, respectively. Near a height of 1 kpc (100 zones from the midplane), the warm gas dominates (at 70–80% of the volume) at the expense of the hot gas, and hot gas completely fills the regions at larger z. The scale heights for the cold, warm, and hot gas are 65, 600, and 300 pc, respectively. Note the density vs. height figure shows a second (low-density) component of hot gas above 1 kpc.

This work was completed with the support of NASA Grant NAGW-2135.

Reference

Dickey, J.M., & Lockman, F.J. 1990, ARA&A, 28, 215

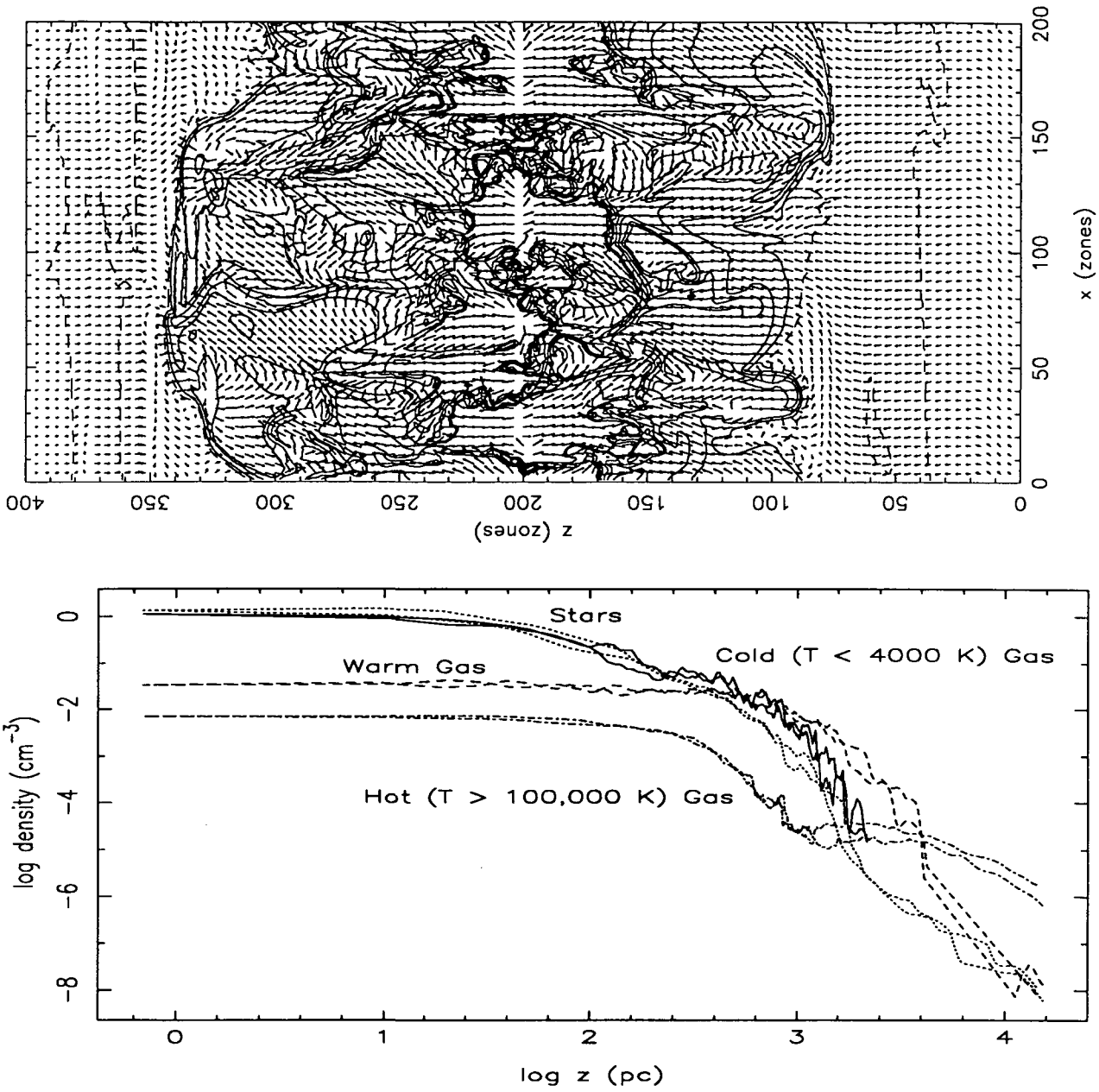

Figure 1. Top plot shows density contours, evenly spaced in log density, and momentum vectors for the intermediate energy injection rate simulation. The middle 200 rows are linearly scaled up to $\pm$ 1 kpc, while the outer 200 rows are geometrically scaled from $\pm$ 1–15 kpc. On the bottom is an averaged density distribution of the three phases of gas and the stars. The gas distributions are averages at five different times as well as at a particular height.

THE VERTICAL DISK STRUCTURE OF THE EDGE-ON SPIRAL GALAXY NGC 3079

S. Veilleux[1], J. Bland-Hawthorn[2], G. Cecil[3], & R. B. Tully[1]

[1] Institute for Astronomy, University of Hawaii, Honolulu, HI 96822
[2] Dept. of Space Physics & Astronomy, Rice University, Houston, TX 77251-1892
[3] Dept. of Physics & Astronomy, University of North Carolina, Chapel Hill, NC 27599-3255

§1. Introduction

NGC 3079 is an edge-on SB(s)c galaxy at a redshift of 1225 km s^{-1} relative to the Local Group. Duric & Seaquist (1988) found a spectacular "figure-eight" radio structure aligned along the minor axis of the galaxy, centered on the nucleus, and extending 3 kpc above and below the plane. The geometry of this structure and the evidence of unusually high nuclear gas velocities (e.g., Heckman, Armus, & Miley 1990; Filippenko & Sargent 1992) suggest that a wind-type outflow from the nucleus is taking place (see also Veilleux et al. 1990). The disk of NGC 3079 is also remarkable: it is extremely rich in H II regions and is the only unambiguous example of a galaxy outside M31 and our own Galaxy to exhibit "Heiles-like" shells (Irwin & Seaquist 1990). Heckman, Armus, & Miley (1980) also identified a nebulosity with a ragged X-shaped morphology formed by a system of lumpy filaments with individual lengths of 3 – 5 kpc. They suggest that this material is ambient halo gas entrained into the boundary layers of the nuclear outflow (see also Hester et al. 1990)

The complex structure of the line emission in NGC 3079 makes this object an ideal target for an imaging spectroscopic study. The present paper reports the preliminary results of such a study.

§2. Observations and Reduction

The Hawaii Imaging Fabry-Perot Interferometer (HIFI; Bland & Tully 1989) was used at the Cassegrain focus of the CFHT 3.6-meter telescope to produce a data cube of this galaxy covering Hα + [N II] $\lambda\lambda$6548, 6583 at a resolution of about 65 km s^{-1}. Order separating filters with flat-topped transmission profiles centered at 6555 Å and 6585 Å and 54 Å FWHM bandpass passed only one etalon order, so true emission line profiles could be synthesized. The resulting data cube is made of 137 images (velocity slices) and represents a total integration time of about 19 hours. These data were parametrized using Gaussian fitting. Spatial smoothing was used to improve the sensitivity to the fainter features. Overall, reliable fits were made to 42 000 spectra.

§3. Results

The present data combine morphological and kinematic information which are of comparable sensitivity and velocity resolution as the radio data of Irwin & Seaquist (1990, 1991). A direct comparison of their data with ours can therefore be made. First, relatively strong Hα and [N II] line emission off the plane of the disk was detected at the south-eastern optical edge of the galaxy, confirming the existence of a warp in the disk of NGC 3079. We also looked for any optical counterparts to the radio shells and filaments identified by Irwin & Seaquist (1990). Possible correspondence between Hα and [N II] features and the *base* of the H I shells B, C, and D and filaments 5, 6, 9, 10, 12, 13, 14, and 15 were found. A few of these features may coincide in position and velocity with the X-shaped structure observed by Heckman, Armus, & Miley (1990). Individual spectra along this structure indicate that [N II]/Hα is not typical of H II regions, reaching values larger than unity in some regions (especially in the north-east quadrant). The *disk* line ratio map also shows that [N II]/Hα has a tendency to decrease with galactocentric radius in the brighter H II regions and to be higher outside of

these H II regions ($\sim$ 0.4) than inside of them ($\sim$ 0.2).

The velocity field derived from the present data is similar but far from identical to the mean velocity field of Irwin & Seaquist (1991). The differences are attributed to extinction effects in the optical. The optical velocity curve is fairly typical of an Sc galaxy, being characterized by a steep rise at the center and a plateau at larger radii. The total velocity amplitude is $\sim$ 400 km s^{-1}. The gas in the shells and filaments appears to follow normal galactic rotation. The line widths in the disk are of order 130 km s^{-1} (FWHM), with a slight tendency to increase towards the center of the galaxy. In some cases, the line widths in the shells and filaments are larger than in the surrounding gas.

§4. Discussion

A number of recent studies have investigated the effects of supernovae explosions on the ISM of spiral galaxies (e.g., Mac Low, McCray, & Norman 1989; Norman & Ikeuchi 1989; Heiles 1990; Koo & McKee 1992a,b, and references therein). The presence of a large superbubble at the center of NGC 3079 and the large number of H I shells in the disk of this galaxy make it a good laboratory to compare the predictions of these models with the observations.

The results of our preliminary analysis indicate that turbulence or shell expansion is causing line broadening in some of the optical filaments. Irwin & Seaquist (1990) arrived at a similar result from their radio data and concluded that the energy deposited in the shells of NGC 3079 is somewhat higher than for shells in the Galaxy. Another important question is the origin of the spatial variations of [N II]/Hα. Clearly, a higher heating rate per ionization is required in the high-[N II]/Hα gas. Photoionization by a diffuse radiation field (Mathis 1986) *cannot* explain [N II]/Hα ratios larger than $\sim$ 0.6. The most likely sources of extra heating are (1) photoionization by the hard ionizing continuum of the active nucleus, (2) photoionization by the hard continuum of the coronal gas ejected into the lower halo by the supernova explosions (e.g. Donahue & Voit 1991; Slavin, Shull, & Begelman 1992), (3) the interaction of the line-emitting gas with high-energy relativistic electrons (e.g., Ferland & Mushotzky 1984), and (4) shocks. Processes (1), (3), and (4) are all likely to be taking place in the central superbubble while the large [N II]/Hα in the disk filaments are likely to be due to processes (2) and (4). The possibility that the high [N II]/Hα ratio is due to a higher metal content cannot yet be excluded (especially in the filaments and the brighter H II regions near the nucleus).

References

Donahue, M., & Voit, G. M. 1991, ApJ, 381, 361.
Duric, N. & Seaquist, E. R. 1988, ApJ, 326, 574.
Ferland, G. J., & Mushotzky, R. F. 1984, ApJ, 286, 42.
Filippenko, A. V., & Sargent, W. L. W. 1992, AJ, 103, 28.
Heckman, T. M., Armus, L., & Miley, G. K. 1990, ApJS, 74, 833.
Heiles C. 1990, ApJ, 354, 483.
Hester, J. J, Kulkarni, S. R., Rand, R. J., & Deich, W. T. 1990, in The Interstellar Disk-Halo Connection in Galaxies, IAU Symposium No. 144, Posters, ed. H. Bloemen (Leiden: Leiden Obs.), p. 51.
Irwin, J. A., & Seaquist, E. R. 1990, ApJ, 353, 469.
_____. 1991, ApJ, 371, 111.
Koo, B.-C., & McKee, C. F. 1992a, ApJ, 388, 93.
_____. 1992b, ApJ, 388, 103.
Mac Low, M.-M., McCray, R., & Norman, M. L. 1989, ApJ, 337, 141.
Mathis, J. S., 1986, ApJ, 301, 423.
Norman, C. A., Ikeuchi, S. 1989, ApJ, 345, 372.
Slavin, J. D., Shull, J. M., & Begelman, M. C. 1992, ApJ, submitted.
Veilleux, S., Bland-Hawthorn, J., Tully, R. B., & Cecil, G. 1990, Bull. A. A. S., 22, 1315.

The Ring Around SN1987A

Crystal L. Martin
Department of Astronomy, University of Arizona
and
David Arnett
Departments of Physics and Astronomy, University of Arizona

MOTIVATION

Stars in the 9-40 $M_\odot$ range play a prominent role in the hydrodynamical and chemical evolution of galaxies. Their stellar winds and supernova explosions are believed to create the hot component of the interstellar medium (ISM). In some galactic disks, the kiloparsec sized superbubbles formed around clusters of massive stars may blow out of the disk plane and release hot, metal enriched gas into the galaxy's halo. Additionally, the expanding shock front of a superbubble in the disk may trigger additional star formation. Furthermore, similar processes probably drive the galactic winds associated with starburst nuclei that enrich the intracluster and intergalactic mediums.

Nonetheless, the explosion of a blue supergiant in the Large Magellanic Cloud (LMC), SN1987A, illuminated the incompleteness of our understanding of massive stars. Evolutionary models of massive stars do not synthesize the observed supergiant populations in either the Milky Way or LMC. Our modeling of the formation of SN1987A's ring will improve our knowledge of both the post-main-sequence evolution of massive stars and their coupling to the ISM in galaxies.

BACKGROUND

It is now generally agreed that SN1987A's progenitor was a blue supergiant (BSG) (Arnett *et al.* 1989) of spectral type B3 Ia, and there is considerable evidence that this star passed through a red supergiant (RSG) stage earlier in its life. Theoretical tracks for low metallicity $20M_\odot$ stars (e.g. Arnett 1991) suggest the progenitor passed through two RSG stages and one BSG stage prior to the final BSG phase. Observationally, the RSG phase is inferred from the narrow UV emission lines seen in spectra of SN1987A taken after May 24, 1987 (Fransson 1989). These line widths and strengths were shown to be consistent with an origin in a low density, (1-4) x 10^4 cm^{-3}, photoionized gas having CNO abundance ratios suggestive of a nucleosynthetic origin via the CNO cycle (Lundqvist & Fransson 1991). Hence, the emerging picture suggests that ashes from the nuclear burning in the interior were mixed into the progenitor's outer layers during a RSG phase and expelled in a slow stellar wind. During the subsequent BSG stage, a faster stellar wind from the hotter, smaller star collided with this circumstellar material. The resulting strong shock front swept up a dense shell (relative to the ISM) of ambient RSG wind which was subsequently photoionized by the UV/soft x-ray burst of the supernova explosion. A shell expansion rate of 15 km/s was derived by Lundqvist and Fransson (1991) from the UV emission lines.

High resolution imaging of the supernova remnant (SNR) has further constrained the morphology of this circumstellar structure. The image taken with ESA's FOC on HST through a narrow [OIII] λ 5007 filter (Panagia *et al.* 1991) reveals a clumpy ellipse of emission with a major axis a bit more than one light year across surrounding the SNR. The radial velocity gradient along the minor axis of the emission strongly suggests that the ellipse on the plane of the sky is actually a ring tilted relative to our line of sight rather than a limb brightened shell (Crotts 1991; Meikle *et al.* 1991). Crotts and Heathcote (1991) derived a ring expansion speed of 10.3 km/s from high-resolution spectra of the nebulosity. Luo and McCray (1991) have shown that the interacting winds scenario can produce an hourglass shaped circumstellar shell with a ring at the waist if the RSG wind has an equator to pole density contrast. Although the cause of such a wind asymmetry is unclear, a low mass secondary in a common envelope phase with the RSG can cause a highly asymmetrical mass-loss profile (Soker, 1992). A binary companion to the progenitor is also one possible cause for the observed asymmetric envelope expansion (Chevalier & Soker 1989).

CALCULATION

We use the PROMETHEUS code (Fryxell *et al.* 1989) to calculate the hydrodynamical interaction of a BSG wind overtaking an asymmetric RSG wind. We calculate one quadrant of a 50 x 100 grid oriented perpendicular to the plane of the ring with an origin at the progenitor star. This calculation is a step toward a 3D calculation which will investigate the stability of the ring. Only the last BSG and RSG phases of the progenitor's wind are modeled since the termination shocks of the winds blown during any previous blue loops and on the main sequence should be at much larger distances than the observed ring. The RSG wind asymmetry is described by a latitudinal density contrast in the RSG wind. We change the inner boundary condition from a RSG wind to a BSG wind abruptly since the acceleration mechanisms for the RSG and BSG winds are believed to be quite different and the stellar models indicate the progenitor evolves from the red to the blue on a time scale that is short in comparison to the time spent at either envelope solution. By choosing a RSG wind density toward the upper end of the estimated range and a BSG wind velocity toward the lower end of the observed range, we can place an upper limit on the duration of the final BSG stage.

RESULTS

The density contours and velocity vectors in Figure 1 illustrate the ring and constricted bubble resulting from an adiabatic calculation of a weak BSG wind crashing into an asymmetric, dense RSG wind with a 10:1 equator to pole density contrast. The ring has reached a radius of 1.85 lt. yr. when the progenitor has been in the final BSG stage for τ_{BSG} = 20, 000 yr. This distance is a factor of three larger than the observed position of the ring, and τ_{BSG} is only 80% of the value predicted by the stellar model of Arnett (1991). Hence we have a discrepancy between the interacting winds model for the ring and the stellar model. We are presently repeating the calculation with the inclusion of additional microphysics. The addition of radiative cooling and ionization losses will work to slow the ring down and increase its density. The results of this calculation will reveal whether or not there really is any discrepancy between the ring formation model and the stellar evolutionary models.

ACKNOWLEDGEMENTS

CLM thanks the University of Arizona's Interdisciplinary Graduate Program and the Universities of Wyoming and Colorado for financial assistance toward attending the Third Teton Summer School.

REFERENCES

Arnett, D. 1991, Ap.J. **383**, 295.

Arnett, W. D. *et al.* 1989, Annu. Rev. Astron. Astrophys. **27**, 629.

Chevalier, R. A. and Soker, N. 1989, Ap.J. **341**, 867.

Crotts, A. P. S. and Heathcote, S. R. 1991, Nature **350**, 685.

Fransson, C. *et al.* 1989, Ap.J. **336**, 429.

Fryxell, B. A. *et al.* 1989, *in Numerical Methods in Astrophysics*, P. R. Woodward, ed., (Academic Press: New York).

Lundqvist, P. and Fransson, C. 1991, Ap.J. **380**, 575.

Luo, D. and McCray, R. 1991, Ap.J. **379**, 659.

Meikle, W. P. S. *et al.* 1991, in *in Proc. ESO/EIPC Workshop on Supernova 1987A and Other Supernovae* (Marciana Marina, Elba, Italy, 1990 September 17 - 22), ed. I. J. Danziger & K. Kjär (Garching: ESO), 595.

Panagia, N. *et al.* 1991, Ap.J. **380**, L23.

Soker, N. 1992, Ap.J. **386**, 190.

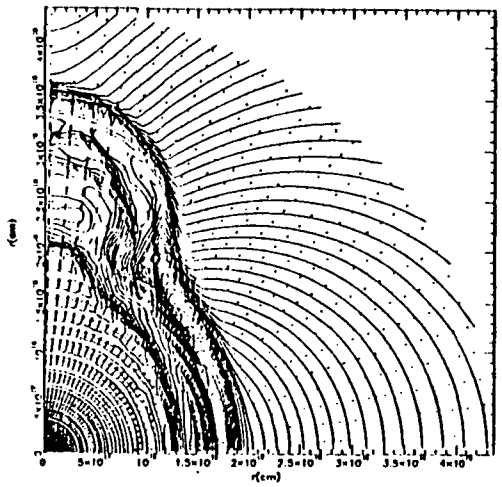

Figure 1

A 'Halo' and a 'Blow-Out' in NGC 253

C.L.Carilli, M.A. Holdaway (NRAO), and P.T.P. Ho (CfA)

We present the discovery of a 'synchrotron halo' in NGC 253. NGC 253 is an inclined, dusty, barred Sc galaxy in the Sculptor Group. It is also one of the prototype nuclear starburst galaxies (Rieke *et al.* 1980, *Ap.J.*238, 24). VLA observations at 327 MHz and 1.4 GHz (Fig. 1) have revealed a synchrotron emitting 'halo' extending 9 kpc above and below the plane of NGC 253 (assuming a distance of 4 Mpc). The spectral index for the radio emission steepens from -0.7 in the disk to -1.0 in the halo. The fractional polarization at 1.4 GHz increases from $\leq$ 2% in the disk up to 20% in the halo, and the magnetic field vectors project parallel to the plane over most of the halo.

The radio continuum images reveal structures in the disk-halo interface which suggest interaction between the disk and halo. The most striking feature is a 'spur' originating at the northeast end of the bar and extending 5 kpc perpendicular to the disk. The spectral index gradient along the spur implies outflow along the feature, with a velocity $\geq$ 53 km sec^{-1} (Fig. 2). Shearing outflow along the spur is also suggested by the magnetic field vectors, which project parallel to its length. Spectral line observations of neutral and ionized hydrogen show excessive 'activity' at the northeast end of the bar (*i.e.* at the base of the spur), with departures from circular motions $\geq$ 30 km sec^{-1} (Puche *et al.* 1991, *A.J.*, 101, 456, Pence 1981, *Ap.J.* 247, 473). And radio continuum and Hα imaging show very active star formation in this region (Fig. 1 and Waller *et al.* 1988, *A.J.* 95, 1057).

Overall, observations suggest that there is outflow from the disk into the halo of NGC 253 along the spur, and that this outflow is driven by the active star formation at the north-east end of the bar. The total kinetic energy in the outflow is $\geq 2\text{x}10^{52} \times (\text{n}_e/10^{-3}\ \text{cm}^{-3})$ ergs, or roughly the energy output of 20 supernovae. The non-thermal radio continuum luminosity from the base of the spur is $\geq$ 30 times that of Cas A.

Figure 1: An optical image of NGC 253 reproduced from the Hubble atlas of galaxies (Sandage and Tammann 1987). The contours are of total intensity from NGC 253 at 0.33 GHz with a resolution of 60″. Contour levels are: -3, 3, 6, 9, 12, 15, 24, 36, 48, 60, 100, 400, 1600, and 3200 mJy/beam. The outer-most contour is for an image convolved to 120″ resolution. The level for this contour is 24 mJy/beam.

Figure 2: The maximum radiative lifetimes for the relativistic electrons as a function of distance from the plane of NGC 253 along the spur. Spectral ages were derived from data at 0.33 and 1.4 GHz, assuming energy losses through synchrotron and inverse Compton radiation (Van der Laan and Perola 1969, *A.A.*, 3, 468, Carilli *et al.* 1991, *Ap.J.*, 383, 554). The slope implies an outflow velocity of 53 $\pm$ 18 km sec^{-1}.

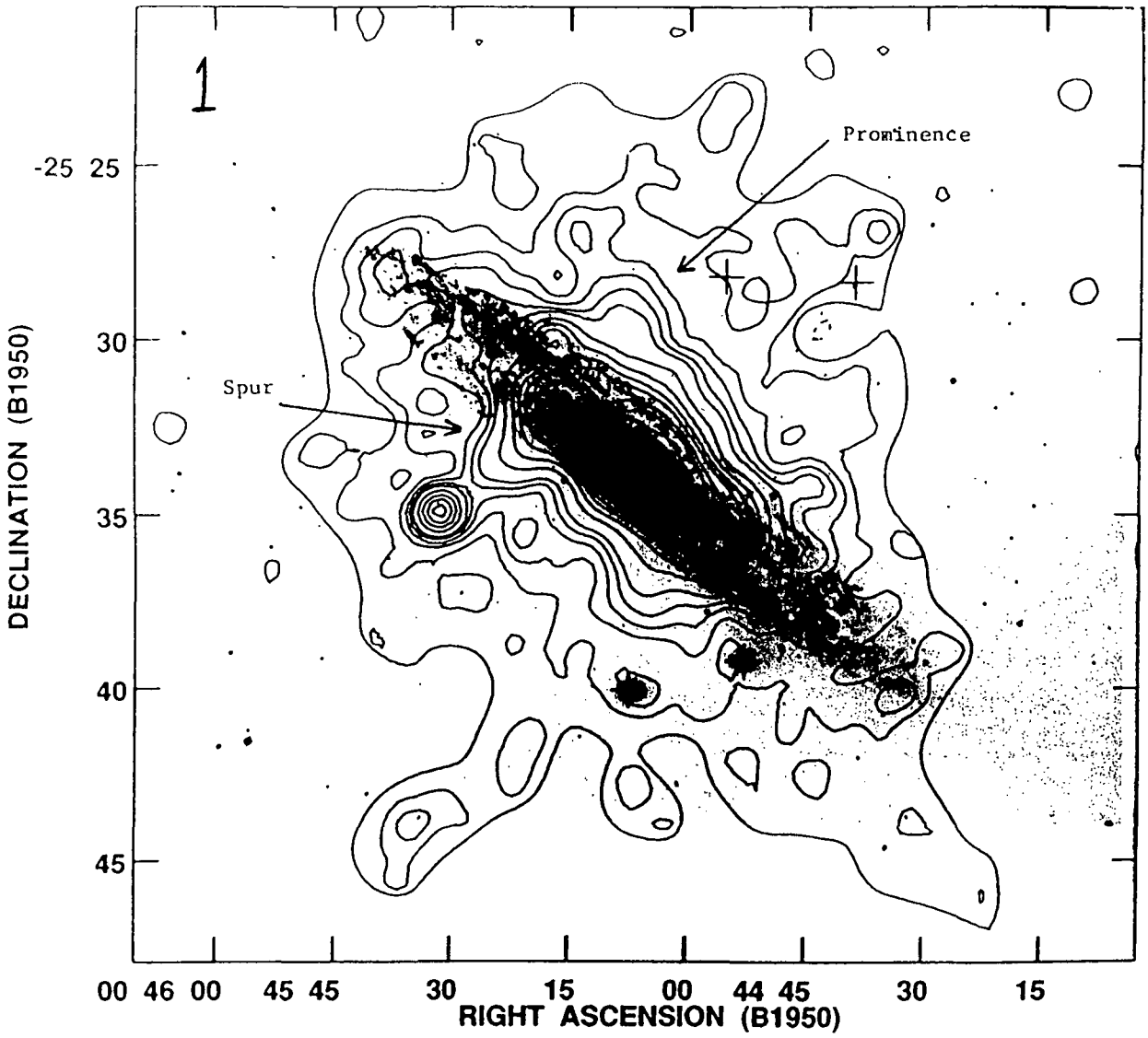
1
Prominence
Spur
-25 25
30
35
40
45
DECLINATION (B1950)
00 46 00
45 45
30
15
00
44 45
30
15
RIGHT ASCENSION (B1950)

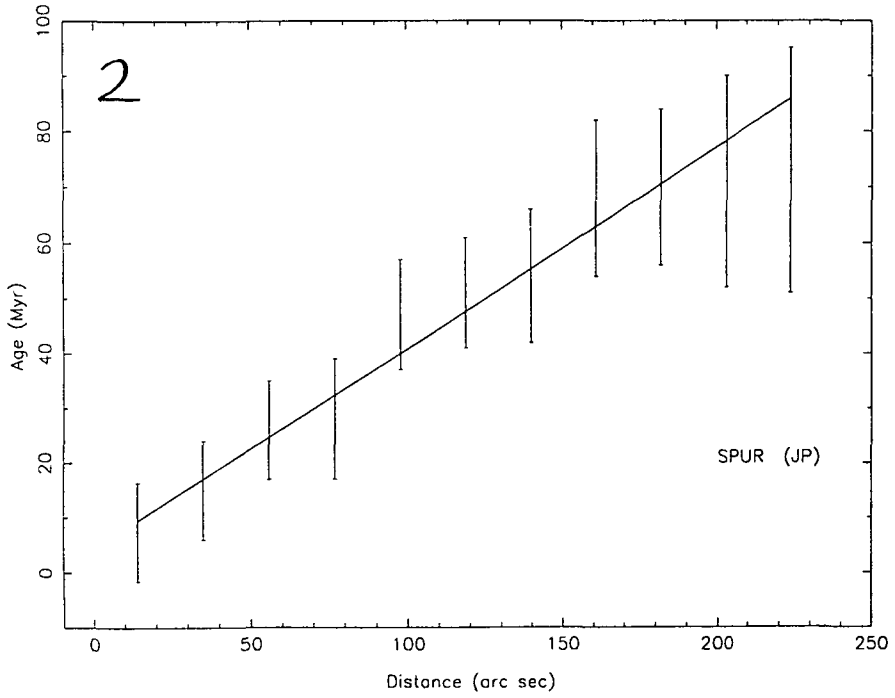
2
Age (Myr)
0
20
40
60
80
100
0
50
100
150
200
250
Distance (arc sec)
SPUR (JP)

Infrared Fine-Structure Line Diagnostics of Shrouded Active Galactic Nuclei

G. M. Voit (Caltech)

Far-infrared spectroscopy of celestial objects will improve dramatically in the coming decade, allowing astronomers to use fine-structure line emission to probe photoionized regions obscured in the optical band by thick clouds of dust. The ultraluminous far-IR galaxies revealed by IRAS, quasar-like in luminosity but smothered in molecular gas, probably conceal either immense starbursts or luminous active nuclei. In both scenarios, these objects ought to produce copious infrared fine-structure emission with several lines comparable to Hβ in luminosity. This paper shows how these lines, if detected, can be used to determine the electron densities and far-IR obscurations of shrouded photoionized regions and to constrain the shape and ionization parameter of the ionizing spectra. The presence of [Ne V] emission in particular will distinguish shrouded AGNs from shrouded starbursts. Since all active galaxies photoionize at least some surrounding material, these diagnostics can also be applied to active galaxies in general and will aid in studying how an active nucleus interacts with the interstellar medium of its host galaxy.

For more details, see the November 10, 1992 edition of the *Astrophysical Journal.*

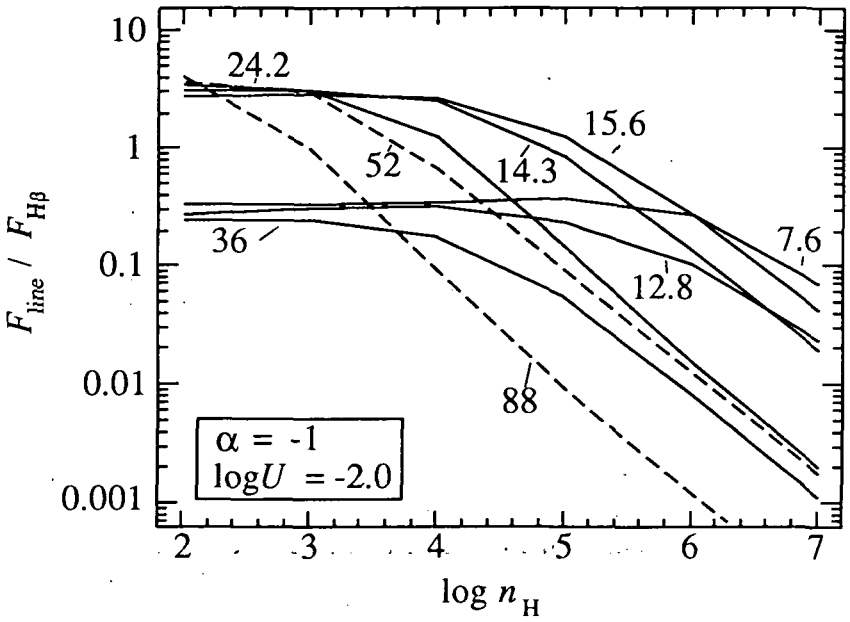

The strongest IR fine-structure lines from a photoionized region radiate as least as much power as the Hβ line, unless the electron density is very high. This figure illustrates the line fluxes, relative to Hβ, for selected fine-structure transitions of oxygen and neon in an AGN-irradiated cloud of ionization parameter log U = -2. Labels on the curves give the wavelength of each transition in microns: [O III] 52 & 88, [Ne II] 12.8, [Ne III] 15.6 & 36.0, [Ne V] 14.3 & 24.2, [Ne VI] 7.6. Note that the critical densities for quenching the neon lines are large (log n ~ 5-6).

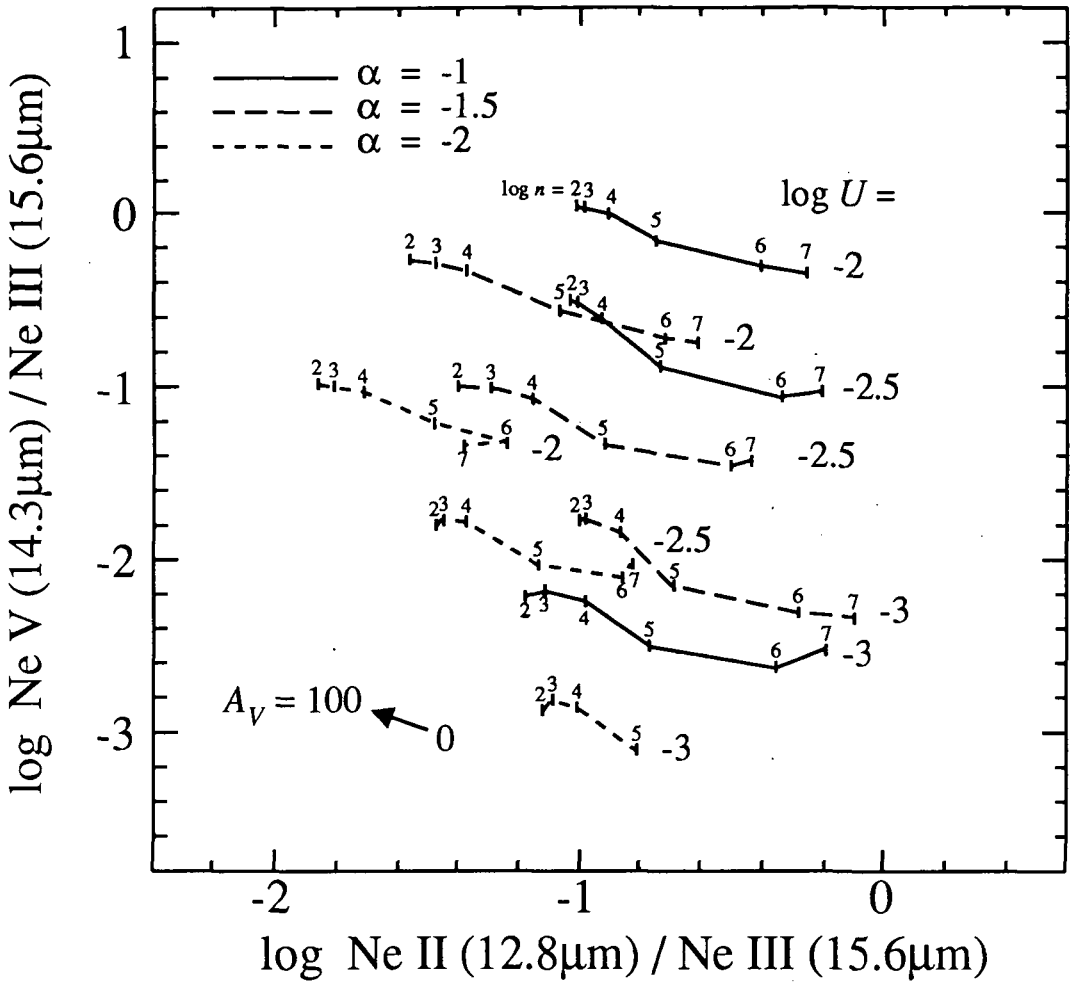

The [Ne II] 12.8μm, [Ne III] 15.6μm, and [Ne V] 14.3μm lines are all reddened by the about the same amount in the ISM and have critical densities that differ by an order of magnitude or less. Thus, they form an excellent ionization-diagnostic trio that probes a wide range of ionization parameters and photon energies. The neon-line plane above shows how these line ratios respond to different spectral shapes (power-laws with a ranging from -1 to -2) and ionization parameters (log U ranging from -2 to -3) over a range of hydrogen densities (log n ranging from 2 to 7). Reddening of 100 V magnitudes produces the shift indicated by the arrow. The [Ne V]/[Ne III] ratio is particularly sensitive to the ionization parameter, and the [Ne II]/[Ne III] ratio is somewhat sensitive to the hardness of the incident spectrum. Stellar H II regions lie far below the pictured portion of the plane, and shocks, with [Ne II]/[Ne III] >> 1, lie far to the right.

THE ABSORPTION AND EMISSION SPECTRUM OF RADIATIVE COOLING GALACTIC FOUNTAIN GAS

ROBERT A. BENJAMIN and PAUL R. SHAPIRO
The University of Texas at Austin

ABSTRACT

We have calculated the time-dependent, nonequilibrium thermal and ionization history of gas cooling radiatively from 10^6 K in a one-dimensional, planar, steady-state flow model of the galactic fountain, including the effects of radiative transfer. Our previous optically thin calculations explored the effects of photoionization on such a flow and demonstrated that self-ionization was sufficient to cause the flow to match the observed galactic halo column densities of C IV, Si IV, and N V and UV emission from C IV and O III] in the constant density (isochoric) limit, which corresponded to cooling regions homogeneous on scales $D \gtrsim 1$ kpc. Our new calculations which take full account of radiative transfer confirm the importance of self-ionization in enabling such a flow to match the data but allow a much larger range for cooling region sizes, i.e. $D_0 \gtrsim 15$ pc. For an initial flow velocity $v_0 \sim 100$ km/s, comparable to the sound speed of a 10^6 K gas, the initial density is found to be $n_{H,0} \sim 2 \times 10^{-2}$ cm^{-3}, in reasonable agreement with other observational estimates, and $D_0 \sim 40$ pc. We also compare predicted Ha fluxes, UV line emission, and broadband X-ray fluxes with observed values. One dimensional numerical hydrodynamical calculations including the effects of radiative cooling are also presented.

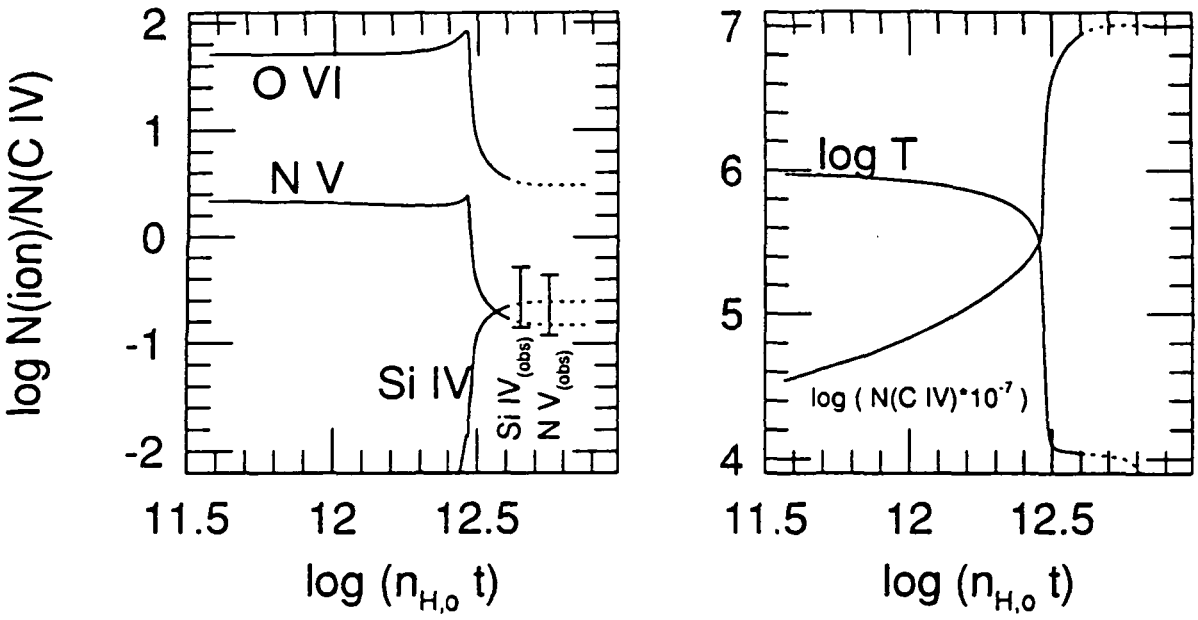

Fig. 1 — (Left panel) Column density ratios N(N V)/N(C IV), N(Si IV)/N(C IV), and N(O VI)/N(C IV) versus ($n_{H,0}t$) (cm^{-3} sec) for a case with D_0=40 pc, v_0=100 km/s, and $n_{H,0}$=1.6x10^{-2} cm^{-3}. Evolution is stopped at the 10^4 K temperature "plateau" stage, when the cooling time becomes much longer than a sound crossing time. Dotted line indicates further evolution if the pressure in this stage remains fixed at the value of the internal pressure of the cooling region at the end of the isochoric, rapid cooling phase. The observed range for the column density ratios is indicated by vertical bars. (Right panel) Plot of temperature and log (10^{-7}N(C IV)) for the same case.

Removing Malmquist Bias from Linear Regressions

Frances Verter
NASA Goddard Space Flight Center

Malmquist bias is present in all astronomical surveys where sources are observed above an apparent brightness threshold (*e.g.,* Malmquist 1920; Tammann 1987). Those sources which can be detected at progressively larger distances are progressively more limited to the intrinsically luminous portion of the true distribution. This bias does not distort any of the measurements, but distorts the sample composition.

We have developed the first treatment to correct for Malmquist bias in linear regressions of astronomical data. This poster presents a demonstration of the corrected linear regression that is computed in four step and illustrated by the two figures below.
Step 1: Create a synthetic *parent sample* of galaxy luminosities in the blue (L_B) and 40-120 μm infrared (L_{FIR}) for which the intrinsic luminosity dispersion and correlation are known.
Step 2: Place the parent galaxies at randomly selected distances and observe them with a detection threshold, thereby creating a *data sample* with Malmquist bias.
Step 3: Compute the linear regression of the data sample both with and without correction for Malmquist bias.
Step 4: Performs steps 2 and 3 repeatedly, generating two distributions of regression results. It will be seen that the peak of the corrected regression fits is much closer to the true functional relationship of the parent population.

In Verter (1992) the corrected regressions are applied to the same galaxy sample that was previously studied by both Lonsdale-Persson and Helou (1987; PH) and by Trinchieri, Fabbiano, and Bandiera (1989; TFB). We show that once Malmquist bias is removed, all the luminosity-luminosity plots agree, to within 2 σ, with a pure increase of galaxy luminosity with galaxy size.

Figure 1 is a parent sample of 200 L_B and L_{FIR} values generated by Monte Carlo simulation. It is assumed that $\log(L_B)$ is described by the Gaussian distribution fit to the Virgo cluster by Sandage, Binggeli, and Tammann (1985), and that $\log(L_{FIR}/L_B)$ is described by the Gaussian distribution fit to UGC galaxies by Bothun, Lonsdale, and Rice (1989). The parent population has a built-in linear correlation between L_B and L_{FIR}.

Figure 2 is one of the possible data samples generated by placing the parent galaxies at various distances and observing them with a surface brightness detection threshold. The observing parameters were chosen to match the previous study by TFB; the galaxy distances are uniformly random between 12 - 60 Mpc, and the detection thresholds are $B_T \leq 13.2$ mag and $f_{FIR} \geq 1.5$ Jy.

The solid line in Figure 1 is the best fit of an ordinary linear regression; it has slope 1.028. The parent population was simulated only once, but the observed data sample was simulated 450 times; the number of detected galaxies was typically between 35 and 55. The dotted line in Figure 2 is the slope of the ordinary linear regression fit to the data samples, $1.386^{+0.081}_{-0.103}$. The dashed line in Figure 2 is the slope of the weighted linear regression fit to the data samples, $1.146^{+0.479}_{-0.296}$. The

lower error bar on the ordinary regressions is too high, by 3 σ, for the fit to be consistent with the linear correlation of the parent sample, whereas the weighted regressions are consistent within 1 σ.

Our method of correcting for Malmquist bias uses a computer program that computes the linear regression with errors in both variables, but instead of the error in each observation we substitute the volume sampled in its measurement. This volume (V_λ) is determined by the distance at which the galaxy surface brightness would fall to the detection threshold. Treating the sampling volume as if it were an error implies that galaxies at larger distances receive less weight in the linear regression, because they are more subject to Malmquist bias. This is illustrated by the sizes of the symbols in Figure 2, which are proportional to $\log(1/V_B V_{FIR})$. Figures 1 and 2 intuitively illustrate why the weighted regression is an improvement: Malmquist bias introduces a disproportionate number of high luminosity pairs into a galaxy sample. An ordinary linear regression is pulled up towards higher slope, but when the observations are weighted the fit favors the more completely sampled galaxies.

Bothun, G. D., Lonsdale, C. J., & Rice, W. 1989, ApJ, 341, 129

Lonsdale Persson, C. J., & Helou, G. 1987, ApJ, 314, 513 (PH)

Malmquist, K. G. 1920, Medd. Lund. Astr. Obs., series 2, no.22

Sandage, A., Binggeli, B., & Tammann, G. A. 1985, AJ, 90, 1759

Tammann, G. A. 1987, in Observational Cosmology, proc. IAU Symp. 124, eds. A. Hewitt, G. Burbidge, & Li Zhi Fang (Dordrecht: D. Reidel) p.151

Trinchieri, G., Fabbiano, G., & Bandiera, R. 1989, ApJ, 342, 759 (TFB)

Verter, F. 1992, ApJ in press

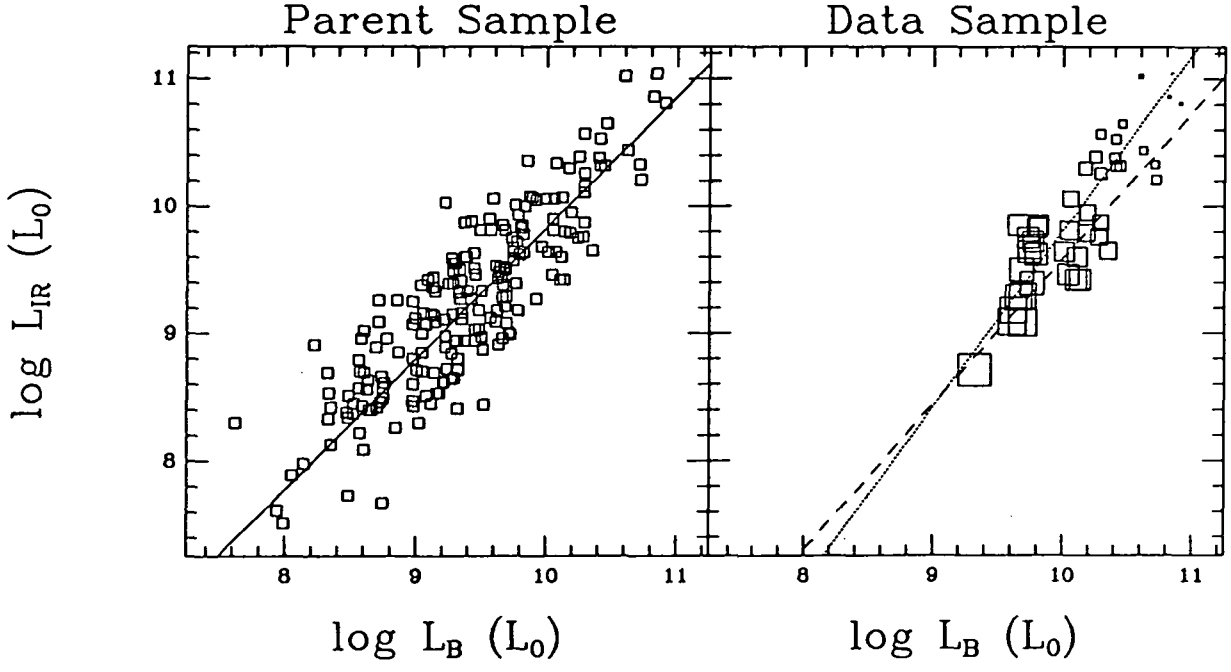

A New "Giant Luminous Arc" Gravitational Lens Associated with a $z = 0.62$ Galaxy Cluster, and the Environments of Distant Radio Galaxies

Mark Dickinson, U. C. Berkeley

In the course of a survey investigating the cluster environments of distant 3CR radio galaxies, I have identified a previously unknown "giant luminous arc" gravitational lens. The lensing cluster is associated with the radio galaxy 3C 220.1 at $z = 0.62$, and is the most distant cluster now known to produce such arcs. I present imaging and spectroscopic observations of the cluster and the arc, and discuss the implications for the cluster mass. At $z > 0.6$ the cluster velocity dispersions implied by such giant arcs may provide an interesting constraint on theories of large scale structure formation.

The parent investigation in which this arc was identified concerns galaxy clusters and radio galaxy environments at $0.35 < z < 0.8$. At the present epoch, powerful FR II radio galaxies tend to be found in environments of poor or average galaxy density [1,2]. In contrast, at the higher redshifts investigated here, richer group and cluster environments are common [3,4]. I present additional data on other clusters from this survey, and discuss its extension to $z > 1$ through a program of near-infrared and optical imaging.

References

1. Longair, M.S., and Seldner, M. (1979), *M.N.R.A.S.*, **189**, 433.
2. Prestage, R.M., and Peacock, J.A. (1988), *M.N.R.A.S.*, *230*, 131.
3. Yates, M.G., Miller, L., & Peacock, J.A. (1989), *M.N.R.A.S.*, **240**, 129.
4. Hill, G.J., & Lilly S.J. (1990), *Ap.J.*, **367**, 1.

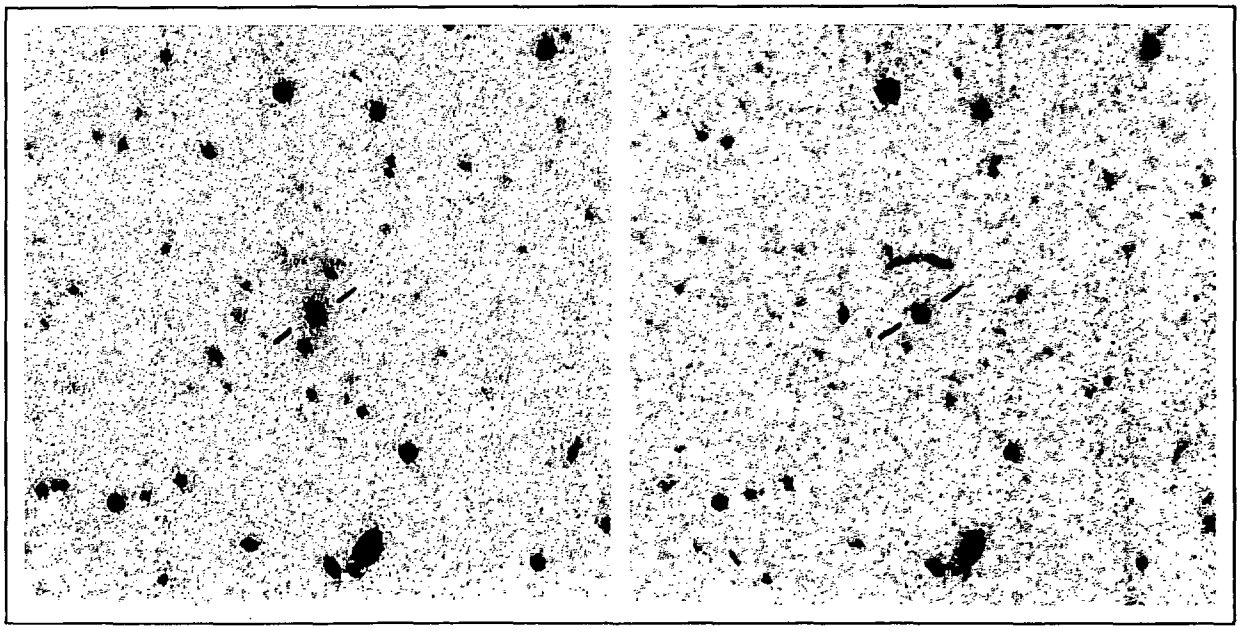

3C 220.1 ($z = 0.62$), its cluster, and the associated gravitational lens arc. The radio galaxy is at the center of curvature of the arc, and is marked. KPNO 4m images: red (left) and blue (right). The field of view is 90 arcseconds on a side.

EMISSION LINE GAS IN EARLY-TYPE GALAXIES: KINEMATICS AND PHYSICAL CONDITIONS

S.E. Deustua (IGPP/LLNL), A.P. Koratkar (STScI) and G. MacAlpine (U. Mich)

Recent studies have found line emission gas in nearby early-type galaxies, but the properties of the emission-line gas in these "normal" galaxies remain enigmatic. In terms of activity in the nucleus, these LINER-like galaxies form an important link between giant H II region galaxies and low-luminosity Seyferts. Despite their large numbers and evolutionary significance, we do not know whether these galaxies form a homogeneous class of objects; nor do we know how the distribution, and kinematics of the line emission gas are affected by the host galaxy's environment or by the properties of the central engine if present.

To address these issues we are conducting a magnitude and volume limited survey of nearby early-type galaxies at Lick Observatory and the Michigan-Dartmouth-MIT Observatory. We have selected $\approx$ 100 galaxies from radio catalogs: the "monsters" from Condon and Broderick (1988) and Condon, Frayer and Broderick (1991), the possibly active galaxies from Wrobel and Heechen (1990) and from Sadler, Jenkins and Kotanyi (1989). A large sample is necessary because while studies of individual "LINERs" have led to a certain understanding of the phenomenon, these studies have not provided a global framework.

Here we present results from our first run of medium resolution ($\sim$ 5Å FWHM) spectroscopy. Kinematic data and line ratios determined along the major and minor axes of 6 galaxies are discussed. The information gleaned from spectroscopic data, when combined with data at other wavelengths, will enable a thorough investigation into the nature of low luminosity nuclear activity.

References

Condon, J.J. and Broderick, J.J., 1988, *A.J.*, **96**, 30.

Condon, J.J., Frayer and Broderick, J.J., 1991, *A.J.*, **101**, 362.

Sadler, E.M., Jenkins, C.R. and Kotanyi, C.G., 1989, *M.N.R.A.S.* , **240**, 591.

Wrobel, J.M., 1991, *A.J.*, **101**, 125.

Wrobel, J.M. and Heeschen D., 1991, *A.J.*, **101**, 148.

Low Redshift Star-Forming Galaxies: What Can They Teach Us About Primeval Galaxies?

D. Calzetti[1,2] and A. L. Kinney[1]
[1] *Space Telescope Science Institute, 3700 San Martin Dr., Baltimore MD 21218, USA*
[2] *Affiliated with the Space Science Department, ESA*

ABSTRACT

The analysis of the UV plus optical spectra of three star-forming galaxies, Mrk 496, Mrk 357, TOL1924-416, obtained by matching the size of the optical aperture with that of IUE, has given unexpected results. These can be summarized as: 1) the dereddened Lyα/Hβ ratios are consistent with the prediction of case B recombination for nebular emission, within the uncertainties; 2) the decrease of the Lyα/Hβ ratio with increasing metallicities is not confirmed in our three objects, although the sample is too small to consider this result definitive. The first result is surprising, mainly because at least the two Markarian galaxies have a large enough HI content to markedly increase the optical depth for the Lyα photons and to trigger their absorption by dust. This finding can probably be explained as an effect of the inhomogeneous distribution of gas and dust within the galaxies. On the basis of these results, we conclude that the detection of the Lyα emission line in searching for primeval galaxies (PGs) can be still considered a valid technique.

The UV+optical spectra (1200Å$\leq \lambda \leq$ 7700Å) of the three metal-poor blue galaxies, Mrk 496, Mrk 357, TOL1924-416, have been assembled by using archival IUE spectra together with new optical observations obtained in an aperture whose size matches that of the IUE aperture. The choice of the aperture has been driven by the necessity of accounting for possible inhomogeneous distributions of the dust present in the galaxies[2]. These three objects, selected because of their Lyα emission, are the first galaxies observed in a IUE-matching optical aperture of a sample of 30 galaxies contained in the *Atlas of Ultraviolet spectra of Star-Forming Galaxies*[5] with high enough redshift to allow observations of the Lyα wavelength region.

The optical spectra has been used to derive: a) the metallicity of the galaxy from the oxygen lines and b) the dust extinction parameter E(B-V) from the observed Hα/Hβ ratio (see Table, where the intrinsic contribution, and the contribution from our Galaxy to the extinction are shown separately).

The estimated E(B-V) has then been used to deredden the Lyα/Hβ line ratio. This ratio is critically dependent not only on the extinction parameter, but also on the adopted extinction law. Since our three galaxies span a range of metallicity, we have used three different extinction laws to deredden the Lyα/Hβ ratios, that is, the Galactic, the LMC and the SMC extinction curves[9,6,7], assuming a crude matching between the average metal content of Mrk 496, Mrk 357, TOL1924-416 and the metal content of the Galaxy, the LMC and the SMC.

The Table shows the dereddened Lyα/Hβ line ratios for the three galaxies. It is evident that such ratios are, within the uncertainties, in the expected range for case B

recombination ($[\mathrm{Ly}\alpha/\mathrm{H}\beta]_{theor} = 23 - 34$), and the agreement is even better if the underlying stellar absorption for the Lyα line is taken into account. In contrast with our result, Hartmann, Huchra & Geller[3] report values for the Lyα/Hβ ratios of the two Markarian galaxies which are 20-30 times below the expectation, due to the underestimation of the E(B-V) value. Our result is also in disagreement with the theoretical expectations for the dust absorption of multiply scattered Lyα photons in an homogeneous gas+dust medium[8]. In fact, the HI column density in front of the two Markarian galaxies is $> 10^{21}$ cm^{-2}, enough to scatter substantially the Lyα photons and to increase the probability of their absorption by dust. The lack of this effect can probably be explained as the result of the uneven distribution of gas and dust inside the galaxy.

From the Lyα/Hβ values reported in the Table, it is also clear that there is no evident anticorrelation between the Lyα/Hβ and the metallicity of the galaxy. The discrepancy between our results and the previous works[4] can be due to the different aperture sizes used in the optical observations. We assume that our estimation of the dust extinction and, consequently, of the Lyα/Hβ line ratios, are more accurate, since we use matching apertures for the UV and optical observations. Neverthless, we are waiting for observations of additional galaxies in the optical before considering this finding as a definitive result.

If the large values of the Lyα/Hβ ratios found here are confirmed, and found to be representative of starburtsting galaxies in general, then the search for Lyα emission from PGs at higher redshifts will continue to be a viable strategy, since the dust in PGs is expected to be of much lower content than in our present examples and there are no hints that it should be homogeneously distributed.

REFERENCES

[1] Burstein, D., & Heiles, C. 1982, AJ, 87, 1165

[2] Calzetti, D., & Kinney, A.L. 1992, in prep.

[3] Hartmann, L.W., Huchra, J.P., & Geller, M.J. 1984, ApJ, 287, 487

[4] Hartmann, L.W., Huchra, J.P., Geller, M.J., O'Brien, P., & Wilson R. 1988, ApJ, 326, 101

[5] Kinney, A.L., Bohlin, R.C., Calzetti, D., Panagia, N., & Wyse R.F.G. 1992, submitted to ApJS

[6] Koornneef, J., & Code, A.D. 1981, ApJ, 247, 860

[7] Lequeux, J., Maurice, E., Prevot, L., Prevot-Burnichin, M.-L., Rocca-Volmerange, B. 1984, *Structure and Evolution of the Magellanic Clouds, IAU Synposium no. 108*, S. van der Bergh and K.S. de Boer eds., p. 405

[8] Neufeld, D.A. 1990, ApJ, 350, 216

[9] Seaton, M.J. 1979, MNRAS, 187, 73p

Galaxy Name	$[O/H]$ solar units	E(B-V)[1] Gal.	E(B-V) intrin.	Lyα/Hβ underedd.	Lyα/Hβ Gal. ext.	Lyα/Hβ LMC ext.	Lyα/Hβ SMC ext.
Mrk 496	−0.05	0.00	0.52 ± 0.15	0.60	$12.4^{+17.3}_{-7.2}$	...	...
Mrk 357	−0.5	0.04	0.26 ± 0.15	1.45	$8.3^{+11.6}_{-4.8}$	$20.8^{+32.2}_{-15.7}$	...
TOL1924-416	−0.7	0.07	0.05 ± 0.10	2.40	$4.8^{+3.8}_{-1.2}$	$5.7^{+8.9}_{-2.1}$	$7.0^{+19.8}_{-3.5}$

Cosmic Evolution of Extragalactic C I, C II, and CO Luminosity

John Bally[1], J. Michael Shull[1,2], and Andrew J. S. Hamilton[2]

[1] Center for Astrophysics and Space Astronomy, APAS Dept., University of Colorado (CU)

[2] Joint Institute for Laboratory Astrophysics, CU & National Institute of Standards and Technology

Carbon is the fourth most abundant element in the Galaxy with an abundance of $\sim 4 \times 10^{-4}$ relative to hydrogen. Of all abundant metals it is the easiest to observe in the interstellar medium (ISM). Carbon can be found in four dominant forms: dust grains, C II, C I, and CO. The latter is the most abundant molecule (next to H_2) in molecular clouds. All three gas-phase forms produce strong sub-mm wavelength emission lines and are the principal tracers of the warm and dense neutral phases of the ISM.

We calculate the gas-phase abundances of neutral carbon (C I), ionized carbon (C II), and carbon monoxide (CO) as a function of cosmic time or redshift z in an idealized scenario of galactic evolution. The total gas-phase abundance of any metal is the product of the fractional abundance of the metal and the total amount of gas remaining in a galaxy. All galaxies are born with metallicity $Z = 0$ and a gas mass fraction, $\mu = M_{\rm gas}/M_{total} \approx 1$ where $M_{total} = M_{gas} + M_{stars}$. As star formation proceeds, a fraction of the mass consumed is locked-up permanently inside long-lived, low-mass stars and stellar remnants (white dwarfs, neutron stars, and black holes). The remaining consumed mass is eventually returned to the ISM via planetary nebulae, red giants, AGB stars, and supernovae, polluted with elements such as carbon, oxygen, and iron. The grain abundance regulates the size and photoelectric heating rate of photodissociation regions (PDRs) in Giant Molecular Clouds, and thus helps determine the strength of the [C II] 158 μm line. The mm and sub-mm wavelength lines of these species may provide a new tool for studies of cosmology, galaxy evolution, and chemical enrichment of the ISM.

Closed Box Model: We use the formalism outlined by Tinsley (1980) to calculate the total gas-phase abundance of carbon as a function of gas mass fraction μ. In a closed-box model of galactic evolution and under the assumption of instantaneous recycling of metal enriched gas for stars above a critical stellar mass, the metallicity of the gas is given by $Z = y \ln(1/\mu)$ where y is the *yield*, the mass of new metals ejected by stars when 1 unit of mass is locked-up into stars. The total ISM abundance of a species such as carbon is given by $M_C = y_C M_{gas} \ln(M_{total}/M_{gas})$ where y_C is the yield of carbon.

Infall rate = star formation rate: If infall of pristine ($Z = 0$) matter plus the mass returned to the ISM by mass loss just balances the star formation rate, the mass of the ISM remains constant. Tinsley (1980) shows than in this case, $Z = y[1 - \exp(1 - 1/\mu)]$ and the abundance of C in the ISM is given by $M_C = y_C M_{gas} [1 - \exp(1 - M_{total}/M_{\rm gas})]$

For simplicity, we assume that the properties of molecular clouds remain constant with increasing redshift, except that the minimum temperature of the clouds, $T_{\rm cl}$, remains somewhat above that of the co-moving temperature of the cosmic microwave background, T_{CMB}. That is $T_{\rm cl} = T_{CMB}(1+z) + T_{\rm off}$. We assume that the fraction of ISM mass in the form of molecular clouds and the fraction of carbon locked up in grains remain constant with changing μ. Then the fraction of gas-phase carbon in the C I, C II, and CO phases is determined by the physics of photodissociation regions. As shown by Langer (1976) and Tielens & Hollenbach (1985), the thickness of the C I-bearing layer in a molecular cloud is, to first order, determined by the attenuation of UV radiation by dust grains. Self-shielding of the CO lines may play a secondary role in determining the location of the C I-to-CO transition.

If the grain properties and fraction of metals in grains are independent of metallicity, then the mass ratios, M(C I)/M(CO) and M(C II)/M(CO), should increase with decreasing Z. This general trend can be tested by observing these species in low-metallicity dwarf galaxies such as the LMC and SMC. Observations of the $z = 2.286$ protogalaxy IRAS F10214+4724 show that the C I lines are about 3 times stronger than the CO lines (Brown & Vanden Bout 1992). The luminosity of spectral lines is determined by excitation conditions within the emitting region. Most CO emission in the Galaxy is produced by gas with volume densities above 10^2 cm^{-3}, and the mm-wave lines of CO are optically thick and thermalized. C I and C II can be excited in: (1) the low-density warm and hot phases of the neutral ISM, where the excitation is sub-thermal and the lines are optically thin; and (2) in the high-density outer layers of molecular clouds

where the lines are nearly thermalized and optical depths approach unity. Reasonable estimates for the parameters of the ISM demonstrate that Galactic C II emission is dominated by warm edges of molecular clouds where the lines are thermalized. A similar argument applies for [C I], which is easier to excite at lower temperatures since the 609 μm line lies only 23.6 K above the ground state. Thus, [C I] is easier to excite than [C II] in PDRs.

The conclusions from our study are:

• The gas-phase carbon abundance as a function of gas mass fraction is relatively insensitive to the galactic evolution model parameters (Fig. 1); the epoch of maximum gas-phase carbon abundance depends mostly on the star formation history of a galaxy.

• In a closed-box model of galactic evolution, the maximum abundance of carbon in the ISM occur when the gas mass fraction of a galaxy $\mu \approx 0.3 - 0.4$.

• The total abundance of carbon in the ISM of galaxies was substantially greater in the past. The star formation histories for galaxies of various Hubble types given by Sandage (1986) imply that the sub-mm line luminosity of early-type galaxies peaks at early epochs, while later Hubble types reach maximum luminosity at progressively later times.

• The total luminosity ratio of [C I]/CO and [C II]/CO increases with decreasing metallicity. The sub-mm fine-structure cooling lines are expected to be relatively brighter than CO in the early Universe and in less chemically evolved galaxies at the present.

REFERENCES

Brown, R. L., & Vanden Bout, P. A. 1992, ApJ (Letters), in press.
Langer, W. D. 1976, ApJ, 206, 699.
Sandage, A. 1986, A&A, 161, 89.
Tielens, A. G. G. M., & Hollenbach, D. J. 1985, ApJ, 291, 722.
Tinsley, B. M. 1980, Fundamentals of Cosmic Physics, 5, 287.

Figure 1. The relative gas-phase concentration of carbon (M_{carbon}/M_{total}) vs. gas mass fraction, $\mu = M_{\rm gas}/M_{total}$ for a closed-box model. The vertical arrows show the present-day value of μ. The yield of carbon, y_C, is normalized to produce a gas phase carbon abundance of 3×10^{-4} ($\mu = 0.05$) at the present.

Figure 2. Carbon content of galaxies of various Hubble types as a function of cosmic time or redshift ($\Omega_o = 1$ universe) for closed-box model and star formation models of Sandage (1986). The present-day gas fraction, μ, is assumed to be only a few percent in early type galaxies, about 10% for Sc spirals, and about 20% for irregulars. The carbon abundances are normalized to the same galactic mass. The maximum gas-phase carbon abundance (and C-line luminosity) occurs when $\mu \approx 0.3 - 0.4$. For early-type galaxies, this corresponds to $z \geq 5$, and at progressively lower redshifts for later Hubble types.

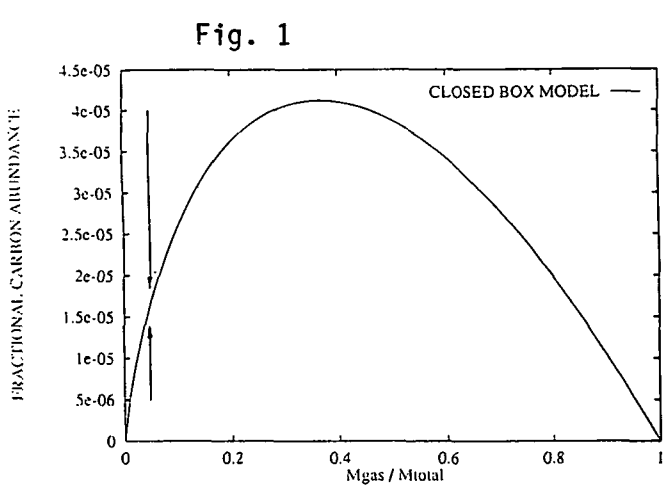

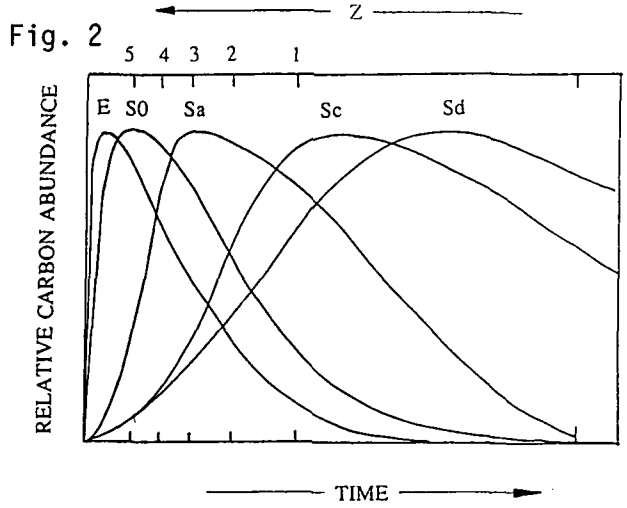

Emission Line Galaxies in a Narrow Strip Toward Perseus.

Nancy E. Ellman, University of California, Santa Cruz.

Many studies have suggested that emission line galaxies have different spatial distributions than non-emission line galaxies. ELGs tend to avoid rich clusters (Dressler, Thompson and Shectman 1985) and may sometimes reside within voids (Balzano and Weedman 1982). This paper describes work in progress on a redshift survey aimed both at determining the angular extent of the structures detected in deep pencil beam survey and at studying the characteristics of galaxies in and around those structures. The current focus is the distribution of emission line galaxies with respect to the rest of the sample.

The data consists of spectra for 190 galaxies in three 40′ fields adjacent to the site of the deep pencil beam survey in Selected Area 68 (Koo, Kron, Szalay 1987). The spectra were obtained using the NESSIE Multifiber Feed and the RC Spectrograph at KPNO, have resolution of 8Å FWHM, (twice that of the original deep survey) and have wavelength range of 4400Å–7230Å. In addition to redshifts, equivalent widths were measured for [OIII], and $H\alpha + [NII]$.

Of the 190 galaxies, 29 exhibited strong [OIII] emission ($W_{5007} > 10$Å). All of those galaxies with a low enough redshift for it to be detectable also showed $H\alpha$ emission. In addition, 17 galaxies with strong $H\alpha + [NII]$ ($W_\lambda > 25$Å) showed only weak or no [OIII] emission. Hence, the emission in these galaxies would not have been detected if they resided at a redshift $z \geq 0.0950$ ($V_R \geq 27000$ km/s.)

Below are wedge plots in RA and Dec of the galaxies in these three fields. Notice the concentrations at $V_R \approx 19000$, 23000 and 33000 km/s, which extend across all 3 fields. From the Dec wedge plot it is apparent that groups or clusters make a significant contribution to the peaks in the velocity distribution, but do not account for all of the overdensity.

The emission line galaxies do not appear to avoid the galaxy concentrations. A KS test gives a probability of 30% that galaxies with strong $H\alpha$ or [OIII] are drawn from the same velocity distribution as those galaxies without strong emission but with a low enough velocity that $H\alpha$ could have been detected. A KS test of the galaxies with and without strong [OIII] over the entire sample gives a probability of only 2% that the galaxies have the same distribution. However, this result could be due to a failure to detect [OIII] galaxies, which may have lower luminosity, at greater distances.

At present we have only rough magnitudes for the galaxies. The survey reaches to $B_J \approx 20$ in two of the fields and to $B_J \approx 20.5$ in the third. The 24 galaxies fainter than $B_J = 20$ appear to lie in the same structures as the brighter galaxies, rather than in the voids.

Future work will include analysis of the distributions of galaxy luminosity, color and surface brightness.

References:

Balzano, V. A., and Weedman D. W. (1982). *Ap. J. Lett.* **255**, L1.

Dressler, A., Thompson, I. A., and Shectman, S. A. (1985). *Ap. J.* **288**, 481.

Koo, D. C., Kron, R. G., and Szalay, A. S. (1987) in *13th Texas Symposium in Relativistic Astrophysics,* ed. M. P. Ulmer (World Scientific, Singapore p. 284)

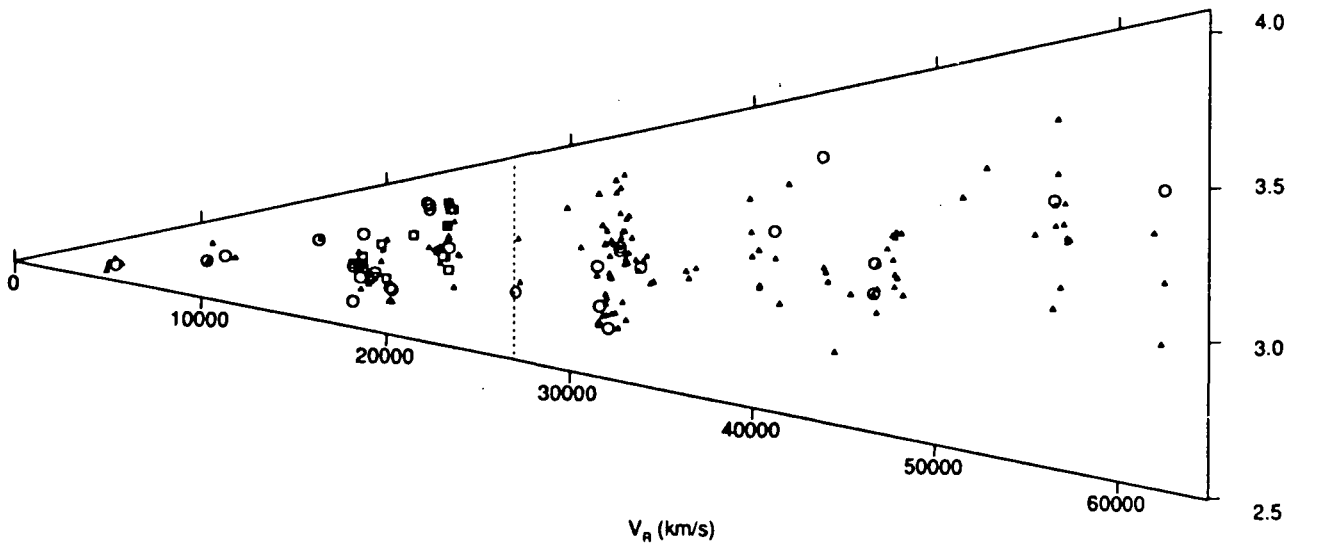

Figure 1: Wedge plot in RA. Circles indicate galaxies with strong [OIII], squares indicate galaxies with strong $H\alpha + [NII]$, but weak or no [OIII], and triangles indicate galaxies with no strong emission. The dotted line shows the velocity to which $H\alpha$ could be deteced. The vertical scale has been stretched by a factor of 15 for clarity.

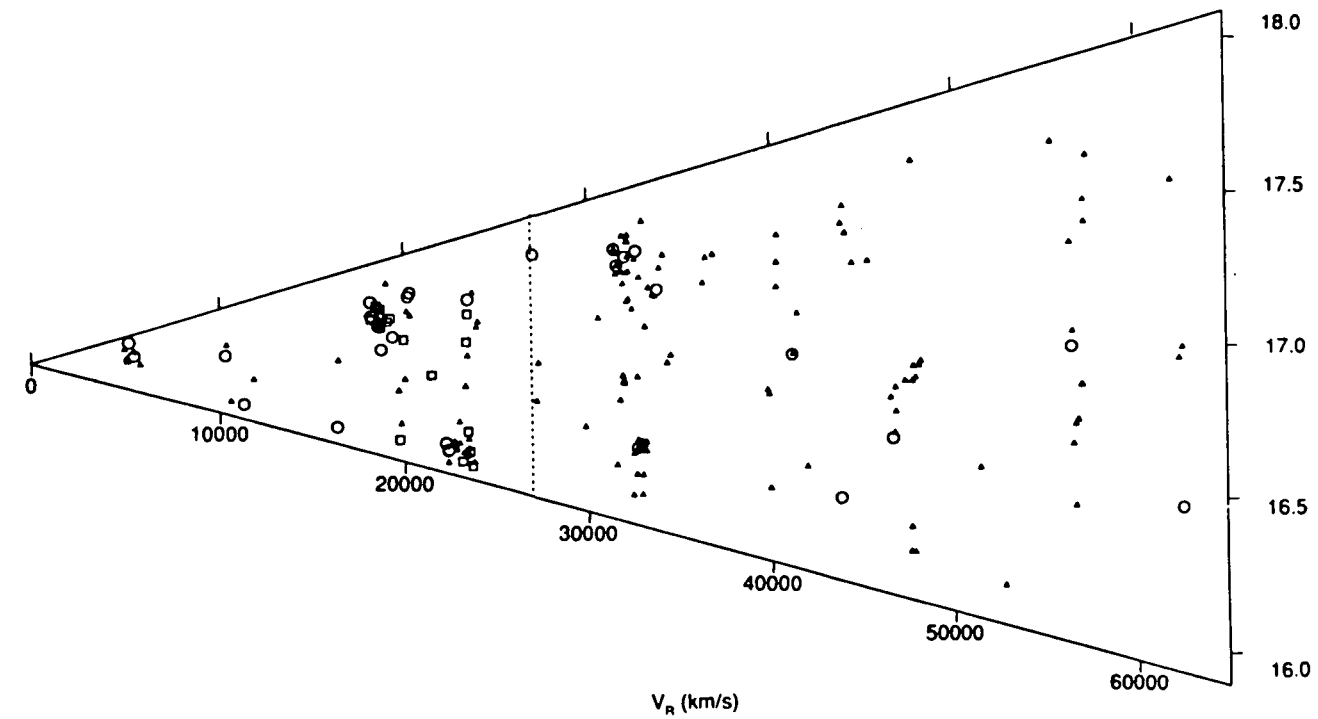

Figure 2: The same as Figure 1., but for a wedge plot in Dec.

A Systematic Investigation of Edge-On Starburst Galaxies: Evidence for Supernova-Driven Superwinds

Matthew D. Lehnert

Space Telescope Science Institute and the Johns Hopkins University

The global wind generated by the collective effect of multiple supernovae and stellar winds from OB associations is a well developed concept both observationally and theoretically (e.g., McCray & Kafatos 1987). On a much larger scale, a starburst, the rapid (<few x 10^8 yrs) formation of many OB associations in a small volume (r<few kpc), with their accompanying stellar winds and high supernovae rate (3 SNe per 10 years in M82, Rieke et al. 1980), should result in a much larger and more vigorous supernova-driven wind, a superwind. Superwinds, while studied theoretically by many authors (e.g., Tomisaka & Ikeuchi 1988; Chevalier & Clegg 1985) and hence is on sound theoretical footing – have only recently been observed (e.g., Heckman, Armus, & Miley 1991). However, most observations are of a few of the nearest starburst galaxies. While these observations provide tremendous insight, we do not as yet understand the global and cosmological significance of galactic superwinds. In order to achieve this depth of understanding, we need to systematize our understanding, that is, we need to determine how prevalent superwinds are and how their properties depend on the star-formation rate and the properties of the galaxies that drive them.

Obtaining such depth in our understanding of superwinds has important consequencies both observationally and theoretically, not only for understanding the properties of starburst galaxies, but indeed, to gain new insight into some of the most outstanding problems of astrophysics. Galactic winds have often been hypothesized to: 1) enrich and heat the inter-galactic medium in clusters, 2) play a critical role in the Hubble Sequence by sweeping cold gas out of proto-bulges/ellipticals, 3) help determine both the mass/metallicity relation between galaxies and the metallicity/radius relation within galaxies, 4) explain some classes of QSO absorption lines, 5) blow away dust and gas in Far-IR Galaxies, possibly facilitating their evolution into optical QSOs, and 6) stimulate the formation of galaxies in the IGM surrounding a newly-formed galaxy and so play a role in the formation of structure in the universe.

We are completing a project designed to realistically assess the global/cosmological significance of superwinds by attempting to systematize our understanding of them (determine their incidence rate and the dependence of their properties on the star-formation that drives them). Specifically, we are analyzing data from an optical spectroscopic and narrow-band imaging survey of an infrared flux-limited sample of about 50 starburst galaxies whose stellar disks are viewed nearly edge-on. This edge-on orientation is crucial because the relevant properties of the superwind can be far more easily measured when the flow is seen in isolation against the sky rather than projected onto the much brighter gas associated with the starburst galaxy itself. These galaxies are all IR "warm" ($S_{60\mu m}/S_{100\mu m}$ >0.4) and have IR luminosities from $\approx 10^9 - 10^{12} L_\odot$ and allow us to discern the properties of galactic superwinds as a function of IR luminosity and hence the star-formation rate. We show that extra-planar emission-line gas is a very common feature of these edge-on galaxies and the properties of the extended emission-line gas (radial pressure profiles that fall as approximately r^{-2}, line ratios becoming more shock/AGN-like as one proceeds out along the minor axis, filamentary and shell-like emission-line morphologies, optical emission-line widths that depend more strongly on the infrared luminosity than on the disk rotation amplitude, etc.) are quantitatively consistent with the superwind theory.

Automata Network Models of Galaxy Evolution

David Chappell and John Scalo
Department of Astronomy
University of Texas at Austin

Two ideas appear frequently in theories of star formation and galaxy evolution: 1. Star formation is nonlocally excitatory, stimulating star formation in neighboring regions by propagation of a dense fragmenting shell or the compression of preexisting clouds, and 2. star formation is nonlocally inhibitory, making HII regions and explosions which can create low-density and/or high temperature regions and increase the macroscopic velocity dispersion of the cloudy gas. Since it is not possible, given the present state of hydrodynamic modeling, to estimate whether one of these effects greatly dominates the other, it is of interest to investigate the predicted spatial pattern of star formation and its temporal behavior in simple models which incorporate both effects in a controlled manner. The present work presents preliminary results of such a study which is based on lattice galaxy models with various types of nonlocal inhibitory and excitatory couplings of the local SFR to the gas density, temperature, and velocity field meant to model a number of theoretical suggestions. These models can be viewed as the descendants of the nearest neighbor excitation/local inhibition cellular automata of Gerola and Seiden. These models are also closely related to discrete models for complex systems as embodied by nonlocal cellular automata, coupled map lattices, and artificial neural networks, all of which are known to exhibit a rich array of phenomena. We are particularly interested in relating our models to the behavior of these relatively well-studied systems, especially with respect to their propensities to exhibit phase transition phenomena and more complex "computational" or "cognitive" behavior (e.g. categorization of a continuous range of environmental stimuli).

The present models evolve on a 2-dimensional square lattice with a constant configuration (i.e. no differential rotation, contraction, etc.). There are no external perturbations; the model is driven entirely by its own internal state. The SFR is controlled by the velocity dispersion, or 'temperature', of the gas. Star formation becomes much more probable at a given site when the 'temperature' falls below a critical threshold value, which is a parameter,

but star formation itself inhibits further star formation in some neighborhood by increasing the 'temperature'. Lattice sites just outside the inhibitory zone around each star are assumed to form a ring of excitation, meant to represent a fragmenting shell which has propagated from the central star. The excitation is performed by simply decreasing the 'temperature' in the ring. Every site's 'temperature' is assumed to cool exponentially with a time constant that is another free parameter. At each site at each time step, the probability for star formation is taken to be a sigmoid function of the velocity dispersion, so that star formation becomes much more likely when the 'temperature' drops below the threshold of the sigmoid function.

The results of this study are as follows. The model exhibits a variety of oscillations, bursts, and irregular patterns in the global star formation rate. The corresponding spatial patterns are equally diverse ranging from well organized global waves to 'foamy' textures of expanding shells. Intermittent, bursty behavior occurs when the cooling time of the gas becomes greater than the propagation time across the lattice. During bursts, a single wave of star formation spreads across the lattice and then dies out. For shorter cooling times more complex behavior results in which oscillatory and irregular SFRs evolve into one another. The relative strength of the excitatory to inhibitory connections controls the geometry of the pattern of star formation. Strong excitatory connections create coherent fronts of star formation while weak ones lead to isolated star formation regions. We suggest that more detailed models can be used with maps of the spatial distribution of star formation (from Hα say) to diagnose the relative importance of inhibitory and excitatory star formation processes in galaxy evolution.

In the future we plan to include the gas density, differential galactic rotation, different connection geometries, and nonperiodic boundary conditions. We will also study the spatio-temporal patterns of star formation more quantitatively using methods drawn from nonlinear dynamics and complex systems.

Page Intentionally Left Blank

ADDITIONAL PAPERS

Page Intentionally Left Blank

Can Cluster Environment Modify the Dynamical Evolution of Spiral Galaxies ?

P. Amram[1], C. Balkowski[2], V. Cayatte[2], M. Marcelin[1], W. T. Sullivan III[3]

[1] Observatoire de Marseille, France
[2] Observatoire de Paris-Meudon, France
[3] Dept. of Astronomy, Universtiy of Washington, USA

Over the past decade many effects of the cluster environment on member galaxies have been established. These effects are manifest in the amount and distribution of gas in cluster spirals, the luminosity and light distributions within galaxies, and the segregation of morphological types. All these effects could indicate a specific dynamical evolution for galaxies in clusters.

Nevertheless, a more direct evidence, such as a different mass distribution for spiral galaxies in clusters and in the field, is not yet clearly established. Indeed, Rubin, Whitmore and Ford (1988) and Whitmore, Forbes and Rubin (1988) (hereafter collectively referred to as RWF) presented evidence that inner cluster spirals have falling rotation curves, unlike those of outer cluster spirals or the great majority of field spirals. If falling rotation curves exist in centers of clusters, as argued by RWF, it would suggest that dark matter halos were absent from cluster spirals, either because the halos had become stripped by interactions with other galaxies or with an intracluster medium, or because the halos had never formed in the first place. Even if they didn't disagree with RWF, Distefano et al (1990) pointed out that the behaviour of the slope of the rotation curves of spiral galaxies (in Virgo) is not so clear. Amram et al. (1992) using a different sample of spiral galaxies in clusters found only 10% of declining rotation curves (2 declining vs 17 flat or rising) in opposition to RWF who find about 40% of declining rotation curves in their sample (6 declining vs 10 flat or rising), we will hereafter briefly discuss the Amram et al. (1992) data paper and compare it to the results of RWF.

We have measured the rotation curves for a sample of 21 spiral galaxies in 5 nearby clusters. These rotation curves have been constructed from detailed two-dimensional maps of each galaxy's velocity field as traced by emission from the Hα line. This complete mapping, combined with the sensitivity of our CFHT 3.60 m.+ Perot-Fabry + CCD observations, allows the construction of high-quality rotation curves. Details concerning the acquisition and reduction procedures of the data are given in Amram et al. (1992). We will now present and discuss our preliminary analysis and compare them with RWF's results.

Following RWF, we characterize the slope of a rotation curve with reference to fiducial points defined relative to the optical radius R_{25}. The "outer gradient" (OG) is the change in rotation velocity between 0.4 and 0.8 R_{25}, normalized to the maximun measured velocity and expressed as a percentage. RWF presented evidence for falling rotation curves in the central regions of clusters, as well as for a marked correlation between OG and r_{cl}, the projected distance of each galaxy from its cluster center. In the figure we present the same plot for our sample; it can been seen that the correlation is not significative. This holds for our sample whether or not we confine ourselves to our 12 galaxies of hightest quality (black dots), or include 9 other galaxies that are questionable (crosses and plus).

The reasons for this discrepancy with RWF probably arise in three distinct arguments : 1) the samples are different, 2) the technics are different and 3) the criteria of selection are different :

1) The RWF's sample contains much more galaxies who are closer to the centers of the clusters. In particular, 2 galaxies located in DC 1842-63 cluster having strong negative value of OG (-26% and -18%) tend to strength the RWF's correlation between r_{cl} and OG. In an other hand, among the 6 galaxies in common, for 2 galaxies (NGC 6045 and UGC 4329) very close from the cluster center, the values of OG disagree. So the other reason for the discrepancy could be the observational technics.

2) Our rotation curves are based on the entire velocity field, as opposed to RWF's data from a 1 arcsec-wide slit along the major axis, for which the emission in the rest of the disk is

ignored (the local non-circular movement are not distinguable from the circular ones and furthermore not taken into account in the rotation curve) and for which gaps in line-emitting gas along the major axis could cause problems. As a consequence of the 2-dimensional field, the deprojection parameters (inclination, position of the dynamical major axis,...) are derived from the dynamics itself. Moreover, the Perot-Fabry + CCD technics is more sensitive than a traditional spectrograph + image tube and photographic plate; for example, this allowed us to measure rotation velocities typically 15 to 30 % father out from the nucleus than RWF and the shape of the rotation curve is computed with much more velocity points.

3) In our plot we have eliminated doubfull galaxies (highly inclined galaxies, galaxies with companion or peculiar, extrapolated rotation curves, ...) and RWF didn't.

We have found no biases in our sample in luminosity, morphological type, size or HI content that might affect our main result of no significant environmental effect. WFR also found that M/L rose much more weakly for galaxies in the inner regions of clusters. They presented this as further strong evidence in favor of a lack of dark halos around inner galaxies. The surface brightness photometry of 10 of our galaxies is being reduced. We have also in preparation a new data paper containing 15 more rotation curves in 2 other clusters which will increase the confidence we have in our result.

REFERENCES

Amram, P., Le Coarer, E., Marcelin, M., Balkowski, C., Sullivan, W.T., III and Cayatte, V. 1992, Astron. Astrophys. Suppl. Ser 1992, 94, 175

Distefano, A., Rampazzo, R., Chincarini, G. and de Souza, R. 1990, Astron. Astrophys. Suppl., 86, 7

Rubin, V.C., Whitmore, B.C. and Ford, W.K.,JR. 1988, Ap. J., 333, 522

Whitmore, B.C., Forbes, D.A. and Rubin, V.C. 1988, Ap. J., 333, 542

Figure. *Outer gradient OG for each galaxy versus its projected radius from its cluster center. Three samples are distinguished : sample 1 (the best quality data) with filled circles and a last-square linear fit (solid line), sample 2 (inclination > 65°) represented by a "x" and sample 3 (questionable due to the presence of companion galaxies, evidence for non-circular motions, or rotation data requiring extrapolation) represented by a "+". The dash-dot-dash line shows the fit published by RWF.*

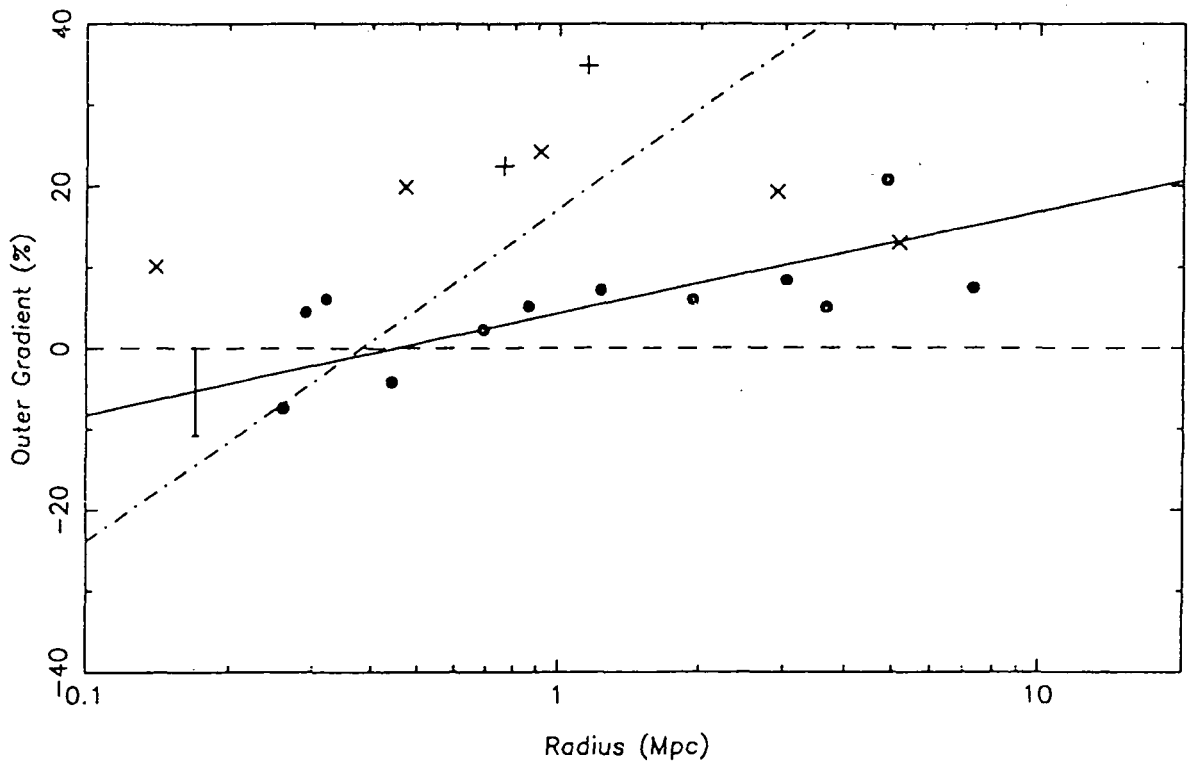

MULTI-FILTER SPECTROPHOTOMETRY SIMULATIONS

Kim A. S. Callaghan, Brad K. Gibson & Paul Hickson
- University of British Columbia -

Introduction

To complement both the multi-filter observations of quasar environments described by Craven *et al.* in these proceedings, as well as the proposed UBC 2.7m Liquid Mirror Telescope (LMT) redshift survey (Hogg *et al.* these proceedings; Gibson & Hickson 1992), we have initiated a program of *simulated multi-filter spectrophotometry.* The goal of this work, still very much in progress, is a better *quantitative* assessment of the multiband technique pioneered by Baum (1962) and Oke (1971), as a viable mechanism for obtaining useful redshift and morphological class information from large scale multi-filter surveys.

Methodology and Preliminary Results

The methodology utilized in our study is qualitatively straightforward (a full *quantitative* discussion is forthcoming - Callaghan *et al.*, in preparation): multi-filter spectrophotometric observations are simulated by adding a representative spectrum for a given galaxy's morphological class and redshift to the sky spectrum and sampling with some specified filter transmission curves. Photon noise is added and a reduced χ^2 minimization routine implemented - *i.e.*, χ^2 is computed by comparing the simulated galaxy spectra against a library of galaxy and stellar templates, the type and redshift leading to the minimum in the χ^2 distribution is assigned as that best representing the physical nature of the object.

The library of comparison templates used here consists of the seven Hubble types included in the Rocca-Volmerange & Guiderdoni (1988) atlas (RVG88), as well as the 81 stellar templates in the Gunn & Stryker (1983) catalog. Unlike previous work, which has rested solely upon comparing against local (*i.e.*, z=0) galaxy templates, we have given the user the option of using a set of templates (again based on the RVG88 atlas) which evolve as a function of lookback time based upon the standard scenarios of spectral evolution as a function of Hubble type, outlined in Guiderdoni & Rocca-Volmerange (1987). The impact of galaxy evolution upon the multi-filter technique is neglected here, but will be detailed in the later Callaghan *et al.* paper.

Our χ^2 program is in many ways akin to the cross-correlation technique so successfully employed by Tonry & Davis (1979) and Ellingson & Yee (1992, in preparation), the primary difference being the latter pair use the continuum-subtracted emission/absorption line spectra in the cross-correlation, whereas the former is optimal for intermediate-band ($\sim 100 - 400$Å) filter set observations (e.g. the 40 filters being used for the UBC 2.7m LMT redshift survey - Gibson & Hickson 1992; the 24 filters utilized in the Craven *et al.* study discussed elsewhere in this volume) for which most of the line information is lost and the continuum is the essential component in the χ^2 calculation.

A series of simulations has been completed, complementing the Craven *et al.* and UBC LMT observations. For brevity, we discuss here some of the preliminary findings from our "Craven" runs: the characteristics of this sample include low signal-to-noise ($s/n = 5.0$), intermediate redshift ($z = 0.4$), and simulated spectrophotometry through the same 24 narrow-band filters as used in the true observations.

The 24-point simulated spectral energy distributions (SEDs) were compared against the set of galaxy templates generated by simply shifting the $z = 0$ templates linearly in $\log F_\nu$ space, the magnitude of the shift necessary to minimize the χ^2 yielding the estimated redshift. In other words, the shape of the SED remains invariant with redshift (*i.e.*, no spectral evolution). Parallel to the *simulation-galaxy template* χ^2 computation, a *simulation-stellar template* χ^2 is also generated and a best assigned stellar type calculated. Late-type stars are invariably assigned as the "best-fit" stellar template, but the χ^2 is always greater than that for the galaxy assignment.

Early-type galaxy redshift assignments accurate to <2% were consistently found, as were type assignment accuracies to a fraction of a Hubble type. Later-type galaxies posed a somewhat more difficult problem in that they possess inherently flatter SEDs, making the determination of redshift more challenging. This was reflected in redshift uncertainties of ~20%, an order of magnitude or so larger than that encountered with the ellipticals. Morphological classification was still accurate to within a Hubble type. This seems reasonable given the similarities between the Sa, Sb, Sc, and Sd (Types 2, 3, 4, and 5, respectively) templates in the RVG88 atlas.

Comments and Summary

Despite apparent similarities between the late-type stellar templates and the galaxy templates, we have not encountered a situation thus far in which a galaxy has been confused with a star. Obviously this is due in part to the number of filters with which we are working (24 for the "Craven" runs). Morphological classification accurate to plus/minus a fraction of a Hubble type seems feasible, even at this low $s/n = 5.0$. Early-type galaxy redshifts accurate to 2%, or better, and late-types to ~20% are also found. Simulations run at signal-to-noise ratios of ~10 indicate that redshifts accurate to a fraction of a percent are obtainable, independent of Hubble class. Because the Craven *et al.*'s filter set has been "tuned" to the redshift of the clusters, their first filter is centered at ~4500Å. Due to this lack of "blue" filters, the all-important 4000Å break in local galaxies will be missed. Our simulations show that at low signal-to-noise ratios, it is possible to assign an anomalously high redshift to any local $z \approx 0$ galaxies that may lie in their cluster fields. Fortunately, the χ^2 is usually poor enough to make the redshift suspect. Future papers in this series will provide a more detailed quantitative error analysis.

References

Baum, W.A. 1962, in *Problems of Extragalactic Research*, ed. G.C. McVittie (New York: MacMillan), p. 390

Gibson, B.K. & Hickson, P. 1992, in *The Space Distribution of Quasars*, ed. D. Crampton (San Francisco: ASP), p. 80.

Guiderdoni, B. & Rocca-Volmerange, B. 1988, A&A, 186, 1

Gunn, J.E. & Stryker, L.L. 1983, ApJS, 52, 121

Oke, J.B. 1971, ApJ, 170, 193

Rocca-Volmerange, B. & Guiderdoni, B. 1988, A&AS, 75, 93

Tonry, J. & Davis, M. 1979, AJ, 84, 1511

LYA AND IR GALAXY COMPANIONS OF HIGH REDSHIFT DAMPED LYA QSO ABSORBERS

Adeline Caulet (ST-ECF/ESA) and Mark McCaughrean (Steward Observatory & MPI Heidelberg)

1. The ancestors of the present-day galaxies

It is true today that not much is known with a solid observational support about the origin and the formation of the present-day gas-rich galaxies. For astronomers, finding our Galaxy ancestor at look back-times of 10 billion years or more would be as thrilling as it has been for paleontologists finding "Lucy" the 4 million years old human ancestor. However, because of galaxy evolution, it will be difficult to recognize the true Galaxian ancestor. A priori, there is no reason for all young forming galaxies to be radio-loud galaxies or even quasars. But the galaxies must form the bulk of their stars at high redshift, with star formation rates (SFR) 10 to 100 times higher than those observed in present-day galaxies. Current SFRs are typically 1 $M_{\odot}$/yr, much too low to produce the stellar mass of galaxies in the Universe lifetime. Intense emission lines Lyα, [OII]λ3727 Å, [OIII]λ5007 Å, Hβ, Hα are predicted to be characteristic signatures of the protogalaxies which are conjectured to be large, massive protogalactic disks with supergiant clouds of ionized gas. The interstellar medium of the protogalaxies is likely to be turbulent, as a result of the considerable energy input from frequent supernovae explosions. A copious amount of dust could be well mixed with the gas and the stars, that absorbs direct stellar light, causes significant scattered light and converts optical stellar light into thermal infrared emission from hot dust.

2. An Infrared Survey of QSO absorption line systems at high redshift

The predicted strong emission lines ([OII], O[III], Hβ, Hα) emitted by young forming galaxies will be redshifted in the infrared J, H, or K bands, at z>1. These lines will be much less extinguished by dust than Lyα, if there is any dust in the primeval galaxies, as Lyα photons are scattered and absorbed by grains within the HII regions (Spitzer 1978). A year ago, we started an IR imaging survey to detect the high z galaxies responsible for the population of QSO heavy-element absorption line systems between z=1.3 and 2.5. The survey samples objects drawn for a more representative portion of the galaxy-luminosity function than the high z radio galaxies and QSO companions where physical conditions are abnormal, perhaps due to their proximity to an active nucleus. The survey extends, in the IR and at higher z, the optical imaging surveys that identified the galaxies producing the QSO Mg II absorption lines at z<1. The low z absorbers are galaxies with star formation activity as evidenced by strong extended [OII] emission and blue continua (Bergeron 1986; Yanny, York, and Williams 1990; Yanny 1990). Unless the low z absorbers are shrouded by dust, their moderate SFRs imply higher SFRs in the more distant absorbers at z>1 to produce all stars in present-day galaxies.

We have used a NICMOS3 HgCdTe 256x256 array detector with the IR camera built by Marcia Rieke on the 2.3m telescope at Steward Observatory to image several QSO fields. The limiting magnitude is K'(2.1μm)= 21.0–21.5 mag per square arcsec for a 3 sigma detection in 3 hours of in-field chopping observations. Each QSO line-of-sight samples several known absorbers with MgIIλ2796–2803 Å and/or CIVλ1548–1551 Å absorption doublets. The equivalent width distributions of the low and high ionization absorption lines of the absorber sample are identical to those of the parent population of all absorbers. This selection process, used already for a spectroscopic survey of MgII absorption lines in CIV-selected absorption systems at high z (Caulet and York 1986, Caulet 1989), gives a methodical approach to observing, reduces the observer biases and makes a more efficient use of telescope time. This selection guarantees that imaging of the sample of QSO fields will provide complete sampling of the whole population of high z QSO absorbers. Included in the sample, the

highly ionized, optically thin CIV absorbers (with weak or no MgII absorption) and the high column HI density damped Lyα systems represent both extremes of the ionization states and of gas density in the QSO heavy-element absorbers, and have never been successfully imaged without ambiguity. The high z damped systems are the "best bet" candidates of the protogalactic disks that evolved into our Galaxy and the other present-day spirals (Wolfe et al. 1986).

Figure 1 is the 5 hour exposure K' image resulting from the combination of a mosaic of 558 individual frames. It shows a candidate z=2.3 cluster of galaxies. One of the galaxies had been discovered previously in Lyα emission with the NASA/GSFC Fabry-Perot Imaging Interferometer during our optical imaging survey of damped Lyα systems (Caulet et al. 1990, Lowenthal et al. 1991). With z=2.313, the Lyα emitting galaxy is a galaxy companion of the z=2.309 damped Lyα system which has been detected only spectroscopically in absorption on the line of sight of the QSO PHL 957. The other small objects clumped around the Lyα galaxy are new candidate galaxies detected in the K' band. We identify also, in the same K' image and near the QSO line of sight, several new galaxy candidates for the damped Lyα system and other intervening QSO absorption systems between z=2 and 3. Follow-up optical and IR spectroscopy of these objects is scheduled for redshift measurement and confirmation of the absorbing galaxies and the cluster members.

References

Bergeron, J. 1986, Astr Ap, 155, L8.

Caulet, A. 1989, ApJ, 340, 90.

Caulet, A., Green, R.F., Woodgate, B.E., and Lowenthal, J.D. 1990, Bull. AAS, 22, 1263.

Caulet, A., and York, D.G. 1986, Bull. AAS, 18, 995.

Lowenthal, J.D., Hogan, C.J., Green, R.F., Caulet, A., Woodgate, B.E., Brown, L., and Foltz, C.B. 1991, ApJ, 377, L73.

Spitzer, L. 1978, in *Physical Processes in the Interstellar Medium* (New York: Wiley).

Wolfe, A.M., Turnshek, D.A., Smith, H.E., and Cohen, R.E. 1986, ApJS, 61, 249.

Yanny, B. 1990, ApJ, 351, 396.

Yanny, B., York, D.G., and Williams, T.B. 1990, ApJ, 351, 377.

Figure 1: K image of PHL 957 field

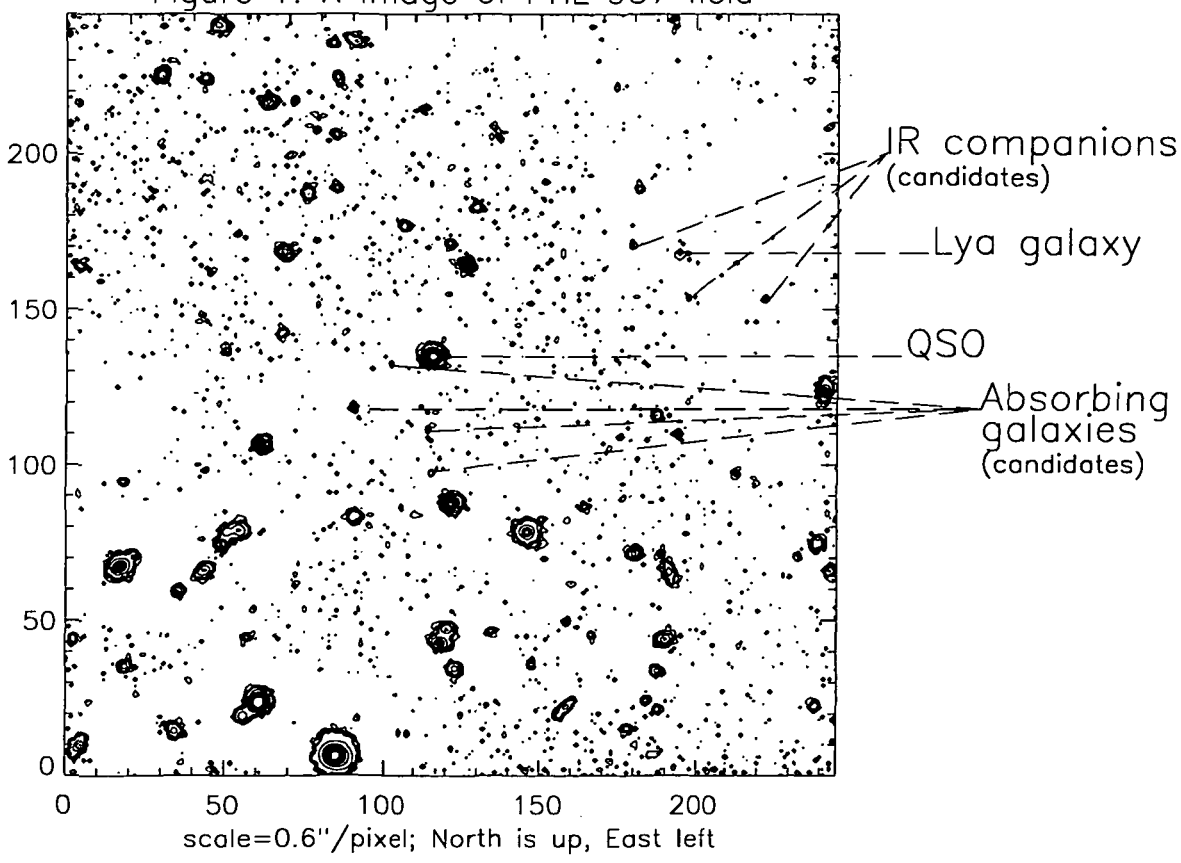

CENTRAL STAR FORMATION IN EARLY-TYPE GALAXIES: IMAGES AND IMPLICATIONS

L. L. Dressel (Applied Research Corporation)
and J. S. Gallagher III (U. of Wisconsin)

INTRODUCTION

We are reporting on an on-going study of strong central star-bursts in early-type galaxies. These galaxies are brighter than m(pg) = 14.5 and are classified as type S0, S0/a, or Sa in the Uppsala General Catalog (UGC, Nilson 1973). All of them have unusually warm, bright far infrared sources for early-type galaxies, with F(100 microns)/F(60 microns) < 2.0 and F(60 microns) > 2.5 Jy (Dressel 1988, Ap. J. 329, L69). Much of the infrared emission comes from the central few arcsec (Telesco, Dressel, and Wolstencroft, in prep). Most of the galaxies were detected at 2380 MHz at Arecibo (Dressel and Condon 1978, Ap. J. Suppl. 36, 53), with flux densities between 15 and 33 mJy. They have diffuse radio sources with a variety of morphologies, typically a few kpc in extent (Dressel, in prep). Long slit spectra through the nucleus show that all have Balmer absorption lines, signifying a large B or A star population, and [OII] 3727 and Balmer emission lines, consistent with ionization by hot young stars (Dressel and Gallagher, in prep). We have made optical continuum and emission line images of the galaxies to use in combination with the above data to study the causes and evolution of strong central star-bursts in early-type disk systems.

DATA

We have used the CCD direct imaging camera on the 2.1 m telescope at Kitt Peak with the TI2 CCD to take images with U, B, R, I, and H alpha + [NII] filters. The CCD has 800 x 800 pixels with a scale of 0.19 arcsec per pixel. The observations were made in October 1991 on three photometric nights with seeing typically 0.9 arcsec. H alpha + [NII], U, I, and composite continuum images of seven galaxies were presented in the poster, to show the distribution of the young and old stellar populations and the overall structure of the galaxies. Descriptions of the individual galaxies are given here:

UGC 00861, NGC 471: type = S0, brightest in multiple system (UGC). The three small UGC companions are within 0.6 diameters. The U isophotes are noticeably asymmetric. The composite continuum image shows a dust lane a few arcsec from the nucleus. The line emission forms a clumpy central ring.

UGC 01157, NGC 632, Mkn 1002: type = S0, pair with UGC 01153 (UGC). The UGC companion, a 15.0 mag E galaxy, is 5 diameters away. The continuum images show a possible bar, inner arms, and irregular outer isophotes. The line emission is centrally concentrated and trefoil-shaped.

UGC 01385, Mkn 2: type = SBa, brightest of 3 (UGC). Two large UGC companion galaxies are 2 and 4 diameters away. The bar and arms are apparent in the continuum images. The line emission is slightly asymmetrically peaked and elongated.

UGC 03201, NGC 1691, Mkn 1088: type = SB0/SBa (UGC). This is a strongly barred galaxy. Most of the line emission is in the center, with an elongated double-peaked morphology suggestive of a clumpy ring. Knots along the arms are also clearly visible.

UGC 03265, NGC 1819, Mkn 1194: type = SB0 (UGC). This is a strongly barred galaxy with classic bar-driven structure. The line emission and the radio continuum emission lie in a clumpy elongated ring.

UGC 12575, NGC 7648, Mkn 531: type = S0 (UGC). The "diamond ring" galaxy. A large off-center clump of star-formation causes strong asymmetry even in the I image. Much structure is visible in the composite continuum image. The composite image and

U image suggest that the clump may be part of an otherwise faint ring.

UGC12618, NGC 7679, Mkn 534, Arp 216: type = S0, pair with UGC 12622, disturbed (UGC); SB0 peculiar: (deVaucouleurs et al. 1976, Second Reference Catalog of Bright Galaxies); Sc/Sa (tides?) (Sandage and Tammann 1981, A Revised Shapley-Ames Catalog of Bright Galaxies). This galaxy is clearly difficult to classify because its properties do not fit neatly into any one Hubble type bin. It has fairly obviously been tidally disturbed by its companion, a disturbed SBa Seyfert galaxy, 3 diameters away. Most of the line emission comes from the complex central region, some from tidal loops.

We have used published IRAS far infrared fluxes and CO fluxes to determine the far infrared luminosities and molecular hydrogen masses of the galaxies. For the three galaxies with no CO observation, the average L(FIR)/M(molecular H) ratio for the CO-detected galaxies was used to estimate the molecular hydrogen mass: < 4, 12, 17 > = 11 (L solar/M solar). Young et al. (1989, Ap. J. Suppl. 70, 699) have found that these parameters are well correlated. For Ho = 50 km/sec/Mpc and a conversion factor of N(cm**-2) = 3.5x10**20 I(CO) (K km/sec), the molecular hydrogen masses of the galaxies range from 3x10**9 to 3x10**10 solar masses, with one upper limit of 8x10**9. We have calculated the star formation rate for a Salpeter IMF from 0.1 to 100 solar masses from the far infrared luminosity using the relation developed by Thronson and Telesco (1986, Ap. J. 311, 98): dM/dt = 6.5x10**-10 L(FIR) solar masses per year. The molecular hydrogen mass has been divided by the deduced star formation rate to see how long the molecular hydrogen would last if it continued to be consumed at the current rate. The hydrogen lifetimes are all less than 4x10**8 years. Even for much lower gas consumption rates or substantial additions to the molecular gas supply, all seven galaxies would meet the defining characteristic of a star "burst": there is not enough gas to support the current star formation rate for a Hubble time.

CONCLUSIONS

The H alpha line images clearly confirm that star formation is occurring in the centers of these early-type galaxies at a high rate. The far infrared luminosities and molecular hydrogen masses imply that the star formation is occurring in a burst that cannot be sustained at the current rate for longer than several hundred million years, if a full Salpeter IMF is formed.

The line emission region is ring-like in morphology in the two most strongly barred galaxies, UGC 03265 and UGC 03201. Several theoretical studies have shown that a barred galaxy can form a ring of molecular gas at an inner Lindblad resonance (e.g., Combes and Gerin 1985, A. and A. 150, 327). This gas presumably forms stars when compression produces sufficient densities.

UGC 12618, the Arp galaxy visibly interacting with a Seyfert galaxy, appears to be a classic case of a tidally induced central star-burst. Many studies have shown that such interactions can channel gas towards the nucleus.

Although the remaining galaxies have comparably strong central star-bursts, judging from their far infrared luminosities and "warm" F(100 micron)/F(60 micron) colors, the causes of the bursts in these galaxies are not as obvious. Some of them have irregular outer isophotes and (apparent) companions, but the companions are generally relatively more distant in projection or smaller than the companion of UGC 12618. Some of the galaxies have bars that are less prominent than that in UGC 03265, and some may have oval distortions or bars that could only be seen in the near infrared.

The burst in UGC 12575, the "diamond ring" galaxy, may require a theory other than tidal disturbance or bar-driven dynamics. The galaxy is fairly isolated and not apparently barred, and the burst is distinctly off-center.

This work was supported in part by NASA grant NAG5-1630.

*Probing the Optical Depth of Spiral Galaxies using Multi-Waveband Observations**

Rhodri Evans

Department of Physics and Astronomy

University of Wales, Cardiff, CF2 3YB, UK†

Abstract

The questions of the optical depth and extinction of galaxies obviously have far-reaching implications; from determining the true stellar content and baryonic mass of galaxies to the origin of the major component of their far infrared radiation. We have investigated whether the reddening of stars can be used to determine the amount and extent of obscuring dust. We find that the amount of reddening is very sensitive to the assumed geometry. The usually assumed case of a screen of dust between the observer and the star produces, for a given optical depth, the maximum amount of reddening. However, for external galaxies such a geometry is clearly wrong. More realistic geometries where the dust and stars are uniformly mixed (a 'slab') or where the dust is sandwiched by unobscured stars (a 'sandwich') produce significantly less reddening. For the slab geometry the reddening rises to a maximum value as the optical depth is increased, and for a sandwich geometry the reddening will actually decrease as the optical depth becomes larger (see Figure 1). The reddening vectors produced by these realistic geometries are compared to multi-waveband observations of individual regions of a sample of eight galaxies. We find evidence for significant optical depths in the central regions of some

---

*This work forms part of a thesis entitled *"Opacity in Spiral Galaxies"* submitted to the University of Wales in Aug. 1992.

†Present address: Dept. of Physics and Astronomy, University of Toledo, Toledo, OH 43606.

of these galaxies, but optical depths of less than unity at ~ 2 scale lengths from the centres. The optical depths derived are in good agreement with other tests such as the measured hydrogen column densities and the far infrared to blue light ratios. However, whereas these two latter approaches are insensitive to the relative distributions of the stars and the dust, the amount of reddening seen in these eight galaxies strongly suggests that the dust to stellar scale height ratio ξ is ≥ 0.5. We find typical blue band extinctions of $A_B = 0.75$-1.0, a factor of 3-4 higher than the RC2 value.

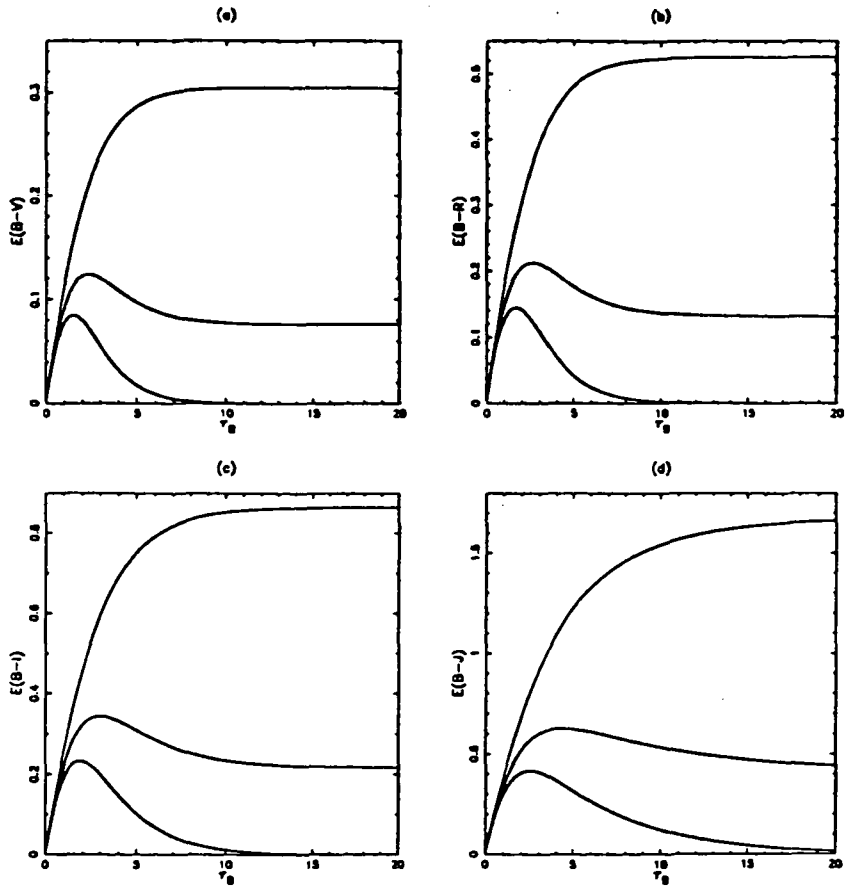

Fig. 1: The colour excess for realistic geometries as a function of B-band optical depth τ_B. In each plot the upper curve is the 'slab', the middle curve is a 'sandwich' with $\xi = 0.25$ and the lower curve is wtih $\xi = 0$.

SPOKES IN RING GALAXIES

Lars Hernquist & Melinda L. Weil
Board of Studies in Astronomy and Astrophysics, University of California, Santa Cruz, CA 95064

Catalogues of peculiar galaxies include several galaxies with luminous rings surrounding nearly vacant areas. Although rare compared to normal galaxies, these "ring" galaxies likely comprise between $\sim$ 0.02-0.2% of all spirals (Athanassoula & Bosma 1985). Many of these objects contain other peculiarities. A noteworthy example is the Cartwheel galaxy, designated AM 0035-335 by Arp and Madore. In addition to a dominant outer ring, the Cartwheel has a more compact inner ring near its center which is linked to the outer one by spoke-like features.

Motivated by observations that many ring galaxies have nearby companions, early simulations of ring formation focussed on interactions between large spirals and less-massive companions. These simulations demonstrated that rings can be produced in disks by an intruder when the stars in the primary rebound radially in response to the gravitational perturbation of the companion (Lynds & Toomre 1976, Theys & Spiegel 1977). Recent work has included the effects of self-gravity, which acts to increase the definition of ring structures. But more complex morphologies, such as the Cartwheel, probably cannot be reproduced without considering gas dynamical effects as well.

Indeed, the Cartwheel galaxy appears quite rich in gas. Its outer ring contains $\gtrsim 10^8 M_\odot$ of ionized gas and its nucleus contains $\lesssim 10^{11} M_\odot$ of neutral gas (Fosbury & Hawarden 1977). Moreover, infrared and visual observations suggest that the color of the Cartwheel shifts radially outwards from red to blue, indicating that star formation has occurred during the expansion of the ring (Appleton & Marcum 1992, Higdon 1992).

We examine the response of self-gravitating primary galaxies consisting of dark matter halos and disks containing both stars and gas to collisions with less massive companions. The primaries were constructed using a technique developed by Hernquist (1991,1992a,b) which makes it possible to realize multi-component systems that are stable and virtually in precise equilibrium. A total of 65,536 particles were employed to represent the primary and 4096 to represent the companion. Half the particles in the primary comprise its halo and the other half its disk. Gas makes up 10% of the disk mass and is represented by 8192 of the disk particles. A system of units is used where the gravitational constant, total disk mass, and disk exponential scale length are unity. Scaling to values appropriate for the Milky Way implies that unit time and velocity correspond to $\sim 1.3 \times 10^7$ years and 260km/sec, respectively. The vertical scale thickness of the disks is 0.2; the halo has core radius of 1 and truncation radius of 10. The gas is initially distributed with the same radial and vertical profiles as the stars but with a vertical scale-thickness of 0.057. A companion with a mass of 1 and scale-length of 0.5 engages in a collision along the initial symmetry axis of the disk. The halo has a mass of 2.9 so that the primary is nearly four times as massive as the companion. The center of masses of the disk and companion are initially separated by 15 length units, where tidal effects are negligible, and approach one another at escape speed. Simulations were performed using a hybrid code capable of evolving systems containing both collisionless material and gas (TREESPH; Hernquist & Katz 1989).

The primary motivation of the present study is to determine whether effects associated with dissipation and self-gravity can account for the unusual morphology of the Cartwheel galaxy. Figure 1 shows the evolution of the gas down the rotation axis of the disk for a few significant times. At late times in the simulation, the disk begins to resemble the Cartwheel. As in other studies of the ring phenomenon, the passing of the companion through the disk induces large radial motions in its stellar distribution. These epicyclic oscillations eventually drift out of phase giving rise to a radial density wave whose crest is reminiscent of observed rings. Initially, the gas responds in a similar manner to the stars, sporting an outwardly propagating ring by t=15. Unlike that in the stellar distribution, however, the ring in the gas appears to be a true material structure. This is due both to shock dissipation in the gas, which allows it to accumulate in thin ridges, and self-gravity which temporarily maintains these features.

As the gas is compressed into a thin ridge near the center of the stellar ring, it becomes mildly self-gravitating and is subject to the "bead" instability. By time t=20 the inner parts of the gas ring have already fragmented into amorphous clumps. Since these clumps partly comprise gas from the inner parts of the disk, which has little angular momentum, they eventually begin to fall back towards the center of the disk. Owing to differential rotation and the effects of tidal forces, the clumps do not remain intact as they fall towards the center and are sheared into radial structures having some curvature. During the final stages of the encounter these features are rather similar in appearance to the spokes in the Cartwheel galaxy. In addition, a second ring begins expanding outwards from the center.

Although we have not attempted to optimize our fit to the Cartwheel, a comparison shows that the spokes in both the Cartwheel and our model are quite clumpy and the material comprising them is not distributed smoothly along their lengths. Moreover, the region between the inner and outer rings in is nearly vacant, aside from the spokes, and both the simulation and the Cartwheel exhibit a secondary inner ring. A failing of the model is the fact that the contrast between the outer ring and the remainder of the galaxy is much greater for the Cartwheel than the simulation. The contrast between the outer ring and inner regions of the galaxy would likely be boosted if the density of gas were to decline less steeply with radius than in the models we constructed.

The simple models used by early investigators reproduce the gross aspects of ring galaxies. The calculation described here, while technically advanced, demonstrates that, for the most part, restricted approaches are adequate to capture most of the essential dynamics. Only if both self-gravity and gas-dynamics are included are the results altered qualitatively. As the gas is compressed in a thin ring, its self-gravity enables it to form transient, but coherent structures which evolve into features which resemble the spokes in the Cartwheel galaxy. Observationally, our models can be further tested by measuring color gradients in the Cartwheel's disk. One might expect the inner regions to be redder than the outer ones since the gas near the center was compressed and fragmented earlier than that in the outer ring. Recent observations suggest that this may in fact be the case. Additional constraints on our models would be provided by detailed observations of gas in the Cartwheel, especially if they establish a physical link between the Cartwheel and one of its neighbors.

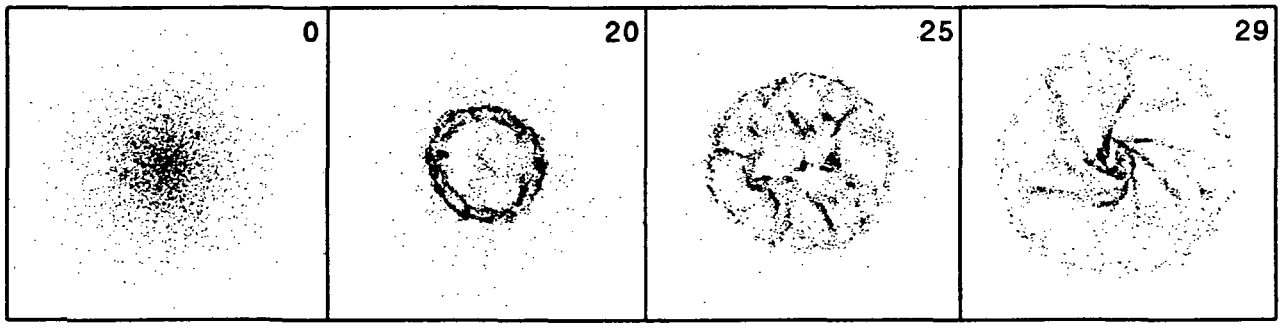

FIGURE 1. Time evolution of gaseous component of primary, seen face-on to the disk plane. Panels measure 15 length units per edge; time is indicated in upper right-hand corner of each.

REFERENCES

Appleton, P.N. & Marcum, P.M., 1992, preprint.
Athanassoula, E., & Bosma, A., 1985. ARA&A 23, 147.
Fosbury, R.A.E. & Hawarden, T.G., 1977. MNRaS 178, 473.
Hernquist, L., 1991. Int. J. Supercomp. Appl. 4, 77.
Hernquist, L., 1992a. ApJ, in press.
Hernquist, L., 1992b. ApJ, in preparation.
Hernquist, L. & Katz, N. 1989. ApJS 70, 419.
Hernquist, L. & Weil, M.L. 1992, in preparation.
Higdon, J.L., 1992, preprint.
Lynds, R. & Toomre, A., 1976. ApJ 209, 382.
Theys, J.C. & Spiegel, E.A., 1977. ApJ 212, 616.

GAS IN MERGING GALAXIES

John E. Hibbard, Jacqueline H. van Gorkom, Steve Kasow, Columbia University.
David J. Westpfahl, New Mexico Institute of Mining and Technology.

SUMMARY

We present observations of the neutral hydrogen, ionized hydrogen, and starlight of galaxies chosen from the "Toomre Sequence" of merging galaxies (Toomre, 1977, in "The Evolution of Galaxies and Stellar Populations"). This sequence is meant to represent the progressive stages of the merger of two disk galaxies into a single elliptical-like remnant. The galaxies in this study span the full range of this sequence.

The stars and atomic gas are very differently distributed, with the stars more widely distributed at early stages, and the gas much more widely distributed at later stages. Large quantities of neutral gas are sent to large radii ($\gtrsim$100 h^{-1}kpc), and still persist even after the central remnant has relaxed to an $r^{1/4}$ light profile.

There are a few times $10^9 M_\odot\, h^{-2}$ of both molecular and atomic gas in each of these systems. Throughout the different stages, about half of the total gas mass lies within the galaxies' optical bodies. The fraction of this mass that is in neutral hydrogen drops rapidly in the later stage mergers, suggesting that atomic gas is processed into molecular gas, stars, and hot gas during the merger and resulting star burst.

Star formation occurs at all stages of the interaction, both within the tails and in the central bodies. In the early stages, the Hα shows many arcs and plumes. In the late stages, there are large H II regions in the tails which are associated with large quantities of neutral hydrogen. There is always a very good correlation between optical, Hα, and H I peaks, with $N_{HI} \gtrsim 3\times10^{20}$cm^{-2} at the location of the H II regions in the tails.

TRENDS

Early Stages: Arp 295 (fig. 1a), NGC 4676="The Mice" (fig. 1b).
Selection: Clearly separated disks bodies; Connecting luminous bridge; Tails or counterarms reaching a few optical diameters (D_{opt}) in length.
Optical: Fainter, thicker optical "plumes" out to several D_{opt}. More widely distributed than H I. **Hα:** Found mostly in main bodies, with loops and plumes, especially along the minor axis (see Arp 295 north, NGC 4676 north). Almost no Hα found in bridges. Hα clumps in tails. **H I:** Confined to bodies and brighter tidal features. Less extended than optical. Reaches a few times D_{opt}. $N_{HI}\gtrsim3\times10^{20}$cm^{-2} at regions with optical and Hα clumps. We note that the break in the tail of NGC 4676 south and subsequent clump in H I is very similar to the H I morphology of NGC 4038/9 = "The Antennae" (Mahoney, van der Hulst, and Burke, in preparation). The later has a very blue dwarf at the end of the arm, whereas in NGC 4676S we find several H II regions.

Middle Stages: NGC 520 + UGC 957 system (fig. 1c).
Selection: Distinct optical bulges embedded in a common luminous envelope; Long, luminous tails. (Note: NGC 4038/9, referenced above, and NGC 3256 and NGC 1467 (English, in preparation) also fall in this category and have similar data available).
Optical: Optical tails end long before H I. Sharp optical cutoffs. Extremely IR luminous. **Hα:** Again, find most Hα in the bodies, with plumes and loops and emission along the minor axis. Also in the regions between the two bulges. Still seen in clumps in tails. **H I:** Gaseous arm is much, much longer than the optical features, with a total H I cross-section 20 times the optical. Central H I absorption. H I minimum along the minor axis, possibly related to the Hα plumes. Column densities $\gtrsim4\times10^{20}$cm^{-2} at regions with optical and Hα clumps (southern tail, at location of UGC 957).

Late Stages: NGC 3921 (fig. 1d), NGC 7252 (fig. 1e).

Selection: Two tails, but only one body. $r^{1/4}$ luminosity profile in the remnant.
Optical: Long, fainter tails, several times D_{opt} in length, which end abruptly. Many loops and shells surrounding the remnant body. **Hα:** The ionized gas in the central remnant is much more smoothly distributed than in the earlier stages, though there are still many knots. There is either Hα or blue colours at the base or spine of the tails. The end of the optical tails coincides with a bright H II region in each of these systems. **H I:** Most, if not all, of the neutral hydrogen is in the tails (the gas which appears near the central regions

can be kinematically associated with the outer regions). Central regions H I poor, CO rich. The end of the optical tails, with the H II regions, have large neutral gas enhancements, with $N_{HI} \gtrsim 4 \times 10^{20} cm^{-2}$. The gaseous tails, however, extend up to twice as far as the optical tails beyond these points.

fig 1a: Arp295
early stage

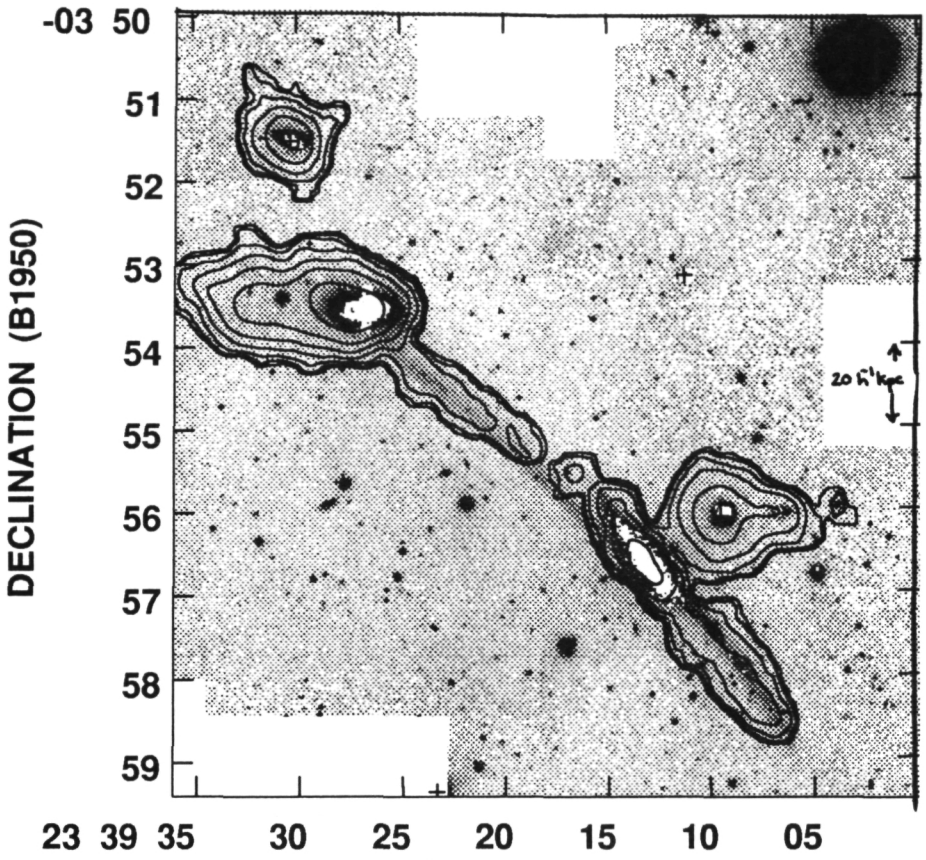

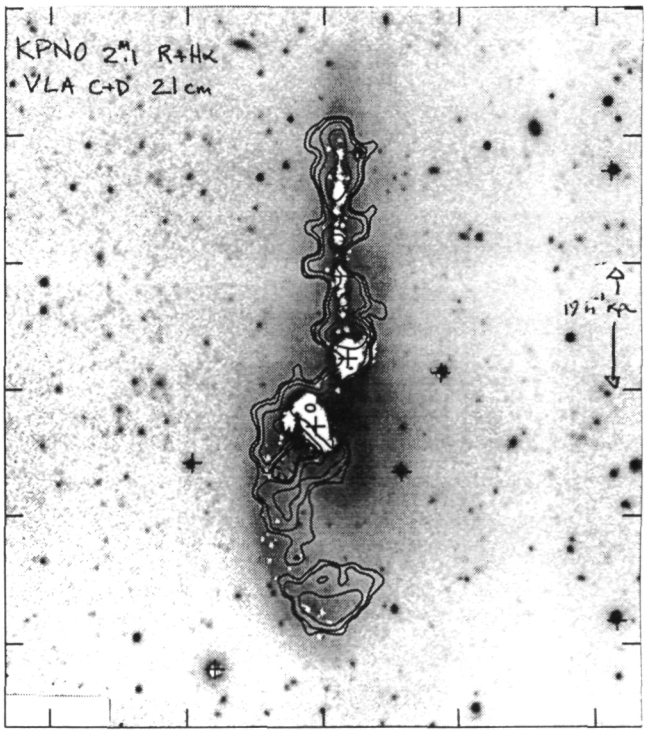

Figure 1 a-e: The 5 interacting systems: Arp 295, NGC 4676, NGC 520, NGC 3921, and NGC 7252. The greyscale shows the deep *KPNO* and *CTIO* broad band *R* images delineating the faint stellar structures, the white shows *KPNO* narrow band Hα imagery, and the contours show *VLA* C+D array observations of the neutral hydrogen. N_{HI} contours are drawn at the following levels, in intervals of $10^{19} cm^{-2}$: 1a,b: (5,10,20,40,80,160); 1c: (2,4,8,16,32); 1d-e: (5,10,15,20,25,30,40).

fig 1b
NGC4676
early stage

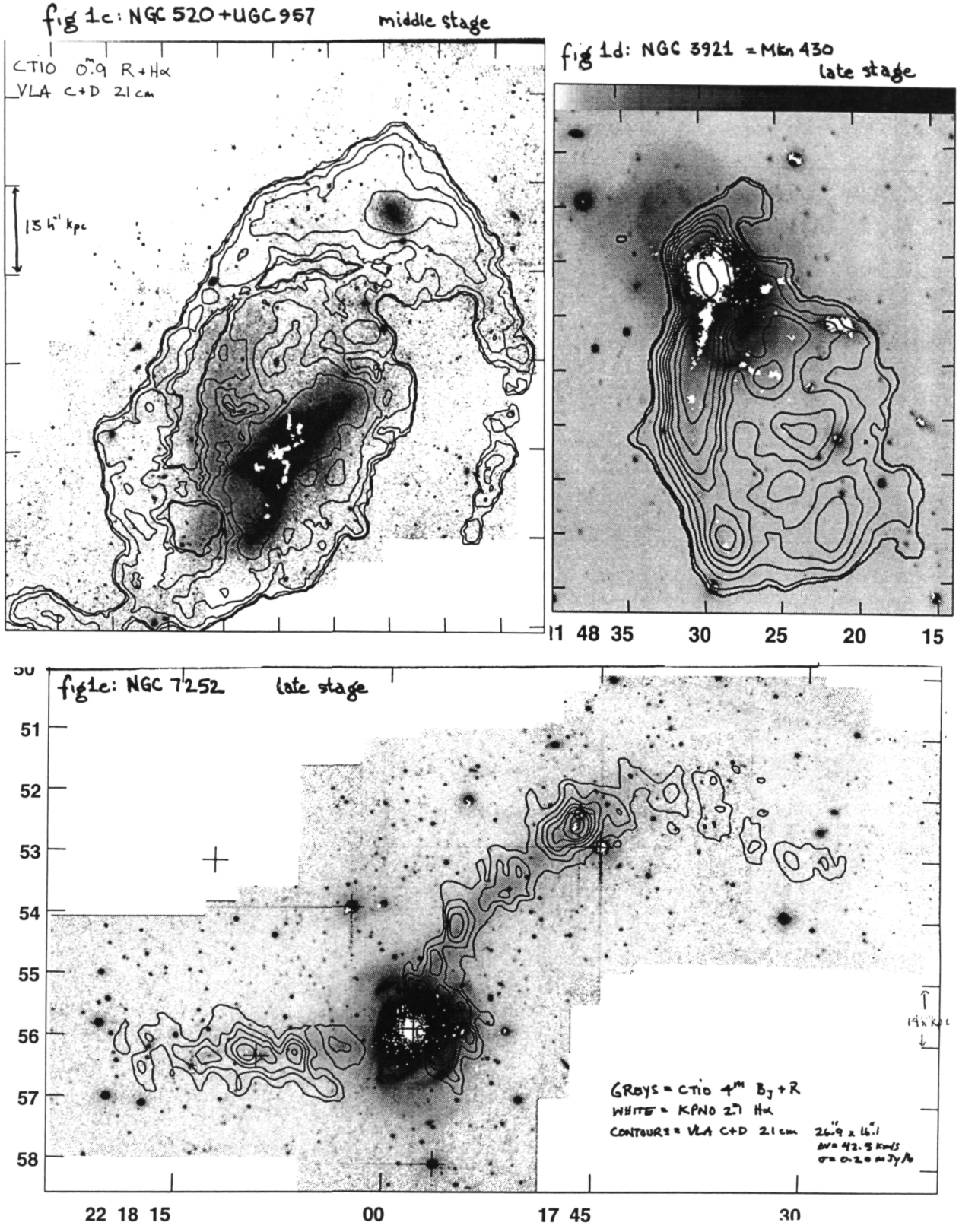
fig 1c: NGC 520+UGC 957
middle stage
CTIO 0.9 R+Hα
VLA C+D 21 cm
13 h⁻¹ kpc
fig 1d: NGC 3921 = Mkn 430
late stage
11 48 35
30
25
20
15
fig 1e: NGC 7252
late stage
50
51
52
53
54
55
56
57
58
22 18 15
00
17 45
30
GRays = CTIO 4m Bj+R
WHITE = KPNO 2.1 Hα
CONTOURS = VLA C+D 21 cm
26.9 x 16.1
ΔV = 42.3 kms
σ = 0.20 mJy/b

The ISM in the M82 Starburst

STEVEN LORD
NASA/Ames Research Center

ABSTRACT

We have observed [O I] (63 μm) and [Si II] (35 μm) in the central 44" (700 pc) of the starburst galaxy M82. The luminosities in these transitions are 7.1×10^7 $L_\odot$ and 6.2×10^7 $L_\odot$, respectively, which are each $\sim$ 0.15% of the bolometric luminosity from this region. The ratios of [O I] line luminosity to [O III], [Si II] (35 μm) and to bolometric luminosities in M82 are similar to those in M42, M17, and Sgr A. These similarities, and the association of the bulk of the [O I] and [Si II] emission with the ionized emission, suggest that the dominant emission mechanism for [O I] and [Si II] in M82 is the same as in these Galactic regions, namely warm gas photodissociated by UV flux from the OB stars responsible for the nearby H II regions. We argue that shock or X ray heated gas or H II plasma is a minor contributor to the intensities of these fine structure lines.

Both the [O I] (63 μm) and the [Si II] (35 μm) spectrum show an asymmetric line profile indistinguishable in shape from those of the [O III] (52 and 88 μm) and [N III] (57 μm) lines and similar to that of the more extended [C II] 158 μm line measured previously in M82. We detect two distinct velocity components, which we attribute to emission from two regions at either end of the central bar, where the bar connects to an orbiting torus of neutral gas seen in H I and CO J=1-0. We model separately the two velocity components and derive the physical conditions in these two regions by the method described in Wolfire *et al.* (1990).

The clouds in these regions are small, R$\sim$1–2 pc, have warm neutral gas surfaces, T$\sim$ 200 K, and are concentrated with volume filling factors of $\sim$ 0.02 and area filling factors of 1–5. The entire central region (R$\sim$ 700 pc) is characterized by a large number, $\sim 5\times10^4$, of $2\times10^3 M_\odot$ clouds with surface densities of $\sim 3\times10^4$ cm^{-3}, illuminated by FUV fluxes 10^4 times the average local interstellar value for the Milky Way. These clouds reside in the harsh conditions

of a starburst nucleus, with photoevaporation times of $\sim 10^6$ yr, and collision timescales only about an order of magnitude longer.

The gas phase Si abundance is high, nearly solar, and the enrichment is probably caused by supernovae-ejected elemental Si or by the destruction of silicate grains by fast supernovae-driven shocks.

DYNAMICS OF THE BARYONIC COMPONENT IN HIERARCHICAL CLUSTERING UNIVERSES

Julio F. Navarro
Physics Department
University of Durham, Durham DH1 3LE, England.

I present self-consistent 3-D simulations of the formation of virialized systems containing both gas and dark matter in a flat universe. A fully Lagrangian code based on the Smoothed Particle Hydrodynamics technique and a tree data structure has been used to evolve regions of comoving radius 2-3 Mpc. Tidal effects are included by coarse-sampling the density field of the outer regions up to a radius ~ 20 Mpc. Initial conditions are set at high redshift ($z > 7$) using a standard Cold Dark Matter perturbation spectrum and a baryon mass fraction of 10% ($\Omega_b = 0.1$). Simulations in which the gas evolves either adiabatically or radiates energy at a rate determined locally by its cooling function were performed. This allows us to investigate with the same set of simulations the importance of radiative losses in the formation of galaxies and the equilibrium structure of virialized systems where cooling is very inefficient. In the absence of radiative losses, the simulations can be re-scaled to the density and radius typical of galaxy clusters. A summary of the main results follow.

We confirm that, in the absence of radiative losses, the spatial distribution of the gas and dark matter in a virialized system is very similar. The gas and dark matter density profiles can be adequately represented by the inner parts of an isothermal sphere ($\rho \propto (1 + (r/r_{core})^{-3\beta_f/2}$, with $\beta_f \sim 0.7$-0.9) although the gas is not completely isothermal ($T_{gas} \propto r^{-1/3}$). No evidence is found for the existence of a core radius in the gas component beyond that artificially imposed by the spatial resolution of the simulations. The average gas temperature matches well the virial temperature of the system ($\beta_T = \sigma^2_{DM}/T_{gas} \sim 1$). If an X-ray emission-weighted gas temperature is used no β discrepancy is present even after a major merger, when the system is far from equilibrium ($\beta_T \sim \beta_f$). This suggests that the β-discrepancy in galaxy clusters is not mainly due to incomplete thermalization of the gas, as previously proposed, but actually reflects either poor velocity dispersion estimates or legitimate low gas temperatures (perhaps due to the effects of cooling).

Radiative cooling is extremely important on galaxy scales. Most of the gaseous mass cools very efficiently at high redshifts and is locked up at the center of small dark matter clumps, where it rapidly settles onto centrifugally supported disk-like structures. Due to their high density, these baryonic cores are hardly disrupted by shocks and may survive longer the mergers of their surrounding dark matter halos. Simple models based on cooling radius arguments at $z = 0$ seriously underestimate the mass of these disks. In this scenario, a galactic disk grows by the mergers of dense gas clumps driven to the center by dynamical friction rather than by the quite infall of material envisaged in earlier models. This process involves a significant loss of angular momentum and large collapse factors. The rotation velocity of the disks is found to systematically overestimate the circular velocity of the surrounding halo (up to 50% for $\Omega_b = 0.1$). The surface density structure of the disks is reasonably fit by an exponential profile and its rotation velocity is flat up to ~ 5 disk scale lengths, in good agreement with the observational properties of disk galaxies.

Star formation can be added in a realistic manner because the thermodynamical properties of the gas are known everywhere, although uncertainties regarding the efficiency of supernovae feedback can not be avoided. Most major galaxies formed through mergers of smaller subunits at recent redshifts ($z < 3$). The derived star formation rates (SFR) were about three times higher at $z \sim 1$ than at the present time, lending support to the interpretation of excess blue counts as due to evolution in both galaxy number density and average star formation rates. The stellar content of halos which have undergone a recent merger ($z < 0.5$) have dynamical and chemical properties which compare favourably with observations of elliptical galaxies.

Figures: 1st row) Gas and dark matter density profiles together with isothermal β model fits (no cooling). 2nd row) Face-on and edge-on views of a gaseous disk at $z = 0$. Box is 100 kpc across (with cooling). 3rd row) Surface density profiles with exponential fits with disk scale lengths 3 and 5 kpc (inner 25 kpc). Rotation velocity of the disk and circular velocity of the system (inner 100 kpc). Insert is a blow-up of the inner 30 kpc.

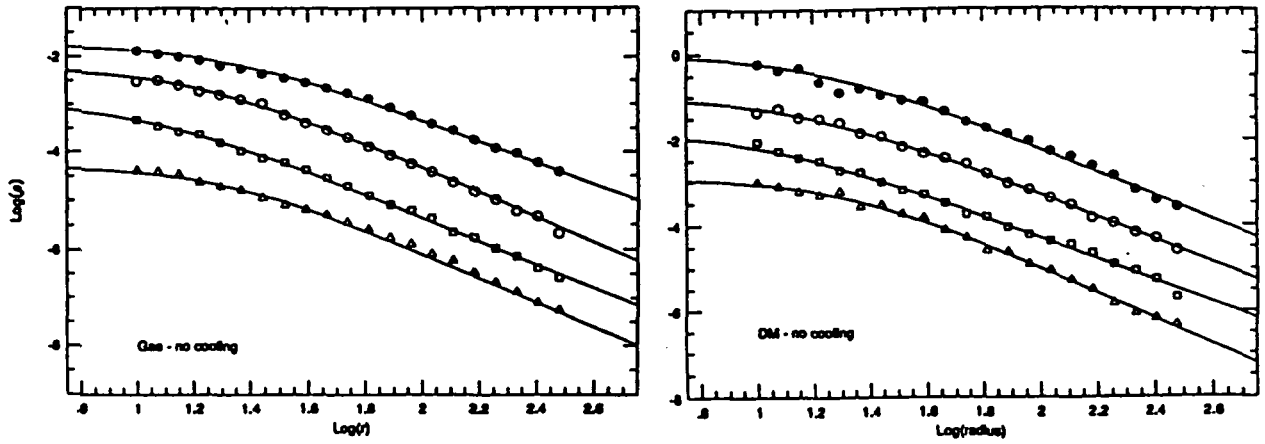
Log(ρ)
Gas - no cooling
Log(r)
DM - no cooling
Log(radius)

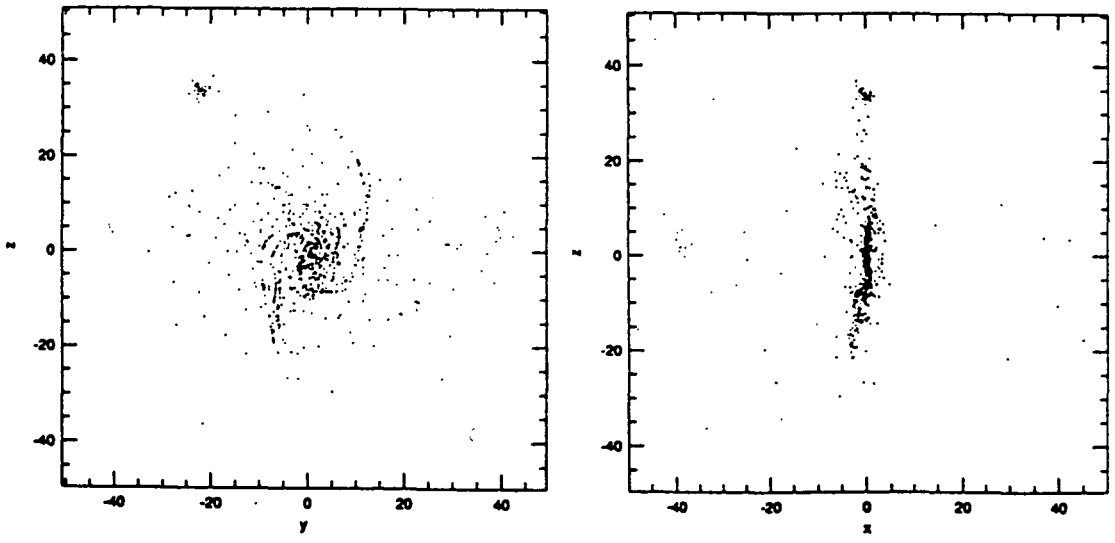
z
y
z
x

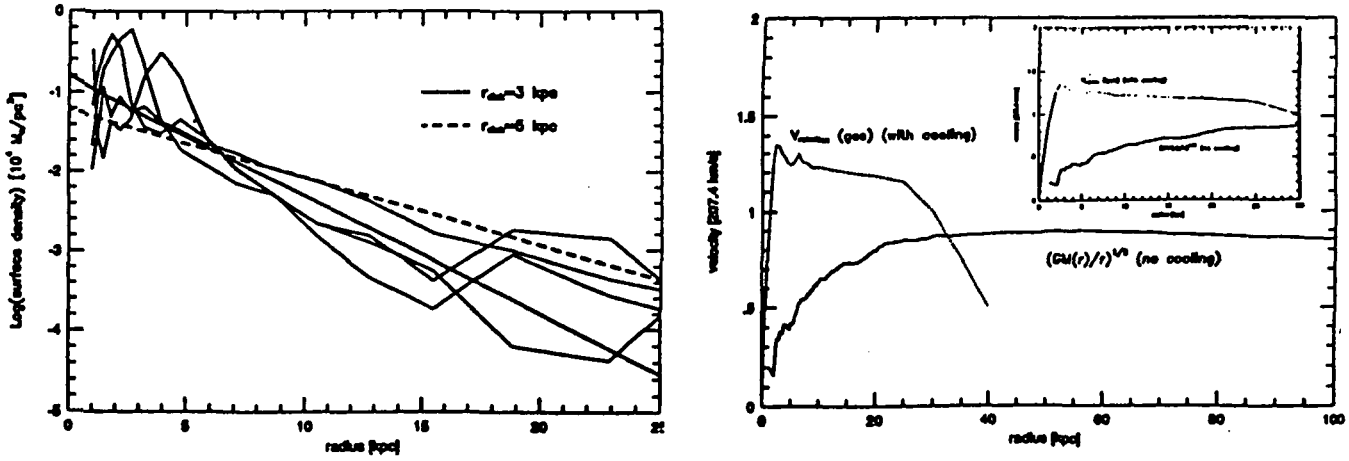
Log(surface density) [10⁶ M⊙/pc²]
r_core=3 kpc
r_core=6 kpc
radius [kpc]
velocity [207.4 km/s]
(GM(r)/r)^1/2 (no cooling)
radius [kpc]

The effects of flaring in HI on the observed velocity field of spirals.

Rob Olling, J.H. van Gorkom
Columbia University, New York

Abstract

This work is part of a larger project in which we want to determine the shapes of dark halos around spiral galaxies. Rotation curves 'probe' the halos in the radial direction. The derived halo mass distributions are badly constrained though (i.e. van Albada et al., 1985). The local halo densities fully determine the width of the gas distribution once the gaseous velocity dispersion is known. There where the dark halo dominates, the Full Width at Half Maximum (FWHM) of the gas layer is proportional to $(\rho_{halo})^{-0.5}$. Therefore, measuring the width of the gas layer probes the halo density directly.

In a dark halo dominated potential, the FWHM of the gas layer increases linearly with radius. This increase of the thickness of the gas layer is known as 'flaring'. Flaring has been found inside the stellar disk (Rupen, 1991). Beyond the edge of the stellar disk, the analysis is hampered by the onset of the warp. Since the galaxy we are studying, NGC 4244, has no significant warp we hope to extend Rupen's analysis into the halo dominated regime.

The usual method to derive a roation curve from an observed 2-dimensional velocity field is to assume that the hydrogen is distributed in infinitely thin rings (eg Begeman, 1989). For a flaring disk, any line of sight samples many different parts of the galaxy, all having different densities and projected velocities. In order to fully exploit the information contained in the gas distribution, we have to understand the effects of flaring on the observables (the spectrum for each point of the galaxy). We have investigated the effects of a flaring disk on the observed velocity field.

It is is obvious that the largest (kinematical) effects are to be expected for low density dark halos at large inclinations.

For low mass galaxies we expect that the flaring of the HI layer will have a major effect on the observed kinematics.

For galaxy with intermediate $V_{max,halo}$ seen at intermediate inclinations, one *overestimates* $Vsin(i)$ typically by a few percent.

For more massive galaxies, any effects arising from the flaring HI layer are minuscule unless the inclination is not too far from 90 degrees.

Introduction

The FWHM of an isothermal gas layer inside the optical disk increases exponentially with distance from the center (Rupen 1991). He shows that (for NGC 4565) the volume mass density decrease is consistent with a constant mass to light ratio for the stars.

We are interested in the flaring of the gas layer beyond the stellar disk. An isothermal gas layer in hydrostatic equilibrium with a dominant dark halo will have a Gaussian vertical distribution. The FWHM of the gas layer is proportional to $(\rho_{halo})^{-0.5}$. For an isothermal halo with $\rho_{halo}(R) \propto 1/R^2$ the FWHM thus increases linearly with radius (under the assumption of a constant gaseous velocity dispersion).

Although very little is known about the shapes of dark halos, there is at least one example (NGC 4650A) where the halo appears to be flattened (Sackett, 1992). The volume density of such a flattened halo is increased with respect to the non-flattened case. Measuring the width of the HI layer will thus set limits on the allowed flattening of the dark halo.

We have constructed a (computer) model which calculates a spectral-line HI cube. Input to this model are the volume mass distributions of the dark and luminous matter and the surface density of the gas. The distribution of the gas is found by solving the equation of hydrostatic equilibrium in the appropriate 'ambient' potential. We use this model to calculated the 'observed' velocity field.

Discussion

To derive the velocity field, some kind of average velocity has to be assigned to each point of the galaxy. One has been doing this by calculating the intensity weighted mean velocity or by making Gaussian fits to to the velocity spectrum at each point. For thin disks either procedure works well, but for thick disks both procedures will return erroneous results. The degree of error depends on the thickness of the hydrogen layer. Indeed for massive galaxies seen at intermediate inclinations, thick disk effects on the observed velocity filed are minimal. The effects of flaring become more significant with increasing inclination and decreasing halo density. To illustrate the effects of a flaring disk, we present in Figure I the side view of a flaring HI layer in an intermediate density dark halo potential seen at an inclination of 70 degrees.

Certainly for less massive galaxies seen at large inclination one needs to derive the thickness of the hydrogen layer, the rotation curve and the total mass distribution simultaneously.

We have used Begeman's (1987) mass model for NGC 3198 to study the effect of flaring in more massive galaxies. We took the rotation curve to be constant for easier interpretation of the calculated velocity field. The very low flaring angle for NGC 3198's dark halo, $\alpha \approx 2.7$ degrees, predicts little or no effects on both the velocity field and the derived rotation curve. This is observed to be true for inclinations of 70 degrees and lower. When inclining the model to 80 degrees, we find that the calculated velocity field shows the characteristic outward curving iso velocity lines (Figure II). The instrinsically flat rotation curve is turned into a slowly rising one Figure III.

We would like to point out that for a falling rotation curve the effects are more severe since not only the gradient in the projection factor, $\cos(\theta)$, but also the gradient in the rotation curve will affect the observed 'average' velocities.

Acknowledgments

We would like to thank Kor Begeman's for his excellent velocity field fitting program and Daniel Puche for implementing it in AIPS.

Albada, T.S. van, Bahchall, J.N., Begeman, K. and Sancisi, R. 1985, *Ap. J.*, **295**, 305.
Begeman, K, 1987, Ph. D. Thesis, University of Groningen
Begeman, K, 1989, Astron. Astrophys., **223**, 47, 1989
Rupen, M.P., 1991, Ph. D. Thesis, Princeton University Observatory
Sackett, P.D., 1992, private communications

Figure I : an edge-on view of a flaring disk

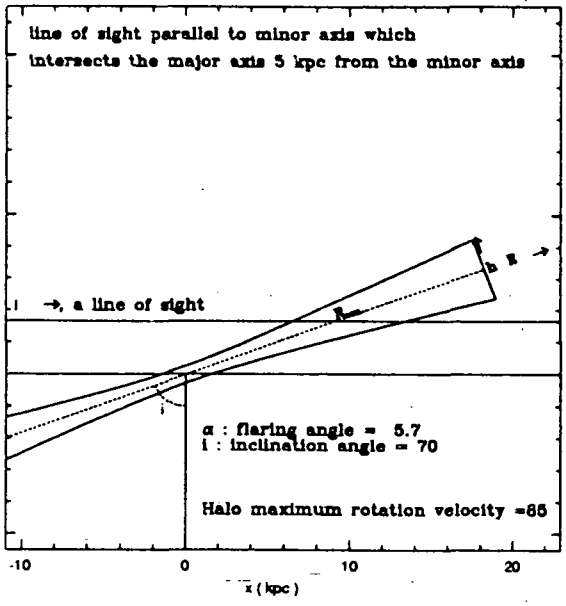

Figure II : Velocity field for 'NGC3918' at i=80

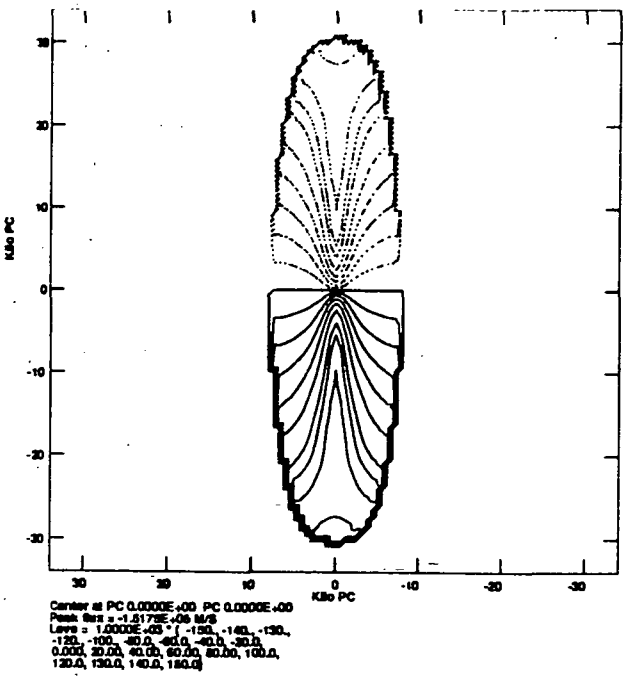

Figure III : Results derived from velocity field

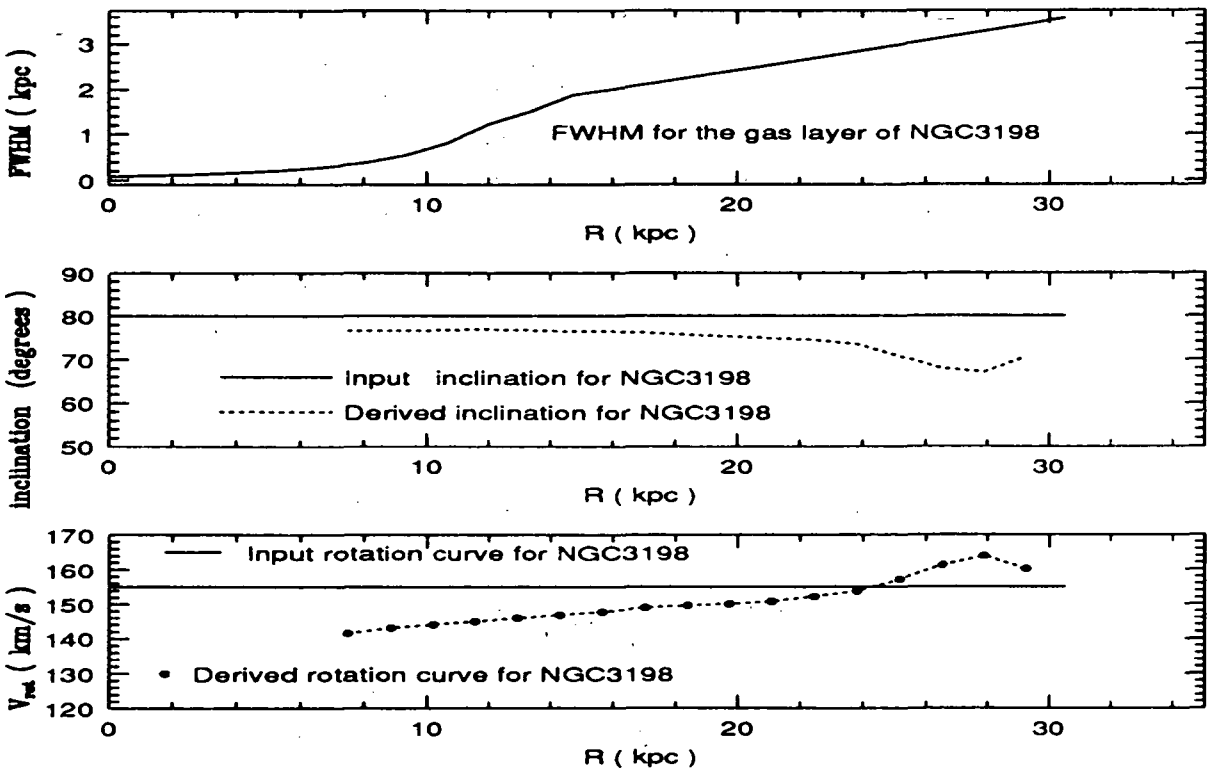

The Lyman Alpha Forest of the High-z Quasar 0000-263

Bryan Penprase[1], Roberto Gilmozzi[2], David Bowen[2], and Piero Madau[2]

[1]IPAC, Caltech MS 100-22, Pasadena, CA 91125.

[2]Space Telescope Science Institute, 3700 San Martin Drive, Baltimore MD 21218.

ABSTRACT. Medium-resolution (δv=45 km s^{-1}) optical spectra of the bright, high-redshift (z=4.1) quasar 0000-263 taken at the ESO 3.5-m NTT telescope were analyzed to determine the distribution of column densities, velocities and line widths of the Lyman-α forest absorption components. The values of N_H, b and z were determined by fitting Voigt profiles to the lines, and convolving with a Gaussian instrumental response function. Over 350 components with log N_H > 13.2 were identified. An analysis of the dependence of the number of components with z reveals that the number evolution of components obeys the power law $dN/dz \propto (1+z)^{\gamma}$, where $\gamma = 0.5 \pm 0.4$ for the sample of 182 lines with log N_H > 14.0. The distribution of component strengths is found to obey $f(N_H) \propto N_H^{-\beta}$, where β = -1.55 for components with $\log(N_H) > 14.7$, and β = -0.68 for the components with $\log(N_H) > 13.5$. A distinct break in the $f(N_H)$ histogram is also observed, at $\log(N_H) \sim 14.7$. The results are briefly considered in the context of theoretical models of quasar Lyman alpha clouds and their evolution.

OBSERVATIONS. Optical spectroscopic observations of the quasar 0000-263 were obtained during two nights at the ESO 3.5-m NTT telescope at Cerro La Silla, Chile. Coadded CCD images of the echelle spectra were flat fielded, cosmic rays were removed, and spectra were extracted and wavelength calibrated. The average FWHM resolution of the spectrograph was 45 km s^{-1}, and the spectrum was sampled at 0.3 Å Intervals. The S/N for the coadded spectrum is estimated to be 10, based on analysis of the line-free region redward of the QSO emission line at 6200 Å. Line-free points of the spectrum blueward of 6200 Å were selected and a 4th degree spline was fitted to remove the continuum. The spectrum, and the continuum fit used are shown in Figure 1. The Lyman-α forest was then analyzed by fitting Voigt profiles convolved with the instrumental response of the spectrograph to the absorption components. The fit chosen was based on the minimization of the residual between observed data and modelled profile, after iterating the parameters N_H,b, and v for each component from an initial component model which was determined interactively. 356 components were found, of which 182 had log(N) > 14.0. The sample should be complete for components with log(N) > 14.0, which is a conservative completeness limit corresponding to an equivalent width threshold of $W_\lambda \sim 700$ mÅ. The components were analyzed to determine if there were statistically significant correlations in the column densities N and Doppler parameter b, and to determine evolutionary trends in dN/dz and in the distribution function of component strengths, $f(N_H)$.

RESULTS. The correlation between N and b values yields a correlation coefficient of R=0.47. The correlation is statistically significant but may be affected by systematic effects intrinsic to line profile modelling of spectra which have many blended components, such as those described by Rauch, et al (1992). After excluding components with $W_\lambda < 0.65$ Å, and b > 90 km s^{-1}, the correlation coefficient was found to decrease to R=0.25. This suggests that the excluded components were responsible for much of the appearance of correlation, although a correlation between b and N for weak components has been predicted from theoretical models of differential ionization of Lyman alpha clouds (Donahue and Shull, 1992).

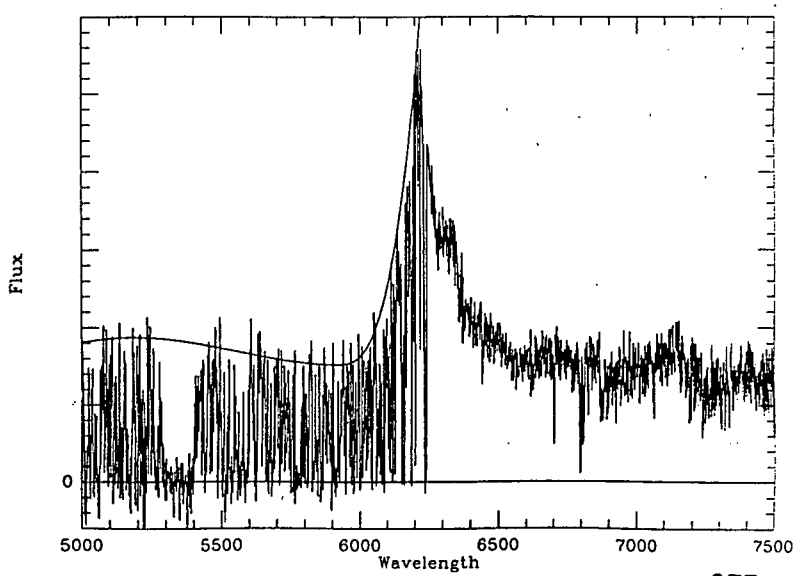

Figure 1: The coadded spectrum of QSO 0000-263, with the continuum fit superimposed. Lyman α components were fit from the wavelengths 5400Å to 6200Å, using modelled Voigt profiles which were convolved with a Gaussian instrumental resolution function, which had a FWHM of δv=45 km s^{-1}.

The distribution function of the component column densities $f(N_H)$ was examined, and the values of $f(N_H)$ for $\log(N_H) > 13.75$ are presented in Figure 2. The function $f(N_H)$ is usually described in terms of a power law $f(N_H) \propto N_H^{-\beta}$, and for the current work we find a value of $\beta = 1.55$ for the strongest components with $\log(N_H) > 14.7$, and a lesser slope of $\beta = 0.7$ for the entire sample. The value of β reported here for the stronger components is consistent with other Lyman α systems, where β is typically 1.5-1.7, (Charlton, et al 1992). While the break in the power law has been predicted by theoretical models to result from changing ionization state of the Lyman α clouds, it may also be due to the weaker lines being incompletely detected due to S/N limitations.

To study the evolution of the number of Hydrogen components N_{comps} with redshift z, we considered redshift intervals of $\delta z = 0.05$ and examined the number of components in each interval. A plot of N vs. (1+z) is shown in Figure 3, for the components with $\log (N_H) > 14.0$. A power law fit was applied to the data, and it was found that $dN/dz \propto (1+z)^{\gamma}$, where $\gamma = 0.5 \pm 0.4$. The fit is shown on Figure 3 with the dashed line. The value of γ derived here is much less than the average value of $\gamma = 2.36 \pm 0.4$ from Bajtlik, Duncan and Ostriker (1988), based on several quasar spectra at the lower redshift redshift range $3.7 > z > 1.7$. The value of $\gamma = 0.5 \pm 0.4$ is however consistent with Lyman limit systems, for which $\gamma = 1.1 \pm 0.4$ for systems with redshifts ranging from $4 > z > 0.4$ (Charlton, et al 1992). It is also worthwhile to note that the value of $\gamma = 0.5$ is consistent with the cosmological model of a constant number of components per unit comoving volume (Sargent, et al 1980; Charlton, et al 1992) where $dN/dz \propto (1+z)/(1+\Omega_0 z)^{1/2}$. For $\Omega_0 = 1$, and assuming pressure and ionization rates constant over the redshift interval considered, the model reduces to $dN/dz \propto (1+z)^{0.5}$, consistent with our observed result. Further observations at higher S/N and at higher spectral resolution are needed to determine if the apparent low value of γ for QSO 0000-263 is indeed real, and whether it does indicate a change in the number evolution of Lyman alpha clouds at high redshift.

References:

Bajtlik, S., Duncan, R.C., and Ostriker, J.P. 1988, *Ap. J.* **327**, 570.
Charlton, J.C., Salpeter, E.E., and Hogan, C.J. 1992, *preprint.*
Donahue, M. and Shull, J.M. 1992, *Ap. J.* **383**, 511.
Rauch, M., Carswell, R.F., Chaffee, F.H., Foltz, C.B., Webb, J.K., Weymann, R.J., Bechtold, J. and Green, R.F., 1992, *Ap. J.* **390**, 387.
Sargent, W.L.W., Young, P.J., Boksenberg, A., and Tytler, D. 1980, *Ap. J. Supp.* **42**, 41.

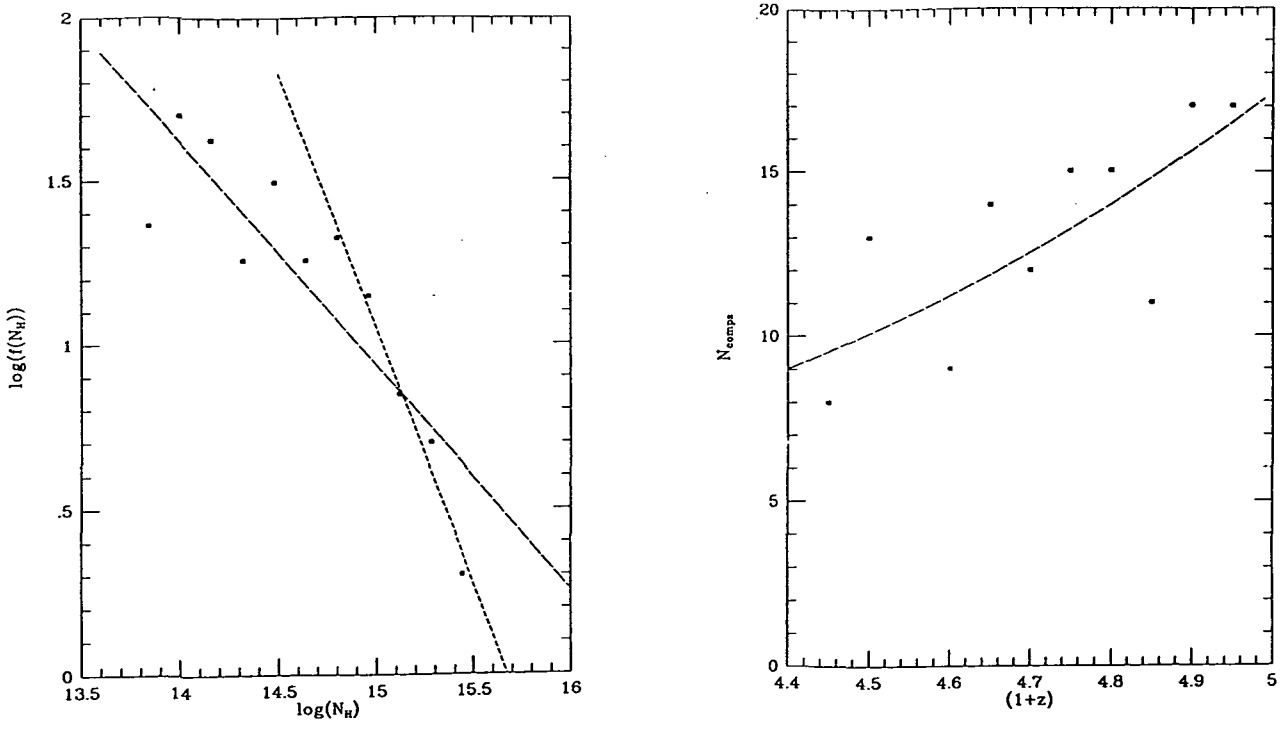

Figure 2: (left) Plot of the histogram function log(f(NH)) with power law fits $f(N_H) \propto N_H^{-\beta}$, with b=1.55 and 0.66.
Figure 3: (right) Plot of the number of components N_{comps} against (1+z), with the best fit $dN_{comps}/dz \propto (1+z)^{0.5}$.

HI in RSA Galaxies

N93-26891

Otto-G. Richter

Space Telescope Science Institute

The original Revised Shapley-Ames galaxy sample of almost 1300 galaxies has been augmented with further bright galaxies from the RSA appendix as well as newer galaxy catalogs. A complete and homogeneous, strictly magnitude-limited all-sky sample of 2345 galaxies brighter than 13.4 in apparent blue magnitude was formed. New 21cm HI line observations for more than 600 RSA galaxies have been combined with all previously available HI data from the literature. This new extentise data act allows detailed tests of widely accepted "standard" reduction and analysis techniques.

Derived global galaxian properties show several clearly non- intrinsic trends with parameters solely related to the observer, like distance, inclination, etc. Separation of the different effects is possible. There are strong indications that procedures commonly used to derive inclinations and internal absorption corrections are far less certain than believed hitherto. From a detailed study of inclinations derived from optical axial ratios it becomes evident that such values are in error by $\pm$ 15-20 degrees, independent of the actual inclination. Even though the error distribution is symmetrical (i.e. the optically derived inclinations don't seem to carry a systematic error) this large error makes claims of exceedingly accurate galaxy distances from the application of the infrared Tully-Fisher relation somewhat suspect.

Variations of the intrinsic flattening of galaxies within the same morphological class can, at best, explain only part of the effect, since the resulting error distribution would not be symmetrical. A more natural (but also more radical) assumption is that of non-circular symmetry in galactic disks at an average ellipticity level of about 0.9 (b/a). While such asymmetries has, so far, paid particular attention to them with regard to the deduction of global properties. If disk galaxies are often triaxial one would expect many objects where the galactic center does not coincide with the geometric center.

Another problematic data correction procedure is the application of a luminosity correction for internal absorption in external galaxies. The RSA correction procedure, based on earlier work by Holmberg, prescribes the largest corrections for early-type (Sa) galaxies with a slow decrease toward late types (Sm/Irr).

The fractional mass contained in the ISM, however, steadily increases from early to late types. If gas-to-dust ratios are meaningful quantities at all, one would expect to see more dust where there is more gas, i.e. in late-type spirals and irregulars. Indeed, it is readily apparent from photographical catalogs of galaxies that late-type galaxies show far more patchiness and dust than early-type galaxies. A correction procedure similar to that proposed by Kodeira and Watanabe seems far more realistic than the traditional formulae. The cause for the apparent failure of the RSA approach might well be variations in bulge-to-disk ratios and disk flattenings among galaxies with similar morphological type. This would cause significant shifts in the Holmberg diagram used to determine the coefficients for the standard formula.

Both corrections discussed above are vital for the Tully-Fisher relation diagram. In those cases where a better determination can be made the scatter around the Tully-Fisher relation seems unaffected. This would imply that a large part of the currently observed scatter is truly intrinsic to the relation. Therefore, results form the Tully-Fisher relation of groups and clusters should be preferred over those using individual galaxies.

A very small but significant fraction of the field galaxy sample so abundant in the RSA appears deficient in neutral hydrogen at levels conventionally associated only with cluster galaxies, i.e. by factors > 2. A more detailed study of the galaxies concerned is needed before any better conclusions can be reached.

Earlier results that the total mass of spiral galaxies (similar to masses among stars) carries the major part ($< 60\%$) of the variance in global properties are confirmed.

Evolution of molecular clouds

M.Sevenster, Sterrewacht Leiden

The evolution of interstellar molecular hydrogen was studied, with a special interest for the formation and evolution of molecular clouds and star formation within them, by a two-dimensional hydrodynamical simulation performed on a rectangular grid of physical sizes on the order of 100 pc. It is filled with an initial density of $\sim$ 1 cm^{-3}, except for one cell ($\sim$ 1 pc^2) at the centre of the grid where an accretion core of $1 - 10^3$ M$_\odot$ is placed. The grid is co-moving with the gridcentre that is on a circular orbit around the Galactic centre and that also is the guiding centre of epicyclic approximation of orbits of the matter surrounding it. The initial radial velocity is zero; to account for differential rotation the initial tangential velocity (i.e. the movement around the galactic centre) is proportional to the radial distance to the grid centre. The rate is comparable to the rotation rate at the Local Standard of Rest. The influence of galactic rotation is noticed by spiral or elliptical forms, but on much longer timescales than selfgravitation and cooling processes. Density and temperature are kept constant at the boundaries and no inflow is alowed along the tangential boundaries.

Cooling is playing an important role in the formation and stability of clouds in a homogeneous medium. Cooling causes a high fragmentation rate because the accreting core is prevented from developing a hot core. For radiative cooling we use an interstellar cooling function for HI gas with an ionization fraction X = 0.1 (Dalgarno & McCray,1972). There is a kink in the curve due to a change of cooling process at T $\sim$ 8000 K that makes an equilibrium between two phases of density and temperature possible (Field, Goldsmith & Habing,1969). Galactic background heating by cosmic-rays, X-rays and grains is calculated for solar neighbourhood conditions (for heavy element- and grain abundances, UV field eg.) (Shull & Woods,1985) and assumed to be a constant parameter throughout the simulation. The heating processes influence the exact form of the two-phase model. Under the influence of a constant, spherical potential well and with radiative cooling and background heating taken into account an apparently random distribution of fragments and filaments of denser, colder matter with hot, low density gas between them arises from a homogeneous medium. Only some of the condensations out of the centre of the potential well are stable and become comparable in size and density to the central core; their exact parameters depend strongly on heating, that maintains temperatures of $\sim$ 20 K in the dense (10 cm^{-3}) clouds.

The research was started with a constant, spherical gravitational potential well imposed on the grid, so the accretion core always kept its original form and mass. These simulations made clear that shapes arise that are far from spherical and mass concentrations that are comparible in size to the accretion core. In order to make a realistic simulation, the potential should be adjusted to the new density distribution. A perturbing self gravitation has been used for this purpose (Icke, 1985), but didn't change the results remarkably. This time a fully self gravitating simulation was made. That means the new potential in a cell is calculated every timestep by adding the attraction of all seperate cells on it. This can be written as a convolution of mass distribution and a point potential, and hence the new potential can easily be found by multiplication in the Fourier domain. As a point potential a smoothened 1/r potential is used.

Under a fully self gravitating potential the initial core evolves via a first stage of flattening of to half its original maximum and a few times its original area. Accretion shocks start plowing through the surrounding matter, heating it to more than 10^3 K. After the shock becomes standing the matter collected is fragmented by cooling, forming over- and underdensities in the post shock ridge. This place seems to be an ideal star birthing region. Eventually a slightly elliptical dense cloud is formed surrounded by a various subcondensations of comparable densities.

The results we found so far thus are promising and in reasonable accordance with observations as well as former research.

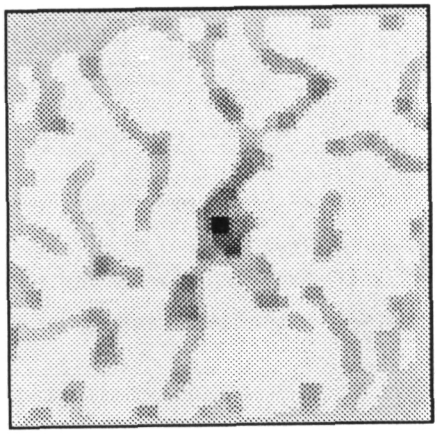

Figure 1.
Fragmentation of a homogeneous medium
by radiative cooling and background heating.

Time evolved : 0.1 Gal.yr.

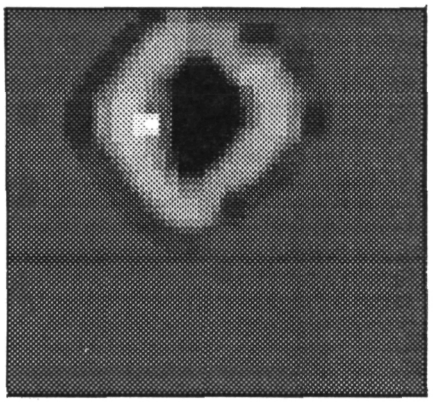

Figure 2.
Dense cores and standing shock
formed under selfgravitation and radiative
cooling from one accretion core.
Time evolved : 0.1 Gal.yr.

References :

A.Dalgarno & R.McCray, 1972; Ann.Rev. of Astr. & Ap., Vol.10, p.375

G.Field, D.Goldsmith & H.Habing, 1969; Ap.J.(Letters), Vol.155, L149

V.Icke, 1985; The growth of molecular clouds by accretion from a smooth galactic disc.

J.Shull & D.Woods, 1985; Ap.J., Vol.288, p50

POWERING THE SUPERWIND IN NGC 253

ALAN WATSON, JAY GALLAGHER
University of Wisconsin – Madison, 475 North Charter Street, Madison, WI 53706.

MICHAEL MERRILL
K.P.N.O., PO Box 26732, Tucson, AZ 85726.

JEAN KEPPEL
603 Pauley Drive, Prescott, AZ 86303.

MARK PHILLIPS
C.T.I.O., Casilla 603, La Serena, Chile 1353.

NGC 253 AS A NUCLEAR STARBURST GALAXY

NGC 253 is a prototypical moderate nuclear starburst galaxy. It is a barred SBc spiral galaxy at a distance of approximately 3 Mpc and can be studied on scales down to 15 pc in the optical and near IR.

It is a bright IRAS source with a flux of 1000 Jy at 60 μm (Rice et al. 1988) and a FIR luminosity of $3 \times 10^{10}\ L_{\odot}$ (Telesco and Harper 1979, Rice et al. 1988). It has a strong Brγ emission line, a signature of ongoing massive star formation (Rieke, Lebofsky, and Walker 1988), and deep CO absorption bands, indicative of the dominance of red supergiants in the near IR. It contains a population of compact radio sources, similar to those seen in M82 (Turner and Ho 1985, Antonucci and Ulvestad 1988, Ulvestad and Antonucci 1991). Optical spectra show that the nucleus is heavily reddened, with a Balmer decrement of approximately 30.

NGC 253 possesses a 'superwind,' seen both in X-ray emission (Fabbiano 1988) and in optical line emission (McCarthy, Heckman, and van Breugel 1987). Nuclear ejection was first suggested by Demoulin and Burbidge (1970) to explain the kinematics of the nuclear region.

NEAR IR OBSERVATIONS

We have obtained J, H, and K images of the entire galaxy at 1.3 arcsec/pixel (18 pc/pixel) using SQIID on the KPNO 1.3m. We have constructed a mosaic of 180 s exposures which traces the galaxy over much of its optical extent. The data were shifted, rotated, magnified, and calibrated following normal practice.

The PtSi detectors in SQIID have a low quantum efficiency (of order 5%) and excellent stability, linearity, and cosmetic quality. To check the quality of the calibration, we compared our images to single-channel measurements (de Vaucouleurs and Longo 1988) in apertures with diameters ranging from 10 arcsec to 100 arcsec and found excellent agreement to around 10%.

C-7

Rieke, Lebofsky, and Walker (1988) published images of the nucleus with a pixel size of 1.2 arcsec. They report that the nucleus was significantly bluer than the circumnuclear region (of order 0.5 mag in $H-K$); we find no trace of this in our data, nor in data taken in October 1991 with SQIID in its current configuration, nor in the data of Forbes et al. (1992). It is possible that seeing or focus effects could blur our colors or that Rieke, Lebofsky, and Walker caught a transitory event, such as a supernova.

We have constructed the $J-H$ and $H-K$ colors for each pixel in our image. We show the color-color diagram for all of the pixels in a region 14 x 14 arcsec centered on the nucleus. The area of the symbol is proportional the the K flux in that pixel. The points clearly form a locus leading from $J-H \approx 0.8$ and $H-K \approx 0.25$ up to much redder colors in the nucleus. We have indicated the standard Milky Way extinction law by an arrow which corresponds to $A_K \approx 0.5$ or $A_V \approx 4.5$. In agreement with Scoville et al. (1985), we interpret the near IR color-color diagram of the nucleus to be due to a dust-shrouded population of red supergiants plus a contribution at K from hot (1000 K) dust.

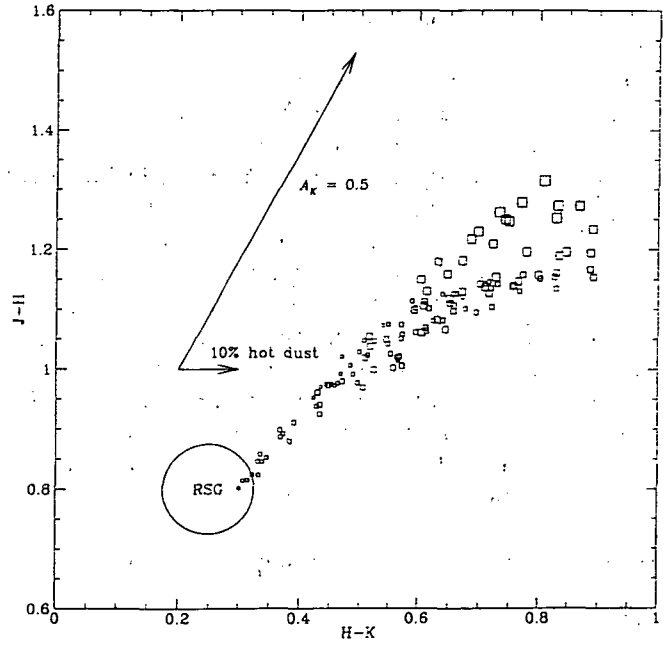

ESTIMATING THE SUPERNOVA RATE

We have obtained the 'dereddened' H magnitude within a radius of 10 arcsec (180 pc) of the nucleus by correcting each pixel for reddening, assuming an intrinsic $J-H$ color of 0.8 for red supergiants. The 'dereddened' H magnitude within 10 arcsec is 7.28, compared the the observed H magnitude of 7.78. (Corrections for extinction are complex, but we consider our correction to be conservative.)

The luminosity of the red supergiants in the nucleus corresponds to about 2% of the bolometric luminosity of NGC 253. The luminosity of massive stars remains roughly constant during their lifetime and they spend a few percent of their life as red supergiants. Assuming a typical red supergiant absolute magnitude at H of -11.0 and a distance of 3 Mpc, the H magnitude of the nucleus corresponds to 4400 red supergiants within 180 pc of the nucleus.

A typical lifetime of a massive star in the red supergiant phase is approximately 10^5 yr, and if we assume continuity over this lifetime we derive a supernova rate of 0.04 yr^{-1} in a 180 pc radius aperture. This is somewhat lower than the rate of 0.1 yr^{-1} to 0.25 yr^{-1} in a 300 pc radius aperture derived from VLA observations of compact sources by Antonucci and Ulvestad (1988). Although our apertures differ in size, our results are directly comparable as most of the compact sources are in the central 10 arcsec. Possible systematic differences between our results may be due to confusion with H II regions and the possibility that the evolution of supernovae in dense environments is not straightforward.

POWERING THE SUPERWIND

From Einstein X-ray observations, Fabbiano (1988) estimates that the temperature and mass of the superwind are of order 10^7 K and about 2×10^7 $M_\odot$. The extent of the wind is at least 4.5 kpc. The wind is highly over-pressurized and is likely to be flowing out at close to the sound speed. This is confirmed by the presence of 300 $km\,s^{-1}$ bulk velocities at the base of the wind seen in long-slit echelle spectra obtained with the CTIO 4m. With these properties, the superwind is being supplied with hot gas on a timescale comparable to the sound crossing time of 10^7 yr. Mass is being supplied to the superwind at a rate of 1.5 $M_\odot\,yr^{-1}$. Energy is flowing into the wind at a rate of about 2×10^{41} $erg\,s^{-1}$ or 6×10^7 $L_\odot$. This corresponds to about 15% of the energy released by supernovae.

This figure should not be over-interpreted. The extinction correction used to derive the supernova rate ignores complications from nebular lines and patchy extinction which will leads us to believe that the true supernova rate wil be somewhat higher than our estimate. Also, the physical properties of the superwind, especially its temperature, are uncertain.

Nevertheless, we can draw two conclusions. It seems inevitable that energy is being efficiently transferred from supernovae in the nucleus into the base of the superwind. The high supernova rate in the nuclear region must lead to an ISM with a global structure vastly different to the ISM in quiescent disks.

We thank Ian Gatley for his help in taking the SQIID images.

REFERENCES

Antonucci, R.J., and Ulvestad, J.S. 1988, ApJ 330, L97.
Demoulin, M.-H., and Burbidge, E.M. 1970, ApJ 159, 799.
Fabbiano, G. 1988, ApJ 330, 672.
Forbes et al. 1992., MNRAS 254, 509.
McCarthy, P.J., Heckman, T.M., and van Breugel, W. 1987, AJ 93, 264.
Scoville, N.Z., et al. 1985, ApJ 289, 129.
Rice, W., et al. 1988, ApJS 68, 91.
Rieke, G.H., Lebofsky, M.J., and Walker, C.E. 1988, ApJ 325, 679.
Telesco, C.M., and Harper, D.A. 1980, ApJ 235, 392.
Turner, J.L., Ho, P.T.P. 1985, ApJ 299, L77.
Ulvestad., J.S., and Antonucci, R.J. 1991, AJ 102, 875.
de Vaucouleurs, A., and Longo, G. 1988, Catalogue of Visual and IR Photometry of Galaxies (University of Texas: Austin).

^{12}CO J=2-1 Map of the Disk of Centaurus A: Evidence for Large Scale Heating in the Dust Lane

W. Wild[1], M. Cameron[2], A. Eckart[2], R. Genzel[2], H. Rothermel[2], G. Rydbeck[3] & T. Wiklind[3]

[1]*European Southern Observatory, La Silla, Chile*
[2]*Max-Planck-Institut für extraterrestrische Physik, W8046 Garching, Germany*
[3]*Onsala Space Observatory, Sweden*

I. Introduction

Centaurus A (NGC 5128) is a nearby (3 Mpc) elliptical galaxy with a prominent dust lane, extensive radio lobes and a compact radio continuum source, suggestive of nuclear activity. As a consequence of its peculiar morphology, this merger candidate has been the subject of much attention, particularly at optical wavelengths. Unfortunately the high and patchy extinction in the disk, aggravated by the warped structure of the dust lane, has severely hindered investigations into the properties of the interstellar medium, particularly with regard to the extent of star formation. Here we present a map of the ^{12}CO J=2-1 line throughout the dust lane which, when combined with a previously measured ^{12}CO J=1-0 map (Eckart *et al.* 1990a) and data on molecular absorption lines observed against the compact non-thermal continuum source (Eckart *et al.* 1990b), offers insight into the excitation conditions of the molecular gas.

II. Results

We mapped the ^{12}CO J=2-1 line with the 15m Swedish-ESO Submillimetre Telescope (SEST) in La Silla, Chile during several observing periods between December 1990 and May 1992. A total of 240 positions, extending over an area of 200″×70″, were measured with the 230 GHz receiver. The beam FHWM is 22″ at this frequency. The grid spacing was typically 8″ in the inner disk and 16″ at the extremities with total integration times of 30 and 4 minutes respectively.

Our map of the ^{12}CO J=2-1 emission, presented in Figure 1, clearly illustrates that strong emission in this line has been detected over a large area of the dust lane. The emission is generally symmetrical about the nucleus but, as in the case of the J=1-0 and IRAS 50μm maps (Eckart *et al.* 1990a), it is not centrally peaked. The striking similarity in the morphologies of the J=2-1, J=1-0 and 50μm maps suggests that the gas and warm dust (T_d ~40K) are probably well coupled. The good spatial sampling of this map has allowed us to undertake an extensive investigation into the kinematics of the gas, particularly in the nuclear vicinity (Rydbeck *et al.* 1992). Here we restrict discussion to the excitation conditions of the gas.

The excitation conditions in the disk can be probed using the J=2-1/J=1-0 ratio, when the J=2-1 map has been convolved to the resolution of the J=1-0 map. This results in a ratio of close to unity at the position of the nucleus, a value which, rather surprising, is also typical of the gas throughout the whole extent of the disk. The ratio of ~1 outside the nucleus contradicts previous conclusions (Eckart *et al.* 1990a) which had been based on comparison with J=2-1 spectra obtained by Phillips *et al.* (1987). Such a high J=2-1/J=1-0 ratio implies that the bulk of the gas in the dust lane is warm (T>15K), dense (n_H ~$2\times10^4\beta$ cm^{-3}, the critical density required to thermalise the J=2-1 level, where β is the escape probability) and, probably partially, optically thick. This conclusion is supported by a measured J=2-1/J=1-0 ^{13}CO ratio of 0.9 at one position in the disk. That the nucleus of Centaurus A does not dominate the ratio map runs contrary to the trend in active galaxies in which the nuclear vicinity generally harbours warmer and denser gas than the disk (*e.g.* Eckart *et al.* 1991; Henkel *et al.* 1991). On the other hand, in all these galaxies, including Centaurus A, the warm dense molecular gas is enclosed within the nuclear bulges.

Only one other galaxy, M82, claims a J=2-1/J=1-0 ratio significantly higher than that measured for Centaurus A (Wild *et al.* 1992). Although NGC 1808, a nearby (10.9 Mpc) spiral

with a peculiar and complex nucleus and numerous 'hotspots', and NGC 4945, a southern edge-on spiral, are characterised by a J=2-1/J=1-0 ratio of $\geq$1 in the nuclear vicinity, this ratio falls to $\sim$0.6 in the disk (Whiteoak *et al.* 1991). In this context, Centaurus A shows excitation characteristics which have more in common with the starburst galaxy IC 342, although even here the J=2-1/J=1-0 ratio falls to $\sim$0.7-0.8 at distances of >500pc from the centre (Eckart *et al.* 1990c). Such a comparison raises the question of the extent of star forming activity in the dust lane. Certainly the dust lane is abundant in HII regions but, on the other hand, the far-IR luminosity and total molecular mass in the central kiloparsec ($1\times10^9 L_\odot$ and $5\times10^7 M_\odot$ respectively) are both a factor of 4 lower than in IC 342. However the star formation efficiencies, $L_{FIR}/M_\odot$, are similar for both galaxies (Eckart *et al.* 1990a) and are comparable to the most active star-forming regions in the disk of the Milky Way.

A more detailed report of this work will be presented elsewhere.

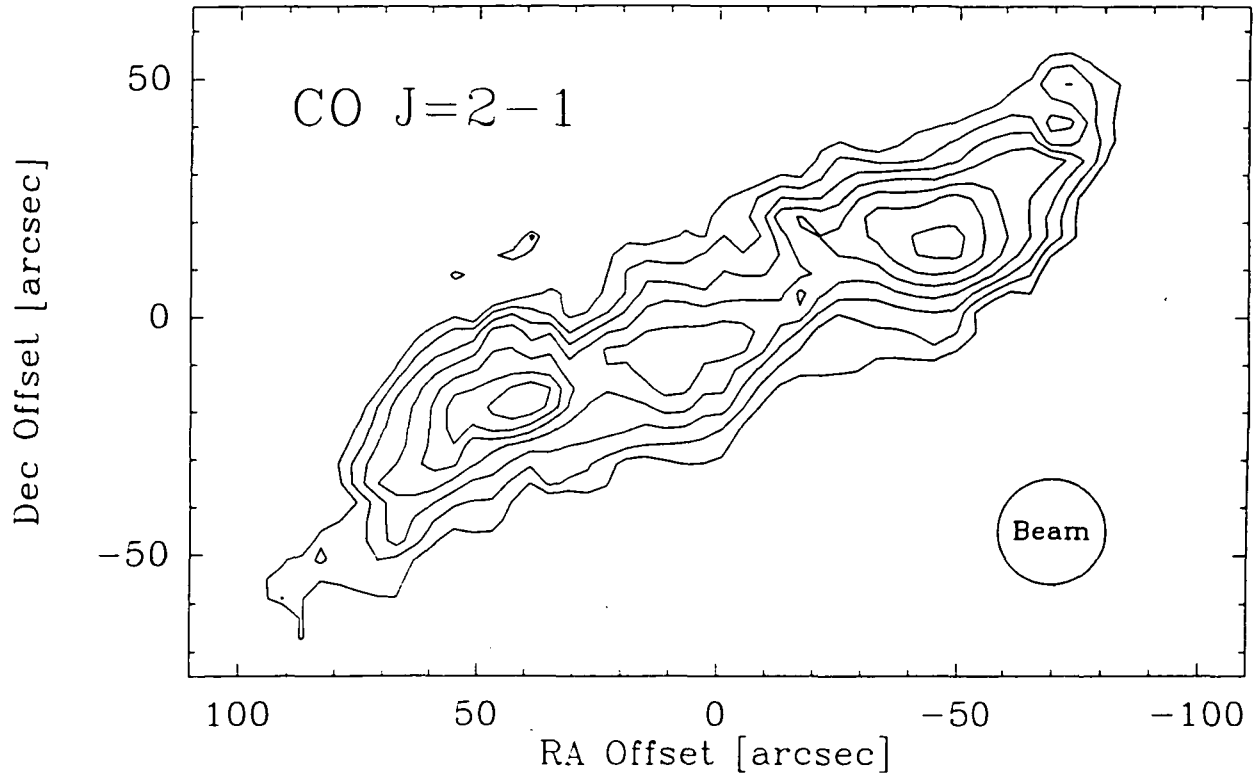

Figure 1: Contour map of the velocity integrated ^{12}CO J=2-1 emission from the dust lane in Centaurus A. Contour levels are 20, 25, ... K kms^{-1} and the peak intensity is 54 K kms^{-1}. Coordinates are offset from the position of the radio continuum source.

REFERENCES

Eckart A., Cameron M., Rothermel H., Wild W., Zinnecker H., Rydbeck G., Olberg M. & Wiklind T., 1990a, *Ap.J.*, **363**, 451

Eckart A., Cameron M., Genzel R., Jackson J.M., Rothermel H., Stutzki J., Rydbeck G. & Wiklind T., 1990b, *Ap.J.*, **365**, 522

Eckart A., Downes D., Genzel R., Harris A.I., Jaffe D.T. & Wild W., 1990c, *Ap.J.*, **348**, 434

Eckart A., Cameron M., Jackson J.M., Genzel R., Harris A.I., Wild W. & Zinnecker H., 1991, *Ap.J.*, **372**, 67.

Henkel C, Baan W.A. & Mauersberger R., 1991, *A&A Rev.*, **3**, 47.

Phillips *et al.*, 1987, *Ap.J.*, **322**, L73

Rydbeck *et al.*, 1992, in preparation.

Whiteoak J.B. *et al.*, 1991, in *Dynamics of Galaxies and their Molecular Cloud Distributions*, p.164, eds: Combes F. & Casoli F.

Wild *et al.*, 1992, *A&A*, accepted.

Page Intentionally Left Blank

AUTHOR INDEX

Page Intentionally Left Blank

REPORT DOCUMENTATION PAGE

Form Approved
OMB No. 0704-0188

1. AGENCY USE ONLY *(Leave blank)*	2. REPORT DATE	3. REPORT TYPE AND DATES COVERED
	January 1993	Conference Publication

4. TITLE AND SUBTITLE

The Evolution of Galaxies and Their Environment

5. FUNDING NUMBERS

188-44-53

6. AUTHOR(S)

D. Hollenbach, H. A. Thronson, and J. M. Shull

7. PERFORMING ORGANIZATION NAME(S) AND ADDRESS(ES)

Ames Research Center
Moffett Field, CA 94035-1000

8. PERFORMING ORGANIZATION REPORT NUMBER

A-93028

9. SPONSORING/MONITORING AGENCY NAME(S) AND ADDRESS(ES)

National Aeronautics and Space Administration
Washington, DC 20546-0001

10. SPONSORING/MONITORING AGENCY REPORT NUMBER

NASA CP-3190

11. SUPPLEMENTARY NOTES

Point of Contact: D. Hollenbach, Ames Research Center, MS 245-3, Moffett Field, CA 94035-1000; (415) 604-4164

12a. DISTRIBUTION/AVAILABILITY STATEMENT

Unclassified — Unlimited
Subject Category 90

12b. DISTRIBUTION CODE

13. ABSTRACT *(Maximum 200 words)*

The Third Teton Summer School on Astrophysics entitled "The Evolution of Galaxies and Their Environment" was held on July 5-10, 1992, to discuss the formation of galaxies, star formation in galaxies, galaxies and quasars at high redshift, and the intergalactic and intercluster medium and cooling flows. Observational and theoretical research on these topics was presented at the meeting and summaries of the contributed papers are included in this volume.

The papers covered a broad range of research on galaxy environment and evolution and focused on such topics as the Cosmic Background Explorer (COBE) observations of the microwave background, the evolution of the large scale structure of the universe, the formation of galaxies, stellar population synthesis and galaxian spectral evolution, the nature of high redshift objects, X-ray observations of galaxies, the intergalactic medium, quasar absorption lines, cooling flows, mergers and interactions among galaxies, galactic clusters and their evolution, star formation in galaxies, galactic winds, and the central energy source for active galaxies. A number of papers examined galaxy morphology and luminosity functions.

Some emphasis was given to the origin and evolution of quasars. A number of papers examined the origin of the Lyman alpha forest of absorption lines from distant quasars, and the implications for the conditions in the intergalactic medium.

14. SUBJECT TERMS	15. NUMBER OF PAGES
Galaxies, Cosmology, Intergalactic medium, Quasars	394
	16. PRICE CODE: A17

17. SECURITY CLASSIFICATION OF REPORT	18. SECURITY CLASSIFICATION OF THIS PAGE	19. SECURITY CLASSIFICATION OF ABSTRACT	20. LIMITATION OF ABSTRACT
Unclassified	Unclassified		

NSN 7540-01-280-5500

GPO 785-158/99054

Standard Form 298 (Rev. 2-89)
Prescribed by ANSI Std. Z39-18
298-102